PATTERNS OF LIFE HISTORY RECORDED IN THE DORSAL RIB HISTOLOGY OF AMNIOTES

AND THEIR IMPLICATIONS FOR BODY SIZE EVOLUTION AND ECOLOGY OF SAUROPOD DINOSAURS

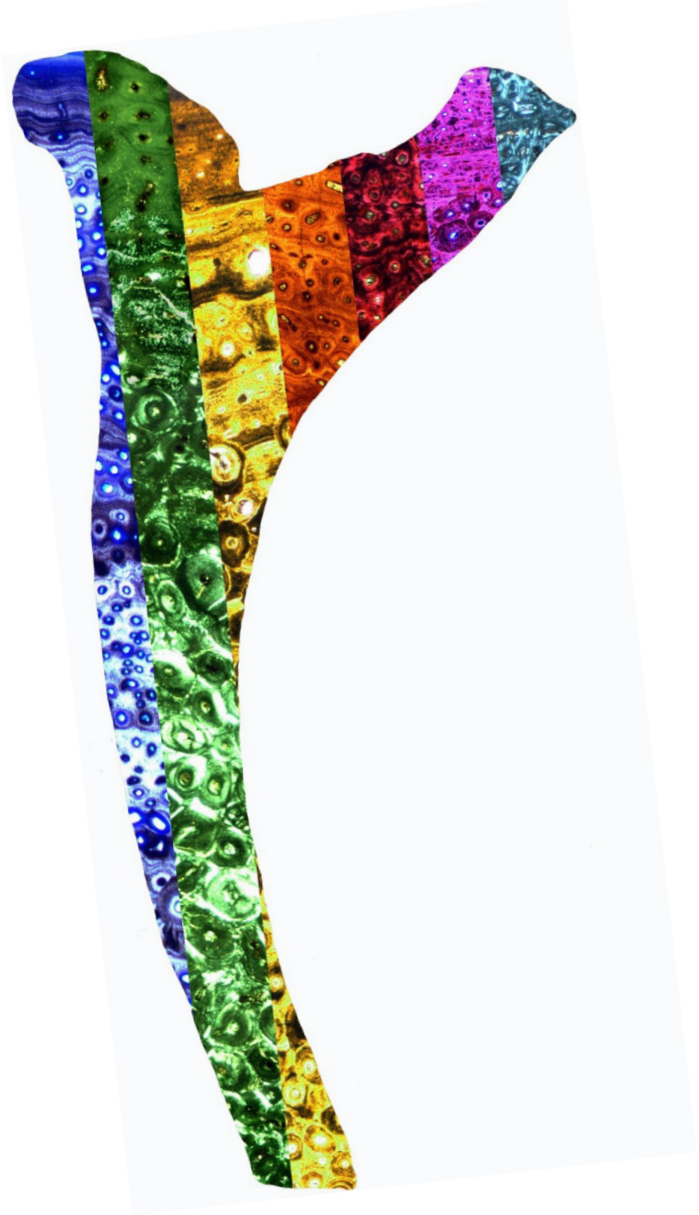

Katja Waskow

Dissertation zur Erlangung des Doktorgrades (Dr. rer. nat.) der
Mathematisch-Naturwissenschaftlichen Fakultät der
Rheinischen Friedrich-Wilhelms-Universität Bonn

Patterns of life history recorded in the dorsal rib histology of amniotes and their implications for body size evolution and ecology of sauropod dinosaurs

Dissertation

zur

Erlangung des Doktorgrades (Dr. rer. nat.)

der

Mathematisch-Naturwissenschaftlichen Fakultät

der

Rheinischen Friedrich-Wilhelms-Universität Bonn

vorgelegt von

Katja Waskow

aus Hagen-Haspe

Bonn, Februar 2019

Angefertigt mit Genehmigung der Matematisch-Naturwissenschaftlichen Fakultät der

Rheinischen Friedrich-Willhelms-Univerität Bonn.

1. Gutachter:	Prof. Dr. P. Martin Sander
2. Gutachterin:	Prof. Dr. Eva Maria Griebeler
Fachnahes Mitglied:	Prof. Dr. J. Wolfgang Wägele
Fachfremdes Mitglied:	Prof. Dr. Tom McCann

Tag der Promotion: 23.05.2019
Erscheinungsjahr: 2019

Hiermit erkläre ich an Eides statt, die vorliegende Arbeit selbstständig verfasst und keine anderen Hilfsmittel als die angegebenen verwendet zu haben. Inhaltlich und wörtlich aus anderen Werken entnommene Stellen und Zitate sind als solche gekennzeichnet.

Katja Waskow

Acknowledgements

First, I would like to express my sincere gratitude to my supervisor Prof. P. Martin Sander for his scientific support, patience, and confidence in me. During the last years his continuous motivation, broad knowledge and out of the box thinking inspired my scientific work, encouraged me to grow as a researcher and helped me writing and finishing this thesis.

Furthermore, my special thanks go to Prof. Eva Maria Griebeler, not only for being my second reviewer, but also for her great mathematical support and ecological knowledge that helped me a lot during growth curve erection and interpretation. Beside my advisors I would like to thank Prof. J. Wolfgang Wägele and Prof. Tom McCann for kindly agreeing to be part of my dissertation committee and for all their efforts connected with this function.

This dissertation is the last contribution to the very successful former DFG Research Unit 533 “Biology of the Sauropod Dinosaurs: The Evolution of Gigantism”. Thus, I want to thank the DFG for funding the first two years of research and all members of the Research Unit for providing me an insight in so many kinds of research and facets of thinking. Nicole Klein and Dorotha Konietzko-Meier are specially acknowledged for my substitution during two maternity leaves that helped me a lot combining scientific and family life.

My special thanks go to Octávio Mateus, Emanuel Tschopp, Cary Woodruff, Kayleigh Wiersma, Shoji Hayashi, Alexandra Houssaye and many others who inspired my work by being constructive and supportive co-authors, on several papers that are part of the outcome of my thesis.

This research would not have been possible without the great support, loan- and sampling permission of a host of people and institutions. Thus, my sincere thanks go to:

Rodney Scheetz (Museum of Earth Sciences, Brigham Young University, Provo, Utah, USA), Glenn Storrs (Cincinnati Museum Center, Cincinnati, USA), Oliver Rieppel, William Simpson, and Kenneth Angielczyk (Field Museum of Natural History, Chicago, Illinois, USA) Daniela Schwarz (Museum für Naturkunde der Humboldt-Universität zu Berlin, Germany), Octávio Mateus (Museu da Lourinhã, Portugal), Jack Horner and Cary Woodruff (Museum of the Rockies, Bozeman, Montana, USA), Ulrich Joger and Ralf Kosma, (Naturhistorisches Museum, Braunschweig, Germany), Adrian Hunt (New Mexico Museum of Natural History and Science), Hans Jakob Siber, Esther Wolfensperger, Ben Pabst, Rabea Lillich, and Nicola Lillich (Sauriermuseum Aathal, Switzerland), Thomas Bolliger (Kulturama Museum des Menschen, ETH Zürich, Switzerland), Randal Irmis and Carolyn Levitt-Bussian (Utah Museum of Natural History, Salt Lake City, Utah, USA), Kelli Trujillo and Laura Vietti (University of Wyoming, USA), and Christopher Norris and Daniel Brinkmann (Yale Peabody Museum, USA).

A histological dissertation always is connected to enormous technical efforts, especially when hundreds of thin sections are needed. Thus, I foremost want to acknowledge the enormous support of Olaf Dülfer, who helped me a lot during thin section production (and sometimes rescue), cast, mold, and reconstruction of the sampled bone elements. Furthermore, I want to thank Rebecca Hofmann, Tanja Wintrich, and Pia Schucht, who also participated in thin sectioning.

It was a great pleasure and scientific benefit to work in Martin Sanders working group for so many years. International networking could not have been easier than simply staying in Bonn to meet all kinds of high-class researchers on all academic levels. Thus, I would like to express my honest thank to all actual and former members of the AG Sander for fruitful discussions and a great working atmosphere with special thanks to my office roommates Tzu-Ruei Yang and Jens Lallensack, as well as Tanja Wintrich who recently finished their theses too and helped me a lot to go to the final stages of this disstertaion.

I am very happy to have many supportive and motivating friends including Janka Brinkkötter, Sashima Läbe, Jessica Mitchell, Kayleigh Wiersma, Marlene Vorderwülbecke, Stephanie Schempershofe, Sylvia Hellige, Meggy Lichtenberg, Patrick Meisner, Melanie Meisner, and Anja Obert whom I want to thank for their cheering ups, helpful comments, and all different kinds of support.

Finally, I would like to thank my family starting with my wonderful mother Marlies Waskow I can always rely on, and my beloved husband Moritz Eisele for enduring my temper and supporting me in so many ways. I want to end by expressing my heartfelt gratitude to my beloved sons Leo Marino and Anton Emilio for opening my heart during tough times and putting a smile on my face.

Summary

This dissertation analysis the potential of dorsal ribs to provide information of ecology and life history traits on both, individual and taxonomical level, mainly using the tool of bone histology. The growth record stored in the dorsal ribs provides information about ontogenetic stage, age at sexual- and skeletal maturity, and in some cases age at death and sex of an individual. The advantages of rib histology in contrast to the normally sampled long bones are especially important for studying sauropods that are primarily in focus of this study. Dorsal ribs of different sauropod taxa from different localities were sampled because the usual sampled long bones like humeri and femora do not develop and preserve cyclicity in all but the outermost cortex. Thus, growth record preservation in ribs that has been proven to be the most complete of all skeletal elements is the best approach to analyze growth of these largest terrestrial animals of all times. In addition to their gigantic size sauropods have the largest size ranges from hatchlings to adults among amniotes. Therefore, their growth rates or growth times analyzed herein must have been close to the maximum that can be approached within the terrestrial realm.

Chapter 1: In the first chapter an introduction into the three main areas of reseach combined in this dissertation is given. The chapter aims to provide an overview about the stages of knowledge on dorsal ribs, sauropods, and histology with special respect to the cyclicity as the main area of interest among all histological features.

Chapter 2: The advantage of ribs as useful element to sample in sauropods has been analyzed and published as result of my diploma thesis. In addition to that this chapter analysis and proofs the utility of dorsal rib histology for growth record examination in other archosaur taxa including different theropod and ornithischian taxa, and crocodiles. In all sampled taxa rib histology reveals an even more complete growth record than the usual sampled long bones indicating that ribs should be also considered for sampling in taxa other than sauropods.

Chapter 3: Similar to long bones, dorsal ribs of graviportal animals like sauropods show a distinct microanatomical pattern. Cortical thickness is increased while a decrease in size of the medullary cavity can be observed. The transition zone between cortex and medullary region is wider and filled with cancellous bone. These specializations most likely evolved for better energy absorption of stresses like compression, bending and torsion. Microanatomical organization in graviportal animals were compared to similar adaptations (osteosclerosis) in secondary aquatic amniotes. The quantitative and qualitative analysis based on a phylogenetic content was performed on a large sample base of fossil and extant amniotes.

Chapter 4: To understand life history and ontogeny of sauropods, dorsal rib samples of juvenile individuals were of special interest. The nearly monospecific Mother´s Day Quarry assemblage of small disarticulated diplodocine specimens has been described as drought induced bone bed yielding only juveniles before. However, accidentally the histological analysis performed on them here, revealed an adult ontogenetic stage, and thus a dwarfed status for most individuals of the assemblage. Additionally, a heterogenous age distribution and the presence of at least two size morphs have been recognized and described.

Chapter 5: The larger diplodocine morphotype of the Mother´s Day Quarry mentioned above is only represented by early sage juveniles and might belong to an average sized diplodocine species. It is not only represented by ribs but also by cranial remains including an almost complete skull and mandible described here. It shows intermingled characters of Macronaria and Diplodocoidea that hint to a recapitulation of phylogeny during ontogeny and to dietary partitioning between juveniles and adults.

Chapter 6: The complete sample base taken for this study provides evidence for different ages at sexual and skeletal maturity in the two mayor sauropod clades. While macronarians on average reached sexual maturity at age 17 and skeletal maturity after 27 years of growth, diplodocoids needed only 12 years to become sexual mature and reached full size at the age of 18 (median). Slight differences between the single taxa of the two mayor clades are observable like, e.g., slightly older ages at main life history events for *Brachiosaurus* than for *Camarasaurus* or ages at sexual and skeletal maturity in a dwarfed diplodocine population that are marginally lower than in other diplodocoids.

Chapter 7: This chapter is the synthesis of this dissertation and aims to review the state of knowledge about life history traits, ecology, and evolution ascertained by analyzing dorsal ribs of different vertebrate taxa. While being underestimated in the past, dorsal ribs begin to be more in focus of scientific interest. The advantages of dorsal ribs over other skeletal elements like humeri and femora that are typically used for histological and microanatomical research are described, summing up well established and new methods and results including individual and taxonomical differences regarding ages at death, sexual- and skeletal maturity, habitat preferences and ecological nice partitioning with focus on sauropods.

Structure of dissertation

The following dissertation is subdivided in several chapters some of which are already published or submitted to different peer reviewed scientific journals. Therefore, some chapters are presented in the format of the journal where they have been published. These papers are included in the contents chapter only with their headings and and main subdivisions (first headings only) because the internal organization and numbering of the published articles differs from the general organization of this thesis. I am the first author of most of the papers presented herein. However, caused by the collaborative nature of some of the studies the contributions of each author are disclosed at the beginning of each chapter. The authorship of Martin Sander in most of the papers is justified by his excellent supervision and proofreading of the manuscripts. Reference lists (if not included in the printed article) are provided at the end of each chapter.

Contents

CHAPTER 4:

HISTOLOGICAL EVIDENCE FOR DWARFISM AND DIFFERENT MORPHOTYPES OF DIPLODOCINE SAUROPODS WITHIN THE UPPER JURASSIC MOTHER'S DAY QUARRY (MORRISON FORMATION, MONTANA, USA) 93

CHAPTER 7:

SYNTHESIS: THE ADVANTAGES OF DORSAL RIB HISTOLOGY – REVIEWING THE STATE OF KNOWLEDGE ABOUT LIFE HISTORY TRAITS, ECOLOGY, AND EVOLUTION OBTAINED BY ANALYZING DORSAL RIBS OF DIFFERENT VERTEBRATE TAXA 321

„Nichts in der Biologie macht Sinn
außer im Licht der Evolution!“

“Nothing in biology makes sense
except in the light of evolution.”

Theodosius Dobzhansky

CHAPTER 1

Introduction

Katja Waskow

This dissertation marks the starting point in analyzing rib histology in more detail focusing mainly on sauropods. Previous knowledge on this special but fruitful and promising new aspect of histological research is rare. In general rib histology has only been studied marginally before (e.g., Erickson, 2005) until recent studies introduced rib histology (Waskow and Sander, 2014; Waskow and Mateus, 2017, (chapter 2)) and rib microanatomy (Canoville et al., 2016; Houssaye et al., 2016a (chapter 3)), as a proper tool for collecting life history data of extinct animals. The following introduction aims to provide an overview about the stage of knowledge in the three main fields of research combined in this study: dorsal ribs, sauropods, and histology with special respect to the cyclicity as the main area of interest among all histological features.

1.1. Dorsal ribs of vertebrates

Even if studied marginally before, dorsal ribs of vertebrates until recent years (Waskow and Sander, 2014; Canoville et al., 2016; Houssaye et al., 2016a (chapter 3); Waskow and Mateus, 2017, (chapter 2)) have never been in focus of scientific interest in both, recent biology and paleontology. Most likely this is caused by their relatively simple shape that in most cases impedes more detailed morphological or taxonomical analysis. Moreover, their shape shows little variation during ontogeny and at first sight they do not affect several areas of research that focus, e.g., on locomotion, nutrition, ecology, or reproduction. Nevertheless, some recent studies start taking ribs more into account to analyze their morphology (Klein and Sichelschmidt, 2014) or ecological adaptations of different taxa using microanatomical patterns (Canoville et al., 2016). Additionally, dorsal ribs of dinosaurs preserve the most complete growth record of all skeletal elements caused by their unique shape (Waskow and Sander, 2014; Waskow and Mateus, 2017, (chapter 2)). The dorsal rib combines the simple shape of a long bone needed for thick cortical bone formation with relatively low resorption in the inner bone region during the expansion in the medullary cavity at the posteromedial side of the proximal rib shaft region. Contrary to that, the expansion of the medullary cavity in long bones destroys significantly more of the early juvenile growth record. By sampling the proximal end of the dorsal rib shaft at the posteromedial side histologically, various life history data can be ascertained. Especially in sauropods that are primarily in focus of this dissertation, dorsal ribs are the only skeletal elements yielding an almost complete growth record needed for skeletochronological

analysis because theirs long bones do not produce and preserve lines of arrested growth (LAGs) in all but the outermost cortex due to relatively higher bone apposition and remodeling rates (Mitchell and Sander, 2014; Waskow and Sander, 2014).

1.1.1. Function and evolution of ribs

In general ribs (latin: costae) are long curved bones of vertebrates forming the rib cage. The primary function of the rib cage is to protect inner organs like heart, lungs, and other internal organs of the thorax. In terrestrial tetrapods they are also very important for breathing. Together with the intercostal musculature they serve in expanding the chest cavity (Romer and Parsons, 1977). In terms of evolutionary development, the first outgrowth of some ventral arches appears in the tail region of the Holocephalia. In Elasmobranchii this first outgrowth that evolved and extend in the system of intermuscular septa becomes divided into a lower haemapophsis and a laterodorsal rib bearing pleurapophysis. On the Sarcopterygian branch the ossification of ribs begins in Dipnoi, and becomes complete in Tetrapods (Gadow, 1933). The primitive anatomical condition in ribs still observable in some fish (e.g., *Polypterus*), is that two sets of ribs (dorsal- and ventral ribs) are connected to the vertebral column. In most fishes (like, e.g., sharks) the dorsal ribs (homologous to the primitive pleurapophysis) commonly are absent and only the ventral ribs (homologous to the primitive haemapophysis) are developed (Gadow, 1933; Romer and Parsons, 1977). Following the conventional doctrine contrary to this, tetrapods only show a single set of ribs that most likely is homologous to the dorsal rib set. More recently Britz and Bartsch (2003) postulated that dorsal ribs in gnathostome vertebra do not exists at all and that the most parsimoneus explanation predicts that all ribs seen in gnathostomata are homologous to the ventral ribs. However, to avoid confusion, the ribs of the vertebrate taxa studied herein are still referred to as dorsal ribs independent of their possible ventral origin. The terminology dorsal rib is frequently used in other respects to distinguish them from more anterior and posterior ribs along the vertebral column like, e.g., cervical, sacral, or caudal ribs.

The evolutionary origin of the two headed rib seen in tetrapods from the single headed fish rib most likely is closely connected to the adaptation to the terrestrial realm. While the dorsal axial musculature became less important resulting in its reduction in size, the dorsal ribs served as an anchor for muscle attachment needed for undulating movement. This enforced a more stable connection of ribs and vertebrae accomplished by the formation of a second rib head. It is still not completely understood whether this formation was performed by either the development of a new second rib head (namely the tuberculum) or by the spitting of the former single wide proximal head into a capitulum and a tuberculum. While the capitulum articulates with the intercentra or intercentral disc, the tuberculum articulates at first with the side of the neural arch, and later in evolutionary development with the diapophysis or dorsal transverse process (Rockwell et al., 1938). In early vertebrates, every vertebra was connected to a pair of ribs. In their descendants however,

the number and morphology of ribs differs greatly between different taxa. While dorsal ribs in mammals were restricted to the thoracic region, some vertebrate taxa like, e.g., snakes have dorsal ribs on every vertebra of the trunk region. Frogs and lampreys in contrast do not show any ribs at all (Romer and Parsons, 1977). Dorsal rib morphology of amniotes can be related to lifestyle and locomotion like, e.g., flying, diving, or digging (Jenkins, 1970; Wake, 1979; Tickle et al., 2007; Canoville et al., 2016)

1.1.2. Ontogenetic formation of ribs

Like all other bony skeletal elements, the bone forming dorsal ribs is a living tissue that (beside of its mechanical functions) is used for production of white and red blood cells in the marrow spaces and as mineral storage (Currey, 2002; Hall, 2005). During its life it undergoes several cycles of formation by osteoblasts (that became osteocytes once surrounded by bone tissue) and resorption by osteoclasts. Initially, the bone tissue itself however, is a replacement tissue. In the early stages of embryonic development, the rib consists of fibrous membranes and avascular cartilage. During ossification (osteogenesis), the cartilage is replaced by bone. Two types of ossification do exist: intermembraneous ossification and endochondral ossification (Gilbert, 2000; Hall, 2005). While intermembraneous ossification, in which compact and spongy bone develops directly from mesenchymal connective tissue, is the only ossification forming flat bones like cranial bones, endochondral ossification replacing cartilage by bone tissue is most important for the initial formation of the rest of the skeleton, including long bones and ribs. The initial cartilage is produced by chondrocytes that differentiated from mesenchymal cells. As more cartilage matrix is produced and calcification begins, nutrients can no longer reach the inner chondrocytes in the avascular cartilage resulting in their death and disintegration of surrounding cartilage. Blood vessels invade the resulting spaces, carying osteogenetic cells needed for bone formation (Gilbert, 2000; Currey, 2002, Hall, 2005). This is how the primary center of ossification is built in the middle region of the bone.

At the same time chondrocytes and cartilage continue to grow at the end of the bone increasing bone length building the epiphyseal centers of ossification, commonly called the growth plate. Secondary In long bones this growth in length occurs at both ends approximately in the same rate (Francillon-Vieillot et al., 1990), while growth in dorsal ribs is directed from proximal to distal. This most likely is caused by the need of the rib head region to stay in function. While the capitulum and tuberculum of the rib are articulated to the dorsal vertebrae during growth, the distal end of the rib has no limitation of growth enabling a more rapid growth in this direction. This assumption is verified by the findings of Waskow and Sander (2014) who found the most complete growth record located at the proximal end of the rib shaft. While ribs are increasing in length they are also increasing in diameter. In this so-called appositional growth osteoblasts produce new bone beneath the periosteum that covers the bone surface.

Simultaneously, osteoclasts resorb older bone tissue lining the medullary cavity to enlarge it (Gilbert, 2000; Hall, 2005). This whole formation process of bone called remodelling initiates shortly before hatching and continues throughout growth. However, because bone is a living tissue bone resorption and formation of bone is not stopped completely after the individual reached skeletal maturity. Remodeling, the formation of secondary or Haversian bone tissue still proceeds. This process where primary bone is resorbed and replaced by newly formed bone material in most taxa is initiated way before growth is completed (Francillon-Vieillot et al., 1990; Mitchell, 2017). Injury, exercise, and mobilization of minerals stored in the bone tissue are often discussed to cause this secondary remodeling (Mitchell, 2017) that is further described in chapter 1.3.2.

1.1.3. Dorsal ribs of sauropods

Sauropods, that are mainly in focus of this dissertation, show rib cages that consist of a set of 10 to 12 ribs on each body side (Osborn and Mook, 1921). However, the difference in rib count at least partially is caused by the interpretation of the last ribs that were already counted to the sacrum in some descriptions. Even if dorsal rib morphology in general does not differ greatly within the rib cage, sauropod taxa (compared to most dinosaurs, mammals and reptiles) do show some differences along the vertebral column, especially in the rib-head region. The angle of capitulum and tuberculum shows some variation from cranial to caudal. While capitulum and tuberculum are situated far apart in the first ribs, they subsequently approach each other posteriorly (Fig. 1). This approach is more rapid in the first four ribs and lesser distinctive in the following (Osborn and Mook, 1921). This enables more accurate position determination within the rib cage in ribs one to four if there were found in isolation.

Only little variation in rib morphology can be observed between different sauropod taxa. However, overall robustness, length, and shaft curvature or rotation together with dorsal rib head morphology variation in some cases allows the assignment to a certain sauropod taxon on family to genus level, especially in rib two to four. In most sauropod taxa rib three to four are the stoutest while rib five in most cases is the longest rib in the whole rib cage (Osborn and Mook, 1921; Waskow and Sander, 2014). Pneumaticity in ribs occurs frequently and most extensive in the head region of Titanosauriform taxa (Wilson and Sereno, 1998; Wedel, 2005). In *Camarasaurus* and most Diplodocoidea no pneumaticity has been observed at all (Wedel, 2005). Only some small foramina leading to internal cavities have been reported for some Diplodocidae like, e.g., *Apatosaurus* (Gilmore, 1936) or *Supersaurus* (Lovelace et al., 2003). In *Brachiosaurus* pneumaticity does occur, however it is not as pronounced as in Titanosauriform taxa (Riggs, 1904; Janensch, 1947; 1950). Pneumaticity influences the completeness of the growth record due to resorption of primary bone tissue during the formation of pneumatic cavities. Thus, mainly non-pneumatic dorsal ribs of *Camarasaurus* and diplodocine taxa are used for sampling in this study.

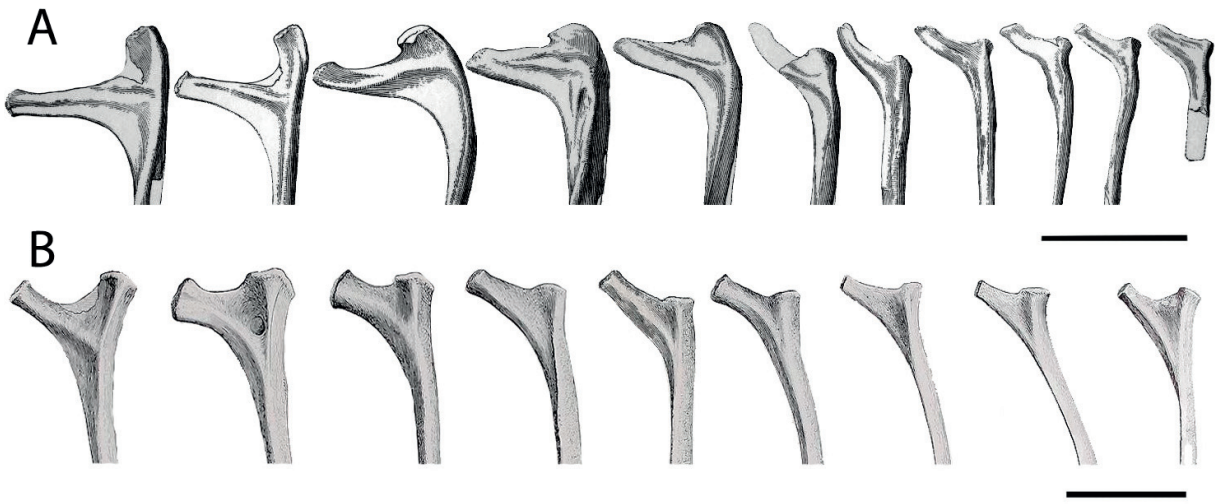

Fig. 1: Drawings of the dorsal rib head region showing the change in morphology and angle between capitulum and tuberculum from anterior to posterior in the two mayjor neosauropod clades Macronaria (*Camarasaurus*) and Diplodocoidea (*Apatosaurus*). Scale bar equals 50 cm. **A**: Dorsal rib head region of *Camarasaurus supremus* modified after Osborn and Mook (1921). Right rib cage mirrored to the left for better comparison. **B**: Dorsal rib head region (left side) of *Apatosaurus louisae* modified after Gilmore (1936).

1.2. Sauropods

Sauropods are the largest terrestrial vertebrates that ever inhabited the planet. They are known from all continental landmasses (Lockley et al., 1994; Upchurch, 1995) including fragmentary remains from Antarctica (Cerda et al., 2012) where most likely more of these giants await their discovery still covered by ice. Stratigraphically their range extends from the Late Triassic (Norian) until the Late Cretaceous (Maastrichtian) (Apesteguía, 2004; Molnar, 2010; Vila et al., 2012). Even if often stated in the literature before (Buffetaut et al., 2000; 2002; Yates and Kitching, 2003; Sander et al., 2004; Apaldetti et al., 2018) true body fossils of sauropods do not occur until the Early Jurassic since the sediments in which the sauropods described to be Triassic in age were found recently were redated to be Jurassic. Nevertheless, tracks of sauropods are known from the Late Triassic verifying their occurrence latest in the Norian (Lallensack, 2018). Hence sauropods dominated ecosystems worldwide for over 100 Ma and were the most successful herbivores of all times.

Even though globally distributed, several sauropod taxa traditionally are described to be endemic caused by the fragmentation of Pangea (Russell, 1993; Upchurch et al., 2002; Wilson, 2005). The prime age of sauropod diversification is often stated to be the Late Jurassic were most of the sauropod genera do occur (Klein et al., 2011; Wilson, 2002). However, this might be caused by the diversity of Late Jurassic outcrops including the enormous, sauropod-rich Morrison Formation of North America (Foster, 2003) and other localities worldwide like, e.g., the Lourinhã Formation of Portugal, Europe (Mateus et al., 2006) and other localities that produced several Late Jurassic sauropod taxa including several sauropod findings in Tendaguru (Africa) (Sander, 2000), Argentina, (South America) (Rauhut, 2006), China, (Asia) (Pi et al., 1996), and Germany, (Europe) (Sander et al., 2006). In

contrast to this there is a bias in the fossil record caused by limited preservation in the Middle Jurassic. However, new findings of Middle Jurassic diplodocoid remains in Asia (that have thought to be restricted to the Late Jurassic of North America before) now challenge this traditional assumption and hint to an earlier dispersal and diversification of sauropods than previously thought (Upchurch and Mannion, 2009; Xu et al., 2018). This is consistent with what should be expected looking at sauropod cladistics. The number of valid sauropod genera increases significantly. While studies published within the last seven years claim the number of valid sauropod taxa to be 175 (Mannion et al., 2011) or 204 (Sander, 2013) According to the Paleobiology Database (www.paleodb.org) in early 2019 289 valid sauropod genera are known 203 of which belong to the Neosauropoda. The two major sister clades studies here consist of 35 genera of Diplodocoidea and 164 genera of Macronaria.

1.2.1. Sauropod phylogeny

The following section mainly focuses on the phylogenetic relationships of the two mayor sister clades of the Eusauropoda comprising the Neosauropoda analyzed in this thesis (Macronaria and Diplodocoidea). A general description of the more basal sauropodomorph and sauropod taxa is given by Upchurch et al. (2007) and Yates et al. (2012). The latest phylogenetic analyses describing the current understanding of the relationships of basal Sauropodomorpha and the origin of Sauropoda is given by Apaldetti et al. (2018). The Phylogenetic relationships of the African taxon *Spinophorosaurus* (the only basal sauropod analyzed herein) are described by Remes et al. (2009). Generally, *Spinophorosaurus* groups between the basal most sauropod *Vulcanodon* (Africa) and more derived Eusauropods including *Jobaria* (Africa) and other Asian genera like *Omeisaurus* or *Mamenchisaurus*. An overview about the relationships between the best-known sauropod taxa and all sauropod taxa analyzed for this dissertation is given in Fig. 2.

1.2.1.1. Historical overview

The first cladistic analysis that tried to classify sauropods in general divided them (as it has done traditionally before) into a broad-toothed and a narrow-toothed group. The narrow-toothed group included diplodocids and titanosaurids whereas the broad-crowned sauropods include *Brachiosaurus* and *Camarasaurus* (Upchurch, 1995). However, this first classification did not consider several important postcranial characteristics, a point of weakness that has been mentioned by McIntosh (1990) before. In the following years Salgado et al. (1997) and Wilson and Sereno (1998) published broader phylogenetic analyses that suggested that the two narrow-toothed groups were distantly related, and that Titanosauria shared a close relationship with *Brachiosaurus*. In their analysis the brought-teeth condition is described as the primitive condition in sauropods whereas narrow-teeth are a derived feature that has evolved at least twice independently in diplodocids and titanosauriformes. With that, these analyses for the first time divided the Neosauropoda in the two still existing neosauropod clades Macronaria and Diplodocoidea. That latter has

been confirmed to be valid by lower level phylogenetic analyses several times (Upchurch, 1998; Wilson, 2002; Upchurch et al., 2004). While the Diplodocoidea include Rebbachisauridae, Dicraeosauridae, and Diplodocidae (the last of which are the main Diplodocoidea sampled for this dissertation), the Macronaria mainly consist of *Camarasaurus*, the dwarfed taxon *Europasaurus* and the Titanosauriformes including the Brachiosauridae, and Titanosauria.

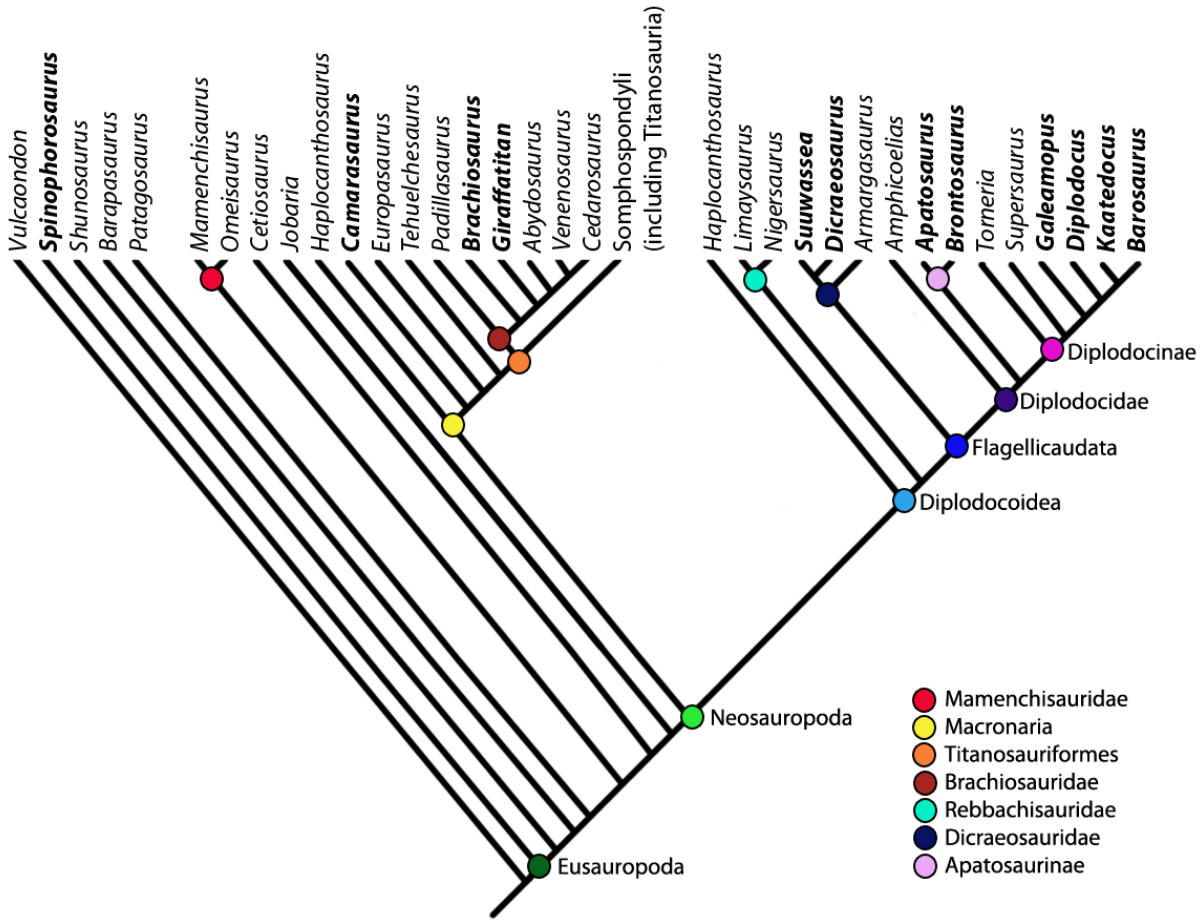

Fig. 2: Phylogenetic relationships of sauropod genera based on combined data of Wilson (2005), Carballido and Sander (2014), and Tschopp et al. (2015) showing the most important genera for this study with focus on the two major clades of the Neosauropoda (Macronaria and Diplodocoidea). Genera of the Somphospondyli including Titanosauria are not listed in more detail because they were not relevant for the study based on their high degree of dorsal rib pneumatisation and the Cretaceous age of most of the taxa. Genera sampled within this dissertation are written in bold.

1.2.1.2. Current phylogenies

New discoveries and reanalysis of already known taxa continue to change our understanding of the sauropod phylogeny. One of the most important clades erected by Allain and Aquesbi (2008) in the course of their description of the new sauropod *Tazoudasaurus naimi* (Allain et al., 2004) is Gravisauria which is defined as the least inclusive clade containing *Vulcanodon karibaensis* and *Saltasaurus loricatus*. Gravisauria had evolved the typical sauropod bauplan that lead to the evolution of gigantism. The clade Sauropoda itself now is defined as the most inclusive clade containing *Saltasaurus loricatus* but not *Melanorosaurus readi* (Yates et al., 2012). In 2013 Sander reviewed the state of knowledge about sauropod evolution and paleobiology including an update on new sauropod finds and phylogenies. The sister taxa Macronaria and Diplodocoidea are comparable in size and identical in lineage durations that begin with the origin of Neosauropoda in the Middle Jurassic and end at the Cretaceous–Paleogene boundary (Wilson, 2002). A detailed phylogenetic analysis of the Diplodocidae on specimen level including the majority of all diplodocids found worldwide has been done by Tschopp et al. (2015). A time calibrated evolutionary tree focusing on Diplodocoidea and their ancestors is given by Xu et al. (2018). More recent phylogenetic analyses of the macronarian clade (mainly preformed to integrate new species like, e.g., *Europasaurus*) have been performed by, e.g., D'Emic (2013), Mannion et al. (2013), Carballido and Sander (2014), Mocho et al. (2014), D´Emic et al. (2016), Carballido et al. (2017), Mannion et al. (2017), Royo-Torres et al. (2017), and Díez Díaz et al. (2018).

1.2.2. Sauropod gigantism

Sauropods are the largest herbivores that ever evolved reaching over 40 meters in length, 17 meters in height, and over 50 metric tons of weight (Sander and Clauss, 2008). Besides these impressive scales, they also had the largest ontogenetic size ranges from hatchlings to skeletal mature individuals. Early trends to gigantism already occur in the late Triassic, e.g., in the recently described clade of Lessemsauridae (Apaldetti et al., 2018; McPhee et al., 2018; Sander and Lallensack, 2018). Lessenmsauridae is a sauropod taxon that evolved among numerous other sauropodomorpha (a paraphyletic assemblage) in a first radiation of the group before the classical sauropod body plan including all characters and traits relevant for true gigantism has evolved within the Gravisauria (Sander, 2013). Environmental conditions differing from today like, e.g., atmospheric oxygen level that are often discussed to enable gigantism can largely be excluded as explanation for gigantism (Sander and Clauss, 2008) because the oxygen level has been even lower than today (Berner et al., 2007). The success of this long-lived taxon that reached and overcame the limits of biology in several ways cannot be explained using monocausal reasons. It is a combination of features including the unique bauplan, long neck, mastication, lung structure and reproduction that has been studied by Sander and colleagues for the last two decades

successfully (Sander and Clauss, 2008; Klein et al., 2011; Sander, 2013). While the long neck enabled sauropods to reach a large area containing food without moving (Sander and Clauss, 2008), the redundancy of mastication furthermore facilitates a maximum input of food and thus energy in a short amount of time (Christiansen, 2000). The avian lung structure, documented in sauropods by pneumaticity occurring in several axial and girdle elements of the skeleton, provides maximum oxygen input (Perry et al., 2009). Finally, sauropods (in contrast to megaherbivore mammals) follow the reproductive r-strategy producing many small offspring that decreases the extinction risk by reducing the population recovery time (Janis and Carrano, 1991; Sander and Clauss, 2008; Werner and Griebeler, 2011). Further life history adaptations that enabled gigantism (ascertained as a result of this thesis) are discussed in chapter 7.

1.2.3. Sauropod reproduction and ontogeny

In general, only little is known about the ontogeny of sauropods mainly caused by the overrepresentation of adult specimens. Besides some exceptions, especially early stage juveniles are extremely rare (Lehman and Coulson, 2002; Carballido et al., 2012). Thus, only little is known about absence or presence of allometric growth in sauropods. However, embryonic bones of sauropods (mainly belonging to titanosauriform taxa of the Cretaceous) are more frequently found and suggest isometric growth, at least in the postcranial skeleton (Chiappe et al., 1998; 2000; Sites, 2005; García and Cerda, 2010; Barret et al., 2016). In contradiction to the numerous Late Jurassic sauropod findings of adults worldwide, nesting sites or embryonic remains of this age are extremely rare (Castanhinha et al., 2009; Britt and Nailor, 1996). Both, egg and clutch size of sauropods are way smaller than what would be expected for a gigantic oviparous animal. However, both can be explained by the need of gas exchange level. To optimize oxygen level, most likely sauropods lay relatively small eggs and limited clutch size to what can be observed in recent reptiles. To optimize the offspring number, it is often been discussed whether one female produces several clutches at a time (Seymour, 1979; Sander et al., 2008; Werner and Griebeler, 2011; Ruxton et al., 2014). Incubation times are thought to be short based on ecological arguments and phylogenetic bracketing of crocodiles and birds (Ruxton et al., 2014; Lee, 2016) However, more recent studies on dinosaur incubation periods based on growth-line counts in embryonic teeth (Erickson et al., 2017) and evolutionary phylogenetic assumptions (Yang and Sander, 2018) suggest longer incubation times for toothed dinosaurs (including sauropods) that are comparable to rates of outgroup and recent reptiles.

For earliest stage sauropods a hatchling weight of about 3.4 kg has been reported that (based on histological analyses) has been increased to over 40 kg within a few weeks (Rogers et al., 2016). Additionally, the authors reported isometric growth of the bone which has been repeatedly stated by other authors before (Bonnan, 2004; Kilbourne and Makovicky, 2010; Sander et al., 2011). More information about the ontogenetic

development of sauropods including changes in tooth morphology connected with dietary changes and niche partitioning at different ontogenetic ages (Woodruff et al., 2018,(chapter 5)) generation times (respectively age of sexual maturity), age at skeletal maturity and longevity (Waskow et al., submitted, (chapter 4); Waskow et al., unpublished, (chapter 6)) has been ascertained by this dissertation and will be analyzed and discussed in more detail in chapter 6 and 7.

1.3. Histology

The histology preserved in bone tissue can be analyzed at different levels of magnification from the microanatomical to the cellular level. While microanatomy of ribs and long bones is used to analyze the ecological adaptation to a certain habitat in different vertebrate taxa in chapter 3, the tissue level representing the level of the expression of the growth marks is in focus of all other histological studies performed in this thesis (chapter 2, 4, 5, and 6) Thus, following description of primary and secondary bone tissue refer to this level of magnification.

1.3.1. Primary bone tissue

The primary bone tissue of vertebrates is the richest source of information about, e.g., ontogenetic age, metabolic rate, ecological adaptation, or life history for extinct animals. Cortical thickness, bone tissue type, vascularization, Sharpey´s fibers, and osteocyte density are among the features used for collecting these data. Cortical thickness plays an important role in bone strength and weight that changes due to ecological adaptation to a special habitat including flying and aquatic or graviportal adaptation (Houssaye et al., 2014; 2015; 2016a, (chapter 3); 2016b). While bone tissue type and amount and direction of vascularization are primarily hinting at basal metabolic rates and bone apposition rates (e.g., Case, 1978; Ricqlés, 1980; Padian et al., 2001; Huttenlocker and Farmer, 2017) direction and number of Sharpeys fibers can be used to detect muscle attachment and strength (e.g., Petermann and Sander, 2013; Kolenda et al., 2018). This in turn can be analyzed in terms of locomotion or breathing. Osteocytes that form by the incorporation of osteoblasts are the mechanosensory cells of bone and thus serve in biomechanical and biochemical functions (Aarden et al., 1994). Their analysis sheds light on growth rates and phylogeny of different taxa (Cubo et al., 2012; Stein and Werner, 2013). Another very important feature of the primary bone tissue is the annularity preserved in there, the study of which is known as skeletochronology. Annual produced growth marks are mainly in focus of this dissertation and thus are described in more detail in chapter 1.4.1 and chapter 1.4.2. For a more detailed description of the different features of primary bone tissue see Francillon-Vieillot et al. (1990) and Chinsamy-Turan (2005; 2011).

1.3.2. Secondary bone tissue

Because bone is a living tissue, all primary bone structures described above are influenced by remodeling and resorption due to the expansion of the medullary cavity, both of which destroy the primary growth-record. Both processes are described in more detail in the three-front model of bone formation (primary bone tissue, secondary bone tissue, and resorption of bone for enlargement of the medullary cavity) of Mitchell and Sander (2014). The formation of secondary osteons usually starts in the inner cortex and proceeds outwards during life until it reaches the outer bone surface. In already remodeled bone areas second, third, or even more generations of secondary osteons can occur. Thus, secondary bone, also known as Haversian bone is also subject to remodeling (Francillon-Vieillot et al., 1990). Even though secondary osteons are one of the first microscopical structures ever described (Havers, 1691) the triggers and function of remodeling are still not completely understood (Currey, 2002; Mitchell et al., 2017; Currey et al., 2017). One theory suggests that dense Haversian bone may repair microcracks in bone resulting from stress and strain (load) during locomotion (Martin and Burr, 1982; García-Aznar et al., 2005; Seeman, 2006). Other theories suggest that the remodeling process is caused by the storage and remobilization of minerals or could be linked with metabolic rate (Ricqlès, 1980; Montoya-Sanhueza and Chinsamy, 2018). However, secondary remodeling (and with that the amount of Haversian bone tissue and generations of secondary osteons) increases with ontogenetic age and thus also can be used to determine the relative ontogenetic stage of an animal (Castanet et al., 1993; Currey, 2002; Mitchell and Sander, 2014), especially in senescent individuals that do not preserve primary bone tissue any more (Mitchell, 2017; Mitchell et al., 2017).

1.4. Cyclicity

Cyclicity is a common natural phenomenon that occurs in sediments, ice, plants, and animals. The best-known example of annual cyclicity are tree-rings. They are caused by climate based seasonal and predictable growth rate changes and are used for dendrochronology, a scientific method of dating trees. Fields of application are ecological climatology, and timing of events, art and architecture (Fritts, 2012; Schweingruber, 2012). The sedimentary equivalent of tree-rings are varves. A varve is a periodically recurring sedimentary unit consisting of at least two differing layers of sediment that were caused by differing current flow strength or rates of sedimentation during a year (usually annual deposition in lacustrine environment) or other periodically recurring time units (Anderson, 1988). Changes in oxygen level in bottom wates during the annual climatic cycle are also discussed to cause varve formation (e.g., Reimers et al., 1990). The same phenomenon of cyclicity is observable in glacier ice where the annual layers of snowfall were compressed under the weight of the following depositions and form visible differing layers of ice that can be analyzed for dating, and various fields of paleoclimatology (Hammer et al., 1986; Dansgaard et al., 1993; Petit et al., 1999). In animals, different forms of cyclicity do occur.

While teeth show daily forming deposition lines in dentine tissue (Cahill, 1970; Erickson, 1996a; b; García and Zurriaguz, 2016) that were first recognized by Owen (1840-1845), their root cementum preserves annual incremental lines similar to the annual forming growth marks in bones (Klevezal and Kleinenberg, 1967). Especially in extinct animals the annual nature of these cycles has been discussed controversial in the past (Chinsamy and Hillenius, 2004; Padian and Horner, 2004). However, now the annual nature of growth marks is generally accepted (Erickson, 2005; Sander et al., 2011) and used as a standard method of aging extant and extinct animals (Hutton, 1986; Caetano, 1990; Castanet and Smirina, 1990; Castanet and Baez, 1991; Ricqlès et al., 1991; Castanet et al., 1993; 2004; Chinsamy, 1994; Smirina and Tsellarius, 1996; Smirina and Ananjeva, 2007; Garcia, 2011; Köhler et al., 2012; Woodward et al., 2014; Klein and Griebeler, 2018). Additionally, the annual nature of cyclicity can be tested by the usage of growth models that are further described in chapter 1.5.2. The single growth models predict certain ages of, e.g., sexual maturity that are within the realm of age estimation generated by the count of growth marks and estimation of missing inner cortical cycles (Griebeler et al., 2013; Klein et al., 2015; Klein and Griebeler, 2016; 2018).

1.4.1. Different types of growth record preservation

In primary bone tissue information about growth is recorded by the formation of growth marks. In general, three different types of cyclical growth do occur (Fig. 3). The best established and most analyzed type of growth mark is a line of arrested growth (LAG). LAGs are dark continuous lines that mark the surface where growth was interrupted during a certain period of the year. They complete a cycle thought to be annual consisting of a fast-growing zone, a slower growing annulus and the LAG itself. Two other forms of annual cyclicity are known. Polish lines have been described by Sander (2000) as growth lines in fibrolamellar bone that are visible in polished sections but not in macroscopic view under the microscope in a thin section. The third type of cyclic growth are modulations that can be described as cyclical repeated variations in tissue type, vascularization, and/or bone apposition rate in primary bone tissue not completed by a visible LAG (Ricqlès, 1983; Sander and Tückmantel, 2003). These other types of annuli are especially important for analyzing sauropod histology as described herein.

It is not completely understood what causes the formation of growth marks. External environmental factors like, e.g., limited sources of nutrition and light during drought or winter seasons as well as genetical causes (e.g., hormonal fluctuations) are often discussed as possible reasons (Klevezahl, 1980; Castanet et al., 1993; Burke and Castanet, 1995). However, the preservation of LAGs in tropical taxa that are not subject to seasonal variation or changes in length of daylight impede external environmental factors as a monocausal explanation for LAG formation (Pal et al., 2009). In some cases, the phenomenon of double or even triple LAGs do occur (Fig. 3 A; Castanet and Smirina, 1990; Castanet et al., 1993;

Castanet, 1994; Castanet et al., 2000; 2004). Double layers are two closely spaced LAGs (that do not represent External Fundamental System (EFS) cycles) showing no visible structures of primary bone tissue between them. Studies about recent animals like frogs (Guarino and Erismis, 2008) and newts (Caetano, 1990) prove that they represent only a single year. Thus, they can be counted as one annual cycle. Even if they seem to be more common in amphibians (Guarino and Erismis, 2008; Caetano, 1990), double LAGs are no indication for exothermy because they do also occur in mammals (Klevezal and Kleinenberg, 1967) and dinosaurs (Waskow and Sander, 2014).

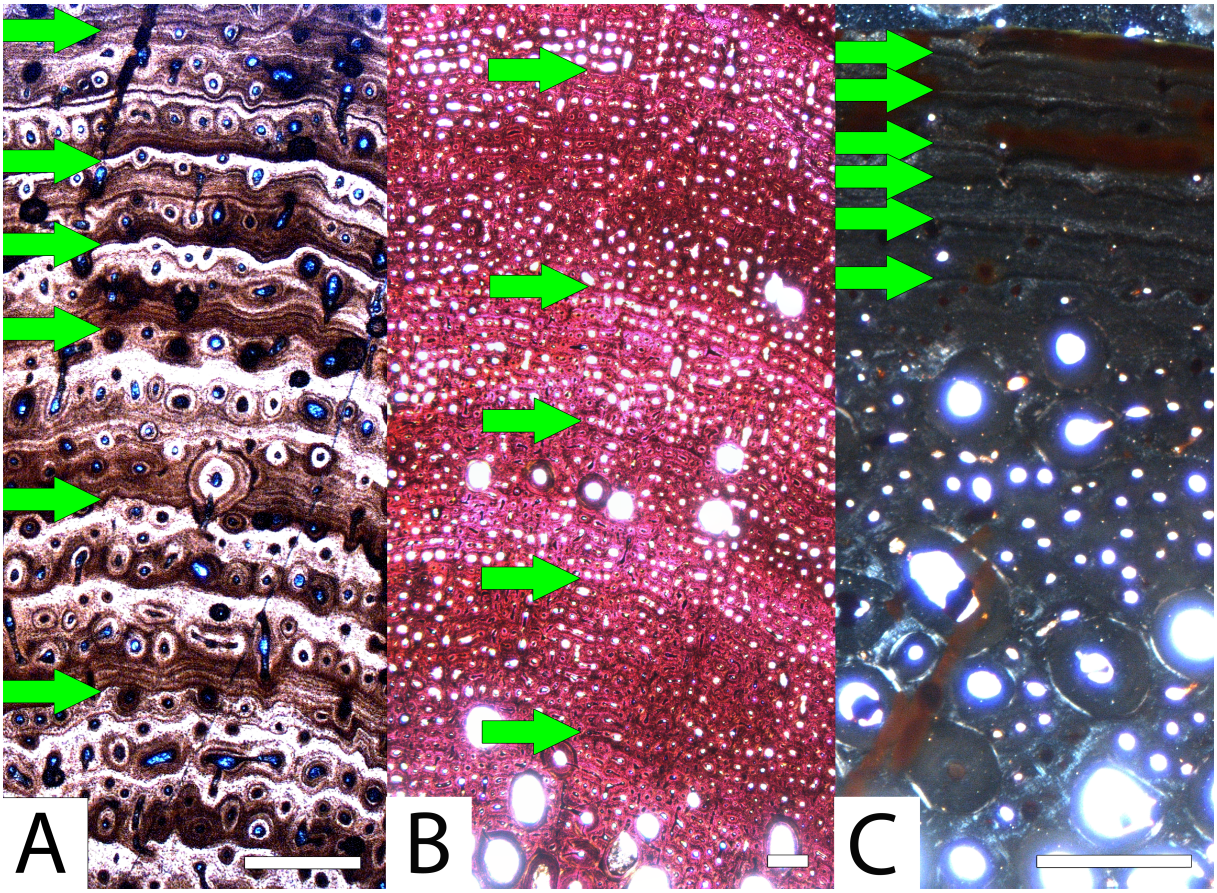

Fig. 3: Different types of growth record preservation. Green arrows indicate growth marks. Scale bars equal 500 µm. **A**: Typical lines of arrested growth (LAGs) preserved in a *Camarasaurus* dorsal rib sample (UMNH 21608). Note the phenomenon of multiple LAGs occurring, e.g., at the first marked growth line near the medullary region (bottom-up). **B**: Modulations of the colour and varcularization pattern occurring in the inner cortical region of a juvenile *Camarasaurus* individual (UW 46212). **C**: External fundamental system (EFS) indicating skeletal maturity in a dorsal rib of a dwarfed diplodocine (CMC VP 9932).

1.4.2. Growth record preservation in sauropods

The first histological studies solely preformed on sauropods to estimate their growth rates were performed on the traditionally sampled long bones (Ricqlès, 1968; 1983; Sander, 2000; Sander and Tückmantel, 2003). Even though cyclicity has been reported in these studies (especially in the outer parts of the cortex) bone apposition rates of sauropod in primary and secondary bone tissue in general are too high to produce and preserve LAGs throughout the whole cortex. Thus, most of the sampled sauropod long bones show mainly incomplete growth record in the primary bone tissue and high amounts of remodeling, even in relatively young adult ontogenetic stages. This caused the erection of histologic ontogenetic stages (HOS) for sauropods to enable estimations of the ontogenetic age of an individual (Klein and Sander, 2008; Mitchell et al., 2017). The only exception of this general pattern of preservation in sauropod long bones known so far is the 60% complete growth record preserved in the ulna of a *Mamenchisaurus* from China that has been described by Wings et al. (2007). Contrary to the poor completeness of skeletochronological information in long bones, better growth record preservation has been reported for other skeletal elements like, e.g., a sauropod pelvis (Reid, 1981). Thus, Waskow and Sander (2014) studied the histology of a complete and articulated *Camarasaurus* rib cage in more detail to estimate the completeness of growth record preservation and best sampling area in sauropod ribs. With up to 87% of growth record preservation their analysis revealed that the proximal rib shaft of anterior dorsal ribs preserves the most complete growth record of all skeletal elements ever sampled.

1.5. Quantification of the histological growth record

1.5.1. Growth curve compilation

Good growth record preservation enables the quantification of growth in a growth curve. This has been done frequently in dinosaur taxa (e.g., theropods or psittacosaurs) that do show cyclicity in the usually sampled long bones (Erickson and Tumanova, 2000; Erickson et al., 2004; 2007; Horner and Padian, 2004; Bybee et al., 2006; Erickson et al., 2009; Cullen et al., 2014; Bo et al., 2016). In these classical growth curves body mass is plotted versus growth time of either one or several individuals. The usage of mass instead of, e.g., length or height has some advantages one of which is comparability to biological studies where mass is commonly used. Additionally, for extinct animals, mass is easier to estimate than, e.g., length (Sander et al., 2011). Mass estimations are usually base on long bone measurements (Anderson et al., 1985; Mazzetta et al., 2004; Campione and Evans, 2012; Campione et al., 2014). The growth time is estimated based on growth cycle count and estimation of missing inner cycles (Erickson et al. 2004; Bybee et al. 2006; Klein and Sander, 2007). The method of plotting mass versus age assumes a linear relationship between

increase in long bone cortical thickness and increase in body mass. This is reasonable for sauropod long bones that have been reported to grow isometrically (Bonnan, 2004; Kilbourne and Makovicky, 2010; Sander et al., 2011) and have a nearly circumferential cross-section at the usually sampled mid shaft. The growth dynamics of dorsal ribs in contrast are much more complicated, impeding direct correlation of mass with age as will be further discussed in chapter 7. Here age is correlated with bone apposition rate that is quantified by measuring the distances between the single LAGs.

1.5.2. Growth curve analysis

After compilation of a long bone-based growth curve, it can be compared to several biological growth models including the von Bertalanffy model, the Gompertz model, the logistic model (LGM) and the Chapman-Richards model, the most commonly used of which is the von Bertalanffy equation (Reiss, 1989; Erickson et al., 2001; Lehman and Woodward, 2008; Griebeler et al., 2013; Werner and Griebeler, 2014; Griebeler and Werner, 2018). Such growth curve models indicate ages at fastest growth, and ages at sexual- (inflection point of the curve) and skeletal maturity (asymptote of the curve). In case of the rib-based growth curves a direct correlation of mass and age and thus comparison to biological growth models is not possible, caused by the complex shape and growth of the rib discussed in chapter 7. Nevertheless, correlation of age versus bone apposition rate (obtained by measuring distances between the single LAGs) allows at least the determination of ages at sexual- and skeletal maturity. These life history data then in turn ca be used for analysis of ecological adaptations including generation times. In sauropods these generation times differ statistically significant between different taxa allowing taxonomic assignment of histological sampled individuals based on their growth curves as will be discussed in Waskow et al. (unpublished, (chapter 6)). Together with other life history data obtained by, e.g., tooth morphology (Woodruff et al., 2018, (chapter 5)) and ontogenetic variation in both morphology and histology (Waskow et al., submitted, (chapter 4); Woodruff et al., 2018, (chapter 5)) age distribution at certain localities obtained by the compilation of growth curves can also hint to ecological niche partitioning at different ontogenetic ages as will be further discussed in chapter 6 and 7.

1.6. Aim of dissertation

This dissertation aims to uncover the potential of dorsal rib material of amniotes for paleontological studies by analyzing it histologically. The following six chapters reveal the advantages of studying these skeletal elements that were former claimed to be uninformative and morphological undiagnostic. Ribs contain almost complete growth records including all important life history information on individual and taxonomical level in all analyzed taxa and turn out to be taxonomically diagnostic elements in terms of histology. In addition to that they show habitational adaptations that yield information on the

environment and lifestyle of extinct animals. Especially in sauropods they are crucial elements to sample because for theses largest terrestrial vertebrates of all times dorsal ribs are the only skeletal elements bearing an almost complete growth record. However, by no means this dissertation claims to have entirely explored the full potential of dorsal rib histology. It should be rather seen as a starting point that might inspire more detailed taxonomical, phylogenetical, environmental, developmental, ontogenetical, habitational, and environmental investigations on ribs of extant and extinct animals in the future.

1.7. References

Aarden, E. M., Nijweide, P. J., and Burger, E. H. (1994). Function of osteocytes in bone. Journal of Cellular Biochemistry 55(3), 287-299.

Allain, R., and Aquesbi, N. (2008). Anatomy and phylogenetic relationships of *Tazoudasaurus naimi* (Dinosauria, Sauropoda) from the late Early Jurassic of Morocco. Geodiversitas 30(2), 345-424.

Allain, R., Aquesbi, N., Dejax, J., Meyer, C., Monbaron, M., Montenat, C., Richir, P., Rochdy, M., Russell, D., and Taquet, P. (2004). A basal sauropod dinosaur from the Early Jurassic of Morocco. Comptes Rendus Palevol 3(3), 199-208.

Anderson, R. Y., and Dean, W. E. (1988). Lacustrine varve formation through time. Palaeogeography, Palaeoclimatology, Palaeoecology 62(1-4), 215-235.

Anderson, J. F., Hall-Martin, A., and Russell, D. A. (1985). Long bone circumference and weight in mammals, birds, and dinosaurs. Journal of Zoology Series A 207, 53-61.

Apaldetti, C., Martínez, R. N., Cerda, I. A., Pol, D., and Alcober, O. (2018). An early trend towards gigantism in Triassic sauropodomorph dinosaurs. Nature Ecology and Evolution 2(8), 1227-1232.

Apesteguía, S. (2004). *Bonitasaura salgadoi* gen. et sp. nov.: A beaked sauropod from the Late Cretaceous of Patagonia. Naturwissenschaften 91(10), 493-497.

Barrett, P. M., Pouech, J., Mazin, J. M., and Jones, F. M. (2016). Teeth of embryonic or hatchling sauropods from the Berriasian (Early Cretaceous) of Cherves-de-Cognac, France. Acta Palaeontologica Polonica 61(3), 591-596.

Berner, R. A., VandenBrooks, J. M., and Ward, P. D. (2007). Oxygen and evolution. Science 316(5824), 557-558.

Bo, Z., Hedrick, B. P., Chunling, G., Tumarkin-Deratzian, A. R., Fengjiao, Z., Caizhi, S., and Dodson, P. (2016). Histologic examination of an assemblage of *Psittacosaurus* (Dinosauria: Ceratopsia) juveniles from the Yixian Formation (Liaoning, China). The Anatomical Record 299(5), 601-612.

Bonnan, M. F. (2004). Morphometric analysis of humerus and femur shape in Morrison sauropods: Implications for functional morphology and paleobiology. Paleobiology 30(3), 444-470.

Britt, B. B., and Naylor, B. G. (1996). An embryonic *Camarasaurus* (Dinosauria, Sauropoda) from the Upper Jurassic Morrison Formation (Dry Mesa Quarry, Colorado). In:

Carpenter, K., Hirsch, K. F., and Horner, J. R., editors. Dinosaur eggs and babies. Cambridge, Cambridge University Press: 256-264.

Britz, R., and Bartsch, P. (2003). The myth of dorsal ribs in gnathostome vertebrates. Proceedings of the Royal Society of London B: Biological Sciences 270(Suppl 1), 1-4.

Buffetaut, E., Suteethorn, V., Le Loeuff, J., Cuny, G., Tong, H., and Khansubha, S. (2002). The first giant dinosaurs: a large sauropod from the Late Triassic of Thailand. Comptes Rendus Palevol 1(2), 103-109.

Buffetaut, E., Suteethorn, V., Cuny, G., Tong, H., Le Loeuff, J., Khansubha, S., and Jongautchariyakul, S. (2000). The earliest known sauropod dinosaur. Nature 407(6800), 72.

Burke, A., and Castanet, J. (1995). Histological observations of cementum growth in horse teeth and their application to archaeology. Journal of Archaeological Science 22(4), 479-493.

Bybee, P. J., Lee, A. H., and Lamm, E. T. (2006). Sizing the Jurassic theropod dinosaur *Allosaurus*: Assessing growth strategy and evolution of ontogenetic scaling of limbs. Journal of Morphology 267(3), 347-359.

Caetano, M. H. (1990). Use and results of skeletochronology in some urodeles (*Triturus marmoratus*, Latreille 1800 and *Triturus boscai*, Lataste 1879). Annales des Sciences Naturelles. Zoologie et Biologie Animale 4(11), 197-199.

Cahill, D. R. (1970). The histology and rate of tooth eruption with and without temporary impaction in the dog. The Anatomical Record 166(2), 225-237.

Campione, N. E., and Evans, D. C. (2012). A universal scaling relationship between body mass and proximal limb bone dimensions in quadrupedal terrestrial tetrapods. BMC Biology 10(1), 60.

Campione, N. E., Evans, D. C., Brown, C. M., and Carrano, M. T. (2014). Body mass estimation in non-avian bipeds using a theoretical conversion to quadruped stylopodial proportions. Methods in Ecology and Evolution 5(9), 913-923.

Canoville, A., Buffrénil, V. de, and Laurin, M. (2016). Microanatomical diversity of amniote ribs: An exploratory quantitative study. Biological Journal of the Linnean Society 118(4), 706-733.

Carballido, J. L., and Sander, P. M. (2014). Postcranial axial skeleton of *Europasaurus holgeri* (Dinosauria, Sauropoda) from the Upper Jurassic of Germany: Implications for sauropod ontogeny and phylogenetic relationships of basal Macronaria. Journal of Systematic Palaeontology 12(3), 335-387.

Carballido, J. L., Marpmann, J. S., Schwarz-Wings, D., and Pabst, B. (2012). New information on a juvenile sauropod specimen from the Morrison Formation and the reassessment of its systematic position. Palaeontology 55(3), 567-582.

Carballido, J. L., Pol, D., Otero, A., Cerda, I. A., Salgado, L., Garrido, A. C., Ramezani, J., Cúneo, N. R., and Krause, J. M. (2017). A new giant titanosaur sheds light on body mass

evolution among sauropod dinosaurs. Proceedings of the Royal Society B 284(1860), 20171219.

Case, T. J. (1978). Speculations on the growth rate and reproduction of some dinosaurs. Paleobiology 4(3), 320-328.

Castanet, J. (1994). Age existimation and longevity in reptiles. Gerontology 40, 174-192.

Castanet, J., and Smirina, E. (1990). Introduction to the skeletochronological method in amphibians and reptiles. Annales des Sciences Naturelles Zoologiques 11, 191–197.

Castanet, J., and Baez, M. (1991). Adaptation and evolution in *Gallotia* lizards from the Canary Islands: Age, growth, maturity and longevity. Amphibia-Reptilia 12(1), 81-102.

Castanet, J., Francillon-Vieillot H., Meunier, F. J., and Ricqlès, A. de (1993). Bone and individual aging. In: Hall, B. K., editor. Bone Volume 7: Bone growth -B. Boca Raton, Florida, CRC Press: 245–283.

Castanet, J., Rogers, K. R., Cubo, J., and Boisard, J. (2000). Periosteal bone growth rates in extant ratites (ostriche and emu). Implications for assessing growth in dinosaurs. Life Sciences 323, 543-550.

Castanet, J., Croci, S., Aujard, F., Perret, M., Cubo, J., and Margerie, E. de (2004). Lines of arrested growth in bone and age estimation in a small primate: *Microcebus murinus*. Journal of Zoology 263(1), 31-39.

Castanhinha, R., Araujo, R., and Mateus, O. (2009). Dinosaur eggshell and embryo localities in Lourinhã Formation, Late Jurassic, Portugal. Journal of Vertebrate Paleontology 29(3): 76A.

Cerda, I. A., Carabajal, A. P., Salgado, L., Coria, R. A., Reguero, M. A., Tambussi, C. P., and Moly, J. J. (2012). The first record of a sauropod dinosaur from Antarctica. Naturwissenschaften 99(1), 83-87.

Chiappe, L. M., Coria, R. A., Dingus, L., Jackson, F., Chinsamy, A., and Fox, M. (1998). Sauropod dinosaur embryos from the Late Cretaceous of Patagonia. Nature 396(6708), 258.

Chiappe, L. M., Dingus, L., Jackson, F., Grellet-Tinner, G., Aspinal, R., Clarke, J., Coria, R. A., Garrido, A., and Loope, D. (2000). Sauropod eggs and embryos from the Late Cretaceous of Patagonia. In: Bravo, A. M., Reyes, T., editors. First international symposium on dinosaur eggs and babies. Isona, Spain, Extended abstacts: 23-29.

Chinsamy, A. (1994). Dinosaur bone histology: Implications and inferences. The Paleontological Society Special Publications 7, 213-228.

Chinsamy-Turan, A. (2005). The microstructure of dinosaur bone: Deciphering biology with fine-scale techniques. Baltimore, Maryland, The Johns Hopkins University Press.

Chinsamy-Turan, A. (2011). Forerunners of mammals: Radiation, histology, biology. Indiana University Press.

Chinsamy, A., and Hillenius, W. J. (2004). Physiology of non-avian dinosaurs. In: Weishampel, D. B., Dodson, P., and Osmólska, H., editors. The Dinosauria, second edition. Berkeley, California, University of California Press: 643-659.

Christiansen, P. (2000). Feeding mechanisms of the sauropod dinosaurs *Brachiosaurus*, *Camarasaurus*, *Diplodocus*, and *Dicraeosaurus*. Historical Biology 14(3), 137-152.

Cubo, J., Le Roy, N., Martinez-Maza, C., and Montes, L. (2012). Paleohistological estimation of bone growth rate in extinct archosaurs. Paleobiology 38(2), 335-349.

Cullen, T. M., Evans, D. C., Ryan, M. J., Currie, P. J., and Kobayashi, Y. (2014). Osteohistological variation in growth marks and osteocyte lacunar density in a theropod dinosaur (Coelurosauria: Ornithomimidae). BMC Evolutionary Biology 14(1), 231.

Currey, J. D. (2002). Bones: Structure and mechanics. Princeton, New Jersey, Princeton University Press, 436 pp.

Currey, J. D., Dean, M. N., and Shahar, R. (2017). Revisiting the links between bone remodelling and osteocytes: Insights from across phyla. Biological Reviews 92(3), 1702-1719.

Dansgaard, W., Johnsen, S. J., Clausen, H. B., Dahl-Jensen, D., Gundestrup, N. S., Hammer, C. U., Hvldberg, C. S., Steffensen, J. P., Sveinbjörnsdottir, A. E., and Bond, G. (1993). Evidence for general instability of past climate from a 250-kyr ice-core record. Nature 364(6434), 218.

D'Emic, M. D. (2013). Revision of the sauropod dinosaurs of the Lower Cretaceous Trinity Group, southern USA, with the description of a new genus. Journal of Systematic Palaeontlogy 11(6), 707-726.

D'Emic, M. D., and Foster, J. R. (2016). The oldest Cretaceous North American sauropod dinosaur. Historical Biology 28(4), 470-478.

Díez Díaz, V., Garcia, G., Pereda-Suberbiola, X., Jentgen-Ceschino, B., Stein, K., Godefroit, P., and Valentin, X. (2018). The titanosaurian dinosaur *Atsinganosaurus velauciensis* (Sauropoda) from the Upper Cretaceous of southern France: New material, phylogenetic affinities, and palaeobiogeographical implications. Cretaceous Research 91, 429-456.

Erickson, G. M. (1996a). Incremental lines of von Ebner in dinosaurs and the assessment of tooth replacement rates using growth line counts. Proceedings of the National Academy of Sciences 93(25), 14623-14627.

Erickson, G. M. (1996b). Daily deposition of dentine in juvenile *Alligator* and assessment of tooth replacement rates using incremental line counts. Journal of Morphology 228(2), 189-194.

Erickson, G. M. (2005). Assessing dinosaur growth patterns: A microscopic revolution. Trends in Ecology and Evolution 20(12), 677-684.

Erickson, G. M., and Tumanova, T. A. (2000). Growth curve of *Psittacosaurus mongoliensis* Osborn (Ceratopsia: Psittacosauridae) inferred from long bone histology. Zoological Journal of the Linnean Society 130(4), 551-566.

Erickson, G. M., Rogers, K. C., and Yerby, S. A. (2001). Dinosaurian growth patterns and rapid avian growth rates. Nature 412(6845), 429.

Erickson, G. M., Zelenitsky, D. K., Kay, D. I., and Norell, M. A. (2017). Dinosaur incubation periods directly determined from growth-line counts in embryonic teeth show reptilian-grade development. Proceedings of the National Academy of Sciences 114(3), 540-545.

Erickson, G. M., Rogers, K. C., Varricchio, D. J., Norell, M. A., and Xu, X. (2007). Growth patterns in brooding dinosaurs reveals the timing of sexual maturity in non-avian dinosaurs and genesis of the avian condition. Biology Letters 3(5), 558-561.

Erickson, G. M., Makovicky, P. J., Currie, P. J., Norell, M. A., Yerby, S. A., and Brochu, C. A. (2004). Gigantism and comparative life-history parameters of tyrannosaurid dinosaurs. Nature 430(7001), 772.

Erickson, G. M., Rauhut, O. W., Zhou, Z., Turner, A. H., Inouye, B. D., Hu, D., and Norell, M. A. (2009). Was dinosaurian physiology inherited by birds? Reconciling slow growth in *Archaeopteryx*. PLoS One 4(10), e7390.

Foster, J. R. (2003). Paleoecological analysis of the vertebrate fauna of the Morrison Formation (Upper Jurassic), Rocky Mountain region, USA: Bulletin 23 (Vol. 23). New Mexico Museum of Natural History and Science.

Francillon-Vieillot, H., Buffrénil, V. de, Castanet, J., Géraudie, J., Meunier, F. J., Sire, Y., Zylberberg, L., and Ricqlès, A. de (1990). Microstructure and mineralization of vertebrate skeletal tissues. In: Carter, J. G., editor. Skeletal biomineralization: patterns, processes and evolutionary trends 1. New York, Van Nostrand Reinhold: 471-530.

Fritts, H. C. (2012). Tree rings and climate. London, New York, San Francisco, Academic Press.

Gadow, H. F. (1933). The evolution of the vertebral column. Cambridge, Cambridge University Press.

García-Aznar, J. M., Rueberg T., and Doblare M. (2005). A bone remodeling model coupling microdamage growth and repair by 3D BMU activity. Biomechanics and Modeling in Mechanobiology 4, 147–167.

Garcia, B. J., (2011). Skeletochronology of the American *Alligator* (*Alligator Mississippiensis*): Examination of the utility of elements for histological study. MSc thesis, Florida State University.

García, R. A., and Cerda, I. A. (2010). Dentition and histology in titanosaurian dinosaur embryos from Upper Cretaceous of Patagonia, Argentina. Palaeontology 53(2), 335-346.

García, R. A., and Zurriaguz, V. (2016). Histology of teeth and tooth attachment in titanosaurs (Dinosauria; Sauropoda). Cretaceous Research 57, 248-256.

Gilbert, S. F. (2000). Developmental biology, 6th Edition. Sunderland, Massachusetts, Sinauer Associates, 56pp.

Gilmore, C. W. (1936). Osteology of *Apatosaurs* with special reference to specimens in the Carnegie Museum. Memoirs of the Carnegie Museum 11(4), 175-300.

Griebeler, E. M., and Werner, J. (2018). Formal comment on: Myhrvold (2016) Dinosaur metabolism and the allometry of maximum growth rate. PLoS ONE 11 (11), e0163205. PloS ONE 13(2), e0184756.

Griebeler, E. M., Klein, N., and Sander, P. M. (2013). Aging, maturation and growth of sauropodomorph dinosaurs as deduced from growth curves using long bone histological data: An assessment of methodological constraints and solutions. PloS ONE 8(6), e67012.

Guarino, F. M., and Erismis, U. C. (2008). Age determination and growth by skeletochronology of *RanaHoltzi*, an endemic frog from Turkey. Italian Journal of Zoology 75 (3), 237-242.

Hall, B. K. (2005). Bones and cartilage: Developmental and evolutionary skeletal biology. New York, Academic Press.

Hammer, C. U., Clausen, H. B., and Tauber, H. (1986). Ice-core dating of the Pleistocene/Holocene boundary applied to a calibration of the 14 C time scale. Radiocarbon 28(2a), 284-291.

Havers, C. (1691). Osteologia nova, or, some new observations of the bones and the parts belonging to them, with the manner of their accretion, and nutrition, communicated to the Royal Society in several discourses (reprinted 1977). Ann Arbor, University Microfilms International.

Horner, J. R., and Padian, K. (2004). Age and growth dynamics of *Tyrannosaurus rex*. Proceedings of the Royal Society of London B: Biological Sciences 271(1551), 1875-1880.

Houssaye, A., Tafforeau, P., and Herrel, A. (2014). Amniote vertebral microanatomy–what are the major trends? Biological Journal of the Linnean Society 112(4), 735-746.

Houssaye, A., Sander, P. M., and Klein, N. (2016b). Adaptive patterns in aquatic amniote bone microanatomy-more complex than previously thought. Integrative and Comparative Biology 56(6), 1349-1369.

Houssaye, A., Tafforeau, P., Muizon, C. de, and Gingerich, P. D. (2015). Transition of Eocene whales from land to sea: Evidence from bone microstructure. PLoS ONE 10(2), e0118409.

Houssaye, A., Waskow, K., Hayashi, S., Cornette, R., Lee, A. H., and Hutchinson, J. R. (2016a). Biomechanical evolution of solid bones in large animals: A microanatomical investigation. Biological Journal of the Linnean Society 117(2), 350-371.

Huttenlocker, A. K., and Farmer, C. G. (2017). Bone microvasculature tracks red blood cell size diminution in Triassic mammal and dinosaur forerunners. Current Biology 27(1), 48-54.

Hutton, J. M. (1986). Age determination of living Nile crocodiles from the cortical stratification of bone. Copeia 1986, 332-341.

Janensch, W. (1947). Pneumatizitat bei Wirbeln von Sauropoden und anderen Saurischien. Palaeontographica (Suppl. 7) 3: 1-25.

Janensch, W. (1950). Die Wirbelsaule von *Brachiosaurus brancai*. Palaeontographica (Suppl. 7) 3: 27-93.

Janis, C. M., and Carrano, M. (1991). Scaling of reproductive turnover in archosaurs and mammals: Why are large terrestrial mammals so rare? Annales Zoologici Fennici, Finnish Zoological Publishing Board, formed by the Finnish Academy of Sciences, Societas Biologica Fennica Vanamo, Societas pro Fauna et Flora Fennica, and Societas Scientiarum Fennica: 201-216.

Jenkins Jr., F. A. (1970). Anatomy and function of expanded ribs in certain edentates and primates. Journal of Mammalogy 51(2), 288-301.

Kilbourne, B. M., and Makovicky, P. J. (2010). Limb bone allometry during postnatal ontogeny in non-avian dinosaurs. Journal of Anatomy 217(2), 135-152.

Klein, N., and Sander, P. M. (2007). Bone histology and growth of the prosauropod dinosaur Plateosaurus engelhardti von Meyer, 1837 from the Norian bone beds of Trossingen (Germany) and Frick (Switzerland). Special Papers in Palaeontology 77, 169–206.

Klein, N., and Sander, P. M. (2008). Ontogenetic stages in the long bone histology of sauropod dinosaurs. Paleobiology 34(2), 247-263.

Klein, N., and Sichelschmidt, O. J. (2014). Remarkable dorsal ribs with distinct uncinate processes from the early Anisian of the Germanic Basin (Winterswijk, the Netherlands). Neues Jahrbuch für Geologie und Paläontologie-Abhandlungen 271(3), 307-314.

Klein, N., and Griebeler, E. M. (2016). Bone histology, microanatomy, and growth of the nothosauroid Simosaurus gaillardoti (Sauropterygia) from the Upper Muschelkalk of southern Germany/Baden-Württemberg. Comptes Rendus Palevol 15(1-2), 142-162.

Klein N., and Griebeler, E. M., (2018). Growth patterns, sexual dimorphism, and maturation modeled in Pachypleurosauria from Middle Triassic of central Europe (Diapsida: Sauropterygia). Fossil Record 21, 137–157.

Klein, N., Remes, K., Gee, C. T., and Sander, P. M. (Eds.) (2011). Biology of the sauropod dinosaurs: Understanding the life of giants. Bloomington, Indiana, Indiana University Press.

Klein, N., Neenan, J. M., Scheyer, T. M., and Griebeler, E. M. (2015). Growth patterns and life-history strategies in Placodontia (Diapsida: Sauropterygia). Royal Society open science 2(7), 140440.

Klevezal, G. A. (1980). Layers in the hard tissues of mammals as a record of growth rhythms of individuals. Report of the International Whaling Commission (Special Issue 3), 89-94.

Klevezal, G. A., and Kleinenberg S. E. (1967)**.** Age determination of mammals by layered structures in teeth and bone. Quebec Fisheries Research Board Translations Series 1024.

Köhler, M., Marín-Moratalla, N., Jordana, X., and Aanes, R. (2012). Seasonal bone growth and physiology in endotherms shed light on dinosaur physiology. Nature 487(7407), 358.

Kolenda, K., Najbar, A., Rozenblut-Kościsty, B., Serwa, E., and Skawiński, T. (2018). Common occurrence of Sharpey's fibres in amphibian phalanges. Zoomorphology 137(2), 329-336.

Lallensack, J. N. (2018). Objective and quantitative methods in the study of dinosaur tracks. Doctoral dissertation, Universitäts-und Landesbibliothek Bonn.

Lee, S. A. (2016). Incubation times of dinosaur eggs via embryonic metabolism. Physical Review E 94(2-1), 022402.

Lehman, T. M., and Coulson, A. B. (2002). A juvenile specimen of the sauropod dinosaur *Alamosaurus sanjuanensis* from the Upper Cretaceous of Big Bend National Park, Texas. Journal of Paleontology 76(1), 156-172.

Lehman, T. M., and Woodward, H. N. (2008). Modeling growth rates for sauropod dinosaurs. Paleobiology 34(2), 264-281.

Lockley, M. G., Meyer, C. A., Hunt, A. P., and Lucas, S. G. (1994). The distribution of sauropod tracks and trackmakers. Gaia 10, 233-248.

Lovelace, D., Wahl, W. R., and Hartman, S. A. (2003). Evidence for costal pneumaticity in a diplodocid dinosaur (*Supersaurus vivianae*). Journal of Vertebrate Paleontology 23, 73A

Mannion, P. D., Allain, R., and Moine, O. (2017). The earliest known titanosauriform sauropod dinosaur and the evolution of Brachiosauridae. PeerJ 5, e3217.

Mannion, P. D., Upchurch, P., Carrano, M. T., and Barrett, P. M. (2011). Testing the effect of the rock record on diversity: A multidisciplinary approach to elucidating the generic richness of sauropodomorph dinosaurs through time. Biological Reviews 86, 157–181.

Mannion, P. D., Upchurch, P., Barnes, R. N., and Mateus, O. (2013). Osteology of the Late Jurassic Portuguese sauropod dinosaur *Lusotitan atalaiensis* (Macronaria) and the evolutionary history of basal titanosauriforms. Zoological Journal of the Linnean Society 168(1), 98-206.

Mateus, O., Walen, A., and Antunes, M. T. (2006). The large theropod fauna of the Lourinhã Formation (Portugal) and its similarity to that of the Morrison Formation, with a description of a new species of *Allosaurus*. Paleontology and geology of the Upper Jurassic Morrison Formation: Bulletin 36, (36, 123).

Martin, R. B., and Burr, D. B. (1982). A hypothetical mechanism for the stimulation of osteonal remodelling by fatigue damage. Journal of Biomechanics 15:137–139.

Mazzetta, G. V., Christiansen, P., and Farina, R. A. (2004). Giants and bizarres: Body size of some southern South American Cretaceous dinosaurs. Historical Biology 2004, 1-13.

McIntosh, J. S. (1990). Sauropoda. In: Weishampel, D. B., Dodson, P., Osmólska, H., editors. The Dinosauria 1. Berkeley, University of California Press: 345-401.

McPhee, B. W., Benson, R. B., Botha-Brink, J., Bordy, E. M., and Choiniere, J. N. (2018). A giant dinosaur from the earliest Jurassic of South Africa and the transition to quadrupedality in early sauropodomorphs. Current Biology 28(19), 3143-3151.

Mitchell, J. (2017). Cortical bone remodeling in amniota: A functional, evolutionary and comparative perspective of secondary osteons (Doctoral dissertation, Universitäts- und Landesbibliothek Bonn).

Mitchell, J., and Sander, P. M. (2014). The three-front model: A developmental explanation of long bone diaphyseal histology of Sauropoda. Biological Journal of the Linnean Society 112(4), 765-781.

Mitchell, J., Sander, P. M., and Stein, K. (2017). Can secondary osteons be used as ontogenetic indicators in sauropods? Extending the histological ontogenetic stages into senescence. Paleobiology 43(2), 321-342.

Mocho, P., Royo-Torres, R., and Ortega, F. (2014). Phylogenetic reassessment *of Lourinhasaurus alenquerensis*, a basal Macronaria (Sauropoda) from the Upper Jurassic of Portugal. Zoological Journal of the Linnean Society 170(4), 875-916.

Molnar, R. E. (2010). Taphonomic observations on eastern Australian Cretaceous sauropods. Alcheringa 34(3), 421-429.

Montoya-Sanhueza, G., and Chinsamy, A. (2018). Cortical bone adaptation and mineral mobilization in the subterranean mammal *Bathyergus suillus* (Rodentia: Bathyergidae): Effects of age and sex. PeerJ 6.

Osborn, H. F., and Mook, C. C. (1921). *Camarasaurus*, *Amphicoelias*, and other sauropods of Cope. Bulletin of the Geological Society of America 30(1), 379-388.

Owen, R. (1840–1845). Odontography; or, a treatise on the comparative anatomy of the teeth; their physiological relations, mode of development, and microscopic structure in the vertebrate animals. Hippolyte Bailliere 1.

Padian, K., and Horner, J. R. (2004). Dinosaur physiology. In: D. B. Weishampel, P. Dodson, and Osmólska, H., editors. The Dinosauria, second edition. Berkeley, California, University of California Press: 660-671.

Padian, K., Ricqlès, A. de, and Horner, J. R. (2001). Dinosaurian growth rates and bird origins. Nature 412(6845), 405.

Pal, A., Swain, M. M., and Rath, S. (2009). Long bone histology and skeletochronology in a tropical Indian lizard, *Sitana ponticeriana* (Sauria: Agamidae). Current Herpetology 28(1), 13-18.

Perry, S. F., Christian, A., Breuer, T., Pajor, N., and Codd, J. R. (2009). Implications of an avian-style respiratory system for gigantism in sauropod dinosaurs. Journal of Experimental Zoology Part A: Ecological Genetics and Physiology 311(8), 600-610.

Petermann, H., and Sander, M. (2013). Histological evidence for muscle insertion in extant amniote femora: Implications for muscle reconstruction in fossils. Journal of Anatomy 222(4), 419-436.

Petit, J. R., Jouzel, J., Raynaud, D., Barkov, N. I., Barnola, J. M., Basile, I., Bender, M., Chappellaz, J., Davis, M., Delaygue, G., Delmotte, M., Kotlyakov, V. M., Legrand, M., Lipenkov, V. Y., Lorius, C., Pépin, L., Ritz, C., Saltzman, E., and Stievenard, M. (1999). Climate and atmospheric history of the past 420,000 years from the Vostok ice core, Antarctica. Nature 399(6735), 429.

Pi, L., Ouyang, H., and Ye, Y. (1996). A new species of sauropod from Zigong, Sichuan, *Mamenchisaurus youngi*. Papers on geosciences contributed to the 30th International Geological Congress, 87-91.

Rauhut, O. W. (2006). A brachiosaurid sauropod from the late Jurassic Cañadón Calcáreo Formation of Chubut, Argentina. Fossil Record 9(2), 226-237.

Reid, R. E. H. (1981). Lamellar-zonal bone with zones and annuli in the pelvis of a sauropod dinosaur. Nature 292(5818), 49.

Reimers, C. E., Lange, C. B., Tabak, M., and Bernhard, J. M. (1990). Seasonal spillover and varve formation in the Santa Barbara Basin, California. Limnology and Oceanography 35(7), 1577-1585.

Reiss, M. J. (1989). The allometry of growth and reproduction. Cambridge, Cambridge University Press, pp. 200.

Remes, K., Ortega, F., Fierro, I., Joger, U., Kosma, R., Ferrer, J. M. M., Ide, O. A., and Maga, A. (2009). A new basal sauropod dinosaur from the Middle Jurassic of Niger and the early evolution of Sauropoda. PLoS ONE 4(9), e6924.

Riggs, E. S. (1904). Structure and relationships of the opisthocoelian dinosaurs. Part II: The Brachiosauridae. Field Columbian Museum. Geological Series 2, 229-248.

Ricqlès, A. de. (1968). Recherches palèohistologiques sur les os longs des tetrapodes. I.- Origine du tissu osseux plexiforme des dinosaurians sauropodes. Annales de Paléontologie 54, 133-145.

Ricqlès, A. de (1980). Tissue structures of dinosaur bone, functional significance and possible relation to dinosaur physiology. In: Thomas, R. D. K., and Olson, E. C., editors. A cold look at the warm-blooded dinosaurs. Westview, Boulder Colorado, AAA selected symposium: 103-139.

Ricqlès, A. de (1983). Cyclical growth in the long limb bones of a sauropod dinosaur. Acta Palaeontologica Polonica 28(1-2).

Ricqlès, A. de, Meunier F. J., Castanet J., and Francillon-Vieillot H. (1991). Comparative microstructure of bone. In: Hall, B. K., editor. Bone, Volume 3, Bone matrix and bone specific products. Ann Arbor, Michigan, CRC Press: 1-78.

Rockwell, H., Evans, F. G., and Pheasant, H. C. (1938). The comparative morphology of the vertebrate spinal column. Its form as related to function. Journal of Morphology 63(1), 87-117.

Rogers, K. C., Whitney, M., D'Emic, M., and Bagley, B. (2016). Precocity in a tiny titanosaur from the Cretaceous of Madagascar. Science 352(6284), 450-453.

Romer, A. S., and Parsons, T. S. (1977). The Vertebrate Body. Philadelphia, PA, Holt-Saunders International.

Royo-Torres, R., Fuentes, C., Meijide, M., Meijide-Fuentes, F., and Meijide-Fuentes, M. (2017). A new Brachiosauridae sauropod dinosaur from the Lower Cretaceous of Europe (Soria province, Spain). Cretaceous Research 80, 38-55.

Russell, D. A. (1993). The role of Central Asia in dinosaurian biogeography. Canadian Journal of Earth Sciences 30(10), 2002-2012.

Ruxton, G. D., Birchard, G. F., and Deeming, D. C. (2014). Incubation time as an important influence on egg production and distribution into clutches for sauropod dinosaurs. Paleobiology 40(3), 323-330.

Salgado, L., Coria, R. A., and Calvo, J. O. (1997). Evolution of titanosaurid sauropods: Phytogenetic analysis based on the postcranial evidence. Ameghiniana 34(1), 3-32.

Sander, P. M. (2000). Longbone histology of the Tendaguru sauropods: Implications for growth and biology. Paleobiology 26(3), 466-488.

Sander, P. M. (2013). An evolutionary cascade model for sauropod dinosaur gigantism-overview, update and tests. PLoS ONE 8(10), e78573.

Sander, P. M., and Tückmantel, C. (2003). Bone lamina thickness, bone apposition rates, and age estimates in sauropod humeri and femora. Paläontologische Zeitschrift 77(1), 161-172.

Sander, P. M., and Clauss, M. (2008). Sauropod gigantism. Science 322(5899), 200-201.

Sander, P. M., and Lallensack, J. N. (2018). Dinosaurs: Four legs good, two legs bad. Current Biology 28(19), R1160-R1163.

Sander, P. M., Mateus, O., Laven, T., and Knötschke, N. (2006). Bone histology indicates insular dwarfism in a new Late Jurassic sauropod dinosaur. Nature 441(7094), 739.

Sander, P. M., Peitz, C., Jackson, F. D., and Chiappe, L. M. (2008). Upper Cretaceous titanosaur nesting sites and their implications for sauropod dinosaur reproductive biology. Palaeontographica Abteilung A, 69-107.

Sander, P. M., Klein, N., Buffetaut, E., Cuny, G., Suteethorn, V., and Le Loeuff, J. (2004). Adaptive radiation in sauropod dinosaurs: Bone histology indicates rapid evolution of giant body size through acceleration. Organisms Diversity and Evolution 4(3), 165-173.

Sander, P. M., Christian, A., Clauss, M., Fechner, R., Gee, C. T., Griebeler, E. M., Gunga, H. C., Hummel, J., Mallison, H., Perry, S. F. and Preuschoft, H., (2011). Biology of the sauropod dinosaurs: The evolution of gigantism. Biological Reviews 86(1), 117-155.

Seeman, E. (2006). Osteocytes–Martyrs for integrity of bone strength. Osteoporosis International 17, 1443–1448.

Schweingruber, F. H. (2012). Tree rings: Basics and applications of dendrochronology. Springer Science and Business Media.

Seymour, R. S. (1979). Dinosaur eggs: Gas conductance through the shell, water loss during incubation and clutch size. Paleobiology 5(1), 1-11.

Sites, A. (2005). Thousand clutches, some of sauropod egg. The sauropods: Evolution and paleobiology, 285.

Smirina, E. M., and Tsellarius, A. Y. (1996). Aging, longevity, and growth of the desert monitor lizard (*Varanus griseus* Daud.). Russian Journal of Herpetology 3(2), 130-142.

Smirina, E. M., and Ananjeva, N. B. (2007). Growth layers in bones and acrodont teeth of the agamid lizard *Laudakia stoliczkana* (Blanford, 1875) (Agamidae, Sauria). Amphibia-Reptilia 28(2), 193-204.

Stein, K. W., and Werner, J. (2013). Preliminary analysis of osteocyte lacunar density in long bones of tetrapods: All measures are bigger in sauropod dinosaurs. PloS ONE 8(10), e77109.

Tickle, P. G., Ennos, A. R., Lennox, L. E., Perry, S. F., and Codd, J. R. (2007). Functional significance of the uncinate processes in birds. Journal of experimental biology 210(22), 3955-3961.

Tschopp, E., Mateus, O., and Benson, R. B. (2015). A specimen-level phylogenetic analysis and taxonomic revision of Diplodocidae (Dinosauria, Sauropoda). PeerJ 3, e857.

Upchurch, P. (1995). The evolutionary history of sauropod dinosaurs. Philosophical Transactions, Royal Society London B 349(1330), 365-390.

Upchurch, P. (1998). The phylogenetic relationships of sauropod dinosaurs. Zoological Journal of the Linnean Society 124(1), 43-103.

Upchurch, P., and Mannion, P. D. (2009). The first diplodocid from Asia and its implications for the evolutionary history of sauropod dinosaurs. Palaeontology 52(6), 1195-1207.

Upchurch, P., Hunn, C. A., and Norman, D. B. (2002). An analysis of dinosaurian biogeography: Evidence for the existence of vicariance and dispersal patterns caused by geological events. Proceedings of the Royal Society of London B: Biological Sciences 269(1491), 613-621.

Upchurch, P., Barrett, P. M., and Dodson, P. (2004). Sauropoda. In: Weishampel, D. B., Dodson, P., and Osmólska, H., editors. The Dinosauria, Second Edition. Berkeley, California, University of California Press: 259–322.

Upchurch, P., Barrett, P. M., and Galton, P. M. (2007). A phylogenetic analysis of basal sauropodomorph relationships: Implications for the origin of sauropod dinosaurs. Special Papers in Palaeontology 77, 57.

Vila, B., Galobart, À., Canudo, J. I., Le Loeuff, J., Dinarès-Turell, J., Riera, V., Parellada, C., and Gaete, R. (2012). The diversity of sauropod dinosaurs and their first taxonomic succession from the latest Cretaceous of southwestern Europe: Clues to demise and extinction. Palaeogeography, Palaeoclimatology, Palaeoecology 350, 19-38.

Wake, D. B. (1979). The endoskeleton: The comparative anatomy of the vertebral column and ribs. Hyman's comparative vertebrate anatomy 192, 237.

Waskow, K., and Sander, P. M. (2014). Growth record and histological variation in the dorsal ribs of *Camarasaurus* sp. (Sauropoda). Journal of Vertebrate Paleontology 34(4), 852-869.

Waskow, K., and Mateus, O. (2017). Dorsal rib histology of dinosaurs and a crocodylomorph from western Portugal: Skeletochronological implications on age determination and life history traits. Comptes Rendus Palevol 16(4), 425-439.

Waskow, K., Wiersma, K., Tschopp, E., Woodruff, D. C., Storrs, G., and Sander, P. M. (submitted). Histological evidence for dwarfism and different morphotypes of diplodocine sauropods within the Upper Jurassic Mother's Day Quarry (Morrison Formation, Montana, USA). Acta Palaeontologica Polonica.

Wedel, M. J. (2005). Postcranial skeletal pneumaticity in sauropods and its implications for mass estimates. In: Curry-Rogers, K.A., and Wilson, J. A. editors. The sauropods: Evolution and paleobiology. Berkeyley, California, University of California Press: 201-228.

Werner, J., and Griebeler, E. M. (2011). Reproductive biology and its impact on body size: Comparative analysis of mammalian, avian and dinosaurian reproduction. PLoS ONE 6(12), e28442.

Werner, J., and Griebeler, E. M. (2014). Allometries of maximum growth rate versus body mass at maximum growth indicate that non-avian dinosaurs had growth rates typical of fast growing ectothermic sauropsids. PloS ONE 9(2), e88834.

Wilson, J. (2002). Sauropod dinosaur phylogeny: Critique and cladistic analysis. Zoological Journal of the Linnean Society 136(2), 215-275.

Wilson, J. A. (2005). Redescription of the Mongolian sauropod *Nemegtosaurus mongoliensis Nowinski* (Dinosauria: Saurischia) and comments on Late Cretaceous sauropod diversity. Journal of Systematic Palaeontology 3(3), 283-318.

Wilson, J. A., and Sereno, P. C. (1998). Early evolution and higher-level phylogeny of sauropod dinosaurs. Society of Vertebate Paleontology Memoires 5: 1-68.

Wings, O., Sander, P. M., Tütken, T., Fowler, D. W. and Sun, G. (2007). Growth and life history of Asia's largest dinosaur. Journal of Vertebrate Paleontology 27(3, Supplement), 167A.

Woodruff, D. C., Carr, T. D., Storrs, G. W., Waskow, K., Scannella, J. B., Nordén, K. K., and Wilson, J. P. (2018). The smallest diplodocid skull reveals cranial ontogeny and growth-related dietary changes in the largest dinosaurs. Scientific Reports 8(1), 14341.

Woodward, H. N., Horner, J. R., and Farlow, J. O. (2014). Quantification of intraskeletal histovariability in *Alligator mississippiensis* and implications for vertebrate osteohistology. PeerJ 2, e422.

Xu, X., Upchurch, P., Mannion, P. D., Barrett, P. M., Regalado-Fernandez, O. R., Mo, J., Ma, J. and Liu, H. (2018). A new Middle Jurassic diplodocoid suggests an earlier dispersal and diversification of sauropod dinosaurs. Nature Communications 9(1), 2700.

Yang, T. R., and Sander, P. M. (2018). The origin of the bird's beak: New insights from dinosaur incubation periods. Biology Letters 14(5), 20180090.

Yates, A. M., and Kitching, J. W. (2003). The earliest known sauropod dinosaur and the first steps towards sauropod locomotion. Proceedings of the Royal Society of London B: Biological Sciences 270(1525), 1753-1758.

Yates, A. M., Wedel, M. J., and Bonnan, M. F. (2012). The early evolution of postcranial skeletal pneumaticity in sauropodomorph dinosaurs. Acta Palaeontologica Polonica 57(1), 85-100.

„Diejenigen, die sich nicht auf neue Methoden einlassen, müssen immer wieder mit den alten Unzulänglichkeiten rechnen."

"Those who do not embark on new methods must always reckon with the old shortcomings."

Sir Francis von Verulam Bacon

CHAPTER 2

Dorsal rib histology of dinosaurs and a crocodylomorph from western Portugal: Skeletochronological implications on age determination and life history traits

published as:

Waskow, K., and Mateus, O. (2017). Dorsal rib histology of dinosaurs and a crocodylomorph from western Portugal: Skeletochronological implications on age determination and life history traits. Comptes Rendus Palevol 16(4), 425-439.

Author contribution:

Histological sampling, research, analysis and manuscript preparation including all text (except large parts of chapter 2.2. Material) and figures were performed by me.

Octávio Mateus provided access, loan and sampling permission for all analysed taxa and wrote major parts of the text for chapter 2.2. Material.

Comptes Rendus Palevol

General Palaeontology, Systematics and Evolution (Evolutionary Processes)

Dorsal rib histology of dinosaurs and a crocodylomorph from western Portugal: Skeletochronological implications on age determination and life history traits

Histologie des côtes dorsales de dinosaures et d'un crocodile de l'Ouest du Portugal : implications squelettochronologiques sur la détermination de l'âge et des traits d'histoire de vie

Katja Waskow [a,*], Octavio Mateus [b,c]

[a] *Steinmann Institute for Geology, Mineralogy, and Paleontology, University of Bonn, Nussallee 8, 53113 Bonn, Germany*
[b] *Departamento de Ciências da Terra, Faculdade de Ciências e Tecnologia, FCT, Universidade Nova de Lisboa, 2829-526 Caparica, Portugal* [c] *Museu Da Lourinhã, Rua João Luis de Moura, 2530-157 Lourinhã, Portugal*

ARTICLE INFO

Article history:
Received 1st December 2014 Accepted after revision 20 January 2017
Available online 19 April 2017

Handled by Michel Laurin

Keywords:
New histological approach for ribs
Determination of ontogenetic stage Skeletal maturity
Age at first reproduction Longevity in dinosaurs

ABSTRACT

Bone histology is an important tool for uncovering life history traits of extinct animals, par-ticularly those that lack modern analogs, such as the non-avian dinosaurs. In most studies, histological analyses preferentially focus on long bones for understanding growth rates and determining age. Here we show, by analyzing ornithischians (a stegosaur and an ornitho-pod), saurischians (a sauropod and a theropod), and a crocodile, rib histology is a suitable alternative. The estimated age for all sampled taxa ranges between 14 to 17 years for *Lour-inhanosaurus antunesi* and 27 to 31 years estimated for *Draconyx loureiroi*. The theropod *Baryonyx* was skeletally mature around 23–25 years of age but showed unfused neurocen-tral sutures, a paedomorphic feature possibly related to aquatic locomotion. Our results show that ribs can contain a nearly complete growth record, and reveal important infor-mation about individual age, point of sexual maturity, and, in some cases, sex. Because ribs are more available than long bones, this method opens new possibilities for studying rare and incomplete fossils, including holotypes.

Mots clés :
Nouvelle approche histologique pour les côtes
Détermination du stade ontogénétique
Maturité squelettique
Âge à la première reproduction
Longévité chez les dinosaures

RÉSUMÉ

L'histologie osseuse révèle d'importantes informations sur les traits d'histoire de vie des animaux éteints n'ayant pas d'analogues modernes, comme les dinosaures non aviens. En général, les os longs sont préférés pour les analyses histologiques. En collectant des données histologiques sur les côtes de différents taxons de vertébrés fossiles tels que des ornithischiens (un stégosaure et un ornithopode), des saurischiens (un sauropode et un théropode) et un crocodile, nous montrons que l'histologie des côtes est un outil approprié pour l'étude des traits d'histoire de vie. Nos résultats montrent que les côtes renferment un enregistrement de la croissance presque complet et, avec cela, d'importantes informations

* Corresponding author.
E-mail addresses: waskow@uni-bonn.de (K. Waskow)

sur l'âge individuel, l'âge de maturité sexuelle et parfois le sexe de l'animal. L'âge estimé de tous les spécimens échantillonnés varie entre 14 et 17 ans (*Lourinhanosaurus antunesi* ; subadultes) et 27 et 31 ans (*Draconyx loureiroi* ; adultes). Le théropode *Baryonyx* a atteint sa maturité squelettique vers 23–25 ans, mais montre des sutures du neurocentre non fusion-nées, une stratégie pédomorphique qui pourrait être liée à la locomotion aquatique. Les côtes étant plus accessibles que les os longs, cette méthode ouvre de nouvelles perspectives pour l'étude de spécimens rares et incomplets, ou même d'holotypes.

1. Introduction

Non-avian dinosaurs are the best-known extinct taxa. Unfortunately, these large creatures lack modern analogs, making it difficult to reconstruct their age and growth. Osteological features like neurocentral fusion are often used to estimate the ontogenetic age of archosaurs. However, even if the closure of neurocentral sutures in pseudosuchians seems to be a plesiomorphic feature (Brochu, 1996; Ikejiri, 2012), the reliability of this diagnosis in other archosaurs is still controversial (Fronimos and Wilson, 2017; Irmis, 2007). Therefore, to obtain information about their life history, the growth record preserved in hard tissues can be used (Castanet, 1994; Castanet et al., 1993). Within the fields of bone histology and skeletochronology, important data can be obtained concerning growth rates, individual age, longevity, skeletal-, and, in some cases, sexual maturity (e.g., Curry, 1999; Enlow and Brown, 1956, 1957, 1958; Griebeler et al., 2013; Horner et al., 1999; Klein and Sander, 2007, 2008; Klein et al., 2009; de Ricqlès, 1975, 1976; de Ricqlès et al., 2001; Sander, 2000; Sander et al., 2011; Woodward et al., 2011a, 2011b). The majority of paleo-histological studies focus on the long bone diaphysis (caused by their nearly circumferential shape, making it possible to infer growth curves). A few former studies, however, have used rib histology of extinct vertebrates (e.g., D'Emic et al., 2015; Erickson et al., 2004; Houssaye and Bardet, 2012; Waskow and Sander, 2014). In contrast to extant reptiles and other non-avian dinosaurs, sauropod long bone histology lacks a skeletochronological significant growth record; thus, rib histology is needed to obtain information about their age, growth, and life cycles. In their histological study on the ribcage of the nearly complete and articulated *Camarasaurus* sp. (SMA 0002), Waskow and Sander (2014) determined that the proxi-mal end of a rib shaft contains the most complete growth record within sauropods. Fossil ribs are generally more frequently preserved and not as important for exhibitions as long bones; thus, they are more easily accessible for analy-ses. The current study focuses on rib histology of different Portuguese vertebrate taxa (mainly non-avian dinosaurs) to determine whether ribs provide sufficient histological data on life history traits of dinosaurs and other vertebrates.

1.1. Growth record preservation in primary bone tissue

Growth in bone tissue is recorded by the formation of annuli. Each annulus represents the bone tissue that was deposited during one year. The most important features concerning annularity used in this study are lines of arrested growth (LAGs), which are clearly developed thin, continuous, dark lines completing the single annuli. These LAGs represent the former surface of the bone where growth was interrupted. Another form of growth lines are polish lines. These more diffuse structures are not observ-able under the microscope, but they are only visible by tilting a polished bone surface, in order to reflect light. They are easy to see with the naked eye (Sander, 2000). Interpretations of the annual nature of the cyclicity pre-served in primary bone tissues of several skeletal elements, like the humerus and femur, have been controversial in the past (e.g., Chinsamy and Hillenius, 2004; Padian and Horner, 2004). Nevertheless, annularity of growth cycles has been demonstrated in long bones, as well as other skeletal elements such as the scapula, coracoid, and ribs of extant and extinct reptiles such as *Alligator mississip-piensis* or varanid squamates (e.g., Erickson et al., 2003; Garcia, 2011; Smirina and Ananjeva, 2007; Smirina and Tsellarius, 1996; Woodward et al., 2014) and extant mam-mals (e.g., several ruminants) with very similar histology to that of non-avian dinosaurs (Köhler et al., 2012). Fur-thermore, counting lines of arrested growth (LAGs) is a standard method of aging both ectothermic (actinoptery-gians, lissamphibians, squamates and crocodillomorphs) and endothermic (mammals) vertebrates (e.g., Altuniş ik et al., 2014; Caetano, 1990; Castanet and Smirina, 1990; Castanet et al., 1993, 2004; Hutton, 1986; Pancharatna and Kumbar, 2013; Snover et al., 2013). Therefore, the annual cyclicity of growth marks is generally accepted for non-avian dinosaurs (Erickson, 2005; Sander et al., 2011). Also, it is well-established that the presence of an External Fundamental System (EFS) indicates skeletal maturity (Chinsamy-Turan, 2005; Erickson, 2005; Sander, 2000; Sander et al., 2011; Turvey et al., 2005). The annular-ity of LAGs within the EFS is, however, controversial. The close spacing of the LAGs with no significant histological elements like osteons or vascular canals in between can be interpreted in different ways: either as a shorter timeframe (more than one LAG deposited in a year) or a longer timeframe (LAGs deposited only every second or third year)(Horner et al., 1999). Additionally, some LAGs might be more distinct than others, and some might be partly erased by the remodeling process.

In some cases, cyclicity only appears as a polish line, which is defined as a growth line in fibrolamellar bone that is visible in a polished section but not in a thin section (Sander, 2000), or as a modulation of bone tissue

not completed by a LAG (de Ricqlès, 1983; Sander et al., 2004).

1.2. Rib histology in non-avian dinosaurs and other vertebrates

In contrast to long bones, ribs have not been a focus of scientific study for decades. Nopcsa (1933), in an innovative study for that time, was the first to analyze dinosaur rib histology using ornithopod ribs. Only a few recent histo-logical papers focused on ribs (e.g., de Buffrénil et al., 1990; D'Emic et al., 2015; Waskow and Sander, 2014). Canoville et al. (2016) published the first quantitative exploratory study about the microanatomical diversity of amniote ribs. A few histological studies compared the dorsal rib histology of some dinosaurs with other skeletal elements (Erickson, 2005; Erickson et al., 2004; de Ricqlès et al., 2008). Most papers that take rib histology into account concern marine vertebrates (e.g., Hayashi et al., 2013; Houssaye, 2009, 2013; Houssaye and Bardet, 2012; Laurin et al., 2007). More recently, Klein et al. (2012) stated that sauropod neck ribs are ossified tendons. The first study focusing exclusively on sauropod rib histology was done by Waskow and Sander (2014). The lack of focus on ribs is primarily because humeri and femora, for example, allow growth curve calculations based on skeletochronology (caused by their nearly cir-cumferential shape).

1.3. Differences in growth records between long bones and ribs

The study of Waskow and Sander (2014) shows that, in contrast to long bones that have most of the growth record preserved in the midshaft region (Currey, 2002; Hall, 2005), ribs, due to their growth trajectory from proximal to distal end, have the most complete growth record at the proximal end of the rib shaft. According to Amprino's rule (Amprino, 1947), the primary bone structure is closely related to the bone apposition rate. This rule has been tested and confirmed in several studies related to verte-brate long bones (Castanet et al., 1996; de Margerie et al., 2004; de Ricqlès et al., 1991), but in ribs, the relative bone apposition rate is also related to morphological changes during ontogeny, as determined by the histological rib sec-tion series of Waskow and Sander (2014). In addition, ribs grow much more slowly than long bones, which causes a difference in bone tissue type, remodeling rate, or number of preserved LAGs, even within the same individual (Horner et al., 2000; Waskow and Sander, 2014; Woodward et al., 2014). The differences in the LAG number counted in different skeletal elements of a same individual can also be explained by different resorption rates during the expansion of the medullary cavity and the difference in the degree and rate of remodeling (Waskow and Sander, 2014). The fast-growing fibrolamellar bone is also more strongly influ-enced by Haversian remodeling than the slower-growing lamellar-zonal bone (Chinsamy-Turan, 2005; Enlow and Brown, 1956). Moreover, the mechanical forces and loads that affect a bone differ in the individual skeletal parts and might therefore influence the primary bone tissue type (Currey, 2002; Dumont et al., 2014). The fact that ribs, in contrast to long bones, do not have an isometric growth could also be an advantage for the growth record preser-vation. Due to the formation of the rib ridge, the medullary cavity seems to expand less on the posteromedial side dur-ing growth, resulting in lesser resorption of the primary bone tissue and therefore more recorded LAGs.

Institutional abbreviations – **ML**: Museu da Lourinhã, Lourinhã, Portugal; **SMA**: Sauriermuseum Aathal, Aathal, Canton Zürich, Switzerland.

2. Material

2.1. Sampled material

The following specimens used for this study repre-sent a phylogenetical broad but incomplete selection of archosaurs including saurischians (Theropoda and Sauropoda), ornitischians (Stegosauria and Ornithopoda) and crocodylomorphs. All samples (excluding the litera-ture data of sauropod SMA 0002) are from the Lusitanian Basin, western Portugal. All but one (*Baryonyx walkeri*) are dated from the Kimmeridgian–Tithonian Lourinhã Forma-tion according to regional stratigraphic context, vertebrate fauna and strontium isotope dating (Mateus et al., 2014). This formation yields dinosaur bones, crocodylomorphs, pterosaurs, mammals, amphibians and other Jurassic ver-tebrates as well as teeth, eggs and tracks (e.g., Araújo et al., 2013; Hendrickx and Mateus, 2014; Milàn et al., 2005), pro-viding a unique window into the terrestrial Late Jurassic fauna of Europe. This study includes dorsal rib histology from the proximal rib shaft of a *Camarasaurus* specimen used in Waskow and Sander (2014), as well as the following dorsal rib samples of specimens from the ML collections.

2.1.1. ML 433: Miragaia longicollum (Stegosauria)

Specimen ML 433 is the holotype of the dacentrurinae stegosaur *M. longicollum* (Mateus et al., 2009), from the Miragaia Member of the Lourinhã Formation, dated from the Kimmeridgian–Tithonian transition (about 152 M.a.) This specimen corresponds to a large individual up to 6.5 m long, with fused neurocentral sutures, and ossified tendons or cartilage located mainly in the ulna. The cervical portion is unusually long for stegosaurs due to the presence of 17 segments, and the most posterior cervical vertebrae being cervicalized dorsal elements (Mateus et al., 2009). Histol-ogy of *Miragaia* has never been studied except for the tail spines by Hayashi et al. (2008).

2.1.2. ML 439: Draconyx loureiroi (Ornithopoda)

Specimen ML 439 is the holotype of camptosaurid ornithopod *D. loureiroi* (Mateus and Antunes, 2001), from the Praia Azul Member of the Lourinhã Formation (Latest Kimmeridgian to earliest Tithonian), and is a poorly-known ankylopollexian, which is partly articulated but poorly pre-served. The neurocentral suture fusion suggests that ML 439 is an adult, but tracks also suggest the occurrence of much larger individuals of ornithopod dinosaurs in the same region (Mateus and Milàn, 2008).

2.1.3. ML 370: Lourinhanosaurus antunesi (Theropoda; Avetheropoda)

Specimen ML 370 is the holotype of *L. antunesi* (Mateus, 1998), also from the Praia Azul Member of the Lourinhã Formation. It is a tetanuran theropod of uncertain affin-ity; recent phylogenetic analyses place *Lourinhanosaurus* as either a basal coelurosaurian (Carrano et al., 2012), a sin-raptorid allosauroid (Benson et al., 2010) or a megalosaurid. The specimen appears to be an adult but no histological study has been done – bone histology has been documented on embryos only (de Ricqlès et al., 2001).

2.1.4. ML 1190: Baryonyx walkeri (Theropoda; Spinosauroidea)

Specimen ML 1190 is the theropod *B. walkeri* (Charig and Milner, 1986) found at Praia das Aguncheiras (Mateus et al., 2011). Stratigraphically, it belongs to the Papo Seco For-mation (early Barremian) of Portugal. It is the only sample from the Early Cretaceous used in this analysis. The body size of this specimen is equivalent to that of the holotype of *B. walkeri* NHM R9951, which is identified as an adult (Charig and Milner, 1986), despite the fact that the neuro-central suture is often, but not always, open and unfused.

2.1.5. ML 426: Crocodylomorph (Crurotarsi)

Specimen ML 426 is a crocodylomorph collected in the late 1980s at Casal da Pedreira, in the vicinity of Lourinhã (Praia Azul Member, Lourinhã Formation, Kimmeridgian–Tithonian boundary). It preserves most of the axial skeleton, a few osteoderms, fragmentary limb ele-ments but no skull. Taking into account the overall anatomy and size of these remains, this crocodylomorph may be a *Goniopholis* (Owen, 1841) but more study is needed. The vertebrae show fused but visible neurocentral sutures, sug-gesting the animal to be an adult.

2.2. Dorsal rib material described in the literature

SMA 0002: *Camarasaurus sp.* (Sauropoda): specimen SMA 0002 is one of the most complete and articulated *Camarasaurus* skeletons ever found. Its assignment to *Camarasaurus* based on several diagnostic features mentioned by Ikejiri (2004), McIntosh (2005), and Upchurch et al. (2004), but this attribution has been recently challenged by Mateus and Tschopp (2013), who identified it as *Cathetosaurus*, based on the morphology of the pelvic gir-dle and dorsal transverse processes. In more recent studies, however, it was again claimed to be a *Camarasaurus* speci-men, based on its autopodial and preliminary unpublished phylogenetic analysis (Tschopp et al., 2015, 2016). The SMA 0002 specimen was found in the Upper Jurassic Morrison Formation (Kimmeridgian), which is situated in the central northern part of Wyoming, USA. It is the stratigraphically oldest *Camarasaurus* in the whole formation (Ayer, 2000; Waskow and Sander, 2014). With three-dimensional preservation, the small but mature individual lacks only the vomers, the splenial bones, the distal end of the tail, and one terminal phalanx of the right pes (Tschopp et al., 2015; Waskow and Sander, 2014). Former histological studies of the long bones and ribs suggest a senescent age of this indi-vidual (Klein and Sander, 2008; Waskow and Sander, 2014), with a growth record of 37 preserved LAGs (Waskow and Sander, 2014).

3. Methods

3.1. Thin sectioning

All samples were taken as complete cross-sections from well-preserved regions of the proximal rib shaft of the different taxa. First, molds of all sampled rib parts were made to enable the reconstruction of the missing bone slice after sampling. These molds were made with a two-component silicone “Provil novo” consisting of the base putty and its catalyst (proportion 1:1). Each rib was pro-tected with a solution of Technovit 4071, a technical polymer. The two components of this polymer (powder and liquid) are usually used in a ratio of 2:1. Here we used a 3:1 ratio to make the liquid suspension more vis-cous to properly mold the whole sampling region of the rib shaft. The protected area then was cut with an automatic rock saw and cut into standard paleo-histological thin sec-tions (see Chinsamy and Raath, 1992; Enlow and Brown, 1956; Lamm, 2007; Wells, 1989). After sawing, the hard-ened Technovit polymer was removed with acetone. Rib pieces were reconnected by putting the rib sections back in the mold and refilling the missing bone material with plaster. The authors decided to use whole cross-sections instead of core drilling (see Stein and Sander, 2009) to be sure that the most complete growth record preserved could be detected. Thin sections were analyzed under a Leica DML P polarizing microscope. The drawings of the sections were made with a Camera Lucida (Schott KL 1500 LCD). Photos were taken with a Leica DFC420 digital camera and processed with Imagic ImageAccess software.

3.2. Measurements for growth record evaluation

In some cases, the center of the medullary region, where the bone growth initiated, is not located in the center of the section itself. Thus, the center of the medullary region was determined following the method of Waskow and Sander (2014) by the intersection of the two imaginary lines connecting the two greatest diameters of the rib. Depending on the region of a section, the distance between two same LAGs vary laterally. We chose to measure the LAG interdistances in the thickest part of the cortex, on the posteromedial side of each section. The percentage of the preserved growth record was calculated by measuring the distance from the medullary region to the surface of the bone at the thickest part of the cortex, and the distance from the first visible LAG to the bone surface. By assum-ing that the first measured distance equals 100% of the growth record, preservation was calculated after the rule of proportion. Based on the assumption that the LAGs are generally more widely spaced in the inner part of the bone (Chinsamy-Turan, 2005), the distance between the center of the medullary region and the first visible LAG was mea-sured and divided by the widest growth cycle to obtain the maximum number of resorbed LAGs.

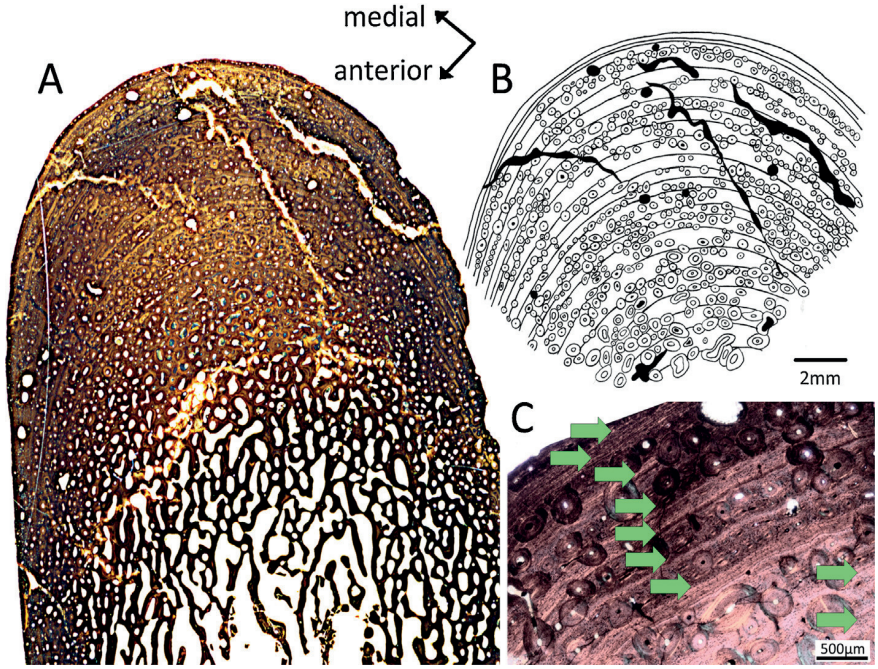

Fig. 1. Histological thin section of the posteromedial side of the dorsal rib of *Miragaia longicollum* (ML 433), which preserves the most complete growth record. A. Scanned image of the entire section. B. Drawing of the visible lines of arrested growth (LAGs) and the secondary osteons influencing the LAGs by destroying, or tracing them. C. Microscopic image of the section (PPL, cross-polarized, magnification?). All LAGs are marked with arrows.
Fig. 1. Section mince histologique du côté postéromédial de la côte dorsale de *Miragaia longicollum* (ML 433), qui préserve l'enregistrement le plus complet de la croissance. A. Image scan de la section entière. B. Dessin des *lines of arrested growth* (LAGs) visibles et des ostéones secondaires influençant les LAGs en les détruisant ou en les suivant. C. Image de la section au microscope (PPL, en polarisation croisée, agrandissement ?). Toutes les LAGS sont marquées par des flèches.

4. Results

4.1. Dorsal rib histological description

4.1.1. ML 433: M. longicollum (Stegosauria)

The well-preserved rib thin section shows a relatively large medullary region filled with spongiosa with reduced intertrabecular spaces in the middle. It is surrounded by a lamellar-zonal bone cortex greatly varying in thickness from 2 to 10 mm. Most primary bone tissue is preserved in the thickest part of the cortex building the rib ridge on the posteromedial side of the bone. The bone tissue is rela-tively poorly vascularized. The canals are predominantly oriented longitudinally. Only a few Sharpey's fibers ori-ented longitudinally, nearly parallel to the bones surface, are visible on the posterolateral side. Including the EFS, 22 annuli are counted, representing 68% of the growth record (Fig. 1). Most of them are preserved as clearly developed LAGs and only the innermost cycles are visible as polish lines (Sander, 2000). The outermost four LAGs, represent-ing the EFS, are closely spaced (distances < 200 µm) with no significant primary bone tissue structures in between. The remodeling rate is relatively low with only about one-third of the primary bone tissue replaced by secondary osteons.

4.1.2. ML 439: D. loureiroi (Ornithopoda)

In contrast to *M. longicollum*, the well-preserved ribs of *D. loureiroi* only have a small medullary region completely filled with dense spongy bone tissue. As in the sample described before, the cortex thickness varies significantly around the section (5 mm to 18 mm). Again, most primary bone tissue is preserved in the posteromedial ridge of the rib (Fig. 2). Near the medullary cavity, fibrolamellar bone slowly changes into slower-growing lamellar-zonal bone towards the bones surface. Overall, the bone tissue is more vascularized than the section of *M. longicollum* described before, although the number of vascular canals (perforat-ing the bone in all three directions) is still moderate. A higher amount of Sharpey's fibers is present with most of them, occurring again at the posterolateral side of the rib. Here, most fibers are oriented longitudinally, although the direction of the fibers changes around the section into sev-eral directions. Thirty growth cycles are counted. Similar to *M. longicollum*, the innermost growth cycles are only visi-ble as polish lines. The outermost three LAGs comprise the EFS. Due to the small size of the medullary region, 86% of the growth record is preserved. There is nearly no corti-cal remodeling in the bone tissue. Only a few secondary osteons are visible, most of which are near the medullary cavity.

4.1.3. ML 370: L. antunesi (Theropoda; Avetheropoda)

In *L. antunesi*, the well-preserved histological section of the rib mainly consists of a large medullary cavity. The center of the medullary cavity is hollow, surrounded by a thick, spongy region. The thin cortex has a consistent thickness (2 mm) and consists of dense, highly vascular-ized primary bone tissue made of primary osteons. On the

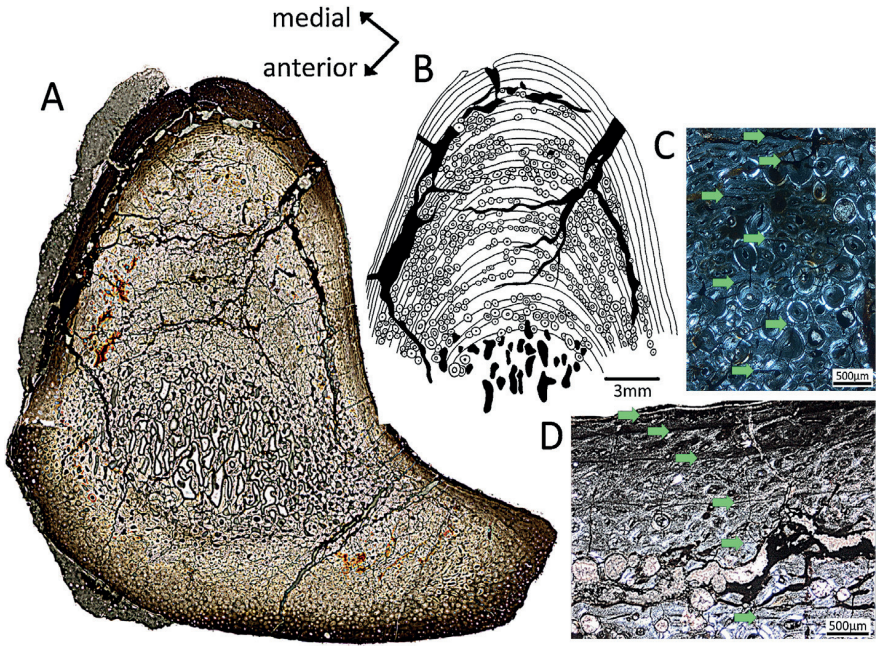

Fig. 2. Histological thin section of the posteromedial side of the dorsal rib of *Draconyx loureiroi* (ML 439), which preserves the most complete growth record. A. Macroscopic scan of the section. B. Drawing of the visible lines of arrested growth (LAGs) and the secondary osteons influencing the LAGs by destroying, or tracing them. C and D. Microscopic images of the section. All LAGs are marked with arrows.
Fig. 2. Section mince histologique du côté postéromédial de la côte dorsale de *Draconyx loureiroi* (ML 439), qui préserve l'enregistrement le plus complet de la croissance. A. Scan macroscopique de la section. B. Dessin des *lines of arrested growth* (LAGs) visibles et des ostéones secondaires influençant les LAGs en les détruisant ou en les suivant. C et D. Images de la section au microscope. Toutes les LAGs sont marquées par des flèches.

anteromedial and posterolateral side, most of the canals are oriented longitudinally and on the anterolateral and pos-teromedial side, some vascular canals are oriented radially. The tissue has a high osteocyte density and shows a vascu-larization similar to that of *D. loureiroii*, described before. A high amount of Sharpey's fibers is visible with most of the fibers oriented obliquely to the bone surface on the anterolateral and posteromedial side. On the opposite sides (anteromedial and posterolateral), Sharpey's fibers are ori-ented longitudinally. Due to the resorption of primary bone tissue caused by the expansion of the medullary cavity, only nine LAGs are preserved in the cortical bone area (Fig. 3). Nevertheless, these nine LAGs represent 57% of the growth record of the individual. There is no EFS visible, even if the last two LAGs seem to be more closely spaced than the others. No secondary osteons can be observed in this sample.

4.1.4. ML 1190: B. walkeri (Theropoda; Spinosauroidea)

All microanatomical patterns of *Baryonyx walker* are very similar to those of *D. loureiroii* described before. The relatively small medullary region is completely filled with cancellous bone. Cortex thickness again varies greatly (5 mm to 12 mm) around the section. Again, the primary bone tissue is well-preserved and moderately vascularized like in *D. loureiroii* and *L. antunesi*. Most vascular canals are oriented radially (especially on the posteromedial side) or longitudinally. Sharpey's fibers are visible and oriented obliquely or inclined to the surface. The 21 LAGs that have been counted represent 81% of the growth record (Fig. 4). The last seven LAGs comprise the EFS. Even if these LAGs seem to be more widely spaced than previously described, there are nearly no observable primary bone tissue struc-tures in between each growth line. In contrast to *L. antunesi*, the number of secondary osteons is relatively high. About two thirds of the cortical bone is remodeled.

4.1.5. ML 426: Crocodylomorph (Crurotarsi)

The elongated medullary region is relatively small and completely filled with cancellous bone. The cortex shows the thickest area on both the posteromedial and anterolateral sides (cortex thickness varies from 1 mm to 4 mm). The well-preserved primary bone tissue consists of lamellar-zonal bone. It is extremely poorly vascularized. Only a few longitudinal canals are visible. Some Sharpey's fibers are visible, mainly on the posterolateral side. Here, their orientation is longitudinal. This orientation becomes more inclined towards the posteromedial and anterolateral sides. Posteromedially, 18 LAGs are preserved, represent-ing 83% of the growth record (Fig. 5). An EFS is not preserved in this individual. Half of the original bone tissue is remod-eled into Haversian bone.

5. Life history data evaluation

In the following section, life history parameters recorded during growth are summarized for every sam-pled taxon. By measuring the distances between the LAGs following the methods of Waskow and Sander (2014), a dia-gram has been created for each individual that shows the

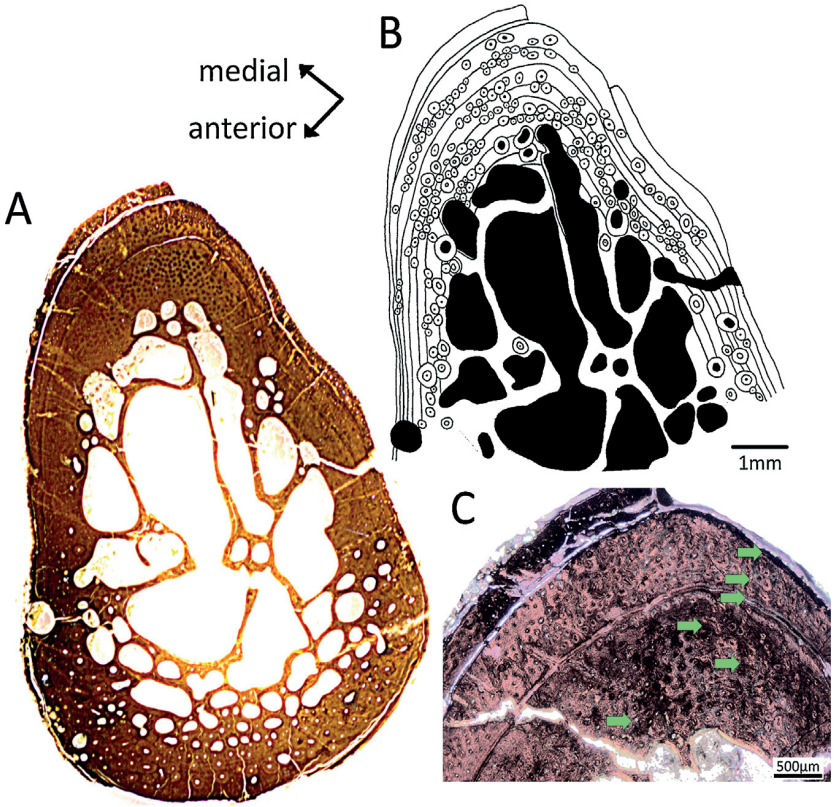

Fig. 3. Histological thin section of the posteromedial side of the dorsal rib of *Lourinhanosaurus antunesi* (ML 370), which preserves the most complete growth record. A. Macroscopic scan of the section. B. Drawing of the visible lines of arrested growth (LAGs) and the secondary osteons influencing the LAGs by destroying, or tracing them. C. Microscopic image of the section. All LAGs are marked with arrows.
Fig. 3. Section mince histologique du côté postéromédial de la côte dorsale de *Lourinhanosaurus antunesi* (ML 370), qui préserve l'enregistrement le plus complet de la croissance. A. Scan macroscopique de la section. B. Dessin des *lines of arrested growth* (LAGs) visibles et des ostéones secondaires influençant les LAGs en les détruisant ou en les suivant. C. Image de la section au microscope. Toutes les LAGs sont marquées par des flèches.

decrease in growth of the rib over somatic time (Figs. 6–10). Due to morphological changes during ontogeny (i.e. ribs are growing from proximal to distal; thus, the sampled prox-imal rib shaft of an adult represents the distal rib shaft when it was juvenile), these graphs are not accurate growth curves and cannot be used for mass estimations (Waskow and Sander, 2014), but they can be used to evaluate life history information. All general estimations requiring fur-ther explanations are discussed in the section following the discussion.

5.1. ML 433: M. longicollum (Stegosauria)

The primary bone tissue type and the low vascularіza-tion in this specimen suggest a relatively low deposition rate. The EFS indicates that the animal reached skeletal maturity before death. Using the method of retrocalcu-lation, we can assume a maximum number of three to four missing growth cycles. Together with the 22 counted annuli, this would raise the age of skeletal maturity to about 25 years. If the EFS is excluded, the animal would have reached full size after 21 to 22 years of growth. Because of the relative completeness of the growth record preserved in the ribs, this is the most complete estimation for skeletal maturity in stegosaurs to date. Previous studies on this group have obtained a less complete growth record, or were only able to erect a general histologic ontogenetic stage (HOS) erected by Klein and Sander (2008) (Hayashi et al., 2009; Redelstorff and Sander, 2009; Redelstorff et al., 2013). Here, a significant decrease in growth is observed after the 11th counted LAG (Fig. 6). This is interpreted as the point of sexual maturity, which would be reached at 14 to 15 years old, that is, long before the animal was skeletally mature.

5.2. ML 439: D. loureiroi (Ornithopoda)

The preserved EFS indicates that the specimen must have been a fully grown individual. A retrocalculation sug-gests that a maximum number of 1-2 growth cycles are missing. Therefore, the animal reached its skeletal maturity after 27 to 31 years of growth, depending on whether the EFS is included or not. Like in the stegosaur *M. longicollum* (see above), a decrease in the rib growth rate is observed (Fig. 7), but it is not as prominent. Between the 11th and 16th counted LAG, this growth rate decrease is observed, and therefore, sexual maturity can be estimated to be reached between the ages of 12 and 17.

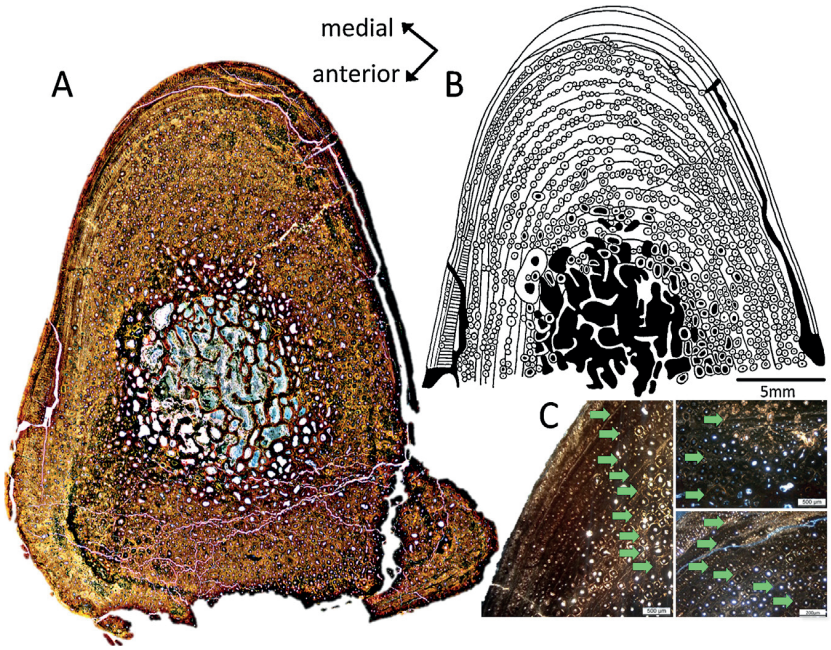

Fig. 4. Histological thin section of the posteromedial side of the dorsal rib of *Baryonyx walkeri* (ML 1190), which preserves the most complete growth record. A. Macroscopic scan of the section. B. Drawing of the visible lines of arrested growth (LAGs) and the secondary osteons influencing the LAGs by destroying, or tracing them. C. Microscopic images of the section. All LAGs are marked with arrows.
Fig. 4. Section mince histologique du côté postéromédial de la côte dorsale de *Baryonyx walkeri* (ML 1190), qui préserve l'enregistrement le plus complet de la croissance. A. Scan macroscopique de la section. B. Dessin des *lines of arrested growth* (LAGs) visibles et des ostéones secondaires influençant les LAGs en les détruisant ou en les suivant. C. Image de la section au microscope. Toutes les LAGs sont marquées par des flèches.

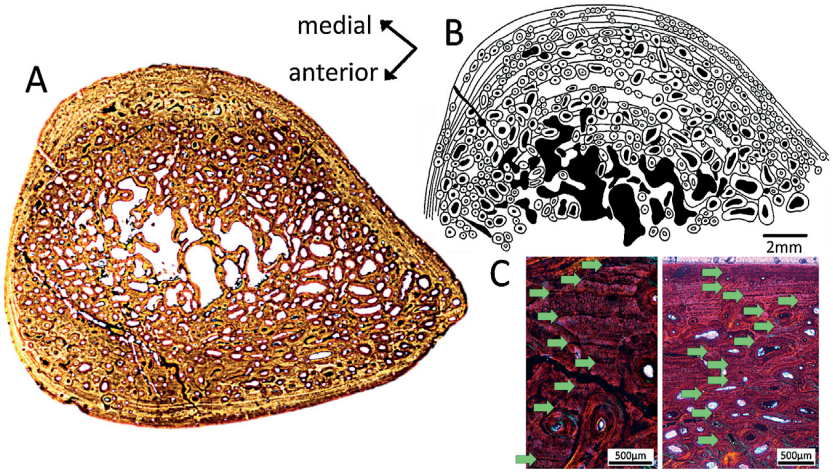

Fig. 5. Histological thin section of the posteromedial side of the dorsal rib of a crocodylomorph (ML 426), which preserves the most complete growth record. A. Macroscopic scan of the section. B. Drawing of the visible lines of arrested growth (LAGs) and the secondary osteons influencing the LAGs by destroying, or tracing them. C. Microscopic images of the section. All LAGs are marked with arrows.
Fig. 5. Section mince histologique du côté postéromédial de la côte dorsale d'un crocodylomorphe (ML 426), qui préserve l'enregistrement le plus complet de la croissance. A. Scan macroscopique de la section. B. Dessin des *lines of arrested growth* (LAGs) visibles et des ostéones secondaires influençant les LAGs en les détruisant ou en les suivant. C. Images au microscope de la section. Toutes les LAGs sont marquées par des flèches.

5.3. ML 370: L. antunesi (Theropoda; Avetheropoda)

Due to the expansion of the large medullary cavity of the specimen ML 370, only 57% of the growth record is pre-served. Depending on the distance between LAGs used for retrocalculation, there are approximately five to eight LAGs missing in the inner cortex. An EFS is missing. The age at death of this skeletally immature individual is suggested to be between 14 and 17 years. Unfortunately, the LAGs counted in this section show up in different parts of the cor-tex. Some LAGs are only visible posteriorly, while others are only visible anteromedially. In contrast to all other sections, not all counted LAGs are visible in the thickest part of the cortex (the posteromedial side of the section), which means

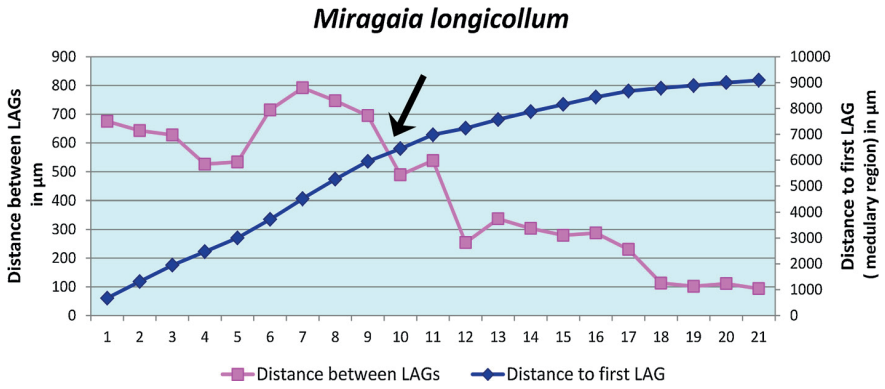

Fig. 6. Qualitative growth curve of *Miragaia longicollum* (ML 433) based on the lines of arrested growth (LAGs) counted in the dorsal rib, plotting cortical thickness increase with age (diamonds) and variation in cycle thickness with age (squares). The black arrow marks a decrease in growth, interpreted as the point of sexual maturity.
Fig. 6. Courbe de croissance qualitative de *Mirgaia longicollum* (ML 433) basée sur les *lines of arrested growth* (LAGs) dénombrées dans la côte dorsale, avec report de l'augmentation des épaisseurs corticales en fonction de l'âge (losanges) et de la variation d'épaisseur du cycle en fonction de l'âge (carrés). La flèche noire représente la diminution de croissance interprétée comme l'indication de la maturité sexuelle.

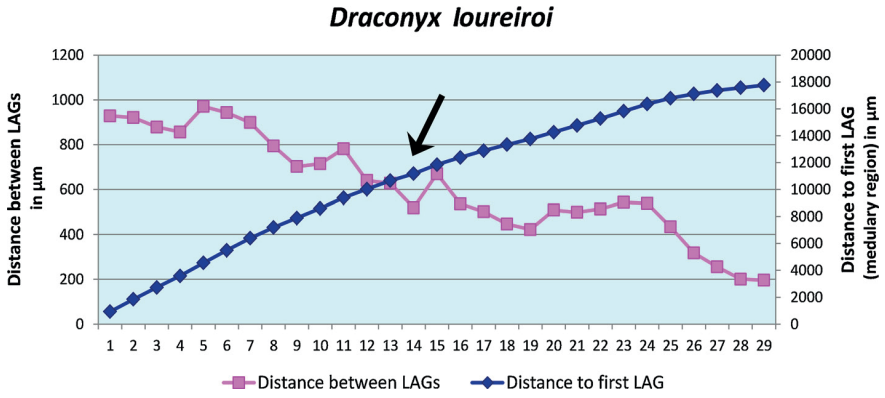

Fig. 7. Qualitative growth curve of *Draconyx loureiroi* (ML 439) based on the lines of arrested growth (LAGs) counted in the dorsal rib, plotting cortical thickness increase with age (diamonds) and variation in cycle thickness with age (squares). The black arrow marks a decrease in growth, interpreted as the point of sexual maturity.
Fig. 7. Courbe de croissance qualitative de *Dragonys loueiroi* (ML 439) basée sur les *lines of arrested growth* (LAGs) dénombrées dans la côte dorsale, avec report de l'augmentation de l'épaisseur corticale en fonction de l'âge (losanges) et de la variation d'épaisseur du cycle avec l'âge (carrés). La flèche noire représente la diminution de croissance interprétée comme l'indication de la maturité sexuelle.

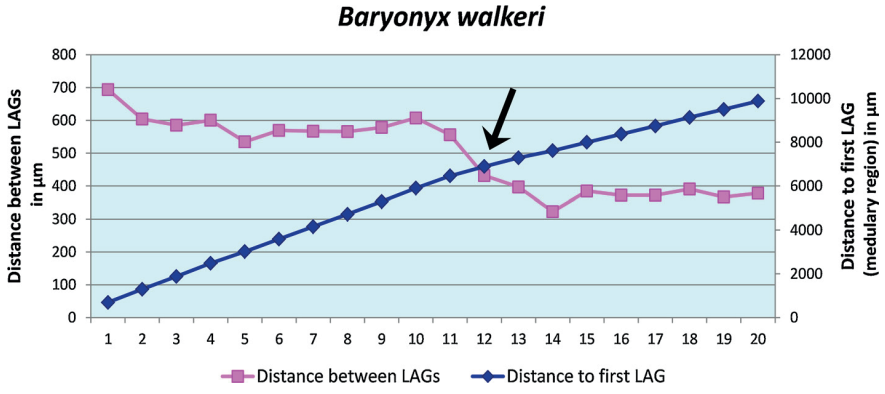

Fig. 8. Qualitative growth curve of *Baryonyx walkeri* (ML 1190) based on the lines of arrested growth (LAGs) counted in the dorsal rib, plotting cortical thickness increase with age (diamonds) and variation in cycle thickness with age (squares). The black arrow marks a decrease in growth, interpreted as the point of sexual maturity.
Fig. 8. Courbe de croissance qualitative de *Baryonyx walkeri* (ML 1190) basée sur les *lines of arrested growth* (LAGs) dénombrées dans la côte dorsale, avec report de l'augmentation de l'épaisseur corticale en fonction de l'âge (losanges) et variation d'épaisseur du cycle avec l'âge (carrés). La flèche noire représente la diminution de croissance, interprétée comme l'indication de la maturité sexuelle.

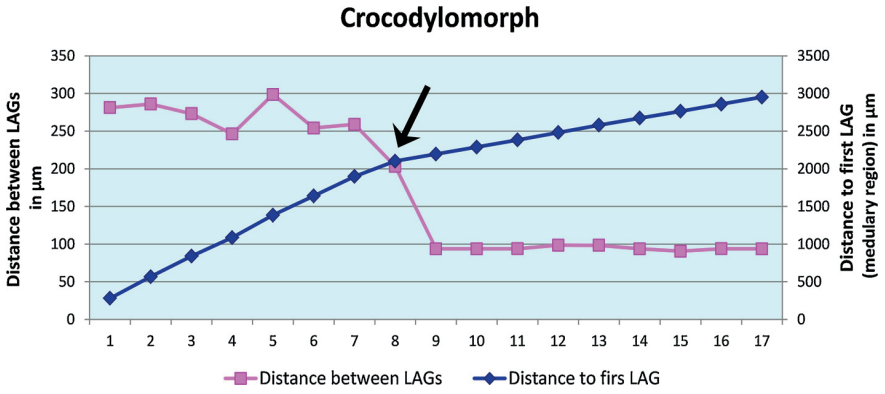

Fig. 9. Qualitative growth curve of a crocodylomorph (ML 426) based on the lines of arrested growth (LAGs) counted in the dorsal rib, plotting cortical thickness increase with age (diamonds) and variation in cycle thickness with age (squares). The black arrow marks a decrease in growth, interpreted as the point of sexual maturity.
Fig. 9. Courbe de croissance qualitative d'un crocodylomorphe (ML 426) basée sur les *lines of arrested growth* (LAGs) dénombrées dans la côte dorsale, avec report de l'augmentation de l'épaisseur corticale en fonction de l'âge (losanges) et variation d'épaisseur du cycle en fonction de l'âge (carrés). La flèche noire représente la diminution de croissance, interprétée comme l'indication de la maturité sexuelle.

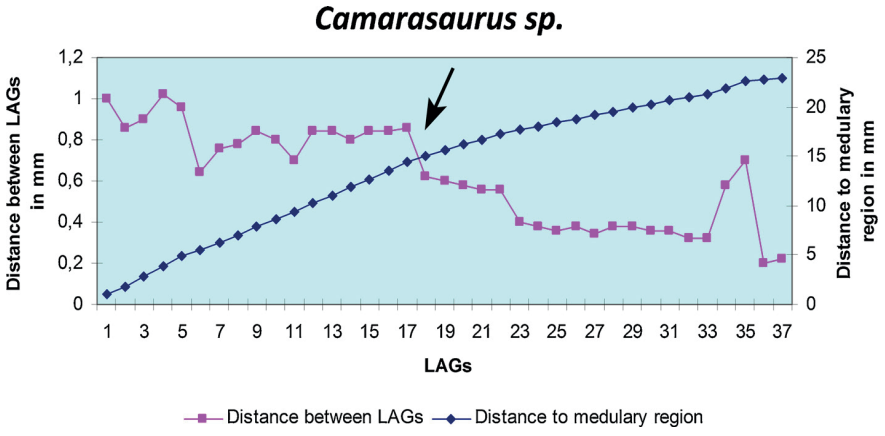

Fig. 10. Qualitative growth curve of *Camarasaurus* sp. (SMA 0002) based on the lines of arrested growth (LAGs) counted in the dorsal rib, plotting cortical thickness increase with age (diamonds) and variation in cycle thickness with age (squares). The black arrow marks a decrease in growth interpreted as the point of sexual maturity.
Fig. 10. Courbe de croissance qualitative de *Camara saurus* sp. (SMA 0002) basée sur les *lines of arrested growth* (LAGs) dénombrées dans la côte dorsale, avec report de l'augmentation de l'épaisseur corticale en fonction de l'âge (losanges) et variation d'épaisseur de cycle avec l'âge (carrés). La flèche noire représente la diminution de croissance interprétée comme l'indication de la maturité sexuelle.

that it was not possible to measure an accurate distance between the single LAGs to generate the growth graph. Therefore, no evidence for the point of sexual maturity is apparent.

5.4. ML 1190: B. walkeri (Theropoda; Spinosauroidea)

The specimen ML 1190 shows a clearly marked decrease in growth in the last 7 LAGs. Therefore, it is most likely that the individual was close to its maximum size. Including two to three missing LAGs computed by retrocalculation, it can be assumed that the animal died between the ages of 23 and 25 years, nearing its skeletal maturity. This is contrary to the anatomical evidence, that is, the neurocentral sutures are unfused, which suggests a rather earlier ontogenetic age. The occurrence of mature traits (based on the rib tis-sues) and subadult traits (partially unfused neurocentral sutures) could be interpreted as a possible paedomorphic trait for this taxon. Paedomorphosis has already been sug-gested in various aquatic or subaquatic tetrapods such as spinosaurids (Ibrahim et al., 2014), plesiosaurs (Araújo et al., 2015; Storrs, 1993) and temnospondyls (e.g., Steyer, 2000), and could be related to a swimming mode of loco-motion. A more detailed analysis including a comparison of bone compactness using software such as Bone Profiler (e.g., Houssaye et al., 2016; Laurin et al., 2011; Steyer et al., 2004) would be useful for a more detailed lifestyle interpre-tation, but is beyond the scope of this study. A significant decrease in the growth rate after the 11th or 12th countable LAG suggests that the point of sexual maturity was reached at an age of 13 to 15 years (Fig. 8).

5.5. ML 426: Crocodylomorph (Crurotarsi)

The bone tissue shows a slow deposition rate. This speci-men did not reach its skeletal maturity before its death. The

missing EFS indicates that the individual was indeed still growing. Considering one to two growth cycles are miss-ing based on retrocalculation, the animal died at an age of 19 to 20 years. After the 9th counted LAG, a decrease in growth is observed (Fig. 9) and interpreted as the point of sexual maturity. In recent crocodiles and alligators, a sig-nificant sexual dimorphism has been observed (Chabreck and Joanen, 1979; Platt, 1996; Platt et al., 2008; Wilkinson and Rhodes, 1997). While the smaller females reach sex-ual maturity after nine to ten years, the larger males need about 20 years to reach the reproduction age. The estimated age of death together with the observed decrease in growth suggests that the small individual ML 426 most likely was a female that reached sexual maturity after 10 to 11 years.

6. Longevity and age determination based on the count of growth cycles in dorsal ribs

It has been shown that animals like crocodiles can live many years after reaching their skeletal maturity (e.g., Klein et al., 2009; Woodward et al., 2011b). Therefore, the num-ber of counted LAGs for each studied individual cannot be equalized with longevity in all samples having an EFS. In contrast, if the animal did not reach its skeletal maturity before its death (which is documented by the absence of an EFS not attributed to preparation or pre-burial damage), its somatic age can be estimated by counting the LAGs and by taking into account the maximum number of LAGs missing due to remodeling or expansion of the medullary cavity. For all skeletally mature vertebrates, the estimated number of LAGs represents the time period they needed to reach full size (Castanet et al., 1993). The question whether the LAGs of the EFS should be included in the count of the LAGs is as controversial as the question of the annuality of the LAGs within the EFS (Horner et al., 1999). However, our diverse sample shows that the difference in the individual size is not significant if the EFS is excluded. By counting the LAGs excluding the EFS, the most reliable individual age before reaching skeletal maturity can be obtained.

7. General discussion

7.1. Viability of dorsal ribs for skeletochronology

While in the past ribs were studied very little, this study shows that dorsal ribs have a reliable growth record con-taining important information about life history traits. The reason to neglect dorsal ribs for histological studies until now may be because ribs have been historically claimed to be more strongly remodeled with secondary osteons than long bones (Enlow and Brown, 1958), given that even juvenile dinosaur individuals were initially claimed to show high amounts of Haversian bone (Nopcsa, 1933). Also, the strong histological variability within ribs has led to their exclusion from life history studies. In the compar-ative histology study by Horner et al. (2000), the ribs were found to be the worst skeletal elements for skeletochronol-ogy, showing the lowest LAGs count of all sampled bones. This can easily be explained by the fact that the authors sampled the wrong part of the rib. All of these reserva-tions have been addressed by the study of Waskow and Sander (2014), who demonstrated that ribs in general have the most complete growth record at the proximal end of the rib shaft where growth initiated, and that (in contrast to the observations in long bones) the younger distal parts are more strongly remodeled than the older proximal ends. This current study further supports these findings. Even if only the proximal end of the rib shaft was sampled for each taxon, the rib histology observed confirms the find-ings of Waskow and Sander (2014). Furthermore, this study extends their observations to more taxa and different onto-genetic stages. Irrespective of the taxon, the rib position within the ribcage, the locomotion type, or the ontogenetic stage of the individual, all sampled taxa show a comparable growth record at this position in the rib. None of the sam-ples were completely remodeled or lacked cyclicity. Even though this study validates ribs to be useful for histologi-cal studies, the major problem of varying bone apposition rates in ribs during ontogeny (also discussed in Waskow and Sander, 2014) still remains unresolved. Therefore, mass based growth curves based on the measurements between cycles of one individual is not reliable without calculating a correction formula. This work is currently in progress by Waskow and Griebeler (in prep.).

7.2. Comparability of the growth record preservation in ribs and long bones

Because ribs were not the focus of histological studies, one could argue that the growth record preserved in ribs might be different from that observed in well-studied long bones. However, Woodward et al. (2014) clearly showed that the growth record in different skeletal elements can be correlated using the example of an extant *A. mississippien-sis*. All samples (even if not including dorsal ribs) show the same number of LAGs with the two closely spaced LAGs at the same relative position. Another more recent research paper by Wiersma et al. (2016) supports a good correla-tion between the growth record of ribs and long bones. The study of Waskow and Sander (2014) additionally shows that it is possible to correlate the growth record between ribs of a single individual independent of the extremely variable outer morphology.

Another point of criticism might be that there are no studies on modern animals verifying that ribs are equally good indicators for overall skeletal maturity as long bones. Because they are not weight-bearing bones, the possibil-ity that their growth might stop earlier due to different restrictions compared to long bones cannot be excluded. However, even though ribs are not weight-bearing bones, to our knowledge, there is no significant allometric change during ontogeny between long bones and the rib cage in archosaurs. This justifies the assumption that these ele-ments have no significant difference in their respective age at skeletal maturity. Additionally, the definition of skeletal maturity is the point where the animal's growth consider-ably slows down or stops. Histologically, this is reached at the beginning of an EFS. At this point, the lines of arrested growth are spaced significantly closer to each other with-out primary osteons, vascularization, etc. in between. For these reasons, these LAGs observed in the rib sections can be identified as the EFS, as it has been done before, for

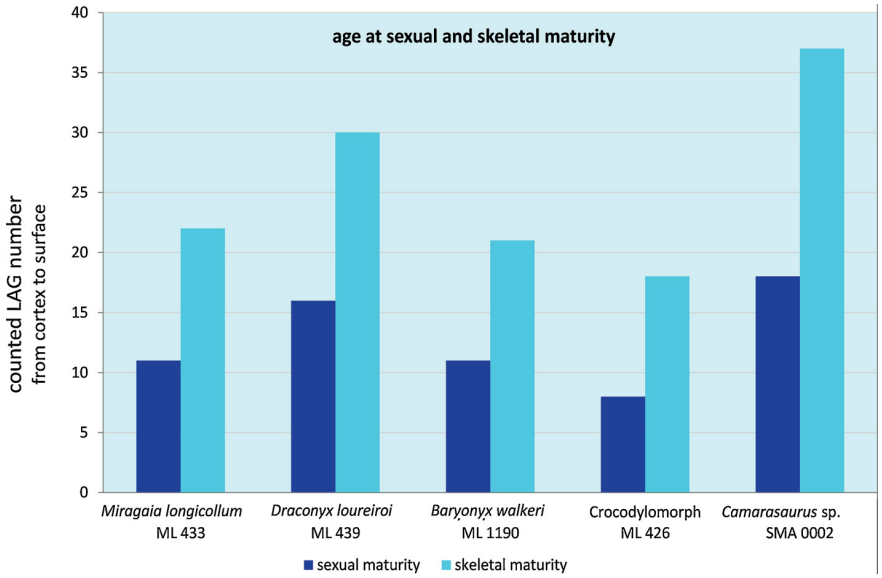

Fig. 11. Graph showing the number of counted growth cycles after which sexual and skeletal maturity were reached in the various taxa studied here.
Fig. 11. Graphique montrant le nombre de cycles de croissance décomptés, après lequel la maturité sexuelle et celle du squelette ont été atteintes dans les différents taxons étudiés ici.

example, by Erickson et al. (2004) and Waskow and Sander (2014). Due to the variation in distance between two given LAGs all around the cortex one could argue that the identifi-cation of an EFS is difficult. Nevertheless the EFS in ribs can be identified doubles and independent of the asymmetric deposition of bone material between the single LAGs, that is caused by morphological changes during ontogeny by look-ing at the area where the bone apposition rate is highest. If the distance between the LAGs here shows the conditions of an EFS its existence can be confirmed. Also, a comparison between the EFS in long bones and ribs of the same individ-ual has been done (at least for sauropods) in the study of Waskow and Sander (2014) with all elements showing an EFS with the same number of LAGs. This additionally rein-forces the assumption that skeletal maturity was reached simultaneously in ribs and long bones. However, the aim of this study is only to show the completeness of the growth record in different archosaur taxa to highlight the research potential of these undervalued skeletal elements. More comparative histological work on bone elements of the same individual, similar to the work of Werning and Nesbitt (2016), Wiersma et al. (2017), and Woodward et al. (2014), needs to be done for extinct archosaurs to underline the importance and comparability of ribs with limb bones.

7.3. Implications for age at sexual maturity

Sexual maturity is a major event in life history, and age estimation at sexual maturity in extinct animals is con-troversial (Chinsamy-Turan, 2005; Curry, 1999; Erickson, 2005; Erickson et al., 2007; Horner et al., 1999; Klein and Sander, 2007, 2008; Sander, 2000). For ecological reasons of survivorship, Dunham et al. (1989) theorized that large non-avian dinosaurs must have required 5 to 20 years to reach their sexual maturity. For sauropods, Sander (2000) argued that sexual maturity can be detected on the basis of a marked decrease in growth, well before the ani-mal was fully grown. This significant decrease in growth corresponds to the inflection point of the growth curve (Griebeler et al., 2013). At this point, it is thought that the animal starts to allocate more resources for its reproduc-tion, which are then no longer available for growth (Case, 1978a, 1978b; Sander, 2000). It is reasonable to assume that sexual maturity in non-avian theropods and ornithischians may occur well before full adult size (Erickson et al., 2007). This is coincident with the findings of Lee and Werning (2008), who reported on medullary bone (found only in breeding females) that occurs in specimens showing the same decrease in growth. This reduction of growth has been directly observed in large, recent reptiles such as tur-tles and crocodiles (Lance, 2003). In our sampled taxa from Portugal, as well as in the sauropod data point from the literature (Waskow and Sander, 2014), the inflection point mentioned above is reached at the halfway point of skeletal maturity (Figs. 10 and 11). We conclude that the decrease in growth rate marks the acquisition of sexual maturity in our study of a heterogeneous group of archosaur taxa including Ornithischia (stegosaurs and ornithopods) as well as Saurischia (theropods and sauropods) and crocody-lomorphs.

8. Conclusions

Dorsal rib histology of all studied taxa shows a nearly complete growth record and is valuable for estimating indi-vidual age at skeletal maturity and, in some cases, age at death. Even with respect to morphological changes dur-ing ontogeny, the point of sexual maturity can also be estimated. In all the studied taxa showing a significant decrease in growth rate, sexual maturity is reached around halfway of skeletal maturity. However, the non-isometric growth of ribs impedes a growth curve calculation for

mass estimation. Therefore, this method cannot replace long bone examination for assessments of other information like maximum annual growth rate or metabolic rate. However, ribs do not typically resorb bone on the posteromedial side, preserving the first LAGs, which most likely are destroyed in long bones due to the expansion of the medullary cavity. As showed by this analysis and previous studies (e.g., D'Emic et al., 2015; Erickson et al., 2004; Houssaye and Bardet, 2012; Waskow and Sander, 2014), ribs record growth better than long bones, and are generally easier to sample. The fact that they are also generally more common in museum collections reinforces their crucial role in bone histology and skeletochronology.

Acknowledgments

We would like to thank Olaf Dülfer (University of Bonn, Bonn, Germany) for technical support and help during the process of thin sectioning, and Aurore Canoville, Jessica Mitchell, Janka Brinkkötter, and Moritz Eisele for their assistance with translation into French, English proofreading, and picture editing during manuscript preparation. We thank Carla Tomás for the skilled preparation of specimens and laboratory management. Many Thanks to the reviewers Armand de Ricqlès, Jean-Sébastien Steyer and Holly Woodward for their helpful reviews, and the editors, with special thanks to Michel Laurin and Jorge Cubo, for their editorial efforts and quick responses. Finally, we would like to thank the DFG for funding. This is contribution 170 of the DFG Research Unit 533 "Biology of the Sauropod Dinosaurs: The Evolution of Gigantism".

References

Altunişik, A., Ergül Kalayci, T., Gül, Ç., Özdemir, N., Tosunoğlu, M., 2014. A skeletochronological study of the smooth new *Lissotriton vulgaris* (Amphibia: Urodela) from an island and a mainland population in Turkey. It. J. Zool. 81 (3), 381–388.

Amprino, R., 1947. La structure du tissu osseux envisagée comme expression de différences dans la vitesse de l'accroissement. Arch. Biol. 58, 315–330.

Araújo, R., Castanhinha, R., Martins, R.M., Mateus, O., Hendrickx, C., Beckmann, F., Schell, N., Alves, L.C., 2013. Filling the gaps of dinosaur eggshell phylogeny: Late Jurassic Theropod clutch with embryos from Portugal. Sci. Rep. 3, 1924.

Araújo, R., Polcyn, M.J., Lindgren, J., Jacobs, L.L., Schulp, A.S., Mateus, O., Olímpio Gonçalves, A., Morais, M.L., 2015. New aristonectine elasmosaurid plesiosaur specimens from the Early Maastrichtian of Angola and comments on paedomorphism in plesiosaurs. Neth. J. Geosci. 94, 93–108, http://dx.doi.org/10.1017/njg.2014.43.

Ayer, J., 2000. The Howe Ranch Dinosaurs. Sauriermuseum Aathal, Zurich (95 p.).

Benson, R.B.J., Carrano, M.T., Brusatte, S.L., 2010. A new clade of archaic large-bodied predatory dinosaurs (Theropoda: Allosauroidea) that survived to the Latest Mesozoic. Naturwissenschaften 97 (1), 71–78.

Brochu, C.A., 1996. Closure of neurocentral sutures during crocodilian ontogeny: implications for maturity assessment in fossil archosaurs. J. Vert. Paleontol. 16, 49–62.

de Buffrénil, V., de Ricqlès, A., Ray, C.E., Domning, D.P., 1990. Bone histology of the ribs of the archaeocetes (Mammalia: Cetacea). J. Vert. Paleontol. 10 (4), 455–466.

Caetano, M.H., 1990. Use and results of skeletochronology in some urodeles *Triturus marmoratus*, Latreille 1800 and *Triturus boscai*, Lataste 1879. Ann. Sci. Nat. Zool. 11, 197–199.

Canoville, A., Buffrénil, V., Laurin, M., 2016. Microanatomical diversity of amniote ribs: an exploratory quantitative study. Biol. J. Linn. Soc. 118 (4), 706–733, http://dx.doi.org/10.1111/bij.12779.

Carrano, M.T., Benson, R.B.J., Sampson, S.D., 2012. The phylogeny of Tetanurae (Dinosauria: Theropoda). J. Syst. Palaeontol. 10.2 (2012), 211–300.

Case, T.J., 1978a. On the evolution and adaptive significance of postnatal growth rates in the terrestrial vertebrates. Quart. Rev. Biol. 53, 243–282.

Case, T.J., 1978b. Speculations on the growth rate and reproduction of some dinosaurs. Paleobiology 4, 320–328.

Castanet, J., 1994. Age existimation and longevity in reptiles. Gerontology 40, 174–192.

Castanet, J., Smirina, E., 1990. Introduction to the skeletochronological method in amphibians and reptiles. Ann. Sci. Nat. Zool. (Paris) II, 191–197.

Castanet, J., Francillon-Vieillot, H., Meunier, F.J., de Ricqlès, A., 1993. Bone and individual aging. In: Hall, B.K. (Ed.), Bone. Volume 7: Bone Growth—B. CRC Press, Boca Raton, FL, USA, pp. 245–283.

Castanet, J., Grandin, A., Abourachid, A., de Ricqlès, A., 1996. Expression of growth dynamic in the structure of the periosteal bone in the mallard, *Anas platyrhynchos*. C. R. Acad. Sci. Paris, Ser. III 319, 301–308.

Castanet, J., Croci, S., Aujard, F., Perret, M., Cubo, J., de Margerie, E., 2004. Lines of arrested growth in bone and age estimation in a small primate: *Microcebus murinus*. J. Zool. 2631, 31–39.

Chabreck, R.H., Joanen, T., 1979. Growth rates of American alligators in Louisiana. Herpetologica, 51–57.

Charig, A.J., Milner, A.C., 1986. *Baryonyx*, a remarkable new theropod dinosaur. Nature 324 (6095), 359–361.

Chinsamy, A., Raath, M.A., 1992. Preparation of bone for histological study. Palaentol. Afr. 29, 39–44.

Chinsamy, A., Hillenius, W.J., 2004. Physiology of non-avian dinosaurs. In: Weishampel, D.B., Dodson, P., Osmólska, H. (Eds.), The Dinosauria, second ed. University of California Press, Berkeley, CA, USA, pp. 643–659.

Chinsamy-Turan, A., 2005. The Microstructure of Dinosaur Bone. Deciphering Biology with Fine-Scale Techniques. The John Hopkins University Press, Baltimore, MD, USA (195 p.).

Currey, J.D., 2002. Bones. Structure and Mechanics. Princeton University Press, Princeton, NJ, USA (436 p.).

Curry, K.A., 1999. Ontogenetic histology of *Apatosaurus* (Dinosauria:Sauropoda): new insights on growth rates and longevity. J. Vert Paleontol. 19, 654–665.

D'Emic, M.D., Smith, K.M., Ansley, Z.T., 2015. Unusual histology and morphology of the ribs of mosasaurs (Squamata). Palaeontology 58 (3), 511–520.

Dumont, M., Borbely, A., Kaysser-Pyzalla, A., Sander, P.M., 2014. Long bone cortices in a growth series of *Apatosaurus* sp. (Dinosauria: Diplodocidae): geometry, body mass, and crystallite orientation of giant animals. Biol. J. Linn. Soc. 112 (4), 782–798.

Dunham, A.E., Overall, K.L., Porter, W.P., Forster, C.A., 1989. Implications of ecological energetics and biophysical and developmental constraints for life history variation in dinosaurs. In: Farlow, J.O. (Ed.), Paleobiology of the Dinosaurs. Geological Society of America Special Paper 238, Boulder, CO, USA, pp. 1–19.

Enlow, D.H., Brown, S.O., 1956. A comparative histological study of fossil and recent bone tissue. Part. I. Texas J. Sci. 8, 405–443.

Enlow, D.H., Brown, S.O., 1957. A comparative histological study of fossil and recent bone tissues. Part II. Texas J. Sci. 9 (2), 186–204.

Enlow, D.H., Brown, S.O., 1958. A comparative histological study of fossil and recent bone tissues. Part III. Texas J. Sci. 10 (2), 187–230.

Erickson, G.M., Makovicky, P.J., Currie, M.A., Norell, S.A., Yerby, C.A., Brochu, C.A., 2004. Gigantism and comparative life history parameters of tyrannosaurid dinosaurs. Nature 430, 772–775.

Erickson, G.M., 2005. Assessing dinosaur growth patterns: a microscopic revolution. Trends Ecol. Evol. 20, 677–684.

Erickson, G.M., de Ricqlès, A., de Buffrénil, V., Molnar, R.E., Bayless, M.K., 2003. Vermiform bones and the evolution of gigantism in Megalania—how a reptilian fox became a lion. J. Vert. Paleontol. 23 (4), 966–970.

Erickson, G.M., Rogers, K.C., Varricchio, D.J., Norell, M.A., Xu, X., 2007. Growth patterns in brooding dinosaurs reveals the timing of sexual maturity in non-avian dinosaurs and genesis of the avian condition. Biol. Lett. 3, 558–561.

Fronimos, J.A., Wilson, J.A., 2017. Neurocentral suture complexity and stress distribution in the vertebral column of a sauropod dinosaur. Ameghiniana 54 (1), 36–49, http://dx.doi.org/10.5710/AMGH.05.09.2016.3009.

Garcia, B.J., 2011. Skeletochronology Of The American Alligator (Alligator Mississippiensis): Examination Of The Utility Of Elements For Histological Study (Master Thesis).

Griebeler, E.M., Klein, N., Sander, P.M., 2013. Aging, maturation and growth of Sauropodomorph dinosaurs as deduced from growth curves using long bone histological data: an assessment of methodological constraints and solutions. PLoS One 8 (6), e67012, http://dx.doi.org/10.1371/journal.pone.0067012.
Hall, B.K., 2005. Bone and Cartilage: Developmental and Evolutionary Skeletal Biology. Elsevier Academic Press, London (787 p.).
Hayashi, S., Carpenter, K., Watabe, M., Mateus, O., Barsbold, R., 2008. Defensive weapons of thyreophoran dinosaurs: histological comparisons and structural differences in spikes and clubs of ankylosaurs and stegosaurs. J. Vert. Paleontol. 28 (Supplement to 3), 89A–90A.
Hayashi, S., Carpenter, K., Suzuki, D., 2009. Different growth patterns between the skeleton and osteoderms of *Stegosaurus* (Ornithischia: Thyreophora). J. Vert. Paleontol. 29 (1), 123–131.
Hayashi, S., Houssaye, A., Nakajima, Y., Chiba, K., Ando, T., Sawamura, H., Inuzuka, N., Kaneko, N., Osaki, T., 2013. Bone inner structure suggests increasing aquatic adaptations in Desmostylia (Mammalia, Afrotheria). PLoS One 8 (4), e59146, http://dx.doi.org/10.1371/journal.pone.0059146.
Hendrickx, C., Mateus, O., 2014. Abelisauridae (Dinosauria: Theropoda) from the Late Jurassic of Portugal and dentition-based phylogeny as a contribution for the identification of isolated theropod teeth. Zootaxa 3759, 1–74.
Horner, J., de Ricqlès, A., Padian, K., 1999. Variation in dinosaur skeletochronology indicators: implications for age assessment and physiology. Paleobiology 25, 295–304.
Horner, J.R., de Ricqlès, A., Padian, K., 2000. Long bone histology of the hadrosaurid dinosaur *Maiasaura peeblesorum*: growth dynamics and physiology based on an ontogenetic series of skeletal elements. J. Vert. Paleontol. 20 (1), 115–129 (doi: 10.1671/0272-4634(2000)020[0115:LBHOTH]2.0.CO;2).
Houssaye, A., 2009. "Pachyostosis" in aquatic amniotes: a review. Integr. Zool. 4 (4), 325–340.
Houssaye, A., 2013. Bone histology of aquatic reptiles: what does it tell us about secondary adaptation to an aquatic life? Biol. J. Linn. Soc. 108 (1), 3–21.
Houssaye, A., Bardet, N., 2012. Rib and vertebral microanatomical characteristics of hydropelvic mosasauroids. Lethaia 45 (2), 200–209.
Houssaye, A., Waskow, K., Hayashi, S., Cornette, R., Lee, A.H., Hutchinson, J.R., 2016. Biomechanical evolution of solid bones in large animals: a microanatomical investigation. Biol. J. Linnean Soc. 117, 350–371, http://dx.doi.org/10.1111/bij.12660.
Hutton, J.M., 1986. Age determination of living Nile crocodiles from the cortical stratification of bone. Copeia 1986, 332–341.
Ibrahim, N., Sereno, P.C., Dal Sasso, C., Maganuco, S., Fabbri, M., Martill, D.M., Iurino, D.A., 2014. Semiaquatic adaptations in a giant predatory dinosaur. Science 345 (6204), 1613–1616.
Ikejiri, T., 2004. Anatomy of *Camarasaurus lentus* (Dinosauria: Sauropoda) from the Morrison Formation (Late Jurassic), Thermopolis, central Wyoming, with PALAEOELECTRONICA.ORG59 determination and interpretation of ontogenetic, sexual dimorphic, and individual variation in the genus. Fort Hays State University, Kansas, UMI (Unpublished Masters Thesis).
Ikejiri, T., 2012. Histology-based morphology of the neurocentral synchondrosis in *Alligator mississippiensis* (Archosauria, Crocodylia). Anat. Rec. (Hoboken) 295 (1), 18–31.
Irmis, R.B., 2007. Axial skeleton ontogeny in the Parasuchia (Archosauria: Pseudosuchia) and its implications for ontogenetic determination in archosaurs. J. Vert. Paleontol. 27, 350–361.
Klein, N., Sander, P.M., 2007. Bone histology and growth of the prosauropod dinosaur *Plateosaurus engelhardti* von Meyer, 1837 from the Norian bone beds of Trossingen (Germany) and Frick (Switzerland). Spec. Pap. Palaeontol. 77, 169–206.
Klein, N., Sander, P.M., 2008. Ontogenetic stages in the long bone histology of sauropod dinosaurs. Paleobiology 34, 247–263.
Klein, N., Scheyer, T., Tütken, T., 2009. Skeletochronology and isotopic analysis of an individual specimen of *Alligator mississippiensis* Daudin, 1802. Fossil Rec. 12, 121–131.
Klein, N., Christian, A., Sander, P.M., 2012. Histology shows that elongated neck ribs in sauropod dinosaurs are ossified tendons. Biol. Lett. 8 (6), 1032–1035.
Köhler, M., Marín-Moratalla, N., Jordana, X., Aanes, R., 2012. Seasonal bone growth and physiology in endotherms shed light on dinosaur physiology. Nature 487, 358–361.
Lamm, E.T., 2007. Paleohistology widens the field of view in paleontology. Microsc. Microanal. 13 (S02, Supplement), 50–51.
Lance, V.A., 2003. Alligator physiology and life history: the importance of temperature. Exp. Gerontol. 38, 801–805.
Laurin, M., Meunier, F.J., Germain, D., Lemoine, M., 2007. A microanatomical and histological study of the paired fin skeleton of the Devonian sarcopterygian *Eusthenopteron foordi*. J. Paleontol. 81 (1), 143–153.
Laurin, M., Canoville, A., Germain, D., 2011. Bone microanatomy and lifestyle: a descriptive approach. C. R. Palevol 10, 381–402.
Lee, A.H., Werning, S., 2008. Sexual maturity in growing dinosaurs does not fit reptilian growth models. Proc. Natl. Acad. Sci. USA 105, 582–587.
McIntosh, J.S., 2005. The genus *Barosaurus* Marsh (Sauropoda, Diplodocidae). In: Tidwell, V., Carpenter, K. (Eds.), Thunder-lizards: the Sauropodomorph Dinosaurs. Indiana University Press, Bloomington, IN, USA, pp. 38–777.
de Margerie, E., Robin, J.-P., Verrier, D., Cubo, J., Groscolas, R., Castanet, J., 2004. Assessing a relationship between bone microstructure and growth rate: a fluorescent labelling study in the king penguin chick (*Aptenodytes patagonicus*). J. Exp. Biol. 207, 869–879.
Mateus, O., 1998. *Lourinhanosaurus antunesi*, a new Upper Jurassic allosauroid (Dinosauria: Theropoda) from Lourinhã, Portugal. Mem. Acad. Cien. Lisboa 37, 111–124.
Mateus, O., Tschopp, E., 2013. *Cathetosaurus* as a valid sauropod genus and comparisons with *Camarasaurus*. J. Vert. Paleontol., Program and Abstracts 2013, 173.
Mateus, O., Antunes, M.T., 2001. *Draconyx loureiroi*, a new camptosauridae (Dinosauria, Ornithopoda) from the Late Jurassic of Lourinhã, Portugal. Ann. Paleontol. 87 (1), 61–73.
Mateus, O., Milàn, J., 2008. Ichnological evidence for giant ornithopod dinosaurs in the Upper Jurassic Lourinha Formation, Portugal. Oryctos 8, 47–52.
Mateus, O., Maidment, S.C., Christiansen, N.A., 2009. A new long-necked 'sauropod-mimic' stegosaur and the evolution of the plated dinosaurs. Proc. Roy. Soc. B: Biol. Sci. 276 (1663), 1815–1821.
Mateus, O., Dinis, J., Cunha, P.P., 2014. Upper Jurassic to Lowermost Cretaceous of the Lusitanian Basin, Portugal – landscapes where dinosaurs walked. Cien. Terra Special issue No. VIII, 1–37.
Mateus, O., Araújo, R., Natário, C., Castanhinha, R., 2011. A new specimen of the theropod dinosaur *Baryonyx* from the Early Cretaceous of Portugal and taxonomic validity of Suchosaurus. Zootaxa 2827, 54–68.
Milàn, J., Christiansen, P., Mateus, O., 2005. A three-dimensionally preserved sauropod manus impression from the Upper Jurassic of Portugal: Implications for sauropod manus shape and locomotor mechanics. Kaupia 14, 47–51.
Nopcsa, F.B., 1933. On the histology of the ribs in immature and half-grown trachodont dinosaurs. Proc. Zool. Soc. London 103 (1), 221–226, http://dx.doi.org/10.1111/j.1096-3642.1933.tb01588.x.
Owen, R., 1841. Report on British fossil reptiles. Rep. Br. Assoc. Adv. Sci. 11, 60–204.
Padian, K., Horner, J.R., 2004. Dinosaur physiology. In: Weishampel, D.B., Dodson, P., Osmólska, H. (Eds.), The Dinosauria, second ed. University of California Press, Berkeley, CA, USA, pp. 660–671.
Pancharatna, K., Kumbar, S.M., 2013. Bone growth marks in tropical wall lizard, *Hemidactylus brooki*. Russ. J. Herpetol. 12 (2), 107–110.
Platt, S.G., (Unpublished PhD Thesis) 1996. The Ecology and Status Morelet's Crocodile in Belize. Clemson University, SC, USA.
Platt, S.G., Rainwater, T.R., Thorbjarnarson, J.B., McMurry, S.T., 2008. Reproductive dynamics of a tropical freshwater crocodilian: Morelet's crocodile in northern Belize. J. Zool. 275 (2), 177–189.
Redelstorff, R., Sander, P.M., 2009. Long and girdle bone histology of *Stegosaurus*: implications for growth and life history. J. Vert. Paleontol. 29 (4), 1087–1099.
Redelstorff, R., Hübner, T.R., Chinsamy, A., Sander, P.M., 2013. Bone histology of the Stegosaur *Kentrosaurus aethiopicus* (Ornithischia: Thyreophora) from the Upper Jurassic of Tanzania. Anat. Rec. (Hoboken) 296 (6), 933–952.
de Ricqlès, A., 1975. Recherches paléohistologiques sur les os longs des tétrapodes VII. — Sur la classification, la signification fonctionnelle et l'histoire des tissus osseux des tétrapodes. Première partie, structures. Ann. Paleontol. 61, 51–129.
de Ricqlès, A., 1976. On bone histology of fossil and living reptiles with comments on its functional and evolutionary significance. In: Bellairs, A.D.A., Cox, C.B. (Eds.), Linnean Society Symposium Series 3. Linnean Society, London, pp. 123–150.
de Ricqlès, A., 1983. Cyclical growth in the long limb bones of a sauropod dinosaur. Acta Palaeontol. Pol. 28, 225–232.
de Ricqlès, A., Meunier, F.J., Castanet, L., Francillon-Vieillot, H., 1991. Comparative microstructure of bone. In: Hall, B.K. (Ed.), Bone. CRC Press, Boca Raton, FL, USA, pp. 1–78.
de Ricqlès, A., Mateus, O., Antunes, M.T., Taquet, P., 2001. Histomorphogenesis of embryos of Upper Jurassic theropods from Lourinhã (Portugal). C. R. Acad. Sci. Paris, Ser. IIa 332, 647–656.

de Ricqlès, A., Padian, K., Knoll, F., Horner, J.R., 2008. On the origin of high growth rates in archosaurs and their ancient relatives: complementary histological studies on Triassic archosauriforms and the problem of a "phylogenetic signal" in bone histology. Ann. Paleontol. 94 (2), 57–76.

Sander, P.M., 2000. Long bone histology of the Tendaguru sauropods: implications for growth and biology. Paleobiology 26, 466–488.

Sander, P.M., Klein, N., Stein, K., Wings, O., 2011. Sauropod bone histology and its implications for sauropod biology. In: Klein, N., Remes, K., Gee, C.T., Sander, P.M. (Eds.), Biology of the Sauropod Dinosaurs: Understanding the Life of Giants. Indiana University Press, Bloomington, IN, USA, pp. 276–302.

Sander, P.M., Klein, N., Buffetaut, E., Cuny, G., Suteethorn, V., Le Loeuff, J., 2004. Adaptive radiation in sauropod dinosaurs: bone histology indicates rapid evolution of giant body size through acceleration. Org. Divers. Evol. 4 (3), 165–173.

Smirina, E.M., Tsellarius, A.Y.T., 1996. Aging, longevity and growth of the desert monitor lizard (*Varanus griseus* Daud.). Russ. J. Herpetol. 3, 130–142.

Smirina, E.M., Ananjeva, N.B., 2007. Growth layers in bones and acrodont teeth of the agamid lizard *Laudakia stoliczkana* (Blanford, 1875) (Agamidae, Sauria). Amphibia–Reptilia 28 (2), 193–204.

Snover, M.L., Balazs, G.H., Murakawa, S.K., Hargrove, S.K., Rice, M.R., Seitz, W.A., 2013. Age and growth rates of Hawaiian hawksbill turtles (*Eretmochelys imbricata*) using skeletochronology. Mar. Biol. 160 (1), 37–46.

Stein, K., Sander, P.M., 2009. Histological core drilling: a less destructive method for studying bone histology. In: Brown, M.A., Kane, J.F., Parker, W.G. (Eds.), Methods in Fossil Preparation: Proc. First Annual Fossil Preparation and Collections Symposium, Petrified Forest National Park, 2008. University of Nebraska State Museum Holbrook, Arizona, pp. 69–80.

Steyer, J.S., 2000. Ontogeny and phylogeny in temnospondyls: a new method of analysis. Zool. J. Linn. Soc. 130, 449–467.

Steyer, J.S., Laurin, M., Castanet, J., de Ricqlès, A., 2004. First histological and skeletochronological data on temnospondyl growth: palaeoecological and palaeoclimatological implications. Palaeogeogr., Palaeoclimatol., Palaeoecol. 206 (3), 193–201.

Storrs, G.W., 1993. Function and phylogeny in sauropterygian (Diapsida) evolution. Am. J. Sci. 293A, 63–90.

Tschopp, E., Wings, O., Frauenfelder, T., Brinkmann, W., 2015. Articulated bone sets of manus and pedes of *Camarasaurus* (Sauropoda, Dinosauria). Palaeontol. Electron. 18 (2), 1–65.

Tschopp, E., Wings, O., Frauenfelder, T., Rothschild, B.M., 2016. Pathological phalanges in a camarasaurid sauropod dinosaur and implications on behaviour. Acta Palaeontol. Pol. 61 (1), 125–134.

Turvey, S.P., Green, O.R., Holdaway, R.N., 2005. Cortical growth marks reveal extended juvenile development in New Zealand moa. Nature 435, 940–943.

Upchurch, P., Barrett, P.M., Dodson, P., 2004. Sauropoda. In: Weishampel, D.B., Dodson, P., Osmólska, H. (Eds.), The Dinosauria, second ed. University of California Press, Berkeley and Los Angeles, California, pp. 259–322.

Waskow, K., Sander, P.M., 2014. Growth record and histological variation in the dorsal ribs of *Camarasaurus* sp. (Sauropoda). J. Vert. Paleontol. 34 (4), 852–869.

Wells, N.A., 1989. Making thin sections. In: Feldmann, R.M., Chapman, R.E., Hannibal, J.T. (Eds.), Paleotechniques. Department of Geological Sciences, University of Tennessee, Knoxville, Tennessee, pp. 120–129.

Werning, S., Nesbitt, S.J., 2016. Bone histology and growth in Stenaulorhynchus stockleyi (Archosauromorpha: Rhynchosauria) from the Middle Triassic of the Ruhuhu Basin of Tanzania. C. R. Palevol 15, 169–181.

Wiersma, K., Canoville, A., Siber, H.-J., Sander, P.M., 2017. Testing hypothesis of skeletal unity using bone histology: the case of the sauropod remains from the Howe-Stephens and Howe Scott quarries (Morrison Formation, Wyoming). Palaeontol. Electron. (submitted).

Wilkinson, P.M., Rhodes, W.E., 1997. Growth rates of American alligators in coastal South Carolina. J. Wildlife Manage. 61, 397–402.

Woodward, H.N., Rich, T.H., Chinsamy, A., Vickers-Rich, P., 2011a. Growth dynamics of Australia's polar dinosaurs. PLoS One 6 (8), e23339, http://dx.doi.org/10.1371/journal.pone.0023339.

Woodward, H.N., Horner, J.R., Farlow, J.O., 2011b. Osteohistological evidence for determinate growth in the American alligator. J. Herpetol. 45 (3), 339–342.

Woodward, H.N., Horner, J.R., Farlow, J.O., 2014. Quantification of intraskeletal histovariability in *Alligator mississippiensis* and implications for vertebrate osteohistology. Peer J 2, e422.

„Wenn manche Tiere auch sehr eigenartig aussehen, so sind sie doch das Beste, das die Natur für einen bestimmten Lebensraum hervorbringen konnte.“

“Although some animals look very strange, they are the best that nature could produce for a particular habitat.”

Wilhelm Schwöbel

CHAPTER 3

Biomechanical evolution of solid bones in large animals: A microanatomical investigation

published as:

Houssaye, A., **Waskow, K.**, Hayashi, S., Cornette, R., Lee, A. H., and Hutchinson, J. R. (2016). Biomechanical evolution of solid bones in large animals: A microanatomical investigation. Biological Journal of the Linnean Society 117(2), 350-371.

Author contribution:

Alexandra Houssaye designed the study, conducted the analyses and wrote major parts of the manuscript.

I participated in data acquisition (CT scans and histological thin-sections) of dorsal rib material of different taxa and their analyses and description in several parts of the manuscript.

Shoji Hayashi and Andrew H. Lee provided additional histological samples and CT scans of dorsal ribs, humeri, and femora of different taxa.

Raphaël Cornette and John R. Hutchinson gave significant input into both, analyses and manuscript preparation. In addition to that John R. Hutchinson also contributed to data aquisition.

All authors contributed to the final version of the manuscript, read it, and approved it.

The LINNEAN SOCIETY BIOLOGICAL Journal of the Linnean Society

Biomechanical evolution of solid bones in large animals: a microanatomical investigation

ALEXANDRA HOUSSAYE[1]*, KATJA WASKOW[2], SHOJI HAYASHI[3], RAPHAËL CORNETTE[4], ANDREW H. LEE[5] and JOHN R. HUTCHINSON[6]

[1] *Département Ecologie et Gestion de la Biodiversité, UMR 7179, CNRS/Muséum National d'Histoire Naturelle, 57 rue Cuvier, CP-55, Paris, 75000, France*
[2] *Steinmann Institut für Geologie, Mineralogie und Paläontologie, Universität Bonn, Nussallee 8, Bonn, 53115, Germany*
[3] *Osaka Museum of Natural History, Higashi-sumiyoshi-ku, Osaka, 546-0034, Japan*
[4] *UMR CNRS/MNHN/UPMC/EPHE 7205, Institut de Systématique, Evolution, Biodiversité (ISYEB), Muséum National d'Histoire Naturelle, 45 rue Buffon, Paris, 75005, France*
[5] *Department of Anatomy, Midwestern University, 19555 N 59th Avenue, Glendale, AZ, 85308, USA*
[6] *Department of Comparative Biomedical Sciences, Structure and Motion Laboratory, The Royal Veterinary College, Hawkshead Lane, Hatfield AL9 7TA, UK*

Received 16 June 2015; revised 20 July 2015; accepted for publication 20 July 2015

Graviportal taxa show an allometric increase of the cross-sectional area of supportive bones and are assumed to display microanatomical changes associated with an increase in bone mass. This evokes osteosclerosis (i.e. an increase in bone compactness observed in some aquatic amniotes). The present study investigates the changes in bones' microanatomical organization associated with graviportality and how comparable they are with aquatically acquired osteosclerosis aiming to better understand the adaptation of bone to the different associated functional requirements. Bones of graviportal taxa show microanatomical changes that are not solely attributable to allometry. They display a thicker cortex and a proportionally smaller medullary cavity, with a wider transition zone between these domains. This inner cancellous structure may enable to better enhance energy absorption and marrow support. Moreover, the cross-sectional geometric parameters indicate increased resistance to stresses engendered by bending and torsion, as well as compression. Adaptation to a graviportal posture should be taken into consideration when analyzing possibly amphibious taxa with a terrestrial-like morphology. This is particularly important for palaeoecological inferences about large extinct tetrapods that might have been amphibious and, more generally, for the study of early stages of adaptation to an aquatic life in amniotes. © 2015 The Linnean Society of London, *Biological Journal of the Linnean Society*, 2016, **117**, 350 371.

ADDITIONAL KEYWORDS: amphibious adaptation – bone mass increase – gigantism – graviportality – osteosclerosis – ribs – stylopod.

INTRODUCTION

Animals with extremely large body masses and with massive pillar-like limbs adapted to support their weight are said to be graviportal (Gray, 1968; Polly & Hall, 2007). Their typically columnar limbs help to resist bending and torsional loads generated by flexion and rotation of the limbs during locomotion (Hildebrand, 1982; Carrano, 1998; Ramsay *et al.*, 2001). The stylopodial elements (humerus, femur) are disproportionately larger at midshaft, and longer overall, relative to the more distal zeugopodials and autopodials. These larger bones are the result of allometric changes that help them to resist gravity (Gregory, 1912; Alexander & Pond, 1992; Polly & Hall, 2007) because body mass (and thus gravitational loading) tends to increase by a factor of eight when body length proportionately increases by a factor of two (Schmidt-Nielsen, 1984).

The allometric increase of the cross-sectional areas of supportive bones is a well-known characteristic of graviportal vertebrates (Ross, 1984). However, further

*Corresponding author. E-mail: houssaye@mnhn.fr

adaptations at the microstructural scale may occur; for example, Doube *et al.* (2011) showed how the trabecular mesh of larger species becomes more robust across a wide range of lineages of terrestrial tetrapods. Oxnard (1990, 1993) posited that there may be a general trend in some graviportal tetrapods to fill in the marrow cavities of the long bones not only to resist compressive loads from gravity, but also to help absorb more kinetic energy when the feet impact the ground (Warner *et al.*, 2013), avoiding 'crushing fractures', as well as providing scaffolding to support the heavy bone marrow itself.

Graviportal long bones are thus considered more massive than in other terrestrial taxa (Polly & Hall, 2007; Sander *et al.*, 2011) and should show an increase in bone mass at the microanatomical scale. Moreover, very massive ribs were observed in sauropods (Waskow & Sander, 2014), which suggests that, although not involved in support, ribs might also be more compact in graviportal taxa. The aforementioned increase in bone mass in graviportal land animals may be analogous to osteosclerosis observed in comparable bones of aquatic amniotes. These secondarily aquatic tetrapods are generally shallow water swimmers relying on a hydrostatic control of buoyancy and body trim (Houssaye, 2009). Thus, ironically, the increased compactness of bones appears to have convergently evolved several times in tetrapods: (1) to maintain appropriate buoyancy and balance in water (a low-gravity environment) compared to land and (2) to improve resistance to gravity, enabling the limits of body size in terrestrial tetrapods to be pushed to greater extremes (Hokkanen, 1986). Indeed, Wall (1983) already observed that some graviportal taxa appear to show an increase in bone deposition, so that they can be mistaken for aquatic taxa, especially bottom-walkers. In the case of mustelids, the functional signal of compact bones in wolverines appears to be associated more with their large body mass than with aquatic habits (Fish & Stein, 1991). Moreover, the (unexplained) high compactness in the ribs of rhinoceroses (De Buffrénil *et al.*, 2010) also illustrates this trend, in combination with varying aquatic habits in extant and extinct rhinocerotoids (Prothero, 1992; Clementz, Holroyd & Koch, 2008).

In the present study, we investigate microanatomical and cross-sectional specializations in the bones of graviportal and other related tetrapod taxa with both qualitative and quantitative methods, and in a phylogenetic context because microanatomical structures can show phylogenetic signals (Cubo *et al.*, 2005). We first seek to evaluate the bone microanatomical changes observable in graviportal taxa, aiming to determine how comparable this pattern is to the specialization observed in aquatic amniotes. We then synthesize our comparative results, aiming to better understand the adaptation of bone to the different functional requirements associated with graviportality in giant tetrapods, and notably focus on how the resulting patterns in graviportal taxa may sometimes be similar to changes associated with buoyancy and body trim control in secondarily aquatic tetrapods.

Institutional abbreviations

AMP, Ashoro Museum of Paleontology, Hokkaido, Japan; BYU, Brigham Young University, Utah, USA; CMC, Cincinnati Museum Center, Ohio, USA; FMNH, Field Museum of Natural History, Chicago, Illinois, USA; HMNS, Hayashibara Museum of Natural Sciences, Okayama, Japan; JRHRVC, uncatalogued research collection of John R. Hutchinson at The Royal Veterinary College, Hatfield, UK; MDE, Musée des Dinosaures, Espéraza, France; MNHN, Museum national d'Histoire naturelle, Paris, France; MPC, Mongolian Paleontological Center, Ulaanbaatar, Mongolia; NHMUK, Natural History Museum, London, UK; NMB, Naturhistorisches Museum Basel, Switzerland; NMW, National Museum of Vienna, Austria; NSM, National Science Museum, Tokyo, Japan; OMNH, Sam Noble Oklahoma Museum of Natural History, USA; OMNH*, Osaka Museum of Natural History, Osaka, Japan; PIMUZ, Paläontologisches Institut und Museum, Universität Zürich, Switzerland; RTMP, Royal Tyrrell Museum of Palaeontology, Drumheller, Canada; SMA, Saurier-museum Aathal, Switzerland; STIPB Steinmann-Institut, Universität Bonn, Germany; UCMP, University of California Museum of Paleontology, USA; UFGK, Ur- und Frühgeschichte Köln, Köln, Germany; UMNH, Utah Museum of Natural History, USA; UMZC, University Museum of Zoology, Cambridge, United Kingdom; YPM, Yale Peabody Museum of Natural History, New Haven, Connecticut, USA; ZFMK, Zoologisches Forschungsmuseum Alexander Koenig, Bonn, Germany; ZMZ, Zoologisches Museum der Universität Zürich, Switzerland.

MATERIAL AND METHODS

Material

The material analyzed consisted of humeri, femora and ribs of a large sample of fossil and extant mammals and reptiles. The taxa were chosen based on availability (including good preservation of the bone mid-diaphysis and feasibility of obtaining good quality digital imaging data, in addition to general accessibility to our research team) with the aim of including large forms and of representing diverse postures and locomotor habits (e.g. terrestrial versus aquatic) (Fig. 1 and Tables 1–3). Our final sample

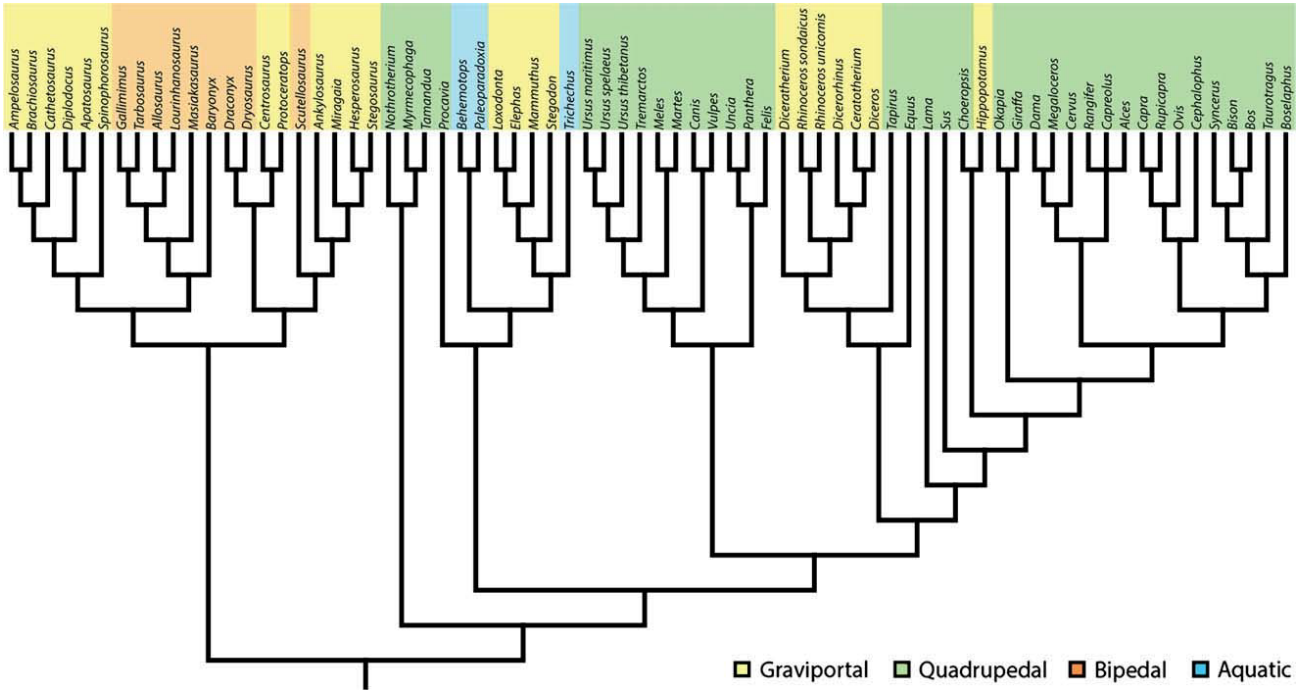

Figure 1. Consensus phylogenetic tree, based on (Sereno, 1999; Gilbert *et al.*, 2006; Remes, 2009; Todd, 2010; Meredith *et al.*, 2011; Steiner & Ryder, 2011; Thompson *et al.*, 2012; Bibi, 2013), with the four groups defined in the present study illustrated [yellow: graviportal; green: quadrupedal (graviportal taxa excluded); orange: bipedal; blue: aquatic].

consisted of 54 humeri of 49 species, 43 femora of 38 species (and two indeterminate theropod dinosaurs; although their phylogenetic position could not be determined precisely, meaning that they could not be incorporated in analyses taking the phylogeny into consideration, they could increase the sample of bipedal taxa), and 25 ribs of 25 species. Stylopodial bones were chosen because they are considered to have a stronger ecological signal than zeugopodial ones (Canoville & Laurin, 2010; Quemeneur, de Buffrénil & Laurin, 2013) and show a much larger cross-sectional area in graviportal taxa (Alexander & Pond, 1992; Carrano, 2001; Campione & Evans, 2012). Complete cross-sectional microanatomical data for stylopodial bones are rare for giant sauropods because of practical constraints imposed by the bone size. Conversely, whole transverse rib sections were available.

Bone section analysis

Some bones were sectioned using standard petrographic thin-section techniques (Houssaye *et al.*, 2008) (Tables 1–3). Others were scanned using high-resolution computed tomography (GEphoenix|X-ray v|tome|xs 240) at the Steinmann-Institut, University of Bonn (Germany) and at the AST-RX platform of the Muséum National d'Histoire naturelle (UMS 2700) or at the Equine Diagnostic Imaging Centre at the Royal Veterinary College (GE Lightspeed), with reconstructions performed using DATOX/RES, phoenix datos|x or MEDVIEW software (MedImage). Image segmentation and visualization were performed from the reconstructed image data using VGSTUDIOMAX, versions 2.0 and 2.2 (Volume Graphics Inc.). These techniques neither introduce artefacts, nor bias interpretation of the results for comparative analyses (Dumont *et al.*, 2013; Houssaye, Tafforeau & Herrel, 2014b). New virtual thin sections were made from the microtomographic data in cross-sectional planes of interest that serve as references for our comparative studies. For long bones, these were diaphyseal transverse sections showing the thickest cortex, and thus were assumed to cross the growth centre (Houssaye *et al.*, 2014a; Nakajima, Hirayama & Endo, 2014). Rib transverse sections were made at approximately the first third of the proximodistal distance along the perimeter of the rib, which has been shown to be the location of the growth centre in ribs (Waskow & Sander, 2014).

Scans of the classical (physical) thin sections, performed at high resolution (i.e. between 6400 and 12 800 dpi) using a V750-M Pro scanner (Epson) and virtual thin sections were transformed into single-bit digital images using PHOTOSHOP CS3 (Adobe Systems) (where black represents bone and white

Table 1. List of the humeri analyzed in the present study

	Taxon	Abbreviation	P	Coll Nb	ST
Diplodocidae	cf. *Apatosaurus* sp.	Ap	G	OMNH 01275	CS
Titanosauria	*Ampelosaurus atacis*	Am	G	MDE C3-270	CS
Tyrannosauridae	*Tarbosaurus* sp.	Tar	B	HMNS 94-10-78	CS
Allosauridae	*Allosaurus fragilis*	All	B	UMNH 3607	CS
Thyreophora	*Scutellosaurus lawleri*	Sc	B	UCMP 13068	CS
Thyreophora	*Scutellosaurus lawleri*	Sc	B	UCMP 130580	CS
Protoceratopsidae	*Protoceratops andrewsi*	Pr	G	MPC-D 100/530	CS (2)
Ceratopsidae	*Centrosaurus apertus*	Cen	G	RTMP 79.14.759	CS
Nothrotheriidae	*Nothrotherium escrivanse*	No	Q	PIMUZ A/V 477	Straehl *et al.* (2013)
Myrmecophagidae	*Tamandua tetradactyla*	Tam	Q	NMB 10420	Straehl *et al.* (2013)
Myrmecophagidae	*Myrmecophaga tridactyla*	My	Q	ZMZ 11119	Straehl *et al.*, (2013)
Desmostylia	*Paleoparadoxia* sp.	Pal	A	AMP AK0011	CS
Trichechidae	*Trichechus manatus*	Tr	A	NSM M 34694	VS
Stegodontidae	*Stegodon aurorae*	St	G	OMNH QV 264	CS
Elephantidae	*Elephas maximus*	El	G	JRHRVC uncatalogued	VS
Elephantidae	*Loxodonta africana*	Lo	G	NHMUK 1939.5.27.1	VS
Felidae	*Felis felis*	Fe	Q	UFGK uncatalogued	VS
Felidae	*Panthera leo*	Pa	Q	MNHN1912-398	Laurin *et al.*, (2011)
Felidae	*Uncia uncia*	Un	Q	NSM M 33876	VS
Canidae	*Canis lupus*	Ca	Q	Unnumbered	Laurin *et al.* (2011)
Canidae	*Vulpes vulpes*	Vu	Q	STIPB M12	VS
Mustelidae	*Meles meles*	Me	Q	STIPB M4002	VS
Ursidae	*Ursus thibetanus*	Ut	Q	ZFMK 81557	VS
Ursidae	*Ursus maritimus*	Um	Q	ZFMK 2005.356	VS
Equidae	*Equus burchelli*	Eq	Q	NMW 28810	Laurin *et al.* (2011)
Tapiridae	*Tapirus terrestris*	Tap	Q	ZFMK 462	VS
Rhinocerotidae	*Diceratherium* sp.	Dic	G	NHMUK PV M7752	VS
Rhinocerotidae	*Diceros bicornis*	Db	G	UMZC H.6481	VS
Rhinocerotidae	*Diceros bicornis*	Db	G	NHMUK M92402	VS
Rhinocerotidae	*Ceratotherium simum*	Ce	G	JRHRVC uncatalogued	VS
Rhinocerotidae	*Ceratotherium simum*	Ce	G	MNHN ZM MO 2005-297	VS
Rhinocerotidae	*Dicerorhinus sumatrensis*	Di	G	UMZC H.6392	VS
Rhinocerotidae	*Dicerorhinus sumatrensis*	Di	G	MNHN ZM AC 1903-300	VS
Rhinocerotidae	*Rhinoceros sondaicus*	Rs	G	MNHN ZM AC A7970	VS
Rhinocerotidae	*Rhinoceros unicornis*	Ru	G	MNHN ZM AC 1960-59	VS
Hippopotamidae	*Choeropsis liberiensis*	Ch	G	ZFMK 65 570	VS
Hippopotamidae	*Hippopotamus amphibius*	Hi	G	UMZC H.10714	VS
Suidae	*Sus scrofa*	Su	Q	STIPB M56	VS
Giraffidae	*Giraffa camelopardalis*	Gi	Q	JRHRVC uncatalogued	VS
Giraffidae	*Okapia johnstoni*	Ok	Q	UMZC H.20302	VS
Cervidae	*Rangifer tarandus*	Ra	Q	STIPB M47	VS
Cervidae	*Capreolus capreolus*	Cp	Q	MNHN CH 221	Laurin *et al.* (2011)
Cervidae	*Alces americanus*	Al	Q	UMZC H.17691	VS
Cervidae	*Cervus elaphus*	Cer	Q	MNHN Unnumbered	Laurin *et al.* (2011)
Cervidae	*Megaloceros* sp.	Meg	Q	UCMP 63524	VS
Cervidae	*Megaloceros giganteus*	Meg	Q	UMZC H.17535	VS
Cervidae	*Dama dama*	Da	Q	STIPB M1	VS
Bovidae	*Cephalophus sylvicultor*	Cep	Q	NHMUK ZD 1961.8.9.80-1	VS
Bovidae	*Ovis ammon*	Ov	Q	NMW 26499	Laurin *et al.*, (2011)

Table 1. *Continued*

	Taxon	Abbreviation	P	Coll Nb	ST
Bovidae	*Rupicapra*	Rup	Q	STIPB M1639	VS
Bovidae	*Capra falconeri*	Cap	Q	NMW 12081	Laurin *et al.* (2011)
Bovidae	*Boselaphus tragocamelus*	Bo	Q	NMW 25399	Laurin *et al.* (2011)
Bovidae	*Taurotragus oryx*	Tau	Q	NMW 61319	Laurin *et al.* (2011)
Bovidae	*Syncerus caffer*	Sy	Q	NHMUK ZD 1874.11.2.4	VS

P, posture; G, graviportal; B, bipedal; Q, quadrupedal; A, aquatic; ST, section type; CS, classical section; VS, virtual section.

cavities) and analyzed using BONE PROFILER (Girondot & Laurin, 2003). Some additional sections, either histological thin sections or virtual thin sections, originate from previous studies (Laurin, Canoville & Germain, 2011; Hayashi *et al.*, 2013; Straehl *et al.*, 2013). Quantitative parameters were measured directly on these images, not only via BONE PROFILER (Girondot & Laurin, 2003, but also via the IMAGEJ plugin BONEJ (Doube *et al.*, 2010), except for maximal diameter (MD) of bone, which was taken directly from the sections. These parameters included Girondot & Laurin, 2003 for details and illustrations of parameters 1–4, and definitions of the measurements 5–9 in BONEJ at http://bonej.org/slice: (1) C: compactness of the whole section (i.e. surface occupied by bone divided by whole sectional area); (2) P: the extent of the medullary cavity as measured by the relative distance from the centre of the section to the point where the most abrupt change in compactness occurs; (3) S: the width of the transitional zone between the compact cortex and the medullary cavity as measured by the reciprocal of the slope of the compactness profile at the inflection point; (4) MD: maximum bone diameter at the level of section (here considered as a proxy for body size); (5) CSA: cross-sectional area; (6) CSS: cross-sectional shape (= I_{max}/I_{min}; the ratio of maximal to minimal second moments of area); (7) J: polar second moment of area (= $I_{max} + I_{min}$); (8) Z_{pol}: polar section modulus (= J/R; representing the strength of a section against torsion; and (9) Per: perimeter of the section (data available in the Appendix, Table A1).

Statistical analyses

All data were $\log_{10}$ transformed prior to analyses (CSA and Z_{pol} were first raised to the power of 0.50 and 0.33, respectively, reducing them to dimensions more comparable to linear values) to meet the assumptions of normality and homoscedasticity required for parametric analyses. Considering that the parameter maximal diameter (MD) is usually considered as an estimate of overall body size (Girondot & Laurin, 2003) and actual body mass data were not available for our specimens, we performed linear regression analyses on the various microanatomical parameters aiming to evaluate the scaling of each parameter versus MD in the dataset. Because of the very strong impact of MD on the parameters Per, CSA and Z_{pol} ($r \sim 0.99$), the later were removed from the analyses to avoid multiplying the same signal. The amount of phylogenetic signal was investigated for the different parameters analyzed. Statistical tests were performed using an approximate 'consensus' phylogeny, derived from several previously published phylogenies (Sereno, 1999; Gilbert, Ropiquet & Hassanin, 2006; Remes, 2009; Todd, 2010; Meredith *et al.*, 2011; Steiner & Ryder, 2011; Thompson *et al.*, 2012; Bibi, 2013) (Fig. 1). We calculated the *K*-statistic *sensu* Blomberg, Garland & Ives (2003), which compares the observed phylogenetic signal in a trait with the signal under a Brownian motion model of trait evolution. Species means were used when several specimens were available for the same species. A *K*-value lower than 1 implies less similarity between relatives than expected under Brownian motion. We then performed linear regression analyses on all parameters aiming to evaluate the allometry in the data. Because a phylogenetic signal generally was detected, we calculated independent contrasts and forced regressions through the origin. We then conducted a principal components analysis (PCA) to explore the distribution of the different taxa in morphospace. Four groups were defined based on their typical limb posture and locomotor habit: (1) Graviportal (i.e. with robust bones with relatively long stylopodia; likely columnar posture); (2) Quadrupedal (graviportal taxa excluded); (3) Bipedal; and (4) Aquatic (with groups 1–3 being predominantly terrestrial taxa). To clearly visualize the trends between the different groups, a between-groups PCA was performed (on the mean values for each group). We also performed a pattern recognition analysis using the cross-validatory *K*-nearest neighbours algorithm

Table 2. List of the femora analyzed in the present study

	Taxon	Abbreviation	P	Coll Nb	ST
Ornithomimidae	*Gallimimus* sp.	Ga	B	HMNS 97-21-378	CS
Allosauridae	*Allosaurus fragilis*	All	B	UMNH 3694	CS
Noasauridae	*Masiakasaurus knopfleri*	Mas	B	FMNH PR 2123	CS
Theropoda	Theropod indet.	Th	B	HMNS 2006-04-356	CS
Theropoda	Theropod indet.	Th	B	HMNS 2006-04-151	CS
Dryosauridae	*Dryosaurus altus*	Dr	B	BYU 13312	CS
Thyreophora	*Scutellosaurus lawleri*	Sc	B	UCMP 170829	CS
Stegosauria	*Stegosaurus* sp.	St	G	YPM 4634	CS
Myrmecophagidae	*Myrmecophaga tridactyla*	My	Q	ZMZ 11119	Straehl *et al.* (2013)
Myrmecophagidae	*Tamandua tetradactyla*	Tam	Q	NMB 10420	Straehl *et al.* (2013)
Elephantidae	*Mammuthus* sp.	Ma	G	UCMP 35984	VS
Elephantidae	*Mammuthus* sp.	Ma	G	NHMUK uncat.	VS
Elephantidae	*Mammuthus* sp.	Ma	G	UCMP V3428	VS
Elephantidae	*Elephas maximus*	El	G	JRHRVC uncatalogued	VS
Elephantidae	*Loxodonta africana*	Lo	G	NHMUK 1939.5.27.1	VS
Felidae	*Felis felis*	Fe	Q	UFGK uncatalogued	VS
Canidae	*Vulpes vulpes*	Vu	Q	STIPB M12	VS
Mustelidae	*Meles meles*	Me	Q	STIPB M4002	VS
Ursidae	*Ursus thibetanus*	Ut	Q	ZFMK 81557	VS
Ursidae	*Ursus maritimus*	Um	Q	ZFMK 2005.356	VS
Tapiridae	*Tapirus terrestris*	Tap	Q	ZFMK 462	VS
Rhinocerotidae	*Ceratotherium simum*	Ce	G	MNHN ZM MO 2005-297	VS
Rhinocerotidae	*Ceratotherium simum*	Ce	G	JRHRVC uncatalogued	VS
Rhinocerotidae	*Ceratotherium simum*	Ce	G	UCMP 125000	VS
Rhinocerotidae	*Dicerorhinus sumatrensis*	Di	G	MNHN ZM AC 1903-329	VS
Rhinocerotidae	*Rhinoceros sondaicus*	Rs	G	MNHN ZM AC A7970	VS
Rhinocerotidae	*Rhinoceros unicornis*	Ru	G	MNHN ZM AC 1960-59	VS
Hippopotamidae	*Choeropsis liberiensis*	Ch	Q	ZFMK 65 570	VS
Hippopotamidae	*Hippopotamus amphibius*	Hi	G	UMZC H.10714	VS
Camelidae	*Lama guanicoe*	La	Q	STIPB M7388	VS
Suidae	*Sus scrofa*	Su	Q	STIPB M56	VS
Giraffidae	*Okapia johnstoni*	Ok	Q	UMZC H.20302	VS
Giraffidae	*Giraffa camelopardalis*	Gi	Q	JRHRVC uncatalogued	VS
Cervidae	*Dama dama*	Da	Q	STIPB M1	VS
Cervidae	*Megaloceros* sp.	Meg	Q	UCMP 63524	VS
Cervidae	*Rangifer tarandus*	Ra	Q	STIPB M47	VS
Cervidae	*Capreolus capreolus*	Cp		STIPB M1452	VS
Cervidae	*Alces americanus*	Al	Q	UMZC H.17691	VS
Bovidae	*Cephalophus sylvicultor*	Cep	Q	NHMUK ZD 1961.8.9.80-1	VS
Bovidae	*Rupicapra*	Rup	Q	STIPB M1639	VS
Bovidae	*Syncerus caffer*	Sy	Q	NHMUK ZD 1874.11.2.4	VS
Bovidae	*Bos taurus*	Bos	Q	NHMUK 47	VS
Bovidae	*Bison bonasus*	Bi	Q	ZFMK 2010-303	VS

P, posture; G, graviportal; B, bipedal; Q, quadrupedal; A, aquatic; ST, section type; CS, classical section; V, virtual section.

(k = 1) (Ripley, 1996; Venables & Ripley, 2002; Cornette *et al.*, 2015) to discriminate between our groups at the same time avoiding possible biases linked to more classical discriminant analyses [notably as a result of the small number of specimens for some groups (Evin *et al.*, 2013)]. Phylogenetic analyses of variance (ANOVAs) and analyses of covariance (ANCOVAs) (when a size effect was detected), as well as phylogenetic multivariate analyses of variance (MANOVAS), were performed as tests to determine whether the group number had a significant correlation with the various parameters analyzed.

All statistical analyses were performed using the statistical software R (R Core Team, 2012) except

Table 3. List of the ribs analyzed in the present study

	Taxon	Abbreviation	P	Coll Nb	ST
Spinosauridae	*Baryonyx* sp.	Ba	B	ML 1190.7c	CS
Sinraptoridae	*Lourinhanosaurus* sp.	Lou	B	ML 370C	CS
Sauropoda	*Spinophorosaurus nigerensis*	Sp	G	Ni 5.40-7ax	CS
Diplodocidae	*Apatosaurus* sp.	Ap	G	BYU 145	CS
Diplodocidae	*Diplodocus* sp.	Di	G	CMC 9932	CS
Camarasauridae	*Cathetosaurus* sp.	Ca	G	SMA 0002	CS
Brachiosauridae	*Brachiosaurus* sp.	Br	G	FMNH 25107	CS
Camptosauridae	*Draconyx* sp.	Dr	B	ML 439	CS
Ankylosauria	Ankylosaurid indet.	An	G	HMNS 94-10-7	CS
Stegosauria	*Miragaia longicollum*	Mi	G	ML 433A	CS
Stegosauria	*Hesperosaurus mjosi*	He	G	HMNS 014	CS
Procaviidae	*Procavia capensis*	Pr	Q	NSM M 3497	VS
Desmostylia	*Behemotops katsuiei*	Be	A	AMP 22	CS
Desmostylia	*Paleoparadoxia* sp.	Pa	A	AMP AK1001	CS
Elephantidae	*Mammuthus primigenius*	Ma	G	ZFMK 98 395	VS
Mustelidae	*Martes foina*	Mar	Q	STIPB M4004	VS
Ursidae	*Tremarctos ornatus*	Tr	Q	ZFMK 97.275	VS
Ursidae	*Ursus spelaeus*	Us	Q	STIPB M6280	VS
Ursidae	*Ursus maritimus*	Um	Q	ZFMK 2005.356	VS
Tapiridae	*Tapirus terrestris*	Ta	Q	ZFMK 462	VS
Tapiridae	*Rhinoceros sondaicus*	Rs	G	MNHN ZM AC A7970	VS
Tapiridae	*Rhinoceros unicornis*	Ru	G	MNHN ZM AC 1960-59	VS
Hippopotamidae	*Choeropsis liberiensis*	Ch	Q	ZFMK 65 570	VS
Bovidae	*Bison bonasus*	Bi	Q	ZFMK 2010-303	VS
Bovidae	*Capra aegagrus*	Cap	Q	UFGK Uncat.	VS

P, posture; G, graviportal; B, bipedal; Q, quadrupedal; A, aquatic; ST, section type; CS, classical section; VS, virtual section.

phylogenetic ANCOVAs that required the use of the PDSIMUL and PDANOVA routines implemented in PDAP (Garland *et al.*, 1993). In the PDSIMUL software, we used Brownian motion as our model for evolutionary change and ran 1000 unbounded simulations to create an empirical null distribution against which the *F*-values from the original data could be compared.

RESULTS

Qualitative analysis

Humerus

Most taxa exhibit humeri showing the standard tubular structure for a tetrapod long bone (i.e. a layer of compact cortex surrounding a large open medullary cavity) (Fig. 2A). The cortex is thicker in the bipedal dinosaurs (the theropods *Tarbosaurus* and *Allosaurus*, and the thyreophoran *Scutellosaurus*) and in the nilgai (*Boselaphus*) and the African buffalo (*Syncerus*; Van Schalkwyk, Skinner & Mitchell, 2004) than in most tubular bones. The pygmy hippopotamus *Choeropsis* [which is only poorly amphibious; Wall (1983)] also displays a tubular bone organization without a particularly thick cortex (Fig. 2B). The tapir shows a wide transition zone between the cortex and the open medullary cavity, and the polar bear shows a thin cortex associated with a wide transition zone (Hayashi *et al.*, 2013). The giant anteater (*Myrmecophaga*) displays a wide loose spongiosa with no open medullary cavity; and the southern tamandua shows a similar organization but with a rather small open medullary cavity. The peculiarity of the microanatomical features of these Xenarthra taxa was already raised in Straehl *et al.* (2013) and Amson *et al.* (2014), matching similar observations of other Xenarthra by Oxnard (1990, 1993).

Among the other taxa, several types of microanatomical organization are observable: (1) the absence of an open medullary cavity but a relatively wide medullary area occupied by a spongiosa (a higher number of, and also thinner, osseous trabeculae compared to the two xenarthrans above); in *Hippopotamus* (Fig. 2C), the sauropods *Ampelosaurus* (Fig. 2D) *Apatosaurus* and the ceratopsid *Centrosaurus* (Fig. 2E); (2), a similar pattern but associated with a much thicker cortex; in *Ceratotherium* (Fig. 2F), *Rhinoceros unicornis* (Fig. 2G),

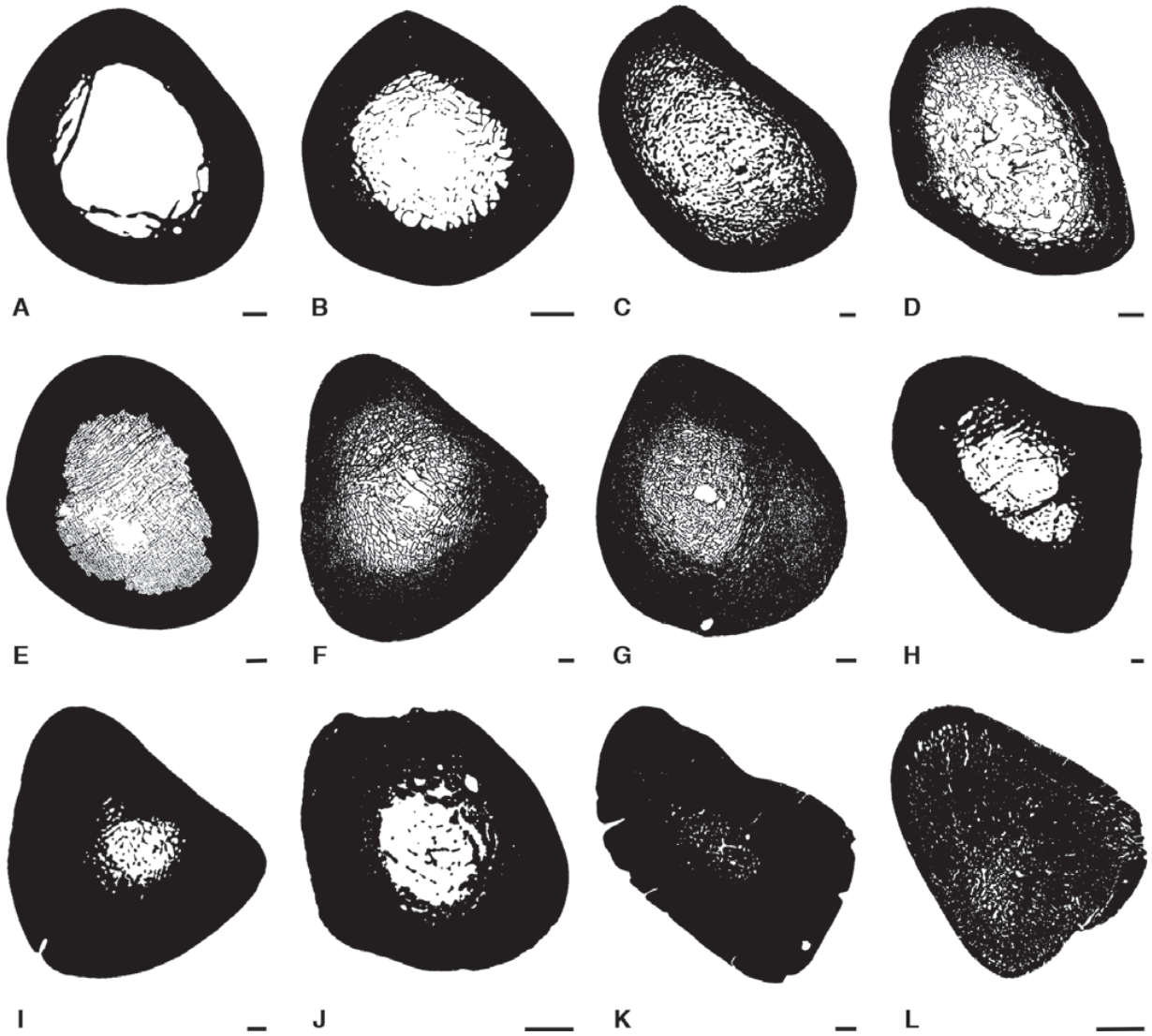

Figure 2. Schematic drawings illustrating the diversity of microanatomical patterns observed in humeri of: (A) *Giraffa camelopardalis*, (B) *Choeropsis liberiensis*, (C) *Hippopotamus amphibious*, (D) *Ampelosaurus atacis*, (E) *Centrosaurus apertus*, (F) *Ceratotherium simum*, (G) *Rhinoceros unicornis*, (H) *Elephas maximus*, (I) *Diceros bicornis*, (J) *Trichechus manatus*, (K) *Paleoparadoxia* sp., and (L) *Dugong dugon*. Scale bars = 5 mm.

and *Rhinoceros sondaicus*, the elephantiform proboscidean *Stegodon*, and with a reduced open medullary cavity, in one specimen of *Dicerorhinus*; (3) a thick cortex and a narrow medullary cavity with only a few thick trabeculae; in the extant proboscideans *Elephas* (Fig. 2H) and *Loxodonta*, the rhinocerotids *Dicerorhinus* (one specimen), *Diceros* (Fig. 2I) and *Diceratherium*, and the ceratopsian *Protoceratops*. The latter (third) kind of bone microanatomical organization was already observed in the sirenian *Trichechus* (Hayashi *et al.*, 2013) (Fig. 2J), whereas the two other relatively slow swimmers sampled, the desmostylian *Paleoparadoxia* (Fig. 2K) and the sirenian *Dugong* (Fig. 2L), display an extremely compact structure with no medullary cavity.

Femur

As observed for the humerus, most taxa display a tubular structure of the femoral midshaft (Fig. 3A). There are substantial variations in the thickness of the cortex, being relatively maximal in *Syncerus* (Fig. 3B) and *Ursus thibetanus*. In the giant anteater, the femur exhibits a pattern similar to its humerus, whereas in the tamandua, the femur shows a better defined and larger open medullary cavity than its humerus. Most other taxa have a cortex with a thickness similar to the maximum values observed in the taxa displaying a tubular structure, although with a spongiosa occupying the whole medullary area; for example, not only in *Ceratotherium* and *R. unicornis* (Fig. 3C), as well as *R. sondaicus* (Fig. 3D), but also in the tapir. Similar to the pattern observed in the humerus, other taxa show a thick cortex and a medullary area occupied by a medullary cavity with no or only a few thick trabeculae; in *Elephas* (Fig. 3E), *Loxodonta*, *Mammuthus* (Fig. 3F), *Hippopotamus* (Fig. 3G), and *Ceratotherium* (one specimen). *Diceratherium* shows a microanatomical organization that is almost tubular, except that a rather poorly extended transition zone between the cortex and the medullary cavity is

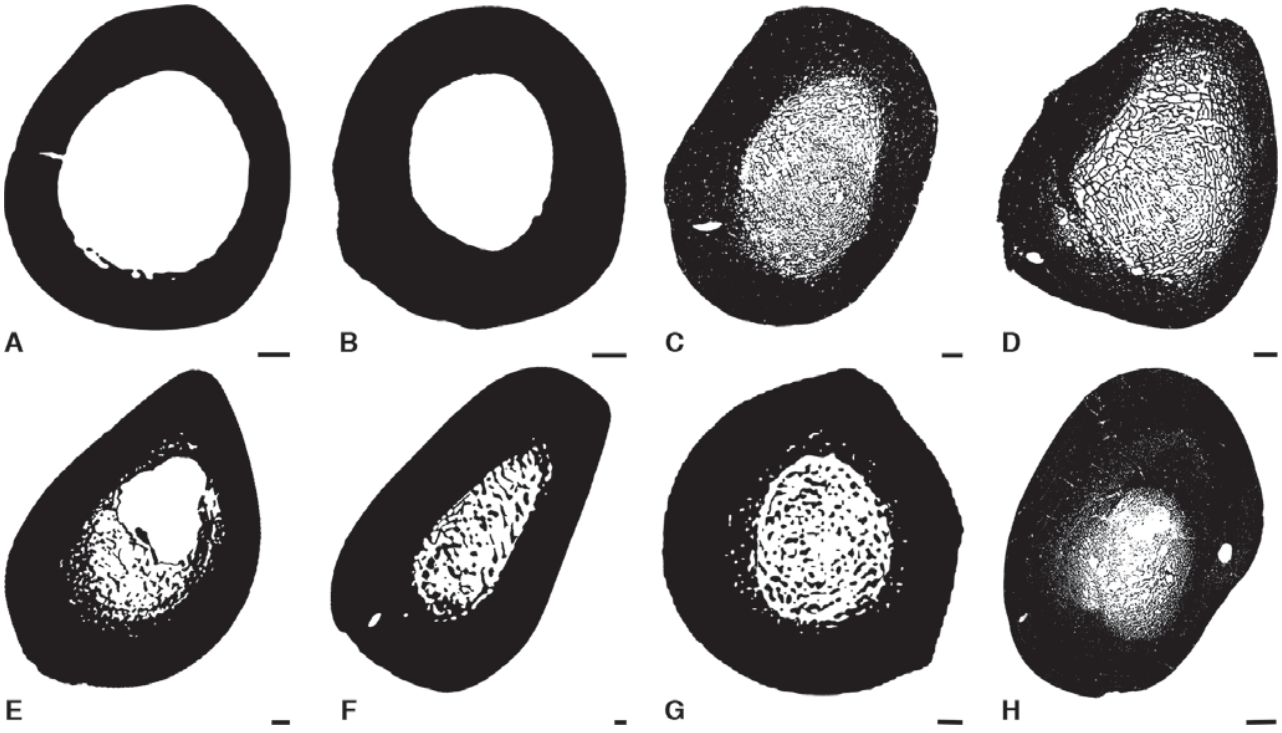

Figure 3. Schematic drawings illustrating the diversity of microanatomical patterns observed in femora of: (A) *Giraffa camelopardalis*; (B) *Syncerus caffer*, (C) *Rhinoceros unicornis*, (D) *Rhinoceros sondaicus*, (E) *Elephas maximus*, (F) *Mammuthus* sp., (G) *Hippopotamus amphibious*, and (H) *Stegosaurus* sp. Scale bars = 5 mm.

occupied by a spongiosa. *Stegosaurus* (Fig. 3H) shows a thick cortex and a reduced medullary area with a small medullary cavity and a lightly built spongiosa.

Rib

In amniotes, there is a wide diversity of rib internal morphologies, notably in the thickness of the cortex and the number of infilling trabeculae, as already highlighted in Hayashi *et al.* (2013). This not only reflects a natural diversity, but also relies on the difficulty of making homologous comparisons with ribs because bone microanatomical features are known to vary both along the rib and between ribs along the ribcage (Waskow & Sander, 2014; Houssaye *et al.*, 2015).

Typically, in our sample, the ribs of quadrupedal taxa show a clear medullary area with no or a few thick trabeculae (Fig. 4A, B). Weakly active swimmers are characterized by a clear increase in bone compactness, which is limited in most desmostylians (Fig. 4C) but extremely high in all sirenians (*Trichechus*, *Dugong*, and *Halitherium*; A. Houssaye, pers. observ.) with an almost complete bone filling. Most dinosaurian taxa sampled, especially graviportal thyreophorans [stegosaurs (Fig. 4D) and ankylosaurs] and sauropods (Fig. 4E, F), but also bipedal taxa (Fig. 4G), display ribs with a thick cortex and no open medullary cavity but a rather dense spongiosa with reduced intertrabecular spaces in most taxa (Fig. 4D, E). However, some dinosaur taxa present a thick cortex but a rather loose inner spongiosa (e.g. the sauropod *Spinophorosaurus* and the moderately large theropod *Lourhinhanosaurus*) (Fig. 4F). The mammoth and *Rhinoceros* (*R. unicornis* and *R. sondaicus*) show an organization grossly similar to that of other large quadrupedal mammals, except that the spongiosa is made of numerous thin trabeculae (Fig. 4H, I).

Quantitative analysis

The *K*-statistics calculated are all much lower than 1 for all three bones analyzed ($0.34 < K < 0.68$ for the humerus, $0.37 < K < 0.55$ for the femur, and $0.39 < K < 0.67$ for the rib) (see Appendix, Table A2). However, randomization tests are unable to reject the possibility of a significant phylogenetic signal in the data, except for the compactness (C), width of the transition zone (S), and aspect ratio (CSS) for the rib. This justifies the need to account for the effects of phylogenetic pseudoreplication (Garland, 2001).

Linear regressions on the independent contrast data show that only the polar moment of area (J) is affected by size (MD) for the three bones, although not strongly. The other parameters show either no or a rather weak impact of size, depending on the bones concerned (see Appendix, Table A2).

Analyses of variance show that only C and the extent of the medulla (P) for the humerus vary significantly (Table 4) depending on the group number (1–4). Analyses of covariance all show a significant signal when phylogeny is not taken into consideration (except J for the rib), although this significance is lost when phylogeny is incorporated (Table 4). Similarly, the multivariate analysis of variance is

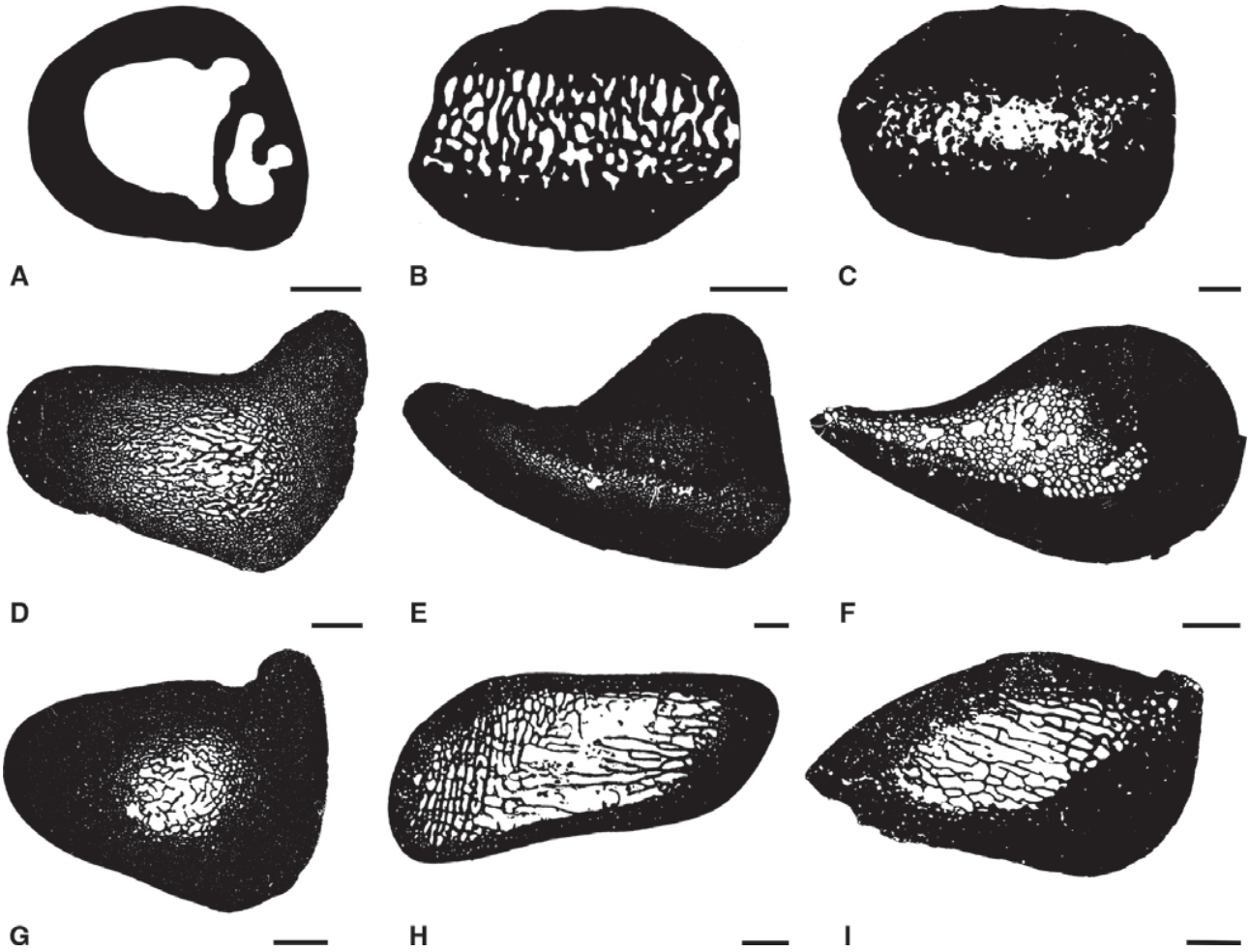

Figure 4. Schematic drawings illustrating the diversity of microanatomical patterns observed in ribs of: (A) *Martes foina*, (B) *Ursus spelaeus*, (C) *Paleoparadoxia* sp., (D) *Miragaia longicollum*, (E) *Cathetosaurus* sp., (F) *Lourinhanosaurus* sp., (G) *Baryonyx* sp., (H) *Mammuthus primigenius*, and (I) *Rhinoceros unicornis*. Scale bars = 5 mm (except for *Martes*: 0.5 mm).

significant for the humeri ($F = 3.33$, $P = 0.013$) but loses significance when phylogeny is taken into consideration ($F = 4.65$, $P = 0.475$). However, the results for the femora and the ribs are not significant when accounting for phylogeny ($F = 4.08$, $P = 0.887$ for the femora; $F = 3.51$, $P = 0.456$ for the ribs) or not ($F = 2.29$, $P = 0.07$ for the femora; $F = 2.44$, $P = 0.07$ for the ribs). Bone compactness is greater in aquatic and graviportal (especially in the femur) taxa, which also show a wider corticomedullary transition (high S; except in the ribs of the graviportal taxa). Aquatic taxa have a more reduced medullary cavity associated with a relatively thicker cortex (lower P). This reduced medullary cavity and thicker cortex are also observed, although to a much lesser extent, in graviportal taxa but only in long bones (especially in the femur) and not in the ribs. The CSS index demonstrates different signals depending on the bone sampled and thus does not appear to be consistent with the locomotor groups. Aquatic, graviportal, and bipedal taxa have higher values of J in the humerus (but lower values in the ribs) compared to quadrupedal taxa. Bipedal taxa display compact ribs with a wide corticomedullary transition and a thicker cortex.

Our PCA of bone microanatomy in the humerus shows that the two main axes explain 75.1% of the variance (53.6% and 21.5%, respectively). This analysis demonstrates which variables covaried: P correlates inversely with C (compactness) and J (polar second moment of area). The smaller medullary cavity in aquatic and graviportal tetrapods is thus consistently associated with a relatively thicker cortex and a higher compactness (Fig. 5A). It is particularly interesting to note that graviportal taxa group together (and with aquatic taxa), being essentially discriminated by the first axis, whereas they are randomly distributed based on PC2 and PC3. Our between-groups PCAs generally show, for all bones, that the first axis mainly discriminates based on bone microanatomical features (C, S, P), and the second axis essentially based on bone shape parameters (CSS and J) (Figs 5B, 6B, 7B). The between-groups PCA for the humerus distinguishes the four groups, with aquatic taxa displaying the strongest compactness, thicker cortex, smaller medullary cavity, and more rounded geometry (CSS closer to 1; as opposed to quadrupedal taxa with CSS diverging from 1). Additionally, graviportal taxa, as opposed to bipedal and aquatic ones, display (for obvious reasons of

Table 4. *F*- and *P*-values obtained for the various analyses of (co)variance

	Phylogenetic ANOVA		ANCOVA		Phylogenetic ANCOVA	
	F	*P*	*F*	*P*	*F*	*P*
Humerus						
C	**11.96**	**0.032**				
S			**5.49**	**0.024**	8.68	0.235
P	**14.16**	**0.015**				
CSS	1.14	0.794				
J			**5.28**	**0.026**	8.58	0.261
Femur						
C			**7.96**	**0.008**	8.84	0.105
S	4.86	0.412				
P			**7.99**	**0.008**	8.78	0.089
CSS			**7.63**	**0.009**	9.00	0.103
J			**8.54**	**0.006**	9.05	0.081
Rib						
C	2.35	0.546				
S	2.44	0.529				
P	7.17	0.111				
CSS	0.77	0.852				
J			4.18	0.053	8.56	0.198

Statistical significance is indicated in bold ($P < 0.05$). ANOVA, analysis of variance; ANCOVA, analysis of covariance.

gravitational support) a higher polar second moment of area (J) and a larger transition zone between the cortex and medullary cavity (Fig. 5B). The two main axes explain 94.9% of the variance (76.1% and 18.8%, respectively). Our K-NN classifications indicate that 74.5% of specimens were well-classified and thus show a clear signal.

Similar to the humerus, our PCA analysis for the femur shows that the two main axes explain 79.0% of the variance in our microanatomical data (59.4% and 19.6%, respectively). Similar covariations are observable between C, and P. However, CSS in this case varies almost antagonistically to P. Again, graviportal taxa group together, being discriminated based essentially on the first axis (Fig. 6A). The between-groups PCA for the femur shows that graviportal taxa are distinct from the other quadrupedal and the bipedal taxa in showing a much higher compactness, proportionally thicker cortex, and higher polar second moment of area (Fig. 6B). Bipedal taxa differ from quadrupedal ones in showing a higher polar second moment of area (J) and less rounded cross-sections (CSS further from 1). The two main axes explain 100% of the variance, 95.0% and 5.0%, respectively, showing that the variation conclusively distinguishes graviportal taxa from the others. Congruent with our results for the humerus, we find from the K-NN classifications that we reliably assigned 69.8% of our specimens to groups a priori.

The PCA analysis for the ribs shows that the two main axes explain 63.0% of the variance (42.6% and 20.4% respectively). In our rib sample, C still varies antagonistically to P, and in a direction almost orthogonal to those of the polar second of moment area and cross-sectional shape (Fig. 7A). Graviportal taxa continue to group together. However, it is interesting to note that the bipedal taxa are within the distribution area of the graviportal ones and that the two aquatic taxa are much closer to the graviportal forms than to the other terrestrial ones. For ribs, the first axis does not clearly distinguish graviportal taxa because aquatic and bipedal ones display a much higher compactness, whereas graviportal taxa display microanatomical features closer to those of the other terrestrial forms. The second axis discriminates graviportal taxa from the other ones, notably based on the more rounded shape of the cross-sections (in contrast to the increased eccentricity evident for the humerus and femur; Carrano, 2001) and higher polar second moment of area. These two main axes explain 96.9% of the variance (61.7% and 35.2%, respectively). For ribs, we obtained a relatively poor result for the K-NN classifications: 46.2% of specimens as well-classified.

Comparisons between the classical and between-groups PCAs show that the same parameters drive the distributions of data for both the mean representatives of the groups and for all individuals.

DISCUSSION

We found that only certain key microanatomical and cross-sectional traits distinguish how humeri, femora, and ribs of tetrapods change their shape and internal bone structure with increasing graviportal or aquatic adaptations. In particular, the ribs show stronger changes of compactness with aquatic habits than with graviportality, which is in accordance with a role in buoyancy and body trim control in shallow waters but no weight-bearing role on land. Otherwise, as we proposed in the Introduction, there are remarkable qualitatively and quantitatively similar patterns in how bones change their internal geometry with lifestyles as different as giant, graviportal land animals versus secondarily aquatic tetrapods, especially increasing bone compactness and reducing medullary cavities along both evolutionary trajectories. As for bipedal taxa, they tend to show a strong change in femoral cross-sectional area and an increased internal robustness in their ribs.

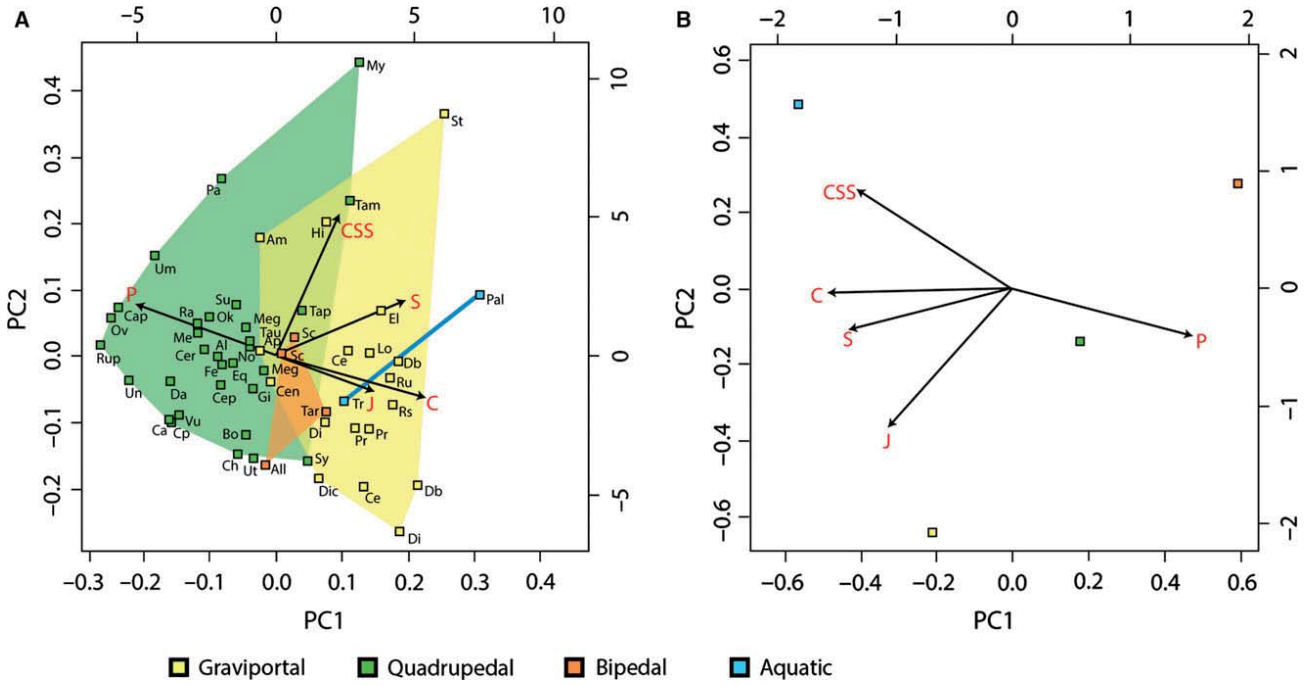

Figure 5. Microanatomical clusters obtained by principal component analyses (PCA) conducted on the humeri of our sample. Graphs showing the distribution of the variance in all taxa examined according to the PCA1 and PCA2 axes. A, classical PCA. B, between-groups PCA. Abbreviations for taxa as in Table 1.

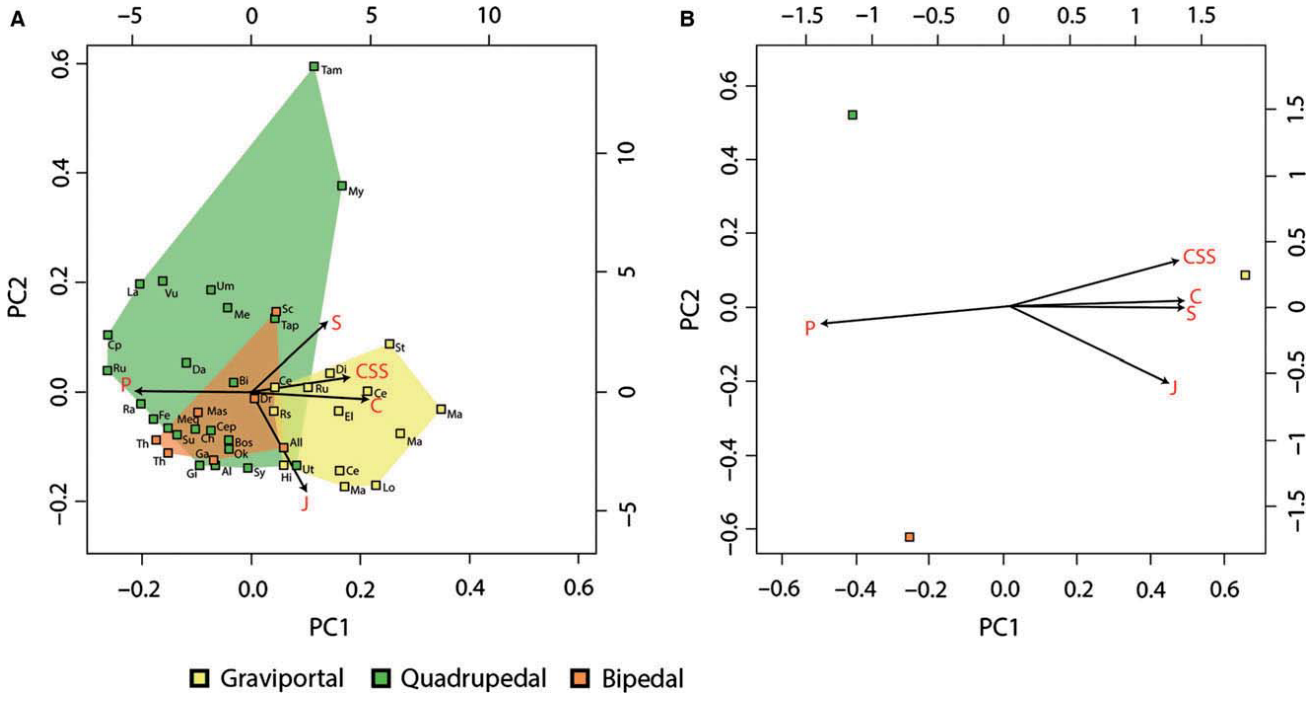

Figure 6. Microanatomical clusters obtained by principal component analyses (PCA) conducted on the femora of our sample. Graphs showing the distribution of the variance in all taxa examined according to the PCA1 and PCA2 axes. A, classical PCA. B, between-groups PCA. Abbreviations for taxa as in Table 2.

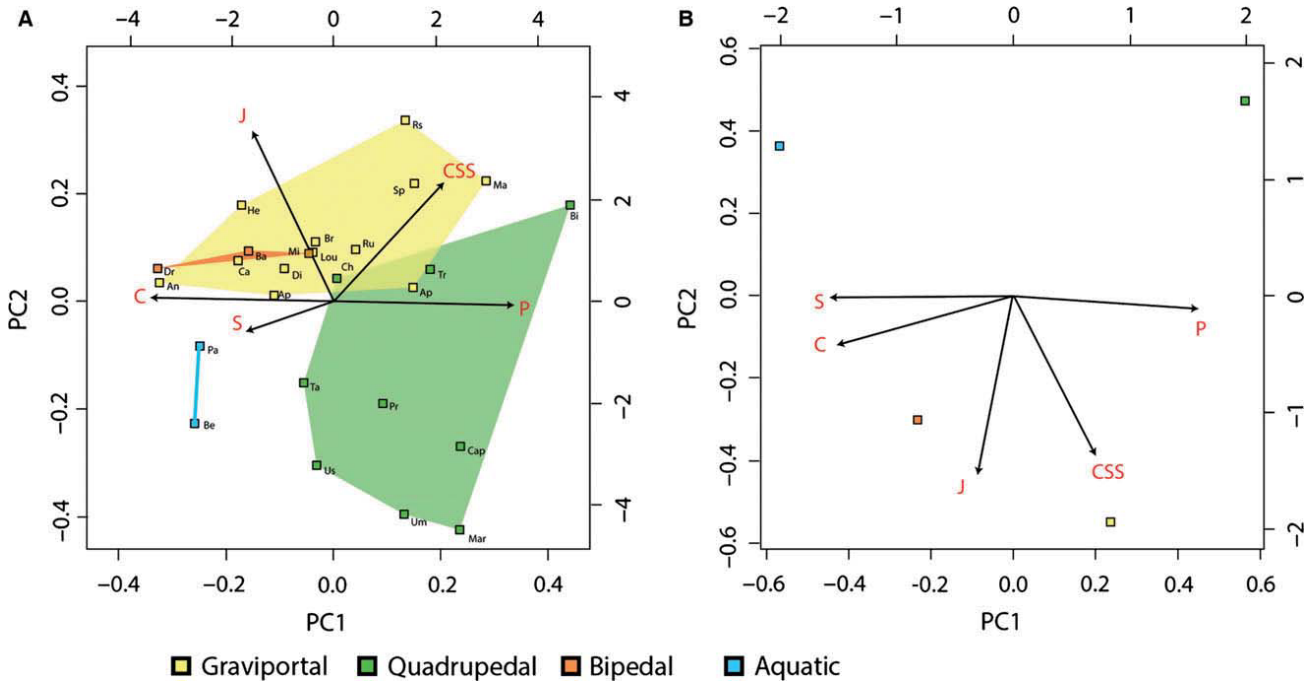

Figure 7. Microanatomical clusters obtained by principal component analyses (PCA) conducted on the ribs of our sample. Graphs showing the distribution of the variance in all taxa examined according to the PCA1 and PCA2 axes. A, classical PCA. B, between-groups PCA. Abbreviations for taxa as in Table 3.

Phylogenetic signal

Our quantitative analyses show that there is a weak phylogenetic signal in the dataset for most parameters. Despite this relative weakness, when phylogeny is taken into consideration, our analyses of (co)variance do not show any significant change between the four groups defined. Although a historical signal is common in bone cross-sectional geometry and microanatomical data, as previously noted (Houssaye *et al.*, 2014b), our findings might also reflect the fact that adaptations to an aquatic lifestyle and to a graviportal morphology occurred only infrequently in amniote evolution, such that the extant taxa showing such adaptations form a few groups on the phylogeny. A more thorough sampling of Tetrapoda might show a different phylogenetic signal in that our dataset of < 75 total species is far from comprehensive. Our results, however, might still reveal the occurrence of fundamental trends of anatomical construction that transcend phylogenetic constraints.

Cross-sectional geometry versus microanatomical parameters

Various comparative studies have focused on long bone sections aiming to analyze the link between bone microanatomical organization and the structural and functional requirements of extant organisms and to make inferences about the lifestyle of extinct taxa (Canoville & Laurin, 2010; Houssaye *et al.*, 2013; Quemeneur *et al.*, 2013; Klein *et al.*, 2015). Of course, individual bones, let alone whole skeletons, of extinct taxa are not always complete. Given the fragmentary nature of fossil material, body size or mass is difficult to estimate precisely. Our aim was to determine how similar the cross-sectional geometry of tetrapod bones is across a continuum encompassing bipedal, quadrupedal, graviportal, and aquatic forms with a particular focus on graviportal taxa. In addition to the microanatomical parameters commonly used, we included some cross-sectional geometry parameters. Because linear regressions on the independent contrast data showed a strong impact of body size (i.e. MD) on parameters Per, CSA, and Z_{pol}, the latter were considered to display redundant information and were removed from further analyses. However, the parameters J and CSS showed their own patterns of variability and are of appreciable interest in such comparative studies (Table 4).

Our comparative analysis highlights different trends of bone adaptation to a graviportal limb construction. Although some parameters were, for some bones, covarying with MD (size parameter), it was never the case for all bones (see Appendix, Table A2); hence, all of the selected parameters display signals that are not solely attributable to size or

allometry. Graviportal taxa are large animals with relatively larger cross-sections in their humeri, femora, and ribs, reflecting greater resistance to compression and tension, as well as greater bone mass, especially in the stylopodia. They are also characterized by a thicker cortex and a proportionally smaller medullary cavity, with a wider transition zone between the cortex and the medullary cavity, notably linked to the filling of the medullary area by a spongiosa with variations in trabecular thickness and size of the intertrabecular spaces. This inner cancellous structure may add benefits for impact energy absorption and marrow support (Oxnard, 1990, 1993). Wall (1983) noted the filling of the medullary cavity in *Ceratotherium*, suggesting a link with the animal's great weight, and the differences in the type of spongiosa between *Ceratotherium* and *Hippopotamus*. Our results also show that graviportal taxa exhibit higher values for the midshaft polar second moment of area, indicating increased resistance to stresses engendered by bending and torsion (O'Neill & Ruff, 2004) that predominate in vertebrate limb bones during locomotion (Ruff, 2002). Our results concerning the two stylopodial limb bones are strongly congruent.

However, rib microanatomical adaptation differs as summarized above. If there is a clear increase in bone mass in the ribs of some graviportal taxa, comparable to that observed in graviportal long bones, a similar phenomenon appears to occur for the bipedal forms sampled but, conversely, not for the rhinoceroses and mammoth. The occurrence of this osseous specialization remains unexplained. Our analyses showed an absence of significant signal in the rib MANOVA and a low K-NN classification power for this bone. Considering the difficulty of making homologous comparisons with ribs (Houssaye & Bardet, 2012; Houssaye *et al.*, 2014b), it appears necessary to increase taxon sampling and to analyze variations along the rib and the ribcage in various taxa, as reported for one sauropod in Waskow & Sander (2014), with the aim of better documenting and understanding rib adaptations to changes of biomechanical constraints.

Distinguishing graviportal and amphibious adaptations

The variations that we have detected among graviportal taxa are interesting; not all graviportal tetrapods converge on the same bone inner morphologies. Alexander & Pond (1992) established that, although elephants, rhinoceroses, and hippopotamus are considered graviportal taxa, elephants strongly differ from the two other groups in their relatively much longer legs (predominated by long stylopodia). The posture and gait of elephants is often mis-characterized as uniformly 'columnar' and restricted to simply walking (Ren *et al.*, 2008, 2010) but is nonetheless very distinct from rhinos and hippos in form and hence likely biomechanical function as well. Similarly, hippos are known only to trot on land, and never gallop, whereas even large extant rhinos can gallop and elephants can or do not (Alexander & Pond, 1992; Ren *et al.*, 2010), and so biomechanical and behavioural disparity exists even between these taxa. Such gross differences between these three groups of extant mammals are not evident at the microanatomical level (see 'Qualitative analysis').

Despite this variability, a clear trend is observed across the graviportal tetrapods examined here. The increase in bone mass (as represented by the infilling of marrow cavities and increased bone compactness; Christiansen, 1999) observed in graviportal taxa, including the amphibious *Hippopotamus*, is more restricted compared to that observed in some other amniotes, especially some shallow water swimmers or bottom-walkers that are almost exclusively aquatic (Hayashi *et al.*, 2013; Houssaye *et al.*, 2013; Klein *et al.*, 2015). Adaptation to a graviportal morphology and related behaviours is thus not to be mistaken for the specialization of bone mass increase observed in these aquatic taxa.

However, it is difficult to determine whether the pattern observed in *Hippopotamus* reflects its graviportal limbs or the benefit of a slight increase in bone mass in its legs enabling their use as ballast and offering stability in water. As a result, both adaptations might be mistaken, or even synergistic, and it seems almost pointless to try to unravel their evolutionary integration. Adaptation to a graviportal limb morphology should thus be taken into consideration when analyzing possibly amphibious taxa displaying a terrestrial-like morphology, and thus notably in the study of the early stages of adaptation to an aquatic life in amniotes. This cautionary note is particularly relevant for interpreting less well understood large extinct forms such as some south American endemic ungulates (A. Houssaye, pers. observ.), some giant xenarthrans and marsupials, *Arsinoitherium* and related giant tethytheres (including basal Proboscidea), and the diversity of large and small Rhinocerotoidea (Antoine *et al.*, 2003; Gheerbrant & Tassy, 2009; Vizcaino *et al.*, 2012).

ACKNOWLEDGEMENTS

We warmly thank O. Dülfer, P. Göddertz, Y. Nakajima, P. M. Sander, R. Schellhorn, and J. Schultz, (Steinmann-Institut, University of Bonn, Bonn,

Germany); C. Bens and J. Lesur (Muséum National d'Histoire Naturelle, Paris, France); N. Klein (Staatliches Museum für Naturkunde, Stuttgart, Germany); O. Mateus (Museu da Lourinha, Lourinha, Portugal); R. Scheetz (Brigham Young University, Utah, USA); W. Simpson (Field Museum of Natural History, Chicago, USA); F. Straehl, T. Scheyer, and M. Sanchez-Villagra (Universität Zurich, Zurich, Switzerland); R. Barsbold, K. Tsogtbaatar, and C. Tsogtbaatar (Mongolian Paleontological Center, Ulaanbaatar, Mongolia); D. Brinkman and M. Fox (Yale Peabody Museum, Yale University, New Haven, USA); S. Ishigaki, M. Saneyoshi, and S. Suzuki (Hayashibara Museum of Natural Sciences, Okayama, Japan); H. Taruno (Osaka Museum of Natural History, Osaka, Japan); T. Ando, H. Sawamura, and T. Shinmura (Ashoro Museum of Paleontology, Ashoro, Japan); S. Kawada, M. Manabe, R. Miyawaki, R. Tajiri, and T. Yamada (National Science Museum, Tokyo, Japan); Y. Kobayashi, K. Nakamura, and H. Nomura (Hokkaido University, Sapporo, Japan); H. Berke (Universität Köln, Köln, Germany); K. Padian and S. Werning (University of California Museum of Paleontology, Berkeley, USA); R. Irmis (Utah Museum of Natural History, Utah, USA); T. Bolliger and H. J. Siber (Sauriermuseum Aathal, Switzerland); G. W. Storrs (Cincinnati Museum Center, Ohio, USA); P. Bybee (Utah Valley University, Provo, USA); R. Cifelli (Sam Noble Oklahoma Museum of Natural History, Norman, USA); D. Eberth (Royal Tyrrell Museum, Drumheller, Canada); M. Watabe (Osaka City University, Japan); M. Lowe (University Museum of Zoology, Cambridge); and R. Sabin (Natural History Museum, Department of Zoology, London) for the loan of specimens, sections or images and technical help. Input on earlier, independent inceptions of this study from S. Shefelbine, M. Doube, M. Laurin, and S. Pierce is appreciated. We thank the Steinmann Institut (University of Bonn, Germany) for providing beamtime and support, UMS 2700 outils et méthodes de la systématique intégrative CNRS-MNHN and AST-RX, Plateau technique d'accès scientifique à la tomographie à rayons X du MNHN, M. Garcia Sanz for performing the scans and reconstructions at the AST-RX platform (MNHN, Paris, France), and UMR 7207 CR2P MNHN CNRS UPMC-Paris6 for 3D imaging facilities. A.H. thanks F. Goussard (MNHN, Paris, France) for discussions about graviportality and A. C. Fabre (Duke University, NC, USA) for help with the statistics. We thank D. Germain (MNHN, Paris, France) and an anonymous reviewer for interesting comments that improved the quality of the manuscript, as well as J. A. Allen for editorial work on the manuscript submitted for publication. A.H. acknowledges financial support received from the ANR-13-PDOC-001 and the A. v. Humboldt Foundation. J.R.H. was funded by grants from the Natural Environment Research Council (UK). Funding was provided by the Japanese Society for the Promotion of Science (JSPS) to S.H. A.H. designed the study. A.H., K.W., S.H., A.H.L., and J.R.H. participated in the data acquisition. A.H. conducted the analyses and drafted the manuscript, with significant input from R.C. and J.R.H., respectively. All authors contributed to, read and approved the final manuscript submitted for publication.

REFERENCES

Alexander R, Pond C. 1992. Locomotion and bone strength of the white rhinoceros, *Ceratotherium simum*. *Journal of Zoology* **227:** 63–69.

Amson E, Argot C, McDonald HG, de Muizon C. 2014. Osteology and functional morphology of the forelimb of the marine sloth *Thalassocnus* (Mammalia, Tardigrada). *Journal of Mammalian Evolution* **22:** 169–242.

Antoine PO, Ducrocq S, Marivaux L, Chaimanee Y, Crochet JY, Jaeger JJ, Welcomme JL. 2003. Early rhinocerotids (Mammalia: Perissodactyla) from South Asia and a review of the Holarctic Paleogene rhinocerotid record. *Canadian Journal of Earth Sciences* **40:** 365–374.

Bibi F. 2013. A multi-calibrated mitochondrial phylogeny of extant Bovidae (Artiodactyla, Ruminantia) and the importance of the fossil record to systematics. *BMC Evolutionary Biology* **13:** 166.

Blomberg SP, Garland T, Ives AR. 2003. Testing for phylogenetic signal in comparative data: behavioral traits are more labile. *Evolution* **57:** 717–745.

Campione NE, Evans DC. 2012. A universal scaling relationship between body mass and proximal limb bone dimensions in quadrupedal terrestrial tetrapods. *BMC Biology* **10:** 60.

Canoville A, Laurin M. 2010. Evolution of humeral microanatomy and lifestyle in amniotes, and some comments on palaeobiological inferences. *Biological Journal of the Linnean Society* **100:** 384–406.

Carrano MT. 1998. The evolution of dinosaur locomotion: functional morphology, biomechanics, and modern analogs. *Paleobiology* **24:** 450–469.

Carrano MT. 2001. Implications of limb bone scaling, curvature and eccentricity in mammals and non-avian dinosaurs. *Journal of Zoology* **254:** 41–55.

Christiansen P. 1999. Scaling of the limb long bones to body mass in terrestrial mammals. *Journal of Morphology* **239:** 167–190.

Clementz MT, Holroyd PA, Koch PL. 2008. Identifying aquatic habits of herbivorous mammals through stable isotope analysis. *Palaios* **23:** 574–585.

Cornette R, Herrel A, Stoetzel E, Moulin S, Hutterer R, Denys C, Baylac M. 2015. Specific information levels in relation to fragmentation patterns of shrew mandibles: do fragments tell the same story? *Journal of Archaeological Science* **53:** 323–330.

Cubo J, Ponton F, Laurin M, de Margerie E, Castanet J. 2005. Phylogenetic signal in bone microstructure of sauropsids. *Systematic Biology* **54:** 562–574.

De Buffrénil V, Canoville A, D'Anastasio R, Domning DP. 2010. Evolution of sirenian pachyosteosclerosis, a model-case for the study of bone structure in aquatic tetrapods. *Journal of Mammalian Evolution* **17:** 101–120.

Doube M, Kłosowski MM, Arganda-Carreras I, Cordelières FP, Dougherty RP, Jackson JS, Schmid B, Hutchinson JR, Shefelbine SJ. 2010. BoneJ: free and extensible bone image analysis in ImageJ. *Bone* **47:** 1076–1079.

Doube M, Kłosowski MM, Wiktorowicz-Conroy AM, Hutchinson JR, Shefelbine SJ. 2011. Trabecular bone scales allometrically in mammals and birds. *Proceedings of the Royal Society of London Series B, Biological Sciences* **278:** 3067–3073.

Dumont M, Laurin M, Jacques F, Pelle E, Dabin W, de Buffrenil V. 2013. Inner architecture of vertebral centra in terrestrial and aquatic mammals: a two-dimensional comparative study. *Journal of Morphology* **274:** 570–584.

Evin A, Cucchi T, Cardini A, Vidarsdottir US, Larson G, Dobney K. 2013. The long and winding road: identifying pig domestication through molar size and shape. *Journal of Archaeological Science* **40:** 735–743.

Fish FE, Stein BR. 1991. Functional correlates of differences in bone density among terrestrial and aquatic genera in the family Mustelidae (Mammalia). *Zoomorphology* **110:** 339–345.

Garland Jr T. 2001. *Phylogenetic Comparison and Artificial Selection*. Hypoxia: Springer, 107–132.

Garland T, Dickerman AW, Janis CM, Jones JA. 1993. Phylogenetic analysis of covariance by computer simulation. *Systematic Biology* **42:** 265–292.

Gheerbrant E, Tassy P. 2009. L'origine et l'évolution des éléphants. *Comptes Rendus Palevol* **8:** 281–294.

Gilbert C, Ropiquet A, Hassanin A. 2006. Mitochondrial and nuclear phylogenies of Cervidae (Mammalia, Ruminantia): Systematics, morphology, and biogeography. *Molecular Phylogenetics and Evolution* **40:** 101–117.

Girondot M, Laurin M. 2003. Bone profiler: a tool to quantify, model, and statistically compare bone-section compactness profiles. *Journal of Vertebrate Paleontology* **23:** 458–461.

Gray J. 1968. *Animal Locomotion*. London: Weidenfield & Nicolson, 479.

Gregory WK. 1912. Notes on the principles of quadrupedal locomotion and on the mechanism of the limbs in hoofed animals. *Annals of the New York Academy of Sciences* **22:** 267–294.

Hayashi S, Houssaye A, Nakajima Y, Chiba K, Ando T, Sawamura H, Inuzuka N, Kaneko N, Osaki T. 2013. Bone Inner Structure Suggests Increasing Aquatic Adaptations in Desmostylia (Mammalia, Afrotheria). *PLoS ONE* **8:** e59146.

Hildebrand M. 1982. *Analysis of Vertebrate Structure, 2nd edn*. New York: John Wiley & Sons.

Hokkanen JE. 1986. The size of the largest land animal. *Journal of Theoretical Biology* **118:** 491–499.

Houssaye A. 2009. 'Pachyostosis' in aquatic amniotes: a review. *Integrative Zoology* **4:** 325–340.

Houssaye A, Bardet N. 2012. Rib and vertebral microanatomical characteristics of hydropelvic mosasauroids. *Lethaia* **45:** 200–209.

Houssaye A, de Buffrenil V, Rage JC, Bardet N. 2008. An analysis of vertebral 'pachyostosis' in *Carentonosaurus mineaui* (Mosasauroidea, Squamata) from the Cenomanian (early Late Cretaceous) of France, with comments on its phylogenetic and functional significance. *Journal of Vertebrate Paleontology* **28:** 685–691.

Houssaye A, Lindgren J, Pellegrini R, Lee AH, Germain D, Polcyn MJ. 2013. Microanatomical and histological features in the long bones of mosasaurine mosasaurs (Reptilia, Squamata) - implications for aquatic adaptation and growth rates. *PLoS ONE* **8:** e76741.

Houssaye A, Scheyer TM, Kolb C, Fischer V, Sander PM. 2014a. A new look at ichthyosaur long bone microanatomy and histology: implications for their adaptation to an aquatic life. *PLoS ONE* **9:** e95637.

Houssaye A, Tafforeau P, Herrel A. 2014b. Amniote vertebral microanatomy – what are the major trends? *Biological Journal of the Linnean Society* **112:** 735–746.

Houssaye A, Tafforeau P, De Muizon C, Gingerich PD. 2015. Transition of Eocene whales from land to sea: evidence from bone microstructure. *PLoS ONE* **10:** e0118409.

Klein N, Houssaye A, Neenan JM, Scheyer TM. 2015. Long bone histology and microanatomy of Placodontia (Diapsida: Sauropterygia). *Contributions to Zoology* **84:** 59–84.

Laurin M, Canoville A, Germain D. 2011. Bone microanatomy and lifestyle: a descriptive approach. *Comptes Rendus Palevol* **10:** 381–402.

Meredith RW, Janečka JE, Gatesy J, Ryder OA, Fisher CA, Teeling EC, Goodbla A, Eizirik E, Simão TL, Stadler T. 2011. Impacts of the cretaceous terrestrial revolution and KPg extinction on mammal diversification. *Science* **334:** 521 524.

Nakajima Y, Hirayama R, Endo H. 2014. Turtle humeral microanatomy and its relationship to lifestyle. *Biological Journal of the Linnean Society* **112:** 719–734.

O'Neill MC, Ruff CB. 2004. Estimating human long bone cross-sectional geometric properties: a comparison of noninvasive methods. *Journal of Human Evolution* **47:** 221–235.

Oxnard C. 1990. From giant ground sloths to human osteoporosis: an essay on the architecture and biomechanics of bone. *Proceedings of the Australasian Society of Human Biology* **3:** 75–96.

Oxnard CE. 1993. Bone and bones, architecture and stress, fossils and osteoporosis. *Journal of Biomechanics* **26:** 63–79.

Polly PD, Hall B. 2007. *Limbs in Mammalian Evolution*. Evolution, Development and Transformation: Fins into Limbs, 245–268.

Prothero J. 1992. Scaling of bodily proportions in adult terrestrial mammals. *American Journal of Physiology-Regulatory, Integrative and Comparative Physiology* **262:** R492–R503.

Quemeneur S, de Buffrénil V, Laurin M. 2013. Microanatomy of the amniote femur and inference of lifestyle

in limbed vertebrates. *Biological Journal of the Linnean Society* **109:** 644–655.

R Core Team. 2012. *R: a language and environment for statistical computing*. Vienna, Austria: R Foundation for Statistical Computing.

Ramsay EC, Henry RW, Csuti B, Sargent E, Bechert U. 2001. Anatomy of the elephant foot. *The Elephant's Foot Prevention and Care of Foot Conditions in Captive Asian and African Elephants* **000:** 9–12.

Remes K. 2009. Taxonomy of Late Jurassic diplodocid sauropods from Tendaguru (Tanzania). *Fossil Record* **12:** 23–46.

Ren L, Butler M, Miller C, Paxton H, Schwerda D, Fischer MS, Hutchinson JR. 2008. The movements of limb segments and joints during locomotion in African and Asian elephants. *Journal of Experimental Biology* **211:** 2735–2751.

Ren L, Miller CE, Lair R, Hutchinson JR. 2010. Integration of biomechanical compliance, leverage, and power in elephant limbs. *Proceedings of the National Academy of Sciences of the United States of America* **107:** 7078–7082.

Ripley BD. 1996. *Pattern Recognition and Neural Networks*. Cambridge: Cambridge University Press.

Ross MD. 1984. The influence of gravity on structure and function of animals. *Advances in Space Research* **4:** 305–314.

Ruff CB. 2002. Long bone articular and diaphyseal structure in old world monkeys and apes. I: locomotor effects. *American Journal of Physical Anthropology* **119:** 305–342.

Sander PM, Christian A, Clauss M, Fechner R, Gee CT, Griebeler EM, Gunga HC, Hummel J, Mallison H, Perry SF, Preuschoft H, Rauhut OWM, Remes K, Tütken T, Wings O, Witzel U. 2011. Biology of the sauropod dinosaurs: the evolution of gigantism. *Biological Reviews* **86:** 117–155.

Schmidt-Nielsen K. 1984. *Scaling: Why is Animal Size So Important?*. Cambridge: Cambridge University Press.

Sereno PC. 1999. The evolution of dinosaurs. *Science* **284:** 2137 2147.

Steiner CC, Ryder OA. 2011. Molecular phylogeny and evolution of the Perissodactyla. *Zoological Journal of the Linnean Society* **163:** 1289–1303.

Straehl FR, Scheyer TM, Forasiepi AM, MacPhee RD, Sánchez-Villagra MR. 2013. Evolutionary patterns of bone histology and bone compactness in xenarthran mammal long bones. *PLoS ONE* **8:** e69275.

Thompson RS, Parish JC, Maidment SC, Barrett PM. 2012. Phylogeny of the ankylosaurian dinosaurs (Ornithischia: Thyreophora). *Journal of Systematic Palaeontology* **10:** 301–312.

Todd NE. 2010. New phylogenetic analysis of the family Elephantidae based on cranial-dental morphology. *Anatomical Record* **293:** 74–90.

Van Schalkwyk O, Skinner J, Mitchell G. 2004. A comparison of the bone density and morphology of giraffe (*Giraffa camelopardalis*) and buffalo (*Syncerus caffer*) skeletons. *Journal of Zoology* **264:** 307–315.

Venables WN, Ripley BD. 2002. *Modern applied statistics with S, 4th edn*. New York: Springer Science & Business Media.

Vizcaino SF, Cassini GH, Toledo N, Bargo MS. 2012. On the evolution of large size in mammalian herbivores of Cenozoic. In: Patterson, BD, Costa, LP, eds. *Bones, Clones, and Biomes: the History and Geography of Recent Neotropical Mammals*. Chicago: University of Chicago Press, 76–101.

Wall WP. 1983. The correlation between high limb-bone density and aquatic habits in recent mammals. *Journal of Paleontology* **57:** 197–207.

Warner SE, Pickering P, Panagiotopoulou O, Pfau T, Ren L, Hutchinson JR. 2013. Size-related changes in foot impact mechanics in hoofed mammals. *PLoS ONE* **8:** e54784.

Waskow K, Sander PM. 2014. Growth record and histological variation in the dorsal ribs of *Camarasaurus* sp. (Sauropoda). *Journal of Vertebrate Paleontology* **34:** 852–869.

Table A1. Raw sectional parameter's data

	C	S	P	MD	CSS	Per	CSA	Z_{pol}	J
Humerus									
cf. *Apatosaurus* sp.	0.754	0.0277021	0.6773825	44	1.62980948	132.712246	933.587221	9715.91318	2.6315E+10
Ampelosaurus atacis	0.5895	0.0445797	0.68067395	66	2.02142078	189.871009	1364.71598	17627.9246	3.4661E+10
Tarbosaurus sp.	0.845	0.0249974	0.3878153	37.3	1.67221876	109.505969	698.90406	5718.97325	2.3263E+10
Allosaurus fragilis	0.709	0.0330969	0.5328786	56.7	1.10104819	182.935439	1664.75	22814.3094	3.9711E+10
Scutellosaurus lawleri	0.767	0.02608405	0.47519445	6.1	1.7453153	17.7631477	16.6803522	23.5649804	2094015360
Scutellosaurus lawleri	0.748	0.03428075	0.49438835	6.2	1.74668323	18.5855037	16.7970183	24.5559238	5587392843
Protoceratops andrewsi	0.87	0.04931345	0.34611915	26.8	1.41403757	81.1489818	402.680359	2465.97302	1.8517E+10
Centrosaurus apertus	0.692	0.0369296	0.603935	71.8	1.39379674	218.887785	2365.52537	43458.9921	4.952E+10
Nothrotherium escrivanse	0.707	0.0402866	0.57175565	42.7	1.43651929	148.460741	821.756914	8453.70593	325626361
Tamandua tetradactyla	0.771	0.1114419	0.45461645	12.8	2.09834287	34.083974	56.3406191	121.873831	67005673
Myrmecophaga tridactyla	0.779	0.08295315	0.5336896	24.9	1.88133605	72.4851798	226.833683	1438.15776	9021375519
Paleoparadoxia sp.	0.991	0.0561819	0.20336195	71.5	2.77611418	230.493596	2337.07392	27463.7247	1.2313E+10
Trichechus manatus	0.847	0.04846035	0.3922043	30.2	1.45781749	92.9795767	483.992514	3250.56812	5306545326
Stegodon aurorae	0.8765	0.0877158	0.4005202	109.1	3.81102574	298.16076	3936.64447	62265.0409	4.3269E+10
Elephas maximus	0.842	0.05249945	0.4070543	111.9	2.06930312	335.060117	5710.41012	129960.413	7.5809E+10
Loxodonta africana	0.815	0.0546215	0.41543035	171.6	1.73850574	530.178544	12797.3272	427162.592	1.0537E+11
Felis felis	0.632	0.02545275	0.60012225	10.1	1.22554728	32.2653093	43.2547398	132.893787	1768862922
Panthera leo	0.559	0.0499733	0.65528645	42.6	2.11840963	119.173266	520.981963	4985.38748	71783189.2
Uncia uncia	0.607	0.0210712	0.6243309	20.7	1.16401539	63.0756768	172.377372	966.14164	657968.171
Canis lupus	0.672	0.02004715	0.56168685	21.1	1.16309786	65.7047044	208.075595	1239.19666	8498570.98
Vulpes vulpes	0.598	0.0197373	0.6285198	10.1	1.47570931	29.8648047	39.5984859	104.166178	3982269159
Meles meles	0.553	0.03390675	0.68812195	14.6	1.39552601	44.2923192	73.4683406	284.012383	2609351126
Ursus thibetanus	0.714	0.0272929	0.5288421	31.5	1.159827	100.361881	473.17172	3752.19453	1.7426E+10
Ursus maritimus	0.416	0.0410072	0.76926415	40	1.52341853	119.725898	397.463989	4367.26597	1593464740
Equus burchelli	0.7345	0.02214605	0.5095534	44.2	1.5861186	131.670874	875.351855	8761.3077	138352866
Tapirus terrestris	0.727	0.0499866	0.52519865	30	1.72634614	88.1248629	383.308657	2600.3148	6874655768
Diceratherium sp	0.813	0.0369669	0.4227705	59.1	1.16365892	198.387776	2056.80276	29796.5587	3.8793E+10
Diceros bicornis	0.866	0.0844297	0.38609245	79.6	1.58133877	248.150212	3388.61777	55565.8038	5.0669E+10
Diceros bicornis	0.937	0.04801215	0.244733	70.2	1.36543122	234.341888	3036.14728	43636.4342	4.6708E+10
Ceratotherium simum	0.771	0.08211185	0.5265021	90.7	1.43941503	288.3035	3983.60004	79227.5561	7.3067E+10
Ceratotherium simum	0.87	0.05897395	0.3785192	89.3	1.09325214	300.785459	4872.58925	96547.1359	4.8186E+10
Dicerorhinus sumatrensis	0.941	0.0405863	0.2476923	50.6	1.19083061	166.252171	1817.73517	21474.0709	3.7758E+10
Dicerorhinus sumatrensis	0.7895	0.05289275	0.47326635	52.8	1.26646699	166.425747	1478.43379	18150.7765	3.6142E+10

Table A1. *Continued*

	C	S	P	MD	CSS	Per	CSA	Z_{pol}	J
Rhinoceros sondaicus	0.869	0.0649185	0.34861485	73.6	1.4770946	225.093211	2874.82772	43475.8748	4.6722E+10
Rhinoceros unicornis	0.8295	0.10740125	0.43134165	80.2	1.35068775	248.573146	3425.67492	50278.2152	5.8381E+10
Choeropsis liberiensis	0.686	0.02613705	0.5673361	32.1	1.14208348	102.677652	504.544357	4460.9078	1.5288E+10
Hippopotamus amphibius	0.702	0.06436875	0.6118456	86.9	2.22530084	259.110707	2960.06361	58736.7668	5.9204E+10
Sus scrofa	0.631	0.02430255	0.6003419	24.9	3.63766796	67.1764533	151.530108	470.787446	413731524
Giraffa camelopardalis	0.648	0.0318064	0.5861701	60.1	1.3791709	189.248725	1641.71544	27914.3916	4.3306E+10
Okapia johnstoni	0.555	0.0244792	0.6607122	45.7	1.69029825	139.005724	704.23744	8566.4574	2.6256E+10
Rangifer tarandus	0.558	0.0235944	0.6583878	28.9	1.61317959	83.6333391	275.257268	2139.65023	5429620027
Capreolus capreolus	0.625	0.021938	0.60333185	10.1	1.1362849	32.7248912	45.80802	137.358736	92764575.6
Alces americanus	0.565	0.0298595	0.6525799	49.1	1.42815576	152.356557	920.674897	12991.7901	3.2602E+10
Cervus elaphus	0.6285	0.02369065	0.60380775	28.8	1.51195302	86.1193287	324.377205	2446.87413	589169148
Megaloceros sp.	0.611	0.0333998	0.6161711	60.9	1.62067849	158.974806	1176.1583	15801.0523	2.6987E+10
Megaloceros giganteus	0.669	0.0298408	0.5681548	64.7	1.53269307	220.053795	2027.47621	38780.6003	5.2045E+10
Dama dama	0.522	0.02269245	0.6856129	23.1	1.27968951	72.8664689	190.865724	1294.75374	7047929850
Cephalophus sylvicultor	0.633	0.02342205	0.6001151	22.2	1.42471846	67.3509822	200.289565	1190.9045	9305931183
Ovis ammon	0.513	0.0217732	0.694616	15.6	1.34806804	48.1066423	83.5143993	376.405659	2116795.15
Rupicapra rupicapra	0.42	0.0150244	0.7568849	17.2	1.3917047	52.134012	81.6721988	446.833074	2114367417
Capra falconeri	0.498	0.01906225	0.70350495	28.4	1.49132452	85.6613597	255.971189	2070.7954	21831850.6
Boselaphus tragocamelus	0.787	0.0231287	0.45428325	36.8	1.29414919	116.299339	745.778222	7044.40382	124366535
Taurotragus oryx	0.658	0.0494474	0.53410215	43.1	1.38002135	135.878333	815.961365	8919.20573	182632556
Syncerus caffer	0.808	0.0289635	0.43155055	52.3	1.2995507	165.045138	1466.04239	18396.2748	3.2326E+10
Femur									
Gallimimus sp.	0.626	0.01513185	0.608222	36.9	1.33771868	115.9	566.5	4206.2	2.4161E+10
Allosaurus fragilis	0.729	0.0221192	0.5134419	112.4	1.63674374	335.9	5713.2	147443.5	3.5867E+10
Masiakasaurus knopfleri	0.58	0.02121475	0.6434122	19.8	1.29015776	63.7	153.1	854.0	1.3766E+10
Theropod indet.	0.502	0.017051	0.7008067	41.2	1.32037643	127.4	565.1	5626.2	2.8162E+10
Theropod indet.	0.54	0.01429215	0.6732442	22.5	1.0760162	77.5	198.7	1425.1	1.2178E+10
Dryosaurus altus	0.679	0.03485535	0.55898	36.5	1.30443411	119.9	604.5	5752.3	2.2719E+10
Scutellosaurus lawleri	0.671	0.0583305	0.54961185	12.5	1.53940758	36.5	58.9	159.3	8200209537
Stegosaurus sp.	0.8085	0.0782049	0.39002595	64.3	2.13506047	188.1	1858.2	22386.4	3.4727E+10
Myrmecophaga tridactyla	0.759	0.05481585	0.5086188	32.1	3.40327161	86.1	257.2	1134.0	613759274
Tamandua tetradactyla	0.791	0.08522145	0.40910385	10.2	1.69541064	29.2	45.3	90.5	42093121.8
Mammuthus sp.	0.846	0.03647935	0.4344998	102.9	3.13793105	286.9	4236.7	82310.2	9.5988E+10
Mammuthus sp.	0.898	0.0417144	0.30821945	139.5	2.7991006	377.6	8182.9	202961.3	6.0301E+10
Mammuthus sp.	0.773	0.01852935	0.469349	172	2.61157026	467.0	10730.1	355466.0	9.3391E+10
Elephas maximus	0.772	0.04417595	0.49480345	104.6	2.07317026	301.2	4433.0	88965.3	6.1659E+10
Loxodonta africana	0.855	0.0214633	0.3784931	165.5	2.22445527	454.4	11261.6	336421.6	9.7378E+10
Felis felis	0.544	0.0085559	0.6707156	9.6	1.36595707	29.4	33.1	95.3	3399123230
Vulpes vulpes	0.5335	0.01825615	0.67841195	10.4	1.51324415	34.6	37.2	114.6	547594549

Table A1. *Continued*

	C	S	P	MD	CSS	Per	CSA	Z_{pol}	J
Meles meles	0.631	0.0369182	0.5998947	11.5	1.38376525	35.7	56.2	183.4	3070758534
Ursus thibetanus	0.81	0.00982685	0.43002335	28.9	1.73903779	85.6	410.2	2770.8	1.2271E+10
Ursus maritimus	0.6205	0.03876555	0.6084135	30	1.20049655	98.0	411.2	3809.8	1978834690
Tapirus terrestris	0.687	0.07560465	0.5819344	33.2	1.39165835	105.4	505.8	4378.5	1.4084E+10
Ceratotherium simum	0.669	0.0672103	0.622467	78.6	1.48712577	261.5	2711.4	50647.7	6.4032E+10
Ceratotherium simum	0.819	0.04376185	0.44526285	92.6	2.36400849	261.2	3305.8	53396.0	3.9675E+10
Ceratotherium simum	0.827	0.0205313	0.4109872	70.2	1.81647539	209.2	2398.3	35430.5	5.4899E+10
Dicerorhinus sumatrensis	0.766	0.04312245	0.47130215	61.2	1.91948758	181.5	1528.5	20208.0	2.275E+10
Rhinoceros sondaicus	0.723	0.04575315	0.60366805	73.7	1.40556288	234.1	2616.2	48087.6	5.142E+10
Rhinoceros unicornis	0.7275	0.053317	0.5596257	80.7	1.80454773	249.3	2936.0	58828.5	4.6366E+10
Choeropsis liberiensis	0.634	0.01526325	0.59966175	34.2	1.10414019	109.7	533.2	5360.4	9571820794
Hippopotamus amphibius	0.795	0.02889215	0.4979548	63.7	1.16492891	256.3	2240.2	35258.4	6.1389E+10
Lama guanicoe	0.4635	0.024248	0.72692475	30.3	1.36976274	102.6	300.4	2972.6	1015895734
Sus scrofa	0.545	0.0112854	0.6690296	34.2	1.52137981	102.3	394.1	3644.9	9550042780
Okapia johnstoni	0.632	0.0201897	0.6005681	38.9	1.38165876	119.5	639.7	7145.1	3.0221E+10
Giraffa camelopardalis	0.576	0.01528705	0.6442233	55.6	1.39735273	171.0	1198.7	19177.7	2.9518E+10
Dama dama	0.55	0.02867115	0.66441365	25.8	1.22672813	79.4	244.6	1776.5	7406863488
Megaloceros sp.	0.511	0.01645135	0.6948783	60.9	1.4557609	179.7	1134.3	18689.6	1.71E+10
Rangifer tarandus	0.457	0.0158873	0.7324255	28.2	1.36118577	85.6	232.8	1947.0	8139493914
Capreolus capreolus	0.479	0.0102065	0.716217	14.3	1.19315486	50.4	67.3	292.9	610496842
Alces americanus	0.6	0.0146826	0.62776955	45.1	1.56269337	137.3	783.8	9945.6	2.9683E+10
Cephalophus sylvicultor	0.641	0.01606835	0.5944464	22.3	1.28379722	68.5	211.7	1254.0	1.201E+10
Rupicapra rupicapra	0.451	0.0128629	0.7357525	16.1	1.11279751	51.8	86.0	452.1	2225878735
Syncerus caffer	0.7295	0.01702025	0.51541685	47	1.16998032	151.3	1172.1	15342.9	2.8095E+10
Bos taurus	0.697	0.0155041	0.5453717	23.9	1.22102366	75.4	278.9	1763.1	1.2888E+10
Bison bonasus	0.545	0.04542365	0.665	63.6	1.67279972	187.6	1294.6	20149.4	3.4872E+10
Rib									
Baryonyx sp.	0.89	0.08	0.30	30.00	2.05721393	100.148738	457.494838	2759.09265	3.9002E+10
Lourinhanosaurus sp.	0.84	0.10	0.43	36.20	2.94968841	103.412843	377.533883	1620.38792	1.2269E+10
Spinophorosaurus nigerensis	0.68	0.10	0.51	64.30	5.24293023	180.244181	984.136504	10296.9323	1.5098E+10
Apatosaurus sp.	0.80	0.12	0.34	52.30	1.91206431	161.38304	1254.99186	8992.05142	1.7632E+10
Diplodocus sp.	0.85	0.10	0.40	35.00	2.26642974	111.715848	572.761252	4088.36102	1.9445E+10
Cathetosaurus sp.	0.96	0.12	0.31	59.00	2.81938572	168.940454	1258.2724	10299.6035	1.1085E+10
Brachiosaurus sp.	0.84	0.08	0.52	95.00	2.27558248	306.694462	3464.24929	59266.0278	4.0623E+10
Draconyx sp.	0.92	0.18	0.15	35.90	2.25213537	125.235139	685.404162	3808.00779	2.5386E+10
Ankylosaurid indet.	0.87	0.11	0.20	194.80	1.08211819	646.756144	23100.5993	1032760.32	2.1431E+11
Miragaia longicollum	0.79	0.18	0.45	35.00	3.04946408	113.178671	501.023041	3652.72539	1.6748E+10
Hesperosaurus mjosi	0.94	0.03	0.17	31.10	3.10419624	94.6496397	448.727188	2419.87863	1.4754E+10
Procavia capensis	0.83	0.02	0.41	2.50	2.13679234	7.92001541	2.88669132	1.5187719	70080185.2

Table A1. *Continued*

	C	S	P	MD	CSS	Per	CSA	Z_{pol}	J
Behemotops katsuiei	0.86	0.23	0.13	37.80	2.39497951	108.216129	590.509343	3944.23796	137165494
Paleoparadoxia sp.	0.90	0.14	0.21	42	1.72804407	127.570034	969.953462	8331.74329	4777344161
Mammuthus primigenius	0.63	0.06	0.70	44	5.60441488	114.676197	436.700994	3741.56522	9189994685
Martes foina	0.62	0.05	0.63	2.10	1.388538	6.46602875	1.78350241	0.9543075	12625274.2
Tremarctos ornatus	0.76	0.02	0.63	13	2.71656427	37.9836519	65.753974	175.399147	2988368288
Ursus spelaeus	0.83	0.19	0.57	21.5	1.60069318	61.9800907	215.670279	883.490901	166320661
Ursus maritimus	0.71	0.08	0.58	12.2	1.60164383	35.2923407	44.5497066	85.3548299	17012499.9
Tapirus terrestris	0.79	0.06	0.46	11.2	1.04693967	37.4879769	77.0831935	227.050027	5875901730
Rhinoceros sondaicus	0.79	0.07	0.51	45.2	7.76616786	124.013311	488.269087	3763.93788	1.8325E+10
Rhinoceros unicornis	0.77	0.09	0.49	35.6	3.1603713	101.108498	407.429533	2304.32458	1.0243E+10
Choeropsis liberiensis	0.79	0.06	0.44	14.3	2.17146526	39.4605088	81.1079705	231.869287	1.0704E+10
Bison bonasus	0.48	0.05	0.74	28.2	5.2118326	74.6373393	130.367116	714.166289	5788305648
Capra aegagrus	0.71	0.14	0.53	11.8	5.92186294	28.1173478	27.5919354	47.1734831	1564692.48

C, compactness of the whole section; P, the extent of the medullary cavity as measured by the relative distance from the centre of the section to the point where the most abrupt change in compactness occurs; S, the width of the transitional zone between the compact cortex and the medullary cavity as measured by the reciprocal of the slope of the compactness profile at the inflection point; MD, maximum bone diameter at the level of section; CSS, cross-sectional shape; Per, perimeter of the section; CSA, cross-sectional area; Z_{pol}, polar section modulus; J, polar second moment of area.

Table A2. Table showing the results of the *K*-statistic analysis and of the linear regressions performed for this study

	Phylogenetic signal		Linear regressions on the independent contrast data	
	K	*P*	*P*	Adjusted r^2
Humerus				
C	0.68	< 0.001*	0.91	.02
S	0.55	< 0.001*	0.01*	0.11
P	0.49	< 0.001*	0.81	.02
MD	0.40	< 0.001*		
CSS	0.34	0.041*	0.09	0.04
J	0.37	0.002*	0.04*	0.07
Femur				
C	0.46	< 0.001*	0.01*	0.16
S	0.55	< 0.001*	0.33	0.00
P	0.47	0.004*	0.01*	0.15
MD	0.37	0.006*		
CSS	0.51	0.007*	< 0.01*	0.32
J	0.45	0.005*	< 0.01*	0.54
Rib				
C	0.47	0.139	0.61	.03
S	0.39	0.550	0.15	0.05
P	0.65	0.016*	0.98	.04
MD	0.67	0.017*		
CSS	0.43	0.282	0.30	0.01
J	0.56	0.038*	< 0.01*	0.35

C, compactness of the whole section; S, the width of the transitional zone between the compact cortex and the medullary cavity as measured by the reciprocal of the slope of the compactness profile at the inflection point; P, the extent of the medullary cavity as measured by the relative distance from the centre of the section to the point where the most abrupt change in compactness occurs; MD, maximum bone diameter at the level of section; CSS, cross-sectional shape; J, polar second moment of area.
*$P < 0.05$.

„Der aufregendste Satz, den man in der Wissenschaft hören kann, der Satz, der neue Entdeckungen ankündigt, ist nicht „Heureka“ (Ich hab’s gefunden.), sondern ‚Das ist aber komisch...‘“

“The most exciting phrase to hear in science, the one that heralds the most discoveries, is not "Eureka!" (I found it!) but ‘That's funny...’”

Isaac Asimov

CHAPTER 4

Histological evidence for dwarfism and different morphotypes of diplodocine sauropods within the Upper Jurassic Mother´s Day Quarry (Morrison Formation, Montana, USA)

submitted as:

Waskow, K., Wiersma, K., Tschopp, E., Woodruff, D. C., Storrs, G., and Sander, P. M. Histological evidence for dwarfism and different morphotypes of diplodocine sauropods within the Upper Jurassic Mother's Day Quarry (Morrison Formation, Montana, USA). Acta Palaeontologica Polonica, (submitted).

Author contribution:

The major part of the research of this paper and analysis of all histological dorsal rib samples that are mainly in focus of this study were designed and performed by me including complete manuscript and figure preparation (excluding contributions of coauthors listed below).

Kaleigh Wiersma performed the histological sampling and descriptions of the long bones (chapter 4.4.2.) including HOS stage classification and Fig. 6.

Emanuel Tschopp performed the reassessment of the morphological description of the MDQ material (chaper 4.4.3) that yields information to the taxonomic assignment (chapter 4.5.5.) to which he also contributed in large parts.

D. Cary Woodruff contributed to the writing of chaper 4.5.7. (Alternative explanations for diminutive size) and was responsible for native speaker proof reading.

Glenn Storrs provided loan and sampling permission for all alalyzed specimens and contributed to native speaker proofreading.

Martin Sanders authorship is justified by his excellent supervision and proofreading of the manuscript.

Histological evidence for dwarfism and different morphotypes of diplodocine sauropods within the Upper Jurassic Mother's Day Quarry (Morrison Formation, Montana, USA)

Katja Waskow [1*], Kayleigh Wiersma [1], Emanuel Tschopp [2,3], D. Cary Woodruff [4,5,6], Glenn Storrs[7], and P. Martin Sander [1]

[1] Steinmann Institute for Geology, Mineralogy, and Paleontology, University of Bonn, Nussallee 8, D-53113, Bonn, Germany. Phone: +49 (0) 228 / 73 600 58.
*waskow@uni-bonn.de

[2] American Museum of Natural History, Division of Paleontology, New York, NY, USA.

[3] Museu da Lourinhã, Lourinhã, Portugal.

[4] Department of Ecology and Evolutionary Biology, University of Toronto, Toronto, ON, Canada.

[5] Royal Ontario Museum, University of Toronto, Toronto, ON, Canada.

[6] Great Plains Dinosaur Museum and Field Station, Malta, MT, USA.

[7] Cincinnati Museum Center, 1301 Western Ave., Cincinnati, OH, USA.

Abstract

Sauropods were the largest terrestrial vertebrates ever discovered. Apart from a few island dwarf taxa found in Europe, only very large species are known to date. Additionally, their fossil record almost completely lacks juveniles. Therefore, the Mother´s Day Quarry (Morrison Formation, Montana, USA), a low-diversity bone bed of over 2000 elements belonging to mainly small-sized diplodocines, is of special interest. The quarry yielded diverse skeletal elements in almost complete disarticulation, previously interpreted as a drought-induced mass mortality event killing only juveniles. Using anterior dorsal rib cross-sections, as well as drill core sections of humeri and femora, we provide histological evidence for a heterogeneous ontogenetic age distribution within this assemblage. A reassessment of the morphology included in this study confirms the existence of small but skeletally mature individuals at the site in addition to juveniles. Because most previously known taxa are of large adult sizes, this indicates the presence of a dwarf taxon among the Morrison Formation sauropods. Island dwarfing as an explanation appears inconsistent with the terrestrial habitats of the Morrison Formation. Nevertheless, the dwarfs may have evolved rapidly on a transient island formed by the transgression of the epicontinental sea from the north. Other explanations for dwarfing such as niche fragmentation, increased competition or different climatic conditions are discussed herein. Additionally, at least two different morphs can be observed within the assemblage based on histological and morphological analysis. Possible explanations are sexual dimorphism, the presence of two species or both.

4.1. Introduction

The enormous size of sauropods, which are known to be the largest vertebrates to ever inhabit the terrestrial environment, appeared very early in the evolutionary history of this clade. Some of the earliest known sauropods from the Late Triassic of Thailand already reached a large body size, documented by the findings of humeri having a total length of over one meter (Buffetaut et al., 2002; Sander et al., 2004). Remains of juvenile individuals are rare (Peterson and Gilmore, 1902; Carpenter and McIntosh, 1994; Schwarz et al., 2007; Whitlock et al., 2010; Melstrom et al., 2016; Hanik et al., 2017; Woodruff et al., 2017; Woodruff et al., 2018, (chapter 5)), a fact that might be related to age segregation and different ecological niche occupation at different ontogenetic ages (Myers and Fiorillo, 2009). Therefore, the occurrence of a monospecific bone bed consisting exclusively of small-sized diplodocine bones described as juveniles (Myers and Storrs, 2007; Storrs et al., 2012), which is histologically analyzed herein, was of special interest. Small sauropod individuals other than juveniles like the relatively small species *Neuquensaurus australis* (Lydekker, 1893), a Late Cretaceous titanosaur from North Patagonia (South America); or *Kaatedocus siberi* (Tschopp and Mateus, 2013), a small diplodocine from the Upper Jurassic of North America are rare. Dwarfism however, evolved some large sauropod taxa into island dwarfs that are only known from Europe, where taxa such as *Europasaurus holgeri* (Sander et al., 2006) and *Magyarosaurus dacus* (Nopcsa, 1914; Le Loeuff, 1993) were discovered.

4.1.1. Dwarfed sauropod taxa of Europe

The occurrence of small endemic sauropod populations in Europe, co-existing with giant taxa in the Jurassic and Cretaceous (Mazzetta et al., 2004; Upchurch et al., 2004; Klein et al., 2011; Sander et al., 2011), has been a result of dwarfing, most likely triggered by the geological formation of islands (Nopcsa, 1914; Sander et al., 2006; Stein et al., 2010). The best conclusive evidence for the occurrence of insular or phyletic dwarfism in sauropods is the endemic assemblage of *Europasaurus holgeri* from the Upper Jurassic of Germany described by Sander et al. (2006). The remains of this basal macronarian, found in the Langenberg Quarry near Oker (Harz Mountains, Lower Saxony), include different ontogenetic stages as well as two different size morphs (Carballido and Sander, 2014; Marpmann et al., 2015). Another European dwarf sauropod is *Magyarosaurus dacus*, a titanosaurid sauropod from the Upper Cretaceous (Maastrichtian) continental formations of the Haţeg Basin of Romania, known exclusively from small individuals ($<10^3$ kg). Island dwarfing as a cause for its diminutive size was first hypothesized by Franz Baron Nopcsa in the early 20th century (Nopcsa, 1914; 1923). Subsequently, some rare finds of isolated, normal-sized sauropod bones questioned this assumption, resulting in the identification of all titanosaur remains from the Haţeg Basin as *Magyarosaurus dacus* by Le Loeuff (1993) and Weishampel et al. (2003). More recently, the histological study of Stein et al. (2010) verified the dwarfed nature of the smaller individuals. Island dwarfism as a possible explanation for

the small size of most of the Romanian sauropod remains, is additionally supported by the occurrence of other relatively small-bodied dinosaur taxa within the same strata (Weishampel et al., 1993; 2003; Benton et al., 2010).

4.1.2. Bone tissue formation and apposition rates in sauropods

In general, normal-sized sauropod long bones consist of fast-growing, highly vascularized, laminar to plexiform bone tissue, also known as fibrolamellar bone, that preserves little if any of the growth record. The general interpretation is that the bones are growing too quickly to produce lines of arrested growth (LAGs), formed during seasonal growth stops (Curry, 1999; Sander, 1999; 2000; Klein and Sander, 2008; Sander et al., 2011). Only the outermost cortex might produce an external fundamental system (EFS), indicating that the animal in question is skeletally mature. The EFS typically consists of closely spaced LAGs, with no significant bone structures such as primary osteons or vascular canals in between. In normal-sized sauropods, the single laminae of the laminar fibrolamellar bone show constant thicknesses of 4-5 laminae/mm (4.8 median) independent of taxon, ontogenetic age, locality, or sampled bone element, indicating structural causal constraints (Sander and Tückmantel, 2003; Hofmann et al., 2014). Additionally, normal-sized sauropod long bones are often heavily remodeled. Therefore, especially in skeletally mature individuals, the samples often consist exclusively of Haversian bone with remodeling beginning in the inner cortex and proceeding to the surface of the bone (Sander, 2000; Klein and Sander, 2008). Mitchell and Sander (2014) described this remodeling as the second front of sauropod long bone formation in their three-front model.

Compared to long bones, sauropod dorsal rib histology differs greatly even in the same individual (Waskow and Sander, 2014). Caused by a lower bone apposition rate, the rib cortex shows well-developed cyclicity with distinct LAGs and less remodeling (Waskow and Sander, 2014; Wiersma et al., in review). Dwarfed sauropods like *Europasaurus* and *Magyarosaurus* show greatly differing bone microstructures. In *Europasaurus,* the long bones show a slower growing bone tissue and a lower bone apposition rate, indicated by clearly developed LAGs, a lower rate of remodeling, and an EFS at small size (Sander et al., 2006; Mitchell and Sander, 2014). In contrast, *Magyarosaurus* shows extremely remodeled bone tissue, even at small sizes, and presumably early ontogenetic stages. The remodeling rate in this Romanian dwarf is much higher in comparison with normal-sized sauropods, with the remodeling front catching up with the first front of primary bone formation early in ontogeny (Stein et al., 2010; Mitchell and Sander, 2014).

Institutional abbreviations – AMNH, American Museum of Natural History, New York City, New York, USA; **BYU**, Museum of Paleontology, Brigham Young University, Provo, Utah, USA; **CM**, Carnegie Museum of Natural History, Pittsburgh, Pennsylvania, USA; **CMC**, Cincinnati Museum Center, Cincinnati, USA; **DFMMh/FV** Dinosaurier-Freilichtmuseum Münchehagen/Verein zur Förderung der Niedersächsischen Paläontologie (e.V.), Germany;

FMNH, Field Museum of Natural History, Chicago, USA; **SMA**, Sauriermuseum Aathal, Switzerland; **SMNS**, Staatliches Museum für Naturkunde, Stuttgart; **USNM**, National Museum of Natural History, Smithsonian Institution, Washington, D.C., USA; **UW**, University of Wyoming, Laramie, USA; **YPM**, Yale Peabody Museum, New Haven, Connecticut, USA.

4.2. Material

4.2.1. The Mother´s Day Quarry diplodocine assemblage

The Mother´s Day Quarry (MDQ) is located in the northern outcrops of the Late Jurassic Morrison Formation of Montana, specifically within the Salt Wash Member, the lower part of the Morrison Formation (Myers and Storrs, 2007). The diplodocine sauropod fossils found there were described as a drought-induced, mass-mortality assemblage of juveniles deposited by a debris flow, triggered by a heavy rainfall (Myers and Storrs, 2007). The young maturational state was assumed based on the small size and gracile nature of the disarticulated bones, and the presence of small, osteologically immature bone elements with open neurocentral synchondroses. Small skull elements showing juvenile characters also indicated the presence of immature individuals (Myers and Storrs, 2007; Storrs et al., 2012). Despite some rare findings of shed theropod teeth (possibly *Allosaurus* sp.), and a recent find of a stegosaur humerus (not yet published), the assemblage consists exclusively of diplodocine fossils. The bones were found in an approximately 3-meter-thick layer of sandstone and siltstone. There are small, reworked rounded bone clasts within the sample (Myers and Storrs, 2007; Storrs et al., 2012), which seem to show that not all the material deposited together within the debris flow was coming from a single event. Based on regional lithologic correlations and personal communications with F. Peterson, Myers and Storrs (2007) suggested a Kimmeridgian age for the quarry. However, this age is affected by uncertainties, that can only be clarified in further stratigraphical analysis. In general, the members of the Morrison Formation are hard to identify in northern Wyoming and Montana (Parrish et al., 2004; Trujillo, 2006), and there are indications for a younger age of the northern outcrops compared to southern ones (Harris and Dodson, 2004; Harris, 2005; Woodruff and Foster, 2017). Most of the bones are found poorly sorted and in nearly complete disarticulation. Nevertheless, some partially articulated skeletal sections (such as fore- and hind limbs with articulated manus and pedes) are also present at the site. The lack of a preferred orientation of the elongate elements strongly implies quick burial of the bones with minimal transportation. Disarticulation in combination with high angle orientation of the long bones indicates a high-energy depositional setting. By counting the most abundant diplodocine bone elements present within the MDQ assemblage, the minimal number of individuals preserved was postulated to be 15 by Myers and Storrs (2007). This number now can be raised to 16 (G.W. Storrs, pers. obs. 2017). All skeletal remains were interpreted to belong to a single species of diplodocine sauropod (Myers and Storrs, 2007).

4.3. Methods

4.3.1. Sampling techniques

All rib samples are from anterior dorsal ribs (position 2-4, determined by morphology) and were taken as complete cross-sections at the proximal end of the rib shaft (Fig. 1). This position was determined to be the area where the most complete growth record is preserved in sauropod dorsal ribs (Waskow and Sander, 2014). The position of the single sections varies only slightly with respect to the preservation of the surface area. Prior to sawing, each rib was protected with a solution of Technovit® 4071, a technical polymer. The two components of this polymer (powder and liquid) are usually used in a ratio of 2:1. Here we used a 3:1 ratio to increase the viscosity of the liquid suspension to properly encase the whole sampling region of the rib shaft. The protected area then was cut with a rock saw. After sawing, the hardened Technovit® polymer was removed with acetone. Long bones were sampled by core drilling at the mid shaft (posterior midshaft in the humeri, anterior midshaft in the femora) of the bones where growth initiated. The method is described in more detail by Stein and Sander (2009). All samples were processed into paleo-histological thin sections by standard petrographic techniques (see Enlow and Brown, 1956; Wells, 1989; Chinsamy and Raath, 1992; Lamm, 2007; Padian and Lamm, 2013). Thin sections were analyzed under a Leica DML P polarizing microscope. Photos were taken with a Leica DFC420 digital camera and processed with Imagic ImageAccess software.

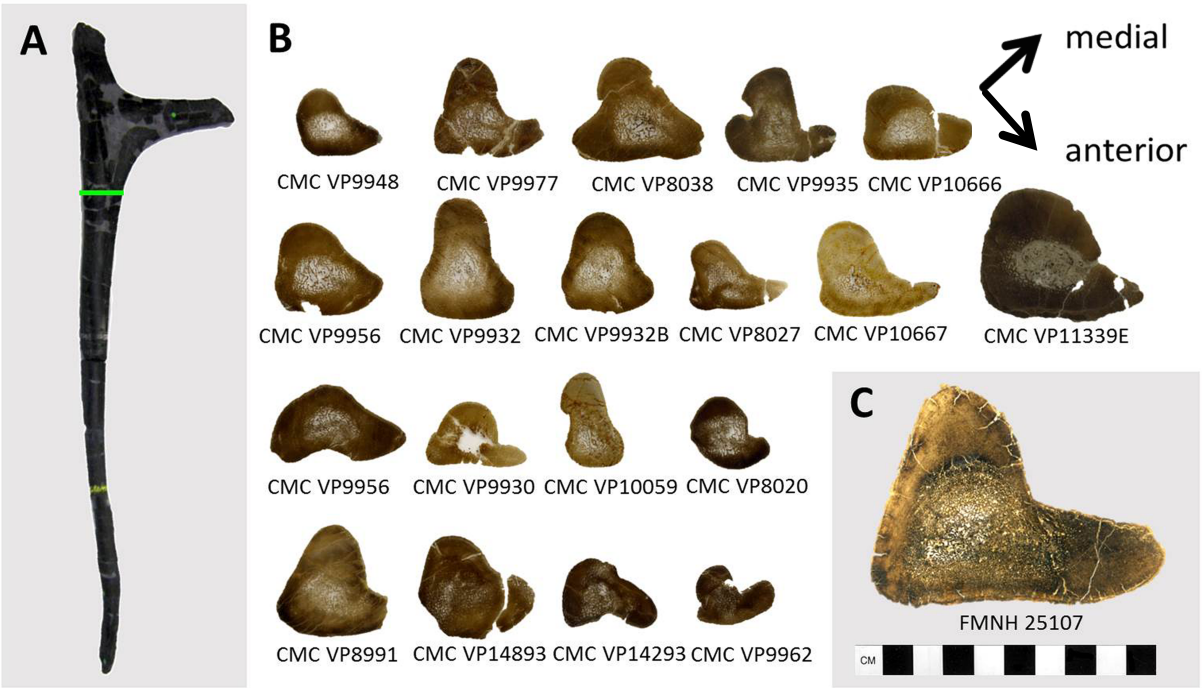

Fig. 1: Sampling position and size comparison of MOR diplodocine dorsal rib cross-sections and an average-sized diplodocine dorsal rib cross-section to the same scale. **A**: Sampling area at the proximal end of the rib shaft (indicated by green bar). **B**: Dorsal rib cross-sections of the MDQ diplodocines. **C**: Normal-sized diplodocine rib cross-section (FMNH 25107). Scale bar equals 10 cm.

4.3.2. Methods used for growth and mass analysis

The percentages of growth record preservation within the single samples were calculated by measuring the distance from the center of the medullary cavity, where growth initiated to the bone surface at the thickest part of the cortex (representing 100%). In the ribs sampled as complete cross-sections, bone profiler version 4.5.8. (Girondot and Laurin, 2003) was used to calculate the center of the medullary cavity. In the case of the long bones, this method was not applicable due to core drilling. Therefore, in these nearly cylindrical bones, the radius (calculated using the formula $2 \cdot \pi \cdot r = U$ and the known circumference) was used to represent 100% of growth record preservation. Based on the distance of the innermost LAG to the surface in relation to the full distance, the percentage of preserved growth record was calculated in both ribs and long bones. Even though the method of Anderson et al. (1985) is often-criticized (e.g., Paul, 1997; Carrano, 2001; Seebacher, 2001; Gunga, 2002), it has shown to be reliable and an accurate way of estimating the mass of an extinct animal (Campione and Evans, 2012). This method was not applicable here, because it requires humerus and femur circumference from the same individual. The MDQ long bone sample represent single bones out of a bone bed, rather than at least partially complete individuals. Thus, the corresponding humeral circumference that is needed for comparison with femur CMC VP 14502, using the Anderson et al. (1985) equation is missing, impeding the set-up of a mass-based growth curve. However, to give a relative indication for the mass of the individuals compared to average-sized sauropods, the mass-range using the smallest and the largest femora present at the site was calculated by the method of Mazzetta et al. (2004) using the smallest and the largest femur present at the site. The growth curve, however, was created based on the distance to the medullary cavity (in case of the long bones represented by the radius) similar to the rib-based growth curves. The maximum number of missing inner cycles due to the expansion of the medullary cavity was calculated by dividing the distance from the innermost LAG to the center of the medullary cavity by the diameter of the broadest growth cycle. Rib-based growth curves for each individual are provided in Waskow et al. (unpublished, (chapter 6)). Even if the errection of histologic ontogenetic stages for ribs is still work in progress by Waskow and Sander, a preliminary classification of the MDQ ribs into rib based histologic ontogenetic stages (RHOS) has been done. To erect RHOS stages histological features such as the degree of vascularization, remodeling, and the amount of Sharpey´s fibers were taken into account. Resulting in the subdivision of 10 different RHOS.

4.3.3. Methods used for the comparison of cervical vertebrae

In sauropods, cervical vertebrae drastically change in shape, size, and morphology from anterior to posterior. Moreover, these changes reflect also ontogenetic development and evolution: anterior cervical vertebrae of adult individuals of derived taxa resemble more posterior elements of juvenile individuals of the same species and of adult individuals of

phylogenetically more basal taxa (Wedel, 2003; Wedel and Taylor, 2013). Therefore, it is difficult to assess morphological variability within a sample and to distinguish ontogenetic from serial variation or taxonomic differences. Herein, we assessed serial variation based on the comparisons with articulated, nearly complete cervical series of *Apatosaurus louisae* (CM 3018; Gilmore, 1936), *Diplodocus carnegii* (CM 84; Hatcher, 1901), *Galeamopus pabsti* (SMA 0011; Tschopp and Mateus, 2017), and *Kaatedocus siberi* (SMA 0004; Tschopp and Mateus, 2013). Morphological features that change throughout the column are the position and shape of the parapophysis, the shape of the ventral edge of the lateral surface, the extension of the lateral pneumatic foramina on the centra, and the development of the posterolateral flanges on the ventral surface. Ontogenetic stages were assessed mainly based on the neurocentral fusion pattern, which can be open, closed, or fused (Ikejiri, 2012; Tschopp and Mateus, 2017). In order to test the existence of two or more morphotypes, we plotted vertebral centrum length against the average elongation index (aEI, centrum length divided by the average or posterior cotyle height and width; Chure et al., 2010), using the four most complete cervical columns (mentioned above) for which these measures and ratios are available as comparison. Because centrum length and elongation were not taken into consideration when assessing serial variation (see above), plotting these two values provides an additional, independent assessment of the variability within the MDQ sample.

4.4. Results

4.4.1. Histological description of the ribs

In total, 19 histological samples were taken from 17 different dorsal ribs, representing the whole size range of anterior dorsal ribs found at MDQ. The maximum diameters of the sections vary between 17 mm and 37 mm and thus are very small compared to average-sized sauropod rib cross-section (Fig. 1).

All rib samples show a thick cortex and a relatively small medullary cavity filled with cancellous bone. In some thin sections, parts of these inner trabeculae are collapsed and compacted due to diagenesis. The intact nature of the bone surface is questionable. No sediment matrix is preserved at the surface of the bone; thus, slight surface damages due to preburial processes or preparation cannot be excluded. The thickest part of the cortex is located at the posteromedial side. Here, the lowest remodeling rate can be observed contrary to the anterolateral side where the strongest remodeling occurs. The primary bone tissue consists of lamellar zonal bone and shows clearly developed LAGs. Most of the vascular canals are oriented longitudinally. Sections CMC VP 8027, CMC VP 10059, CMC VP 10667, and CMC VP 14893 show extremely vascularized bone tissue with at most one to two LAGs preserved, indicating a juvenile ontogenetic stage for these individuals. In these aforementioned sections, the amount of Sharpey´s fibers is very low and no remodeling can be observed (Fig. 2). Section CMC VP 14293 shows well vascularized bone tissue with 5-6

LAGs preserved. In contrast, sections CMC VP 8020, CMC VP 8038, CMC VP 8991, CMC VP 9930, CMC VP 9932, CMC VP 9935, CMC VP 9956, CMC VP 9977, and CMC VP 10666 show a clearly developed EFS and 12 to 23 preserved LAGs, which represent about 50 to 73% of the growth record in most cases (Fig. 3 and 4).

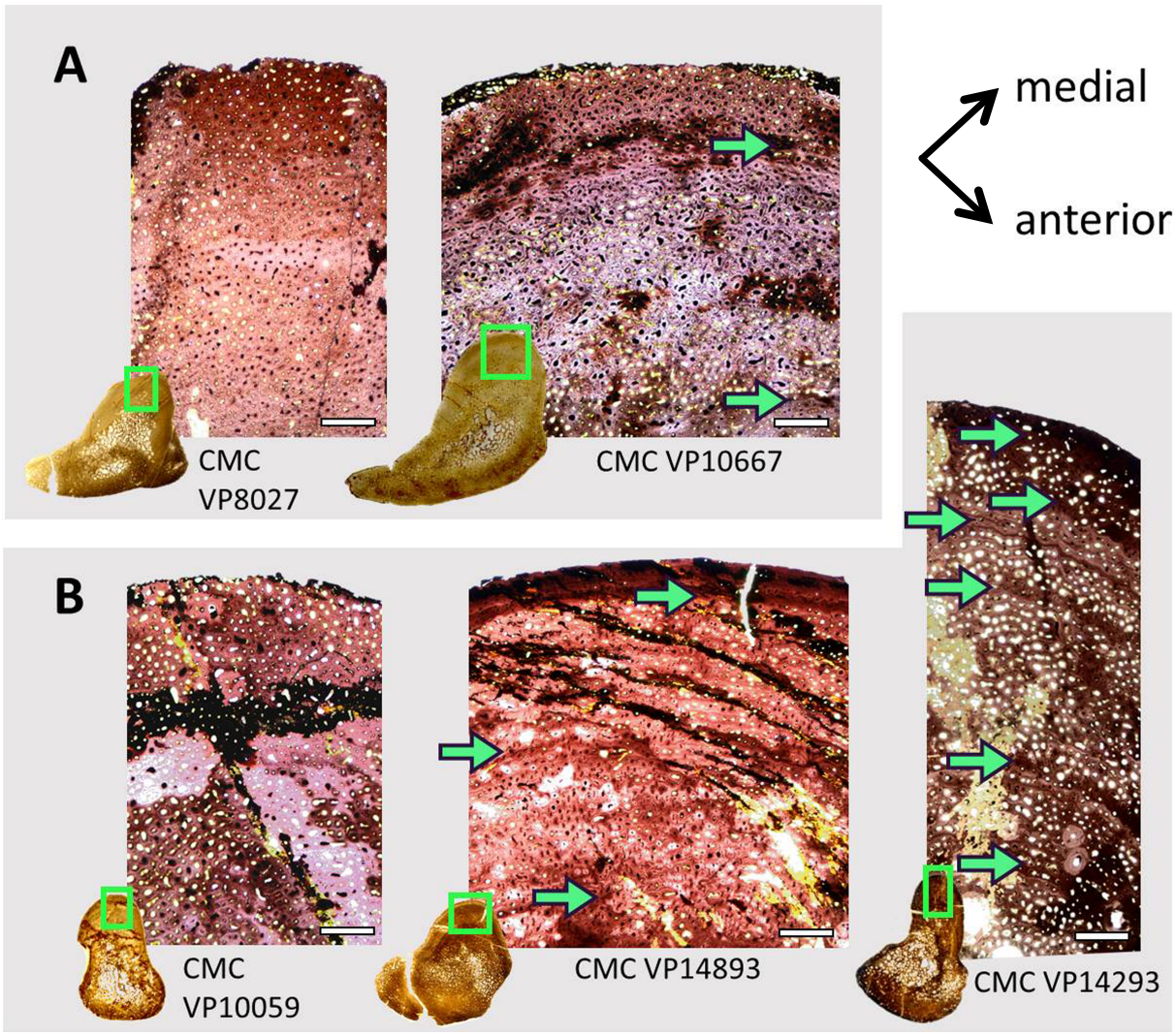

Fig. 2: Histological cross sections (polarized light) of the dorsal ribs of the MDQ diplodocines showing juvenile bone tissue of a relatively early ontogenetic stage. Scan of the complete cross section in the lower left corner. Histological picture representing the thickest part of the cortex at the posteromedial side (area indicated by green boxes). Green arrows indicate LAGs. White scale bars equal 500µm. A: possible morphotype 1 (larger individuals), B: possible morphotype 2 (smaller individuals).

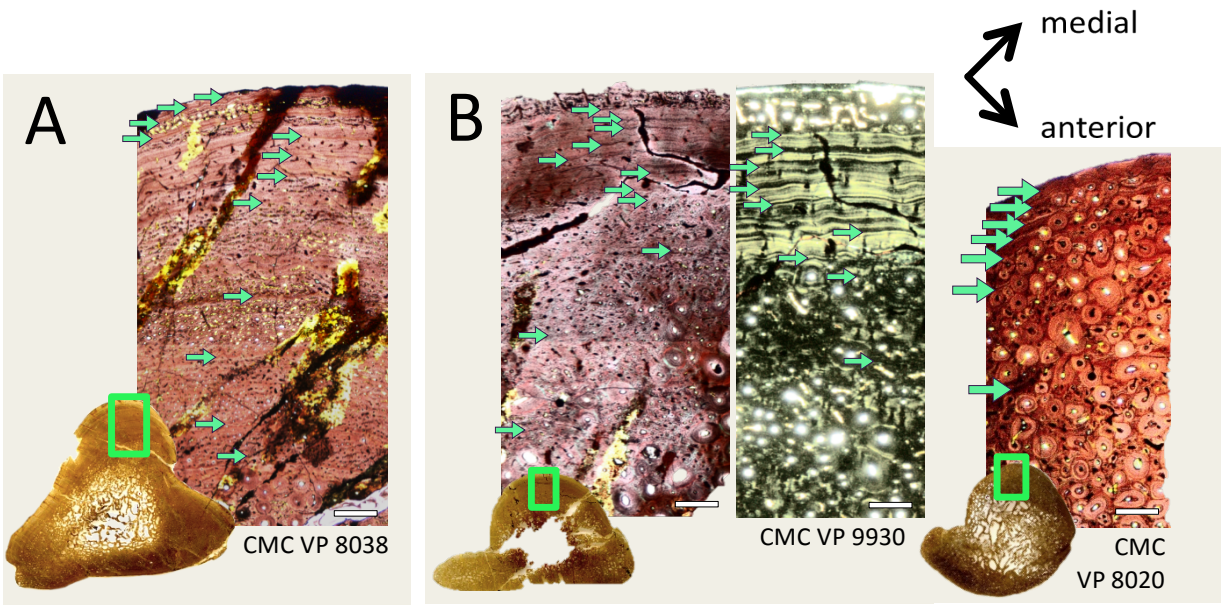

Fig. 3: Histological cross-sections of the dorsal ribs of the MDQ diplodocines showing a clearly developed EFS and stronger remodeled bone tissue indicating skeletal maturity. Scan of the complete cross-section in the lower left corner. Histological picture representing the thickest part of the cortex at the posteromedial side (area indicated by green boxes). Green arrows indicate LAGs. White scale bars equal 500 µm. **A**: Possible morphotype 1 (larger individuals). **B**: Possible morphotype 2 (smaller individuals). Enlarged Polarized picture of section CMC VP 9930 showing the EFS and pathological structure above in more detail.

In general, these sections are highly vascularized; however, the vascularization correlates inversely with the number of preserved LAGs (higher vascularization in sections with a lower LAG count vs. lower vascularization with higher LAG counts). In the sections preserving an EFS, the amount of Sharpey´s fibers is much higher. The direction of the fibers changes from parallel to the bone surface on the posteromedial side, to oblique to the surface anterolaterally. In some small areas (mostly occurring anterolaterally), fibers are only visible as small black spots because they are oriented perpendicular to the section (Fig. 4). The medullary region in most cases consists of Haversian bone tissue. The heaviest remodeled samples of this adult ontogenetic stage show a maximum of 2 to 3 generations of secondary osteons in the inner cortex, and the number of secondary osteons decreases towards the periosteal surface (Fig. 4). Sections CMC VP 9948, CMC VP 9962, and CMC VP 11339 all show the highest degree of Haversian tissue, with almost no primary bone tissue preserved within the cortex. Nevertheless, remains of an EFS are visible in all three samples. Small portions of primary bone material at the posteromedial side show LAGs and less developed vascularization. Some secondary osteons tracing the former LAGs allow a partial reconstruction of the growth record. In general, the size of the secondary osteons is very small (100-200 µm) and up to 4 generations of secondary osteons can be observed (Fig. 4).

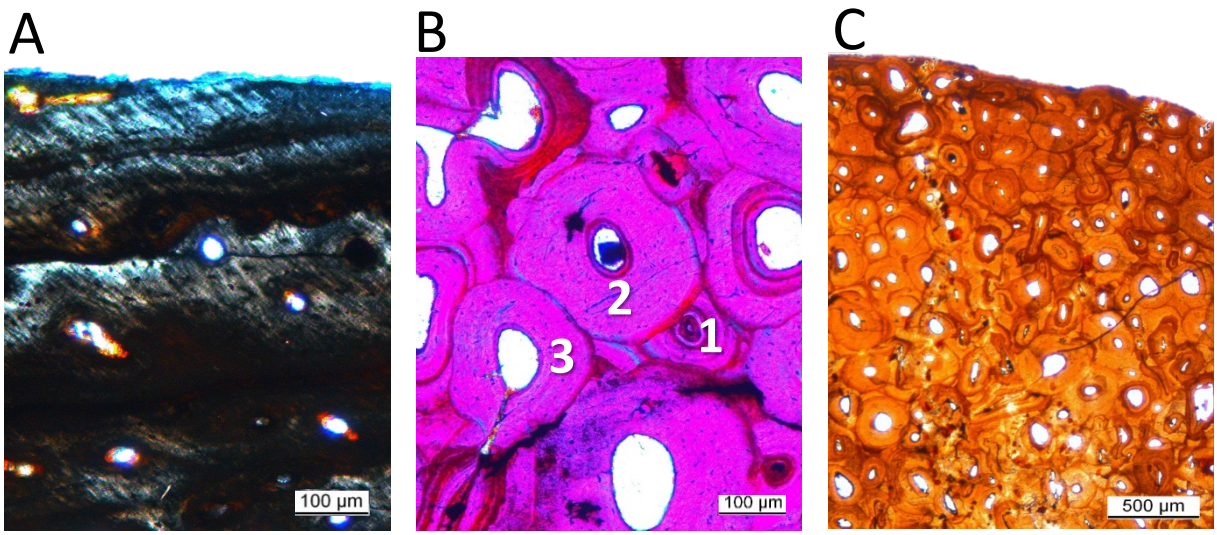

CMC VP 9935 CMC VP 8038 CMC VP 9962

Fig. 4: Histological cross-sections of the dorsal ribs of the MDQ diplodocines. **A**: Polarized light picture showing Sharpey´s fibers in the upper part of the cortex. **B**.: Stronger remodeled bone tissue of the inner cortex showing three generations of secondary osteons. Different generations of secondary osteons are numbered. **C**: Haversian bone tissue of the strongest remodeled sections.

4.4.2. Histological description of the long bones

In total, three humeri and five femora including the smallest and largest samples available were sampled by core drilling (the smallest humerus found at the site has not been sampled because it was prepared to go on display). The size of the sampled humeri ranges from 506 mm (CMC VP 14350) to 820 mm (CMC VP 10347) in length, the femoral length ranges from 595 mm (CMC VP 8661) to 1140 mm (CMC VP 14502). Almost all femora are strongly deformed. Most of them are crushed anteroposteriorly, some others in transverse direction. It cannot be excluded that the proximodistal length has been affected by deformation, impeding the erection of robustness indices. All sampled MDQ long bones exhibit a laminar to plexiform primary bone tissue also known as fibrolamellar bone (Sander et al., 2011; Padian and Lamm, 2013) in some cases interrupted by clearly developed LAGs- and well-developed primary and secondary osteons. The external bone surface seems to be intact (assuming there was no pre-burial damage) in most of the samples, which was corroborated by the presence of sedimentary matrix on the bone surface. The cortex is relatively thick compared to average-sized sauropods, and the medullary cavity is proportionally small, and composed of spongy bone trabeculae. Sharpey´s fibers are rarely observed at all. In all humeri and femora, the vascular canal orientation ranges from laminar to longitudinal; some rare reticular canals occur. The laminae are comparably thin at 6-8 lamina per mm. The clearly defined primary osteons are almost filled with laminar bone. Only sections CMC VP 10347 and CMC VP 15667 possess a nearly completely remodeled cortex with hardly any primary bone tissue visible, and thus these samples only exhibit remnant primary structures. Even if the primary bone is preserved, secondary osteons are present in every sample, mostly in the form of multiple generations of varying degrees

within the innermost cortex. In the femur CMC VP 8861, up to 30% of the cortex is remodeled, while in CMC VP 14004, up to 60% of the cortex is remodeled. Apart from sections taken from CMC VP 8057, CMC VP 10347, and CMC VP 14502, no growth marks can be observed. The femur CMC VP 14502 shows what is likely the formation of an EFS, which consists of three LAGs. In this sample the outer bone surface is compromised, thus the former presence of more outermost LAGs in the EFS cannot be excluded. Proceeding into the inner cortex, the EFS is preceded by seven clearly developed LAGs and two slightly obscured ones. In the innermost cortex, five additional incomplete cycles are visible. In total, the record cycle count for CMC VP 14502 is 17, representing approximately 48% of the individual growth record (Fig. 5). Although the femur CMC VP 8057 only possesses three observable LAGs, an EFS is present. In the humerus CMC VP 10347, even though the cortex is highly remodeled, 8 LAGs can still be observed. Additionally, this specimen possesses an unusual resorption zone in the outermost cortex; we attribute this oddity as being pathologic in origin, e.g., a callus (Fig. 3).

In average sized sauropods, the relative ontogenetic stage of the individual can be estimated using histologic ontogenetic stages (HOS) erected by Klein and Sander (2008), which are then correlated with biological ontogenetic stages (BOS) (Sander et al., 2011). Even if this classification might be not completely applicable to dwarfed species due to their slower growth (Sander et al., 2006; Mitchell et al., 2017), we here classify the long bone samples of the MDQ sauropods into HOS and BOS to erect relative ontogenetic stages for all sampled individuals (Table 1).

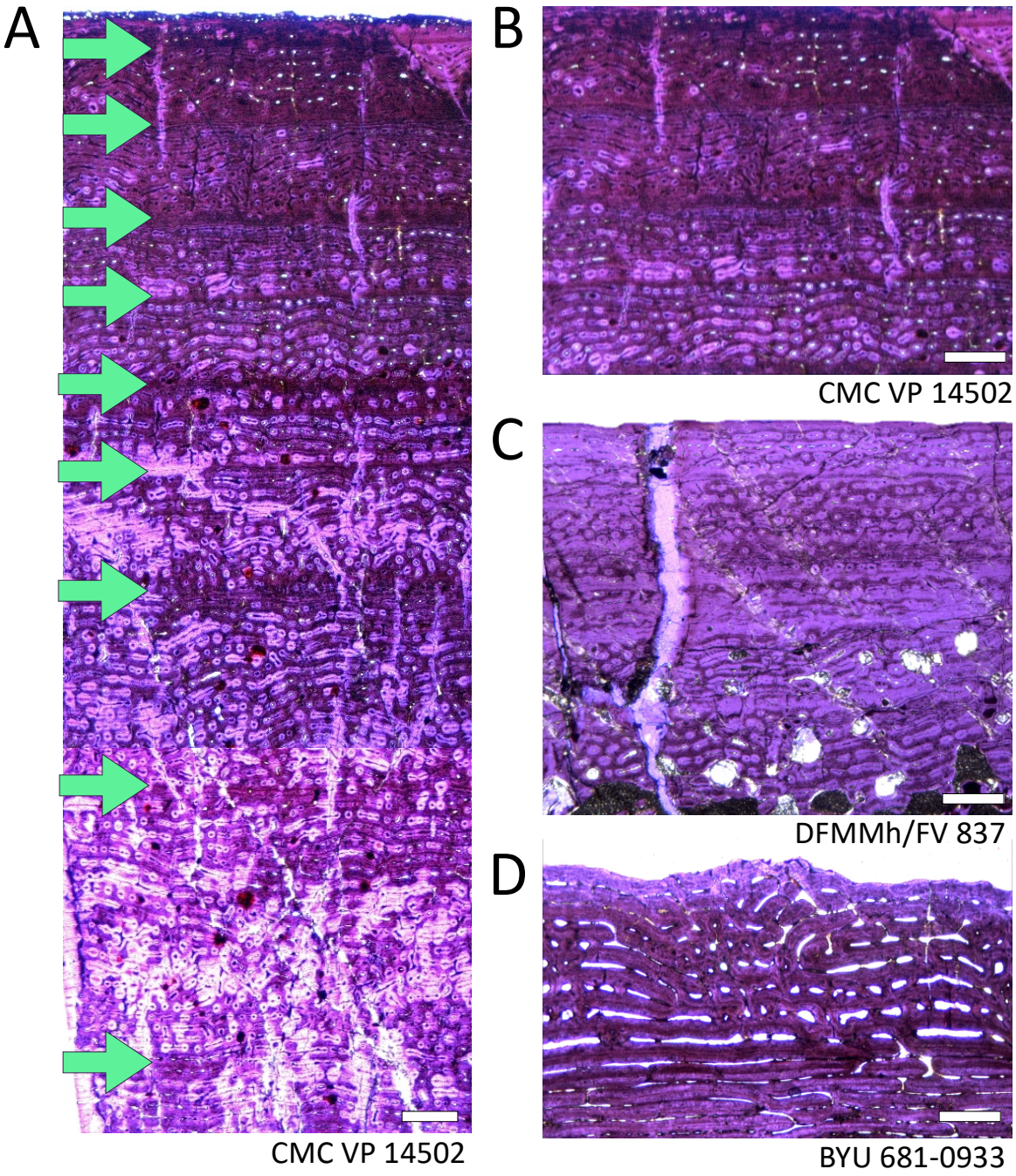

Fig. 5: Histological pictures (polarized light) of the long bones of the MDQ diplodocines in comparison to other dwarf and normal sized sauropods. White scale bars equal 500 µm. **A**: Thin section of femur CMC VP 14502 showing clearly developed LAGs indicated by green arrows and an EFS indicating skeletal maturity. **B**: Outer cortex of femur CMC VP 14502. **C**: Outer cortex of *Europasaurus* femur (DFMMh/FV 837). **D**: Outer cortex of a normal sized diplodocid (BYU 681-0933). Note the difference in lamina thickness.

Specimen	Sampled bone	Bone length (mm)	Bone circumference (mm)	Vascular canals	Primary osteons	Secondary osteons	HOS	BOS	LAGs	EFS
CMC VP14350	Humerus (l)	506	215	Laminar longitudinal	Almost completely filled	Dense in inner cortex	10	Adult I to Adult II	-	-
CMC VP14423	Humerus (l)	640	290	Laminar longitudinal	Almost completely filled	Dense in inner cortex	10	Adult I to Adult II	-	-
CMC VP13047	Humerus (l)	820	300	Laminar longitudinal	Almost completely filled	Dense, cortex completely remodeled	13	Adult III	-	-
CMC VP8861	Femur (l)	595	275	Laminar longitudinal	Almost completely filled	Relatively young, 30% of cortex is remodeled	9	Adult I	-	-
CMC VP14004	Femur (r)	920	400	Laminar longitudinal Some irregular	Dense in inner cortex, more open in outer cortex	Dense, 60% of cortex is remodeled	11	Adult II	-	-
CMC VP8057	Femur (r)	955	320	Longitudinal laminar	Completely filled	Only in innermost cortex	12	Adult II to Adult III	3	yes
CMC VP15667	Femur (r)	990	370	Laminar longitudinal	Almost completely filled	Dense, cortex completely remodeled	13	Adult III	-	-
CMC VP14502	Femur (r)	1140	400	Longitudinal laminar	Almost completely filled	Only in innermost cortex	10	Adult I to Adult II	7 clear, possibly 2 more	Possibly started
SMA 0015 David	Femur (l)	1340	-	Laminar longitudinal	Almost Completely filled	Only in innermost cortex	10	Adult I to Adult II	4	-

Table 1: List of the sampled sauropod long bones at the Cincinnati Museum Center with measurements of length and circumference, vascular orientation, primary and secondary osteons, HOS and BOS, LAGs, and the presence of an EFS. Note that the bone tissue type usually consists of two letters: the first one representing the main bone tissue type that is present in the cortex, and the second one only within the innermost or outermost cortex. Bone length is here defined as the largest proximal-distal distance within each bone. Note that the circumference measurements were taken while the bones were partially covered by plaster jackets. For comparison, measurements and histological features of an average sized sauropod femur (SMA 0015 nicknamed `David´) are given as well.

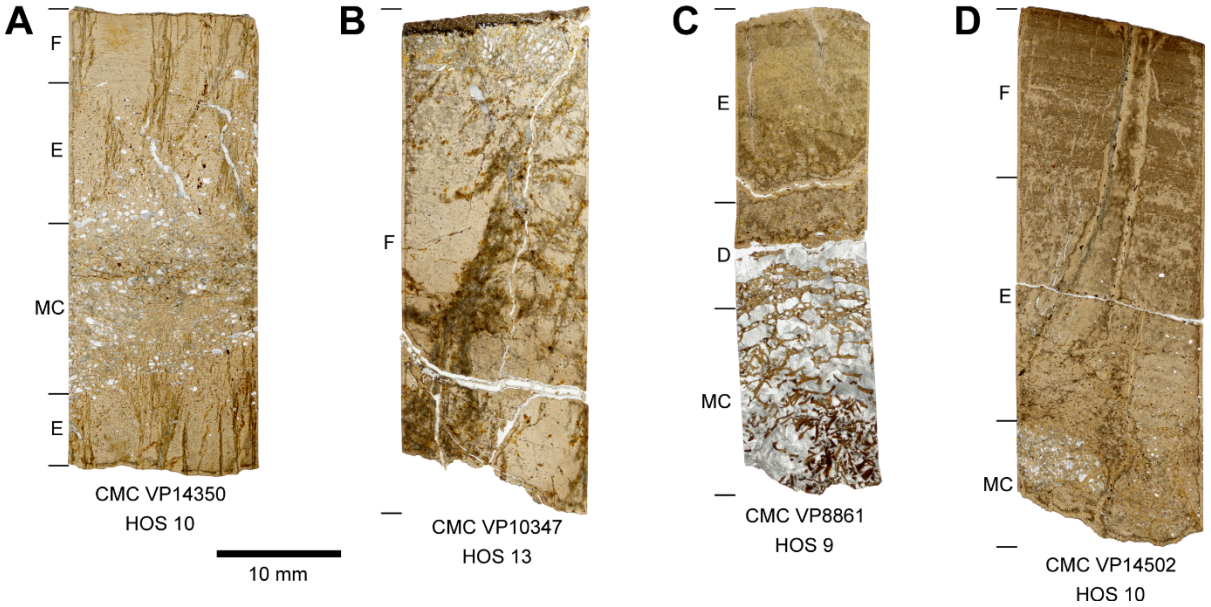

Fig. 6: High resolution scans of thin sections showing the different ontogenetic stages of **A**: the histologically youngest and **B**: oldest humerus of the MDQ diplodocid sample. **C**: The histologically youngest and **D**: oldest femur of the MDQ diplodocid sample. For all samples, the bone tissue types (Klein and Sander, 2008) are indicated to the left, and the histological ontogenetic stages (Klein and Sander, 2008) below. Abbreviations: MC: Medullary cavity. Scale bar equals 10 mm.

Humeri CMC VP 14350 and CMC VP 14423 both primarily exhibit bone tissue type E with bone tissue type F laid down in the outer cortex. This correlates to HOS 10 and BOS Adult I to Adult II. The humerus CMC VP 10347 shows entirely Haversian bone tissue, which is bone tissue type G, and correlates with HOS 13 and BOS Adult III. Femur CMC VP 8861 is the smallest femur sample and shows primarily bone tissue type E with tissue type D laid down in the inner cortex, indicating HOS 9 and BOS Adult I (Fig. 6). The second smallest femur, CMC VP 14004, primarily possesses bone tissue type E with tissue type F present in the outer cortex. This correlates to HOS 11 and BOS Adult II. The femur CMC VP 8057 consists only of bone tissue type F and possesses an EFS, denoting HOS 12 and BOS Adult II to Adult III. The second largest femur, CMC VP 15667, like humerus CMC VP 10347, shows entirely Haversian bone and is therefore HOS 13 and BOS Adult III. The femur CMC VP 14502 is the largest femur in the sample and consists of primarily bone tissue type E with tissue type F laid down in the outer cortex, which correlates with HOS 10 and BOS Adult I to Adult II.

4.4.3. Morphological reassessment of the MDQ material

Based on the histological results the morphology of the material was analyzed again, especially regarding features relevant for individual ontogenetic age and size, as well as taxonomic assignment.

4.4.3.1. Skull

Among the five partial skulls, four (CMC VP 8061, CMC VP 8724, CMC VP 14073, and CMC VP 14129) share features with *Kaatedocus siberi*. These include 1) a well-developed,

narrow sagittal nuchal crest on the supraoccipital; 2) a high ratio of basal tubera width to occipital condyle width; 3) dorsoventrally expanded distal ends of the paroccipital processes, which also bear an oblique ridge extending from dorsomedial to ventrolateral; and 4) the presence of a bony shelf that connects the bases of the basipterygoid processes (Fig. 7) Tschopp and Mateus, 2013; Tschopp et al., 2015). However, one of these specimens (CMC VP 14073) has transversely concave posterior surfaces of the basal tubera, whereas this surface is generally flat to slightly convex in *Kaatedocus* (Tschopp and Mateus, 2013; Tschopp et al., 2015). A fifth, more complete skull (CMC VP 14128; currently being described by Woodruff et al., 2018, (chapter 5)) has a less developed sagittal nuchal crest compared to *Kaatedocus* but shares with the latter the presence of a lateral projection on the dorsal end of the lacrimal, and an anteroposteriorly long frontal, so that the prefrontal does not approach the parietal in dorsal view. Additionally, this skull has a tapered and long anterior process of the squamosal – the opposite of what was reported as an autapomorphy of *Kaatedocus* (Tschopp and Mateus, 2013; Woodruff et al., 2018, (chapter 5)). Therefore, while expressing some morphologies in common with *Kaatedocus*, CMC VP 14128 likely does not belong to this genus.

4.4.3.2. Vertebrae

Based on morphological features that have not been reported to be influenced by serial or ontogenetic variation to date, two morphotypes could be identified among the cervical vertebrae from Mother's Day Quarry. Generally, middle to posterior cervical centra have pneumatic foramina that are subdivided into an anterior and a posterior pneumatic fossa. This subdivision can be incipient (in the smallest specimens), formed by a distinct, narrow lamina extending from anterodorsal to posteroventral, or a relatively wide bony shelf, which has an anteroposterior length that is only slightly shorter than the two fossae it separates (Fig. 7). The subdivision of the pneumatic foramina into two or more subfossae occurs during ontogeny (Wedel, 2003; Carballido and Sander, 2014; Woodruff et al., 2017), so that the small vertebrae with an incipient subdivision are most likely juvenile individuals. However, the difference in morphology of the subdivision in larger vertebrae (i.e. the lamina or the bony shelf) does not depend on vertebral elongation or size, indicating that two different morphs exist among the material. In order to test this further, we plotted cervical vertebral centrum length against the average elongation index (aEI, Fig. 8).

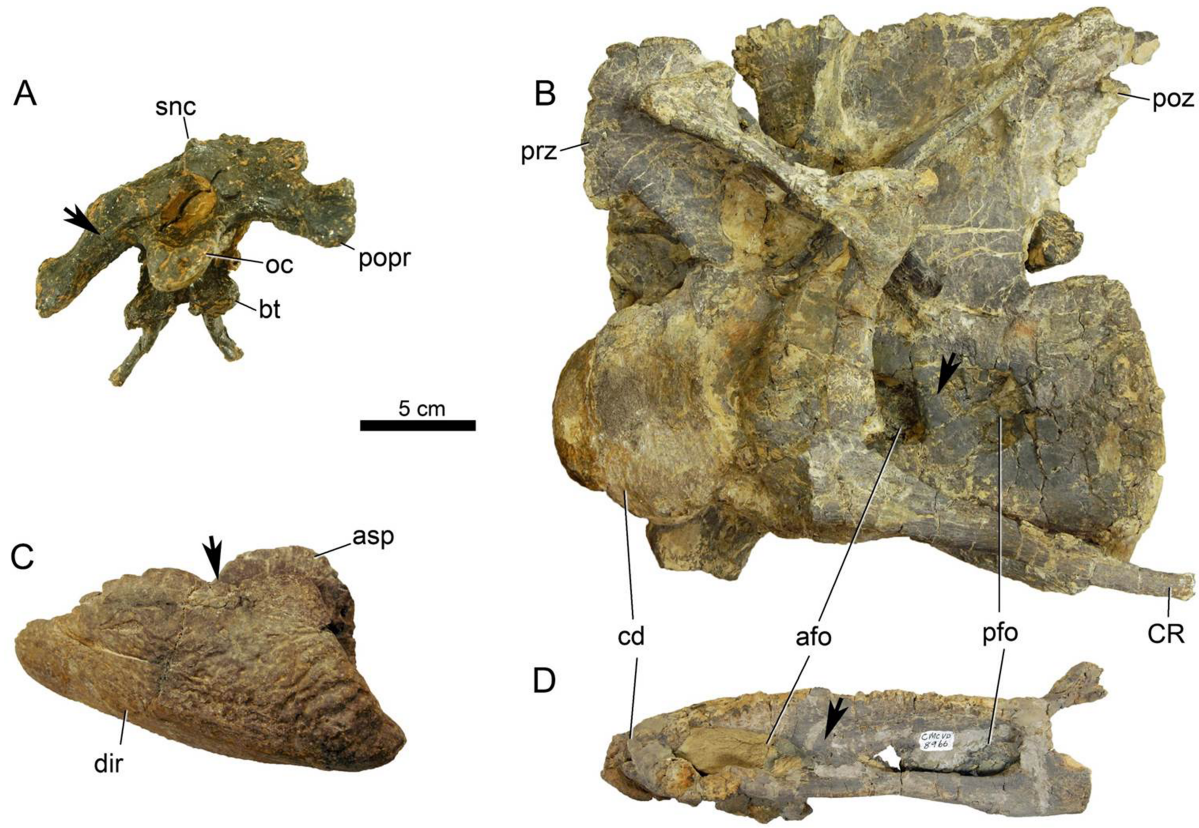

Fig. 7: Morphological evidence for systematic assignment and the presence of two morphotypes among the Mother's Day Quarry diplodocines. **A**: The braincase (CMC VP 14129) has a narrow, distinct sagittal nuchal crest, wide basal tubera compared to the occipital condyle, and a ridge on the posterior surface of the paroccipital processes (arrow), similar to *Kaatedocus siberi*. **B**: The cervical vertebrae (**B**: CMC VP 9766, **D**: CMC VP 8966) show distinct patterns of pleurocoel subdivision into anterior and posterior pneumatic fossae, which can be separated by a lamina (arrow in B) or a wide bony shelf (arrow in D). **C**: Some (but not all) astragali show a groove on the dorsal surface of the ascending process, which becomes more pronounced towards the distal roller (arrow in C). Note that the neural spine is incomplete in B, and that CMC VP 8966 (D) has an open neurocentral synchondrosis. All elements scaled to same length. Scale bar equals 5 cm. Abb.: afo, anterior pneumatic fossa; asp, ascending process; bt, basal tubera; cd, condyle; CR, cervical rib; dir, distal roller; oc, occipital condyle; pfo, posterior pneumatic fossa; popr, paroccipital process; poz, postzygapophysis; prz, prezygapophysis; snc, sagittal nuchal crest.

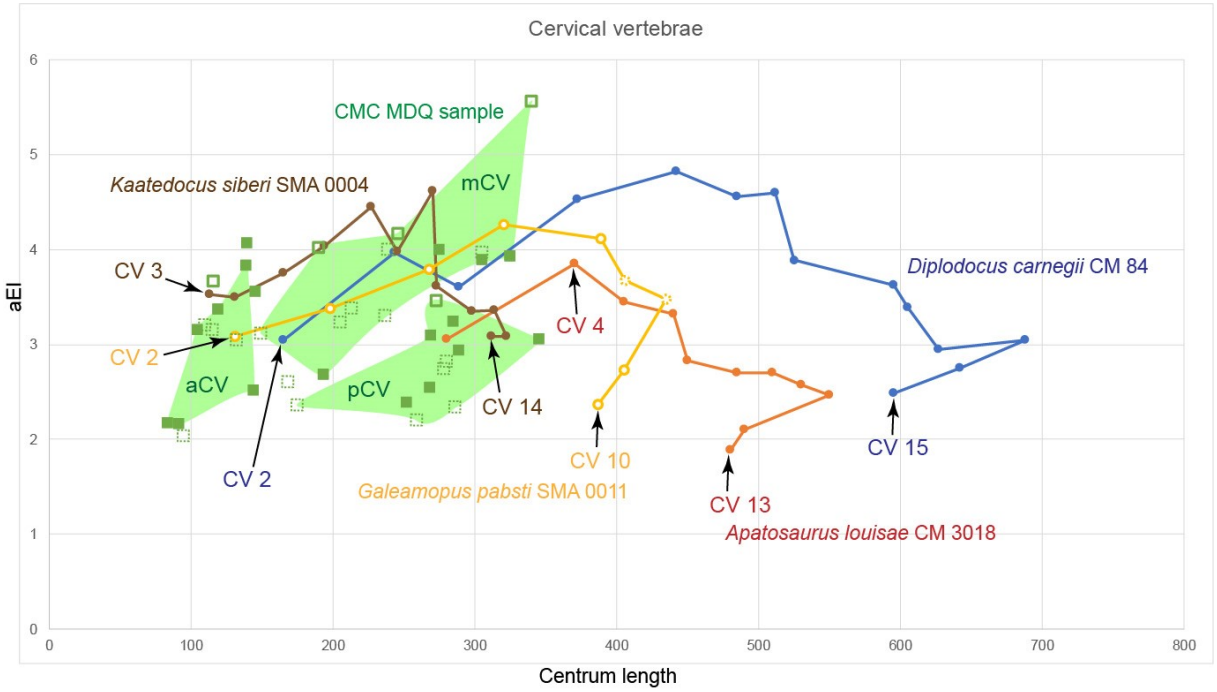

Fig. 8: Cervical vertebral ratios in diplodocine sauropods. The sample of elements from the Mother's Day Quarry (MDQ; green squares) is plotted together with four diplodocine specimens with nearly complete, articulated necks (connected brown, blue, yellow, and red dots). Dotted and closed squares/circles represent elements with open or closed neurocentral synchondroses, whereas filled squares/dots represent elements with fused neurocentral synostoses. The light green areas connect MDQ elements that could be clearly attributed to anterior (aCV), middle (mCV), or posterior cervical vertebrae (pCV) based on morphological features explained in the text. Elements lying outside these areas could not be unambiguously attributed to a single cervical subregion. Note the generally similar shape of the curves, and the rather random distribution of open, closed and fused elements within the MDQ sample. Data of reported diplodocine specimens taken from Hatcher (1901: CM 84), Gilmore (1936: CM 3018), Tschopp and Mateus (2013: SMA 0004; and 2017: SMA 0011).

Of the four known genera plotted together with the MDQ sample, the general distribution of the MDQ cervical vertebrae resembles most the sequence of *Kaatedocus siberi* SMA 0004. However, the MDQ sample shows a very large variation in aEI, which exceeds the one between the four plotted genera. This variability can hardly be explained by ontogenetic changes, because elements with open, closed, and fused neurocentral synchondroses and -ostoses scatter across the entire range of centrum lengths and aEI. Thus, it seems more plausible to explain the variability through the presence of at least two distinct morphotypes. These morphotypes can be mostly distinguished by vertebral centrum elongation, rather than by size. In contrast, the dorsal vertebrae show an inverse correlation of size and neurocentral fusion: the largest elements have open neurocentral synchondroses, whereas the fused elements are generally smaller (Supplementary Tab. 1).

4.4.3.3. Other postcranial skeletal elements

The long bones of the MDQ diplodocines (especially humeri and femora) vary in overall robustness (Supplementary Tab. 2) supporting the presence of two different morphotypes. Variations in the astragali additionally underline skeletal differences of

different individuals within the assemblage. Some astragali show a groove with a distinctly concave posteroventral edge of the ascending process (e.g., CMC VP 7994; Fig. 7), as present in *Galeamopus pabsti* (Tschopp and Mateus, 2017), which is missing in other specimens (e.g., CMC VP 7037; E. Tschopp, pers. obs. 2017).

4.5. Discussion

Based on the Mazzetta et al. (2004) equation using femur length, the MDQ diplodocines range in mass between 991.9 and 3,001.4 kg, which is far less than estimates for normal-sized sauropods, reaching masses several times heavier, such as 6153.4 kg for *Diplodocus carnegii* (CM 84) (Colbert, 1962; Henderson, 1999; Gunga et al., 2008; Stoinski et al., 2011; Woodruff et al., 2017). Based on the histology and morphology data described above, the MDQ material includes several skeletally mature animals, contrary to what has been reported before (Myers and Storrs, 2007; Storrs et al., 2007; Myers and Fiorillo, 2009; Woodruff and Fowler, 2012). In a previous study by Woodruff et al. (2017), the histology of some of the MDQ diplodocines (strictly the MOR material) was analyzed, revealing a juvenile ontogenetic stage of the sampled specimens ranging from 2 to 7 years of age. Although seeming to indicate an immature assemblage, the samples of Woodruff et al. (2017) also exhibited bone tissue morphologies of normal-sized sauropods. These results, contrary to this study, were not in conflict with the previous interpretations that the MDQ consists exclusively of normal-sized juvenile individuals. However, the differing results between the two histological studies could be explained by a combination of smaller sample size (four, from dorsal ribs and femora (Woodruff et al., 2017) vs. 27, from dorsal ribs, femora and humeri (this analysis)) and/or the presence of different taxa or size morphs within the MDQ locality (see below). The following chapters describe the single lines of evidence for this in more detail.

4.5.1. Implications of the histology

Due to the differing growth records, most of the dorsal rib samples likely represent different individuals rather than different bones of the same individual (Fig. 9). Only sections CMC VP 8991, CMC VP 9932, CMC VP 9935, and CMC VP 10666 may represent the same individual based on their size, similar histology, and overlapping growth records (Fig. 10). As shown in previous studies (Waskow and Sander, 2014; Wiersma et al., in review) such an assignment based on histology is possible and reliable. In general, the histology of the sampled dorsal rib material differs greatly from what was expected. Instead of typical juvenile bone, a majority of the samples show an EFS, indicating skeletal maturity (Sander, 2000; Erickson, 2005; Waskow and Mateus, 2017, (chapter 2); Fig. 3). Up to 23 LAGs representing up to 73% of the growth record are preserved within single dorsal ribs, also indicating an older individual age for most of the specimens (Fig. 9). The single growth records will be discussed in more detail below. The decrease in vascularization and the

increasing number of Sharpey´s fibers also hints at an older ontogenetic age in most of the specimens (Klein and Sander, 2008; Chinsamy-Turan, 2005). The remodeling rate, as well as the overall histology of the samples exhibiting an EFS is comparable to what has been previously described for dorsal ribs of skeletally mature sauropods (Waskow and Sander, 2014). Additionally, some samples – consisting nearly exclusively of Haversian bone – show an even more derived stage of bone remodeling and are thus indicative for a senescent individual age. Histology thus reveals the presence of a small sauropod taxon within North America during the Late Jurassic.

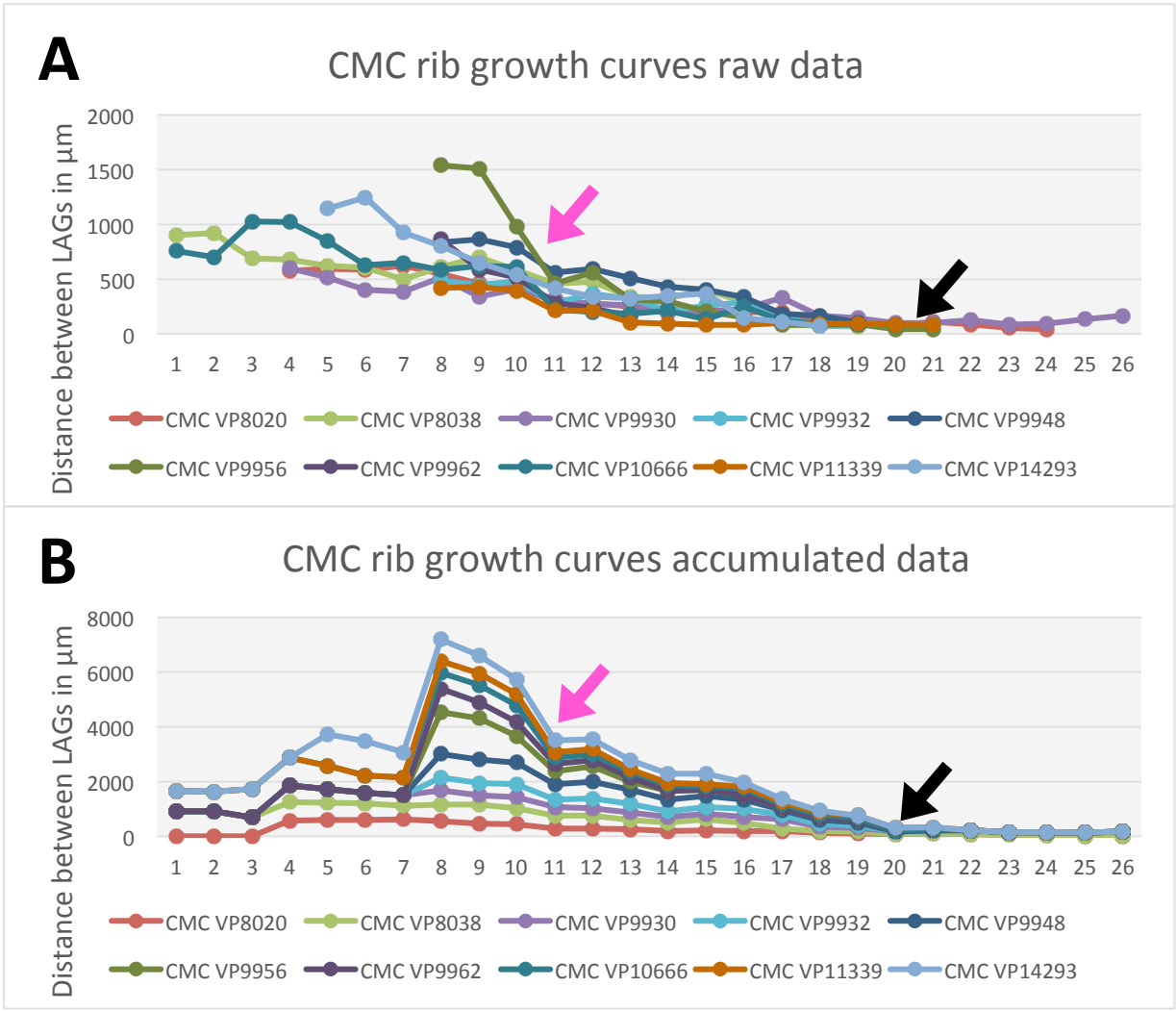

Fig. 9: Growth curves based on the record preserved in the dorsal ribs of the MDQ diplodocines. Purple arrows indicate point of sexual maturity, black arrows indicate point of skeletal maturity. **A**: Raw data graph showing the measured distances between the single LAGs. **B**: Accumulation of measured distances. Note that the flattening at the beginning of the curve is not significant because it is caused by missing inner cycles, and thus missing data points in the innermost cortex.

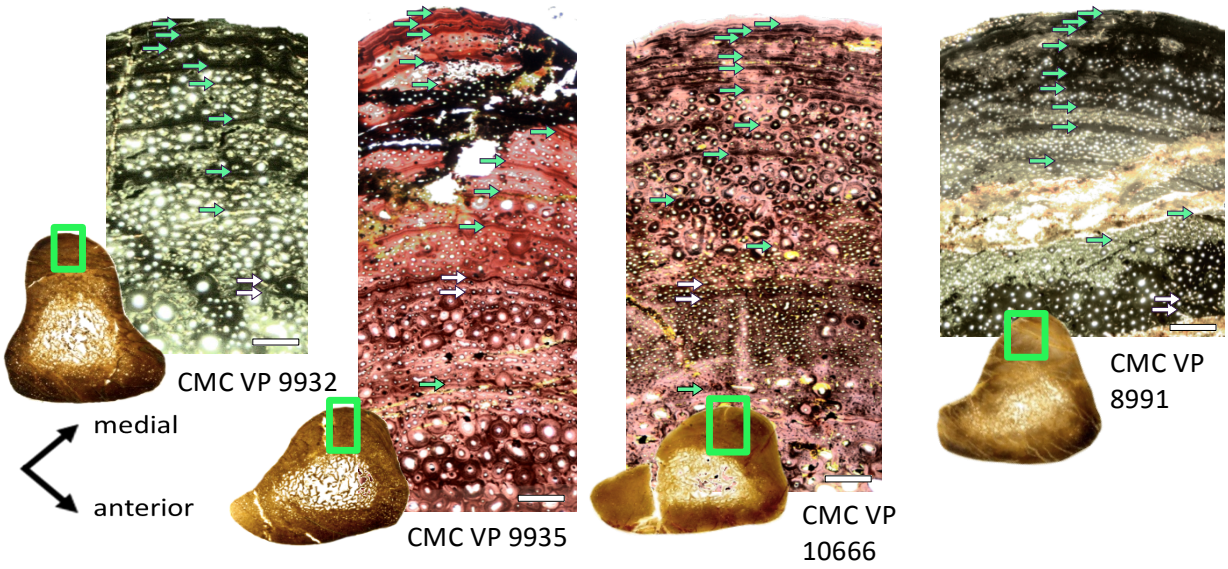

Fig. 10: Histological comparison of four different dorsal ribs representing most likely the same MDQ diplodocine individual (polarized light pictures) underlining the significance of histology as a tool for testing rib affiliation to one or several individuals. Note the similarities in bone tissue type and growth record between the different sections. Green boxes indicate picture area. Green arrows indicate LAGs. White scale bars equal 500 µm. The distinctive double LAGs are marked with white arrows in each slide. Scan of the complete cross-section in the lower left corner.

Nevertheless, at least some samples show a highly vascularized bone structure with fewer LAGs, typical for juveniles (Fig. 2). Surprisingly, the size of these samples is approximately the same (in some cases even larger) compared to samples exhibiting an EFS, indicating the existence of two size morphs. The comparison of maximum cortical thickness with RHOS reveals a poor correlation of age with body size. This further corroborates the existence several size morphs (Fig. 11). However, because the exact position of the sampled ribs within the rib cage is not known, more statistical analysis is needed to verify this assumption histologically. The long bone histology of the MDQ diplodocines supports the existence of a dwarf taxon, showing a much more mature primary bone tissue than what would be expected in a juvenile. These specimens additionally show a remodeling rate typical for adult individuals indicating an older ontogenetic age for these specimens (Table 1). However, a good correlation between relative HOS and bone length (deducing body size) is lacking, supporting the existence of at least two different size morphs (Fig. 12). The humeri were plotted to their corresponding femur length based on ratios found in the literature (Janensch, 1961; McIntosh, 1990; Remes, 2006; Klein and Sander, 2008). Note that most of the CMC specimens plot below the other diplodocines. The lack of a tight correlation between HOS and bone length supports the existence of different morphotypes in the CMC sample. However, sample size is too small to reveal a clear pattern.

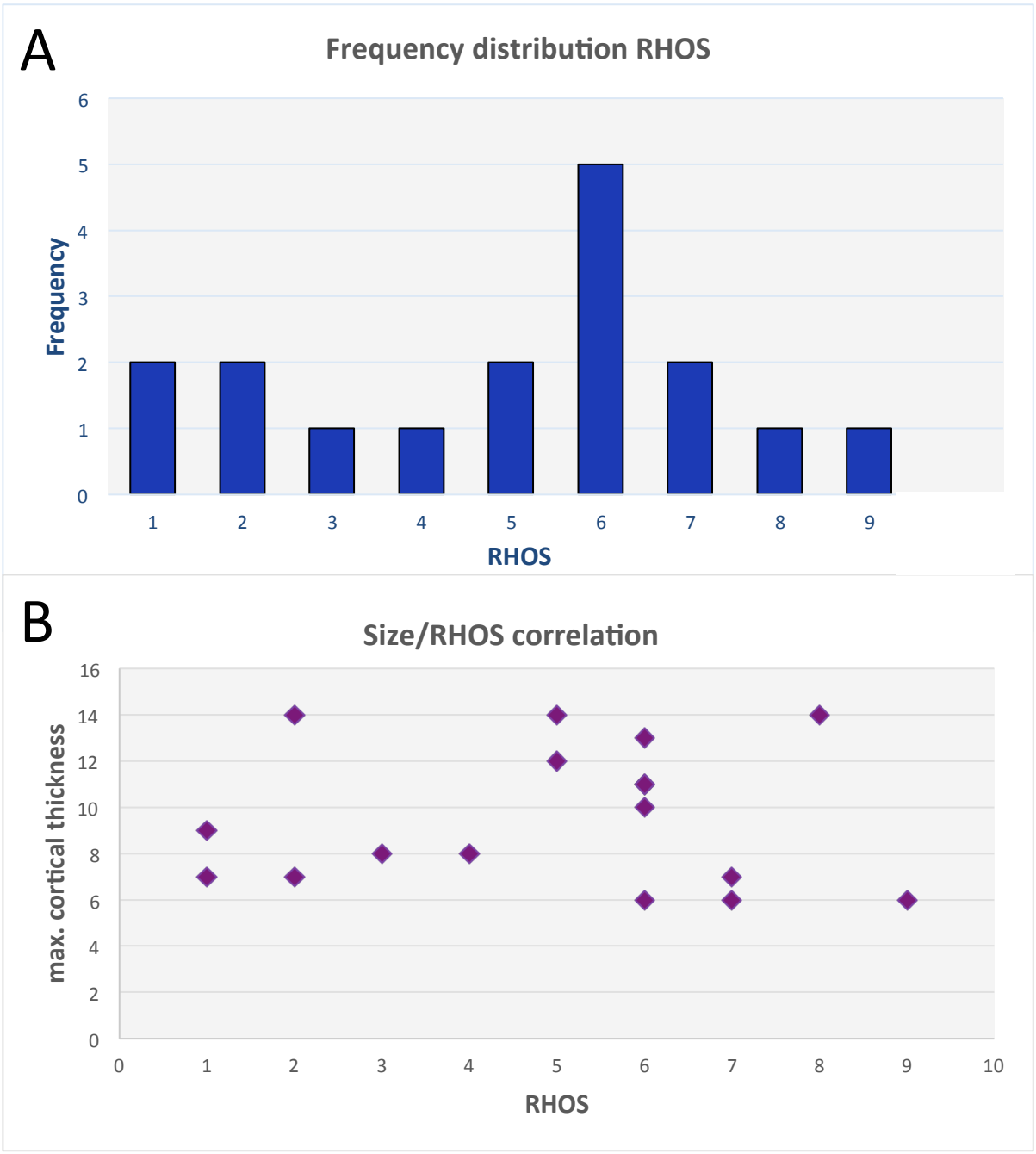

Fig. 11: Comparison of the different rib histological ontogenetic stages (RHOS) observed in the dorsal rib cross-sections of the MDQ diplodocines. **A**: Frequency distribution, indicating a catastrophic event as mortality cause (majority of adult individuals; very few juveniles and senescent specimens). **B**: Maximal cortical thickness measured at the posteromedial side of the rib (size/age correlation) indicating the presence of several size morphs.

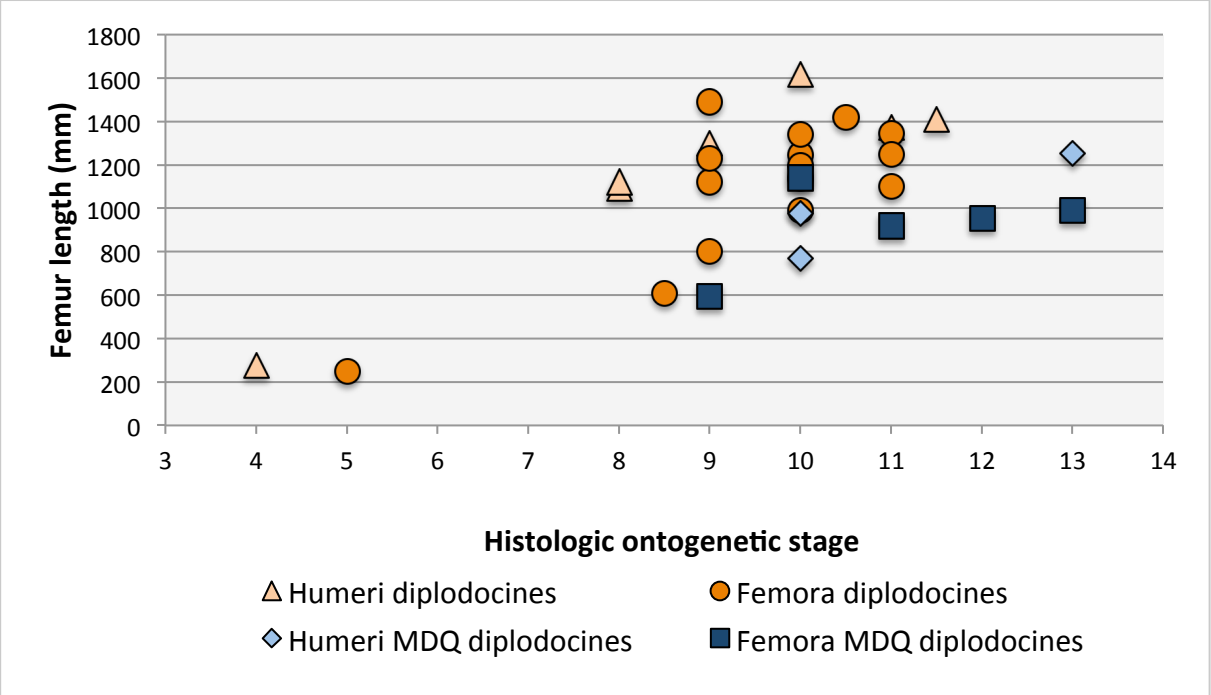

Fig. 12: Histologic ontogenetic stage (HOS) vs. femur length correlation of average-sized diplodocines and MDQ diplodocine samples. Orange triangles represent normal-sized diplodocine humeri, red dots represent average-sized diplodocine femora. Light blue diamonds represent CMC humeri, dark blue squares represent CMC femora. Note that humeri were calculated to their corresponding femur length based on ratios found in the literature (Janensch, 1961; McIntosh, 1990; Remes, 2006; Klein and Sander, 2008). HOS stages 1 and 2 were not included in this diagram since they are lacking in this sample. Note that most of the CMC specimens plot below the other diplodocines. The lack of a tight correlation between HOS and bone length supports the existence of different morphotypes in the MDQ sample. However, due to the small sample size, a clear pattern cannot be recognized.

4.5.2. Comparison of long bone tissue types of normal-sized and dwarfed sauropods

The bone microstructure of dwarfed sauropod long bones differs from the one that has been observed in normal-sized sauropods (Sander et al., 2006; Stein et al., 2010). In contrast to larger-sized sauropods that grew too quickly to produce LAGs in their long bones that have the highest bone apposition rates of all skeletal elements due to their large diameter (Klein and Sander, 2008; Sander et al., 2011), some long bones of the MDQ sauropods show a remarkably complete growth record, with up to an estimated 48% preservation (CMC VP 14502). The presence of LAGs in these specimens indicate seasonal growth, opposed to what has been observed in average-sized sauropods. A similar growth record has also been observed in *Europasaurus holgeri* (Sander et al., 2006; Cerisara, 2017). In both taxa (*Europasaurus* and the MDQ diplodocines), the relative ontogenetic age that would be estimated based on the primary bone tissue differs from the one that is indicated by the remodeling rate within the same sample. The primary bone is usually comprised of an ontogenetically more mature bone tissue type, whereas the remodeling front would indicate a younger individual. The difference between the dwarfed species, however, is the thickness of the cortex in general. Whereas *Europasaurus* has a relatively thin cortex compared to

normal-sized sauropods, the MDQ diplodocines show a relative cortical thickness comparable to average-sized sauropods.

There is also a distinctive difference in lamina thickness between normal-sized sauropods and dwarfs. In *Europasaurus* and the MDQ diplodocines the lamina density is approximately 6-8 lamina per mm (Fig. 5). Even if it has not been stated by the authors within the text, this difference already occurs in the literature (Hofmann et al., 2014) with the lamina density of *Europasaurus* (6-7 lamina/mm) being higher than the lamina density of other macronarians such as *Giraffatitan* (listed as *Brachiosaurus* in Hofmann et al., 2014) and *Camarasaurus* (4-5 lamina/mm). As the study of Stein and Prondvai (2014) suggests, the primary indicator of high bone growth rates is vascular density and/or porosity, which in turn might be directly linked to lamina thickness (Hofmann et al., 2014). Thus, the reduction of lamina thickness might indicate a reduction of the growth rate. The secondary remodeling of the MDQ sauropod long bones again shows a considerable similarity to that of *Europasaurus*. The remodeling rate of the dwarfs, represented by the second front in the three-front model of Mitchell and Sander (2014), seems to differ from their larger counterparts. Whereas the long bones of the MDQ sauropods studied here show a slower remodeling rate similar to *Europasaurus* (Cerisara, 2017), the remodeling rate of *Magyarosaurus dacus* seems to be increased. This Romanian dwarf taxon shows exclusively Haversian bone tissue even in relatively early ontogenetic stages. Stein et al. (2010) explained this unusually high remodeling rate as an effect of phyletic dwarfism. This indicates that the HOS described by Klein and Sander (2008) cannot be applied to the long bones of dwarfed sauropods and new HOS stages for dwarfed species should be created (Cerisara, 2017).

4.5.3. Growth record analysis

Most of the sampled dorsal ribs and at least one of the long bone samples show a remarkably complete growth record that can be analyzed in terms of sexual and skeletal maturity (Fig. 9, 13) as previously shown (Waskow and Sander, 2014; Waskow and Mateus, 2017, (chapter 2). When including the estimated number of missing growth cycles (based on retro-calculation), the estimated age of sexual maturity ranges between 10 and 13 years of age. The graphs indicate, that sexual maturity was reached well before skeletal maturity, specifically at about 50% of the growth time and about 75% of final size. This has been shown by other analyses for extant (Lance, 2003) and extinct animals (Erickson et al., 2007; Griebeler et al., 2013; Waskow and Sander, 2014; Tschopp and Mateus, 2017; Waskow and Mateus, 2017, (chapter 2)). In the MDQ diplodocines skeletal maturity was reached approximately 7 to 10 years later than sexual maturity at an age between 16 and 18 years, indicated by the beginning of the EFS (age at sexual maturity excludes LAGs of the EFS). This is similar but not equal to the findings of Waskow and Sander (2014) and Woodruff and Foster (2017), who estimated slightly older ages at sexual- and skeletal maturity for

Camarasaurus sp. individuals based on dorsal rib histology. The morphologic change in ribs during ontogeny, influenced by bone apposition rate, thus far impedes the analysis of the age of maximum growth. However, by virtue of its almost circular cross-section, the femur CMC VP 14502, shows the best-preserved long bone growth record (Fig. 5, 13). From retro-calculation, 3 to 4 innermost cycles are estimated to be missing in this femur. This implies an age of sexual maturity of 11 to 13, years and an age of skeletal maturity of 18 to 19 years corresponding well with the data observed in the dorsal rib growth record.

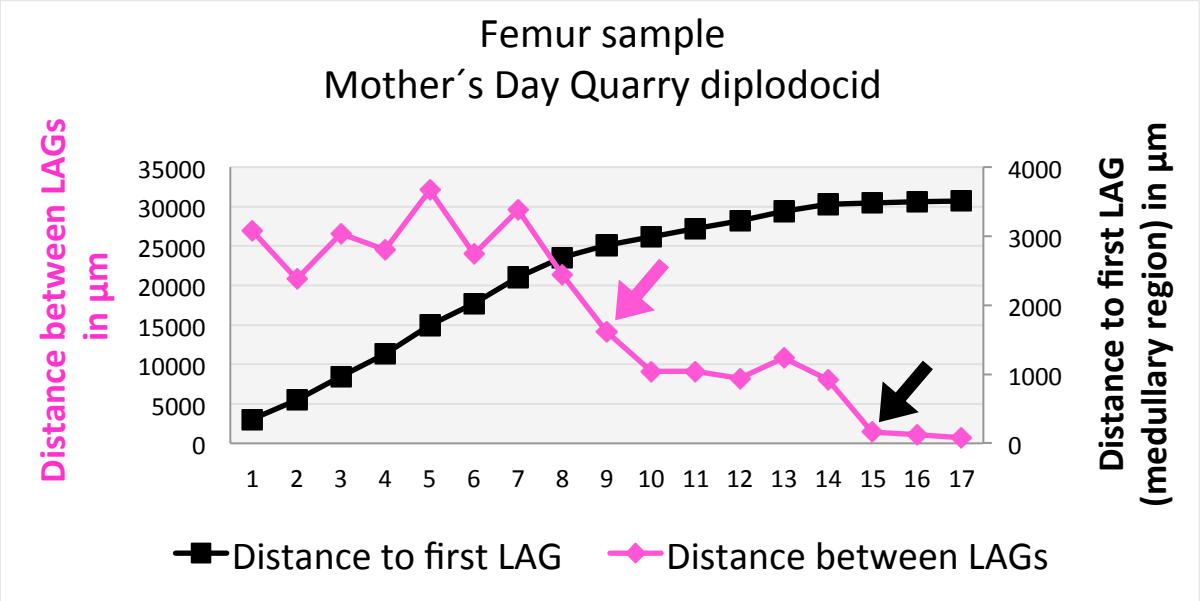

Fig. 13: Growth curve based on growth record preservation in the femur sample CMC VP 14502 of the MDQ diplodocines. Purple arrow indicates point of sexual maturity, black arrow indicates point of skeletal maturity.

4.5.4. Different size morphs

Histologic ontogenetic staging of the dwarfed sauropods based on both dorsal ribs and long bones, reveals a poor correlation with body size (Fig. 11). This indicates the existence of at least two different size morphs. Based on the variability in rib thickness along the ribcage and the uncertainties concerning the position within the ribcage of the single samples these findings are indicative but more statistical analysis is needed to verify them histologically. Further evidence for two distinct size morphs comes from the dorsal vertebrae. Diplodocoid dorsal vertebrae do not significantly change in size and elongation along the column, apart from the anterior-most dorsal vertebral centra (see, e.g., Hatcher, 1901; Gilmore, 1936; McIntosh, 2005). Among the MDQ dorsal vertebrae, size is inversely correlated with neurocentral fusion: the largest elements have open neurocentral synchondroses, whereas the fused elements are generally smaller (Supplementary Tab. 2). All these differences as well as adult size variation could be explained by sexual dimorphism, the existence of several co-occurring sauropod species, or both. The size-morphs could also represent different stages of dwarfing in one species preserved by successive depositional

events, yet the sedimentological character of the deposit as described in the literature indicates a single depositional event (Myers and Storrs, 2007; Storrs et al., 2012). In contrast to that, the age distribution within the histologic sample (mostly adults and only a few juvenile and senescent individuals) indicates a single catastrophic event (Fig. 11). However, there are small, reworked bone clasts within the sample (Myers and Storrs, 2007; Storrs et al., 2012), which seem to show that not all the material deposited together within the debris flow was coming from a single event. Thus, more sedimentological analyses would be needed to clarify theses queries. Another explanation for the strong size variation within the assemblage is the existence of strong developmental plasticity in final body size (Sander and Klein, 2005; Woodruff and Foster, 2017) possibly related to the dwarfing process of this taxon. Developmental trends in vertebral synostosis do appear among vertebrates (Brochu, 1996; Ikejiri, 2010) and dinosaurs (Gilmore, 1925; Carr, 1999; Gallina, 2011; 2012; Carballido and Sander, 2014; Tschopp and Mateus, 2017). However, recent studies have shown that there are numerous dinosaur specimens exhibiting variability in neurocentral fusion, and it remains unknown if these represent taxonomic differences or plasticity within the various species. Although neurocentral fusion clearly takes place during ontogeny, the absence of fusion alone is thus not completely reliable as an indicator for a juvenile ontogenetic age. An assessment of the ontogenetic age of a specimen should therefore always be complemented by additional age indicative features (Bailleul et al., 2016; Woodruff et al., 2017). However, complete fusion of the cervical vertebral column appears to be consistently delayed after sexual maturity in sauropods (Tschopp and Mateus, 2017), so that at least vertebrae with closed neurocentral synostoses can be interpreted to belong to adult individuals. In contrast, in a dwarfed sauropod, lack of fusion could also be interpreted as a paedomorphic (Ibrahim et al., 2014) or size-related biomechanical feature (Woodruff et al., 2017).

4.5.5. Systematic assignment of the Mother´s Day Quarry sauropods

In the past, Myers and Storrs (2007) and Storrs et al. (2012) attributed the MDQ material to early ontogenetic stages of *Diplodocus* (Marsh 1878), based on general gracility of limb bones and vertebral elongation, but did not discuss specific apomorphic features that could be identified in the material. More recently, diplodocine diversity has been shown to be higher than previously thought, and new taxa have been recognized especially in the northern areas of the Morrison Formation (Tschopp and Mateus, 2013; 2017; Tschopp et al., 2015). Furthermore, Myers and Storrs (2007) and Storrs et al. (2012) assumed that all these skeletons represent early ontogenetic stages of *Diplodocus* sp. However, this study shows that most of the sampled individuals have an older ontogenetic age, which questions a simple referral to the larger-sized genus *Diplodocus*. 12 of the 17 sampled ribs show an EFS, at least two to three generations of secondary osteons and a decrease in vascularization, indicating a subadult to adult ontogenetic stage. The other five represent juveniles of two distinct size morphs. The larger one possibly could have grown to normal adult sauropod size. Given that at least two size morphs are present within the MDQ assemblage, the

presence of two different taxa is at least possible. A reassessment of the morphology of the specimens at CMC for the current study confirmed the presence of at least two morphotypes, one of which can most likely be referred to *Kaatedocus siberi* described by Tschopp and Mateus (2013). This species, however, is only known from skull material and cervical vertebrae (Tschopp et al., 2015), so that it is currently impossible to refer post-cervical axial and appendicular material to this species. Based on the definition of a dwarf as a species having only large ancestors (Boucot, 1976), *Kaatedocus* with respect to the phylogenetic position of the taxon within the phylogenetic tree found by Tschopp and Mateus (2017), is a dwarf itself (Fig. 14).

A recent study of Woodruff et al. (2018, (chapter 5)) analyzed the cranial remains of the smallest known diplodocid skull (CMC VP 14128) also from the MDQ, and provide evidence for a young ontogenetic stage of the individual and the assignment to *Diplodocus* sp. Even if CMC VP 14128 is lacking long bones or dorsal ribs for typical histological comparison, it is very likely that this individual represents a juvenile of a normal-sized sauropod possibly represented by the larger morphotype described herein. Nevertheless, also the presence of two large sized morphs representing different genera is possible. To prove the possible assignments to *Diplodocus* and/or *Kaatedocus*, a more detailed morphological comparison of the single skeletal elements is needed. This then raises the question as to whether the MDQ harbored distinct size morphs of the same taxon, or two distinct taxa denoted by stature, or both. However, the example of *Europasaurus* shows that the occurrence of two different size morphs is already known in dwarfed sauropods, and may equally signify sexual dimorphism (Marpmann et al., 2015). The exact determination of the taxonomic assignment of the MDQ diplodocids needs a more detailed analysis including morphological and histological comparison with *Kaatedocus* and *Diplodocus*. To be more conservative at this time, the MDQ sauropods should be referred to as Diplodocinae indet.

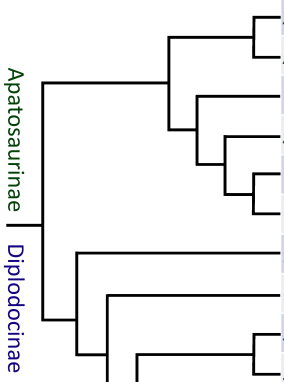

Taxon	Femur pdL	CV 10 cL	Specimen	Reference
Apatosaurus ajax	1870	-	YPM 1860	Benson et al., 2014
Apatosaurus louisae	1785	530	CM 3018	Gilmore, 1936
Brontosaurus excelsus	1790	-	YPM 1981	McIntosh, 1995
Amphicoelias altus	1930	-	AMNH FARB 5764	Osborn, 1898
Brontosaurus parvus	1710	475	UW 15556	Gilmore, 1936
Brontosaurus yahnahpin	-	-	-	
Kaatedocus siberi	**757**	**273**	SMA 0004	Tschopp and Mateus, 2013
Tornieria africana	1380	-	SMNS 12140	McIntosh, 2005
Supersaurus vivianae	-	-	-	-
Supersaurus lourinhanensis		-	-	-
Leinkupal laticauda	-	-	-	-
Galeamopus hayi	1448	-	-	McIntosh, 2005
Galeamopus pabsti	>1160	387	SMA 0011	Tschopp and Mateus, 2017
Barosaurus lentus	1440	737	AMNH FARB 6341	McIntosh, 2005
Diplodocus carnegii	1542	595	CM 84	Hatcher, 1901
Diplodocus hallorum	1575	-	USNM 10865	McIntosh, 2005

Fig. 14: Phylogeny of diplodocid sauropods (modified from Tschopp and Mateus, 2017), with maximum femur lengths reported for the species and centrum lengths for cervical vertebra (CV) 10 of the same specimens as the mentioned femora (where such a vertebra was found associated with the femur). The femur length of *Kaatedocus siberi* (in grey) was estimated based on the average ratio of femur to CV 10 centrum length (cL) in the four diplodocid specimens where this ratio is known (AMNH FARB 6341, CM 84, CM 3018, UW 15556, see measurements in fig). This estimate is reasonable, given that the cervical vertebral elongation of *K. siberi* is intermediate between apatosaurines and diplodocines (see Tschopp and Mateus, 2013; Tschopp et al., 2015).

4.5.6. Indications for insular dwarfism in the Mother´s Day Quarry assemblage

The dwarfing of a large ancestor in both recent and fossil animals, often can be explained by insular dwarfism (Van Valen, 1973; Lomolino, 1985; Anderson and Handley, 2002; Keogh et al., 2005; Weston and Lister, 2009; Lomolino et al., 2013; Gómez-Robles, 2016). Island dwarfism is also known in sauropods, with, e.g., *Europasaurus* and *Magyarosaurus* representing European examples of island dwarfing. However, the existence of island dwarfism within the terrestrial realm of the Morrison Formation may at first seem unrealistic. However, looking at the paleogeography of this region, the existence of a transient island, formed within the Jurassic epicontinental Sundance Seaway (Logan, 1900; Willis, 1910; Crickmay, 1931) in the northern parts of the Morrison Formation cannot be excluded. Even if geological evidence for the existence of a transient island in the northern parts of the Morrison Formation is hard to ascertain, some facts indicate that the dwarfing of the MDQ diplodocines might be related to an island. The presence of individuals representing all different ontogenetic stages from young juveniles to senescent individuals in one assemblage is atypical for sauropods that were believed to have strong age segregation. Large sauropods were likely occupying different ecological niches and habitats at different ages, caused by their enormous size range through ontogeny (Lockley et al., 2002; Myers and Fiorillo, 2009; Codron et al., 2012). The open habitats where the larger-sized subadults

and adults likely congregated generally represent depositional systems more conductive towards fossilization than the likely juvenile inhabited forested environments. Environmental segregation correlated with age segregation has previously been proposed to as one explanation for the general lack of markedly immature sauropods within the fossil record (Myers and Fiorillo, 2009). The MDQ assemblage in contrast shows a high variety of ontogenetic stages documented by the RHOS stages preserved in the ribs (Fig. 11) and the wide range of long bone size. Even if most of the sampled humeri (the smallest of which has not been sampled) show adult to subadult ontogenetic stages, there are several morphological lines of evidence for the presence of juveniles at the site including juvenile skull material (Woodruff et al., 2018, (chapter 5)) and cervical vertebrae showing incipient lamination (Schwarz et al., 2007; Carballido and Sander, 2014). This variety in ontogenetic stages present at one site may be a supportive indication for their dwarfed status. Because of their reduced size, the selection pressure for inhabiting different niches at different ontogenetic ages may no longer have been given. The age distribution in a diplodocine dominated death assemblage, as well as the occurrence of different adult-size morphs is very similar to what has been observed in the coeval German island dwarfed sauropod *Europasaurus holgeri* (Sander et al., 2006; Carballido and Sander, 2014; Marpmann et al., 2015). Additional similarities between the two dwarf assemblages can be seen in their histology (see above). This needs to remain speculative in the absence of hard geological evidence for islands in the region at the time.

4.5.7. Alternative explanations for diminutive size

The state of knowledge about the regional geology does not support the existence of an island – as opposed to *Europasaurus* which even derives from marine sediments (Sander et al., 2006), but there are other examples of stature differences that can be observed in correlation to geography. A review of the stegosaurs from the northern extent of the Morrison Formation (Maidment et al., 2017) showed that the smallest stegosaur, *Hesperosaurus mjosi*, was restricted to this region. Maidment et al. (2017) noted that larger overall size correlated with drier arid environments, and the inverse with wetter climates in extant animals. Based on the coastal setting of the northern Morrison environment adjacent to the Sundance Seaway, Maidment et al. (2017) hypothesized that this trend in stegosaur size was environmentally correlative. Thus, a similar pattern could be true for the MDQ diplodocines, although local geology suggests a generally arid climate.

Other Morrison Formation localities do not record a similar pattern to that observed in the MDQ. In Livingston, Montana, approx. 190 km west of the MDQ, immature *Diplodocus* sp. specimens approximately 12 years old with femora length of approx. 1243 mm, and a skeletally mature *Apatosaurus* sp. with a femur length of 1542 mm are known (Woodruff and Curry-Rogers, 2014; Woodruff et al., 2017). The size of these specimens appears more typical, so how could we explain such a difference? Difference in size based on the ecological

environment of a species (e.g., forest environments vs. open habitats) cannot be excluded. Forest elephants are often cited as a modern example for diminutive size caused by different habitat. However, recent analysis showed that there is no observable skeletal size difference between savannah-elephants and forest elephants (Morgan and Lee, 2003). Within North American cervids it can be observed that coastal white-tailed deer (*Odocoileus virginianus*) have an average body mass of 77 kg, whereas their interior counterparts have an average body mass exceeding 100 kg (Geist, 1998). The smallest statured sub-species, the Key Deer (*Odocoileus virginianus clavium*), living only in the Florida Keys, has an average body mass of 20-34 kg (Geist, 1998) and is in fact an island dwarf. This indicates that there might be a smooth size transition between inland, coastal and island forms. The observed size differences in diplodocines from the MDQ and other Morrison localities may indicate that Montana harbored normal-sized and regionally smaller-statured diplodocines. Smaller statured dinosaur taxa within this region other than mentioned above have not yet been recognized (such as, e.g., a dwarfed *Allosaurus* sp.) but could serve as a test for this hypothesis. Potentially, this island assemblage might have been integrated with another average statured population of juveniles (of the same or a similar genus) during a northward regression of the seaway complicating the interpretation even further by producing an assemblage that records both sizes. Even if not statistically valid, the poor correlation between RHOS and size (Fig. 11), and the presence of juvenile average-sized (Myers and Storrs, 2007; Storrs et al., 2012; Woodruff et al., 2018, (chapter 5)) and small individuals of all ontogenetic stages indicates the presence of at least two different diplodocine taxa.

4.6. Conclusions

The presence of an EFS in many of the sampled dorsal ribs of the MDQ diplodocines provides the first evidence for the presence of a dwarfed sauropod in North America, possibly caused by isolation of a local population on a geologically transient island. Further analysis of the long bone histology in comparison to normal-sized sauropods and dwarfs like *Europasaurus* and *Magyarosaurus,* underline these findings based on the reduced laminar thickness and a well-represented growth record in the long bones atypical for sauropods, due to their rapid rate of bone formation and remodeling. The analysis of both dorsal rib and long bone growth curves show that the diminutive stature was reached by reducing local bone apposition rate, a proxy for overall growth rate, rather than growth time. Sexual maturity was reached at half of the growth time (including the growth recorded in the EFS) at an age of about 10-12 years. Skeletal maturity was reached much later at an age of approximately 17-18 years. This is a similar life history as observed in normal-sized diplodocines. The histological analysis suggests the existence of two or more differently sized diplodocine morphs within the MDQ assemblage. Possibly caused by migration of average-sized juvenile diplodocines on a former island sustaining a population of dwarfed relatives. A morphological reassessment of the skeletal remains supports the existence of several size morphs, including large juveniles and dwarfed adult individuals that in addition to that show possible sexual size dimorphism.

4.7. Acknowledgements

This research would not have been possible without the accommodating loan and sampling permission of the Cincinnati Museum Center. We are grateful to Enrica Sarotto for her help and support during collection work of Emanuel Tschopp at CMC, and to Olaf Dülfer, Tanja Wintrich, and Pia Schucht (University of Bonn) for thin sectioning. Our special thanks go to Riccardo Cerisara and the members of Martin Sander´s working group for fruitful discussion. Finally, we want to thank the DFG for funding. Emanuel Tschopp is currently funded through a Theodore Roosevelt Memorial Fund and Division of Paleontology Postdoctoral Fellowship at Richard Gilder Graduate School of the American Museum of Natural History, New York. This is contribution no. 173 of the DFG Research Unit 533 "Biology of the Sauropod Dinosaurs: The Evolution of Gigantism".

4.8. References

Anderson, J. F., Hall-Martin, A., and Russell, D. A. (1985). Long bone circumference and weight in mammals, birds, and dinosaurs. Journal of Zoology Series A 207, 53-61.

Anderson, R. P., and Handley, C. O. (2002). Dwarfism in insular sloths: Biogeography, selection, and evolutionary rate. Evolution 56(5), 1045-1058.

Bailleul, A. M., Scannella, J. B., Horner, J. R., and Evans, D. C. (2016). Fusion patterns in the skulls of modern archosaurs reveal that sutures are ambiguous maturity indicators for the Dinosauria. PloS ONE 11(2), e0147687.

Benson, R. B. J., Campione, N. E., Carrano, M. T., Mannion, P. D., Sullivan, C., Upchurch, P., and Evans D. C. (2014). Rates of dinosaur body mass evolution indicate 170 million years of sustained ecological innovation on the avian stem lineage. PLoS Biology 12(5), e1001853.

Benton, M. J., Csiki, Z., Grigorescu, D., Redelstorff, R., Sander, P. M., Stein, K., and Weishampel, D. B. (2010). Dinosaurs and the island rule: The dwarfed dinosaurs from Hateg Island. Palaeogeography, Palaeoclimatology, Palaeoecology 293(3-4), 438-454.

Boucot, A. J. (1976). Rates of size increase and of phyletic evolution. Nature 261(5562), 694-696.

Brochu, C. A. (1996). Closure of neurocentral sutures during crocodilian ontogeny: Implications for maturity assessment in fossil archosaurs. Journal of Vertebrate Paleontology 16, 49-62.

Buffetaut, E., Suteethorn, V., Le Loeuff, J., Cuny, C., Tong, H., and Khansubha, S. (2002). The first giant dinosaurs: A large sauropod from the Late Triassic of Thailand. Comptes Rendus Palevol 1, 103-109.

Campione, N. E., and Evans, D. C. (2012). A universal scaling relationship between body mass and proximal limb bone dimensions in quadrupedal terrestrial tetrapods. BMC Biology 10(1), 60.

Carballido, J. L., and Sander, P. M. (2014). Postcranial axial skeleton of *Europasaurus holgeri* (Dinosauria, Sauropoda) from the Upper Jurassic of Germany: Implications for sauropod ontogeny and phylogenetic relationships of basal Macronaria. Journal of Systematic Palaeontology 12(3), 335-387.

Carpenter, K., and McIntosh, J. (1994). Upper Jurassic sauropod babies from the Morrsion Formation. In: Carpenter, K., Hirsch, K., and Horner, J. R., editors. Dinosaur eggs and babies. Cambridge, Cambridge University Press: 265-278.

Carr, T. D. (1999). Craniofacial ontogeny in Tyrannosauridae (Dinosauria, Coelurosauria). Journal of Vertebrate Paleontology 19, 497-520.

Carrano, M. T. (2001). Implications of limb bone scaling, curvature and eccentricity in mammals and non-avian dinosaurs. Journal of Zoology 254, 41-55.

Cerisara, R. (2017). Long bone histology of *Europasaurus holgeri:* Insights into the dwarfing process. MSc thesis, University of Bonn.

Chinsamy-Turan, A. (2005). The microstructure of dinosaur bone: Deciphering biology with fine-scale techniques. Baltimore, Maryland, The Johns Hopkins University Press.

Chinsamy, A., and Raath, M. A. (1992). Preparation of bone for histological study. Palaeontologia Africana 29, 39-44.

Chure, D., Britt, B. B., Whitlock, J. A. and Wilson, J. A. (2010). First complete sauropod dinosaur skull from the Cretaceous of the Americas and the evolution of sauropod dentition. Naturwissenschaften 97(4), 79-391.

Codron, D., Carbone, C., Müller, D. W. H., and Clauss, M. (2012). Ontogenetic niche shifts in dinosaurs influenced size, diversity and extinction in terrestrial vertebrates. Biology Letters 8(4), 620-623.

Colbert, E. H. (1962). The weights of dinosaurs. American Museum Novitates 2076, 1-16.

Crickmay, C. H. (1931). Jurassic history of North America: Its bearing on the development of continental structure. Proceedings of the American Philosophical Society 70(1), 15-102.

Curry, K. A. (1999). Ontogenetic histology of *Apatosaurus* (Dinosauria: Sauropoda): New insights on growth rates and longevity. Journal of Vertebrate Paleontology 19(4), 654-665.

Enlow, D. H., and Brown, S. O. (1956). A comparative histological study of fossil and recent bone tissue. Texas Journal of Science 8, 405-443.

Erickson, G. M. (2005). Assessing dinosaur growth patterns: A microscopic revolution. Trends in Ecology and Evolution 20(12), 677-684.

Erickson, G. M., Curry Rogers, K., Varricchio, D. J., Norell, M. A., and Xu, X. (2007). Growth patterns in brooding dinosaurs reveals the timing of sexual maturity in non-avian dinosaurs and genesis of the avian condition. Biology Letters 3, 558-561.

Gallina, P. A. (2011). Notes on the axial skeleton of the titanosaur *Bonitasaura salgadoi* (Dinosauria-Sauropoda). Anais da Academia Brasileira de Ciências 83(1), 235-245.

Gallina, P. A. (2012). Histología ósea del titanosaurio *Bonitasaura salgadoi* (Dinosauria: Sauropoda) del Cretácico superior de Patagonia. Ameghiniana 49(3), 289-302.

Geist, V. (1998). Deer of the world: Their evolution, behaviour, and ecology. Shropshire, Swanhill Press.

Gilmore, C. W. (1925). A nearly complete articulated skeleton of *Camarasaurus*, a saurischian dinosaur from the Dinosaur National Monument. Memoirs of the Carnegie Museum 10, 347-384.

Gilmore, C. W. (1936). Osteology of *Apatosaurs* with special reference to specimens in the Carnegie Museum. Memoirs of the Carnegie Museum 11(4), 175-300.

Girondot, M., and Laurin, M. (2003). Bone profiler: A tool to quantify, model, and statistically compare bone-section compactness profiles. Journal of Vertebrate Paleontology 23(2), 458-461.

Gómez-Robles, A. (2016). Palaeoanthropology: The dawn of *Homo floresiensis*. Nature 534(7606), 188-189.

Griebeler, E. M., Klein, N., and Sander, P. M. (2013). Aging, maturation and growth of sauropodomorph dinosaurs as deduced from growth curves using long bone histological data. PloS ONE 8(6), e67012.

Gunga, H.-C., Suthau, T., Bellmann, A., Stoinski, S., Friedrich, A., Trippel, T., Kirsch, K., and Hellwich, O. (2008). A new body mass estimation of *Brachiosaurus brancai* Janensch, 1914 mounted and exhibited at the Museum of Natural History (Berlin, Germany). Fossil Record 11(1), 33-38.

Gunga, H.-C., Kirsch, K., Johannes, B., Röcker, L., Rittweger, J., Heinrich, E.-D., Schultze, H.-P., Wiedemann, A., Albertz, J., and Clarke, A. (2002). The dimensions of *Brachiosaurus brancai* (Museum of Natural History, Berlin) and their physiological implications. Naturwissenschaften 21, 144-145.

Hanik, G. M., Lamanna, M. C., and Whitlock, J. A. (2017). A juvenile specimen of *Barosaurus* Marsh, 1890 (Sauropoda: Diplodocidae) from the Upper Jurassic Morrison Formation of Dinosaur National Monument, Utah, USA. Annals of the Carnegie Museum 84(3), 253-263.

Harris, J. D. (2005). A review of Morrison Formation paleogeography and tests for time-transgression and faunal provincialism. Geological Society of America 37, 13-14.

Harris, J. D., and Dodson, P. (2004). A new diplodocoid sauropod dinosaur from the Upper Jurassic Morrison Formation of Montana, USA. Acta Palaeontologica Polonica 49(2), 197-210.

Hatcher, J. B. (1901). *Diplodocus* (Marsh): Its osteology, taxonomy, and probable habits, with a restauration of the skeleton. Memoirs of the Carnegie Museum 1, 1-63.

Henderson, D. M. (1999). Estimating the masses and centers of mass of extinct animals by 3-D mathematical slicing. Paleobiology 25(1), 88-106.

Hofmann, R., Stein, K., and Sander, P. M. (2014). Constraints on the lamina density of laminar bone architecture of large-bodied dinosaurs and mammals. Acta Palaeontologica Polonica 59(2), 287-294.

Ibrahim, N., Sereno, P. C., Dal Sasso, C., Maganuco, S., Fabbri, M., Martill, D. M., and Iurino, D. A. (2014). Semiaquatic adaptations in a giant predatory dinosaur. Science 345(6204), 1613-1616.

Ikejiri, T. (2010). Morphology of the neurocentral junction during postnatal growth of *Alligator* (Reptilia, Crocodylia). PHD thesis. University of Michigan.

Ikejiri, T. (2012). Histology-based morphology of the neurocentral synchondrosis in *Alligator mississippiensis* (Archosauria, Crocodylia). The Anatomical Record 295(1), 18-31.

Janensch, W. (1961). Die Gliedmaßen und Gliedmaßengürtel der Sauropoden der Tendaguru-Schichten. Palaeontographica (Supplement) 7(3), 177-235.

Keogh, J. S., Scott, I. A., and Hayes, C. (2005). Rapid and repeated origin of insular gigantism and dwarfism in Australian tiger snakes. Evolution 59(1), 226-233.

Klein, N., and Sander, P. M. (2008). Ontogenetic stages in the long bone histology of sauropod dinosaurs. Paleobiology 34(2), 247-263.

Klein, N., Remes, K., Gee, C. T., and Sander, P. M. (2011). Biology of the sauropod dinosaurs: Understanding the life of giants. Bloomington, Indiana University Press.

Lamm, E. T. (2007). Paleohistology widens the field of view in paleontology. Microscopy and Microanalysis 13(S02), 50-51.

Lance, V. A. (2003). *Alligator* physiology and life history: The importance of temperature. Experimental Gerontology 38(7), 801-805.

Le Loeuff, J. (1993). European titanosaurids. Revue de Paleobiologie 7, 105-117.

Lockley, M., Schulp, A. S., Meyer, C. A., Leonardi, G., and Mamani, D. K. (2002). Titanosaurid trackways from the Upper Cretaceous of Bolivia: Evidence for large manus, wide-gauge locomotion and gregarious behaviour. Cretaceous Research 23(3), 383-400.

Logan, W. N. (1900). A North American epicontinental sea of Jurassic age. The Journal of Geology 8(3), 241-273.

Lomolino, M. V. (1985). Body size of mammals on islands: The island rule reexamined. The American Naturalist 125(2), 310-316.

Lomolino, M. V., Geer, A. A., Lyras, G. A., Palombo, M. R., Sax, D. F., and Rozzi, R. (2013). Of mice and mammoths: Generality and antiquity of the island rule. Journal of Biogeography 40(8), 1427-1439.

Lydekker, R. (1893). Contributions to the study of the fossil vertebrates of Argentina. I. The dinosaurs of Patagonia. Anales del Museo de La Plata. Paleontologia Argentina 2, 1-14.

Maidment, S. C. R., Woodruff, D. C., and Horner, J. R. (2017). A new specimen of the ornithischian dinosaur *Stegosaurus mjosi* from the Upper Jurassic Morrison Formation of Montana, USA, and implications for growth and size in *Stegosaurus*. Journal of Vertebrate Paleontology 38(1), e1406366.

Marpmann, J. S., Carballido, J. L., Sander, P. M. and Knötschke, N. (2015). Cranial anatomy of the Late Jurassic dwarf sauropod *Europasaurus holgeri* (Dinosauria, Camarasauromorpha): Ontogenetic changes and size dimorphism. Journal of Systematic Palaeontology 13(3), 221-263.

Marsh, O. C. (1878). Principal characters of American Jurassic dinosaurs. Part I. American Journal of Science (3)16, 411-416.

Mazzetta, G. V., Christiansen, P., and Farina, R. A. (2004). Giants and bizarres: Body size of some southern South American Cretaceous dinosaurs. Historical Biology 2004, 1-13.

McIntosh, J. S. (1990). Sauropoda. In: Weishampel, D. B., Dodson, P., and Osmolska, H., editors. The Dinosauria. Berkeley, California. University of California Press: 345-401.

McIntosh, J. S. (1995). Remarks on the North American sauropod *Apatosaurus* Marsh. In: Sun, A., and Wang, Y., editors. Sixth Symposium on Mesozoic Terrestrial Ecosystems and Biota. Beijing, China, China Ocean Press: 119-123.

McIntosh, J. S. (2005). The genus *Barosaurus* Marsh (Sauropoda, Diplodocidae). In: Tidwell, V., and Carpenter, K., editors. Thunder-Lizards. The sauropodomorph dinosaurs. Bloomington, Indiana, Indiana University Press: 38-77.

Melstrom, K. M., D´Emic, M. D., Chure, D. and Wilson, J. A. (2016). A juvenile sauropod dinosaur from the Late Jurassic of Utah, USA, presents further evidence of an avian style air-sac system. Journal of Vertebrate Paleontology 36(4), e1111898.

Mitchell, J., and Sander, P. M. (2014). The three-front model: A developmental explanation of long bone diaphyseal histology of Sauropoda. Biological Journal of the Linnean Society 112(4), 765-781.

Mitchell, J., Sander, P. M., and Stein, K. (2017). Can secondary osteons be used as ontogenetic indicators in sauropods? Extending the histological ontogenetic stages into senescence. Paleobiology 43(2), 321-342.

Morgan, B. J., and Lee, P. C. (2003). Forest elephant (*Loxodonta africana cyclotis*) stature in the Réserve de Faune du Petit Loango, Gabon. Journal of Zoology 259(4), 337-344.

Myers, T. S., and Storrs, G. W. (2007). Taphonomy of the Mother's Day quarry, Upper Jurassic Morrison Formation, south-central Montana, USA. Palaios 22, 651-666.

Myers, T. S., and Fiorillo, A. R. (2009). Evidence for gregarious behavior and age segregation in sauropod dinosaurs. Palaeogeography, Palaeoclimatology, Palaeoecology 274, 96–104.

Nopcsa, F. (1914). Über das Vorkommen der Dinosaurier in Siebenbürgen. Verhandlungen der Zoologisch-Botanischen Gesellschaft 54, 12-14.

Nopcsa, F. (1923). On the geological importance of the primitive reptilian fauna of the uppermost Cretaceous of Hungary; with a description of a new tortoise (*Kallokibotium*). Quarterly Journal of the Geological Society of London 79, 100-116.

Osborn, H. F. (1898). Additional characters of the great herbivorous dinosaur *Camarasaurus*. Bulletin of the American Museum of Natural History 10, 219-233.

Padian, K., and Lamm, E. T. (2013). Bone histology of fossil tetrapods: Advancing methods, analysis, and interpretation. Berkeley California, University of California Press.

Parrish, J. T., Peterson, F., and Turner, C. E. (2004). Jurassic 'savannah' - Plant taphonomy and climate of the Morrison Formation (Upper Jurassic, Western USA). Sedimentary Geology 167(3), 137-162.

Paul, G. (1997). Dinosaur models: The good, the bad, and using them to estimate the mass of dinosaurs. In: Wolberg, D. L., Stump, E., and Rosenberg, G. D., editors. Dinofest International: Proceedings of a Symposium Sponsored By Arizona State University. The Academy of Natural Sciences, Philadelphia: 39-45.

Peterson, O. A., and Gilmore, C. W. (1902). *Elosaurus parvus*, a new genus and species of Sauropoda. Annals of the Carnegie Museum 1, 490-499.

Remes, K. (2006). Revision of the Tendaguru sauropod *Tornieria africana* (Fraas) and its relevance for sauropod paleobiogeography. Journal of Vertebrate Paleontology 26(3), 651-669.

Sander, P. M. (1999). Life history of the Tendaguru sauropods as inferred from long bone histology. Mitteilungen aus dem Museum für Naturkunde der Humboldt-Universität Berlin, Geowissenschaftliche Reihe 2, 103-112.

Sander, P. M. (2000). Long bone histology of the Tendaguru sauropods: Implications for growth and biology. Paleobiology 26(3), 466-488.

Sander, P. M., and Tückmantel, C. (2003). Bone lamina thickness, bone apposition rates, and age estimates in sauropod humeri and femora. Paläontologische Zeitschrift 76(1), 161-172.

Sander, P. M., and Klein, N. (2005). Developmental plasticity in the life history of a prosauropod dinosaur. Science 310(5755), 1800-1802.

Sander, P. M., Mateus, O., Laven, T., and Knötschke, N. (2006). Bone histology indicates insular dwarfism in a new Late Jurassic sauropod dinosaur. Nature 441 739-741.

Sander, P. M., Klein, N., Stein, K., and Wings, O. (2011). Sauropod bone histology and its implicatios for sauropod biology. In: Klein, N., Remes, K., Gee, C. T., and Sander, P. M., editors. Biology of the sauropod dinosaurs. Bloomington, Indiana, Indiana University Press: 276-302.

Sander, P. M., Klein, N., Buffetaut, E., Cuny, G., Suteethorn, V., and Le Loeuff, J. (2004). Adaptive radiation in sauropod dinosaurs: Bone histology indicates rapid evolution of giant body size through acceleration. Organisms, Diversity and Evolution 4, 165-173.

Schwarz, D., Ikejiri, T., Breithaupt, B. H., Sander, P. M. and Klein, N. (2007). A nearly complete skeleton of an early juvenile diplodocid (Dinosauria: Sauropoda) from the Lower Morrison Formation (Late Jurassic) of north central Wyoming and its implications for early ontogeny and pneumaticity in sauropods. Historical Biology 19(3), 225-253.

Seebacher, F. (2001). A new method to calculate allometric length-mass relationships of dinosaurs. Journal of Vertebrate Paleontology 21(1), 51-60.

Stein, K., and Prondvai, E. (2014). Rethinking the nature of fibrolamellar bone: An intergrative biological revision of sauropod osteohistomorphogenesis. Biological Reviews 89(1), 24-47.

Stein, K., and Sander, P. M. (2009). Histological core drilling: A less destructive method for studying bone histology. In: Brown, M. A., Kane, J. F., and Parker, W. G., editors. Lithodendron: The occasional papers of Petrified Forest National Park 1. Methods in fossil preparation: Proceedings of the First Annual Fossil Preparation and Collections Symposium: 69-80.

Stein, K., Csiki, Z., Rogers, K. C., Weishampel, D. B., Redelstorff, R., and Sander, P. M. (2010). Small body size and extreme cortical bone remodeling indicate phyletic dwarfism in *Magyarosaurus dacus* (Sauropoda: Titanosauria). Proceedings of the National Academy of Sciences, USA 107(20), 9258-9263.

Stoinski, S., Suthau, T., and Gunga, H.-C. (2011). Reconstructing body volume and surface area of dinosaurs using laser scanning and photogrammetry. In: Klein, N., Remes, K., Gee, C. T., and Sander, P.M., editors. Biology of the sauropod dinosaurs: Understanding the life of giants. Life of the Past (series ed. Farlow, J. O.). Bloomington, Indiana, Indiana University Press: 94-104.

Storrs, G. W., Oser, S. E., and Aull, M. (2012). Further analysis of a Late Jurassic dinosaur bone-bed from the Morrison Formation of Montana, USA, with a computed three-dimensional reconstruction. Earth and Environmental Science Transactions of the Royal Society of Edinburgh 103(3-4), 443-458.

Trujillo, K. C. (2006). Clay mineralogy of the Morrison Formation (Upper Jurassic-Lower Cretaceous), and its use in long distance correlation and paleoenvironmental analysis. New Mexico Museum of Natural History and Science Bulletin 36, 17-23.

Tschopp, E., and Mateus, O. (2013). The skull and neck of a new flagellicaudatan sauropod from the Morrison Formation and its implication for the evolution and ontogeny of diplodocid dinosaurs. Journal of Systematic Palaeontology 11(7), 853-888.

Tschopp, E., and Mateus, O. (2017). Osteology of *Galeamopus pabsti* sp. nov. (Sauropoda: Diplodocidae), with implications for neurocentral closure timing, and the cervico-dorsal transition in diplodocids. PeerJ 5, e3179.

Tschopp, E., Mateus, O., and Benson, R. B. J. (2015). A specimen-level phylogenetic analysis and taxonomic revision of Diplodocidae (Dinosauria, Sauropoda). PeerJ 3, e857.

Upchurch, P., Barrett, P. M., and Dodson, P. (2004). Sauropoda. In: Weishampel, D. B., Dodson, P., and Osmólska, H., editors. The Dinosauria. 2nd Edition. Berkeley, California, University of California Press: 259-322.

Waskow, K., and Sander, P. M. (2014). Growth record and histological variation in the dorsal ribs of *Camarasaurus* sp. (Sauropoda). Journal of Vertebrate Paleontology 34(4), 852-869.

Waskow, K., and Mateus, O. (2017). Dorsal rib histology of dinosaurs and a crocodylomorph from western Portugal: Skeletochronological implications on age determination and life history traits. Comptes Rendus Palevol 16(4), 425-439.

Wedel, M. J. (2003). The evolution of vertebral pneumaticity in sauropod dinosaurs. Journal of Vertebrate Paleontology 23(2), 344-357.

Wedel, M. J., and Taylor, M. P. (2013). Neural spine bifurcation in sauropod dinosaurs of the Morrison Formation: Ontogenetic and phylogenetic Implications. PalArch's Journal of Vertebrate Palaeontology 10(1), 1-34.

Weishampel, D. B., Norman, D. B., and Grigorescu, D. (1993). *Telmatosaurus transsylvanicus* from the Late Cretaceous of Romania: The most basal hadrosaurid dinosaur. Palaeontology 36, 361-385.

Weishampel, D. B., Jianu, C. M., Csiki, Z., and Norman, D. B. (2003). Osteology and phylogeny of *Zalmoxes* (n.g.), an unusual euornithopod dinosaur from the latest Cretaceous of Romania. Journal of Systematic Palaeontology 1(2), 1-56.

Wells, N. A. (1989). Making thin sections. In: Feldmann, R. M., Chapman, R. E., and Hannibal, J. T., editors. Paleotechniques. Paleontological Society Special Publication Cambridge: 120-129.

Weston, E. M., and Lister, A. M. (2009). Insular dwarfism in hippos and a model for brain size reduction in *Homo floresiensis*. Nature 459(7243), 85-88.

Whitlock, J. A., Wilson, J. A., and Lamanna, M. C. (2010). Description of a nearly complete juvenile skull of *Diplodocus* (Sauropoda: Diplodocoidea) from the Late Jurassic of North America. Journal of Vertebrate Paleontology 30(2), 442-457.

Wiersma, K., Canoville, A., Siber, H.-J., and Sander, P. M. (in review). Testing hypothesis of skeletal unity using bone histology: The case of the sauropod remains from the Howe-Stephens and Howe Scott quarries (Morrison Formation, Wyoming). Palaeontologia Electronica.

Willis, B. (1910). Principles of paleogeography. Science 31(790), 241-260.

Woodruff, D. C., and Fowler, D. W. (2012). Ontogenetic influence on neural spine bifurcation in Diplodocoidea (Dinosauria: Sauropoda): A critical phylogenetic character. Journal of Morphology 273(7), 754-764.

Woodruff, D. C., and Curry Rogers, K. A. (2014). Diplodocid sauropods from the Late Jurassic Morrison Formation of Montana. Journal of Vertebrate Paleontology, SVP Program and Abtsract Book.

Woodruff, D. C., and Foster, J. R. (2017). The first specimen of *Camarasaurus* (Dinosauria: Sauropoda) from Montana: The northernmost occurrence of the genus. PloS ONE 12(5), e0177423.

Woodruff, D. C., Fowler, D. W., and Horner, J. R. (2017). A new multi-faceted framework for deciphering diplodocid ontogeny. Palaeontologia Electronica 20(3), 1-53.

Woodruff, D. C., Carr, T. D., Storrs, G. W., Waskow, K., Scannella, J. B., Nordén, K. K., and Wilson, J. P. (2018). The smallest diplodocid skull reveals cranial ontogeny and growth-related dietary changes in the largest dinosaurs. Scientific Reports 8(1), 14341.

Neurocentral fusion pattern Mother's Day Quarry diplodocines

Dorsal vertebrae

Specimen	Element	Serial position	Neurocentral fusion	Pleurocoel subdivision	naL
CMC VP14458	Vertebra	aDV	fused	double	75
CMC VP14369A	Vertebra	aDV	fused	-	67,8
CMC VP1440	Vertebra	aDV	fused	-	78
CMC VP9733	Arch	aDV	open	-	71
CMC VP9848	Centrum	aDV	open	double	70,3
CMC VP8714	Arch	mDV	open	-	116,6
CMC VP12194	Arch	mDV	open	-	78,7
CMC VP10104	Centrum	mDV to pDV	open	-	86,3
CMC VP8713	Centrum	mDV to pDV	open	single	77
CMC VP10103	Centrum	mDV to pDV	open	incipient	86
CMC VP10102	Centrum	mDV to pDV	open	single	70
CMC VP8706	Vertebra	mDV to pDV	fused	double	88,8
CMC VP7913	Centrum	mDV to pDV	open	double	112,3
CMC VP8028A	Centrum	mDV to pDV	open	single	105,2
CMC VP8028B	Centrum	mDV to pDV	open	single	110
CMC VP8981	Centrum	mDV to pDV	open	single	130
CMC VP10106	Centrum	mDV to pDV	open	double	83,8
CMC VP10598A	Vertebra	pDV	fused	-	74

Supplementary Tab. 1: Neurocentral fusion pattern and size of diplodocine dorsal vertebrae from Mother's Day Quarry. The neurocentral fusion pattern terminology follows Ikejiri (2012). Pleurocoel subdivision is given where visible. Abbreviations: aDV, anterior dorsal vertebrae; mDV, mid-dorsal vertebrae; naL, neural arch length (measured at the point of fusion, so that also elements with open synchondroses could be measured and compared; in mm); pDV, posterior dorsal vertebrae.

Humeri Mother's Day Quarry

Specimen	pdL	prW	minW	diW	RI	HOS
CMC VP 7746	715	310	118	220	0,30	
CMC VP 8301	734	310	115	230	0,30	
CMC VP 8663	802	298	118	224	0,27	
CMC VP 8971	796	315	113	188	0,26	
CMC VP 9834	428	229	75	152	0,36	
CMC VP 10347	820	285	123	180	0,24	13
CMC VP 14350	506	190	70	105	0,24	10
CMC VP 14423	640	271	110	187	0,30	10

Femora Mother's Day Quarry

Specimen	pdL	prW	minW	diW	RI	HOS
CMC VP 8057						12
CMC VP 8861						9
CMC VP 15667	953	294	148	284	0,25	13
CMC VP 14004						11
CMC VP 14502						10
CMC VP 14594	840	184	107	169	0,18	

Supplementary Tab. 2: Measurements (in mm) and HOS of preserved diplodocine humeri and femora from Mother's Day Quarry, where deformation would not be misleading. Abbreviations: diW, distal transverse width; HOS, histological ontogenetic stage; minW, minimum transverse width (usually close to midshaft); pdL, proximodistal length; prW, proximal transverse width; RI, Robustness Index (sensu Wilson & Upchurch 2003: average of prW, minW, and diW divided by pdL).

„In jedem Individuum erblickt die Natur sich selbst aus einem besondern Gesichtspunkte.“

“In each individual, nature sees itself from a special point of view.”

Johann Gottlieb Fichte

CHAPTER 5

The smallest diplodocid skull reveals cranial ontogeny and growth-related dietary changes in the largest dinosaurs

published as:

Woodruff, D. C., Carr, T. D., Storrs, G. W., **Waskow, K**., Scannella, J. B., Nordén, K. K., and Wilson, J. P. (2018). The smallest diplodocid skull reveals cranial ontogeny and growth-related dietary changes in the largest dinosaurs. Scientific Reports 8(1), 14341.

Author contribution:

D. Cary Woodruff designed the study and performed most of manuscript preparation including the morphological description of the specimen. Contributions of other authors are listed below.

Thomas D. Carr and Klara K. Nordén created and analyzed the phylogenetic models (chapter 5.2.4., 5.9.1., 5.9.6.).

Glenn W. Storrs collected the specimen.

I contributed in the histological descriptions of the cervical ribs (5.3.2.5.) most of which are described in the supplementary material (chapter 5.9.3) and preparation of chapter 5.4.3. (possible dwarfism).

John B. Scanella created the transformation grid (chapter 5.2.3.).

John P. Wilson photographed the specimen and created the photogrammetric models (chapter 5.9.7).

All authores contributed in manuscript preparation and proofreading of the final version.

SCIENTIFIC REPORTS

OPEN

The Smallest Diplodocid Skull Reveals Cranial Ontogeny and Growth-Related Dietary Changes in the Largest Dinosaurs

D. Cary Woodruff[1,2,3], Thomas D. Carr[4], Glenn W. Storrs[5], Katja Waskow[6], John B. Scannella[7], Klara K. Nordén[8] & John P. Wilson[9]

Sauropod dinosaurs were the largest terrestrial vertebrates; yet despite a robust global fossil record, the paucity of cranial remains complicates attempts to understand their paleobiology. An assemblage of small diplodocid sauropods from the Upper Jurassic Morrison Formation of Montana, USA, has produced the smallest diplodocid skull yet discovered. The ~24 cm long skull is referred to cf. *Diplodocus* based on the presence of several cranial and vertebral characters. This specimen enhances known features of early diplodocid ontogeny including a short snout with narrow-crowned teeth limited to the anterior portion of the jaws and more spatulate teeth posteriorly. The combination of size plus basal and derived character expression seen here further emphasizes caution when naming new taxa displaying the same, as these may be indicative of immaturity. This young diplodocid reveals that cranial modifications occurred throughout growth, providing evidence for ontogenetic dietary partitioning and recapitulation of ancestral morphologies.

With their titanic bodies and long necks and tails, sauropods are perhaps the most recognizable non-avian dinosaurs. *Diplodocus* is one of the best-known sauropod taxa, represented by over 100 specimens since its discovery in 1878[1]. Whereas the postcrania of *Diplodocus* are well represented, cranial remains are exceedingly rare. An adult *Diplodocus* might attain a body length in excess of 30 m[1], but its skull was well under 1 m[2]. To date only three of these skulls are hypothesized to be from immature animals[3–5], thus biasing our understanding of this taxon's ontogeny, ecology, and evolution towards adult specimens. While few, these immature skulls reveal insights into cranial allometry through ontogeny and suggest that *Diplodocus* and its Diplodocidae kin underwent radical ontogenetic change. Such changes would have significant effects on the ecology of immature Diplodocidae and the life history of these animals.

The smallest of the three immature skulls (CM 11255) is 29.2 cm in length, slightly over half of the adult cranial length[3]. Although this specimen reveals critical ontogenetic components, the cranial attributes of much younger diplodocids have remained unknown. Here we describe a new immature cf. *Diplodocus* skull (CMC VP14128), which, with a total cranial length of ~24 cm, represents the smallest known example. This important new specimen reveals hitherto unknown aspects of immature diplodocid anatomy, and shows that juveniles are not merely smaller versions of adults (*sensu* Whitlock *et al.*[3]). Our primary objectives are to test the taxonomic identity of the specimen using phylogenetic analyses, comparative qualitative and quantitative methods, and discuss the ecological implications of cranial ontogeny in diplodocids. We use immature and mature to refer specifically to developmental history, while juvenile, sub-adult, and adult are used as maturational colloquialisms.

[1]Department of Ecology and Evolutionary Biology, University of Toronto, Toronto, ON, Canada. [2]Royal Ontario Museum, University of Toronto, Toronto, ON, Canada. [3]Great Plains Dinosaur Museum, Malta, MT, USA. [4]Department of Biology, Carthage College, Kenosha, WI, USA. [5]Cincinnati Museum Center, Cincinnati, OH, USA. [6]Steinmann Institute for Geology, Mineralogy, and Paleontology, University of Bonn, Bonn, Germany. [7]Museum of the Rockies, Montana State University, Bozeman, MT, USA. [8]Department of Ecology and Evolutionary Biology, Princeton University, Princeton, NJ, USA. [9]Department of Paleontology, Badlands Dinosaur Museum, Dickinson Museum Center, Dickinson, ND, USA. Correspondence and requests for materials should be addressed to D.C.W. (email: sauropod4@gmail.com)

Received: 3 November 2017

Accepted: 24 August 2018

Published online: 11 October 2018

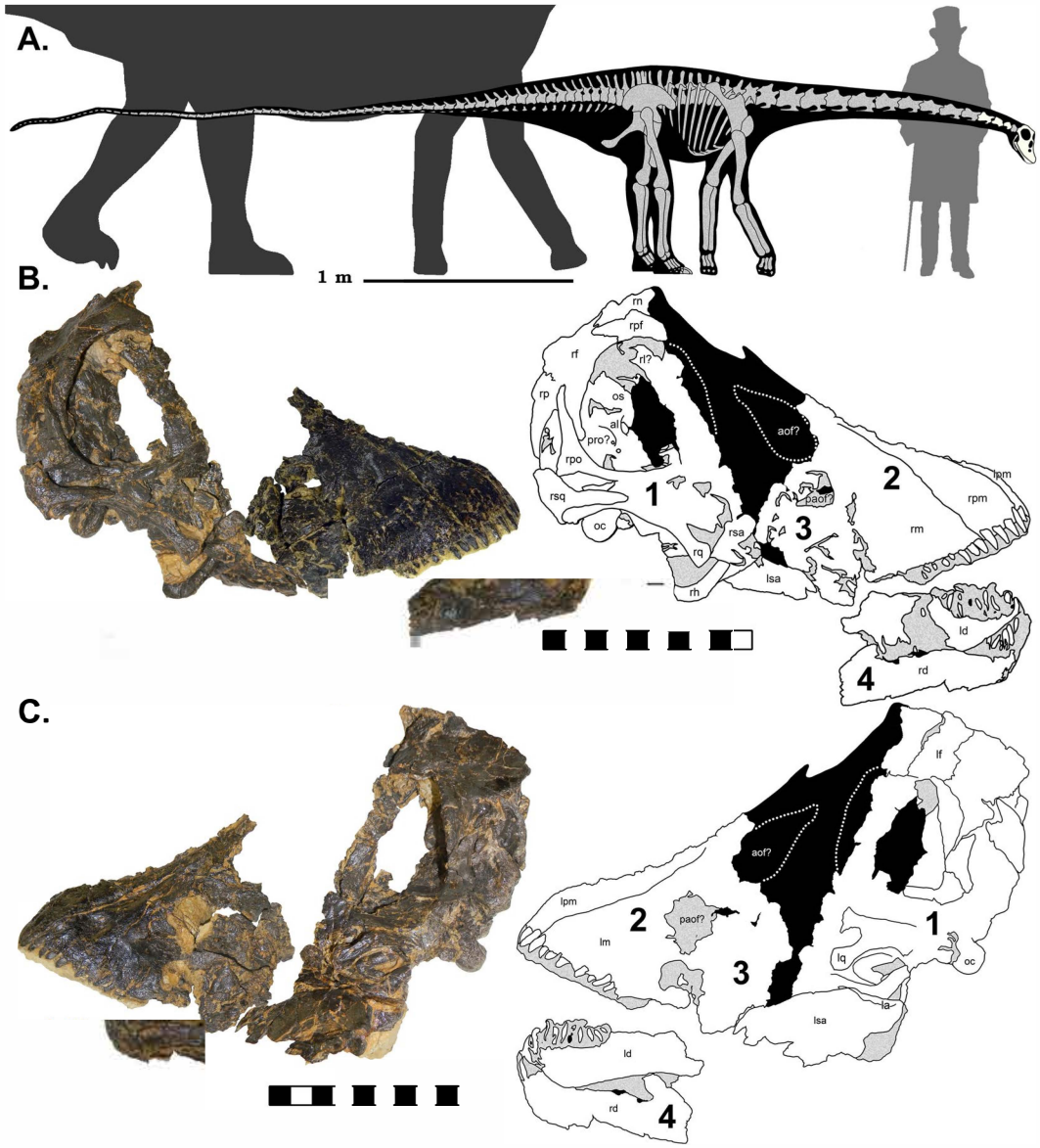

Figure 1. Skeletal reconstruction of CMC VP14128 to scale with a mature *D. carnegii* (dark grey). Grey bones are missing, while those in ivory are those present in CMC VP14128. Skeletal reconstruction based on the *Diplodocus* by S. Hartman. Silhouettes by S. Hartman and PhyloPic (Creative Commons Attribution-ShareAlike 3.0 Unported; http://phylopic.org/image/3cb1d5bf-7db5-4db2-82a6-4c39f6a4441b/; https://creativecommons.org/licenses/by-sa/3.0/), modifications made. Skeletal reconstruction of CMC VP14128 redrawn from *D. carnegii* skeletal by S. Hartman (http://www.skeletaldrawing.com/sauropods-and-kin/diplodocus). Human scale is Andrew Carnegie at his natural height of 1.6 m. Skeletal and silhouettes to scale. (**B**) CMC VP14128 in right lateral view with accompanying schematic. (**C**) CMC VP14128 in left lateral view with accompanying schematic. Schematics by DCW. The four portions of the skull numbered on accompanying schematics. Lateral views and schematics to scale. a: angular, al: alisphenoid, aof: antorbital fenestra, d: dentary, f: frontal, h: hyoid, l: lacrimal, m: maxilla, n: nasal, oc: occipital condyle, os: orbitosphenoid, p: parietal, paof: preantorbital fenestra, pf: prefrontal, pm: premaxilla, po: postorbital, pro: prootic, q: quadrate, sa: surangular, sq: squamosal. L and r before bone denotes if it is left or right.

Material and Methods

Specimens. CMC VP14128 was collected in 2010 from the Mother's Day Quarry (MDQ) of south central Montana (MOR locality no. M-166). The MDQ is a monodominant bone bed containing the remains of at least sixteen small diplodocines[6,7] (recorded femur lengths between 59.5 cm–120 cm[5,8]). While five partial braincases have previously been collected from the MDQ, CMC VP14128 is the only complete skull found at the site. The skull of CMC VP14128 is preserved in four major segments (Fig. 1). CMC VP14128 also preserves one half of the proatlas and at least four anterior cervical vertebrae that were clustered with the cranial remains. A second, similarly sized, isolated, and less distorted braincase (CMC VP14129) was also found in the opposite side of the same field jacket.

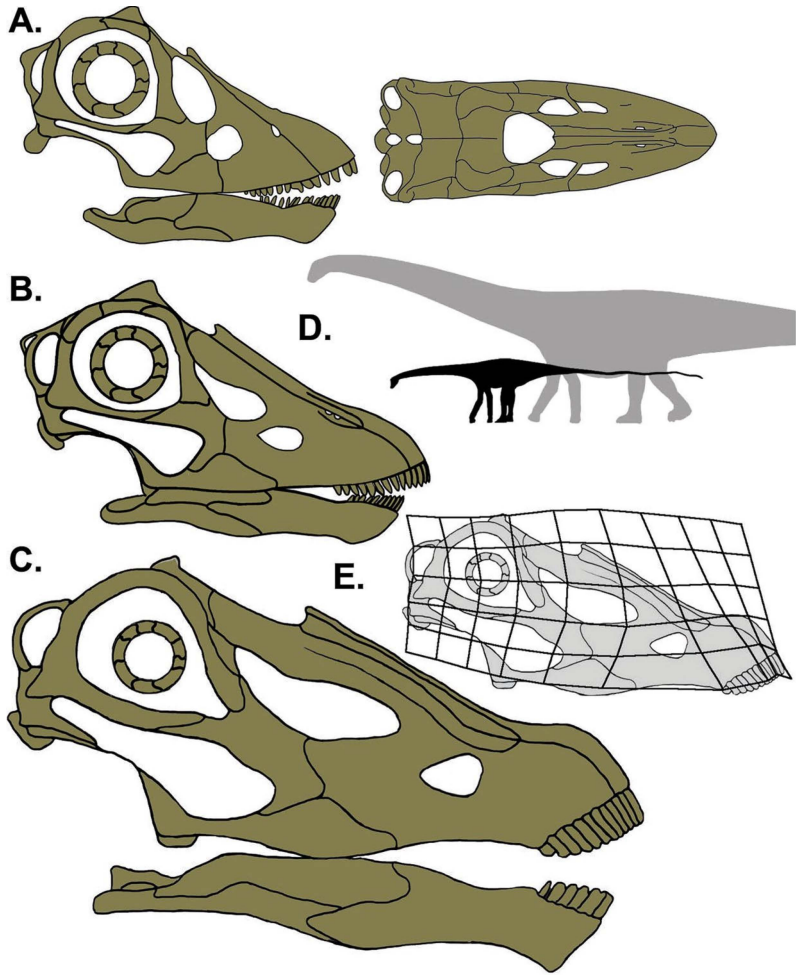

Figure 2. Cranial ontogeny in *Diplodocus* sp. (**A**) CMC VP14128; (**B**) CM 11255 (redrawn from Whitlock *et al.*[3]); (**C**) CM 11161 (redrawn from Wilson and Sereno[69]). Skull drawings by K. Scannella. Skulls to scale. (**D**) Silhouettes of CMC VP14128 and a mature *D. carnegii* to illustrate body length differences between skulls of A and C size. *Diplodocus* silhouette by S. Hartman and PhyloPic (Creative Commons Attribution-ShareAlike 3.0 Unported; http://phylopic.org/image/3cb1d5bf-7db5-4db2-82a6-4c39f6a4441b/; https://creativecommons.org/licenses/by-sa/3.0/), modifications made. Skeletal reconstruction of CMC VP14128 redrawn from *D. carnegii* skeletal by S. Hartman (http://www.skeletaldrawing.com/sauropods-and-kin/diplodocus). (**E**) Transformation grid highlighting the ontogenetic cranial changes. Adult skull is the same in part C (Wilson and Sereno[69]).

Skull length estimates. Anteroposterior skull length was estimated using a linear regression of skull length to lower jaw length in diplodocid genera (Fig. S3). Scaling the anterior and posterior portions of the lower jaw of the immature *Diplodocus* SMM P84.15.3 results in a total jaw length of 19.9 cm, which indicates approximately 5 cm of missing cranial bone. As the cranial dimensions of smaller (and presumably younger) specimens do not develop isometrically (*sensu* Whitlock *et al.*[3]), from CMC VP14128 it appears that the surangular is proportionally smaller and that most of the lower jaw is represented. This approach produces a conservative estimate of 1 cm of missing bone, which results in a jaw length of 15.6 cm and a skull length of 24.3 cm. This shorter estimate is supported by the preservation of the paired dentaries, posterior portions of the jaw and associated ceratobranchial.

Transformation grid. A transformation grid (Fig. 2E) highlighting shape changes between CMC VP14128 and an adult *Diplodocus* was produced using the program tpsSplin[8]. Landmarks were placed on the line drawings of CMC VP14128 and CM 11255 presented in Fig. 2, using the programs tpsUtil[9] and tpsDig264[10] (see Fig. S4).

Phylogenetic analyses. We tested the taxonomic identity of CM VP14128 by including it in the phylogenetic analyses of Whitlock[11] and Tschopp *et al.*[12]. As CMC VP14128 is predominantly represented by cranial material, in addition to the full analyses incorporating all skeletal characters, we also phylogenetically analyzed CMC VP14128 using only cranial characters. An approach such as thus is certainly not fool-proof, nor should the results be unanimously accepted to represent unequivocal relationships – we simply took this approach to examine what, if any, effects might occur from such extensive missing data. We also combined the matrices (excluding redundant characters) into a single data set – 540 characters for the cranial + postcranial matrix (115 scorable

characters – 21% accounted for, 79% missing), and 153 characters for the cranial only matrix (98 scorable characters – 64% accounted for, 36% missing).

Although cranial and vertebral characters identify CMC VP14128 as a diplodocid, it possesses features seen in more inclusive clades, including an extended tooth row, proportionally small antorbital fenestra, and dorsoventrally tall maxilla and premaxilla, which are seen in derived Eusauropoda and basal Macronaria. Paradoxically, if portions of the skull and vertebrae (such as the spatulate teeth and extended tooth row versus the centrum which lack a strong ventral curvature and possess posteriorly elongate postzygapophyses, see below) of CMC VP14128 had been discovered separately, they could have been misidentified.

Furthermore, recent analyses indicate that diplodocids, and potentially all sauropods, underwent allometric growth, and consequently radical ontogenetic trajectories[3,5,13,14]. The documentation of specimens that fill voids in our understanding of sauropod ontogeny is critical. As Rozhdestvensky[15] noted, derived immature individuals can appear more morphologically similar to basal adults than to their own adult form; thus, this developmental aphorism reveals the multifaceted importance of such specimens.

Within the Morrison Formation, some relatively small body size diplodocids have been used to establish new genera (including *Suuwassea*[16] and *Kaatedocus*[17]), and the taxonomy of some has changed in different analyses (e.g. *Suuwassea*[11,12,16,18–20]). When examined using phylogenetic analyses, while there is more recent taxonomic consensus (again *Suuwassea*[11,12,20]) some previous analyses placed such taxa in more basal positions[18,19]. A similar phenomenon has also been seen in other dinosaurian clades[21–26]. Therefore, CMC VP14128 present the opportunity to assess the phylogenetic position of a demonstrably immature animal in a numerical cladistic analysis. Given the presence of plesiomorphic characters, we predict that it will be recovered in a position basal to *Diplodocus*. For this purpose, we used recent phylogenetic analyses as a starting point[11,12] and analyzed the matrices using parsimony and Bayesian algorithms.

Institutional Abbreviations. AMNH, American Museum of Natural History, New York, NY; BYU, Brigham Young University, Provo, UT; CM, Carnegie Museum of Natural History, Pittsburgh, PA; CMC, Cincinnati Museum Center, Cincinnati, OH; HMNS, Houston Museum of Natural Science, Houston, TX; HMN, Humbolt Museum für Naturkunde, Berlin, Germany; MOR, Museum of the Rockies, Bozeman, MT; SMA, Sauriermuseum Aathal, Aathal, Switzerland; SMM, Science Museum of Minnesota, Saint Paul, MN; USNM, United States National Museum, Washington D.C.

Results

Description and comparisons.

Skull. Most of the bones are identifiable, but portions of the maxillae, jugals, nasals, and lacrimals are damaged or missing.

The cranium of CMC VP14128 has diagnostic features of Diplodocidae including: a long prefrontal, paroccipital process with a rounded ventrolateral end, external nares that are retracted and dorsally-facing, a tooth row that does not extend the full length of the maxilla and dentary, low coronoid eminence, and absence of a squamosal-quadratojugal contact. Additionally, the morphology of the basal tubera (robust, triangular, and protruding posteroventrally from the basicranium), the presence of subnarial and maxillary foramina, and the largely peg-like teeth, while not exclusive to Diplodocidae, such morphologies and their combination are commonly observed in diplodocines.

To narrow down the taxonomic identity of CMC VP14128, we compared it with the four Morrison Formation genera of Diplodocinae: *Barosaurus*, *Diplodocus*, *Galeamopus*, and *Kaatedocus*. *Diplodocus* is known from eight complete skulls (CM 11255, CM 3452, CM 11161, MOR 7029, SMM P84.15.3, USNM 2672, USNM 2763), *Kaatedocus* from three skull (AMNH 7530 SMA 0004, SMA D-16/3[12,17]), and *Galeamopus* is reported from at least three partial skulls (AMNH 969, SMA 0011, and HMNS 175[12,27]). Fragmentary cranial remains of *Barosaurus* are reported from the Howe Quarry[12] and recently have been recovered from the Aaron Scott Site in the San Raphael Swell of Utah (CMC VP15544). A tooth row not restricted to the anteriormost portion of the skull is present in CMC VP14128, *Kaatedocus* (SMA 0004), and *Galeamopus* (SMA 0011). The premaxillae of the newest and smallest specimen, CMC VP14128, express the Massopoda condition of four teeth - seen in *Diplodocus* and *Kaatedocus*. In contrast, the reconstructed skull of the *Galeamopus pabsti* holotype has five[27]. The exact morphology of the prefrontal in CMC VP14128 is difficult to determine due to taphonomic distortion, but it appears to exhibit the typical diplodocid posterior hook[27]. The anterior portion of the antorbital fenestra seems to be dorsally situated to the preantorbital fossa as seen in CM 11255, *Galeamopus*[12,27] and possibly in *Kaatedocus*[17], although the damaged margin in CMC VP14128 makes this observation tentative. The posterior margin of the postorbital is gracile and more forked – as in *Diplodocus* and *Kaatedocus*, in contrast to less forked in *Galeamopus*[12,27]; whereas the dorsomedial process is long and tapered as in *Diplodocus* and *Kaatedocus*[3,4,17], but not *Galeamopus*[27]. The squamosal in CMC VP14128 has a tapered and long anterior process approaching the quadrate, as in *Diplodocus* and *Galeamopus*, and not *Kaatedocus* – an autapomorphy of this genus[17]. Due to taphonomic damage and distortion, the morphology of the sagittal nuchal crest cannot be accurately discerned in CMC VP14128 (distinct and narrow vs. wide[11,12]). In contrast, a distinct crest is found in both *Kaatedocus* and *Galeamopus hayi*[12,27], and CMC VP14129 does exhibit this feature (see Materials and Methods). Therefore the weight of evidence indicates a referral to *Diplodocus* over the other taxa.

Mandible. The relative proportions of the dentary and surangular are very similar to the lower jaw of the larger, and slightly more mature *Diplodocus* (CM 11255[3]). Assuming similar proportions of mandibular bones in a mature *Diplodocus* to CMC VP14128, the skull would have been disproportionally stretched (see Material & Methods). Instead, CMC VP14128 indicates that in early ontogeny, the bones of the lower jaw were not directly proportionate to those of an adult (e.g. dentary to total jaw length). Regarding the dentary, the dorsoventral thickness post symphysis is more uniform as in *Diplodocus* and *Kaatedocus*[3,12], opposed to strongly tapered as

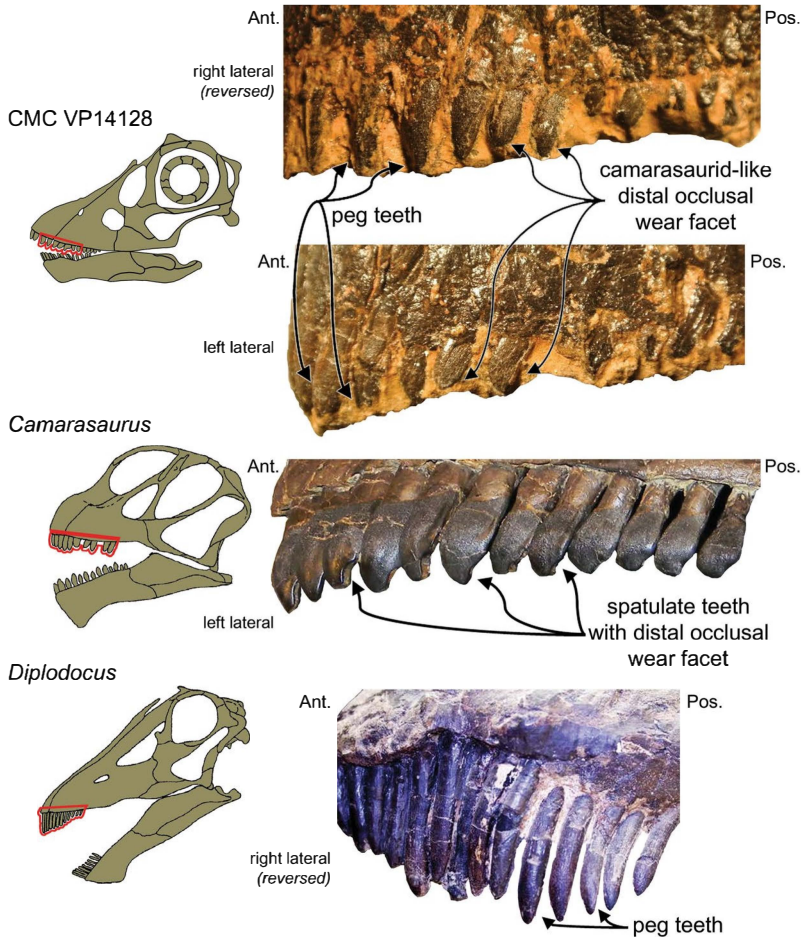

Figure 3. The dental morphotypes in CMC VP14128. Pre- and maxillary teeth of CMC VP14128 in right and left lateral. Drawing by K. Scannella. Red outlines highlight the zoomed in views on the right. Note the combination of diplodocid peg and camarasaurid spatulate tooth forms. *Camarasaurus* sp. with the spatulate tooth form (SMA 0002). *Diplodocus longus* with the peg tooth form (USNM 2672). *Camarasaurus* and *Diplodocus* skull modified from McIntosh[70]. Skulls not to scale.

in *Galeamopus*[27]. One of the most interesting features of the lower jaw is the tooth row (Fig. 1B,C). As expressed in the upper jaw, the lower tooth row extends more posteriorly than seen in more mature specimens. In the right dentary of CMC VP14128, the tooth row (which is posteriorly obscured and damaged) is located along the anterior most ~1.5 cm. The left tooth row, however, clearly spans ~6.5 cm of the dentary; approximately 46% the length of the dentary compared to 22% in adults. Comparable to the adult condition, CM 11255 was hypothesized[3] to have had 10–11 dentary teeth, whereas CMC VP14128 possesses 13. This dental variation may represent intraspecific variation[28], considering that the dentary formula of CMC VP 14128 is the same as in immature camarasauromorphs[28] and that ontogenetic dental formula reduction is documented in other dinosaurs[29,30].

Dentition. The dental formula of CMC VP14128 is 4.8/13; the dental formula of the more mature CM 11255 has a formula of 4.8–9/10–11 dentary teeth, which is comparable to the adult condition of CM 11161 that has a formula of 4.9/11–12[31].

The premaxillary teeth of CMC VP14128 exhibit the typical diplodocine condition: long, slightly inclined, pointed, and narrow-crowned – the so-called peg-like condition. However, from the second maxillary tooth posteriorly, the teeth are apicobasally short, with mesiodistally wide and more labial convex crowns. Several teeth have a *Camarasaurus*-like distal occlusal wear facet (Fig. 3). This relatively basal tooth morphology is consistent with the overall basal-expression form of the cranium.

Maturational state of CMC VP 14128. CMC VP14128 establishes the immature condition for many features of the skull, jaws, dentition, and anterior cervical vertebrae far beyond what has been previously known. We summarize those changes here, and make note of immature features that correspond to the plesiomorphic character states of Diplodocoidea (for a greater discussion on the possibility of ontogenetic recapitulation, please consult the Supplementary Information).

Size. The estimated skull length of CMC VP14128 is 24.29 cm, which is ~40% the length of the largest adult *Diplodocus* skull (USNM 2673, ~60 cm). Cranial size differences observed between CMC VP14128 and adult skulls attest to changing body size through ontogeny (Fig. 2). The cranial size difference between CMC VP14128 and CM 11255 – ~5 cm – seems minor, yet the understanding of sauropodomorph paleobiology is dependent on their relative scale. Understanding minor skeletal nuances can have vast ontogenetic repercussions. A mere 25 cm difference in femoral length separates a 6 m 6-year-old from a 27 m 24-year-old *Diplodocus* (5).

While we do not have complete *Diplodocus* specimens, we have composites and referable material enabling us to draw some conclusions about adult proportions. Specifically, here we use *D. carnegii* CM 84 which is a composite, but represents the informal standard for the genus[32]. Nevertheless, using a ratio from CM 84 assumes isometric growth – contrary to the ontogenetic record of Dinosauria – therefore we should view the resulting estimates as nothing more than generalized proportions.

Using this adult cranial:body length ratio predicts a maximum body length of 9 m for CMC VP14128 and 10.9 m for CM 11255, a difference that would be even greater with a more realistic allometric skull-body length ratio; yet even this isometric trend indicates a minimum difference of nearly 2 m in body length, expressed in ~5 cm of cranial length-difference. While we await more specimens to fill in these crucial ontogenetic intervals, assuming size covaries with age at this locality (see Discussion), we hypothesize that CMC VP14128 was within the recorded MDQ ages of two – six years of age[5] and had a body length well under the isometrically calculated 9 m (Fig. 1).

Tooth count. CMC VP14128 has a high dentary tooth count – 13 – in contrast to the lower tooth count – 11 – seen in larger, presumably more mature specimens, such as CM 11161 (see description above). This variation in tooth count, while limited in sample size, may be indicating a trend of dentary tooth count reduction, which is seen in other immature dinosaurs[29,30,33]. Therefore, the high dentary tooth count of CMC VP14128 indicates its juvenile growth stage. Also, basal eusauropods tend to have a dentary tooth count higher than 11[34,35].

Neurocentral synostosis. Three cervical vertebrae with neural arches are preserved with CMC VP14128. In two of the cervical vertebrae (labeled 2 and 3 in Fig. S1) the arches are completely separate from their centra. One vertebra (labeled 1 in Fig. S1) has a fused arch with sutural contacts that are seen on the anterior- and posterior-most margins. The corresponding sutures in a skeletally mature *Diplodocus* (such as CM 84) are completely closed.

Cervical centrum pneumatization. The cervical centra of CMC VP14128 are excavated by shallow, simple, and weakly divided fossae, typical for young animals, as compared to highly complex fossae and foramina with numerous accessory laminae in adults such as *D. carnegii* CM 84[5,13,36–38].

Cervical rib histology. In the absence of chronologically-informative bones (such as sauropod dorsal ribs that provide an almost complete growth record[39–41]), a cervical rib of CMC VP14128 was sectioned to obtain an estimate of the relative maturity of the specimen based on patterns of remodeling – in like manner to the Histologic Ontogenetic Stage[42]. However, we must cautiously note that the origin and development of cervical ribs is still ongoing research (JRH and DCW in prep.). As cervical ribs incorporate a complex developmental relationship of metaplastic and osteogenic processes[43,44], at this time we should only compare rates of secondary remodeling (Fig. S2).

Progressing through maturity in diplodocid cervical ribs, there are dramatic changes in tissue composition. In the smallest specimen (SMA 0009) the tissue is composed entirely of highly vascular primary tissue. Progressing to CMC VP14128 the tissue is composed of secondary reconstructions and primary tissue – features indicative of metaplasia[45]. Finally, within a sub-adult *Diplodocus* (MOR 592), the tissue consists of regular bony tissues - a core of Haversian bone, periosteally grading from secondary to primary osteons (see greater discussion in the Supplementary Material).

While the ontogenetic development of cervical ribs must be studied in further detail, this analysis supports the hypothesis that they develop via metaplasia from a collagenous to an osseous tissue[43,44]. Thus, the cervical rib of CMC VP14128, conforming to this developmental pathway, further supports our maturational interferences of immaturity for this specimen.

Systematic Paleontology
Saurischia Seeley 1887
Sauropodomorpha von Huene 1932
Sauropoda Marsh 1878
Diplodocoidea Marsh 1884
Flagellicaudata Harris and Dodson 2004
Diplodocidae Marsh 1884
cf. *Diplodocus* Marsh 1878.

Comparative description. The Morrison Formation preserves three sauropod clades: Diplodocoidea, Camarasauridae, and Brachiosauridae. The lack of only spatulate teeth, an inclined posterior portion of the premaxilla, projecting external naris, cervical ribs shorter than centrum, and rectangular not rhomboidal cervical vertebrae profiles in CMC VP14128 are more diplodocoid than macronarian morphologies. Although many of the diagnostic characters in the sauropod skull are proportionally or ontogenetically variable[46] some of the morphologies within CMC VP14128 are different from those expressed in the adult. While a few traits could be outside of the typical adult expressions, we hypothesize that characters/conditions of CMC VP14128 will at least largely associate with a known genus (as previously demonstrated in *Europasaurus*[47]).

CMC VP14128 is referable to Diplodocidae based on the presence of: a long posterior process of the prefrontal, teeth that do not span the length of the maxilla and dentary, a low coronoid eminence on the mandible, lack of crown-to-crown occlusion, cervical rib length that is shorter than the corresponding centrum length, and external nares that are retracted and face dorsally. CMC VP14128 is not referable to *Apatosaurus* given the presence of a basipterygoid recess, a basipterygoid process that lacks an anteroventral flare, and enlarged cervical ribs that do not project below the centrum. Likewise, CMC VP14128 is not referable to *Barosaurus*, based on the presence of long postzygapophyses, anteroposteriorly narrow neural spines, and a strongly posteriorly-angled centrum cotyles. CMC VP14128 has its strongest affinities with the slender diplodocines, including *Diplodocus*, *Galeamopus*, and *Kaatedocus*; however, the distribution of shared features is inconsistent, obscuring its lower-level identity. However, based on the number of shared characteristics, CMC VP14128 is most referable to *Diplodocus* than either *Galeamopus* or *Kaatedocus*.

However, it must be stated that specimens previously assigned to *Diplodocus*, and how we phylogenetically recognize and identify this genus are being reexamined[12,32]. Some historically recognized *Diplodocus* specimens are now being referred to other genera – such as USNM 2673 possibly representing *Galeamopus*[12] and even CM 11255 to *Barosaurus*[48]. Additionally, some Morrison Formation taxa have little to any known or described cranial material (*Barosaurus*, *Dystrophaeus*, *Haplocanthosaurus*, *Supersaurus*, *Suuwassea*), therefore there are several taxa we cannot adequately compare CMC VP14128 to or assess. Additionally, while Whitlock[11] identified three cranial autapomorphies for *Diplodocus* (preantorbital fenestra with well-defined fossa, pterygoid medial to ectopterygoid on transverse palatal hook, teeth inclined anteriorly relative to axis of jaw) since no skulls to date are unquestionably associated with post-crania, Tschopp *et al.*[12] questioned these characters. While the latest phylogenetic analysis of Diplodocidae would advocated that no unambiguous diplodocinae cranial synapomorphies are recognized[12], the exact taxonomic assignment of CMC VP14128 within Diplodocinae remains uncertain. With the current lack of no known diplodocinae synapomorphies[12], one could taxonomically identify CMC VP14128 simply as diplodocinae indeterminate. However, given the predominance of similar morphologies between CMC VP14128 and *Diplodocus* sp. in comparison to the other Morrison Formation diplodocids, we tentatively opt to refer CMC VP14128 to cf. *Diplodocus*. While both identifications (diplodocinae indeterminate and cf. *Diplodocus*) are testable hypotheses, we currently believe that it is more fruitful and more constructive for future works to support/refute our identification of CMC VP14128 as cf. *Diplodocus* versus reanalyzing starting from a subfamily level identification.

Phylogenetic analyses. *Separate data sets.* The cranial + postcranial parsimony and Bayesian analyses of the Whitlock[11] data set recovered CMC VP14128 as the basalmost member of Dicraeosauridae, while the cranial only analysis recovered CMC VP14128 as the sister species of Dicraeosauridae, and *Dicraeosaurus* + *Amargasaurus*, respectively. The cranial + postcranial parsimony and Bayesian analyses of the Tschopp *et al.*[12] data set recovered CMC VP14128, as a diplodocine more derived than *Diplodocus*, while the cranial only analysis recovered CMC VP14128 in a polytomy within Flagellicaudata.

Combined data set. In the combined cranial + postcranial parsimony and Bayesian typology, there is a degree of basal uncertainty (no united Macronaria), yet there is a structured and organized Diplodocoidea (Fig. 4). In the parsimony typology, CMC VP14128 is recovered as the sister species to *Diplodocus*, while in the Bayesian analysis, it is recovered as a derived member of Flagellicaudata and basal to Diplodocidae. For the combined cranial only analyses, the typologies are similar to that of the cranial + postcranial analyses. There are distinct Rebbachisauridae, Dicraeosauridae, and Diplodocidae branches, and CMC VP14128 is recovered as the sister taxon to *Diplodocus*. Apart from minor changes in posterior probability, the Bayesian topology is very similar to the earlier analysis[12]. It likewise recovers CMC VP14128 in a flagellicaudatan polytomy in which Dicraeosauridae forms one branch. Yet we would caution that while these two analyses superficially produce similar results, the low support for groupings indicates that these relations are not definitive.

The minutia between the parsimony and Bayesian analyses do vary, but in general the encompassing skeletal analyses do little to elucidate the taxonomic identify of CMC VP14128. In the analysis of Whitlock[11], CMC VP14128 is recovered in the same dicraeosaurid position, while in the analysis of Tschopp *et al.*[12] taxonomy is slightly more refined as CMC VP14128 is recovered as a derived diplodocine versus a flagellicaudatan polytomy, and finally in the combined analysis, CMC VP14128 is still recovered as a diplodocoid. Certainly the encompassing analyses do reveal much more overall taxonomic resolution, but said resolution is largely irrespective to CMC VP14128. A cranial only approach could appear redundant or unnecessary, yet given the vastly differing phylogenetic placements between the matrices used herein, we would suggest that an elemental or regional styled analyses can be used to further check or verify specimens that are recovered in seemingly unusual or suspect positions.

Discussion

Phylogeny. Parsimony analyses of CMC VP14128 produced a conflict. One resulted in only a generic level association with *Diplodocus*, while the other advocated a unique basal position. If our cranial-only analyses represent true phylogenetic patterns, then relatively small morphological matrices (in terms of number of characters, percentage of each character region, and/or taxa) can be sensitive to inclusion of juvenile specimens[5], as demonstrated by the more basal positioning of CMC VP14128. This is expected as even a few characters that change with ontogeny will have a large effect on the outcome of the analysis. In the larger[12] and combined analyses, CMC VP14128 is recovered amongst other flagellicaudatans (including diplodocids), albeit in large polytomies, agreeing with our previous diagnosis. This suggests including additional characters can override the effect of a few characters that are ontogenetically biased, but as paleontological phylogenetic analyses are often based on small datasets, this bias can be significant.

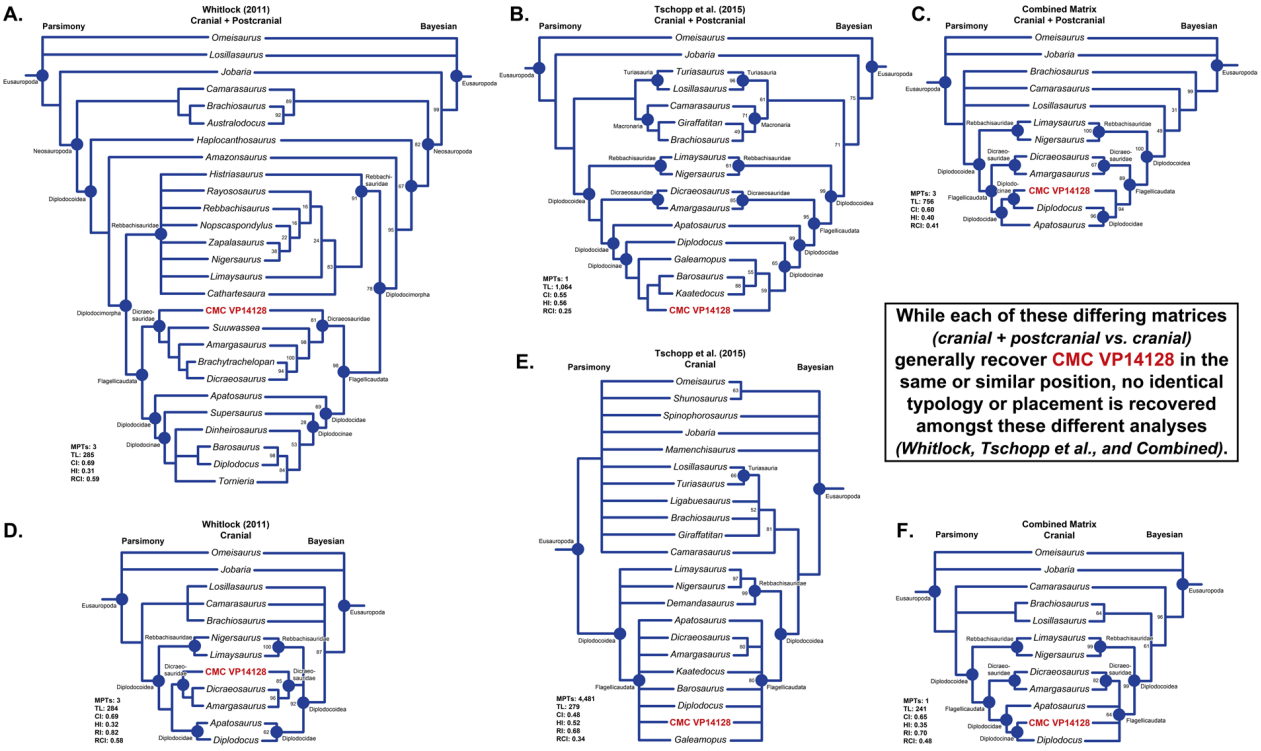

Figure 4. Dendrograms of parsimony (left column) and Bayesian (right column) phylogenetic analyses. (**A**–**C**) Consist of cranial and postcranial characters, while (**D**,**E**) consist of only cranial characters. (**A** and **D**) CMC VP14128 coded into the matrix of Whitlock[11]. (**B** and **E**) CMC VP14128 coded into the matrix of Tschopp *et al.*[12]. (**C** and **F**) CMC VP14128 coded into a combined matrix.

In regard to the plesiomorphic characters in CMC VP14128, we theorize these might be evidence of recapitulation; i.e., the ephemeral presence of plesiomorphic characters that transition into their derived states by adulthood. Recapitulation has been documented in other basal[49,50] and derived[47,51–53] immature sauropods. Morphologies in CMC VP14128 – such as the posterior tooth row, lower jaw proportions, and rounded snout – could be recapitulatory in origin (see Supplementary Material); yet given the relationship between cranial attributes and feeding strategy, these morphologies could also derive from ontogenetic ecomorphological relationships (see below). More specimens and analyses are need to substantiate either possibility, and we note that these hypotheses are not mutually exclusive.

Despite the presence in CMC VP14128 of phylogenetically plesiomorphic features that are not seen in adult *Diplodocus*, this does not mean that the entire skeleton of CMC VP14128 is plesiomorphic, (or that it is a misidentified basal taxon), since the specimen does have characters of *Diplodocus*. Instead, this combination of characters is evidence that 1: not all parts of the skeleton develop at the same rate, and 2: regardless of rate, ontogenetic skeletal changes followed the phylogenetic progression from plesiomorphic to derived states. Recognition of this phenomenon strongly cautions against diagnosing new taxa based on small statured specimens displaying a combination of basal and derived characters, which might instead be evidence of immaturity. Interestingly, similar findings were reported by Tschopp *et al.*[12] regarding "*Elosaurus*" *parvus* (CM 566). While originally thought to be a valid taxon, "*Elosaurus*" is now regarded as an immature *Brontosaurus parvus*[12] (however, while this analysis believes this maturational inference is highly likely, we cautiously note that this hypothesis has not been histologically tested). Including CM 566 into a specimen-level analysis, Tschopp *et al.*[12] recovered the specimen not only within the species *B. parvus*, but also as the basalmost specimen. We would agree with Tschopp *et al.*[12] that more studies are needed to address this issue, and this further highlights the multifaceted relationship between ontogenetically variable characters and taxonomic recovery.

Ecomorphology and behavior implications. The unique cranial and dental characters seen in the immature CMC VP14128 suggests resource partitioning between juvenile and adult *Diplodocus*. Like the immature *Diplodocus* CM 11255[3], CMC VP14128 has a mediolaterally narrow snout, in stark contrast to more mature individuals that express a wide and squared snout. These differences have been hypothesized to indicate dietary niche-partitioning through ontogeny[3], and the narrow snout of CMC VP14128 is consistent with the hypothesis that immature diplodocids had a selective feeding strategy, while fully mature animals were ground-level browsers[3]. CMCVP14128 also has spatulate teeth and an extended tooth row. Spatulate teeth are more efficient for coarse vegetation and bulk feeding, and non-spatulate teeth are beneficial for softer foliage and browsing[54,55]. This combination of dental morphologies in CMC VP14128 may indicate that very immature diplodocids were feeding on a greater variety of plant materials, and orally processed them differently than their more mature counterparts.

Figure 5. Life reconstruction of CMC VP14128. Note the cranial morphologies interpreted to denote differing feeding strategies: in CMC VP14128 the narrow snout with posteriorly elongated and morphologically varied tooth row for bulk feeding vs. the widened snout with anteriorly restricted peg-shaped teeth for ground-level browsing in adults. Also note the camouflaged ontogenetic color change suggesting young diplodocids may have sought forested refuge. Reconstruction by A. Atuchin.

However, previous studies show that nutrition selectivity is problematic in animals exceeding a certain size and that there is a selection pressure towards browsing for large herbivores[56,57]. Another recent analysis[58] showed that narrow, short, and rounded macronarian snouts were more efficient for forested environments while broader and longer diplodocoid snouts suggest open, ground-level browsing. This could also be interpreted as indicators of different ecological environments, implying macronarians would have been adapted for more forested environments while diplodocids were more specialized for open environments. Therefore, the plesiomorphic macronarian-like characters seen in CMC VP14128 could also indicate that juvenile diplodocids lived in more forested environments than the adults that (restricted and protected by their size) were most likely browsing in more open habitats. Foraging in forests would have provided the juveniles with protective cover from predators, a danger that colossal adults would not share.

The skull and tooth morphology of *Diplodocus* suggests that these animals transitioned through distinct feeding roles over their lifespan. This inference is supported by a study of *Alligator mississippiensis* tooth change through ontogeny[59]. Dental changes coincided with changes in diet[59–61], thus dental allometry could be attributed to dietary partitioning.

Though it is currently unknown which specific plant species Morrison Formation sauropods ate, based on $\delta^{13}C$ relationships between modern plant equivalents and tooth enamel implies that *Diplodocus* may have fed on ferns and horsetail, while *Camarasaurus* was generalized, feeding on a wide range of foliage, including ferns, horsetails, conifers, and cycads[62]. An immature *Diplodocus* may have fended for itself (or possibly as part of an age-segregated herd[63]) and fed on differing foliage to gain more nutrients during critical development.

The ontogenetic change in dental morphologies observed within *Diplodocus* also gives evidence for the lack of parental care in sauropods (along with nest structures and histology[14,64]). If adults fed hatchlings - potentially the foliage they ate - then there would be no reason for the changes in tooth morphology. Evidence of precocial juvenile sauropods was also found in a recent histologic assessments of a very immature titanosaur. Furthermore, the extreme size differences between parent and hatchlings could have resulted in high infant mortalities due to trampling.

The differences in cranial morphology between CMC VP14128 and more mature *Diplodocus* specimens (such as CM 11255; Whitlock *et al.*[3]) highlights extreme cranial changes that occurred rapidly over a short increase in size. In addition to the narrow snout, the proportionally enlarged braincase and extremely large orbits are both infantile attributes observed in many other immature vertebrates. The more box-like cranial condition and the extended tooth row in CMC VP14128 are reminiscent of the co-occurring camarasaurid condition. If these characters represents recapitulation, we could hypothesize that dietary generalization is the more basal condition and increasing specialization the more derived.

Possible dwarfism? Instead of a juvenile, CMC VP14128 could represent an unknown Morrison Formation dwarf taxon. Two separate investigations of age determinant histology and morphology of the MDQ material produced different results[5,41]. The bone tissue types in the first analysis indicate average sized immature diplodocids with typically expressed tissues[5], yet many of the specimens of the second analysis exhibit tissues indicating skeletal maturity[41]. In comparing histology, this is not simply the case of incorrect tissue interpretations (DCW and KW pers. obs.) – the varying tissue morphologies indicate a more complex story for the MDQ.

The regional geology does not support the presence of an island depositional system – an extensive marine unit with localized terrestrial deposits. Nevertheless, regional geography or environment could explain a possible size difference. In the case of stegosaur specimens from the northern extent of the Morrison Formation, larger overall size (*Stegosaurus*) appears correlated with arid environments, and smaller size with wetter climates (*Hesperosaurus*[65]). Based on the coastal setting adjacent to the Sundance Seaway, this trend in stegosaur size was hypothesized to be environmentally correlated[65]. A similar pattern might hold true for the MDQ diplodocids.

Other Morrison Formation localities in Montana record more typical sized specimens of *Apatosaurus* and *Diplodocus*[5,66]. This regional size difference, and size difference within the MDQ[41], may represent regional variation. Such regional differences are present in a modern group of herbivores, cervids. The North American coastal White-tailed Deer (*Odocoileus virginianus*) have an average body mass 77 kg, while their interior counterparts have an average body mass in excess of 100 kg[67]. The smallest sub-species, the Key Deer (*Odocoileus virginianus clavium*) represents an example of island dwarfing has an average body mass of 34 kg[67]. Therefore, these size differences between localities may indicate variably-sized regional diplodocid populations. In spite of these findings CMC VP14128 is almost certainly not a regional dwarf because it lacks autapomorphies. The morphologies we assigned to ontogeny could hypothetically be used to erect autapomorphies, however we strongly caution that the onus is on such an analysis to demonstrate that no attributes are related to ontogenetic variation as proposed herein. Alternatively, opposed to the dwarf morphotype observed by Waskow *et al.*[41], CMC VP14128 may represent the larger morph present at the site.

Conclusions

Within Dinosauria, there are small bodied taxa that display basal and derived characters and occupy unusual basal phylogenetic positions. The validity and position of such taxa has been disputed[21–26,68,69], and regarding sauropodomorph phylogeny, we would advocate that the combination of basal and derived characters and basal phylogenetic recovery should be recognized as an indicator of an immature ontogimorph – instead of a distinct taxon. In light of the current wealth of information pertaining to dinosaur ontogeny, we can no longer assume that all morphological differences correspond with phylogenetic distinctiveness. Accounting for ontogeny could prove as test for our phylogenies. Recognizing the ontogenetic age of immature specimens provides important insights into the life history of these animals. The immature *Diplodocus* specimen CMC VP14128 extends our understanding of the ontogeny of the genus and the evolution of diplodocids into new areas, where:

(1) The combination of basal and derived characters in the juvenile is broadly congruent with the phylogenetic transition from eusauropods to diplodocoids.
(2) The plesiomorphic tooth morphology is retained in immature *Diplodocus* and lost with maturity, and we predict this growth pattern will be seen in all other diplodocoids.
(3) As first proposed by Whitlock *et al.*[3], tooth and skull morphology indicate that during growth *Diplodocus* inhabited different trophic levels/niches, where juveniles were generalists (i.e., browsers; Fig. 5) and more mature individuals were specialists (i.e., ground-level browsing), a pattern that we predict is ancestral for Diplodocoidea.

References

1. Foster, J. *Jurassic West: The Dinosaurs of the Morrison Formation and their World*. (Indiana University Press, 2007).
2. Berman, D. & McIntosh, J. S. Skull and relationships of the Upper Jurassic sauropod *Apatosaurus* (Reptilia, Saurischia). *Ann. Carnegie Museum* **8**, 1–35 (1978).
3. Whitlock, J. A., Wilson, J. A. & Lamanna, M. C. Description of a nearly complete juvenile skull of *Diplodocus* (Sauropoda: Diplodocoidea) from the Late Jurassic of North America. *J. Vertebr. Paleontol.* **30**, 442–457 (2010).
4. Erickson, B. History of the Poison Creek expedition 1976–1990: With description of *Haplocanthosaurus* postcranials and a subadult diplodocid skull. *Sci. Museum Minnesota Monogr.* **8**, 1–34 (2014).
5. Woodruff, D. C., Fowler, D. W. & Horner, J. R. A new multi-faceted framework for deciphering diplodocid ontogeny. *Palaeontol. Electron.* **20.3.43A**, 1–53 (2017).
6. Myers, T. S. & Storrs, G. W. Taphonomy of the Mother's Day Quarry, Upper Jurassic Morrison Formation, south-central Montana, USA. *Palaios* **22**, 651–666 (2007).
7. Storrs, G. W., Oser, S. E. & Aull, M. Further analysis of a Late Jurassic dinosaur bone-bed from the Morrison Formation ofMontana, USA, with a computed three-dimensional reconstruction. *Earth Environ. Sci. Trans. R. Soc. Edinburgh* **103**, 443–458 (2013).
8. Rohlf, F. TpsSplin ver 1.22. *Stony Brook, NY* (2016).
9. Rohlf, F. TpsUtil ver. 1.64. *Stony Brook, NY* (2013).
10. Rohlf, F. J. tpsDig2, digitize landmarks and outlines, version 2.10. *Dep. Ecol. Evol. State Univ. New York Stony Brook* (2015).
11. Whitlock, J. A. A phylogenetic analysis of Diplodocoidea (Saurischia: Sauropoda). *Zool. J. Linn. Soc.* **161**, 872–915 (2011).
12. Tschopp, E., Mateus, O. & Benson, R. B. J. A specimen-level phylogenetic analysis and taxonomic revision of Diplodocidae (Dinosauria, Sauropoda). *PeerJ* **3**, e857 (2015).
13. Carballido, J. L. & Sander, P. M. Postcranial axial skeleton of *Europasaurus holgeri* (Dinosauria, Sauropoda) from the Upper Jurassic of Germany: Implications for sauropod ontogeny and phylogenetic relationships of basal Macronaria. *J. Syst. Palaeontol.* **12**, 335–387 (2014).
14. Rogers, K. C., Whitney, M., D'Emic, M. & Bagley, B. Precocity in a tiny titanosaur from the Cretaceous of Madagascar. *Science.* **352**, 450–453 (2016).
15. Rozhdestvensky, A. K. Growth changes in Asian dinosaurs and some problems of their taxonomy. *Paleontol. žurnal* **3**, 95–109 (1965).
16. Harris, J. D. The significance of *Suuwassea emilieae* (Dinosauria: Sauropoda) for flagellicaudatan intrarelationships and evolution. *J. Syst. Palaeontol.* **4**, 185–198 (2006).
17. Tschopp, E. & Mateus, O. The skull and neck of a new flagellicaudatan sauropod from the Morrison Formation and its implication for the evolution and ontogeny of diplodocid dinosaurs. *J. Syst. Palaeontol.* **11**, 853–888 (2013).
18. Rauhut, O. W. M., Remes, K., Fechner, R., Cladera, G. & Puerta, P. Discovery of a short-necked sauropod dinosaur from the Late Jurassic period of Patagonia. *Nature* **435**, 670–672 (2005).
19. Lovelace, D. M., Hartman, S. A. & Wahl, W. R. Morphology of a specimen of *Supersaurus* (Dinosauria, Sauropoda) from the Morrison Formation of Wyoming, and a re-evaluation of Diplodocid phylogeny. *Arq. do Mus. Nac.* **65**, 527–544 (2007).
20. Whitlock, J. A. & Harris, J. D. The dentary of *Suuwassea emilieae* (Sauropoda: Diplodocoidea). *J. Vertebr. Paleontol.* **30**, 1637–1641 (2010).
21. Carr, T. D. & Williamson, T. E. Diversity of late Maastrichtian Tyrannosauridae (Dinosauria: Theropoda) from western North America. *Zool. J. Linn. Soc.* **142**, 479–523 (2004).
22. Fowler, D. W., Woodward, H. N., Freedman, E. A., Larson, P. L. & Horner, J. R. Reanalysis of '*Raptorex kriegsteini*': A juvenile tyrannosaurid dinosaur from Mongolia. *PLoS One* **6** (2011).
23. Campione, N. E., Evans, D. C. Jr, J, S., Cuthbertson, R. & Holliday, C. Cranial growth and variation in Edmontosaurs (Dinosauria: Hadrosauridae): implications for latest Cretaceous megaherbivore diversity in North America. *PLoS One* **6**, e25186 (2011).

24. Frederickson, J. A. & Tumarkin-Deratzian, A. R. Craniofacial ontogeny in *Centrosaurus apertus*. *PeerJ* **2**, e252 (2014).
25. Scannella, J. B., Fowler, D. W., Goodwin, M. B. & Horner, J. R. Evolutionary trends in Triceratops from the Hell Creek Formation, Montana. *Proc. Natl. Acad. Sci.* **111**, 10245–10250 (2014).
26. Fowler, E. A. F. & Horner, J. R. A new brachylophosaurin hadrosaur (Dinosauria: Ornithischia) with an intermediate nasal crest from the Campanian Judith River Formation of northcentral Montana. *PLoS One* **10** (2015).
27. Tschopp, E. & Mateus, O. Osteology of *Galeamopus pabsti* sp. nov. (Sauropoda: Diplodocidae), with implications for neurocentral closure timing, and the cervico-dorsal transition in diplodocids. *PeerJ* **5**, e3179 (2017).
28. Gilmore, C. W. A nearly complete articulated skeleton of *Camarasaurus*, a saurischian dinosaur from the Dinosaur National Monument, Utah. *Mem. Carnegie Muse*um (1925).
29. Carr, T. D. Craniofacial ontogeny in Tyrannosauridae (Dinosauria, Coelurosauria). *J. Vertebr. Paleontol.* **19**, 497–520 (1999).
30. Carr, T. D., Varricchio, D. J., Sedlmayr, J. C., Roberts, E. M. & Moore, J. R. A new tyrannosaur with evidence for anagenesis and crocodile-like facial sensory system. *Sci. Rep*. **7** (2017).
31. Yu, C. The skull of *Diplodocus* and the phylogeny of the Diplodocidae. PhD thesis, (University of Chicago, 1993).
32. Tschopp, E. & Mateus, O. Case 3700: *Diplodocus* Marsh, 1878 (Dinosauria, Sauropoda): proposed designation of *D. carnegii* Hatcher, 1901 as the type species. *Bull. Zool. Nomencl.* **73**, 17–24 (2016).
33. Wang, S. *et al*. Extreme ontogenetic changes in a ceratosaurian theropod. *Curr. Biol.* **27**, 144–148 (2017).
34. He, X., Li, K. & Cai, K. The Middle Jurassic dinosaur fauna from Dashanpu, Zigong, Sichuan: *Omeisaurus tianfuensi*s. Sauropod dinosaurs (2). *Sichuan Publ. House Sci. Technol* (1988).
35. Ouyang, H. & Ye, Y. The first mamenchisaurian skeleton with a complete skull *Mamenchisaurus youngi*. *Sichuan Publ. House Sci. Technol* (2002).
36. Wedel, M. J. The evolution of vertebral pneumaticity in sauropod dinosaurs. *J. Vertebr. Paleontol.* **23**, 344–357 (2003).
37. Wedel, M. J. Vertebral pneumaticity, air sacs, and the physiology of sauropod dinosaurs. *Paleobiology* **29**, 243–255 (2003).
38. Wedel, M. J. In *The sauropods: evolution and paleobiology* (eds Rogers, K. C. & Wilson, J.) 201–228 (University of California Press, 2005).
39. Waskow, K. & Sander, P. M. Growth record and histological variation in the dorsal ribs of Camarasaurus sp. (Sauropoda). *J. Vertebr. Paleontol.* **34**, 852–869 (2014).
40. Waskow, K. & Mateus, O. Dorsal rib histology of dinosaurs and a crocodylomorph from western Portugal: Skeletochronological implications on age determination and life history traits. *Comptes Rendus Palevol* **16**, 425–439 (2017).
41. Waskow, K., Wiersma, K., Tschopp, E., Woodruff, D. C. & Sander, P. M. Histological evidence for dwarfism and slow growth in Late Jurassic diplodocoid sauropods from the Upper Jurassic Mother's Day Quarry (Morrison Formation, Montana, USA). *Paleobiology*.
42. Klein, N. & Sander, M. Ontogenetic stages in the long bone histology of sauropod dinosaurs. *Paleobiology* **34**, 247–263 (2008).
43. Cerda, I. A. *et al*. Novel insight into the origin of the growth dynamics of sauropod dinosaurs. *PLoS One* **12** (2017).
44. Klein, N., Christian, A. & Sander, P. M. Histology shows that elongated neck ribs in sauropod dinosaurs are ossified tendons. *Biol. Lett.* **8**, 1032–1035 (2012).
45. Horner, J. R., Woodward, H. N. & Bailleul, A. M. Mineralized tissues in dinosaurs interpreted as having formed through metaplasia: A preliminary evaluation. *Comptes Rendus - Palevol* **15**, 183–203 (2016).
46. Chure, D., Britt, B. B., Whitlock, J. A. & Wilson, J. A. First complete sauropod dinosaur skull from the Cretaceous of the Americas and the evolution of sauropod dentition. *Naturwissenschaften* **97**, 379–391 (2010).
47. Marpmann, J. S., Carballido, J. L., Sander, P. M. & Knötschke, N. Cranial anatomy of the Late Jurassic dwarf sauropod *Europasaurus holgeri* (Dinosauria, Camarasauromorpha): Ontogenetic changes and size dimorphism. *J. Syst. Palaeontol.* **13**, 221–263 (2015).
48. Melstrom, K. M., D'emic, M. D., Chure, D. & Wilson, J. A. A juvenile sauropod dinosaur from the Late Jurassic of Utah, U.S.A., presents further evidence of an avian style air-sac system. *J. Vertebr. Paleontol.* **36** (2016).
49. Reisz, R. R., Scott, D., Sues, H. D., Evans, D. C. & Raath, M. A. Paleontology: Embryos of an early Jurassic prosauropod dinosaur and their evolutionary significance. *Science (80-.).* **309**, 761–764 (2005).
50. Reisz, R. R., Evans, D. C., Sues, H. D. & Scott, D. Embryonic skeletal anatomy of the sauropodomorph dinosaur *Massospondylus* from the lower Jurassic of South Africa. *J. Vertebr. Paleontol.* **30**, 1653–1665 (2010).
51. Chiappe, L. M., Salgado, L. & Coria, R. A. Embryonic skulls of titanosaur sauropod dinosaurs. *Science* **293**, 2444–2446 (2001).
52. García, R. A. & Cerda, I. A. Dentition and histology in titanosaurian dinosaur embryos from Upper Cretaceous of Patagonia, Argentina. *Palaeontology* **53**, 335–346 (2010).
53. García, R. A. *et al*. Paleobiology of titanosaurs: Reproduction, development, histology, pneumaticity, locomotion and neuroanatomy from the South American Fossil Record. *Ameghiniana* **52**, 29–68 (2015).
54. Fiorillo, A. R. Dental microwear patterns of the sauropod dinosaurs *Camarasaurus* and *Diplodocus*: evidence for resource partitioning in the Late Jurassic of North America. *Hist. Biol.* **13**, 1–16 (1998).
55. D'Emic, M. D., Whitlock, J. A., Smith, K. M., Fisher, D. C. & Wilson, J. A. Evolution of High Tooth Replacement Rates in Sauropod Dinosaurs. *PLoS One* **8** (2013).
56. Hummel, J. *et al*. *In vitro* digestibility of fern and gymnosperm foliage: implications for sauropod feeding ecology and diet selection. *Proc. R. Soc. B Biol. Sci.* **275**, 1015–1021 (2008).
57. Westoby, M. An Analysis of Diet Selection by Large Generalist Herbivores. *Am. Nat.* **108**, 290–304 (1974).
58. Whitlock, J. A. Inferences of diplodocoid (Sauropoda: Dinosauria) feeding behavior from snout shape and microwear analyses. *PLoS One* **6** (2011).
59. Gignac, P. M. Biomechanics and the ontogeny of feeding in the American alligator: reconciling factors contributing to intraspecific niche differentiation in a large-bodied vertebrate. (Florida State University, 2010).
60. Dodson, P. Functional and ecological significance of relative growth in Alligator. *J. Zool.* **175**, 315–355 (1975).
61. Bailleul, A. M., Scannella, J. B., Horner, J. R. & Evans, D. C. Fusion patterns in the skulls of modern archosaurs reveal that sutures are ambiguous maturity indicators for the Dinosauria. *PLoS One* **11** (2016).
62. Tütken, T. In *Biology of the Sauropod dinosaurs: understanding the life of giants* (eds Klein, N., Remes, K., Gee, C. T. & Sander, P. M.) 57–79 (Indiana University Press, 2011).
63. Myers, T. S. & Fiorillo, A. R. Evidence for gregarious behavior and age segregation in sauropod dinosaurs. *Palaeogeogr. Palaeoclimatol. Palaeoecol.* **274**, 96–104 (2009).
64. Chiappe, L. M. *et al*. Nest Structure for Sauropods: Sedimentary Criteria for Recognition of Dinosaur Nesting Traces. *Palaios* **19**, 89–95 (2004).
65. Maidment, S. C. R., Woodruff, D. C. & Horner, J. R. A new specimen of the ornithischian dinosaur *Hesperosaurus mjos*i from the Upper Jurassic Morrison Formation ofMontana, USA, and implications for growth and size in Morrison stegosaurs. *J. Vertebr. Paleontol*. **e1406366** (2018).
66. Woodruff, D. C. & Rogers, K. C. Diplodocid Sauropods From The Late Jurassic Morrison Formation Of Montana. *SVP Conf. 2014* Abstract (2014).
67. Geist, V. *Deer of the world: their evolution, behaviour, and ecology*. (Stackpole books, 1998).
68. Scannella, J. B. & Horner, J. R. *Torosaurus* Marsh, 1891, is *Triceratops* Marsh, 1889 (Ceratopsidae: Chasmosaurinae): Synonymy through ontogeny. *J. Vertebr. Paleontol.* **30**, 1157–1168 (2010).
69. Wilson, J. & Sereno, P. C. Early Evolution and Higher Level Phylogeny of Sauropod Dinosaurs. *J. Vertebr. Paleontol.* **18**, 1–68 (1998).
70. McIntosh, J. S. In *The Dinosauria* (eds Weishampel, D. B., Dodson, P. & H., O.) 345–401 (University of California Press, 1990).

Acknowledgements

Thanks to the Cincinnati Museum Center Dinosaur Field School participants, the U.S. Bureau of Land Management (permit M 99231), and to S. Oser for initiating this research. K. Curry Rogers provided invaluable descriptive assistance. J. Horner and the Museum of the Rockies provided financial support associated with transportation and preparation. E.T. Lamm created the histologic thin sections of CMC VP14128. K. Scannella produced the cranial drawings of CMC VP14128 used in Figs 2, 3, 4, and SI Fig. 4. A. Atuchin produced the exquisite life restoration of CMC VP14128 in Fig. 5. Thanks to C. Ancell and B. Harmon for the preparation and casting. E. Tschopp and J. Whitlock provided invaluable reviews that greatly improved this work.

Author Contributions

G.W.S. collected the specimen, D.C.W. described the specimen, D.C.W., T.D.C., G.W.S., K.W., J.B.S., K.K.N. and J.P.W. wrote the manuscript, T.D.C. and K.K.N. created and analyzed the phylogenetic models, J.B.S. created the transformation grid, J.P.W. photographed the specimen and created the photogrammetric models.

Additional Information

Supplementary information accompanies this paper at https://doi.org/10.1038/s41598-018-32620-x.

Competing Interests: The authors declare no competing interests.

Publisher's note: Springer Nature remains neutral with regard to jurisdictional claims in published maps and institutional affiliations.

The Smallest Diplodocid Skull Reveals Cranial Ontogeny and Growth-Related Dietary Changes in the Largest Dinosaurs

D. Cary Woodruff[1,2,3]*, Thomas D. Carr[4], Glenn W. Storrs[5], Katja Waskow[6], John B. Scannella[7], Klara K. Nordén[8], John P. Wilson[9]

Supplementary information

Phylogenetic analysis

We tested the taxonomic identity of CM VP14128 by including it in the phylogenetic analyses of Whitlock[11] and Tschopp *et al.*[12]. Additionally, we used modified matrices from Whitlock[11] and Tschopp *et al.*[12] consisting of only cranial characters. Finally, we combined these matrices (a cranial + postcranial and a cranial only matrix), as a larger matrix may circumvent problems with ontogenetically changeable characters.

Cranial + postcranial characters

We included CM VP14128 in the data matrix that combined the matrices of Whitlock[11] and Tschopp *et al.*[12] that included two outgroup taxa, 10 ingroup taxa, and 540 characters; following that analysis, *Omeisaurus* and *Jobaria* were designated as outgroup taxa. We ran the matrix in PAUP with the characters unordered under a branch and bound search, a furthest addition sequence, zero length branches were collapsed, and the 'MulTrees' option was in effect.

For the "Combined Matrix Cranial + Postcranial" matrix we obtained three most parsimonious trees, each with a tree length of 756 steps, with a CI (excluding uninformative characters) of 0.60, an HI (excluding uninformative characters) of 0.40, and an RCI of 0.41. We obtained a strict consensus tree that showed a resolved Diplodocoidea and an unresolved polytomy of basal neosauropods. The position of CM VP14128 is resolved as the sister species of *Diplodocus*, a relationship supported by the common possession of the following unambiguously optimized characters: tooth crown aligned along jaw axis such that the crowns do not overlap, cervical vertebrae possess a longitudinal sulcus on their ventral surface, a lamina divides the pleurocoel on the cervical vertebrae, paired pneumatic fossae are present on the ventral surface of the anterior cervicals, posterior cervical neural arches lack an accessory spinal lamina , and the anterior and mid-caudal centra possess a ventral longitudinal hollow. The characters in code form that support the position of CM VP14128: 68 (0 to 1), 79 (0 to 1), 82 (0 to 1), 89 (0 to 1), 98 (1 to 0), 144 (0 to 1).

We included CM VP14128 in the data matrix of Tschopp *et al.*[12], and we followed their procedure in ordering 23 characters (see Tschopp *et al.*[12]) and in designating *Shunosaurus* as the outgroup taxon. The matrix includes 22 taxa and 477 characters. We ran the matrix in PAUP under a branch and bound search, a furthest addition sequence, zero length branches were collapsed, and the 'MulTrees' option was in effect.

For this matrix we obtained a single most parsimonious tree that has a CI of 0.55, and HI of 0.56, an RCI of 0.25, and a tree length of 1,064 steps. The position of CM VP14128 is resolved as the sister species of *Kaatedocus* + *Barosaurus*, which is supported by five unambiguously resolved characters: 24 (0 to 1), 32 (1 to 0), 74 (0 to 1), 87 (1 to 0), 154 (1 to 0).

Finally, we included CM VP14128 in the data matrix "Whitlock 2011 Cranial + Postcranial" [Cary: insert how you want to identify this matrix instead of the file name I've used], which includes 27 taxa and 192 characters, *Omeisaurus* and *Jobaria* were designated as outgroups and we followed the same procedures as for the other analyses.

We obtained three most parsimonious trees, each with a CI of 0.69, HI of 0.31, and and RCI of 0.59, and a length of 285 steps. The position of CM VP14128 is resolved as the sister species of the (*Suuwassea* (*Amargasaurus* (*Brachytrachelopan* + *Dicraesaurus*))) clade. The position of CM VP14128 is supported by five unambiguously optimized characters: 24 (1 to 0), 37 (0 to 1), 40 (0 to 1), 45 (0 to 1), 60 (0 to 1).

Cranial only characters

Using one published parsimony analysis dataset[11] recovered a topology nearly identical to that originally recovered, where CMC VP 14128 is recovered as the basalmost member of Dicraeosauridae (Fig. 4). While the Bayesian analysis of this matrix recovered relatively high support for CMC VP 14 128 as a sister to *Amargasaurus* and *Dicraeosaurus* (Dicraeosauridae), while the diplodocids *Diplodocus* and *Apatosaurus* fall out as a sister to this branch.

Next, we coded CMC VP 14128 into a second diplodocoid matrix[12], but with an increased number of characters (127 vs. 76) and taxa/specimens (81 vs. 26). Theoretically, such an increased amount of information should result in greater phylogenetic resolution. Both this analysis and the Bayesian analysis recovered a similar topology in that all members of Flagellicaudata, including CMC VP 14128, were recovered together in a singular, unresolved polytomy (Fig. 4).

The combining of matrices entails bringing together the taxa and characters to create a larger, more encompassing matrix[71]. Accounting for shared characters, our combined matrix consisted of 153 cranial characters. Regarding taxa, we only used those that both analyses shared. While maximum parsimony is currently the most popular method used for morphological datasets, Bayesian methods have alternatively been argued to show a higher accuracy[72–74]. We hence analyzed the data with both methods.

For the parsimony analysis we coded CMC VP 14128 and incorporated it into Whitlock's[11] phylogenetic analysis of Diplodocoidea. Following that work we designated *Omeisaurus* and *Jobaria* as outgroups and excluded the redundant taxa *Rayosaurus* and *Nopscaspondylus*. The data matrix was constructed in MacClade[75] and executed in PAUP v.4.0[76]. We ran a branch-and-bound search with the characters unordered and unweighted under ACCTRAN optimization.

In the resulting basal dicraeosaurid location, the unambiguously optimized characters that support this position includes: presence of frontal contribution to the supratemporal fenestra; prominent and ventrally directed process from the squamosal extending from its posteroventral margin; postparietal foramen present; a narrow, sharp, and distinct sagittal crest of the supraoccipital; and subtriangular cross-section of the dentary, tapering sharply towards its ventral extreme.

Next, we coded CMC VP 14128 into the matrix of Tschopp *et al*.[12]. Like Whitlock[11], Tshopp et al.[12] also examined the phylogenetic relationship of diplodocids, but with an increased number of characters (127 vs. 76) and taxa/specimens (81 vs. 26). Theoretically, such an increased amount of information (if phylogenetically informative) – here in the form of characters and comparative individuals – should result in greater phylogenetic resolution. Bayesian analyses were run in MrBayes v3.2[77]. As the dataset did not include constant characters we applied the Mkv model[78]. For each data set we ran the analysis for 2 million generations (four chains, two runs) with a sampling frequency of 1,000. Priors were kept to standard settings. We tested both a model with equal rates of character change, and a model with variable rates (gamma distribution). The support for each model was then evaluated using the Bayes factor, with a value over 10 considered as strong support for either model[79]. We checked log-likelihood scores to ensure the analysis had reached a stable phase (visually examining plots). Convergence between runs was judged when ESS (Estimated Sample Size) was greater than 200, PSRF (Potential Scale Reduction Factor) was 1, and average standard deviation of split frequencies was less than 0.1. The trees generated during the first 10,000 generations were discarded as burn in for the compilation of the majority-rule consensus tree.

Vertebrae

The post-cranial remains of CMC VP 14128 comprise vertebrae consisting of an incomplete proatlas and at least four anterior cervicals (Fig. S1 and Fig. S2). Taphonomically, it is interesting to note that although the skull, proatlas, and anterior cervicals are preserved, the median bones (atlas and axis vertebrae) are missing. The vertebrae bear morphologies diagnostic of the Morrison Formation members of Diplodocidae, and are clearly dissimilar from the sympatric macronarians (*Brachiosaurus* – better cervicals known from the African *Giraffatitan*, HMN SII[80]), *Camarasaurus* [such as BYU 9047[81]]). While the vertebrae of CMC VP 14128 are anteroposteriorly long (as also in *Giraffatitan*), macronarian cervicals have a strong ventral curvature to the centra with angled condyles, cotyles, and neural arches that result in largely rhomboidal lateral profiles[80,81] – inconsistent with the rectangular diplodocid condition[12,17,27,82–84].

The centra are accamerate to slightly procamerate, and the pneumatic fossae are simple and weakly divided by an accessory lamina (conditions observed in immature diplodocids[5]). The cervical centrum length is approximately two times longer than cotyle width. The ventral surfaces of the centra exhibit a slight lateral concavity, and all lack an anteroposterior ventral keel (as seen in *Apatosaurus*[83,84]). Unlike the diplodocinae *Barosaurus* (AMNH 6341[85]), in lateral view the cotyle is strongly angled dorsally to the centrum. In the one complete neural arch, the prezygapophyses do not project anterior to the condyle, yet the postzygapophyses are anteroposterioly long (unlike *Barosaurus*) and project posteriorly well past the cotyle, and display prominent epipophyses (*Diplodocus* conditions[82]). The diapophysis is strongly posteriorly oriented, while the angle between the prezygapophyses and neural spine is V-shaped and very steep (*Diplodocus* conditions[82]). The neural spines are not bifurcated (a spinal feature ubiquitous in all diplodocids); although this lack of bifurcation is attributable to the specimen's ontogenetic status[5,86,87]).

All cervical ribs in articulation or associated are shorter than their respective centra (a condition expressed in Diplodocidae; although rare, cervical ribs longer than the centra have infrequently been observed in some immature diplodocids([87]; pers. obs. DCW). The cervical ribs exhibit an overall gracile morphology. They do not project strongly ventrally from the centrum, nor do they exhibit a pronounced ventrolateral process or a robust anterior process (conditions typically observed in *Apatosaurus*[83,84]. The shaft of each cervical rib exhibits a slight ventral curvature, maintains a general uniform width, and tapers gradually (a condition more typical of the Diplodocinae than Apatosaurinae conditions). Likewise, the minor mediolateral width of the capitulum (nearly 1.5 times smaller than the length of the tuberculum) produces a dorsoventrally narrow and oval-shaped costotransverse ansa (more analogous to *Diplodocus carnegii*[82] than *Apatosaurus ajax*[84]).

Of the represented cervical vertebrae, three are preserved in good condition. In two of these the neural arch is completely unfused, and in only one of these is there a fragmentary portion of the arch. The best preserved cervical has a fused arch with sutural contacts only visible on the anterior- and posterior-most margins (Fig. S1). While developmental trends in vertebral synostosis do appear within sauropods[48,88], numerous dinosaur specimens – including CMC VP 14128 – exhibit variability, and therefore indicate this feature's plasticity and ambiguity regarding the use of fusion alone as an ontogenetic indicator.

Cervical rib histology

As demonstrated within sauropod dorsal ribs[39] and cervical ribs[44], serial location is critical for accurate comparisons. The microstructure from the anterior and posterior regions greatly differs as the cervical rib documents the transition from osteological to tendinous tissues[44]. All samples were taken as near mid-shaft as possible. Cross-sectional shape differences likely reflect some of this variation in sample locations (the MOR 592 sample – Fig. S3 C – is the most anterior of the set), yet variation within the sampled region should still produce comparable sections.

In a cervical rib of the smallest diplodocid postcranium known to date (the taxonomically debated SMA 0009), the tissue is composed entirely of highly vascular primary tissue (Fig. S3 A). Amongst the numerous collagen fibrils and fibroblast lacunae are Haversian canals with resorptive edges. Within CMC VP 14128 we see interstitial material and structures initially resembling secondary osteons. However, upon closer inspection these structures lack osteocyte lacunae and canaliculi, and they do not possess a true cement line. Demarcated borders exist, but range from sinuous to not fully encompassing (Fig. S3 B). Instead we identify these features as secondary reconstructions[45]. In examining the interstitial material, it is a very fibrous or woven-looking tissue. Like the secondary reconstructions, this tissue is devoid of lacunae and is entirely composed of irregularly sized and spaced hypermineralized collagen fibrils; as such we identify this as primary tissue[45]. As secondary reconstructions and primary tissue are indicative of metaplasia, we suggest that the cervical rib of CMC VP 14128 is largely – if not entirely – composed of metaplastic tissues. Finally, in a 12 year old *Diplodocus*[86], we see the core of the cervical rib is composed of Haversian bone, and periosteally grading from multiple to single generational secondary osteons, with primary osteons constituting the outermost tissue (Fig. S3).

Phylogenetic recapitulation during ontogeny

As discussed in the main article, CMC VP 14128 possesses phylogenetically plesiomorphic features that are not seen in adult *Diplodocus*. While these traits could derive from ecomorphological relationships, they could alternatively represent phylogenetic recapitulation. Recapitulation, as used here, refers to the presence of plesiomorphic character states that are seen in early stages of ontogeny that are seen to be replaced later in growth by their derived character states. Therefore, two criteria are required to pass the test to qualify as recapitulated characters, namely 1) the equivalents of the phylogenetic characters are seen in growth, and 2) the derived state must be preceded by the plesiomorphic state.

For example, CMC VP 14128 possesses several features that are equivalent to plesiomorphic character states relative to Diplodocoidea that are replaced in growth by the descendant character states; these include: narrow and short snout (wide and long in adults), dorsoventrally tall maxilla and premaxilla (long and low in adults), small antorbital fenestra (large in adults), mesiodistally long tooth rows (mesially limited in adults), spatulate maxillary teeth (peg-like in adults), and simply pneumatized cervical centra (complexly pneumatic in adults). Since the juvenile features seen in CMC VP 14128 correspond to the non-diplodocoid condition, as is seen in sauropod phylogeny, then this would support the hypothesis of recapitulation in the post-hatching growth of *Diplodocus*.

Additionally, the change in the ecomorphotype of the skull from the juvenile to adult condition is consistent with the phylogenetic progression, which is the predicted pattern if recapitulation is at work. Otherwise, a matching pattern between ontogeny and phylogeny would not be seen. Therefore, the phylogenetic transition is incorporated into the developmental pathway, and, as a result, constrains the growth pattern. As a result of this phenomenon, the juveniles and adults are ecomorphologically separated from each other and so they do not compete for the same resources.

References

5. Woodruff, D. C., Fowler, D. W. & Horner, J. R. A new multi-faceted framework for deciphering diplodocid ontogeny. *Palaeontol. Electron.* **20.3.43A,** 1–53 (2017).

11. Whitlock, J. A. A phylogenetic analysis of Diplodocoidea (Saurischia: Sauropoda). *Zool. J. Linn. Soc.* **161,** 872–915 (2011).

12. Tschopp, E., Mateus, O. & Benson, R. B. J. A specimen-level phylogenetic analysis and taxonomic revision of Diplodocidae (Dinosauria, Sauropoda). *PeerJ* **3,** e857 (2015).

17. Tschopp, E. & Mateus, O. The skull and neck of a new flagellicaudatan sauropod from the Morrison Formation and its implication for the evolution and ontogeny of diplodocid dinosaurs. *J. Syst. Palaeontol.* **11,** 853–888 (2013).

27. Tschopp, E. & Mateus, O. Osteology of *Galeamopus pabsti* sp. nov. (Sauropoda: Diplodocidae), with implications for neurocentral closure timing, and the cervico-dorsal transition in diplodocids. *PeerJ* **5,** e3179 (2017).

39. Waskow, K. & Sander, P. M. Growth record and histological variation in the dorsal ribs of *Camarasaurus* sp. (Sauropoda). *J. Vertebr. Paleontol.* **34,** 852–869 (2014).

44. Klein, N., Christian, A. & Sander, P. M. Histology shows that elongated neck ribs in sauropod dinosaurs are ossified tendons. *Biol. Lett.* **8,** 1032–1035 (2012).

45. Horner, J. R., Woodward, H. N. & Bailleul, A. M. Mineralized tissues in dinosaurs interpreted as having formed through metaplasia: A preliminary evaluation. *Comptes Rendus - Palevol* **15,** 183–203 (2016).

71. Brusatte, S. L. & Carr, T. D. The phylogeny and evolutionary history of tyrannosaurid dinosaurs. *Sci. Rep.* **6,** 1–8 (2016).

72. Wright, A. M. & Hillis, D. M. Bayesian Analysis Using a Simple Likelihood Model Outperforms Parsimony for Estimation of Phylogeny from Discrete Morphological Data. *PLoS One* **9,** (2014).

73. O'Reilly, J. E. *et al.* Bayesian methods outperform parsimony but at the expense of precision in the estimation of phylogeny from discrete morphological data. *Biol. Lett.* **12,** 20160081 (2016).

74. Puttick, M. N. *et al.* Uncertain-tree: discriminating among competing approaches to the phylogenetic analysis of phenotype data. *Proc. R. Soc. B Biol. Sci.* **284,** 20162290 (2017).

75. Mindell, P. MacClade: Analysis of Phylogeny and Character Evolution. *Auk* **111,** 1035–1036 (1994).

76. Swofford, D. L. PAUP*: Phylogenetic Analysis Using Parsimony (*and Other Methods). *Sinauer Assoc. Sunderland, Massachusetts.* 1–142 (2002).

77. Ronquist, F. *et al.* Mrbayes 3.2: Efficient bayesian phylogenetic inference and model choice across a large model space. *Syst. Biol.* **61,** 539–542 (2012).

78. Lewis, P. O. A likelihood approach to estimating phylogeny from discrete morphological character data. *Syst. Biol.* **50,** 913–925 (2001).

79. Kass, R. E. & Raftery, A. E. Bayes factors. *J. Am. Stat. Assoc.* **90,** 773–795 (1995).

80. Janensch, W. Die wirbelsäule von *Brachiosaurus brancai*. *Palaeontogr. (Supplement 7)* **3,** 27–93 (1950).

81. McIntosh, J. S., Miller, W. E., Stadtman, K. L. & Gillette, D. D. The Osteology of *Camarasaurus lewisi* (Jensen, 1988). *BYU Geol. Stud.* **41,** 73–115 (1996).

82. Hatcher. *Diplodocus* Marsh, its osteology, taxonomy, and probable habits, with a restoration of the skeleton. *Mem. Carnegie Museum* **1,** 1–64 (1901).

83. Gilmore, C. W. Osteology of *Apatosaurus*, with special reference to specimens in the Carnegie Museum. *Mem. Carnegie Museum* **11,** 175–300 (1936).

84. Upchurch, P., Tomida, Y. & Barrett, P. M. A new specimen of *Apatosaurus ajax* (Sauropoda: Diplodocidae) from the Morrison Formation (Upper Jurassic) of Wyoming, USA. *Natl. Sci. Museum Monogr.* **26,** 1–108 (2004).

85. McIntosh, J. S. in *Thunder-lizards: The Sauropodomorph Dinosaurs* 38–77 (2005).

86. Woodruff, D. C. & Fowler, D. W. Ontogenetic influence on neural spine bifurcation diplodocoidea (dinosauria: Sauropoda): A critical phylogenetic character. *J. Morphol.* **273,** 754–764 (2012).

87. Mannion, P. D., Upchurch, P., Mateus, O., Barnes, R. N. & Jonese, M. E. H. New information on the anatomy and systematic position of *Dinheirosaurus lourinhanensis* (Sauropoda: Diplodocoidea) from the Late Jurassic of Portugal, with a review of European diplodocoids. *Journal of Systematic Palaeontology* **10,** 521–551 (2012).

88. Hanik, G. M., Lamanna, M. C. & Whitlock, J. A. A Juvenile Specimen of *Barosaurus* Marsh, 1890 (Sauropoda: Diplodocidae) from the Upper Jurassic Morrison Formation of Dinosaur National Monument, Utah, USA. *Ann. Carnegie Museum* **84,** 253–263 (2017).

Figure captions

Supp. Info. Figure 1: Post cranial remains of CMC VP 14128. For both vertebrae A (right lateral), B (left lateral), C (anterior), D (dorsal), E (ventral), F (posterior). Note the numbering of the cervical vertebrae (1-2) does not correspond serially, merely a numerical way to denote each element.

Supp. Info. Figure 2: Post cranial remains of CMC VP 14128. A (right lateral), B (left lateral), C (anterior), D (dorsal), E (ventral), F (posterior). Note the numbering of the cervical

vertebrae (3-4) does not correspond serially, merely a numerical way to denote each element. The centrum of cervical 4, proatlas, and cervical ribs only shown in a single plane.

Supp. Info. Figure 3: Histology of diplodocid cervical ribs. Blue boxes denote the magnified areas to the right of each specimen. A. SMA 0009; B. CMC VP 14128; C. MOR 592. H.C. w/ Scal. Ed. = Haversian canals with scalloped edges; Col. Fib. = collagen fibrils; 2^{nd} Rec. = secondary reconstructions; Pri. Tis. = primary tissue; Pri. Ost. = primary osteons; 2^{nd} Ost. = secondary osteons. Note the hypothesized ontogenetic development from a metaplastic to osseous tissue. Specimens not to scale.

Supp. Info. Figure 4: A. Linear regression of diplodocid lower jaws to skull length. B. Linear regression of diplodocid skull to estimated body length.

Supp. Info. Figure 5: CM VP14128 (top) with overlay grid and landmark locations (red circles). Adult *Diplodocus* (bottom; redrawn from *17*) with transformed grid and landmark locations (red circles). Drawings by K. Scannella.

Supp. Info. Figure 6: The second specimen found in the field jacket with CMC VP 14128, CMC VP 14129. Note that CMC VP 14129 was found on the opposing side of the jacket, and no other material was found with this specimen. A (dorsal), B (right lateral), C (left lateral), D (ventral), E (anterior), F (posterior).

Measurement Figure 1: Select measurements for Part 1 (consult Fig. 1 for numbering scheme) of CMC VP 14128. Colors for each measurement correspond to the lines in the corresponding image.

Measurement Figure 2: Select measurements for Parts 2 and 3 (consult Fig. 1 for numbering scheme) of CMC VP 14128. Colors for each measurement correspond to the lines in the corresponding image.

Measurement Figure 3: Select measurements for Part 4 (consult Fig. 1 for numbering scheme) of CMC VP 14128. Colors for each measurement correspond to the lines in the corresponding image. Drawings by K. Scannella.

Character Matrices (*excel spreadsheets*)

Photogrammetric model 1: (*3D pdf*)

Photogrammetric model 2: (*3D pdf*)

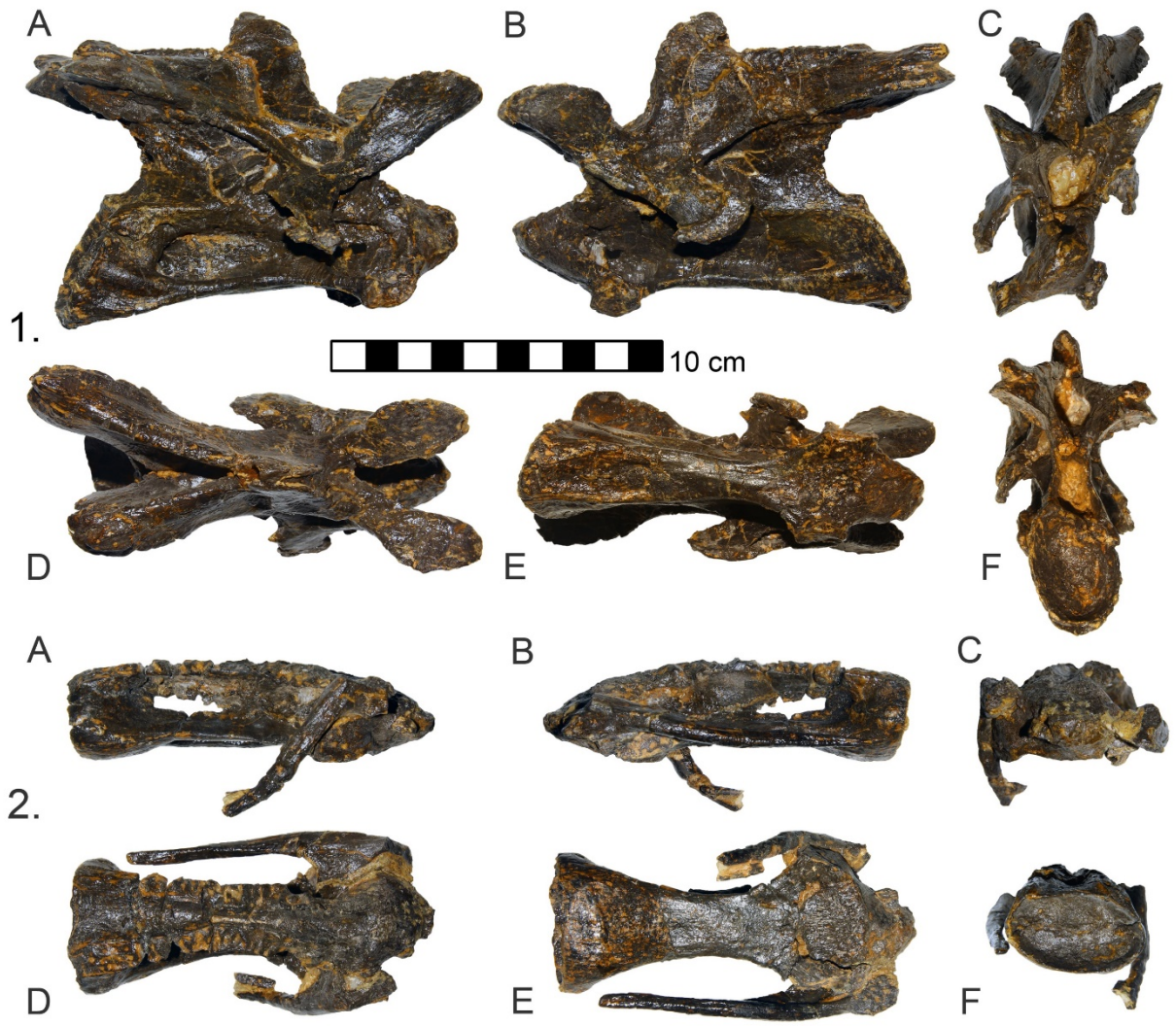

S.I. Fig. 1

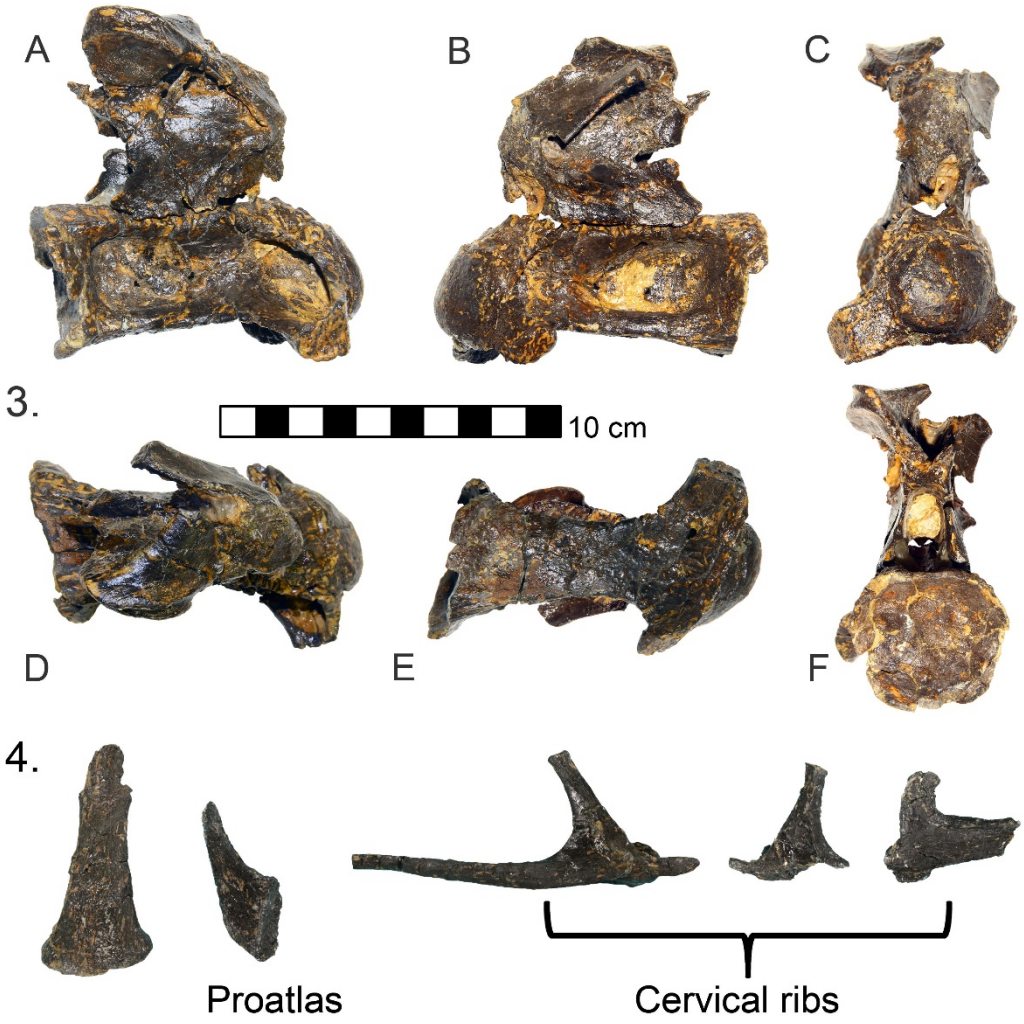

S.I. Fig. 2

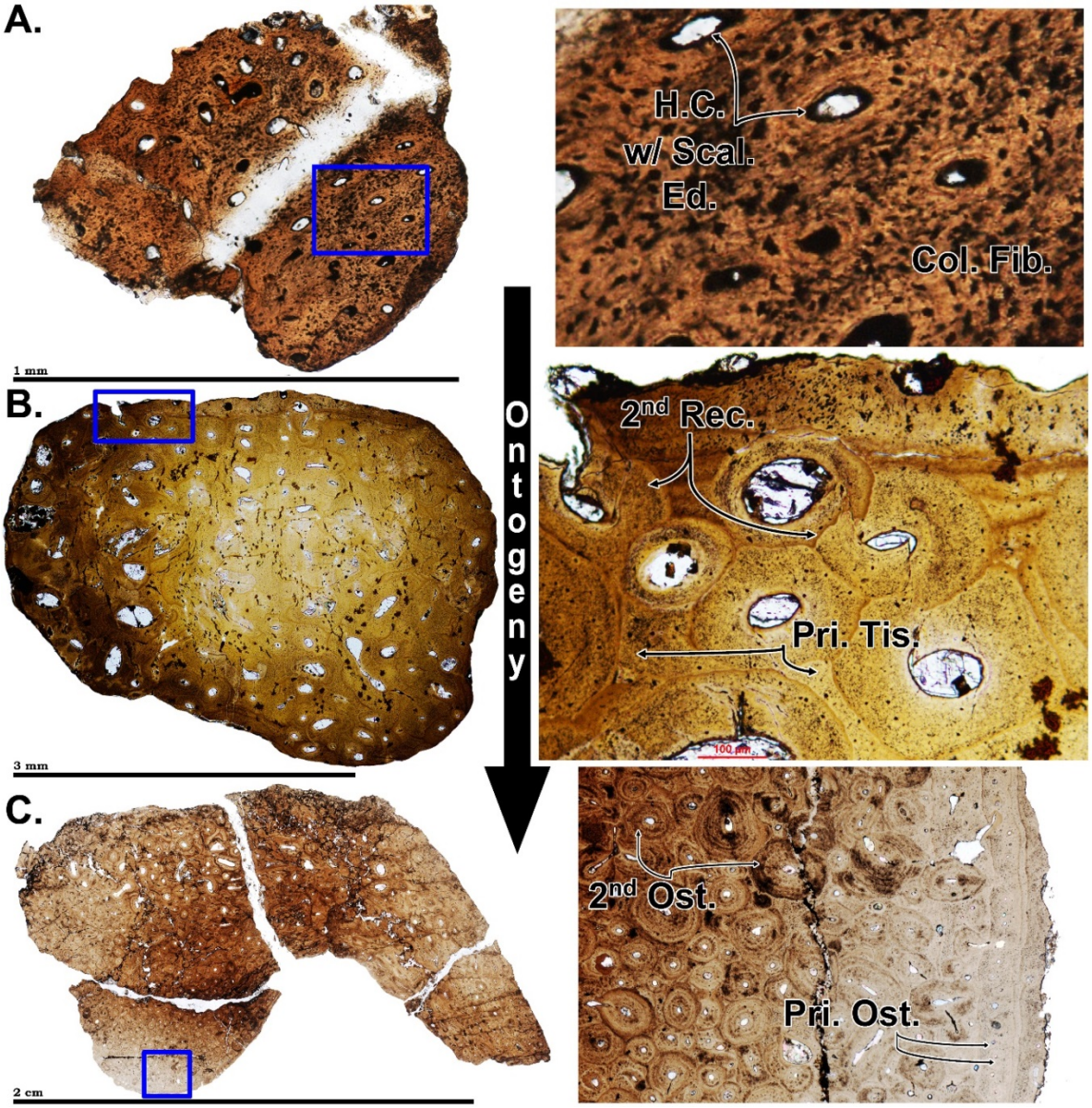
A.
1 mm
B.
3 mm
C.
2 cm
Ontogeny
H.C.
w/ Scal.
Ed.
Col. Fib.
2nd Rec.
Pri. Tis.
2nd Ost.
Pri. Ost.

S.I. Fig. 3

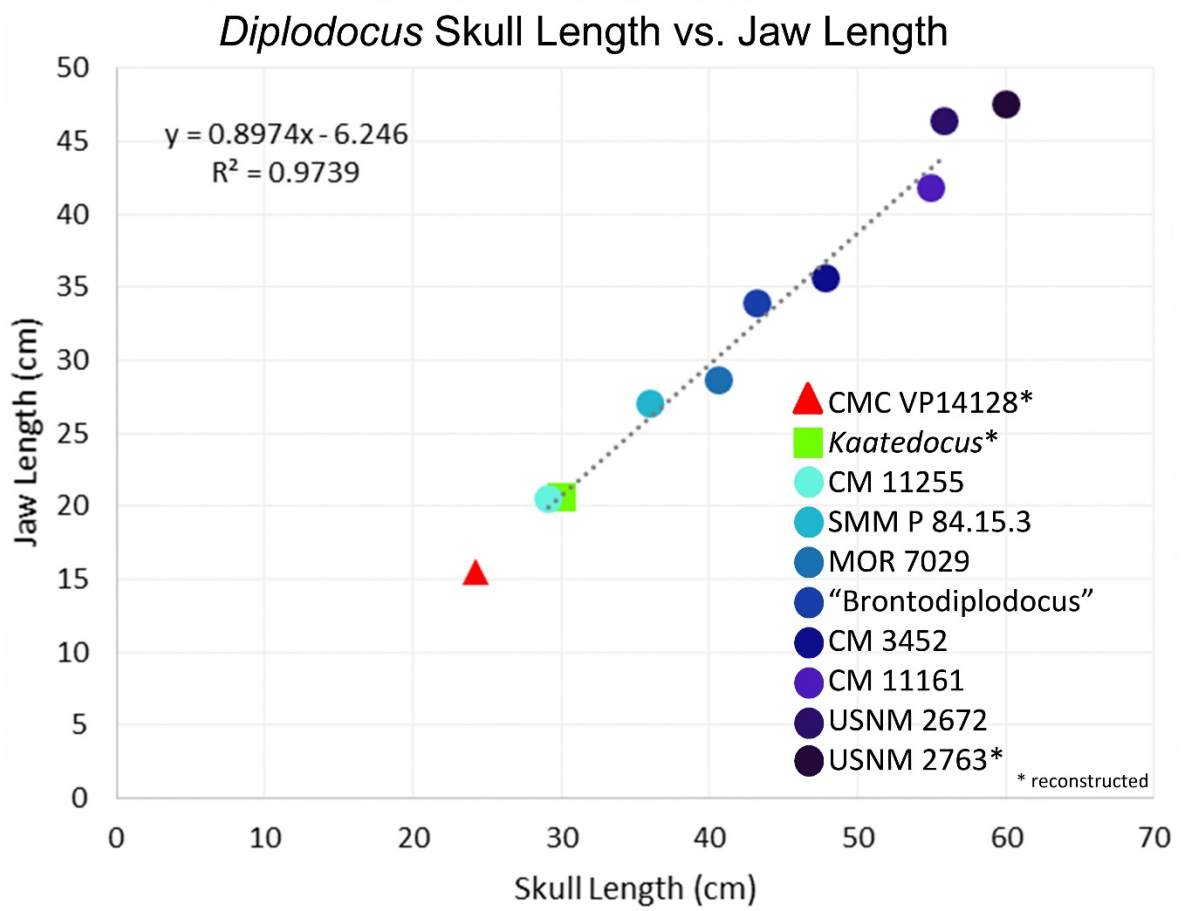
Diplodocus Skull Length vs. Jaw Length
y = 0.8974x - 6.246
R² = 0.9739
Jaw Length (cm)
Skull Length (cm)
CMC VP14128*
*Kaatedocus**
CM 11255
SMM P 84.15.3
MOR 7029
"Brontodiplodocus"
CM 3452
CM 11161
USNM 2672
USNM 2763*
* reconstructed

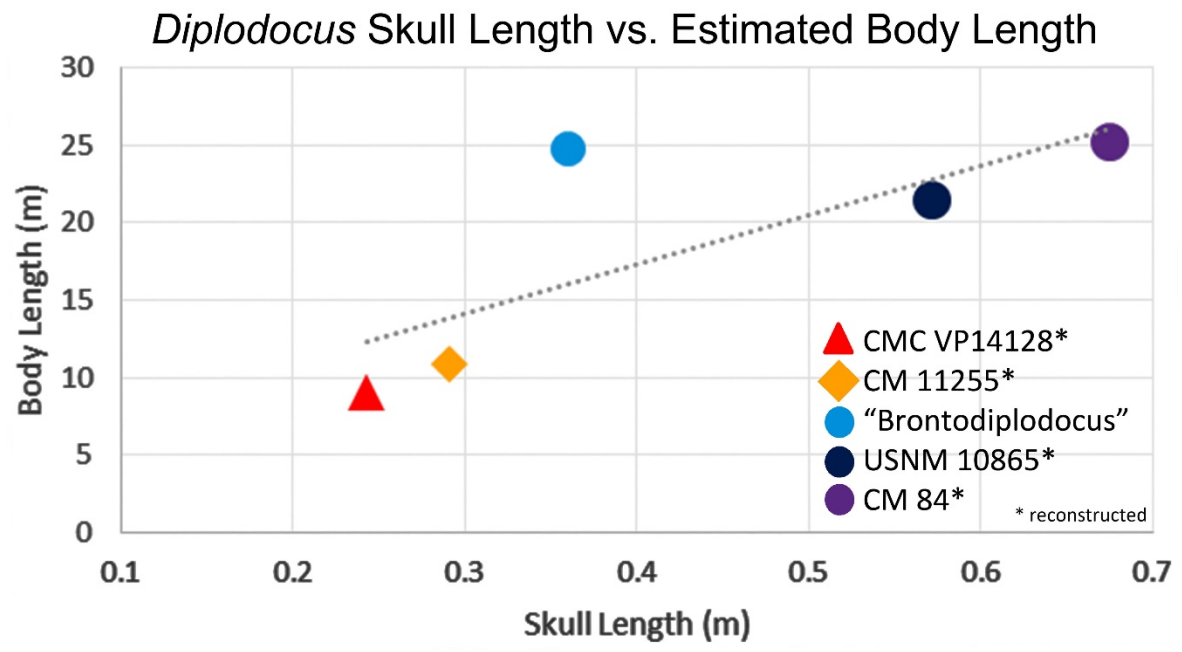
Diplodocus Skull Length vs. Estimated Body Length
Body Length (m)
Skull Length (m)
CMC VP14128*
CM 11255*
"Brontodiplodocus"
USNM 10865*
CM 84*
* reconstructed

S.I. Fig. 4

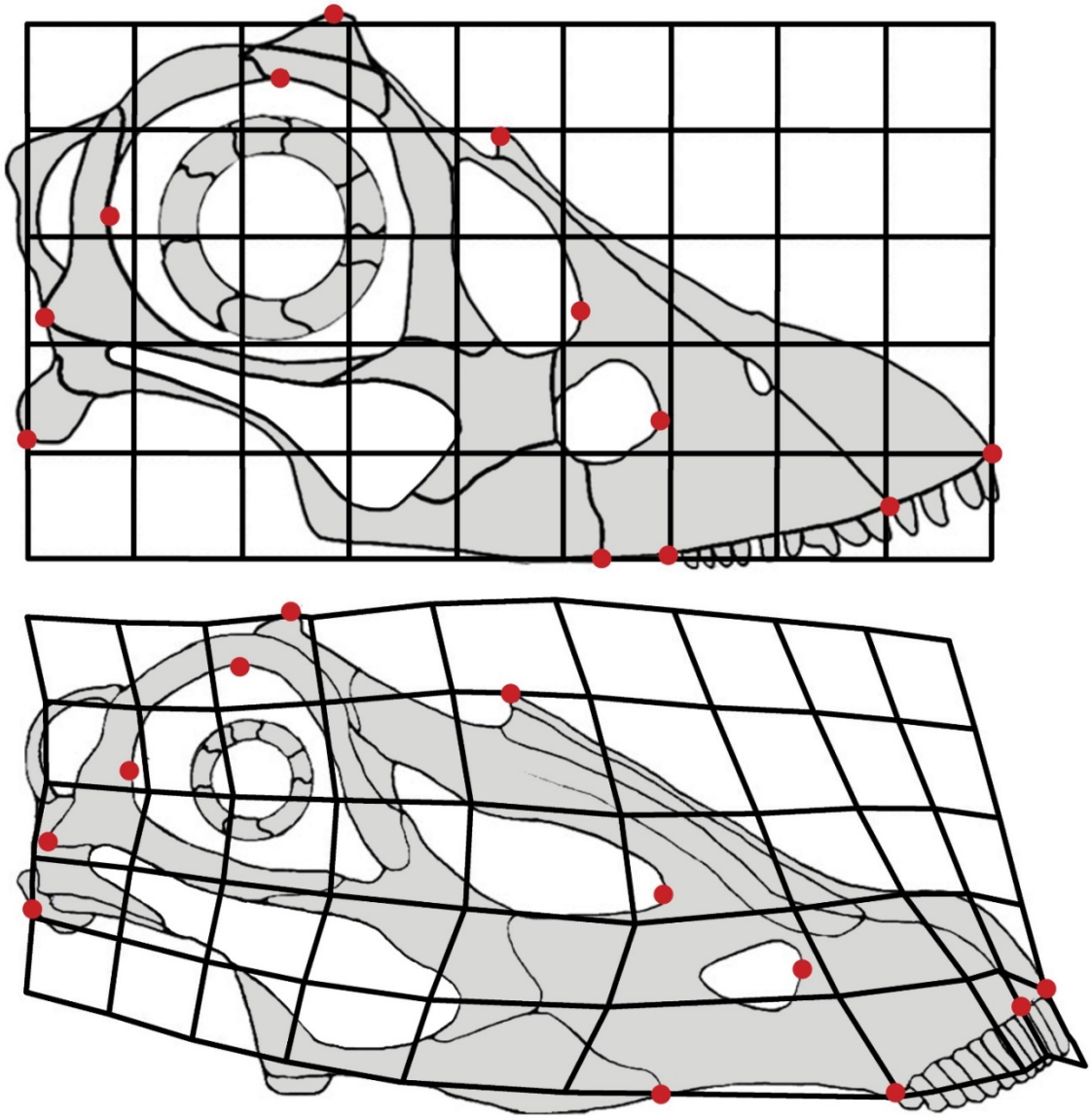

S.I. Fig. 5

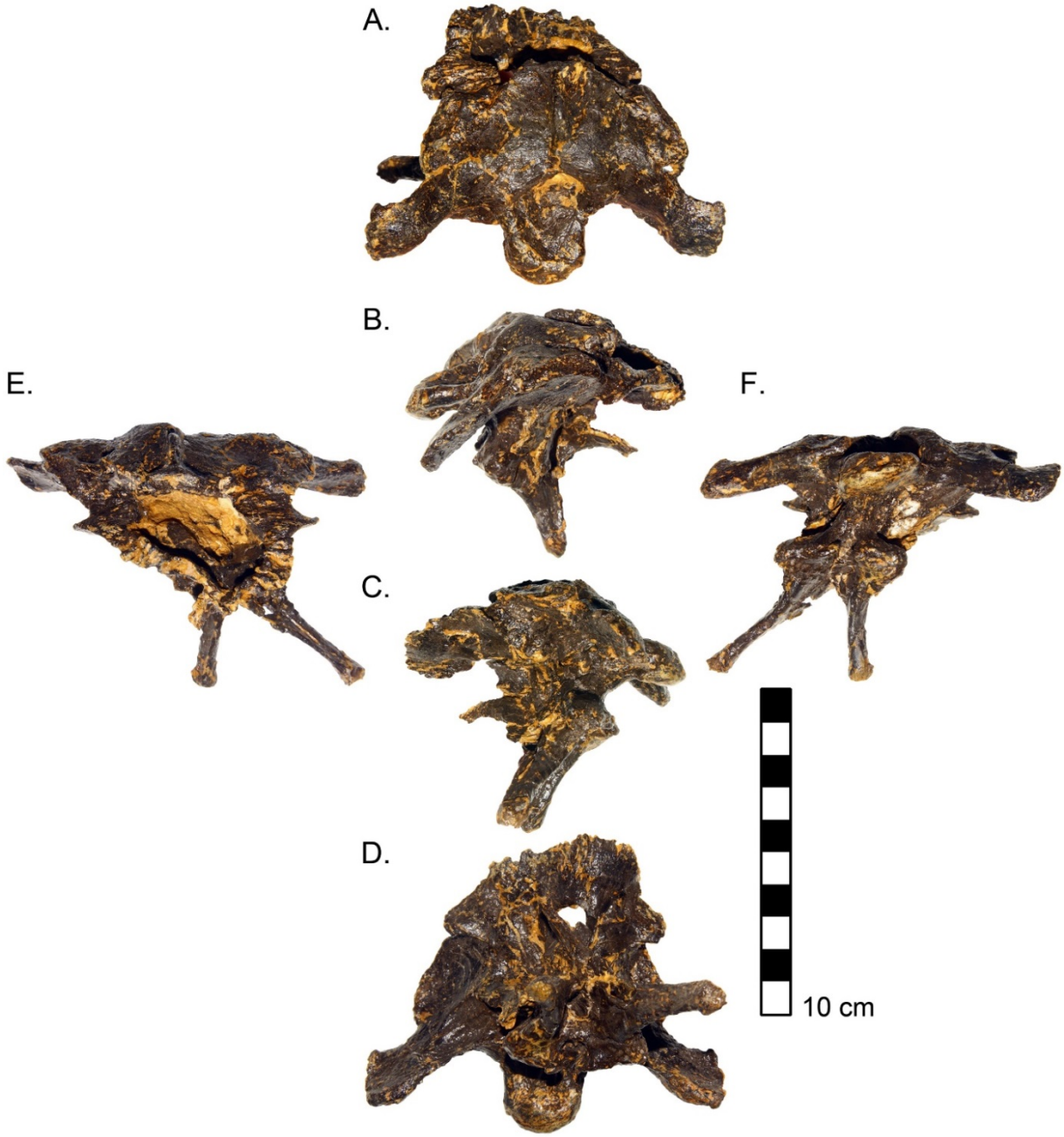

S.I. Fig. 6

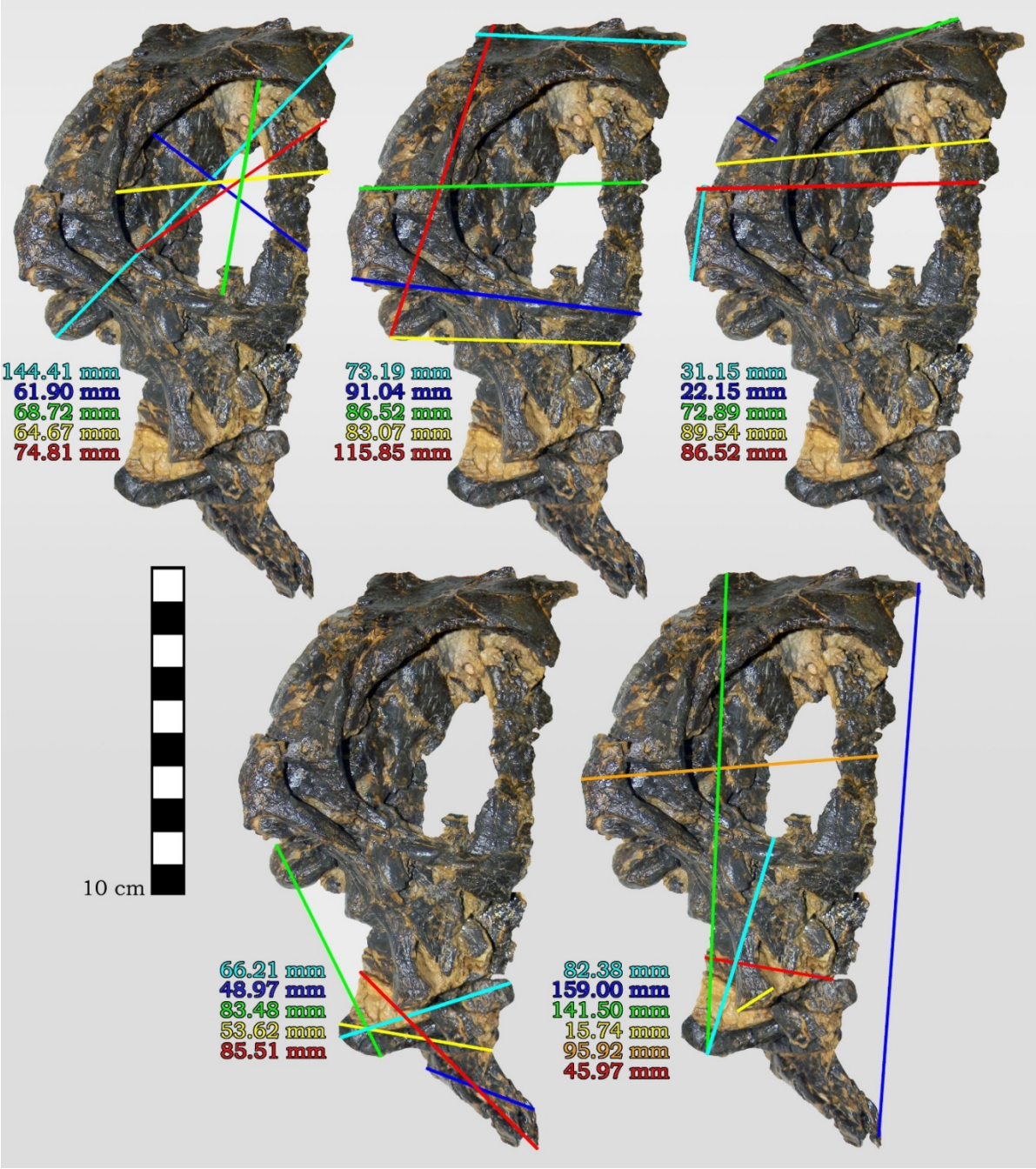

Measurement Fig. 1

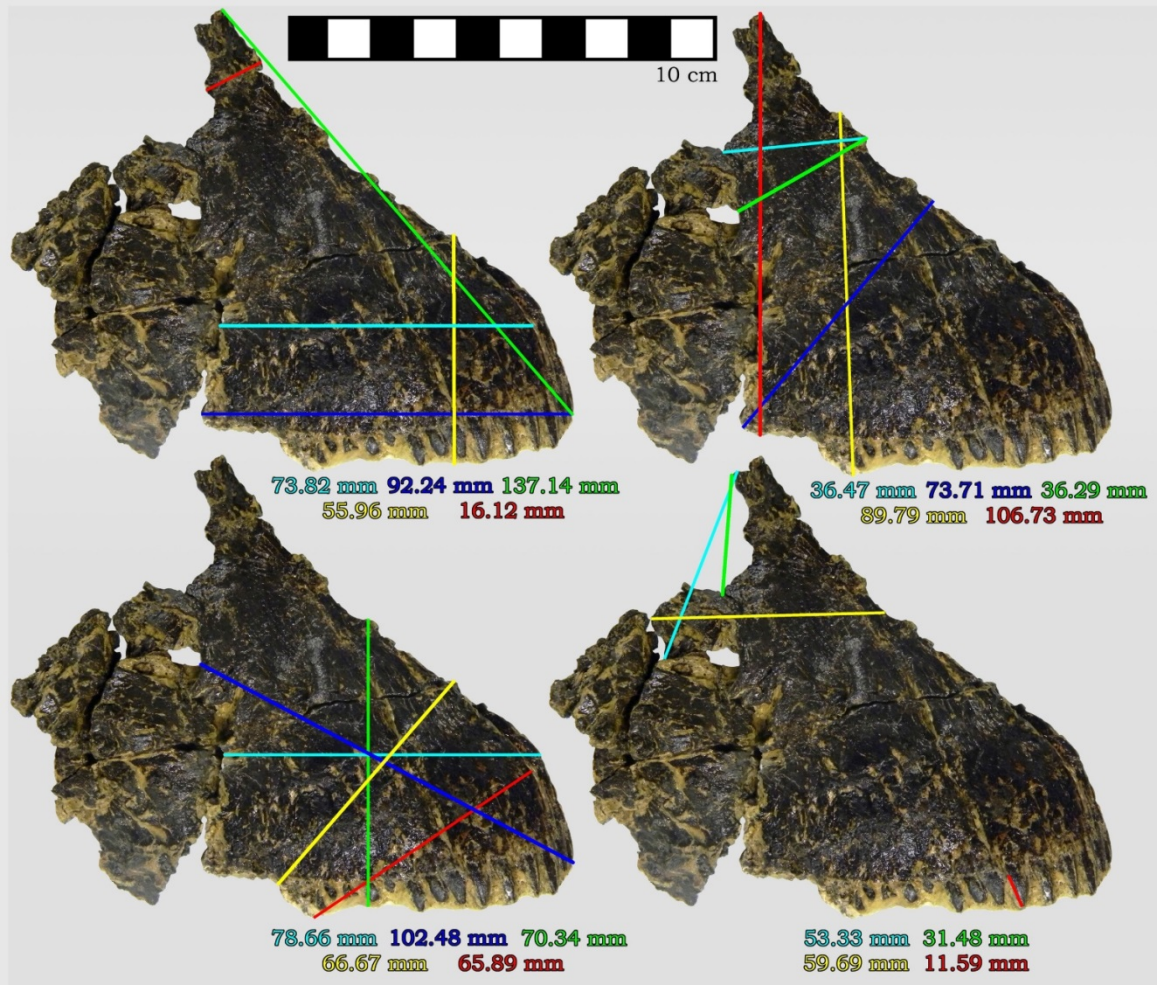

Measurement Fig. 2

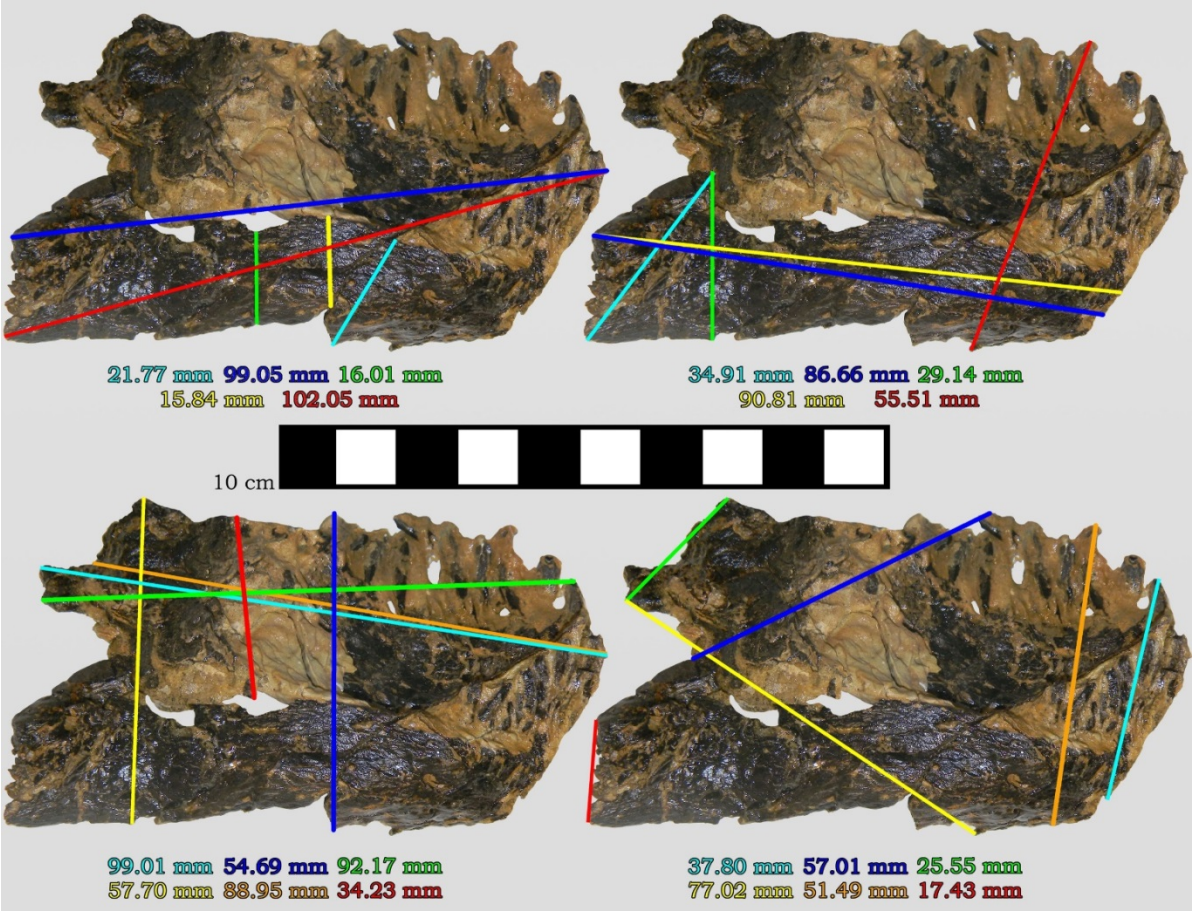

Measurement Fig. 3

„Die Zeit ist die wichtigste Zutat
im Rezept des Lebens.“

“Time is the most important ingredient
in the recipe of life.”

Charles Darwin

CHAPTER 6

Life history traits of different Jurassic sauropod taxa – Dorsal rib histology reveals differences in ages at sexual and skeletal maturity between macronarians and diplodocoids

unpublished:

Waskow, K., Griebeler, E. M, and Sander, P.M. Life history traits of different Jurassic sauropod taxa – Dorsal rib histology reveals differences in ages at sexual and skeletal maturity between macronarians and diplodocoids.

Author contribution:

This study was designed and performed by me, including sampling, histological description and analysis of all skeletons studied herein, and main manuscript and figure preparation.

Eva Maria Griebeler performed the statistical analysis including partially text writing of related chapters and proofreaded the manuscript.

Martin Sanders authorship is justified by his excellent supervision and proofreading of the manuscript.

Life history traits of different Jurassic sauropod taxa – Dorsal rib histology reveals differences in ages at sexual and skeletal maturity between macronarians and diplodocoids

Katja Waskow[1], Eva Maria Griebeler[2], and P. Martin Sander[1]

[1] Steinmann Institute for Geology, Mineralogy, and Paleontology, University of Bonn, Nussallee 8, D-53113, Bonn, Germany. Phone: +49 (0) 228 / 73 600 58.
*waskow@uni-bonn.de

[2] Institute of Organismic and Molecular Ecology, Evolutionary Ecology, Johannes Gutenberg University, Johann Joachim Becher Weg 13, D55128 Mainz, Germany.

Abstract

Sauropod dinosaurs are not only the largest terrestrial vertebrates to ever walk the earth, they also had the largest size differences seen between hatchlings and adults among amniotes. Therefore, their life history traits and growth rates are of special interest to evolutionary ecologists. Skeletochronology, using histological growth marks in long bones like humeri and femora, is frequently used to construct growth curves in dinosaurs and other tetrapods by plotting age vs. bone size. However, this approach is difficult to apply in sauropods because formation rates of primary and secondary bone tissue in the long bones are too high to produce and preserve lines of arrested growth (LAGs) in all but the outermost cortex. Previous studies have shown that sauropod dorsal ribs in contrast commonly preserve a remarkably complete growth record. Therefore, this study analyses the growth record preserved in ribs of 15 different Jurassic sauropod taxa represented by 66 different individuals (including 13 type specimens) from 14 different localities. Sexual and skeletal maturity, two major events in an animal's life, are clearly visible in each individual growth record and indicated by two significant decreases in annual bone apposition rate and thus growth rate. The analysis shows that the life history of diplodocoid sauropods differs from their sister taxon, the macronarians. On average, diplodocoids reached sexual maturity after 10 to 15 years of growth and skeletal maturity at an age of 17 to 22 years, while macronarians took 16 to 23 years to become sexually mature and reached skeletal maturity at an age of 25 to 34 years (excluding cycles in the external fundamental system (EFS)). These statistically significant differences in sexual and skeletal maturity between macronarians and diplodocoids are successfully applied for taxonomic assignment of indetermined sauropod rib samples to one of the two clades. The age distribution in the sample base is adult-dominated, suggesting that adult large sauropods may have inhabited different environments than their juveniles, and that these environments were more appropriate for fossil preservation. An exception is an assemblage of dwarfed sauropods found in the

Mother´s Day Quarry (Wyoming, USA) showing a heterogenous age distribution including several juveniles. The general absence of coexisting adults and juveniles in large sized sauropods within a habitat could suggest ecological niche partitioning of different ontogenetic stages in space and might have been triggered by size difference rather than by phylogeny.

6.1. Introduction

Growth rates of the largest terrestrial animals to ever inhabit the earth are in focus of scientific interest since their discovery in the 19th century (Case, 1978; Curry, 1999; Sander, 1999; 2000; Sander and Tückmantel, 2003; Upchurch et al., 2004a; Sander et al., 2006; 2011; Klein and Sander, 2008; Lehman and Woodward, 2008; Klein et al., 2009; Griebeler et al., 2013; Erickson, 2014; Waskow and Sander, 2014; Myhrvold, 2016; Cerda et al., 2017; Griebeler and Werner, 2018). Because sauropods are extinct and lack good modern analogs, the only way to obtain more information about their life history traits is to use the skeletochronological growth record preserved in hard tissues (Castanet et al., 1993; Castanet, 1994). Previous histological sauropod studies mainly focused on the usually sampled long bones (Sander, 1999; 2000; Sander and Tückmantel, 2003; Klein and Sander, 2008; Griebeler et al., 2013; Hedrick et al., 2014; Cerda et al., 2017). Unfortunately, the quality and quantity of growth record preservation in sauropod long bones is relatively poor compared to other dinosaur taxa (Erickson and Tumanova, 2000; Horner et al., 2000; Padian et al., 2001; Erickson, 2005; Klein and Sander, 2007; Cerda et al., 2017). The higher bone apposition rates of primary bone tissue, especially early in ontogeny, impedes the formation of LAGs and other cyclical bone growth marks. Additionally, the remodeling rate of sauropod long bones seems to be increased compared to other skeletal elements of the same individual or remodeling rates in long bones of other dinosaur taxa (Klein and Sander, 2008; Lehman and Woodward, 2008; Waskow and Sander, 2014). This increased bone formation rate of the primary and secondary bone front described in the three-front model of Mitchell and Sander (2014) impedes growth record preservation in sauropod long bones. So far, the best growth record preserved in a sauropod long bone was found in a *Mamenchisaurus* ulna (Wings et al., 2007). However, in their abstract the authors report even in this specimen growth record preservation has only started at 40% of final size. Additionally, it is questionable if the estimated growth patterns are representative for the whole taxon. The preservation of LAGs in long bones is untypical for sauropods and thus could also be a pathological effect only occurring in this one individual.

In contrast to long bones, dorsal ribs have been shown to preserve an almost complete growth record and to be a reliable tool for skeletochronology. Rib histology provides almost complete growth records, including paleobiological information about growth rates, ages at sexual and skeletal maturity, and in some cases even sex (Waskow and Sander, 2014; Waskow and Mateus, 2017, (chapter 2)). Although the annual nature of

cyclicity in extinct taxa, such as dinosaurs, has been discussed controversially in the past (Chinsamy and Hillenius, 2004; Padian and Horner, 2004), it is a standard method of aging extant and extinct animals (Hutton, 1986; Caetano, 1990; Castanet and Smirina, 1990; Castanet and Baez, 1991; Ricqlès et al., 1991; Castanet et al., 1993; 2004; Chinsamy, 1994; Smirina and Tsellarius, 1996; Erickson et al., 2003; Smirina and Ananjeva, 2007; Garcia, 2011; Köhler et al., 2012; Woodward et al., 2014; Klein and Griebeler, 2018). Therefore, the annual cyclicity of growth marks is generally accepted for non-avian dinosaurs (Erickson, 2005; Sander et al., 2011). The estimation of age at sexual maturity in extinct animals is frequently discussed in the literature (Curry, 1999; Horner et al., 1999; Sander, 2000; ChinsamyTuran, 2005; Erickson, 2005; Erickson et al., 2007; Klein and Sander, 2007; 2008). For ecological reasons of survivorship, Dunham et al. (1989) theorized that large non-avian dinosaurs must have required 5 to 20 years to reach sexual maturity. The onset of sexual maturity can be histologically detected on the basis of a marked decrease in growth, well before the animal was fully grown, and corresponds to the inflection point of the growth curve (Reiss, 1989; Sander, 2000; Lee and Werning, 2008; Ritz et al., 2010; Griebeler et al., 2013; Waskow and Sander, 2014; Waskow and Mateus, 2017, (chapter 2); Klein and Griebeler, 2018). As at this age the animal started to allocate resources for reproduction, and thus these were not available for growth anymore and growth rate decreased (Case, 1978a; 1978b; Reiss, 1989; Sander, 2000). Unfortunately, dorsal ribs (in contrast to long bones) do not grow isometrically. Caused by their general growth direction from proximal to distal, the local bone apposition rate at the proximal rib shaft varies. This impedes a mass-based growth curve erection from a rib of a single individual (Waskow and Sander, 2014). Thus, in this study, as many sauropod individuals as possible (representing different ontogenetic stages) were sampled to create reliable growth curves for different sauropod taxa based on several individuals and estimate ages of important events within the life of the single taxa. Individuals including an articulated or associated long bone for size estimation were preferred. The study focusses on Jurassic sauropod taxa based on the taxonomic diversity in sauropods during the late Jurassic (especially in the North American Morrison Formation where most of the samples were found). Another reason for using Jurassic taxa instead of, e.g., Cretaceous ones is the lower amount of pneumatisation in Jurassic sauropod ribs when compared to Cretaceous taxa most of which belong to the Titanosauriformes that do show stronger pneumatisation along the axial skeleton. This pneumatization potentially destroys the growth record by expansion of pneumatic cavities.

Institutional Abbreviations:

ANS: Academy of Natural Sciences, Philadelphia, Pennsylvania, USA; **BYU**: Museum of Earth Sciences, Brigham Young University, Provo, Utah, USA; **CM:** Carnegie Museum of Natural History, Pittsburgh, Pennsylvania, USA **CMC**: Cincinnati Museum Center, Cincinnati, USA; **FMNH**: Field Museum of Natural History, Chicago, Ilinois, USA; **MfN**: Museum für Naturkunde, Berlin, Germany; **ML**: Museu da Lourinhã, Lourinhã, Portugal; **MOR**: Museum of

the Rockies, Bozeman, Montana, USA; **NMB**: Staatliches Naturhistorisches Museum Braunschweig, Germany; **NMMNH**: New Mexico Museum of Natural History and Science, Albuquerque, USA; **SMA**: Sauriermuseum Aathal, Aathal, Canton Zürich, Switzerland; **UMNH**: Utah Museum of Natural History, Salt Lake City, Utah, USA; **UW**: University of Wyoming, USA; **YPM**: Yale Peabody Museum, New Haven, Connecticut, USA.

6.2. Methods

6.2.1. Selection of samples and sampling area

Because ribs are bad indicators for the body size of an individual, alternative size proxies are needed to erect a rib-based growth curve for the different sauropod taxa. Therefore, preferably specimens including a femur were chosen for sampling. However, based on their gigantic size, most sauropod remains were found incomplete and in disarticulation. Thus, the number of specimens where skeletal unity of rib and femur can be ascertained is low. To increase the sample size, also individuals lacking femora were included. In these cases, femur length was estimated by measuring corresponding humerus length (if available) based on ratios found in the literature (Janensch, 1961; McIntosh, 1990b; Remes, 2006; Klein and Sander, 2008). For most Diplodocoids humerus length equals 65% of femur length. In *Brachiosaurus* and *Camarasaurus* this ratio would have been higher based on the relatively long forelimbs and thus humeri (especially in *Brachiosaurus*). However, estimations of humerus length was not necessary in these taxa because all articulated dorsal rib samples taken for this study include a femur. The position of the rib within the rib cage, as well as the relative sampling position within the rib cage, is crucial for the completeness of the growth record. Prior analysis of Waskow and Sander (2014) of a complete and articulated *Camarasaurus* sp. rib cage showed that the best sampling position is the proximal end of the rib shaft of the second or third dorsal rib with the best growth record preservation occuring at the posteromedial side (Fig. 1). Thus, if possible, the rib samples were selected by their relative position within the rib cage and cut at the proximal rib shaft. Unfortunately, in most cases the exact determination of the position of each rib within the ribcage was not possible, due to disarticulation of the samples. However, in sauropods the morphology of the rib head, and the angles between capitulum, tuberculum, and rib shaft differ from cranial to caudal within the rib cage (Osborn and Mook, 1921; Gilmore, 1936; Jensen 1987; Waskow and Sander, 2014). Thus, at least the relative position within the rib cage could be tested prior to sampling for all ribs having the rib head region preserved. In order to get a good sample base, also fragmentary ribs consisting only of proximal shafts were included. In cases where the proximal end of the rib shaft was damaged or missing, ribs were sampled slightly more distal, but still proximal to the mid shaft region. Nearly all rib samples were taken as complete cross-sections to get the most complete growth record.

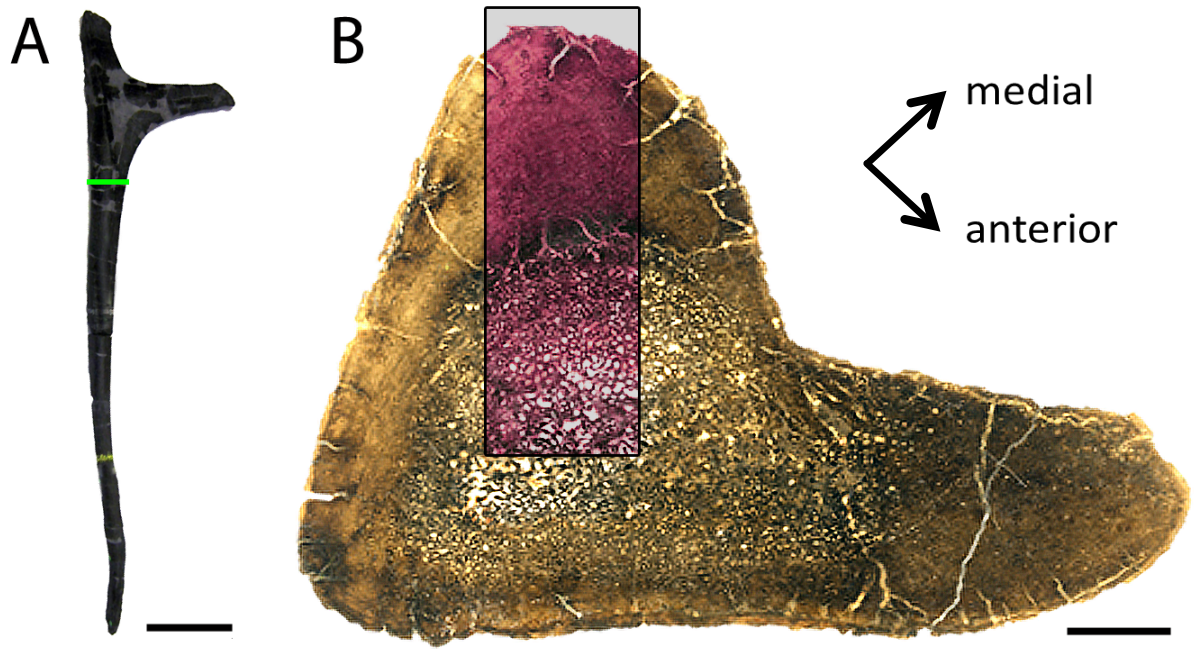

Fig. 1: Area of best growth record preservation in dorsal ribs of sauropods. **A**: Photograph of *Camrarasaurus* sp. (SMA 0002) dorsal rib marking the best sampling position within a sauropod rib (indicated by green bar). Scale bar equals 20 cm. **B**: Scan of a dorsal rib thin section of *Brachiosaurus altithorax* (FMNH 25107) marking the area of best growth record preservation on the posteromedial side of the rib (indicated by purple area). Scale bar equals 1 cm.

6.2.2. Thin sectioning methods

Prior to cutting, the area of the cutting plane of each rib was surrounded with Technovit 4071 to protect the fossils from breaking during sawing. This resin was chosen because it is easy to remove with acetone after sawing. The two-component technical polymer (powder and liquid) normally is used in a 2:1 ratio. Here it was used in a ratio of 3:1 to make the liquid suspension more viscous. The protected area then was cut with a rock saw and processed into standard paleohistological thin sections (see Enlow and Brown, 1956; Wells, 1989; Chinsamy and Raath, 1992; Lamm, 2007). The sample base includes very large samples that reach up to 12,5 cm in rib diameter at the broadest position. In general, thin sections of larger size (greater than 7,5cm) were processed like normal-sized samples, but larger glass slides and more accuracy in terms of evenness of the slide in the final grinding were needed.

6.2.3. Methods used for growth record analysis

Annual cycles were counted at the thickest part of the cortex which is located posteromedially (Fig. 1). Three different types of cyclicity occur in the rib cross-sections. The innermost cycles are often only preserved as polish lines, which are defined as a growth lines that are visible in a polished section but not in a thin section (Sander, 2000), or as a modulation of bone tissue not completed by a LAG (Ricqlès, 1983; Sander et al., 2004).

Because modulations and polish lines have been interpreted as annual cycles before (Sander, 2000; Sander and Tückmantel, 2003), if present they were taken into account for estimations of sexual and skeletal maturity. In the mid to outer cortex, most of the growth record is preserved as clearly developed LAGs. In skeletally mature individuals the growth record is completed by an external fundamental system (EFS) because it is well established that the presence of an EFS indicates skeletal maturity (Chinsamy-Turan, 2005; Erickson, 2005; Sander, 2000; Sander et al., 2011; Turvey et al., 2005). The annularity of LAGs within the EFS is controversial. The close spacing of the LAGs with no significant histological elements like osteons or vascular canals in between can be interpreted in different ways: either as a shorter timeframe (more than one LAG deposited in a year) or a longer timeframe (LAGs deposited only every second or third year) (Horner et al., 1999). Therefore, the LAGs preserved within the EFS have always been excluded in the estimations of age at skeletal maturity. In some samples small sediment grains are still sticking to the bone surface, excluding surface damages caused by preparation. However, this does neither exclude preburial damage due to scavengers or decay, nor damage due to weathering prior to collection of the fossil bone in the field.

The individual growth time of each sampled sauropod (representing age at death in skeletally immature individuals) was estimated by counting the preserved cyclicity (inculding LAGs of the EFS) in each sample and adding the retrocalculated number of missing growth cycles in the inner cortex and medullary region. Under the assumption, that the thickness of the single growth cycles generally decreases from the center of the bone towards the surface, i.e., with time, the number of missing cycles was estimated by measuring the distance from the innermost LAG to the center of the medullary cavity and dividing it by the thickness of the broadest growth cycle. This method of retrocalculation has been used by several authors in the past before (Horner et al., 1999; Erickson, 2001; Padian et al., 2001; 2004; Horner and Padian, 2004; Klein and Sander, 2007). The percentage of individual growth record preservation was estimated by measuring the distance from the center of the medullary cavity, where growth initiated to the bone surface at the thickest part of the cortex (representing 100%). This distance then was compared to the distance between the innermost LAG and the surface. The center of the medullary cavity was calculated by using bone profiler version 4.5.8 (Girondot and Laurin, 2003). Age at sexual maturity was estimated based on the significant decrease in growth, visible in each skeletally mature sauropod rib sample. This decrease in growth represents the inflection point of the growth curve (Sander, 2000; Lee and Werning, 2008; Ritz et al., 2010; Griebeler et al. 2013).

6.2.4. Statistical analysis

We compared ages at sexual and skeletal maturity of macronarians and diplodocids for articulated, disarticulated, and pooled articulated and disarticulated ribs. Therefore, we used generalized linear regression models of the Poisson family, with a power function as link function. In each model, the discrete trait (age at sexual or skeletal maturity) is predicted from the continuous femur length and the categorical variable taxon (macronarian, diplodocoid) for each of the rib sets. Both, ages at sexual and skeletal maturity had skewed distributions (Poisson family) and allometric studies had observed an increase in age at sexual and skeletal maturity with increasing body size (femur length, power function as link function, Griebeler et al., 2013). Only specimens with a corresponding femur length were included in this analysis. Specimens without femur length, but with an estimate on sexual and skeletal maturity (*Apatosaurus* sp. (UW 46211), dwarfed diplodocine samples (CMC, MOR 790), *Camarasaurus* sp. "Alf" (SMA 0274), *Camarasaurus* sp. (YPM VP 060121)) were used to validate whether they were correctly taxonomical assigned (Macronaria vs. Diplodocoidea).

To test for differences in frequency of adults and juveniles between sampling localities, we applied the χ^2 test to analyze 2 x 2 contingency tables. All statistical analysis was conducted in STATISTICA 10 (Stat Soft. Inc. 2011).

6.3. Material

In total 267 dorsal rib samples, labeled with 74 different specimen numbers, were sampled. Based on skeletochronological correlation the samples represent 66 different sauropod individuals. The sample base includes 15 taxa, and 13 type specimens that were taken from 13 different Middle and Late Jurassic localities. Prior to sampling, the exact number of sampled individuals was hard to ascertain due to the disarticulation of many of the finds. Nevertheless, recently a study of Wiersma et al. (in review) showed for long bones that bone histology is a useful tool for assigning isolated bones at the individual level. For rib histology this is also feasible and even more reliable due to the higher resolution of the growth record of each animal. A more detailed study concerning this matter is currently in progress by Waskow and Sander. Thus, it was possible to ascertain that all samples in this study represent different individuals. The sample base consists of one basal sauropod rib sample (*Spinophorosaurus nigeriensis*), many different diplodocid samples including *Apatosaurus, Diplodocus, Barosaurus, Brontosaurus*, and *Galeamopus* as well as a few dicraeosaurids, including the holotype of *Suuwassea emilieae*. The macronarian samples mainly pertains to different *Camarasaurus* species and are complemented by some *Brachiosaurus* and *Giraffatitan* samples. Titanosauria were not sampled because the primary growth record in the proximal part of the dorsal ribs was destroyed by a high degree of pneumatization in this region (Wedel, 2005; Cerda et al., 2012). A few isolated Sauropoda

indet. dorsal rib samples were also included in the study. Quarry maps (if available) are provided for all specimens found in articulation or association to a femur or humerus for size estimation to prove the likelihood of skeletal unity for the individuals in question (Fig. 2, S.I. Fig. 1 - 10) If several ribs showing a high probability of belonging to the same individual as the measured long bone were available, one to three of these ribs were selected for sampling.

The order of the following listing is based on the phylogeny of Tschopp et al. (2015) on genus level. The order of the listing within a certain taxon is based on completeness of the individual starting with the most complete specimen. Type specimens are always mentioned first independent of their completeness.

6.3.1. Basal sauropod dorsal rib samples

***Spinophorosaurus nigeriensis* (NMB 1698):** NMB 1698 is the paratype of *Spinophorosaurus nigeriensis*, and the only basal sauropod within the sample base of this analysis. The partial skeleton was found north of Aderbissinat (Republic of Niger) in Jurassic sediments of uncertain age (Remes et al., 2009). The skeletal remains include a partial skull, a complete set of right dorsal ribs, some girdle elements, several vertebrae, and chevrons, a humerus and an isolated pedal phalanx (Fig. 2).

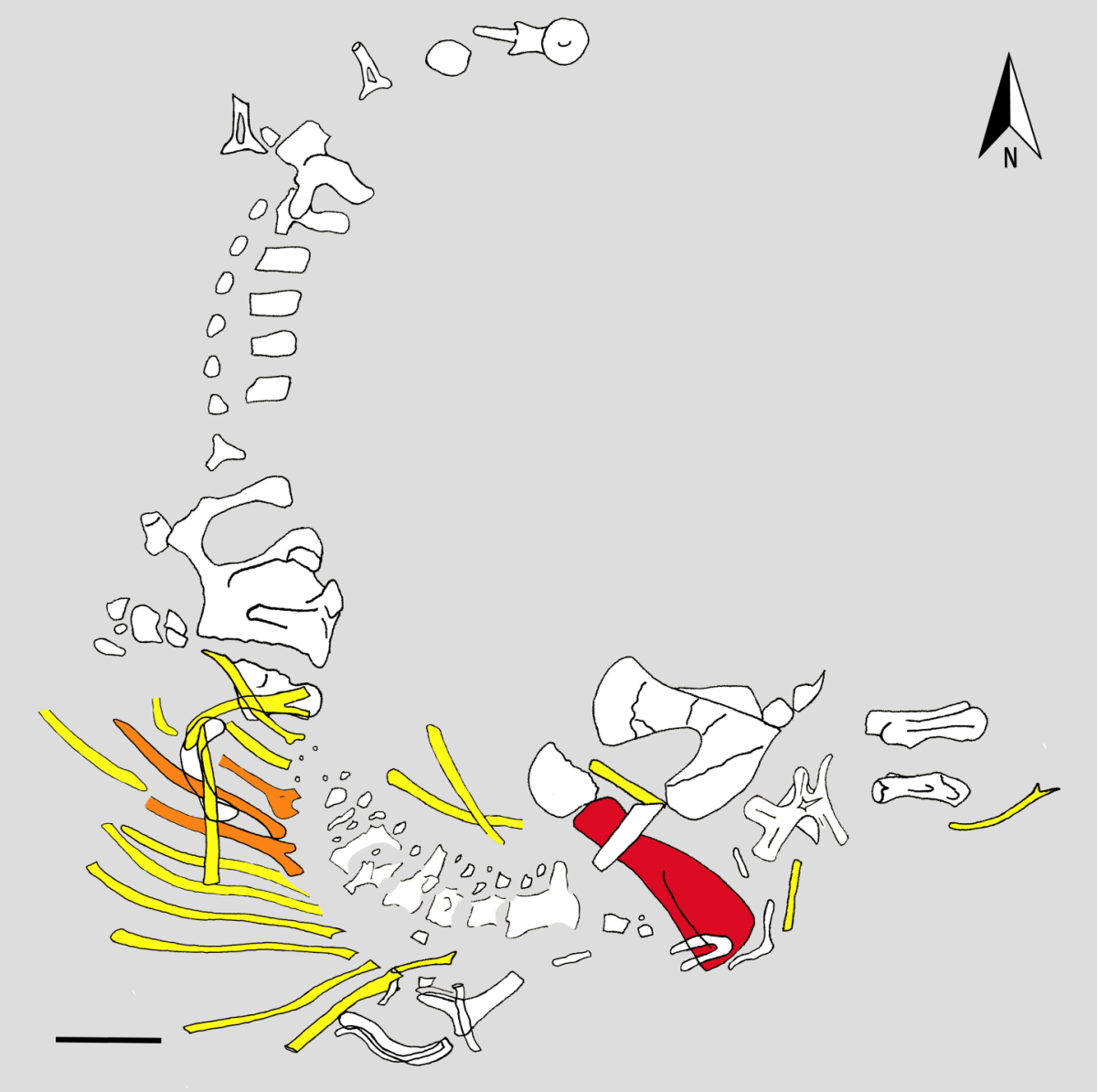

Fig. 2: Quarry map of the paratype of *Spinophorosaurus nigeriensis* (NMB-1698-R) found north of Aderbissinat (Republic of Niger) in Jurassic sediments of uncertain age. Ribs are marked in yellow. Based on rib morphology the sampled rib element most likely belongs to one of the ribs of the articulated trunk region marked in orange. Long bone used for size estimation is marked in red. Scale bar equals 30 cm.

6.3.2. Macronarian dorsal rib samples

***Camarasaurus lewisi* (BYU 9047):** The *Camarasaurus* samples include BYU 9047 the holotype of *Camarasaurus lewisi* that had been described originally by Jensen (1988) as *Cathetosaurus lewisi* before McIntosh et al. (1996) assigned it to *Camarasaurus lewisi*. In their osteological description McIntosh et al. (1996) described BYU 9047 as a senescent individual. The specimen was excavated in 1967 by James A. Jensen in the Dominguez Jones Quarry located in Mesa County (Colorado, USA) from the lower half of the Brushy Basin Member of the Morrison Formation. The partial skeleton consists of one tooth, complete cervical vertebrae 1 to 8, and heavily damaged cervical vertebrae 9 to 12, dorsal vertebrae 8 to 12, sacrum, caudal vertebrae 1 to 26, 18 chevrons, right humerus, radius, ulna, distal

carpal, partial right manus, partial left ilium, left pubis, and both ischia (Ikejiri, 2005). Unfortunately, no scientifically accurate quarry map exists for the Dominguez Jones Quarry and the holotype of *Camarasaurus lewisi*. However, the nearly perfect articulation of specimen BYU 9047 is well documented by photographs in the publication of Jensen (1988).

***Camarasaurus grandis* (YPM VP 001901):** YPM VP 001901 is the holotype of *Camarasaurus grandis* (Tschopp et al., 2015) initially described as holotype of *Apatosaurus grandis* (Marsh, 1877). According to Ikejiri et al. (2005), YPM VP 001901 is a juvenile specimen based on unfused neurocentral sutures. It was found at the Brushy Basin Member of the Morrison Formation at Como Bluff (Reed´s Quarry 1, Albany County, Wyoming, USA) together with the remains of the former paratype of *Apatosaurus grandis* YPM VP 001905 and two other specimens (YPM VP 001900, initially described as holotype of *Morosaurus impar*, and YPM VP 001902). All four skeletons now were referred to the genus *Camarasaurus* (Tschopp et al., 2015). There are some uncertainties about the exact assignment of some bones to either YPM VP 001901, YPM VP 001902, or YPM VP 001905 (Tschopp et al., 2015; Ostrom and McIntosh, 1966). No quarry map or scientific drawing of the exact discovery position of the isolated bones exists, complicating the assignment of some bones to certain individuals. The partial articulation of the specimens YPM VP 001901 an YPM VP 001905 is only documented by the letter correspondence of William Harlow Reed and Othniel Charles Marsh of 1878 in which Reed states the articulation in addition to some very rough hand drawings of some parts of the skeletons. The unequivocal remains of YPM VP 001901 include a basioccipital, several dorsal vertebrae, a partial sacrum, caudal vertebrae 1 to 27, the left pectoral girdle and forelimb elements, the right scapulacoracoid, left sternal plate, the left femur, tibia, fibula, and ribs (Ikejiri, 2005), enabling size comparison for growth curve compilation.

***Camarasaurus grandis* (YPM VP 001905):** YPM VP 001905 is the paratype of *Camarasaurus grandis.* The specimen is the former paratype of *Apatosaurus grandis* and was found in Reed´s Quarry 1 (Como Bluff, Morrison Formation, Wyoming, USA) together with the remains of the *Camarasaurus grandis* holotype YPM VP 001901 and another specimen of the same species (YPM VP 001902). The remains that can be assigned to YPM VP 001905 include a nearly complete skull, all cervical vertebrae, most or all dorsal vertebrae, a partial sacrum (formerly assigned to YPM VP 001900, the former holotype of *Morosaurus impar*), 12 anterior to mid caudal vertebrae, some chevrons, coracoids, scapulae, left humerus, right ulna, right ischium, femora, tibiae, fibulae, and some pes elements (Ikejiri, 2005).

***Camarasaurus* sp. (SMA 0002):** The most complete *Camarasaurus* specimen within the whole sample base is SMA 0002. The nearly complete specimen nicknamed “E.T.” was found in perfect articulation in the Howe Stephens Quarry (Morrison Formation) in Wyoming (USA) by the excavation team of Hans Jakob ‘Kirby’ Siber (Sauriermuseum Aathal, Switzerland). Only the vomers, the splenial bones, the distal most end of the tail, and one terminal phalanx of the right pes is missing (S.I. Fig. 1). Its completeness enables mass estimations for the specimen. Although SMA 0002 is a comparably small individual, its osteology, and bone

histology reveal a derived ontogenetic age (Klein and Sander, 2008; Tschopp et al., 2014; Waskow and Sander, 2014).

***Camarasaurus* sp. (SMA 0274):** The *Camarasaurus* sp. skeleton SMA 0274 nicknamed "Alf" is a partial individual found at the Howe Scott Quarry (Morrison Formation) (Wyoming, USA) by the Sauriermuseum team. The scattered but associated bones that were interpreted to belong to the individual consist of several isolated cervical and dorsal vertebrae, dorsal ribs, and partial pelvic girdle elements. No long bones are preserved. The individual itself has been sold to the private collector Felix Beyeler. Who is member of the development association VFSMA of the Sauriermuseum. The histological thin section analyzed herein however, is stored in the collection of the Steinmann Institute (University of Bonn, Germany).

***Camarasaurus* sp. (UW 46215):** UW 46215 is a partial articulated *Camarasaurus* specimen found in association in the same road cut near Laramie (Morrison Formation, Wyoming, USA) as the *Apatosaurus* UW 46211 and *Camarasaurus* UW 46212 (S.I. Fig. 2). Based on neurocentral suture fusion, UW 46215 is an adult individual consisting of a scapulacoracoid, femur, eight articulated cervical vertebrae, and several partially articulated ribs (S.I. Fig. 2).

***Camarasaurus* sp. (UW 46212):** UW 46212 is a partial *Camarasaurus* sp. skeleton that was found in association together with *Apatosaurus* UW 46211 and *Camarasaurus* UW 46215 (see above). It consists of many partially articulated dorsal, sacral, and caudal vertebrae, the sacrum, and associated ribs. Unfortunately, no long bones are preserved (S.I. Fig. 2). All but the last 22 caudal vertebrae show open neurocentral sutures. The sacrum is completely unfused, indicating a juvenile ontogenetic stage for UW 46212.

***Camarasaurus* sp. YPM VP 000619:** The remains of YPM VP 000619, a *Camarasaurus* sp. individual initially referred to as *Morosaurus* sp. (Madsen et al., 1995), mainly consist of a partial skull including the left premaxilla, maxilla, the right dentary and braincase, and some rare postcranial remains including dorsal rib fragments partial vertebrae and partial sacrum. Long bone remains are not preserved, impeding size estimation for growth curve construction. The specimen was collected by James William Lambuth in 1891 in Jefferson County (Colorado, USA) in the Upper Jurassic Morrison Formation (Madsen et al., 1995).

***Camarasaurus* sp. (UMNH samples):** 18 isolated ribs, most likely *Camarasaurus,* found at the Cleveland-Lloyd Dinosaur Quarry, Utah, USA, (Morrison Formation) were sampled (UMNH 5289, UMNH 5302, UMNH 20518, UMNH 21606, UMNH 21608, UMNH 24220, UMNH 24298, UMNH 24384, UMNH 24386, UMNH 24801, UMNH 24802, UMNH 24803, UMNH 24804, UMNH 24805, UMNH 24806, UMNH 24807, UMNH 24808, UMNH 24809). Based on the correlation of the growth records between the ribs, the 18 UMNH samples belong to 12 different *Camarasaurus* individuals, thus only samples representing different individuals were included in the analysis.

***Camarasaurus* sp. (YPM VP 060121):** YPM VP 060121 is an isolated partial rib assigned to *Camarasaurus* sp. The rib, stored at the Yale Peabody Museum, was collected by Reed in the Como Bluff Quarry 4 (Albany County, Wyoming, USA), an Upper Jurassic Morrison Formation locality.

***Brachiosaurus altithorax* (FMNH P25107):** FMNH P25107 is the holotype of *Brachiosaurus altithorax* and the type species of the genus. The partial skeleton consists of the last seven dorsal vertebrae, the sacrum, the first two caudal vertebrae, left coracoid, and fragmentary left ilium, right humerus, ilium and femur, and several dorsal ribs (Taylor, 2009). No quarry maps exist for the specimen. However, the good articulation of the remarkably complete holotype specimen is well documented by photos of the excavation in 1900 stored in the Field Museum of Natural History. It was collected from the Morrison Formation of the Grand River valley of western Colorado (USA) by the Field Columbian Museum (now Field Museum of Natural History) paleontological expedition. This expedition was led by Elmer S. Riggs who subsequently described the specimen (Riggs, 1901; 1903a; 1904). The holotype is slightly larger and more robust than the brachiosaurids found in Tendaguru (Africa) initially described as *Brachiosaurus brancai* (Janensch 1914; 1950; 1961). Later on, the latter has been generically separated from the American genus *Brachiosaurus* based on morphological reanalysis and is now referred to as *Giraffatitan brancai* (Paul, 1988; Taylor, 2009). In the type specimen of *Brachiosaurus altithorax* the lack of suture fusion in the coracoid led to the assumption that FMNH P25107 was a subadult individual (Taylor, 2009).

Cf. *Brachiosaurus altithorax* (SMA 0009): The by far smallest sauropod in the whole sample base is SMA 0009 (nicknamed “Baby Toni”). This remarkably complete and articulated juvenile postcranial sauropod skeleton (S.I. Fig. 3) was found at the Howe Stephens Quarry (Morrison Formation) and initially described by Schwarz et al. (2007) as juvenile diplodocid. After further preparation, Carballido et al. (2012) hypothesized its affiliation to the Brachiosauridae. This assumption has been corroborated by the analysis of Tschopp et al. (2015) who included the SMA 0009 specimen into their diplodocid analysis based on its initial description. The only known brachiosaurid species from the Morrison Formation is *Brachiosaurus altithorax* thus an affiliation of SMA 0009 to this species is very likely.

***Brachiosaurus altithorax* (SMA 0314):** The only remain of an adult *Brachiosaurus* found by the Siber team is the isolated rib SMA 0314. It was found in the Howe Stephens Quarry of the Morrison Formation in Wyoming (USA) and has been identified by its typical broad and thin plank-like shape. In contrast to most other samples, core drilling was used to sample this rib. A size estimation for the individual was not possible due to missing articulated or associated long bone elements.

Cf. *Gitaffatitan* (J 12): The isolated dorsal rib J 12 was found in the Upper Saurian Marls of Tendaguru (Tansania). It was excavated by Janensch during the Geman Tendaguru expedition between 1909 and 1913 and is stored in the MfN. The site produced exclusively

isolated bones accumulated due to normal mortality events such as starvation, seasonal drought, disease, old age, and weakness (Heinrich, 1999). Long bones and girdle elements found at the site are assignable to *Giraffatitan brancai* (Sander, 2000). Thus, sample J 12 most likely belongs to this taxon. However, because of the missing articulation an exact size estimation of the specimen is not possible.

6.3.3. Diplodocoidea dorsal rib samples

***Suuwassea emilieae* (ANS 21122):** ANS 21122 is the holotype of *Suuwassea emilieae* initially described by Harris and Dodson (2004) as indeterminate flagellicaudatan. Further analyses of the specimen differing in results suggested affinities to Diplodocidae (Gallina and Apesteguía, 2005; Rauhut et al., 2005; Remes, 2006; Lovelace et al., 2007) and Dicraeosauridae (Salgado et al., 2006) until the discovery of the dentary of the holotype identified ANS 2112 as dicraeosaurid sauropod (Whitlock and Harris, 2010; Tschopp and Mateus, 2013). Phylogenetic analyses confirmed this assignment and described the specimen as the basal most dicraeosaurid known to date (Whitlock, 2011; Tschopp et al., 2015). The remains of the holotype ANS 21122 consist of a partial skull, several cranial, cervical, dorsal, and caudal vertebrae, ribs, a complete scapulocoracoid, a humerus, a partial tibia, a complete fibula, and a partial pes (S.I. Fig. 4). They were found in Southern Carbon County (Montana, USA) in a layer most likely equivalent to the Brushy Basin Member of the Morrison Formation. More detailed information about the exact finding locality are not provided to avoid non-scientific exploitation because *Suuwassea emilieae* was found on public land (Harris and Dodson, 2004). The histology of some skeletal elements of the specimen has already been described by Hedrick et al. (2014) and Woodruff (2015) and revealed a subadult ontogenetic age of the specimen.

***Dicraeosaurus sattleri* (M31):** The remains of the holotype of *Dicraeosaurus sattleri* (stored at the MfN) were found in the M pit of the Upper Saurian Marls in Tendaguru (Tansania). The specimen was excavated during the German Tendaguru expedition led by Werner Janensch in 1909. It includes two cervical vertebrae, four complete and three incomplete dorsal vertebrae, the sacrum, 7 anterior vertebrae, and one mid caudal vertebra, several incomplete dorsal rib remains, five chevrons, two ilia, two pubes, one ischium, and two femora (Janensch, 1929). No quarry map exists for the individual. However, all skeletal elements were found in association or partly articulation and there is no overlap in skeletal elements (Janensch 1929). Thus, it is very likely that the femur used for size estimation belongs to the same individual as the dorsal rib sample.

***Apatosaurus ajax* (YPM VP 001860):** The *Apatosaurus* samples include YPM VP 001860 the holotype of *Apatosaurus ajax* (Marsh, 1877) which in addition is the type species of the genus. The nearly complete specimen was found in the Upper Brushy Basin Member of the Jurassic Morrison Formation near Morrison (Gunnison County, Colorado, USA) in the eastern foothills of the Rocky Mountains (Ostrom and McIntosh, 1966; Upchurch et al., 2004b).

During collection and shipping it became intermingled with YPM VP 001840, the holotype of *Atlantosaurus immanis* (McIntosh, 1995; Tschopp et al., 2015) now proposed to be a new species by Tschopp et al. (2015). As a result, it was difficult to distinguish the two individuals, even though they come from different quarries. Following the suggestions of Berman and McIntosh (1978) and McIntosh (1995), Tschopp et al. (2015) were able to distinguish which elements of the mingled taxa comprise the holotype individual of *Apatosaurus ajax* mainly based on bone color. The only material not confidently referable to either specimen is a braincase, the assignment of which does not influence this study. Thus, a relative reliable age and size estimate based on dorsal rib growth record and femur length is possible for YPM VP 001860.

***Apatosaurus louisae* (SMA 0269):** The remains of SMA 0269 (nicknamed "Arapahoe") were identified as *Apatosaurus louisae* by Hans Jakob 'Kirby' Siber and his team who found the skeleton between the years 2010 and 2014 in the Dana Quarry (Morrison Formation, Ten Sleep, Wyoming, USA). The remains labeled with SMA 0269 consist of several cervical, dorsal, and caudal vertebrae and a nearly complete set of dorsal ribs, the complete stylopodium and zeugopodium, pubis, and ischium. Unfortunately, the skeleton is a composite of at least four individuals. Nevertheless, at least six dorsal vertebrae, several ribs, and the right forelimb and hindlimb seem to belong to a single individual (S.I. Fig. 5). Thus, only the remains of this individual will be referred to as SMA 0269 herein.

***Apatosaurus* sp. (UW 46211):** UW 46211 is a by far less complete *Apatosaurus* skeleton found in 2006 together with a two *Camarasaurus* specimens (UW 46212 and UW 46215), and some *Allosaurus* remains a few miles from Laramie (Wyoming, USA) during gas pipeline constructions (S.I. Fig. 2). The quarry now known as the McKinsey-REX Quarry is located in the Upper Jurassic Morrison Formation. The specimen consists of an articulated sacrum including the last four dorsal vertebrae, three more articulated dorsal-, and 15 anterior articulated caudal vertebrae, as well as a few more disarticulated caudals. Based on its osteology this specimen is thought to be subadult.

***Apatosaurus* sp. (MOR 957):** The partial *Apatosaurus* sp. skeleton MOR 957 was found at the Big Horn Thunder Lizard Quarry (Morrison Formation, Wyoming, USA). Stratigraphically the Quarry is located immediately below the Howe Quarry. The Museums of the Rockies excavated the skeletal remains, including a femur enabling size estimation for the individual. A quarry map proving articulation and thus skeletal unity of the individual exists. However, it was not available to the authors before submission of this thesis.

***Apatosaurus* sp. (YPM VP 004832):** The remains of YPM VP 004832 include a right pubis, some vertebrae, and dorsal rib fragments most likely belonging to *Apatosaurus* sp. (Ostrom and McIntosh, 1966). They were found by Reed and Carlin in 1878 in Albany County (Wyoming, USA) in the outcrops of the Upper Jurassic Morrison Formation. Unfortunately, complete long bones of the individual are not preserved, impeding size estimations.

***Brontosaurus excelsus* (YPM VP 001980):** YPM VP 001980 is the holotype of *Brontosaurus excelsus* (Marsh 1879a). It was found in the Atlantosaurus beds of Wyoming in the Como BIuff area (Reed´s Quarry 10), east of Medicine Bow (Morrison Formation, Wyoming, USA) during the late 1870s. Initially it consisted of several vertebrae, the sacrum, left ilium, and chevrons. During the following years more, postcranial material was added to the type specimen (Marsh, 1879b; 1881; 1896; McIntosh, 1995). The complete remains include mid and posterior cervical vertebrae including cervical ribs, dorsal vertebrae dorsal and sternal ribs, sacrum, anterior and midcaudal vertebrae partial including chevrons, forelimbs excluding autopodia, pectoral and pelvic girdle, and the complete hindlimbs. No detailed quarry map exists for the specimen, but its articulation has been stated by Reed in his letter correspondence with Marsh. During the last century it has been synonymized with *Apatosaurus* (Riggs, 1903b; Gilmore, 1936; McIntosh, 1990a; 1995; Upchurch et al., 2004b) until the phylogenetic analysis of Tschopp et al. (2015) revealed *Brontosaurus* as a valid genus. The nearly complete postcranial skeleton is still one of the best preserved diplodocid specimens ever discovered and was the first to be published with a reconstruction of the entire skeleton (Marsh, 1883).

***Brontosaurus excelsus* (YPM VP 001981):** Initially, the partial postcranial skeleton YPM VP 001981 has been described as the holotype of *Brontosaurus amplus* (Marsh, 1881). It includes dorsal vertebrae and ribs, the sacrum, the anterior most caudal vertebrae including chevrons, pectoral and pelvic girdle, forelimbs, and hindlimbs including bones of both pes and manus. It was found in Reed´s Quarry 11 near the finding locality of YPM VP 001980 (Morrison Formation, Wyoming, USA). Equally to the latter, YPM VP 001981 has been synonymized with *Apatosaurus* (Gilmore, 1936; McIntosh, 1990a; 1995; Upchurch et al., 2004b) Although it has never been described in more detail. The recent phylogenetic analysis of Tschopp et al. (2015) clearly grouped the specimen to the species *Brontosaurus excelsus.*

Apatosaurinae indet. (BYU 18531): One of the most complete Apatosaurinae specimens sampled is BYU 18531 labeled as *Apatosaurus* cf. *excelsus*. However, the analysis of Tschopp et al. (2015) groups it close to *Apatosaurus ajax* and proposed its species identification as *Brontosaurus parvus* but a more detailed taxonomical description of this specimen in the literature is still missing. It was found in the Mill Canyon, Grand County, (Utah, USA) and collected from the Brushy Basin Member (Morrison Formation) in 2008. The nearly complete specimen is largely articulated (S.I. Fig. 6).

***Galeamopus pabsti* (SMA 0011):** The remains of SMA 0011, the holotype of *Galeamopus pabsti* (Tschopp and Mateus, 2017), include an almost complete disarticulated skull, 13 cervical vertebrae, the first two dorsal vertebrae, the last six presacral vertebrae, several cervical, dorsal-, and sternal ribs, a partial sacrum, both scapulae and coracoids, both humeri, the left ulna, radius and manus, the right ilium, both pubes, the left proximal ischium, the left femur, tibia, fibula, and nearly complete pes found at the Howe Scott

Quarry (Wyoming, USA). The Quarry is located between the Howe Stephens Quarry and the Howe Quarry. Stratigraphically, its position is within the Upper Jurassic Morrison Formation slightly above the Howe Stephens Quarry. The remains of SMA 0011 (nicknamed "Max") described by Tschopp and Mateus (2017) consist of two partially articulated skeletons found 34 meters away from each other (S.I. Fig. 7) that were interpreted to belong to the same individual based on matching size, no overlap of elements, and a similar pattern of neurocentral closure of vertebrae (Tschopp and Mateus, 2017). Bone histology of different skeletal elements including several ribs however, indicates that some elements of the holotype of *Galeamopus pabsit* belong to other individuals. Nevertheless, articulation and association of bones allows to hypothesize skeletal unity for at least the two partial skeletons (S.I. Fig. 7). Based on the histological results, now the partial skeletons representing different individuals were referred as SMA 001101 and SMA 001102. The individual assignment to certain animals of all histologically sampled skeletal elements labeled with SMA 0011 has been described in more detail by Wiersma et al. (in review). Size and neurocentral fusion of both partial skeletons have been described as juvenile to subadult in the literature (Tschopp et al., 2015; Tschopp and Mateus, 2017). The histology of scapula, humerus, and femur of SMA 0011 has been described by Klein and Sander (2008). Their analysis revealed a subadult age (histologic ontogenetic stage (HOS 8 to 9) for humerus and femur, and a variable degree of remodeling in the scapula. Thus, long bone histology indicates sexual maturity but not skeletal maturity for SMA 001101, the individual the femur belongs to (Klein and Sander, 2008).

***Diplodocus hallorum* (NMMNH P 3690):** The holotype specimen NMMNH P 3690 was originally described as *Seismosaurus halli* (Gillette, 1991). The assignment to a new genus differing from *Diplodocus* was mainly based on an overestimated size. Size in turn was ascertained on an incorrect assignment of the position of some midcaudal vertebrae (Curtice, 1996; Herne and Lucas, 2006). Later on, Gillette (1994) himself corrected the species name to *Seismosaurus hallorum* because he did not apply the correct Latin ending in his initial description (Gillette, 1991). However, several reanalyses of the specimen suggested its assignment to the genus *Diplodocus* (Lucas et al., 2006; Lovelace et al., 2007). The recent phylogenetic analysis of Tschopp et al. (2015) verified these findings and assigned NMMNH P 3690 to *Diplodocus hallorum*, retaining it as a valid species of *Diplodocus* The skeletal remains of the individual were found 16 km west of San Ysidro (New Mexico, USA) in the Brushy Basin Member of the Morrison Formation. They include 25 caudal and sacral vertebrae, a partial pelvis, five chevrons, several ribs, and a partial femur that was found as float at the same locality but seems to belong to the same individual (Gillette, 1991; Lucas et al., 2004). Unfortunately, both ends of the NMMNH P 3690 femur are slightly damaged (most likely caused by scavengers). Thus, the stated femur size of 1800 mm that was used herein for this study is based on estimates. The length of the femur as preserved is 1680 mm, which compares well to sizes of other skeletal elements of the holotype specimen (Herne and Lucas, 2006; Lucas et al., 2004). Both, the femur, and a thoracic rib of the

holotype were sampled histologically and show the same ontogenetic age which additionally underlines skeletal unity of the two elements.

***Diplodocus carnegii* (CM 94):** CM 94 is a paratype of *Diplodocus carnegii* (Hatcher, 1901). It was found in the Sheep Creek Quarry (Morrison Formation, Wyoming, U.S.A) together with the holotype of the species (CM 84). Although partially articulated (S.I. Fig. 8), unfortunately, the partial skeleton labeled with CM 94 consists of at least two different individuals because it includes two pairs of ischia in addition to mid-caudal vertebrae, forelimb elements, a tibia, fibula, one dorsal rib, and partial pes (Hatcher, 1901; Tschopp et al., 2015). The partial skeletons of the holotype CM 84 and the paratype CM 94 are mounted together in the Carnegie Museum of Natural History. Casts of this composite skeleton are on display in numerous museums worldwide (Holland, 1906; McIntosh, 1981; Rea, 2004; Nieuwland, 2010), which made this *Diplodocus* one of the best studied dinosaur (e.g., Stevens and Parrish, 1999; Bedell and Trexler, 2005; McIntosh, 2005; Carrano, 2006; Harris, 2006; Taylor et al., 2009; Whitlock, 2011; Woodruff and Fowler, 2012; Tschopp and Mateus, 2013; Wedel and Taylor, 2013; Taylor and Wedel, 2016; Tschopp and Mateus, 2016). Thus, *Diplodocus carnegii* is suggested to be the type specimen of the genus (Tschopp and Mateus, 2016). For growth curve compilation, the femur length of the slightly larger holotype (CM 84) was used.

***Diplodocus* sp. (MOR 592):** MOR 592 is a partial articulated young adult *Diplodocus* sp. individual. It consists of an almost complete cervical, and partial dorsal vertebrae series showing fused or partially fused neurocentral sutures (Woodruff and Fowler 2012). It includes a femur, enabling growth curve construction, and was found in the O'Hair- near the Strickland Creek Quarry (Morrison Formation, Montana, USA). In previous works the O'Hair Quarry was referred to as the Strickland Creek Quarry as well (Cooley and Schmidt, 1998; Turner and Peterson, 1999) before the MOR team decided to rename this part of the Quarry in honor of the Landowners. Although a quarry map of the individual exists and confirms skeletal unity for the individual (D. C. Woodruff, pers. com. 2018), it was not available for the authors before submission of this thesis. The fair articulation of the specimen is also stated by Woodruff and Fowler (2012).

***Barosaurus lentus* (YPM VP 000429):** The partial skeleton YPM VP 000429 is the holotype of *Barosaurus lentus* and the type species of the genus. It was found in 1890 in the eastern portions of the Black Hills (Morrison Formation outcrops) at the Hatch Ranch (Piedmont Butte, Meade County, South Dakota, USA) and was excavated in 1898. It includes three complete and one incomplete posterior cervical vertebra, six dorsal vertebrae, 19 caudal vertebrae, three chevrons, approximately ten dorsal ribs, left sternal plate, and partial remains of a scapula, sacrum, illium, ischium, femur, tibia, and fibula (Lull, 1919; Tschopp et al. 2015; Taylor and Wedell, 2016). Althoughmost of the bones were found in disarticulation it is very likely that they belong to a single individual that has been scattered by carnivores (a tooth of which has been found in the quarry as well) and erosion. Additionally, it cannot be excluded that single bones of the specimen were collected by public visitors in the nine years

between its finding and excavation (Lull, 1919). A quarry map including rib findings can be found in Lull (1919). Nevertheless, size estimation based on long bone length for growth curve calculation was not possible due to the incompleteness of all limb bone remains.

Diplodocinae indet. (SMA 0013): The partial but well-articulated postcranial skeleton SMA 0013 (nicknamed "Brösmeli") was found in 1993 and 1994 at the Howe Stephens Quarry (Morrison Formation, Wyoming, USA) by Hans Jakob 'Kirby' Sibers team from the Sauriermuseum Aathal (Switzerland). Initially the Diplodocine individual included a cervical and dorsal vertebral column, several associated long bones and ribs, as well as several isolated but associated vertebrae, and chevrons (S.I. Fig. 9). Unfortunately, most of the skeletal remains have been destroyed by a fire in the Dinopark Münchehagen (Germany) where the individual was on display. The remaining elements were sold to Aart Walen, a private preparator.

Diplodocinae indet. (ML 418): The remains of ML 418 found at Moita dos Ferreiros (Lourinhã, Portugal) initially consisted of a mid to posterior cervical vertebra, a middorsal vertebra, a partial tibia, and some dorsal rib fragments of late Kimmeridgian to early Tithonian age. The cervical vertebrae, however, got lost due to bad preservation. The skeletal remains of this individual were referred to as *Dinheirosaurus* by Antunes and Mateus (2003). Later on, it has been assigned to *Apatosaurus* sp. by Mateus (2005). Mannion et al. (2012) noted that it cannot be adequately assigned to either of these two genera because it lacks important autapomorphic skeletal elements. And referred to it as Diplodocidae indet. The phylogenetic analysis of Tschopp et al. (2015) found the specimen as sister taxon of *Galeamopus* in all trees and identified ML 418 as Diplodocinae indet. Long bone remains for accurate size estimation are not preserved.

Diplodocinae indet. (CMC): The 17 diplodocine dorsal rib samples (CMC VP 8020, CMC VP 8027, CMC VP 8038, CMC VP 8991, CMC VP 9930, CMC VP 9932, CMC VP 9935, CMC VP 9948, CMC VP 9956, CMC VP 9962, CMC VP 9977, CMC VP 10059, CMC VP 10666, CMC VP 10667, CMC VP 11339, CMC VP 14293, CMC VP 14893) found in the Mother´s Day Quarry (Wyoming, USA) are part of a nearly monospecific bonebed and were collected from the Saltwash Member of the Morrison Formation. Initially the assemblage of mostly disarticulated bones has been described as mass mortality event killing exclusively juveniles (Myers and Storrs, 2007; Storrs et al., 2012). However, the recent study of Waskow et al. (submitted, (chapter 4)) revealed a heterogeneous age distribution within the assemblage. Most of the sampled specimens show an EFS documenting their adult ontogenetic stage. Additionally, the authors state the presence of at least two different morphotypes within the assemblage, one of which most likely represents the dwarfed genus *Kaatedocus.* Morphological reassessments of the Mother's Day Quarry indicate the presence of normal-sized diplodocine juveniles at this locality in addition to a population of dwarfs (Waskow et al., submitted, (chapter 4); Woodruff et al., 2018, (chapter 5)). Based on skeletochronological and histological similarities rib samples CMC VP 8991, CMC VP 9932,

CMC VP 9935, and CMC VP 10666 most likely represent the same individual (Waskow et al., submitted, (chapter 4)). Thus, only section CMC VP 10666 preserving the most complete growth record of all four samples was included in this study.

Diplodocinae indet. (MOR 790): MOR 790 is another sauropod rib from the Mother´s Day Quarry (Morrison Formation). It was sampled by the Museum of the Rockies (Bozeman, Montana, USA) prior to the sampling series of Waskow et al. (submitted, (chapter 4)) described above. Because this sample seems to belong to the larger and younger diplodocine morphotype present at the site, it was included into the sample base as well.

Diplodocidae indet. (SMA 0008): SMA 0008 is a partial postcranial, well-articulated skeleton found in 1995 in the Upper Jurassic Morrison Formation at Spring Hill Quarry (Wyoming, USA) by Hans Jakob `Kirby´ Siber and his team from the Sauriermuseum Aathal. The individual nicknamed "Aurora" includes a complete dorsal vertebral column found in perfect articulation, the sacrum, several long bones including both femora, and 15 ribs as well as several smaller elements (e.g., chevrons) that might belong to the same individual (S.I. Fig. 10). The articulation of ribs and long bones enables a reliable age and size estimation for this individual. Although SMA 0008 has never been scientifically described in more detail, at least some studies concerning sauropod histology and morphology included this specimen and referred to it as Diplodocidae indet. (Klein and Sander, 2008; Tschopp, 2013).

6.3.4. Sauropoda indet. dorsal rib samples

Sauropoda indet. (FMNH 25112): The partial but articulated skeleton FMNH 25112 (former specimen number 7163) was collected from the Grand River Valley, near Fruita, (Mesa County, Colorado, USA) in 1901 in a geological horizon equivalent to the Como Beds of Wyoming (Morrison Formation) explored by Riggs. He described the specimen as *Apatosaurus excelsus* (Riggs, 1903b). It includes all dorsal vertebrae, 18 caudals, chevrons, dorsal ribs, sacrum, and the right femur (Riggs, 1903b; Upchurch et al., 2004a) Although no quarry map exists, the good articulation of the specimens is documented by photographs shown in Riggs (1903b). It is one of the few sauropod non-type specimens adequately described. One century later, Upchurch et al. (2004a) questioned Riggs' assignment. They proposed that FMNH 25112 might belong to another *Apatosaurus* species not described yet. The phylogenetic analysis of Tschopp et al. (2015) found FMNH 25112 being difficult to assign. They described the specimen as Diplodocid indet. with possible affiliations to *Apatosaurus*, *Brontosaurus*, or *Diplodocus* that needs a more detailed analysis.

Sauropoda indet. (YPM VP 007447): YPM VP 007447 is an isolated rib that was collected in Albany County (Wyoming, USA) in the Upper Jurassic Morrison Formation. According to the Yale Peabody Museum of Natural History database it was collected between 1974 and 2008 by John McIntosh, Peter Dodson, and Robert Bakker.

Sauropoda indet. (YPM VP 060120): YPM VP 060120 is another isolated sauropod rib fragment found in the Como Bluff Quarry 4 (Albany County, Wyoming, USA), that was collected by Reed in the Upper Jurassic Morrison Formation. Especially the head region of the rib is too incomplete to allow a more detailed taxonomic assignment.

Sauropoda indet. (YPM VP 001911): The sauropod dorsal rib YPM VP 001911 to date is specified as *Camarasaurus*. A very old label glued to the bone however, identifies it as *Brontosaurus*. Most likely the rib was collected at Como Bluff (Morrison Formation) and labeled by Williston who worked for Marsh back in the 1870s to 1880s. Caused by its long collection history it is not possible to determine who relabeled the specimen and for what reason. Thus, an exact assignment solely based on collection history is not possible.

Sauropoda indet. (Sa 14, Sa 21, Sa 22): All three samples stored in the MfN were found in the Middle Saurian Marls. The site produced fossil bones from different sauropods including *Dicraeosaurus* and *Giraffatitan* in addition to several isolated theropod and sauropod teeth. The only femur preserved within the assemblage has been assigned to *Giraffatitan* (D. Schwarz, pers. com. 2018). However, there is no articulation of the single rib elements to the femur, impeding a size estimation for these individuals.

6.4. Results

In general, the dorsal rib histology of all sampled sauropod taxa seems to be very uniform, independent of taxonomy and size of the individual. All samples show a relative thick cortex. The inner cortex transforms gradually into cancellous bone without a sharp boundary by the size of the erosion cavities gradually increasing from the inner cortex to the medullary region. All ribs have a medullary region filled with cancellous bone. For the majority of rib samples, an open medullary cavity was not observed. The highest amount of primary bone tissue preservation occurs on the posteromedial side of the sampled proximal dorsal rib shaft region. Independent of ontogenetic age, here the remodeling rate is lower than in any other region of the cross-section. To the contrary, posteromedially the highest amount of Sharpey´s fibers is visible. The orientation of the fibres changes from parallel to the bone surface on the posteromedial side to oblique to the surface anterolaterally.

Most of the vascular canals and primary osteons are also orientated longitudinally in all samples. Consequently, they are only represented as circular spots in the histological cross-section. A few radial canals are also visible. Circumferential canals do not occur in any of the dorsal rib samples. While ontogenetically younger individuals show a higher degree of vascularization and a low count of Sharpey´s fibers, in ontogenetically older individuals the degree of vascularization decreases in contrast to the increasing amount of Sharpey´s fibers. The number of secondary osteons increases with age. However, even senescent individuals still show primary bone tissue and a low amount of Haversian bone. In all sections, the primary bone tissue of the cortex consists of fibrolamellar bone that becomes metaplastic-

like in the regions with high amounts of Sharpey´s fibers. The bone tissue is interrupted by many distinctive LAGs. This results in a nearly complete preservation of the growth record that will be described for each individual in more detail below.

In all following descriptions, ages at sexual and skeletal maturity are defined based on the two distinct decreases in growth rate occurring in the individual's growth record. Cyclicity of the EFS itself was excluded for counting ages at skeletal maturity. The growth time of the individual represents all countable cycles (including the EFS) in addition to the number of missing cycles in the inner cortex and medullary region that had been estimated by retrocalculation. See methods chapter for a more detailed description of all life history data estimate techniques. For all individuals not showing a completely developed EFS, age at death could be estimated. In contrast, the longevity of fully-grown animals could not be estimated because it cannot be excluded that the animal lived on after growth has stopped completely.

6.4.1. Growth record analysis of basal sauropod taxa

***Spinophorosaurus nigeriensis* (NMB 1698):** Based on its growth record (Fig. 3), the paratype of *Spinophorosaurus nigeriensis* was a fully-grown individual that had just reached skeletal maturity at the time of death. The deposition of the EFS had started but had not been completed before its death. In some areas small sediment grains are still sticking to the bone surface, excluding surface damages caused by preparation. 18 LAGs, representing 68% of the complete growth record, are preserved and only one can be assigned to the EFS. Based on retrocalculation estimates, at most four innermost cycles are missing. Thus, the overall growth time of the individual was 22 years. Because the formation of the EFS was not completed, the individual died in its 22th year of life. NMB 1698 reached sexual maturity at an age of 13 years (Fig. 4).

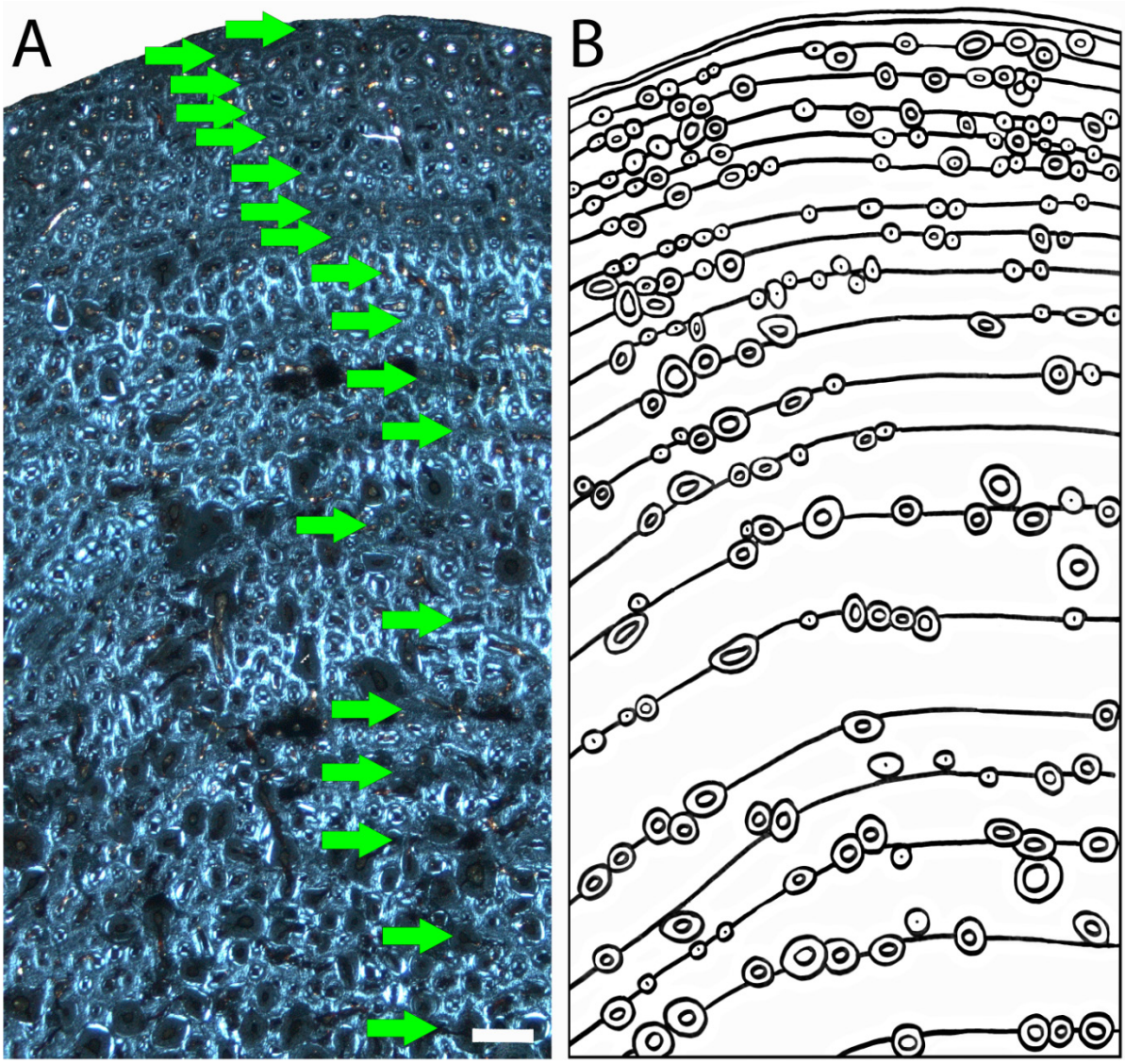

Fig. 3: Growth record preservation (LAGs and modulations) in the histological cross-section of the dorsal rib of *Spinophorosaurus nigeriensis* (NMB 1698). **A**: Polarized light photograph. Green arrows indicate growth marks. Scale bar equals 500 µm. **B**: Drawing of the visible growthmarks and the secondary osteons influencing the LAGs by destroying or tracing them.

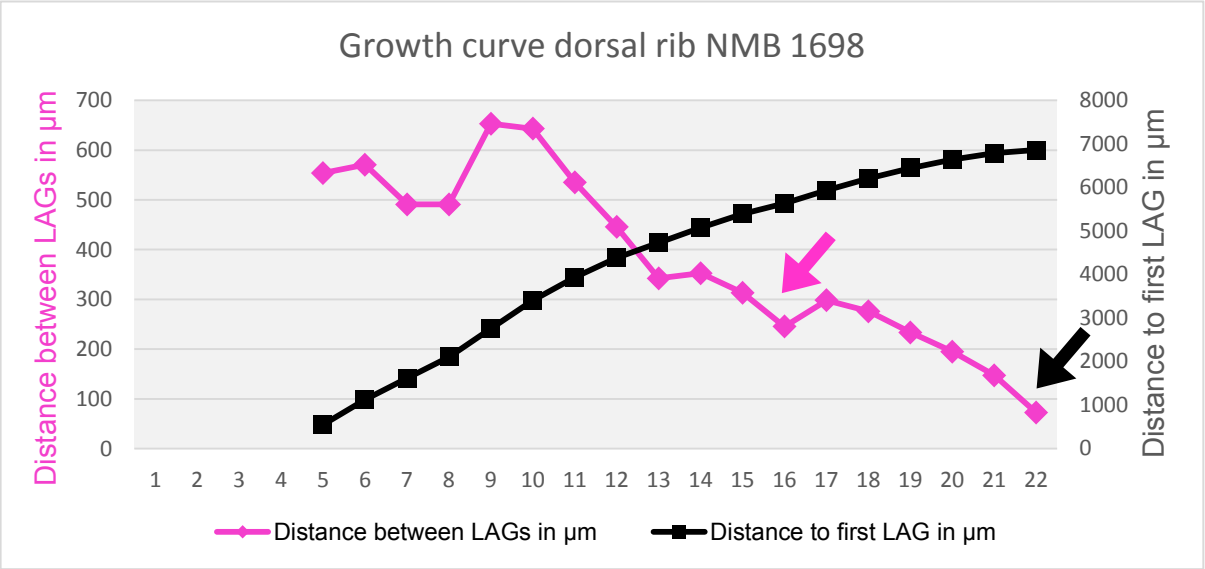

Fig. 4: Growth curve based on growth record preservation in the dorsal rib of *Spinophorosaurus nigeriensis* (NMB 1698). Due to retrocalculation estimates four innermost cycles are missing thus measurements start with the first countable cycle most likely representing the fifth year of the animal's life. Purple arrow indicates point of sexual maturity, black arrow indicates point of skeletal maturity.

6.4.2. Growth record analysis of macronarian taxa

***Camarasaurus lewisi* (BYU 9047):** Specimen BYU 9047 was a senescent individual showing a well-developed EFS and a relatively high amount of Haversian bone tissue in the innermost cortex. The EFS includes eight to 10 LAGs, depending on which LAGs are considered part of the EFS. Caused by the close distance between the EFS LAGs and the lack of structures like primary osteons or vascularity between them, discrimination of annual deposited LAGs vs. double or triple LAGs becomes nearly impossible. In some areas the outer bone surface is still covered with sediment grains, indicating no damage by preparation. Nevertheless, loss of some outermost EFS cycles due to preburial damage cannot completely be excluded. In total, 31 cycles are preserved, representing 68% of the growth record. Most of the innermost cycles are only visible as modulations even in the more remodeled areas (Fig. 5). The maximum number of resorbed LAGs due to remodeling and expansion of the medullary cancellous bone region is six, resulting in an overall growth time of 37 years. Even if decreases in growth are not as significant as in other sampled individuals, growth record analysis indicates, that the animal reached sexual maturity at 16 years of age, and skeletal maturity after 27 to 29 years of growth (Fig. 6).

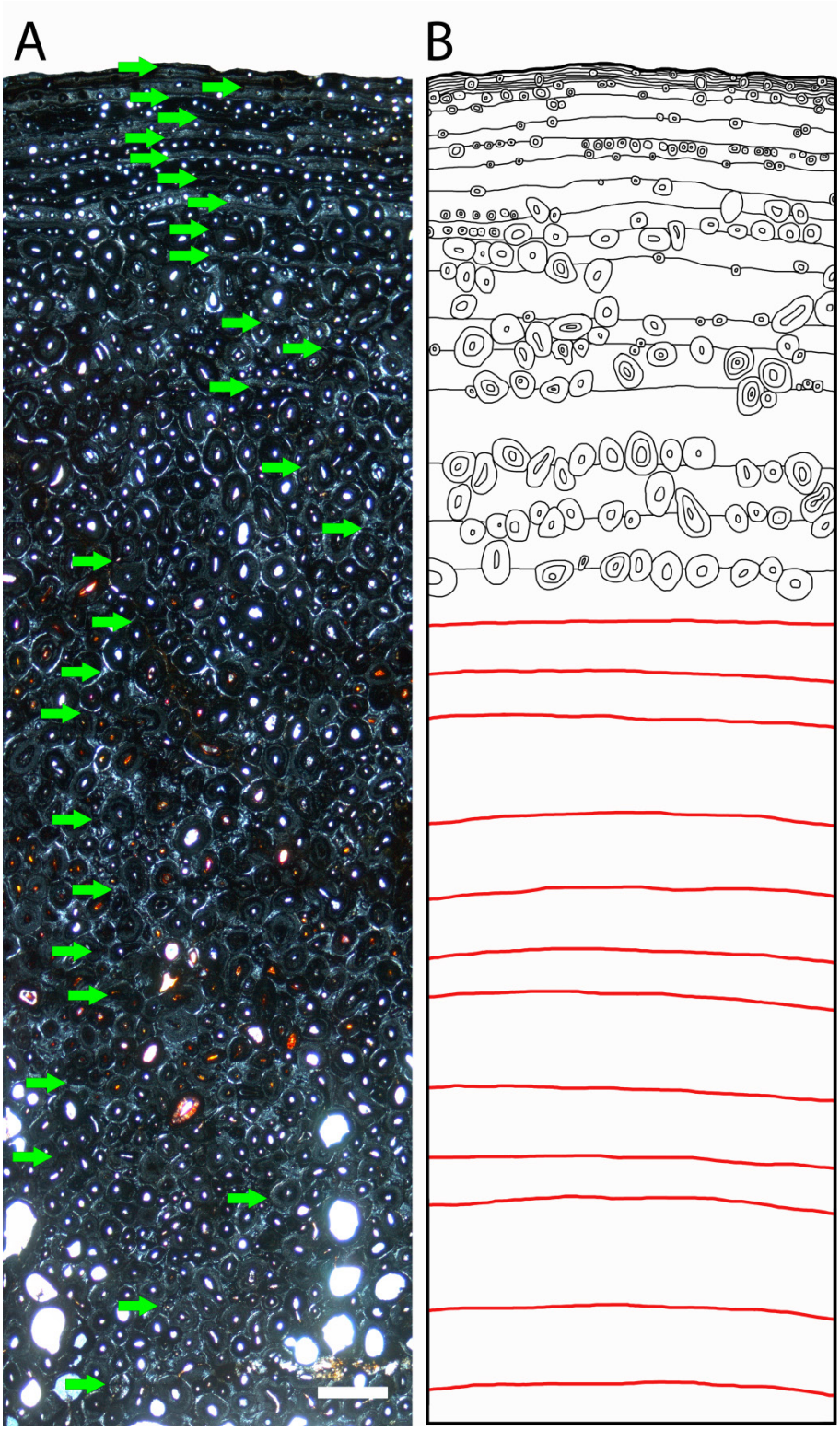

Fig. 5: Growth record preservation in the histological cross-section of the dorsal rib of *Camarasaurus lewisi* (BYU 9047). **A**: Polarized light photograph. Green arrows indicate growth marks. Note that not all LAGs of the EFS are marked with arrows due to magnification of the figure. Scale bar equals 500 µm. **B**: Drawing of the visible growthmarks and the secondary osteons influencing the LAGs by destroying or tracing them. Polish lines not visible under the microscope are marked in red.

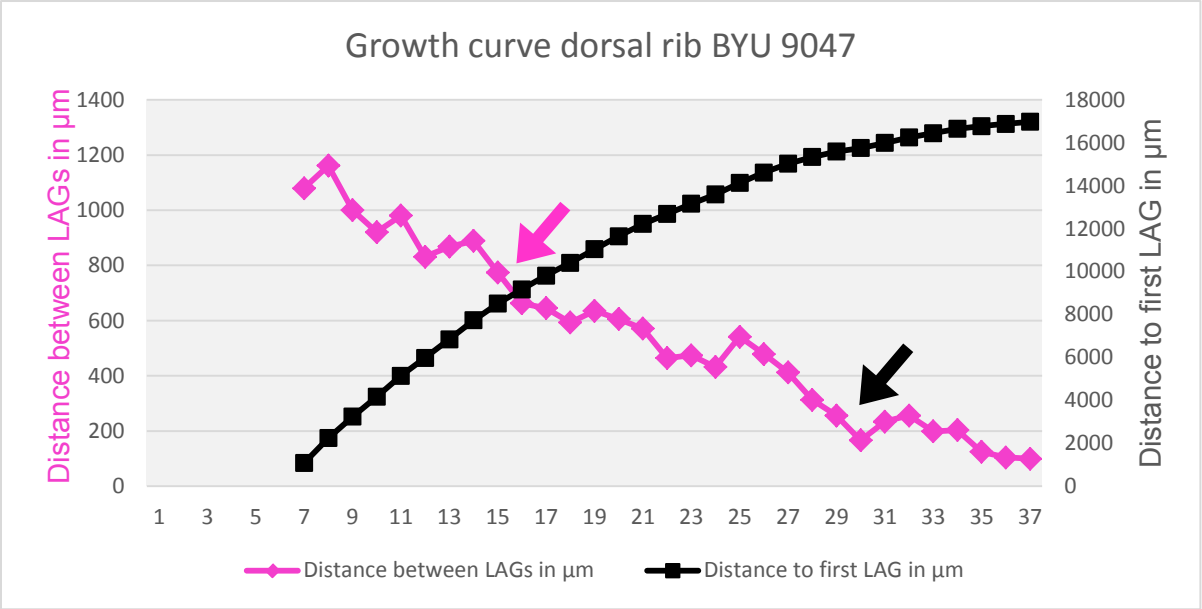

Fig. 6: Growth curve based on growth record preservation in the dorsal rib of *Camarasaurus lewisi* (BYU 9047). Due to retrocalculation estimates six innermost cycles are missing thus measurements start with the first countable cycle most likely representing the seventh year of the animal´s life Purple arrow indicates point of sexual maturity; black arrow indicates point of skeletal maturity.

***Camarasaurus grandis* (YPM VP 001901):** In total 17 LAGs (representing 76% of the growth record) are preserved in the dorsal rib of YPM VP 001901 (S.I. Fig. 11). Minor sedimentary remains exclude preparational damage, however not preburial decay. Retrocalculation estimates suggest the loss of the innermost three cycles. The sample lacks an EFS, indicating that skeletal maturity was not reached before death that occurred at 20 years of age. Sexual maturity was reached after 17 years of growth, indicated by a decrease in growth after the 14th cycle (S.I. Fig. 57). Note that the dorsal rib described here is catalogued as part of the holotype YPM VP 001901. However, its growth record (S.I. Fig. 57 and 58) indicates that it might possibly belong to the paratype YPM VP 001905 instead (see description below).

***Camarasaurus grandis* (YPM VP 001905):** *Camarasaurus* YPM VP 001905 shows 17 LAGs preserved in its dorsal rib cortex, representing 76% of the growth record (S.I. Fig. 12). Retrocalculation suggests the loss of three cycles to remodeling. No EFS is observable, indicating that the animal had not reached skeletal maturity before its death. The decrease in growth after the 14th cycle, however, indicates that sexual maturity was reached at the age of 17 years (S.I. Fig. 58). The animal died in its 21st year of life. Histology, skeletochronology, and life history estimates are identical to the growth record described for YPM VP 001901 (S.I. Fig. 57 and 58), indicating that both rib samples most likely belong to the same individual. Both specimens (the holotype of *Camarasaurus grandis* (YPM VP 001901) as well as the paratype of *Camarasaurus grandis* (YPM VP 001905)) were found in the same quarry. Thus, missassignment of a dorsal rib to either YPM VP 001901 or YPM VP 001905 solely based on location in the quarry is possible. Unfortunately, it was not possible to determine the exact discovery positions of the single ribs sampled here, impeding a more accurate assignment of both ribs to either the holotype or the paratype.

***Camarasaurus* sp. (SMA 0002):** The dorsal rib histology of *Camarasaurus* SMA 0002 has already been described in detail by Waskow and Sander (2014) who analyzed all ribs of the right rib cage in detail. In total 40 samples were taken, covering all parts of the ribs including the capitulum and the complete shaft from proximal to distal. In the dorsal rib sample of specimen SMA 0002 that provided the most complete growth record (found at the proximal shaft of the 3dr rib) 37 cycles are preserved representing 87% of the complete growth record. Although the relatively uneven bone surface of SMA 0002 does not preclude preburial damage, surface destruction due to preparation can be excluded by the presence of sediment grains still sticking to the surface. Assuming one or two innermost LAGs might be missing (based on retrocalculation), the growth time estimate (Including EFS cycles) for the individual is 38 to 39 years. Excluding the LAGs in the EFS, age at skeletal maturity was 34 years. Based on the growth curve, sexual maturity was reached earlier in ontogeny after 18-19 years of growth. In addition to the growth record, the relatively high number of secondary osteons in the innermost cortex (which is untypical for ribs) attests to a senescent ontogenetic stage of this individual. Thus, the estimated growth time of nearly 40 years is unlikely to represent longevity.

***Camarasaurus* sp. (SMA 0274):** The histology of SMA 0274 reveals a senescent ontogenetic age of the individual. A clearly developed EFS is visible consisting of five closely spaced LAGs (S.I. Fig. 13). Small sediment remains on the bone surface exclude preparation damages. In total 22 cycles can be counted, including ten cycles only visible as polish lines in the inner cortex. The innermost cortex is completely remodeled, restricting the preserved growth record to 67%. Retrocalculation estimates compute the loss of 11 cycles, resulting in an overall growth time of 33 years. Sexual maturity was reached after 19 years of growth and skeletal maturity with 28 years of age (S.I. Fig. 59). Histology reveals a bone tissue of derived ontogenetic age. This implies that the Individual most likely had lived on many years after growth has stopped completely.

***Camarasaurus* sp. (UW 46215):** Skeletochronology and dorsal rib histology of sample UW 46215 reveal an adult but not fully-grown ontogenetic age of the specimen. In total 18 cycles are preserved, representing 55% of the growth record (S.I. Fig. 14). Retrocalculation estimates indicate the loss of six additional cycles due to remodeling and expansion of the medullary cancellous bone region. Although no clear EFS is visible, the decrease in cycle thickness occurring close to the outer sample surface, indicates that UW 46215 was about to reach skeletal maturity but has not completed growth before death. Thus, the estimated growth time of 24 years most likely represents age at death. However, it should be mentioned that coarse bone surface damages are visible indicating that the outermost bone layer might be lost due to preparation or preburial damage. Thus, it cannot be excluded that a former EFS might be missing in the sample, which would raise the ontogenetic stage of the animal to the fully-grown level. In either case, sexual maturity had already been reached at

the age of 17 years indicated by a distinct decrease in growth occurring after the 11th countable cycle (S.I. Fig. 60).

***Camarasaurus* sp. (UW 46212):** *Camarasaurus* UW 46212 shows typical juvenile bone tissue interrupted by 10 clearly developed LAGs representing 80% of the growth record (S.I. Fig. 15). The bone surface might have been slightly influenced by preparation because no sediment grains still sticking to the surface are visible. No EFS or clear decrease in growth is visible, indicating that the animal in question has neither reached skeletal nor sexual maturity (S.I. Fig. 61). The estimated maximum number of missing LAGs in the inner cortex is 4. Thus, UW 46212 most likely died at the age of 14.

***Camarasaurus* sp. (YPM VP 000619):** *Camarasaurus* YPM VP 000619 is a juvenile individual showing nine clearly developed LAGs representing 52% of the growth record (S.I. Fig. 16). Sedimentary remains on the bone surface indicate the completeness of the outermost cortex. Retrocalculation estimates compute the loss of six innermost cycles. Thus, the animal most likely died at the age of 14 years. No clear decrease in growth is visible, indicating that the animal reached neither sexual nor skeletal maturity. The comparison with other *Camarasaurus* individuals presumes that YPM VP 000619 was close to achieve sexual maturity.

***Camarasaurus* sp. (UMNH samples):** Most of the 18 UMNH samples belong to adult, skeletal mature individuals. Only sample UMNH 24802 shows a less ontogenetical derived bone tissue including 11 clearly developed cycles that represent 54% of the growth record (S:I: Fig. 17). Growth time and age at death have been estimated to be 16 years (including 5 missing innermost cycles) for this individual. Based on its growth record UMNH 24802 was close to reach sexual maturity as indicated by as slight decrease in growth observable in the outermost cycles (S.I. Fig. 62). All other UMNH samples show growth times varying between 30 and 37 years and EFS varying between 3 and 10 cycles respectively (S.I. Fig. 18-27). Most of the sampled individuals show growth times of 30 to 31 years and reached skeletal maturity at the age of 26 to 27. Based on the distinct decrease in growth occurring in each growth record of the UMNH samples, sexual maturity on average was reached after 18 to 20 years of growth (S.I. Fig. 63-76) Distinct skeletochronological similarities that are unique in the single individuals (Wiersma et al., in review; Waskow and Sander, in prep.) indicate that samples UMNH 5289 and UMNH 5302 belong to the same individual (S.I. Fig. 63 and 64). The same is true for samples UMNH 21606, UMNH 21608, and UMNH 24804 (S.I. Fig. 65-67) and samples UMNH 24384, and UMNH 24801 (S.I. Fig. 68 and 69), representing two other individuals (Fig. 7). Thus, only samples UMNH 5302, UMNH 21608, and UMNH 24384 preserving the most complete growth record for the three different individuals respectively, were included in this study.

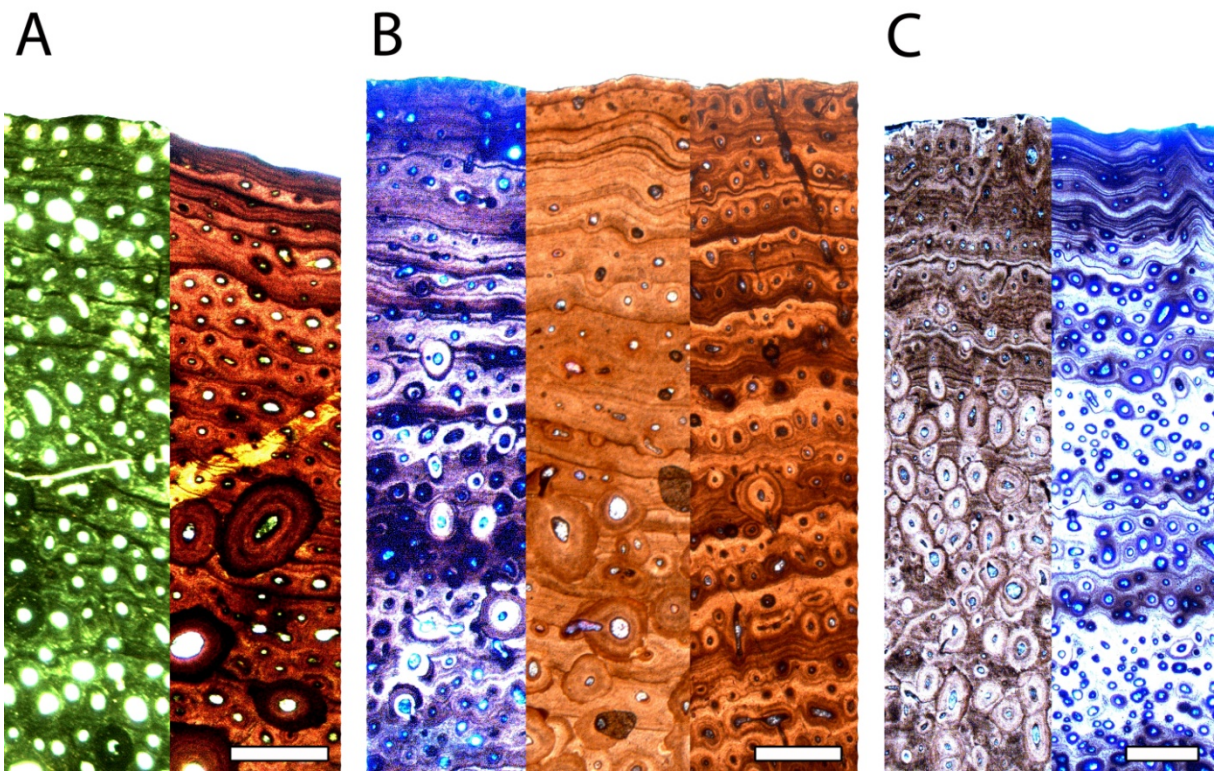

Fig. 7: Histology of seven different *Camarasaurus* sp. (UMNH) samples representing three different individuals. Note the simmiliarity of the single growth records (similar spacing between LAGs) as well as the similar remodeling, and vasculatisation patterns. Growth curves for all seven samples are given in the supplementary informations (S.I. 63-69). Scale bars equal 500 µm. **A**: Photograph of samples UMNH 5289 (polarized light) and UMNH 5302 representing the same individual. **B**: Photograph of samples UMNH 24804 (polarized light), UMNH 21606, and UMNH 21608 represnting the same individual. **C**: Photograph of samples UMNH 24384 and UMNH 24801 (polarized light) representing the same individual.

***Camarasaurus* sp. (YPM VP 060121):** The isolated rib fragment YPM VP 060121 shows 24 cycles, 12 of which are preserved as modulations. 65% of the original growth record is preserved (S.I. Fig. 28). Based on retrocalculation 7 innermost cycles have been resorbed. The specimen reached skeletal maturity at the age of 28 as indicated by an EFS consisting of three closely spaced LAGs that raise the total growth time to 31 years. However, the loss of some outermost EFS cycles due to preparation or preburial damage cannot be excluded. Sexual maturity was reached after 20 years of growth (S.I. Fig. 77).

***Brachiosaurus altithorax* (FMNH P25107):** FMHN P25107 is the largest rib within the sample base. The type specimen of *Brachiosaurus altithorax* shows 35 cycles (S.I. Fig. 29). Seven of these build a clearly developed EFS, indicating skeletal maturity. Grains preserved on the outer bone surface indicate that no preparational damage has influenced the number of cycles within the EFS. Preburial decay, however, cannot be excluded completely. The preservation of an EFS disproves the assumption of Taylor (2009) who stated that FMNH P25107 possibly represents a subadult individual based on the lack of suture fusion in the coracoid. 77% of the growth record are preserved. The estimated maximum number of missing innermost cycles is five. Thus, according to the growth record *Brachiosaurus altithorax* reached sexual maturity after 17 years of growth and skeletal maturity at the age

of 32 (S.I. Fig. 78). The overall growth time estimated to be 40 years, the age at death however might have been older.

***Brachiosaurus altithorax* (SMA 0009):** The smallest articulated specimen of the whole sample base only shows one LAG preserved in its cortex (S.I. Fig. 30). No resorption or remodeling is visible in the inner cortex. Thus, the one preserved cycle represents 100% of the growth record. No sediment grains are sticking to the surface. Slight surface damage due to preparation cannot be excluded. In contrast, preburial damage is very unlikely because the preservation and nearly perfect articulation of the young juvenile animal itself hint to a quick burial. Thus, the animal must have been in its second year of life.

***Brachiosaurus altithorax* (SMA 0314):** The drill core sample of the isolated dorsal rib SMA 0314 shows a clearly developed EFS consisting of 12 closely spaced LAGs (S.I. Fig. 31). Thus, skeletal maturity can be confirmed for the individual. Unfortunately, the untypical thin and plank like shape of this particular rib even in the proximal end impedes estimations of growth record completeness and number of missing cycles. Cancellous bone dominates the inner bone structure. Therefore, no estimations on age at sexual or skeletal maturity can be given.

Cf. *Giraffatitan* (J 12): J12 shows 30 LAGs representing 60% of the growth record (S.I. Fig. 32). Fortunately, the drill core sample includes the medullary region allowing retrocalculation. The loss of at most 9 innermost cycles due to remodeling can be assumed. The complete growth time of the animal was 39 years, not necessarily representing its longevity, that might have lasted even longer. The distinct decrease in growth occurring after the 13th cycle indicates that sexual maturity was reached after 22 years (S.I. Fig. 79). The deposition of an EFS consisting of five closely spaced LAGs indicates that skeletal maturity was reached at the age of 34 years. The loss of more outermost EFS cycles due to preparation is unlikely because some sedimentary remains are still visible on the bone surface.

6.4.3. Growth record analysis of diplodocoid taxa

***Suuwassea emilieae* (ANS 21122):** The dorsal rib histology of the holotype *Suuwassea emilieae* reveals an adult, but not fully-grown ontogenetic stage for the specimen. 56% of the growth record is preserved. The growth record consists of 16 cycles of which eight are developed as LAGs (Fig. 8). The remaining eight cycles are only visible as modulations. Retrocalculation suggests the loss of three innermost cycles raising the total growth time of the animal to 19 years. Although the decrease in cycle thickness indicates that the animal was close to the deposition of an EFS, skeletal maturity was not reached during its lifetime. Thus, the estimated growth time represents age at death. A significant decrease in growth after the 12th cycle (and thus 15 years) marks onset of sexual maturity (Fig. 9). Note that due to the lack of a preserved femur, femur length was estimated based on humerus length (752 mm).

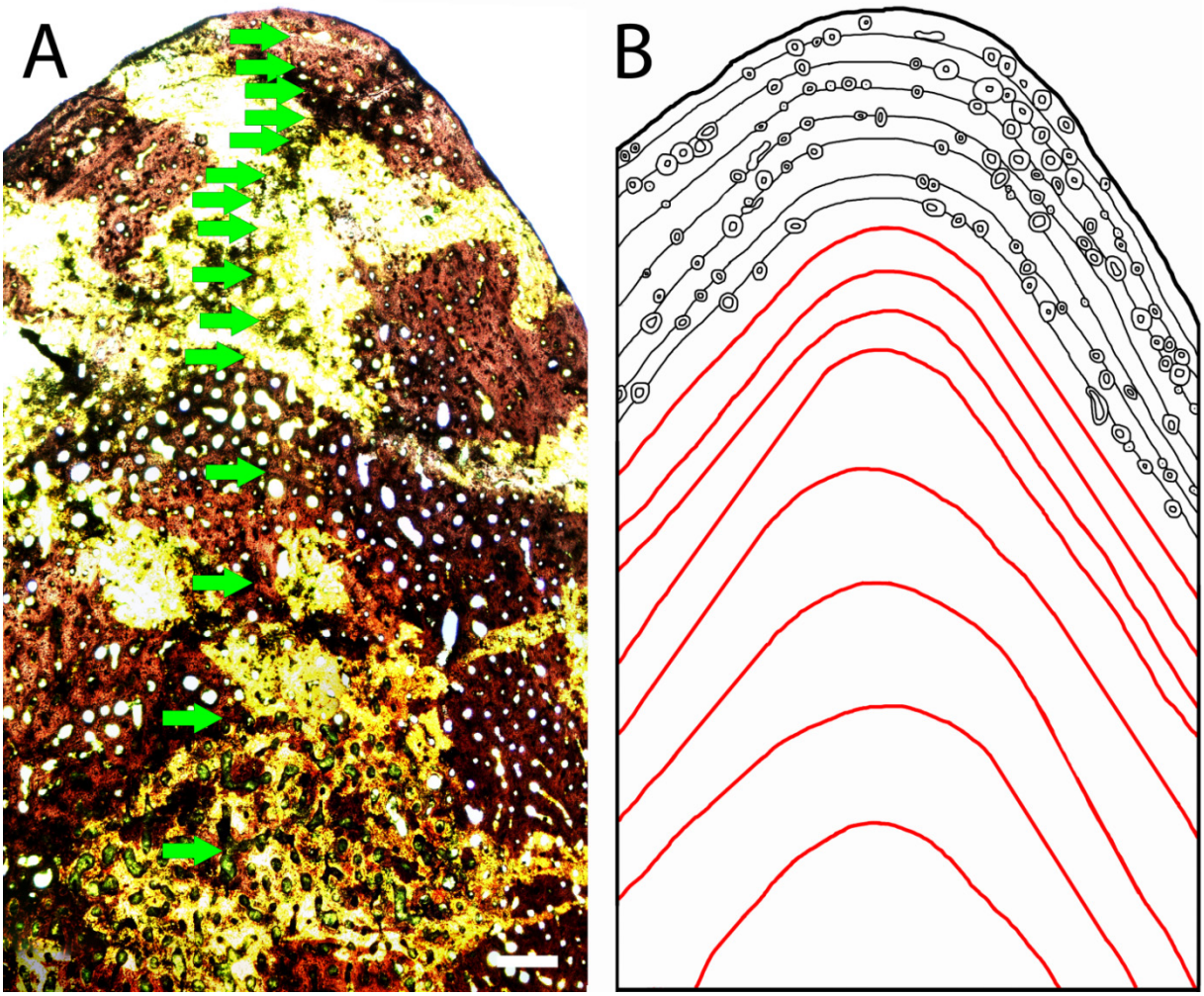

Fig. 8: Growth record preservation in the histological cross-section of the dorsal rib of *Suuwassea emilieae* (ANS 21122) **A**: Polarized light photograph. Green arrows indicate growth marks. Scale bar equals 500 µm. **B**: Drawing of the visible growthmarks and the secondary osteons influencing the LAGs by destroying or tracing them. Polish lines not visible under the microscope are marked in red.

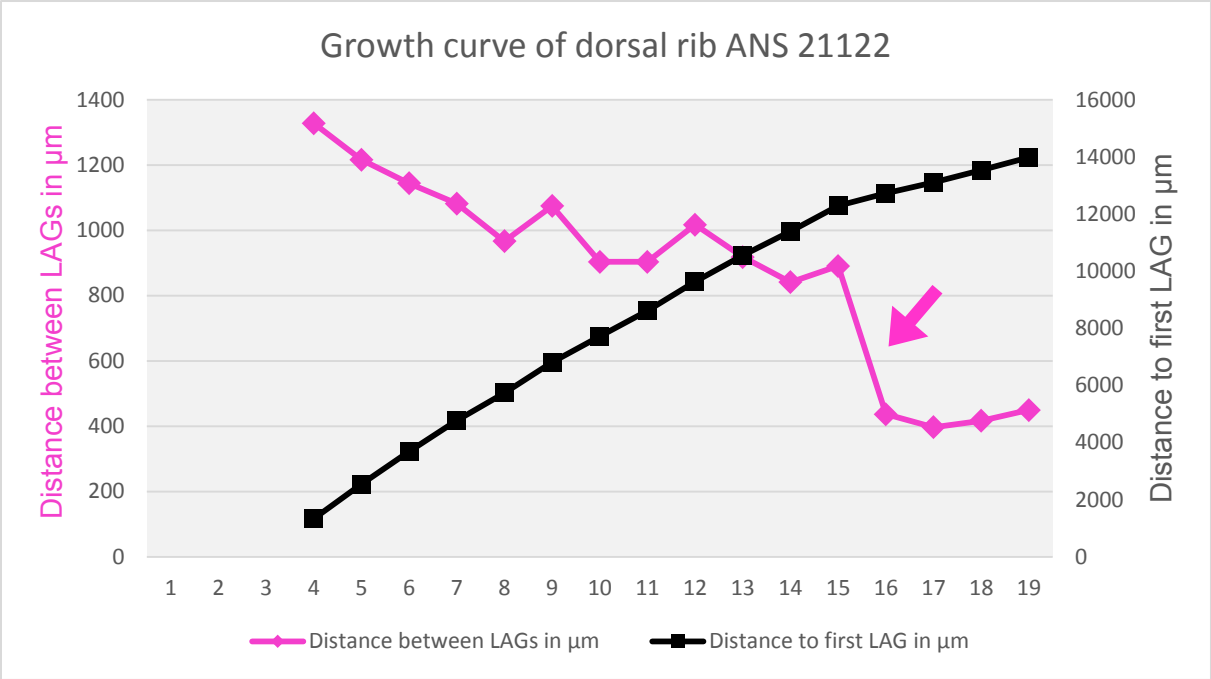

Fig. 9: Growth curve based on growth record preservation in the dorsal rib of *Suuwassea emilieae* (ANS 21122). Purple arrow indicates point of sexual maturity. Note that skeletal maturity has not been reached before death in this individual.

***Dicraeosaurus sattleri* (M 31):** M 31 is one of the few dorsal ribs in the whole sample base where no clear growth record can be observed. Contrary to the other samples, M 31 has a large medullary cavity most of which is filled with trabeculae merging slowly into a thin cortex (S.I. Fig. 33). In general, the bone tissue is heavily remodeled, suggesting an old ontogenetic stage of the individual. Sparsely remains of a former EFS are visible in the outermost cortex indicating skeletal maturity. M 31 is the only *Dicraeosaurus* specimen in the whole sample base. Thus, the difference in growth record preservation might be based on higher pneumatisation observable in the ribs of *Dicraeosaurus* compared to other Diplodocoidea. Pneumatisation of the axial sleketon in *Dicraeosaurus* has been reported before by Schwarz and Fritsch (2006). Additionally, the method used for the sampling differs. Contrary to most other samples, core drilling has sampled the dorsal rib of M 31. Thus, it cannot be excluded that a complete cross-section might contain more skeletochronological information. However, the rib of *Dicraeosaurus sattleri* is relatively small so that the drill core sample equals nearly 50% of a complete cross-section. The sample was taken exactly at the position containing the most complete growth record in all other samples. Therefore, sampling technique as an explanation for missing growth record information is unlikely.

***Apatosaurus ajax* (YPM VP 001860):** The holotype of *Apatosaurus ajax* is an adult individual that shows 20 clearly developed growth cycles representing 77% of the growth record (S.I. Fig. 34). Only two innermost cycles might be missing due to expansion of the medullary cancellous bone region. The growth time of the animal can be estimated to be 22 years. Age at death might have been higher. However, the general histology of the sample indicates a relatively early adult ontogenetic age for YPM VP 001860. Skeletal maturity is indicated by an EFS consisting of four closely spaced LAGs and was reached at the age of 18 years. Based

on growth curve analysis sexual maturity was achieved after 12 years of growth (S.I. Fig. 80). The loss of some outermost EFS LAGs due to preparation cannot be excluded because no sedimentary remains are left on the outer bone surface.

***Apatosaurus louisae* (SMA 0269):** Skeletochronology of SMA 0269 reveals a adult but not fully grown ontogenetic age for the specimen. 14 cycles are preserved in the dorsal rib cortex representing 79% of total growth record (S.I. Fig. 35). Most of the broad cycles are preserved as modulations. Due to the relatively young ontogenetic age of the specimen only two innermost cycles were lost based on retrocalculation estimates. No EFS can be observed indicating that skeletal maturity was not reached before death. Thus, the estimated 16 years of growth most likely also represent age at death. Sexual maturity in contrast has been reached at the age of 10 years as indicated by a distinct decrease in growth occurring after the eighth countable cycle (S.I. Fig. 81).

***Apatosaurus* sp. (UW 46211):** Specimen UW 46211 is a sexual and skeletal mature individual that shows 12 cycles most of which are developed as modulations (S.I. Fig. 36). The completeness of the growth record is 45%. Based on retrocalculation estimates, the missing 55% of the record consisted of at most eight additional cycles that would raise the overall growth time to 20 years. Skeletal maturity was reached at the age of 17 years as indicated by an EFS consisting of three LAGs. Preparational damages of the outermost EFS cannot be excluded because the sample lacks sedimentary remains still sticking to the bone surface. Sexual maturity, as indicated by a distinct decrease in growth after the 4th countable cycle was reached at the age of 12 years (S.I. Fig. 82).

***Apatosaurus* sp. (MOR 957):** The dorsal rib histology of MOR 957 shows 14 well developed LAGs representing 74% of the growth record (S.I. Fig. 37). Retrocalculation estimates the loss of two innermost cycles due to remodeling. Skeletal maturity has not been reached, as no EFS is visible. Small sedimentary remains on the bone surface neglect surface damage due to preparation. The adult but not fully grown individual most likely died at the age of 16 years. It reached sexual maturity at the age of 14 years. This is indicated by the significant decrease in growth after the 12th countable cycle (S.I. Fig. 83).

***Apatosaurus* sp. (YPM VP 004832):** *Apatosaurus* YPM VP 004832 is a senescent individual that shows 19 growth cycles of which 14 are developed as LAGs (S.I. Fig. 38). Five additional cycles are only visible as modulations even in the strong remodeled parts of the mid to inner cortex. The growth record completeness is 56%. At most 5 innermost cycles are missing based on retrocalculation, raising the overall growth time to 24 years. The high amount of Haversian bone tissue however, hints to an even higher age at death. The animal was skeletal mature as indicated by a clear developed EFS consisting of 7 LAGs. The loss of further outermost EFS cycles due to preburial damage or preparation cannot be excluded. Skeletal maturity had been reached at the age of 17 years (excluding EFS cycles). Growth curve analysis reveals an age at sexual maturity of 13 years for the individual (S.I. Fig. 84).

***Brontosaurus excelsus* (YPM VP 001980):** Skeletochronology and histology of the holotype specimen of *Brontosaurus excelsus* hint to a juvenile to subadult ontogenetic stage of the specimen. Eight cycles can be observed in the dorsal rib cortex which are developed as clearly visible LAGs or polish lines (S.I. Fig. 39). The loss of four additional innermost cycles is indicated by retrocalculation. Thus, the animal most likely died at the age of 12 years without reaching sexual or skeletal maturity. Nevertheless, the decrease in cycle thickness indicates that YPM VP 001980 was close to reach sexual maturity.

***Brontosaurus excelsus* (YPM VP 001981):** Specimen YPM VP 001981 shows a clearly developed growth record preserved in its dorsal rib. Most of the 21 counted cycles (S.I. Fig. 40) are developed as modulations and best visible with naked eye. 80% of the growth record is preserved. The missing 20% were resorbed during the formation of the medullary region that (based on retrocalculation estimates) destroyed a maximum number of two innermost cycles. Sexual maturity was reached with 14 years of age (S.I. Fig. 85). The individual became skeletal mature at the age of 20 years. Including the two cycles preserved within the EFS the overall growth time of the animal was 22 years, presumably representing its age at death.

Apatosaurinea indet. (BYU 18531): The skeletochronology of this apatosaurine specimen shows 18 cycles representing 58% of the growth record (S.I. Fig. 41). Retrocalculation estimates the loss of at most seven innermost cycles that would increase total growth time to 25 years. The outermost cortex shows an EFS consisting of four closely spaced LAGs, indicating skeletal maturity. No mineral grain remains are observable on the bone surface, thus the loss of additional outermost EFS cycles cannot be excluded. Skeletal maturity had been reached after at most 21 years of growth. The significant decrease in growth occurring after the 8th cycle indicates that sexual maturity had been achieved at the age of 15 years (S.I. Fig. 86). In comparison to other diplodocoids, the estimated ages at sexual and skeletal maturity confirm the assignment of BYU 18531 (that according to Tschopp et al. (2015) most likely can be referred to as *Brontosaurus parvus*) to the diplodocoid clade.

***Galeamopus pabsti* (SMA 0011):** Dorsal rib skeletochronology of the holotype specimen SMA 0011 suggests an adult but not fully-grown ontogenetic stage for the individual. 11 clearly developed cycles most of which are preserved as modulations are visible (S.I. Fig. 42), representing 54% of the growth record. At most four former cycles have been resorbed due to expansion of the medullary cancellous bone region. Thus, the growth time which coincides with the individual's age at death can be estimated to be 15 years. Based on a distinct decrease in growth occurring after the eighth countable cycle, sexual maturity has already been reached at the age of 12 years (S.I. Fig. 87). Skeletal maturity has not been achieved before death, because no EFS can be observed.

***Diplodocus hallorum* (NMMNH P 3690):** *Diplodocus hallorum* (former *Seismosaurus hallorum*) is an adult individual showing 17 preserved cycles (S.I. Fig. 43), representing 48% of the complete growth record in its dorsal rib cortex. 11 cycles are developed as LAGs, the

other six are better visible in grazing light as modulations. An EFS consisting of seven LAGs as well as a relatively high amount of Haversian bone tissue in the inner cortex indicate a senescent ontogenetic age for the individual. Small sediment grains sticking to the bone surface exclude the loss of additional outermost EFS cycles due to preparation. Based on retrocalculation estimates remodeling and expansion of the medullary region destroyed nine innermost cycles. Thus, total growth time can be estimated to be 26 years. Age of death in contrast, is hard to ascertain. The derived histology indicates that the animal might have lived on for several years after growth was completed. Skeletal maturity was reached at the age of 19 years (excluding the EFS). Sexual maturity was achieved after 14 years of growth indicated by growth record analysis showing a decrease in growth after the fifth countable cycle (S.I. Fig. 88).

***Diplodocus carnegii* (CM 94):** The holotype of *Diplodocus carnegii* shows a nearly complete growth record consisting of 21 LAGs representing 91% of the growth record (S.I. Fig. 44). Based on retrocalculation estimates only one innermost LAG might be missing. The individual reached sexual maturity at the age of 12, and skeletal maturity after 19 years of growth (S.I. Fig. 89). The age estimate at skeletal maturity excludes the EFS consisting of three closely spaced cycles. The complete individual growth time is 22 years.

***Diplodocus* sp. (MOR 592):** Specimen MOR 592 was a young adult individual showing 17 cycles in its dorsal rib cortex. Four of these are preserved as LAGs. The innermost 13 cycles are only visible as modulations (S.I Fig. 45). In total 63% of the growth record is preserved. Based on retrocalculation four innermost cycles are missing due to expansion of the medullary cancellous bone region. The formation of an EFS has just started but has not been completed before death. Thus, the growth time of 21 years, in this case can be interpreted as age at death in the young adult *Diplodocus* individual. It had reached sexual maturity at the age of 12, and skeletal maturity at the age of 19 years (S.I. Fig. 90). The dorsal rib histology of MOR 592 has been briefly been described before by Woodruff (2015) who claimed a subadult ontogenetic stage for the individual. However, this interpretation was based on a much smaller sample size. The much larger sample size in this study, however, allows a comparison of ages at major life history events (sexual and skeletal maturity) of MOR 592 to other diplodocoids. These suggest that the two outermost closely spaced LAGs do indeed represent the beginning of an EFS. No sediment grains are preserved on the bone surface. Therefore, neither preburial nor preparational damage could be excluded.

***Barosaurus lentus* (YPM VP 000429):** The holotype of *Barosaurus lentus* shows 16 cycles in its dorsal rib cortex representing 56% of the total growth record (S.I. Fig. 46). Eight innermost cycles have been resorbed as indicated by retrocalculation estimates. Overall growth time can be estimated to be 24 years for this sample. Because growth most likely was completed before death, age at death cannot be determined. An EFS consisting of three closely spaced LAGs indicates skeletal maturity of the individual that was reached after 21 years of growth. Although the lack of sedimentary remains on the bone surface generally

hints to a possible loss of additional outermost EFS cycles, the smooth surface structure makes preparational damages unlikely. Sexual maturity had been achieved at the age of 13 years. This is indicated by the distinct decrease in growth occurring after the 5th countable cycle (S.I. Fig. 91).

Diplodocine indet. (SMA 0013): SMA 0013 was an adult diplodocine individual. The growth record covers 59% and consists of 19 well developed cycles (S.I. Fig. 47). Retrocalculation estimates the loss of three additional innermost cycles due to the expansion of the medullary cavity. Consequently, the growth time can be calculated to be 22 years. An EFS consisting of five closely spaced LAGs is present in SMA 0013 indicating that skeletal maturity had been reached at the age of 17 years. The bone surface shows relatively coarse damages caused by preparation. Hence, the loss of some outermost EFS cycles cannot be excluded. A distinct decrease in growth occurring after the 10th countable cycle indicates that sexual maturity was reached at the age of 13 years (S.I. Fig. 92).

Diplodocine indet. (ML 418): Although tissue preservation is relatively poor, the dorsal rib histology of ML 418 reveals an old ontogenetic age of the individual. The innermost cortex shows relatively intense remodeling. Nevertheless, 23 cycles representing 76% of the growth record are preserved (S.I. Fig. 48). The maximum number of missing innermost cycles has been estimated to be three based on retrocalculation raising the overall growth time to 26 years. A well-developed EFS consisting of four closely spaced LAGs indicates skeletal maturity of the individual that has been reached after 22 years of growth (excluding the EFS). Sedimentary remains still sticking to the surface exclude preparational damage and thus the loss of further outermost EFS cycles. Sexual maturity had been reached by the individual after 15 years of growth (S.I. Fig. 93). These estimates for age at sexual and skeletal maturity match the estimates of other diplodocoids better than the estimates for macronarians sampled here, as discussed in detail below. Therefore, the assignment of ML 418 to the diplodocoid clade determined by several authors before (Antunes and Mateus, 2003; Mateus, 2005; Mannion et al., 2012; Tschopp et al., 2015) can be confirmed by histology (see next chapter and discussion).

Diplodocinae indet. (CMC): In contrast to most other samples, the isolated sauropod rib samples collected in the Mother´s Day Quarry show a heterogeneous age distribution from very young juveniles that have not accomplished their first year of life to senescent individuals showing remains of an EFS and extremely remodeled bone tissue. However, most of the sampled individuals are young adults (indicated by a clearly developed EFS) that reached sexual maturity after 13 to 15 years (S.I. Fig. 94-103) and skeletal maturity with 16 to 17 years of age (excluding EFS cycles). These estimations were based on 50 to 73% complete growth records accomplished by retrocalculation of missing inner cycles. In most cases no sediment matrix is preserved at the surface of the bone; thus, slight surface damages due to preburial processes or preparation cannot be excluded. The sample size versus age variation indicates the presence of at least two size morphs within the sample

base including, one dwarfed taxon and young juveniles of average-sized sauropods. A more detailed description of the histology of the Mother´s Day Quarry diplodocines including figures is given by Waskow et al. (submitted, (chapter 4)).

Diplodocinae indet. (MOR 790): MOR 790 shows highly vascularized juvenilee bone tissue interrupted by four clearly developed cycles best visible in macroscopic view (S.I. Fig. 49). Retrocalculation indicates the loss of at most four additional cycles. Accordingly, the animal most likely died at the age of eight years and had neither reached sexual nor skeletal maturity before its death.

Diplodocid indet. (SMA 0008): SMA 0008 shows 12 clearly developed cycles most of which are visible as modulations (S.I. Fig. 50). 38% of the growth record is preserved. Based on retrocalculation nine innermost cycles have already been resorbed, raising the total growth time to 21 years. A clear EFS consisting of three closely spaced LAGs is visible in the outermost cortex indicating that skeletal maturity was reached at 18 years of age. Sexual maturity was achieved much earlier after 13 years of growth (S.I. Fig. 104). The loss of further EFS cycles due to preparation cannot be excluded because the bone surface lacks sedimentary remains.

6.4.4. Growth record analysis of Sauropoda indet. samples

Sauropoda indet. (FMNH 25112): The dorsal rib histology of FMNH 25112 differs greatly from all other macronarian or diplodocid samples. Most of the inner structure consists of cancellous bone ranging all the way from the medullary region to the bone surface. In some small areas a very thin outermost cortex can be observed consisting of an EFS and showing at least five closely spaced cycles (Fig. 10). Thus, skeletal maturity can be confirmed for the individual. By contrast, age at sexual maturity is not documented in the incomplete growth record. The extreme difference in bone histology of this specimen to both, macronarians and diplodocids, might corroborate its assignment to another sauropod taxon. In fact, a similar histology, showing equally large bone trabeculae and high remodeling rates can be observed in sample M31 assigned to as *Dicraeosaurus sattleri* and in the indetermined sauropod Sa 22 (see description below).From a histological point of view, an assignment of FMNH 25112 to a taxon closely related, or equal to *Dicraeosaurus* is at least possible contrary to what one would expect based on its geographic finding position. *Dicraeosaurus* is only known from the Tendaguru beds of Africa. Consequently, the assignment of FMNH 25112 to this taxon would make it the first evidence for this group in North America.

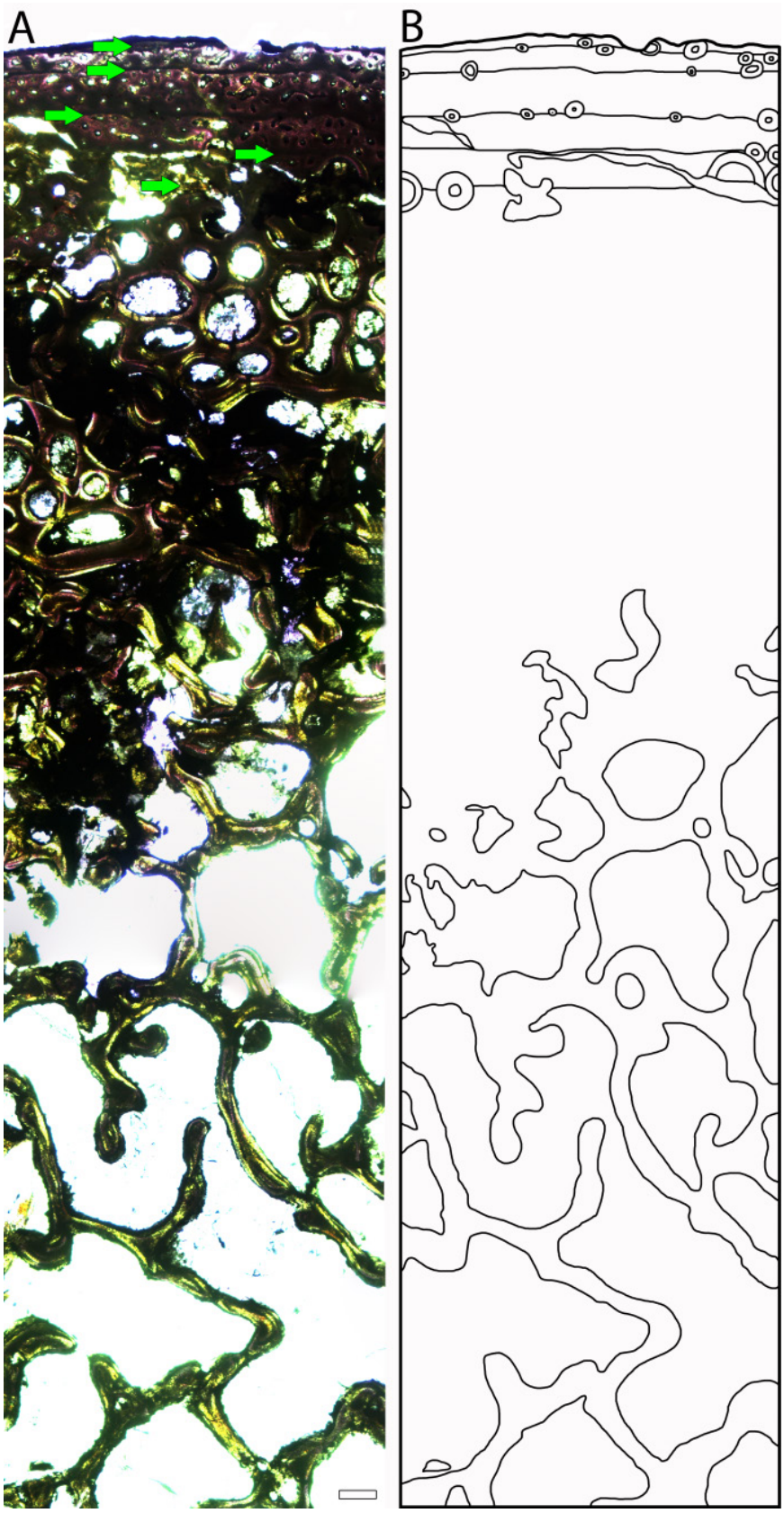

Fig. 10: External fundamental system (EFS) in the histological dorsal rib cross-section of Sauropoda indet. (FMNH 25112). **A**: Polarized light photograph. Green arrows indicate LAGs forming the EFS. Scale bar equals 500 µm. **B**: Drawing of the visible growth marks of the EFS and the secondary osteons influencing the LAGs by destroying or tracing them. Note the large cancellous bone area similar to the *Dicraeosaurus* sample M31.

Sauropoda indet. (YPM VP 007447): 60% of the growth record of YPM VP 007447 are preserved. The complete number of cycles including the seven missing innermost cycles estimated by retrocalculation is 27. 13 of the 20 cycles preserved are only visible as well-developed modulations. Only the outermost 10 cycles are LAGs, eight of these built the EFS (S.I. Fig. 51). The inner cortex shows intense remodeling compared to other dorsal rib samples indicating a senescent ontogenetic age of the individual. This is consistent with the high number of LAGs observable in the EFS. The loss of some additional outermost cycles cannot be excluded because the outer bone surface shows irregularities that hint to preburial damage. The animal reached sexual maturity after 13 years of growth and skeletal maturity at the age of 19 years (S.I. Fig. 105). These estimates fit to the life history data derived for other diplodocoids sampled herein. Thus, the isolated dorsal rib sample YPM VP 007447 can be assigned to Diplodocoidea based on its histology (see following chapter and Discussion).

Sauropoda indet. (YPM VP 060120): Rib sample YPM VP 060120 shows 22 cycles representing 70% of the total growth record. The outermost 13 cycles as well as the 16th cycle are developed as LAGs (S.I. Fig. 52). The other cycles are only, but clearly visible as modulations with naked eye. Based on retrocalculation, three innermost cycles are missing due to the expansion of the medullary region. Hence, the growth time of the individual was 25 years. Because relatively few remodeling occurs within the inner cortex, this estimate most likely represents, or at least is close to the age at death. An EFS consisting of seven closely spaced LAGs indicates skeletal maturity that was reached at the age of 18 years. Small remains of fine minerals visible at the outer bone surface indicate that no outermost EFS cycles were lost due to preparation. Preburial damage however, cannot be excluded completely. Sexual maturity was reached at the age of 14 years based on the growth curve (S.I. Fig. 106). These two estimates on major events in life history of the individuals fit perfectly to those obtained for other diplodocines like *Diplodocus*, *Apatosaurus*, *Barosaurus* or *Brontosaurus*. Accordingly, sample YPM VP 060120 former assigned as Sauropoda indet. now can be referred to as Diplodocine indet. based on its skeletochronology (see next chapter and discussion).

Sauropoda indet. (YPM VP 001911): As described in the material chapter, it is questionable if the sample YPM VP 001911 belongs to *Camarasaurus*, a macronarian, or to *Brontosaurus*, a representative of the diplodocoid clade. The growth record reveals the preservation of 16 cycles representing 69% of the growth record (S.I. Fig. 53). The animal had reached skeletal maturity before its death as indicated by an EFS consisting of three very closely spaced LAGs. Retrocalculation estimates presume the loss of four innermost cycles raising the total growth time to 20 years. YPM VP 001911 reached sexual maturity with 12 and skeletal maturity with 17 years of age (S.I. Fig. 107). These estimates are within the range of other diplodocoids ascertained within this study. Therefore, the older labeling of the specimen that assigned it to *Brontosaurus* is more reasonable (see next chapter and discussion).

Sauropoda indet. (Sa 22): The primary bone tissue of sample Sa22 is almost completely remodeled up to the outermost cortex. Nevertheless, remains of an EFS and some cyclicity is visible at the border area of the drill core sample. The EFS consists of 5 closely spaced LAGs indicating skeletal maturity which are followed by one wider spaced cycle (S.I. Fig. 54). As core drilling had not reached the center of the medullary region and due to intense remodeling it is neither possible to estimate the exact percentage of growth record preservation nor the number of missing cycles. Both, incompleteness of the growth record and missing estimations of former cycle count impede the taxonomic assignment of the specimen to the macronarian or diplodocoidean clade based on life history traits (see next chapter and discussion). Nevertheless, the unusually high remodeling rate in this rib indicates an assignment to *Dicraeosaurus* rather than to *Giraffatitan* (both of which are the two sauropod taxa found at the Sa 22 locality). *Dicraeosaurus sattleri* sample M31 (described above) is the only sample in the whole sample base that shows remodelling patterns similar to Sa 22. Nevertheless, this assumption needs further confirmation based on a larger *Dicraeosaurus* sample base.

Sauropoda indet. (Sa 14): Sauropod dorsal rib sample Sa 14 shows a clearly developed growth record consisting of 26 LAGs (S.I. Fig. 55). Due to the sampling technique (core drilling that did not reach the medullary region) The cortex was not sampled entirely. Thus, it is neither possible to estimate the percentage of growth record preservation nor the number of missing LAGs. In turn, no estimates for age at skeletal and sexual maturity can be given, impeding its comparison to Diplodocoidea or Macronaria based on life history data estimates (see next chapter and discussion). However, the relatively high number of LAGs in the outermost to lower-mid cortex indicates a more probable assignment to the macronarian clade and thus to *Giraffatitan* the only macronarian found at the site. Although more accurate life history estimates for the individual are difficult to obtain, the achievement of skeletal maturity is indicated by an EFS consisting of five closely spaced LAGs.

Sauropoda indet. (Sa 21): Like in sample Sa 14 the growth record of Sa 21 is incomplete. Core drilling sampled the sauropod dorsal rib. Due to overall preservation the sample was taken not exactly at the position of best growth record preservation. Nevertheless, the remains of 20 LAGs can be counted (S.I. Fig. 56). The estimation of the percentage of growth record preservation and of the number of missing LAGs are not possible due to the sampling position. Thus, again no estimation of the age at sexual and skeletal maturity can be given. An EFS consisting of three LAGs indicates skeletal maturity of the individual. Like in sample Sa 14 the relatively high cycle count of 20 in the upper cortex hints to a more reasonable assignment of the animal to the macronarian clade and thus to *Giraffatitan*.

Model			Constant			Femur length			Taxon	
	N	DF	W	p	DF	W	p	DF	W	p
a) Articulated ribs										
ASM~femur length + taxon	17	1	9.282	**0.002**	1	0.009	0.924	1	3.319	0.068
SM~femur length + taxon	11	1	10.675	**0.001**	1	0.001	0.973	1	11.194	< **0.001**
b) Disarticulated ribs										
ASM~femur length + taxon	17	1	1.763	0.184	1	1.148	0.284	1	6.214	**0.013**
SM~femur length + taxon	18	1	1.869	0.172	1	1.112	0.292	1	7.261	**0.007**
c) Articulated and disarticulated ribs pooled										
ASM~femur length + taxon	34	1	11.691	< **0.001**	1	0.007	0.935	1	15.625	< **0.001**
SM~femur length + taxon	29	1	16.761	< **0.001**	1	0.638	0.424	1	24.917	< **0.001**

Table 1: Results on an effect of femur length and taxon (macronarian, diplodocoid) on age at onset of sexual- and skeletal maturity. We fitted a generalized linear model of the Poisson family to data and used a power function (allometric relation) as link function. In this model the discrete trait (ASM or SM, both in years) is predicted from the continuous femur length (mm) and the categorical variable taxon. The models clearly demonstrate an effect of the taxon on ASM and SM, but no femur effect for our sample. Analysis was conducted for a) articulated ribs, b) disarticulated ribs, and c) articulated and disarticulated ribs pooled. ASM = age at sexual maturity, SM = age at skeletal maturity, N = sample size, DF = degrees of freedom, W = Wald statistics, p = p value.

6.4.5. Discrimination of Diplodocoidea and Macronaria from ages at sexual and skeletal maturity

Our statistical tests show, that discrimination of Diplodocoidea and Macronaria based on ages at sexual and skeletal maturity is possible (Tab. 1). An allometric effect (femur length) on ages at sexual and skeletal maturity is not indicated by all generalized linear models for our sample (Fig. 11). The described taxon effect (Diplodocoidea, Macronaria) was highly significant for the disarticulated samples as well as for the pooled articulated and disarticulated samples. For the smaller sample size of ribs found in articulation with the rest of the skeleton it was only marginally significant. All ages at sexual and skeletal maturity as well as femur lengths of articulated and disarticulated specimens passed to this analysis are listed in Table 2. Ribs belonging to articulated specimens indicate that sexual maturity was reached at an age between 10 and 15 years in Diplodocoidea, and between 16 and 19 years of age in Macronaria. In disarticulated specimens age at sexual maturity was estimated to be 13 years in Diplodocoidea and 17 to 23 years in Macronaria. For pooled articulated and

disarticulated specimens, age at sexual maturity ranges between 10 and 15 years in Diplodocoidea and between 16 and 23 years in Macronaria.

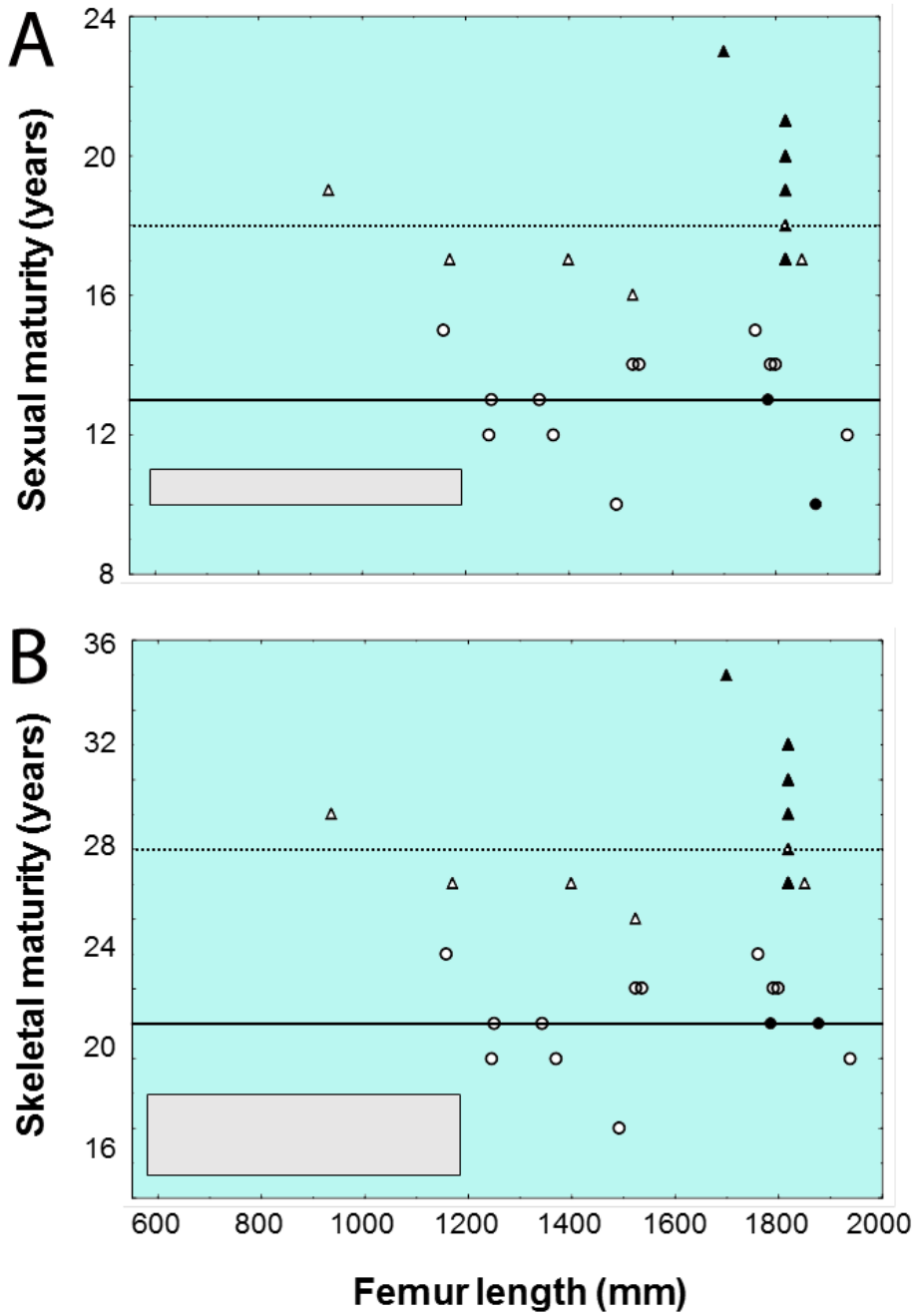

Fig. 11: Ages at onset of sexual- (**A**) and skeletal maturity (**B**) against femur length in macronarians and diplodocoids studied (Table 2). Generalized linear models (GLM) indicate no influence of femur length but an effect of the taxon (macronarians and diplodocoids) on both maturation ages in our sample. Macronarians = triangles, diplodocids = circles, articulated specimen = open symbols, disarticulated specimen = filled symbols, dotted line = median for macronarian specimen, solid line = median for diplodocoid specimen, grey rectangle = dwarfed diplodocoids (disarticulated specimens, no individual estimates of femur length, marked grey area equals possible size range generated from isolated femora measurements found at the same quarry).

In articulated specimens, skeletal maturity was reached between 17 and 21 years of age in Diplodocoidea and between 27 and 34 years in Macronaria. For disarticulated specimens, age at skeletal maturity ranges between 17 and 21 years in Diplodocoidea and between 25 and 34 years in Macronaria. For pooled articulated and disarticulated specimens, age at skeletal maturity was reached after 17 to 21 years of growth in Diplodocoidea and between 25 and 34 years in Macronaria.

The ages at sexual and skeletal maturity of rib samples not articulated to a long bone for size estimates including *Apatosaurus* sp. UW 46211 (12 and 17 years) and the dwarfed diplodocine samples CMC, and MOR 790 (10-11 and 15-18 years) fitted well to those of other Diplodocoidea with known femur length but were considerably smaller than those of Macronaria with available femur lengths. Likewise, ages at sexual and skeletal maturity of *Camarasaurus* sp. "Alf" SMA 0274 (19 and 28) and of *Camarasaurus* sp. YPM VP 060121 (20 and 28 years) also missing articulated long bones for size estimation fitted well to those seen in Macronaria individuals of known femur lengths (Table 2).

Using the differences in age at sexual and skeletal maturity seen between Diplodocoidea and Macronaria, now sauropod ribs material of uncertain taxonomic affinities (based on morphology) can be assigned to one of the two clades. This has been done for the indeterminate sauropod rib material of our sample (YPM VP 007447, YPM VP 060120, Sa 14, Sa 21, Sa 22). Thus, applying these differences, samples Sa 14 and Sa 21 described as Sauropoda indet. now can be referred to as Macronaria indet. (most likely *Giraffatitan*, consistent with their locality). Respectively, Sauropoda indet. samples YPM VP 001911, YPM VP 060120, and YPM VP 007447 now can be assigned to Diplodocoidea. Former assignments of samples to a certain taxon that are tainted with uncertainties can be confirmed or disproven as it has been done for samples ML 418, BYU 18531, and YPM VP 001911.

6.4.6. Comparison of age structures found at different localities

To compare age structures of populations from different localities, we classified ontogenetic stages of specimen into two classes, adults and juveniles (Table 2). Adults are sexual mature specimens that must not have reached skeletal maturity. By contrast, juvenile individuals died before reaching sexual maturity. Out of 16 *Camarasaurus* specimens (all UMNH specimens in Table 1, disarticulated ribs, Macronaria) only one was a juvenile that was close to reach sexual maturity, whereas out of 18 samples comprising the dwarfed Diplodocoidea sample (all CMC specimens and MOR 790 in Table 1) six were early-stage juveniles. This difference in the age structure observed is marginally significant (χ^2 test: χ^2 = 3.800, df = 1, p = 0.051).

Genus and species	Rib number	Preservation	Femur length (mm)	ASM (years)	SM (years)	Taxon	Ontogenetic stage
Camarasaurus lewisi	BYU 9047	articulated	1525	16	27	M	adult
Camarasaurus grandis	YPM VP 1901/1905	articulated	1170	17		M	adult
Camarasaurus sp.	UW 46215	articulated	1400	17		M	adult
Camarasaurus sp.	SMA 0002	articulated	935	19	34	M	adult
Brachiosaurus altithorax	FMNH P25107	articulated	1850	17	32	M	adult
Apatosaurus ajax	YPM VP 1860	articulated	1940	12	18	D	adult
Apatosaurus louisae	SMA 269	articulated	1492	10		D	adult
Apatosaurus sp.	MOR 957	articulated	1537	14		D	adult
Brontosaurus excelsus	YPM VP 1981	articulated	1790	14	20	D	adult
Brontosaurus parvus	BYU 18531	articulated	1760	15	21	D	adult
Galeamopus pabsti	SMA 0011	articulated	1370	12		D	adult
Diplodocidae „Aurora“	SMA 0008	articulated	1250	13	18	D	adult
Diplodocinae „Broesmeli“	SMA 0013	articulated	1344	13	17	D	adult
Diplodocus sp.	MOR 592	articulated	1245	12	19	D	adult
Diplodocus carnegii	CM 94	articulated	1525	14	19	D	adult
Diplodocus hallorum	NMMNH P 3690	articulated	1800	14	19	D	adult
Suuwassea emiliae	ANS 21122	articulated	1157	15		D	adult
Camarasaurus	UMNH 5289	disarticulated	1820*	17	27	M	adult
Camarasaurus	UMNH 5302	disarticulated	1820*	17	26	M	adult
Camarasaurus	UMNH 20518	disarticulated	1820*	20	25	M	adult
Camarasaurus	UMNH 21606	disarticulated	1820*	21	27	M	adult
Camarasaurus	UMNH 21608	disarticulated	1820*	21	27	M	adult
Camarasaurus	UMNH 24298	disarticulated	1820*	17	26	M	adult
Camarasaurus	UMNH 24384	disarticulated	1820*	19	26	M	adult

Genus and species	Rib number	Preservation	Femur length (mm)	ASM (years)	SM (years)	Taxon	Ontogenetic stage
Camarasaurus	UMNH 24386	disarticulated	1820*		27	M	adult
Camarasaurus	UMNH 24801	disarticulated	1820*	19	26	M	adult
Camarasaurus	UMNH 24802	disarticulated				M	juvenil
Camarasaurus	UMNH 24803	disarticulated	1820*	20	27	M	adult
Camarasaurus	UMNH 24804	disarticulated	1820*	21	27	M	adult
Camarasaurus	UMNH 24805	disarticulated	1820*	17	27	M	adult
Camarasaurus	UMNH 24806	disarticulated	1820*	17	26	M	adult
Camarasaurus	UMNH 24807	disarticulated	1820*	18	27	M	adult
Camarasaurus sp. "Alf"	SMA 0274	disarticulated	5	19	28	M	adult
Camarasaurus sp.	YPM VP 060121	disarticulated	1060-1660*	20	28	M	adult
cf. *Giraffatitan*	SMA 0274	disarticulated	1700*	23	34	M	adult
Apatosaurus sp.	YPM VP 4832	disarticulated	1785**	13	17	D	adult
Apatosaurus sp.	UW 46211	disarticulated		12	17	D	adult
Barosaurus lentus	YPM VP 429	disarticulated	1877**	13	21	D	adult
Diplodocinae indet. (dwarfed)	CMC VP 8020	disarticulated	590-1140*	10	17	D	adult
Diplodocinae indet. (dwarfed)	CMC VP 8027	disarticulated				D	juvenil
Diplodocinae indet. (dwarfed)	CMC VP 8038	disarticulated	590-1140*	11	18	D	adult
Diplodocinae indet. (dwarfed)	CMC VP 8991	disarticulated	590-1140*	10	15	D	adult
Diplodocinae indet. (dwarfed)	CMC VP 9930	disarticulated	590-1140*	11	17	D	adult
Diplodocinae indet. (dwarfed)	CMC VP 9932	disarticulated	590-1140*	11	16	D	adult

Genus and species	Rib number	Preservation	Femur length (mm)	ASM (years)	SM (years)	Taxon	Ontogenetic stage
Diplodocinae indet. (dwarfed)	CMC VP 9935	disarticulated	590-1140*	11	17	D	adult
Diplodocinae indet. (dwarfed)	CMC VP 9948	disarticulated	590-1140*	11	16	D	adult
Diplodocinae indet. (dwarfed)	CMC VP 9956	disarticulated	590-1140*	11	16	D	adult
Diplodocinae indet. (dwarfed)	CMC VP 9962	disarticulated	590-1140*		17	D	adult
Diplodocinae indet. (dwarfed)	CMC VP 10059	disarticulated				D	juvenil
Diplodocinae indet. (dwarfed)	CMC VP 10666	disarticulated	590-1140*	10	16	D	adult
Diplodocinae indet. (dwarfed)	CMC VP 10667	disarticulated				D	juvenil
Diplodocinae indet. (dwarfed)	CMC VP 11339	disarticulated	590-1140*	11	15	D	adult
Diplodocinae indet. (dwarfed)	CMC VP 14293	disarticulated				D	juvenil
Diplodocinae indet. (dwarfed)	CMC VP 14893	disarticulated				D	juvenil
Diplodocinae indet. (dwarfed)	MOR 790	disarticulated				D	juvenil

Table 2: Specimens used to study differences between age at sexual and skeletal maturation and age-structures at different localities. * = length of a femur found in the surrounding (only applicable to disarticulated ribs), ** = length estimated from a humerus found in the surrounding (only applicable to disarticulated ribs), range given for femur length or no estimate of femur length given = specimens were used to check whether their ASM and SM values fit to their taxonomic status (validation of our discrimination method for macronarians and diplodocids), ASM = age at sexual maturation, SM = age at skeletal maturation, Taxon = macronarian (M) or diplodocid (D), ontogenetic stage = juvenile (sexual maturation not preserved in the growth record) or adult (sexual maturation preserved in the growth record).

6.5. Discussion

6.5.1. Comparison of dorsal rib and long bone histology

All dorsal rib samples show a relatively thick cortex typical for graviportal animals (Houssaye et al., 2016). Like observed in long bones (Klein and Sander, 2008; Mitchell and Sander, 2014), the number of secondary osteons increases with age in ribs. However, the remodeling rate of the dorsal ribs is much lower than in long bones (Klein and Sander, 2008; Waskow and Sander, 2014; Waskow and Mateus, 2017, (chapter 2)). According to Amprino´s rule (Amprino, 1947), the primary bone structure is closely related to the bone apposition rate. This rule has been tested and confirmed for vertebrate long bones in several studies (Castanet et al., 1996; Margerie et al., 2004; Ricqlès et al., 1991). In ribs however, the relative bone apposition rate is also related to morphological changes during ontogeny. The distal rib shaft of the juvenile becomes incorporated in the proximal rib shaft in an older ontogenetic stage. This causes differing bone apposition rates around the rib shaft due to the formation of, e.g., the prominent rib bulge on the posteromedial side of the proximal to mid rib shaft (Waskow and Sander, 2014; Waskow and Mateus, 2017, (chapter 2); Waskow et al., submitted, (chapter, 4)). In addition, ribs grew much slower, i.e., deposited much less bone tissue in a given location, compared to long bones, which causes a difference in bone tissue type, or number of preserved LAGs, even within the same individual (Horner et al., 2000; Waskow and Sander, 2014; Woodward et al., 2014). This difference might influence the remodeling rate as well resulting in the preservation of a high amount of primary bone tissue. However, because we still do not understand the true nature of remodeling, this is only an assumption. Contrary to long bones, the primary bone tissue of ribs is interrupted by clearly developed LAGs. Additionally, the innermost growth record of dorsal ribs was not resorbed during the formation of a medullary cavity (as it is the case in long bones) because it is largely absent in dorsal ribs of sauropods. This results in nearly complete growth records that are even more complete than the ones observed in the long bones of other dinosaurs (Erickson, 2005; Erickson and Tumanova, 2000; Horner et al., 2000; Klein and Sander, 2007).

6.5.2. Growth record implications for life history traits

The two significant decreases in growth occurring in all skeletally mature sauropod samples can be interpreted as the onset of sexual maturity (first decrease in growth rate) and skeletal maturity (second decrease in growth rate) (S.I. Fig. 57-107), as it has been done in other studies before (Sander, 2000; Griebeler et al., 2013; Waskow and Sander, 2014; Waskow and Mateus, 2017, (chapter 2)). The second decrease represents the start of the EFS. All EFS cycles have been excluded for estimation of skeletal maturity. Longevity in skeletally mature individual showing a completely developed EFS is hard to ascertain because it cannot be excluded that the animal lived on for several years after growth had stopped completely. Sexual maturity in all sampled individuals and taxa was reached after

about half of the growth time of skeletal maturity. This is consistent with the findings of other studies concerning age at sexual maturity in different archosaur taxa (Erickson et al., 2007; Lee and Werning, 2008; Griebeler et al., 2013; Waskow and Sander, 2014; Waskow and Mateus, 2017, (chapter 2)), including recent reptiles such as turtles and crocodiles (Lance, 2003).

6.5.3. Differences in growth between macronarians and diplodocoids

We found a significant difference in the onset of sexual- and skeletal maturity between the two different sauropod clades (Table 2). While macronarians on average reached sexual maturity after approximately 18 years (median) and skeletal maturity after 27 years (median) of growth, their sister taxon the diplodocoids grew much faster, reaching sexual maturity on average after 13 years (median) and skeletal maturity after 18 to 19 years (median) of growth (Fig. 12).

This, at least partially, may explain the differences in growth time estimations for sauropods in the literature. While Ricqlès (1980) estimated 43 years of growth for the macronarian *Bothriospondylus madagascariensis* based on a half grown humerus, most age estimations for diplodocoids like, e.g., *Apatosaurus* were lower (Curry, 1999; Erickson et al., 2001; Griebeler et al., 2013). Although varying greatly in general, most of the estimates on sexual and skeletal maturity from these previous studies fit to those presented here, when taxonomic differences were considered. Differences in life history traits between different sauropod taxa have been reported in the literature before (e.g., Sander, 2000; Lehman and Woodward, 2008). Sander (2000) reported on differences in histology between the four sauropod taxa found in Tendaguru. This study, however, was performed on long bones and thus was mainly based on differences in bone tissue type and primary bone tissue structures rather than on complete growth records. Thus, it only compared sizes at sexual maturity of the four taxa rather than ages.

While the results of Sander (2000) are consistent with the data presented here, the study of Lehman and Woodward reported dissimilarities (e.g., longer growth times for the diplodocoid *Apatosaur*us than for *Janenschia* or *Alamosaurus*, both of which belong to the macronarian clade). However, the study of Lehman and Woodward (2008) was based on different postcranial sauropod bone elements and a histological comparison of these is problematic. The different bone apposition rates in different bone elements of the same individual results in differences in bone tissue type, growth record preservation, and remodeling (see short comparison of dorsal rib and long bone histology above). These differences and their causes are not completely understood, and more research is needed here. Additionally, the analysis of Lehman and Woodward (2008) assumes proportional growth of all analyzed skeletal elements during ontogeny, which is unlikely, especially for animals covering an extreme size range from hatchling to adult. Allometric growth of the long bones relative to the rest of the body should be expected and has already been

reported for sauropods (Rozhdestvensky, 1965; Ikejiri, 2004; Whitlock et al., 2010; Carballido et al., 2012; Carballido and Sander, 2014; Rogers et al., 2016; Woodruff et al., 2017; Woodruff et al., 2018).

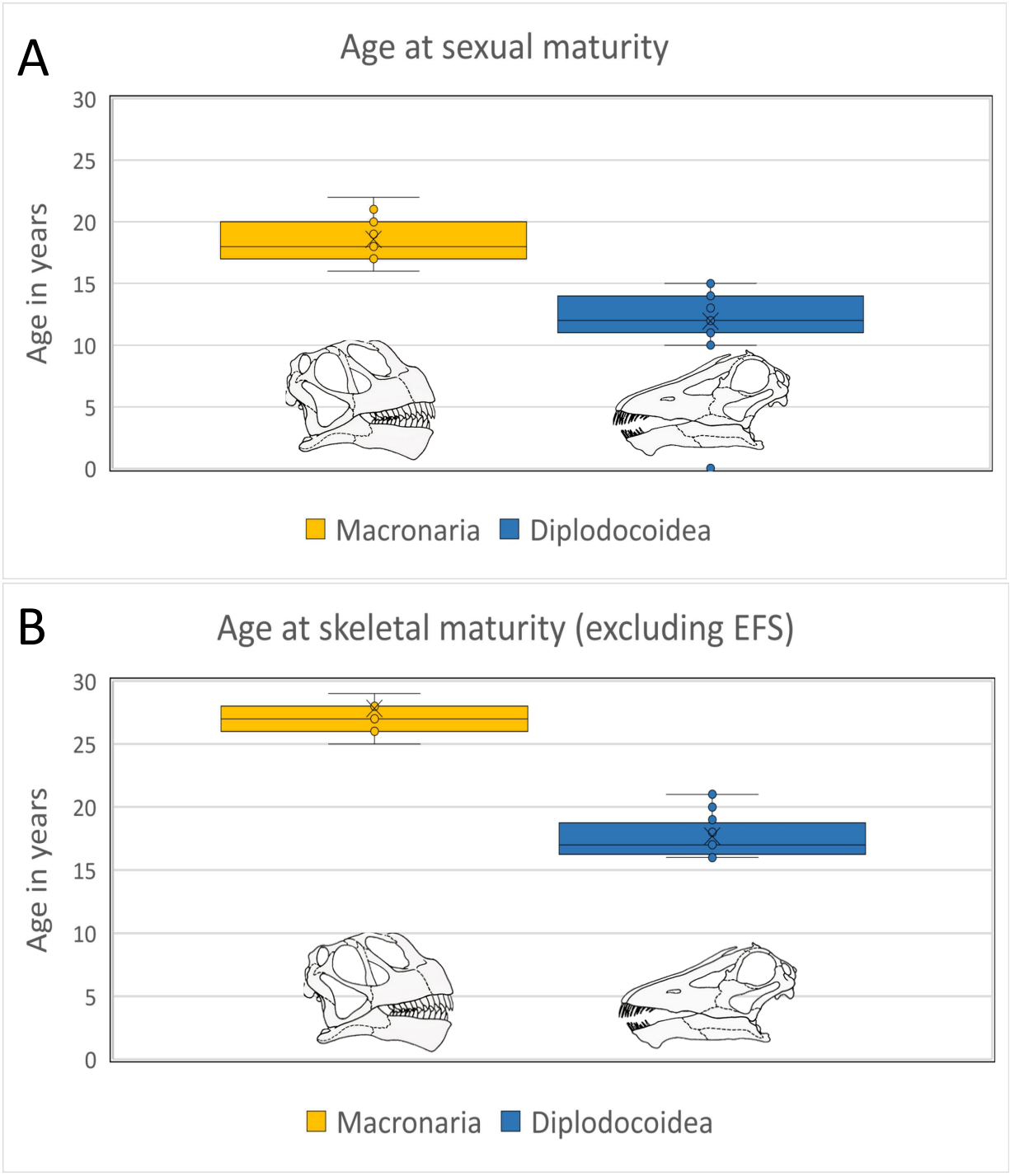

Fig. 12: Differing ages at sexual- and skeletal maturity in the two main Neosauropoda clades (Macronaria and Diplodocoidea). **A**: Age at sexual maturity varying between 16 to 22 (18 years median) in macronarians and 10 to 15 (13 years median) in diplodocids. **B**.: Age at skeletal maturity varying between 25 to 29 (27 years median) in macronarians and 16 to 21 (18 to 19 years median) in diplodocids.

Griebeler et al. (2013) also studied the growth record in two *Apatosaurus* sp. femora (SMA 0014, BYU 60117328) and one *Camarasaurus* sp. femur (CM 36664). Their estimated ages at sexual and skeletal maturity for these two diplodocoids and the one macronarian fit only partially to those found in this study. Onset of sexual maturity in *Apatosaurus* sp. SMA 0014 was at about 8 years, and in *Apatosaurus* sp. BYU 60117328 it was at about 13 years, whereas in *Camarasaurus* sp. CM 36664, at 17 years it was higher than in the two *Apatosaurus* sp. specimens. Skeletal maturity was reached in *Apatosaurus* sp. SMA 0014 between 22 and 28 years, in *Apatosaurus* sp. BYU 60117328 between 16 and 18 years, and in *Camarasaurus* sp. CM 36664 between 16 and 24 years. While the high range on age at skeletal maturity of *Apatosaurus* sp. SMA 0014 matches that found in this study on diplodocoids, ages for *Apatosaurus* sp. BYU 60117328 and *Camarasaurus* sp. CM 36664 are lower than expected from our study of the two sauropod clades. Overall lower onsets of sexual and skeletal maturity documented in these sauropod femora compared to the ribs studied here can be attributed to the general incompleteness of femoral growth records and the resulting overestimated numbers of growth cycles missing in their cortex as determined by retrocalculation. An important consideration when considering the reliability of the long bone results is that the samples in that study were rather the exception in showing growth marks at all, that typically are absent from sauropod long bone. Thus, atypical presence of growth marks in these long bones could be due to untypically slow growth or an atypical physiology of the affected individuals.

6.5.4. Differences in growth between single taxa within the two major clades

Differences in timing of major life history events are not only observable between the macronarians and diplodocoids, but also between different taxa of the same clade. While all sampled UMNH *Camarasaurus* specimens found at the same locality show similar ages at sexual maturity (18-19 years on average) and skeletal maturity (26-27 years on average), other *Camarasaurus* individuals show slightly higher ages. *Camarasaurus* SMA 0002, for instance, most likely reached skeletal maturity at the age of 34 years, and sexual maturity at the age of 19 years. However, the assignment of this individual to the genus *Camarasaurus* has been questioned by Mateus and Tschopp (2013). Although a more recent phylogenetic analysis of Tschopp et al. (2015) assigned the individual to *Camarasaurus* sp. again. The skeletochronological differences here allows to address the comparably small SMA 0002 individual at least to another *Camarasaurus* species differing from *Camarasaurus lewisi* (BYU 9047) or the UMNH *Camarasaurus* individuals. The few brachiosaurid samples analyzed show higher ages (34 years for age at skeletal maturity and 23 years for age at sexual maturity) than the camarasaurids. The reason for that might be either the scaling relationship between body mass and longevity or taxonomically differing points at sexual and skeletal maturity. In any case these differences would allow taxonomic assignment of fragmentary rib remains to one of the taxa in question if this trend turns out to be statistically significant. However, more *Brachiosaurus* samples are needed to test this

hypothesis. A similar pattern can be observed in the diplodocoideans. While most of the normal-sized diplodocines show on average ages of 18 to 20 years at skeletal maturity and 12 to 14 years at sexual maturity, the dwarfed diplodocine population of the MDQ has slightly younger ages for both (growth times of 16 to 17 years to reach skeletal, and 10 to 11 years to reach sexual maturity). Thus, one could argue that dwarfing evolved by a shortening of ontegeny, i.e., progenesis. However, because the differences in age at sexual and skeletal maturity between average sized and dwarfed diplodocines do not differ greatly scaling relationships between body mass and longevity might also be an explanation for their slightly differing life history.

6.5.5. Taxonomic assignment of indeterminate sauropod rib material based on histology

The reported difference in ages at sexual and skeletal maturity between macronarians and diplodocoids can be used for a taxonomic determination of Sauropoda indet. dorsal rib material. For the ribs of known taxonomic status lacking information on femur length, the assignment of the specimens to a sauropod clade based on ages at sexual and skeletal maturity was correct. Thus, the taxonomic status of all sampled Sauropoda indet. samples have been tested based on their life history information. Although the dorsal rib histology of most basal sauropods has not been studied yet, the assignment to a large sauropod not belonging to the Neosauropoda can be excluded for our Sauropoda indet. samples based on their geological age and geographical context.

In some cases, histology reveals taxonomic differences that might allow even more specific assignments. The unusually high remodeling rate observed in *Dicraeosaurus sattleri* (M31) can also be observed in sample Sa 22 and FMNH 25112, the taxonomic assignment of which is uncertain. However, the sauropod remains found at the Sa 22 site include *Giraffatitan* and *Dicraeosaurus*. The high remodeling rate and the cancellous bone structure representing the second and third front of the three-front model of Mitchell and Sander (2014) is increased in the *Dicraeosaurus* sample. Assuming this is a taxon-related character of *Dicraeosaurus* or closely related taxa, the large bone trabeculae and high amount of Haversian bone tissue might indicate the assignment of Sa 22 and FMNH 25112 to this clade. However, this hypothesis needs further verification based on more dicraeosaurid samples. Nevertheless, the small body size of *Dicraeosaurus* supports an assignment of at least Sa 22 to this genus. *Dicraeosaurus* is known to be one of the smallest non-dwarf sauropod species. An exceptionally high remodeling rate (based on long bones) has also been observed in the small-sized European sauropod *Magyarosaurus* (Stein et al., 2010). *Magyarosaurus* was interpreted as a dwarf species based on its adult ontogenetic stage and smaller size, that shows even stronger remodeling. However, the overall trend of reduced size combined with higher remodeling rates can be observed in both taxa even if it is significantly different in its intensity (Sander et al., 2006; Cerisara, 2017). Thus, comparably high remodeling rates in

sauropods might be related to small size and triggered by overall body size that overlie general differing phylogenetic trends.

6.5.6. Age distribution in sauropods and its implications for ecology

Conspicuously, in nearly all localities most of the samples represent adult or at least subadult individuals (Fig. 13). The only exception is the CMC diplodocid samples of the Mother´s Day Quarry (MDQ). These diplodocids belong to a dwarfed population that is not comparable to the normal sized sauropods because it most likely evolved under different ecological conditions that are further discussed in Waskow et al. (submitted, (chapter 4)). When comparing the MDQ locality to that from which the UMNH *Camarasaurus* specimens originate, the CMC diplodocid sample comprised a considerable higher proportion of juveniles (although only marginally significant). A heterogenous age distribution including many early stage juveniles has been reported for the dwarf sauropod *Europasaurus* as well (Scheil, unpublished). However, these findings were not included in the statistical analysis performed here because the large sample size *Europasaurus* would have imbalanced the sample size between dwarf and average sized samples.

We considered increasing the average-sized age distribution sample size, by using literature data, e.g., the ontogenetic age distribution mentioned by Foster (2007) but decided against doing so so for several reasons. Foster did not include all quarries of the Morrison Formation in his analysis, but only localities yielding juvenilee sauropod material. The majority of sauropod quarries in the Morrison Formation however produced only adult average-sized sauropods. This preselection of localities by Foster thus distorts the general outcome of the actual age distribution we see in the fossil record. Additionally, Foster did not state the discrimination of juveniles and adults clearly. The only explanatory note on discrimination between juveniles and adults Foster made is that all specimens <50% of average size were considered as juveniles. The definition of average sauropod size however is not stated at all. It can only be assumed that the largest specimen of a certain taxon was used as size scale equaling 100%. However, this study as well as the analysis of Waskow and Mateus (2017, (chapter 2)) and Sander (2000), revealed that sexual maturity was reached long before skeletal maturity. Thus, many of the specimens described as juveniles by Foster might have already been sexual mature and thus considered adults in our analysis. Finally, the sauropod taxa used in Fosters analysis are only represented by very few individuals per taxon in each locality. Quarries like this most likely represent accumulations of skeletal remains over time rather than real populations and were thus excluded for our ontogenetic age distribution analysis.

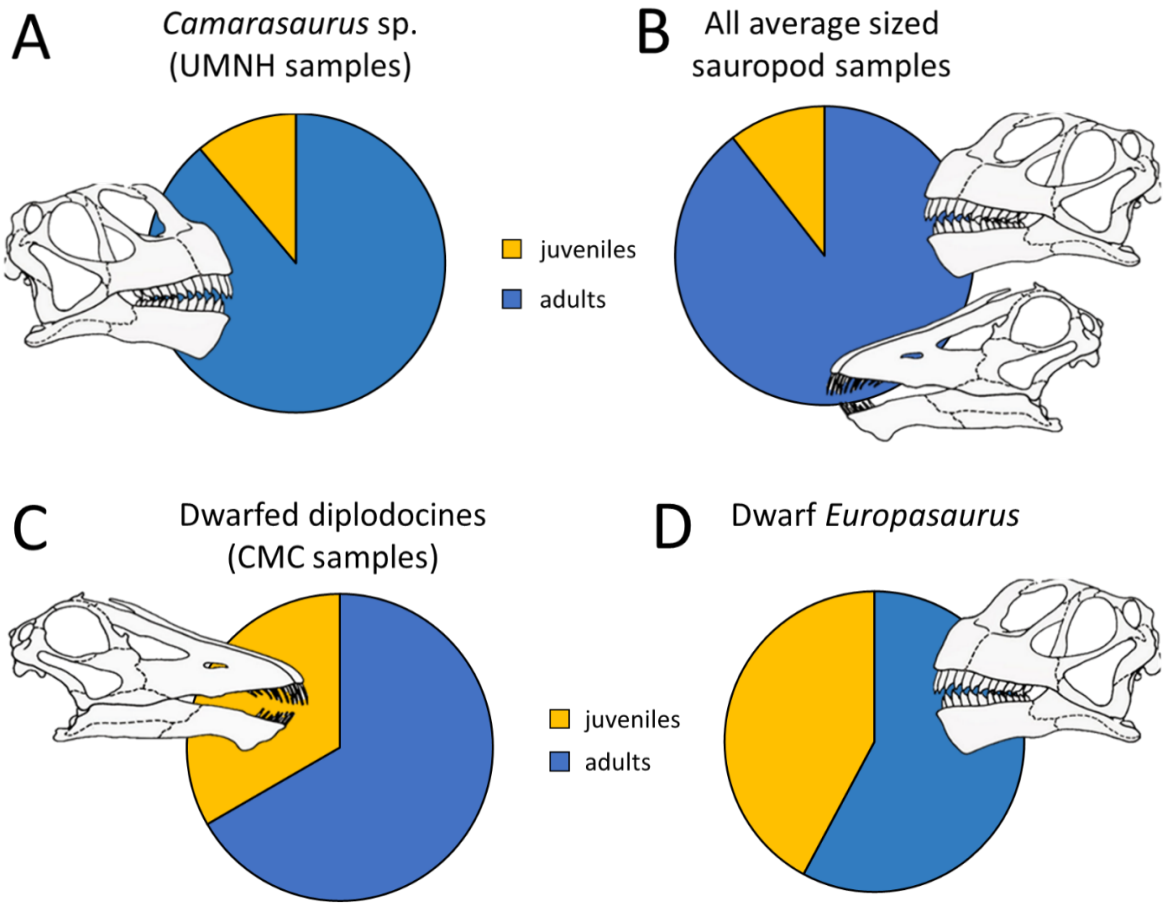

Fig. 13: Age distribution generated from dorsal rib growth records in different sauropod localities. Note the difference in age distribution between average size sauropod localities (A and B) and quarries yielding dwarfed sauropods (C and D). **A**: Age distribution in the *Camarasaurus* sp. (UMNH) sample base found at the Cleveland Lloyd Dinosaur Quarry (Utah, USA). **B**: Age distribution of all average size sauropod samples taken for this study (including 13 different localities most of which are located in the Upper Jurassic Morrisom Formation). **C**: Age distribution in the dwarfed diplodocine assemblage (CMC) found at the Mother´s Day Quarry (Montana, USA). **D**: Age distribution in the dwarfed macronarian *Europasaurus* assemblage found at the Langenberg Quarry (Oker, Germany) as generated by the study of Scheil (2018).

The striking absence of young juveniles of average-sized sauropods from the fossil record shown by our study has been already noted in the literature before (Lehman and Coulson, 2002; Carballido et al., 2012). Most likely it resulted from age segregation in sauropods which was caused by the occupation of different ecological niches at different ontogenetic ages and thus sizes. Taphonomical processes including mechanical separation of smaller-sized individuals can be excluded by the preservation of adult skeletal elements covering a large size range. Especially large skeletal elements like long bones of juveniles should be expected to be equally abundant in places where isolated smaller bones (e.g., small tail vertebrae) of adult can be found. In addition to that rare findings of articulated young juveniles like SMA 0009 prove, that sauropod skeletons of young ontogenetic age in general are completely ossified and thus do have the potential of being preserved.

Age segregation in sauropods as an explanation for an overrepresentation of adult individuals in the fossil record has been discussed in the literature before by Myers and Fiorillo (2009). The extreme size difference between hatchlings and adults could have prevented the occurrence of both at the same locality, because hatchlings and small juveniles would have been in danger of being trampled by their own parents. Additionally, diet might have differed between ontogenetic stages. Huge size differences between juveniles and adults might imply a use of food plants of different height, and energy content of food plants could have added to niche partitioning between juveniles and adults. It might have been more energy-efficient for young juveniles to feed selectively on energy-rich plant parts such as young shoots and reproductive structures (to obtain the energy for their large annual mass gain); larger individuals, due to their size, most likely were restricted to bulk feeding (Hummel et al., 2008; Sander et al., 2010; Gee, 2011).

6.5.7. Selective advantages of different life history strategies in macronarians and diplodocoids

The difference in ages at sexual and skeletal maturity of similar-sized individuals in the two different clades (Fig. 12) are also important from an ecological point of view. The classical K-selection versus r-selection concept (Pianka 1970) predicts that in stable environments intraspecific competition favors, among others, a delayed reproduction (longer generation time), decreased clutch size, increased size of offspring, and parental care in organisms, whereas in unstable environments (r-selection) intraspecific competition is low and thus early onset of maturity, large clutch sizes, small offspring and no parental care are favored over evolutionary time. From this concept, the findings of this study predict that the macronarians that reached sexual maturity later within their life than similar-sized diplodocoids might have lived in more stable environments. However, a complete test of whether the life history strategy of macronarian is indeed closer to that expected under K-selection than that of diplodocoids needs an assessment of differences in the other traits. Unfortunately, nothing is known about egg sizes, clutch sizes, and numbers of clutches per year in diplodocoids. Most of the sauropod egg material containing embryonic remains were assigned to titanosauriformes and thus to the macronarian clade (Garcia et al., 2006; Royo-Torres, 2007; Grellet-Tinner et al., 2011; Mohabey and Samant, 2013; Junior et al., 2017; Hechenleitner et al., 2018). This underrepresentation of diplodocoids is mainly due to the lack of Jurassic sauropod egg material.

Not only intraspecific competition, but also predation is a main agent of mortality in natural populations. Smaller-bodied animals experience a higher predation rate than larger-bodied animals (Sinclair et al. 2003, Owen-Smith and Mills 2008). Thus, stronger predation pressure can select for an early reproduction within the life of an organism in order to enable a successful reproduction before death. This selection scenario would suggest that diplodocoids experienced stronger predation pressure than macronarians. High juvenile

mortality from predation might also explain the low frequencies of sauropod juveniles in the fossil record. The higher frequency of juveniles in The MDQ dwarfed diplodocids and the island dwarf *Europasa1urus* (Carballido and Sander, 2014; Scheil, unpublished) would suggest that mortality caused by predation was lower in their environments (e.g., an island) than for sauropod in general.

6.6. Conclusions

Dorsal rib histology is an important tool for estimating individual ages at sexual and skeletal maturity. This is especially true for sauropods that do not preserve skeletochronological information of an equal quality in their long bones. All sampled sauropod taxa reached sexual maturity well before skeletal maturity, and the growth time was half of that needed to become skeletally mature. A significant difference in age at the onset of sexual maturity and skeletal maturity is observed between macronarians and diplodocoids. Macronarians reached sexual maturity after 16 to 23 years of growth, and skeletal maturity after 25 to 34 years of growth, while the diplodocoids became sexual mature at the age of 10 to 15 years, and skeletal maturity was between 17 to 22 years of age. These differences in two major life history events enabled us to assign indet. rib samples to either the macronarians or the diplodocoids. For animals that have not reached skeletal maturity the exact age at death (Cyclicity including EFS growth marks + estimated number of missing cycles) can be determined. However, estimations of longevity for senescent individuals showing a fully developed EFS is not possible because we do not have any recording of individual lifetime after the completition of skeletal maturity. The overrepresentation of subadult to adult individuals in the fossil record indicates different ecological niches at different ages and sizes for sauropods. Only dwarfed populations like the diplodocines of the Mother´s Day Quarry seem to have inhabited the same environment throughout their lifespans. Thus, niche partitioning at different ontogenetic stages seems to be triggered by size rather than by phylogeny. Phylogenetically independent adaptations related to size and possibly to ecology can be observed in the histology of both clades. Dwarfed populations like the MDQ dwarfs (Diplodocoidea) and *Europasuarus* (Macronaria) show histological patterns and life history traits similar to average-sized sauropods combined with reduced bone apposition rates. In contrast to this some small taxa like *Dicraeosaurus* (Diplodocoidea) and *Magyarosaurus* (Macronaria) show extremely high remodeling rates in their ribs and long bones. The differences in life history traits and histology described here might be useful to obtain more ecological information on different sauropod taxa in the future.

6.7. Acknowledgements

This research is would have not been possible without the great support, loan and sampling permission of the following persons and institutions: Rodney Scheetz (Museum of

Earth Sciences, Brigham Young University, Provo, Utah, USA), Glenn Storrs (Cincinnati Museum Center, Cincinnati, USA), Oliver Rieppel, William Simpson, and Kenneth Angielczyk (Field Museum of Natural History, Chicago, Illinois, USA) Daniela Schwarz (Museum für Naturkunde der HumboldtUniversität zu Berlin, Germany), Octávio Mateus (Museu da Lourinhã, Portugal), Jack Horner and Cary Woodruff (Museum of the Rockies, Bozeman, Montana, USA), Ulrich Joger and Ralf Kosma, (Naturhistorisches Museum, Braunschweig, Germany), Adrian Hunt (New Mexico Museum of Natural History and Science), Hans Jakob 'Kirby' Siber, Esther Wolfensperger, Ben Pabst, Rabea Lillich, and Nicola Lillich (Sauriermuseum Aathal, Switzerland), Thomas Bolliger (Kulturama Museum des Menschen, Zürich, Switzerland), Randal Irmis and Carolyn Levitt-Bussian (Utah Museum of Natural History, Salt Lake City, Utah, USA), Kelli Trujillo and Laura Vietti (University of Wyoming, Laramie, USA), and Christopher Norris and Daniel Brinkmann (Yale Peabody Museum, USA). Many thanks to Emanuel Tschopp for sharing detailed information about the sampled sauropod individuals, especially concerning taxonomy, morphology, and long bone measurements and to Michael Scheil for sharing his unpublished data about age distribution in *Europasaurus*. Further we want to thank Olaf Dülfer, Tanja Wintrich, and Pia Schucht (University of Bonn, Germany) for help during thin sectioning preparation and rib reconstruction as well as the members of the Sander lab for fruitful discussion. This is contribution number 175 of the DFG Research Unit 533 "Biology of the Sauropod Dinosaurs: The Evolution of Gigantism".

6.8. References

Amprino, R. (1947). La structure du tissu osseux envisagée comme expression de différences dans la vitesse de l'accroissement. Archives de Biologie 58(4), 317-330.

Antunes M. T., and Mateus, O. (2003). Dinosaurs of Portugal. Comptes Rendus Palevol 2(1), 77-95.

Bedell, M. W., and Trexler, D. L. (2005). First articulated manus of *Diplodocus carnegii*. In: Tidwell, V., and Carpenter, K., editors. Thunder-Lizards. The sauropodomorph dinosaurs. Bloomington, Indiana, Indiana University Press: 302 pp.

Berman, D. S., and McIntosh, J. S. (1978). Skull and relationships of the Upper Jurassic sauropod *Apatosaurus* (Reptilia, Saurischia). Bulletin of the Carnegie Museum of Natural History 8, 1-35.

Caetano, M. H. (1990). Use and results of skeletochronology in some urodeles *Triturus marmoratus*, Latreille 1800 and *Triturus boscai*, Lataste 1879. Annales des Sciences Naturelles Zoologiques 11, 197-199.

Carballido, J. L., and Sander, P. M. (2014). Postcranial axial skeleton of *Europasaurus holgeri* (Dinosauria, Sauropoda) from the Upper Jurassic of Germany: Implications for sauropod ontogeny and phylogenetic relationships of basal Macronaria. Journal of Systematic Palaeontology 12(3), 335-387.

Carballido, J. L., Marpmann, J. S., Schwarz-Wings, D., and Pabst, B. (2012). New information on a juvenile sauropod specimen from the Morrison Formation and the reassessment of its systematic position. Palaeontology 55(3), 567-582.

Case, T. J. (1978a). Speculations on the growth rate and reproduction of some dinosaurs. Paleobiology 4, 320-328.

Case, T. J. (1978b). On the evolution and adaptive significance of postnatal growth rates in the terrestrial vertebrates. The Quarterly Review of Biology 53(3), 243-282.

Carrano, M. T. (2006). Body-size evolution in the Dinosauria. In: Carrano, M., Gaudin, T. J., Blob, R. W. and Wible, J. R., editors. Amniote paleobiology: Perspectives on the evolution of mammals, birds, and reptiles. Chicago, Illinois, University of Chicago Press: 225-268.

Castanet, J. (1994). Age estimation and longevity in reptiles. Gerontology 40, 174-192.

Castanet, J., and Smirina, E. (1990). Introduction to the skeletochronological method in amphibians and reptiles. Annales des Sciences Naturelles Zoologiques (Paris) II:191-197.

Castanet, J., and Baez, M. (1991). Adaptation and evolution in *Gallotia* lizards from the Canary Islands: Age, growth, maturity, and longevity. Amphibia-Reptilia 12, 81-102.

Castanet, J., Francillon-Vieillot, H., and Bruce, R. C. (1996). Age estimation in desmognathine salamanders assessed by skeletochronology. Herpetologica, 160-171.

Castanet, J., Francillon-Vieillot, H., Meunier, F. J., and Ricqlés, A. de. (1993). Bone and individual aging. In: Hall, B. K., editor. Bone, Volume 7: Bone Growth - B. Boca Raton, Florida, CRC Press: 245-283.

Castanet, J., Croci, S., Aujard, F., Perret, M., Cubo, J., and Margerie, E. de. (2004). Lines of arrested growth in bone and age estimation in a small primate: *Microcebus murinus*. Journal of Zoology 263(1), 31-39.

Cerda, I. A., Salgado, L., and Powell, J. E. (2012). Extreme postcranial pneumaticity in sauropod dinosaurs from South America. Paläontologische Zeitschrift 86(4), 441-449.

Cerda, I. A., Chinsamy, A., Pol, D., Apaldetti, C., Otero, A., Powell, J. E., and Martínez, R. N. (2017). Novel insight into the origin of the growth dynamics of sauropod dinosaurs. PloS ONE 12(6), e0179707.

Cerisara, R. (2017). Long bone histology of *Europasaurus holgeri*: Insights into the dwarfing process. MSc thesis, University of Bonn.

Chinsamy, A. (1994). Dinosaur bone histology: Implications and inference. In: Rosenberg, G. D., and Wolberg, D. L., editors. Dino Fest. Paleontological Society, Special Publication 7: 213-227.

Chinsamy-Turan, A., (2005). The microstructure of dinosaur bone. Deciphering biology with fine-scale techniques. Baltimore, Maryland, The John Hopkins University Press: 195p.

Chinsamy, A., and Raath, M.A., (1992). Preparation of bone for histological study. Palaentolgia Aficana 29, 39-44.

Chinsamy, A., and Hillenius, W. J. (2004). Physiology of non-avian dinosaurs. In: Weishampel, D. B., Dodson, P. and Osmólska, H., editors. The Dinosauria, second edition. Berkeley, California, University of California Press: 643-659.

Cooley, J. T., and Schmitt, J. G. (1998). Sedimentology and stratigraphy – An anastomosed fluvial system in the Morrison Formation (Upper Jurassic) of southwest Montana. Modern Geology 22(1), 171-208.

Curry, K. A. (1999). Ontogenetic histology of *Apatosaurus* (Dinosauria: Sauropoda): New insights on growth rates and longevity. Journal of Vertebrate Paleontology 19(4), 654-665.

Curtice, B. (1996). Codex of diplodocid caudal vertebrae from the Dry Mesa dinosaur quarry. MSc thesis, Brigham Young University.

Dunham, A. E., Overall, K. L., Porter, W. P., Forster, C. A., (1989). Implications of ecological energetics and biophysical and developmental constraints for life history variation in dinosaurs. In: Farlow, J. O., editor. Paleobiology of the dinosaurs. Boulder, Colorado, Geological Society of America Special Paper 238: 1-19.

Enlow, D. H., Brown, S. O., (1956). A comparative histological study of fossil and recent bone tissue. Part. I. The Texas Journal of Science 8, 405-443.

Erickson, G. M. (2005). Assessing dinosaur growth patterns: A microscopic revolution. Trends in Ecology and Evolution 20(12), 677-684.

Erickson, G. M. (2014). On dinosaur growth. Annual Review of Earth and Planetary Sciences 42, 675-697.

Erickson, G. M., and Tumanova, T. A. (2000). Growth curve of *Psittacosaurus mongoliensis* Osborn (Ceratopsia: Psittacosauridae) inferred from long bone histology. Zoological Journal of the Linnean Society 130(4), 551-566.

Erickson, G. M., Curry Rogers, K. and Yerby, S. A. (2001). Dinosaurian growth patterns and rapid avian growth rates. Nature 412, 429-433.

Erickson, G. M., Ricqlès, A. de, Buffrénil, V. de, Molnar, R. E., and Bayless, M. K., (2003). Vermiform bones and the evolution of gigantism in Megalania–how a reptilian fox became a lion. Journal of Vertebrate Paleontology 23 (4), 966-970.

Erickson, G. M., Rogers, K. C., Varricchio, D. J., Norell, M. A., and Xu, X. (2007). Growth patterns in brooding dinosaurs reveals the timing of sexual maturity in non-avian dinosaurs and genesis of the avian condition. Biology Letters 3, 558-561.

Foster, J. (2007). The Jurassic west: The dinosaurs of the Morrison Formation and their world. Bloomington, Indiana, Indiana University Press: 389p.

Gallina, P., and Apesteguía, S. (2005). *Cathartesaura anaerobica* gen. et sp. nov., a new rebbachisaurid (Dinosauria, Sauropoda) from the Huincul Formation (Upper Cretaceous), Río Negro, Argentina. Revista del Museo Argentino de Ciencias Naturales nueva serie 7(2), 153-166.

Garcia, B. J., (2011). Skeletochronology of the American *Alligator* (*Alligator Mississippiensis*): Examination of the utility of elements for histological study. MSc thesis, Florida State University.

Garcia, G., Marivaux, L., Pélissié, T., and Vianey-Liaud, M. (2006). Earliest Laurasian sauropod eggshells. Acta Palaeontologica Polonica 51(1).

Gee, C. T. (2011). Dietary options for the sauropod dinosaurs from an integrated botanical and paleobotanical perspective. In: Klein, N., Remes, K., Gee, C. T., and Sander, P. M., editors. Biology of the sauropod dinosaurs: Understanding the life of giants. Bloomington, Indiana, Indiana University Press: 34-56.

Gillette, D. D. (1991). *Seismosaurus halli*, gen. et sp. nov., a new sauropod dinosaur from the Morrison Formation (Upper Jurassic/Lower Cretaceous) of New Mexico, USA. Journal of Vertebrate Paleontology 11(4), 417-433.

Gillette, D. D. (1994). Seismosaurus: The earth shaker. Columbia University Press.

Gilmore C. W. (1936). Osteology of *Apatosaurus* with special reference to specimens in the Carnegie Museum. Memoirs of the Carnegie Museum 11(4), 175-300.

Girondot, M., and Laurin, M. (2003). Bone profiler: A tool to quantify, model, and statistically compare bone-section compactness profiles. Journal of Vertebrate Paleontology 23(2), 458-461.

Grellet-Tinner, G., Sim, C. M., Kim, D. H., Trimby, P., Higa, A., An, S. L., Oh, H. S., Kim, T., and Kardjilov, N. (2011). Description of the first lithostrotian titanosaur embryo in ovo with Neutron characterization and implications for lithostrotian Aptian migration and dispersion. Gondwana Research 20(2-3), 621-629.

Griebeler, E. M., and Werner, J. (2018). Formal comment on: Myhrvold (2016) Dinosaur metabolism and the allometry of maximum growth rate. PLoS ONE 11 (11), e0163205. PloS ONE 13(2), e0184756.

Griebeler, E. M., Klein, N., and Sander, P. M. (2013). Aging, maturation, and growth of sauropodomorph dinosaurs as deduced from growth curves using long bone histological data: An assessment of methodological constraints and solutions. PloS ONE 8(6), e67012.

Harris, J. D. (2006). The axial skeleton of the dinosaur *Suuwassea emilieae* (Sauropoda: Flagellicaudata) from the Upper Jurassic Morrison Formation of Montana, USA. Palaeontology 49(5), 1091-1121.

Harris, J. D., and Dodson, P. (2004). A new diplodocoid sauropod dinosaur from the Upper Jurassic Morrison Formation of Montana, USA. Acta Palaeontologica Polonica 49(2).

Hatcher J. B. (1901). *Diplodocus* (Marsh): Its osteology, taxonomy, and probable habits, with a restoration of the skeleton. Memoirs of the Carnegie Museum 1, 1-63.

Hechenleitner, E. M., Fiorelli, L. E., Martinelli, A. G., and Grellet-Tinner, G. (2018). Titanosaur dinosaurs from the Upper Cretaceous of La Rioja province, NW Argentina. Cretaceous Research 85, 42-59.

Hedrick, B. P., Tumarkin-Deratzian, A. R., and Dodson, P. (2014). Bone microstructure and relative age of the holotype specimen of the diplodocoid sauropod dinosaur *Suuwassea emilieae*. Acta Palaeontologica Polonica 59(2), 295-304.

Heinrich, W. D. (1999). The taphonomy of dinosaurs from the Upper Jurassic of Tendaguru (Tanzania) based on field sketches of the German Tendaguru expedition (1909-1913). Fossil Record 2(1), 25-61.

Herne, M. C., and Lucas, S. G. (2006). *Seismosaurus hallorum*: Osteological reconstruction from the holotype. Bulletin of the New Mexico Museum of Natural History and Science 36, 139-148.

Holland, W. J. (1906). The osteology of *Diplodocus* Marsh: With special reference to the sestoration of the Skeleton of *Diplodocus carnegii* Hatcher, presented by Mr. Andrew Carnegie to the British Museum, May 12, 1905. Authority of the Board of Trustees of the Carnegie Institute.

Horner, J. R., and Padian, K. (2004). Age and growth dynamics of *Tyrannosaurus rex*. Proceedings of the Royal Society of London B: Biological Sciences 271(1551), 1875-1880.

Horner, J. R., Ricqles, A. de, and Padian, K., (1999). Variation in dinosaur skeletochronology indicators: Implications for age assessment and physiology. Paleobiology 25, 295-304.

Horner, J. R., Ricqlès, A. de, and Padian, K. (2000). Long bone histology of the hadrosaurid dinosaur *Maiasaura peeblesorum*: Growth dynamics and physiology based on an ontogenetic series of skeletal elements. Journal of Vertebrate Paleontology 20(1), 115-129.

Houssaye, A., Waskow, K., Hayashi, S., Cornette, R., Lee, A. H., and Hutchinson, J.R. (2016). Biomechanical evolution of solid bones in large animals: A microanatomical investigation. Biological Journal of the Linnean Society 117, 350-371.

Hummel, J., Gee, C. T., Südekum, K. H., Sander, P. M., Nogge, G., and Clauss, M. (2008). In vitro digestibility of fern and gymnosperm foliage: Implications for sauropod feeding ecology and diet selection. Proceedings of the Royal Society of London B: Biological Sciences 275(1638), 1015-1021.

Hutton, J. M. (1986). Age determination of living Nile crocodiles from the cortical stratification of bone. Copeia 1986, 332-341.

Ikejiri, T. (2004). Relative growth and timing of ontogenetic changes in *Camarasaurus* (Dinosauria, Sauropoda). Journal of Vertebrate Paleontology 24(3), 74p.

Ikejiri, T. (2005). Distribution and biochronology of *Camarasaurus* (Dinosauria, Sauropoda) from the Jurassic Morrison Formation of the Rocky Mountain region. New Mexico Geological Society Field Conference Guidebook, Geology of the Chama Basin 56, 367-379.

Janensch, W. (1914). Bericht über den Verlauf der Tendaguru-Expedition. Archiv für Biontologie 3(1), 15-58.

Janensch W. (1929). Die Wirbelsaule der Gattung *Dicraeosaurus*. Palaeontographica 1(2), 37-133.

Janensch, W. (1950). Die Wirbelsule von *Brachiosaurus brancai*. Palaeontographica, Supplement 7(1), 27-92.

Janensch, W. (1961). Die Gliedmaßen und Gliedmaßengürtel der Sauropoden der Tendaguru-Schichten. Palaeontographica-Supplementbände, 177-235.

Jensen, J. A., (1988). A fourth new sauropod dinosaur from the Upper Jurassic of the Colorado Plateau and sauropod bipedalism: Great Basin Naturalist 48, 121-145.

Junior, J. C. S., Martinelli, A. G., Ribeiro, L. C., and Marinho, T. S. (2017). Description of a juvenile titanosaurian dinosaur from the Upper Cretaceous of Brazil. Cretaceous Research 76, 19-27.

Klein, N., and P. M. Sander. (2007). Bone histology and growth of the prosauropod dinosaur *Plateosaurus engelhardti* von Meyer, 1837 from the Norian bone beds of Trossingen (Germany) and Frick (Switzerland). Special Papers in Palaeontology 77, 169-206.

Klein, N., and Sander, P. M. (2008). Ontogenetic stages in the long bone histology of sauropod dinosaurs. Paleobiology 34(2), 247-263.

Klein N. and Griebeler E. M., (2018). Growth patterns, sexual dimorphism, and maturation modeled in Pachypleurosauria from Middle Triassic of central Europe (Diapsida: Sauropterygia). Fossil Record 21, 137-157.

Klein, N., Sander, P. M., and Suteethorn, V. (2009). Bone histology and its implications for the life history and growth of the Early Cretaceous titanosaur *Phuwiangosaurus sirindhornae*. Geological Society of London Special Publication 315, 217-228.

Köhler, M., Marin-Moratalla, N., Jordana, X., and Aanes, R., (2012). Seasonal bone growth and physiology in endotherms shed light on dinosaur physiology. Nature 487, 358-361.

Lamm, E. T., (2007). Paleohistology widens the field of view in paleontology. Microscopy and Microanalysis 13 (S02, Supplement), 50-51.

Lance, V. A. (2003). *Alligator* physiology and life history: The importance of temperature. Experimental Gerontology 38(7), 801-805.

Lee, A. H. and Werning, S. (2008). Sexual maturity in growing dinosaurs does not fit reptilian growth models. Proceedings of the National Academy of Sciences 105(2), 582-587.

Lehman, T. M., and Coulson, A. B. (2002). A juvenile specimen of the sauropod dinosaur *Alamosaurus sanjuanensis* from the Upper Cretaceous of Big Bend National Park, Texas. Journal of Paleontology 76(1), 156-172.

Lehman, T. M., and Woodward, H. N. (2008). Modeling growth rates for sauropod dinosaurs. Paleobiology 34(2), 264-281.

Lovelace, D. M., Hartman, S. A., and Wahl, W. R. (2007). Morphology of a specimen of *Supersaurus* (Dinosauria, Sauropoda) from the Morrison Formation of Wyoming, and a re-evaluation of diplodocid phylogeny. Arquivos do Museu Nacional, Rio de Janeiro 65(4), 527-544.

Lucas, S. G., Herne, M. C., Heckert, A. B., Hunt, A., and Sullivan, R. (2004). Reappraisal of *Seismosaurus*, a late Jurassic sauropod dinosaur from New Mexico. The Geological Society of America.

Lucas, S. G., Spielmann, J. A., Rinehart, L. F., Heckert, A. B., Herne, M. C., Hunt, A. P., Foster, J. R., and Sullivan, R. M. (2006). Taxonomic status of *Seismosaurus hallorum*, a Late Jurassic sauropod dinosaur from New Mexico. New Mexico Museum of Natural History and Science Bulletin 36, 149-162.

Lull, R. S. (1919). The sauropodous dinosaur *Barosaurus* Marsh. Memoirs of the Connecticut Academy of Arts and Sciences 6, 1-42.

Madsen, J. H., McIntosh, J. S., and Berman, D. S. (1995). Skull and atlas-axis complex of the Upper Jurassic sauropod *Camarasaurus* Cope (Reptilia: Saurischia). Carnegie Museum of Natural History.

Mannion, P. D., Upchurch, P., Mateus O., Barnes R. N., Jones, M. E. H. (2012). New information on the anatomy and systematic position of *Dinheirosaurus Lourinhãnensis* (Sauropoda: Diplodocoidea) from the Late Jurassic of Portugal, with a review of European diplodocoids. Journal of Systematic Palaeontology 10, 521-551.

Margerie, E. D. de, Robin, J. P., Verrier, D., Cubo, J., Groscolas, R., and Castanet, J. (2004). Assessing a relationship between bone microstructure and growth rate: A fluorescent labelling study in the king penguin chick (*Aptenodytes patagonicus*). Journal of Experimental Biology 207(5), 869-879.

Marsh, O. C. (1883). Principal characters of American Jurassic dinosaurs. Part VI: Restoration of *Brontosaurus*, (with plate I). American Journal of Science (1880-1910) 26(152), 81.

Marsh, O. C. (1877). Notice of some new dinosaurian reptiles from the Jurassic Formation. American Journal of Science 14(3), 514-516.

Marsh, O. C. (1879a). Principal characters of American Jurassic dinosaurs. Pt. II, American Journal of Science, Series 3, 17, 86-92.

Marsh, O. C. (1879b). Notice of new Jurassic reptiles. American Journal of Science, Series 3, 18, 501-505.

Marsh, O. C. (1881). Principal characters of American Jurassic dinosaurs. American Journal of Science, Series 3, 21, 417-423.

Marsh, O. C. (1896). The dinosaurs of North America. U.S. Geological Survey, 16'th Annual Report 1894(95), 133-244.

Mateus, O. (2005). Dinossauros do Jurássico Superior de Portugal, com destaque para os saurísquios. PhD thesis, Universidade Nova de Lisboa.

Mateus, O., and Tschopp, E. (2013). *Cathetosaurus* as a valid sauropod genus and comparisons with *Camarasaurus*. In SVP 73rd Annual Meeting, Program and Abstracts. Supplement to the online Journal of Vertebrate Paleontology October (Vol. 173).

McIntosh, J. S. (1981). Annotated catalogue of the dinosaurs (Reptilia, Archosauria) in the collections of Carnegie Museum of Natural History.

McIntosh, J. S. (1990a). Species determination in sauropod dinosaurs with tentative suggestions for their classification. In: Carpenter, K., Currie P. J., editors. Dinosaur systematics: Perspectives and approaches. New York, Cambridge University Press: 53-69.

McIntosh, J. S. (1990b). Sauropoda. In: Weishampel, D.B., Dodson, P., Osmólska, H., editors. The Dinosauria 1. Berkeley, University of California Press: 345-401.

McIntosh, J. S. (1995). Remarks on the North American sauropod *Apatosaurus* Marsh. Short Papers, 119-123.

McIntosh, J. S. (2005). The genus *Barosaurus* Marsh (Sauropoda, Diplodocidae). In: Tidwell, V., and Carpenter, K., editors. Thunder-Lizards. The sauropodomorph dinosaurs. Bloomington, Indiana, Indiana University Press: 38-77.

McIntosh, J. S., Miller, W. E., Stadtman, K. L., and Gillette, D. D. (1996). The osteology of *Camarasaurus lewisi* (Jensen, 1988). Brigham Young University Geology Studies 41, 73-115.

Mitchell, J., and Sander, P. M. (2014). The three-front model: A developmental explanation of long bone diaphyseal histology of Sauropoda. Biological Journal of the Linnean Society 112(4), 765-781.

Mohabey, D. M., and Samant, B. (2013). Deccan continental flood basalt eruption terminated Indian dinosaurs before the Cretaceous-Paleogene boundary. Geological Society of India Special Publication 1, 260-267.

Myers, T. S., and Storrs, G. W. (2007). Taphonomy of the Mother's Day quarry, Upper Jurassic Morrison Formation, south-central Montana, USA. Palaios 22, 651-666.

Myers, T. S., and Fiorillo, A. R. (2009). Evidence for gregarious behavior and age segregation in sauropod dinosaurs. Palaeogeography, Palaeoclimatology, Palaeoecology 274(1), 96-104.

Myhrvold, N. P. (2016). Dinosaur metabolism and the allometry of maximum growth rate. PloS ONE 11(11), e0163205.

Nieuwland, I. (2010). The colossal stranger. Andrew Carnegie and *Diplodocus* intrude European culture, 1904–1912. Endeavour 34(2), 61-68.

Osborn, H. F., and Mook, C. C. (1921). *Camarasaurus*, *Amphicoelias*, and other sauropods of Cope. Memoirs of the American Museum of Natural History, New Series 3, 249-387

Ostrom, J. H., and McIntosh, J. S. (1966). Marsh's dinosaurs: The collections from Como Bluff. Yale, University Press.

Owen-Smith, N., and Mills, M. G. (2008). Shifting prey selection generates contrasting herbivore dynamics within a large-mammal predator–prey web. Ecology 89(4), 1120-1133.

Padian, K., and Horner, J. R. (2004). Dinosaur physiology. In: Weishampel, D. B., Dodson, P., and Osmólska, H., editors. The Dinosauria, second edition. Berkeley, California, University of California Press: 660-671.

Padian, K., Ricqlès, A. de, and Horner, J. R. (2001). Dinosaurian growth rates and bird origins. Nature 412(6845), 405.

Paul, G. S. (1988). The brachiosaur giants of the Morrison and Tendaguru with a description of a new subgenus, *Giraffatitan*, and a comparison of the world´s largest dinosaurs. Hunteria 2, 1-14.

Pianka, E. R. (1970). On r-and K-selection. The American Naturalist 104(940), 592-597.

Rauhut, O. W., Remes, K., Fechner, R., Cladera, G., and Puerta, P. (2005). Discovery of a short-necked sauropod dinosaur from the Late Jurassic period of Patagonia. Nature 435(7042), 670-672.

Rea, T. (2004). Bone wars. The excavation and celebrity of Andrew Carnegie's dinosaur. Pittsburgh, Pennsilvania, University of Pittsburgh Press: 288pp.

Reiss, M. J. (1989). The allometry of growth and reproduction. Cambridge, Cambridge University Press: 200p.

Remes, K. (2006). Revision of the Tendaguru sauropod dinosaur Tornieria africana a (Fraas) and its relevance for sauropod paleobiogeography. Journal of Vertebrate Paleontology 26(3), 651-669.

Remes, K., Ortega, F., Fierro, I., Joger, U., Kosma, R., Marín Ferrer, J. M., Ide, O. A., and Maga, A. (2009). A new basal sauropod dinosaur from the Middle Jurassic of Niger and the early evolution of Sauropoda. PLoS ONE 4(9), e6924.

Rozhdestvensky, A. K. (1965). Growth changes in Asian dinosaurs and some problems of their taxonomy. Paleontologičeskij žurnal 3, 95-109.

Riggs, E. S. (1901). The largest known dinosaur. Science 13(327), 549-550.

Riggs, E. S. (1903a). *Brachiosaurus altithorax*, the largest known dinosaur. American Journal of Science 15, 299-306.

Riggs, E. S. (1903b). Structure and relationships of opisthocoelian dinosaurs, part I: *Apatosaurus* Marsh. Field Columbian Museum Publications, Geological Series 4(2), 165-196.

Riggs, E. S. (1904). Structure and relationships of opisthocoelian dinosaurs: The Brachiosauridae. Field Columbian Museum. Geological Series 2, 229-248.

Ricqlès, A. de. (1980). Tissue structures of dinosaur bone, functional significance and possible relation to dinosaur physiology. In: Thomas, R. D. K., and Olson, E. C., editors. A cold look at the warm-blooded dinosaurs. Westview, Boulder, Colorado, AAAS Selected Symposium: 103-139.

Ricqlès, A. de. (1983). Cyclical growth in the long limb bones of a sauropod dinosaur. Acta Palaeontologica Polonica 28, 225-232.

Ricqlès, A. de, Meunier, F. J., Castanet, J., and Francillon-Vieillot, H. (1991). Comparative microstructure of bone. In: Hall, B. K., editor. Bone, Volume 3, Bone Matrix and Bone Specific Products. Ann Arbor, Michigan, CRC Press: 1-78.

Ritz, J., Griebeler, E. M., Huber, R. and Clauss, M. (2010). Body size development of captive and free ranging African spurred tortoises (*Geochelone sulcata*): High plasticity in reptilian growth rates. Herpetological Journal 20, 213-216

Rogers, K. C., Whitney, M., D'Emic, M., and Bagley, B. (2016). Precocity in a tiny titanosaur from the Cretaceous of Madagascar. Science 352, 450-453.

Royo-Torres, R. (2007). La evolución de los dinosaurios saurópodos en la Península Ibérica. Libro de Resuménes 23.

Salgado, L., de Souza Carvalho, I., and Garrido, A. C. (2006). Zapalasaurus bonapartei, un nuevo dinosaurio saurópodo de la Formación La Amarga (Cretácico Inferior), noroeste de Patagonia, Provincia de Neuquén, Argentina. Geobios 39(5), 695-707.

Sander, P. M. (1999). Life history of the Tendaguru sauropods as inferred from long bone histology. Mitteilungen aus dem Museum für Naturkunde der Humboldt-Universität. Berlin, Geowissenschaftliche Reihe 2, 103-112.

Sander, P. M. (2000). Longbone histology of the Tendaguru sauropods: Implications for growth and biology. Paleobiology 26(3), 466-488.

Sander, P. M., and Tückmantel, C. (2003). Bone lamina thickness, bone apposition rates, and age estimates in sauropod humeri and femora. Paläontologische Zeitschrift 77(1), 161-172.

Sander, P. M., Mateus, O., Laven, T., and Knötschke, N. (2006). Bone histology indicates insular dwarfism in a new Late Jurassic sauropod dinosaur. Nature 441(7094), 739.

Sander, P. M., Gee, C. T., Hummel, J., and Clauss, M. (2010). Mesozoic plants and dinosaur herbivory. Plants in mesozoic time: Morphological innovations, phylogeny, ecosystems, 331-359.

Sander, P. M., Klein, N., Stein, K., and Wings, O. (2011). Sauropod bone histology and its implications for sauropod biology. In: Klein, N., Remes, K. Gee, C. T., and Sander, P. M., editors. Biology of the sauropod dinosaurs. Bloomington and Indianapolis, Indiana, Indiana University Press: 259-322.

Sander, P. M., Klein, N., Buffetaut, E., Cuny, G., Suteethorn, V., and Le Loeuff, J. (2004). Adaptive radiation in sauropod dinosaurs: Bone histology indicates rapid evolution of giant body size through acceleration. Organisms, Diversity and Evolution 4 (3), 165-173.

Scheil, M., Wings, O., Knötschke, N. and Sander, P.M. The age structure of the *Europasaurus* assemblage from the Langenberg Quarry (Kimeridgian, Upper Jurassic, Lower Saxony, Germany). MSc thesis, University of Bonn.

Schwarz, D., and Fritsch, G. (2006). Pneumatic structures in the cervical vertebrae of the Late Jurassic Tendaguru sauropods *Brachiosaurus brancai* and *Dicraeosaurus*. Eclogae Geologicae Helvetiae 99(1), 65-78.

Schwarz, D., Ikejiri, T., Breithaupt, B. H., Sander, P. M., and Klein, N. (2007). A nearly complete skeleton of an early juvenile diplodocid (Dinosauria: Sauropoda) from the Lower Morrison Formation (Late Jurassic) of north central Wyoming and its

implications for early ontogeny and pneumaticity in sauropods. Historical Biology 19(3), 225-253.

Sinclair, A. R. E., Mduma, S., and Brashares, J. S. (2003). Patterns of predation in a diverse predator–prey system. Nature 425(6955), 288.

Smirina, E. M., and Tsellarius, A. Y. T. (1996). Aging, longevity and growth of the desert monitor lizard (*Varanus griseus* Daud.). Russian Journal of Herpetology 3, 130-142.

Smirina, E. M., and Ananjeva, N. B. (2007). Growth layers in bones and acrodont teeth of the agamid lizard *Laudakia stoliczkana* (Blanford, 1875) (Agamidae, Sauria). Amphibia-Reptilia 28 (2), 193-204.

Stein, K., Csiki, Z., Rogers, K. C., Weishampel, D. B., Redelstorff, R., and Sander, P. M. (2010). Small body size and extreme cortical bone remodeling indicate phyletic dwarfism in *Magyarosaurus dacus* (Sauropoda: Titanosauria). Proceedings of the National Academy of Sciences, USA 107 (20), 9258-9263.

Stevens, K. A., and Parrish, J. M. (1999). Neck posture and feeding habits of two Jurassic sauropod dinosaurs. Science 284(5415), 798-800.

Storrs, G. W., Oser, S. E., and Aull, M. (2012). Further analysis of a Late Jurassic dinosaur bone-bed from the Morrison Formation of Montana, USA, with a computed three-dimensional reconstruction. Earth and Environmental Science Transactions of the Royal Society of Edinburgh 103(3-4), 443-458.

Taylor, M. P. (2009). A re-evaluation of *Brachiosaurus altithorax* Riggs 1903 (Dinosauria, Sauropoda) and its generic separation from *Giraffatitan brancai* (Janensch 1914). Journal of Vertebrate Paleontology 29(3), 787-806.

Taylor, M. P., and Wedel, M. J. (2016). The neck of *Barosaurus*: Longer, wider and weirder than those of *Diplodocus* and other diplodocines. PeerJ Preprints 4, e67v2.

Taylor, M. P., Wedel, M. J., and Naish, D. (2009). Head and neck posture in sauropod dinosaurs inferred from extant animals. Acta Palaeontologica Polonica 54(2), 213-220.

Trujillo, K. C., Foster, J., Demar, D., and Bilbey, S. A. (2011.) An exceptionally large juvenile *Camarasaurus* from the Morrison Formation (Upper Jurassic) of Albany County, WY, USA. Journal of Vertebrate Paleontology 28(3), 205p.

Tschopp, E. (2013). Evolution of diplodocid sauropod dinosaurs with emphasis on specimens from Howe Ranch, Wyoming (USA). Ph.D. thesis, Universidade Nova de Lisboa.

Tschopp, E., and Mateus, O. (2013). The skull and neck of a new flagellicaudatan sauropod from the Morrison Formation and its implication for the evolution and ontogeny of diplodocid dinosaurs. Journal of Systematic Palaeontology 11(7), 853-888.

Tschopp, E., and Mateus, O. (2016). Case 3700 *Diplodocus* Marsh, 1878 (Dinosauria, Sauropoda): Proposed designation of *D. carnegii* Hatcher, 1901 as the type species. The Bulletin of Zoological Nomenclature 73(1), 17-24.

Tschopp, E., and Mateus, O. (2017). Osteology of *Galeamopus pabsti* sp. nov. (Sauropoda: Diplodocidae), with implications for neurocentral closure timing, and the cervico-dorsal transition in diplodocids. PeerJ 5, e3179.

Tschopp, E., Mateus, O., and Benson, R. B. (2015). A specimen-level phylogenetic analysis and taxonomic revision of Diplodocidae (Dinosauria, Sauropoda). PeerJ 3, e857.

Tschopp, E., Wings, O., Frauenfelder, T., and Rothschild, B. M. (2014). Pathological phalanges in a camarasaurid sauropod dinosaur and implications on behaviour. Acta Palaeontologica Polonica 61(1), 125-134.

Turner, C. E., and Peterson, F. (1999). Biostratigraphy of dinosaurs in the upper Jurassic Morrison Formation of the western interior, USA. Vertebrate paleontology in Utah 99, 77-114.

Turvey, S. P., Green, O. R., and Holdaway, R. N. (2005). Cortical growth marks reveal extended juvenile development in New Zealand moa. Nature 435, 940-943.

Upchurch, P., Barrett, P. M., and Dodson, P. (2004a). Sauropoda: Historical review. In: Weishampel, D. B., Dodson, P., and Osmólska, H., editors. The Dinosauria. 2nd edition. Berkeley, California, University of California Press, Berkeley: 259-273.

Upchurch, P., Tomida, Y., and Barrett, P. M. (2004b). A new specimen of *Apatosaurus ajax* (Sauropoda: Diplodocidae) from the Morrison Formation (Upper Jurassic) of Wyoming, USA. National Science Museum Monographs 26, i-118.

Waskow, K., and Sander, P. M. (2014). Growth record and histological variation in the dorsal ribs of *Camarasaurus* sp. (Sauropoda). Journal of Vertebrate Paleontology 34(4), 852-869.

Waskow, K., and Mateus, O. (2017). Dorsal rib histology of dinosaurs and a crocodylomorph from western Portugal: Skeletochronological implications on age determination and life history traits. Comptes Rendus Palevol 16(4), 425-439.

Waskow, K., Wiersma, K., Tschopp, E., Woodruff, D. C., Storrs, G., and Sander, P. M. (submitted). Histological evidence for dwarfism and different morphotypes of diplodocine sauropods within the Upper Jurassic Mother's Day Quarry (Morrison Formation, Montana, USA). Acta Palaeontologica Polonica.

Wedel, M. J. (2005). Postcranial skeletal pneumaticity in sauropods and its implications for mass estimates. In: Curry-Rogers, K.A., and Wilson, J. A. editors. The sauropods: Evolution and paleobiology. Berkeyley, California, University of California Press: 201-228.

Wedel, M. J., and Taylor, M. P. (2013). Neural spine bifurcation in sauropod dinosaurs of the Morrison Formation: Ontogenetic and phylogenetic implications. PalArch's Journal of Vertebrate Palaeontology 10(1).

Wells, N. A. (1989). Making thin sections. In: Feldmann, R. M., Chapman, R. E., Hannibal, J. T., editors. Paleotechniques. Knoxville, Tennessee, Department of Geological Sciences, University of Tennessee: 120-129.

Whitlock, J. A. (2011). A phylogenetic analysis of Diplodocoidea (Saurischia: Sauropoda). Zoological Journal of the Linnean Society 161(4), 872-915.

Whitlock, J. A., and Harris, J. D. (2010). The dentary of *Suuwassea emilieae* (Sauropoda: Diplodocoidea). Journal of Vertebrate Paleontology 30(5), 1637-1641.

Whitlock, J. A., Wilson, J. A., and Lamanna, M. C. (2010). Description of a nearly complete juvenile skull of *Diplodocus* from the Late Jurassic of North America. Journal of Vertebrate Paleontology 30, 442-457.

Wiersma, K., Canoville, A., Siber, H. J., and Sander, P. M. (in review). Testing hypothesis of skeletal unity using bone histology: The case of the sauropod remains from the Howe Stephens and Howe Scott quarries (Morrison Formation, Wyoming). Palaeontologia Electronica.

Wings, O., Sander, P. M., Tütken, T., Fowler, D. W., and Sun, G. (2007). Growth and life history of Asia's largest dinosaur. Journal of Vertebrate Paleontology 27(3).

Woodruff, D. C. (2015). A new multi-faceted framework for deciphering diplodocid ontogeny PhD thesis, Montana State University.

Woodruff, D. C., and Fowler, D. W. (2012). Ontogenetic influence on neural spine bifurcation in Diplodocoidea (Dinosauria: Sauropoda): A critical phylogenetic character. Journal of Morphology 273(7), 754-764.

Woodruff, D. C., Fowler, D. W., and Horner, J. R. (2017). A new multi-faceted framework for deciphering diplodocid ontogeny. Palaeontologica Electronica 20.3.43A, 1-53.

Woodruff, D. C., Carr, T. D., Storrs, G. W., Waskow, K., Scannella, J. B., Nordén, K. K., and Wilson, J. P. (2018). The smallest diplodocid skull reveals cranial ontogeny and growth-related dietary changes in the largest dinosaurs. Scientific reports 8(1), 14341.

Woodward, H. N., Horner, J. R., and Farlow, J. O. (2014). Quantification of intraskeletal histovariability in *Alligator mississippiensis* and implications for vertebrate osteohistology. Peer J 2, e422.

6.9. Supplementary information

6.9.1. Quarry maps

The following figures show all available quarry maps of specimens found in articulation or association to a femur or humerus (that are not figured within the main manuscript). Long bones were used for size estimation to prove the likelihood of skeletal unity for the individuals in question. If several ribs showing a high probability of belonging to the same individual as the measured long bone were available, one to three of these ribs were selected.

***Camarasaurus* sp. (SMA 0002)**

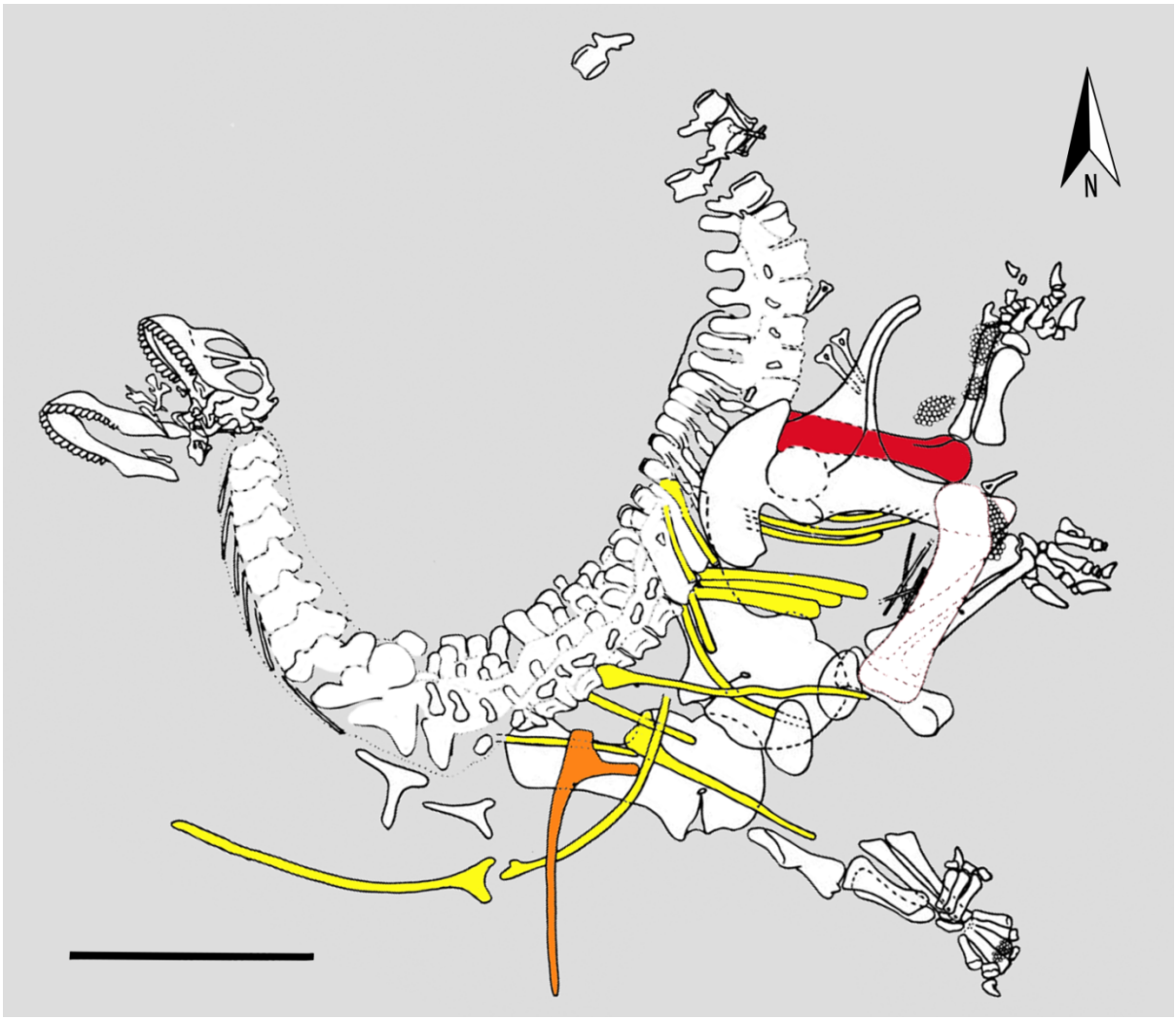

S.I. Fig. 1: Quarry map of *Camarasaurus* sp. (SMA 0002) found at the Howe Stephens Quarry in the Upper Jurassic Morrison Formation. Ribs are marked in yellow. Sampled rib used for this study is marked in orange. Note that in general all dorsal ribs of the right rib cage are sampled in different positions from proximal to distal. For more detailed description see Waskow and Sander (2014). Femur used for size estimation is marked in red. Scale bar equals 1 m.

Camarasaurus sp. individuals UW 46215 and UW 46212, and _Apatosaurus_ sp. UW 46211

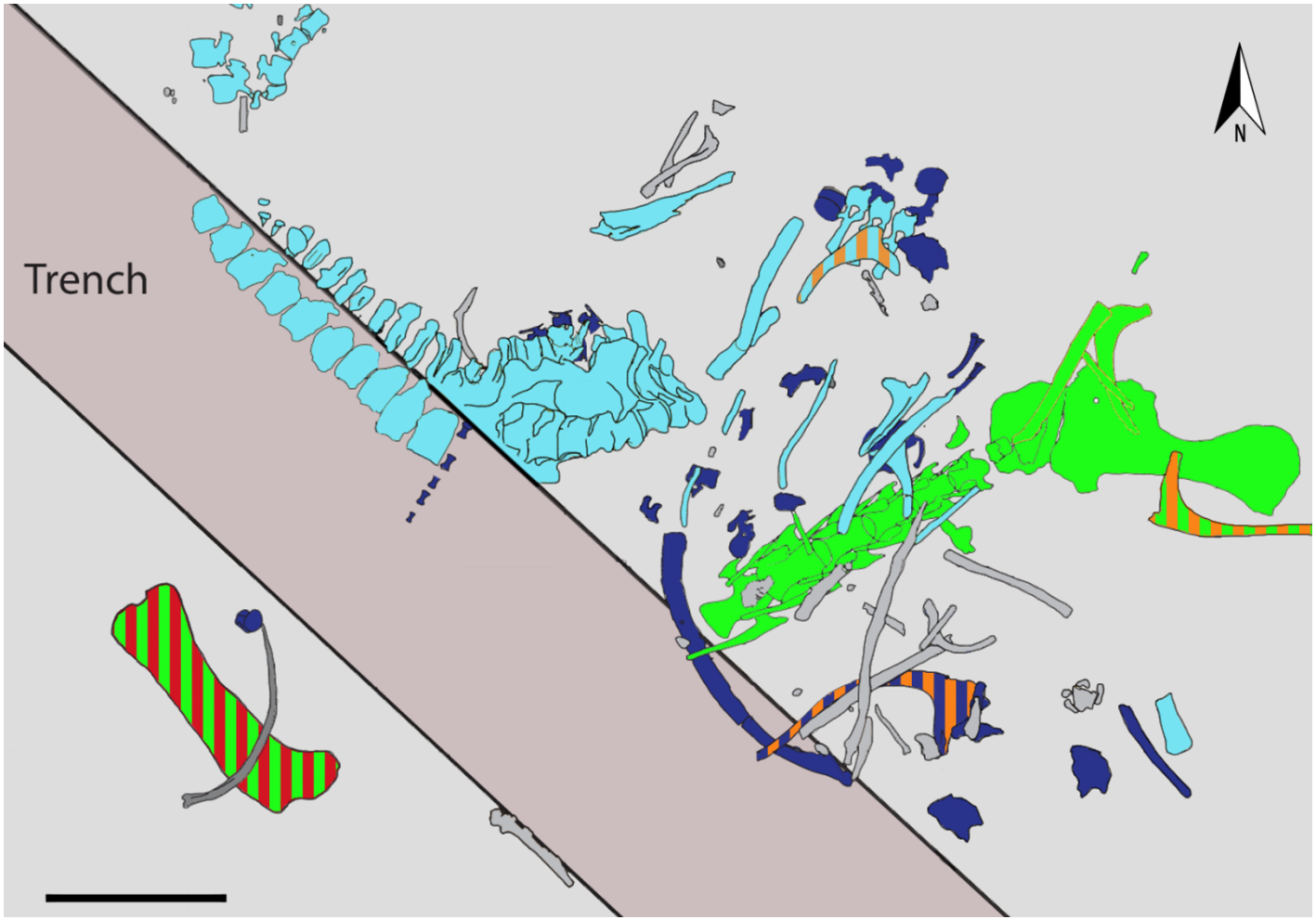

S.I. Fig. 2: Quarry map of two *Camarasaurus* sp. individuals UW 46215 and UW 46212, and *Apatosaurus* sp. UW 46211 found at the McKinsey-REX Quarry in the Upper Jurassic Morrison Formation modified after (Trujillo, 2011). Dark grey bar marks the trench line build for gas pipeline constructions. Bones marked in green belong to the adult *Camarasaur* individual (UW 46215). Red striation marks the femur of the individual used for size estimation. Bones marked in blue belong to the subadult *Apatosaurus* sp. (UW 46211). Bones marked in dark purple belong to the juvenile *Camarasuarus* sp. (UW 46212). Orange striation marks the dorsal ribs used for sampling. Scale bar equals 1 m.

***Brachiosaurus altithorax* (SMA 0009)**

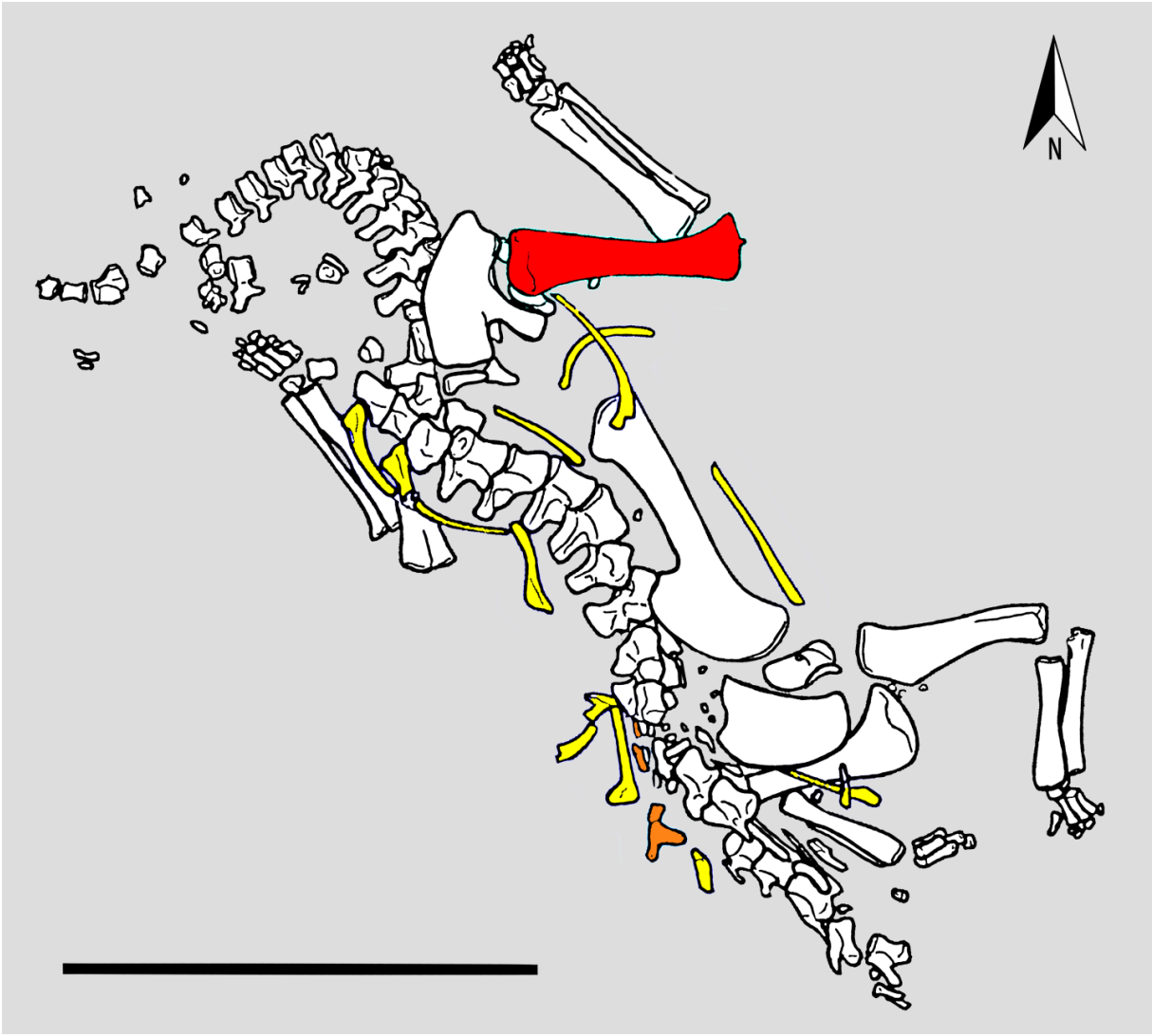

S.I. Fig. 3: Quarry map of youngest articulated juvenile sauropod sampled within this study (SMA 0009) found in the Howe-Stephens Quarry (Upper Jurassic Morrison Formation). The specimen most likely can be assigned as *Brachiosaurus altithorax*. Ribs are marked in yellow. The sampled rib is marked in orange. Femur used for size estimation is marked in red. Scale bar equals 30 cm.

***Suuwassea emilieae* (ANS 21122)**

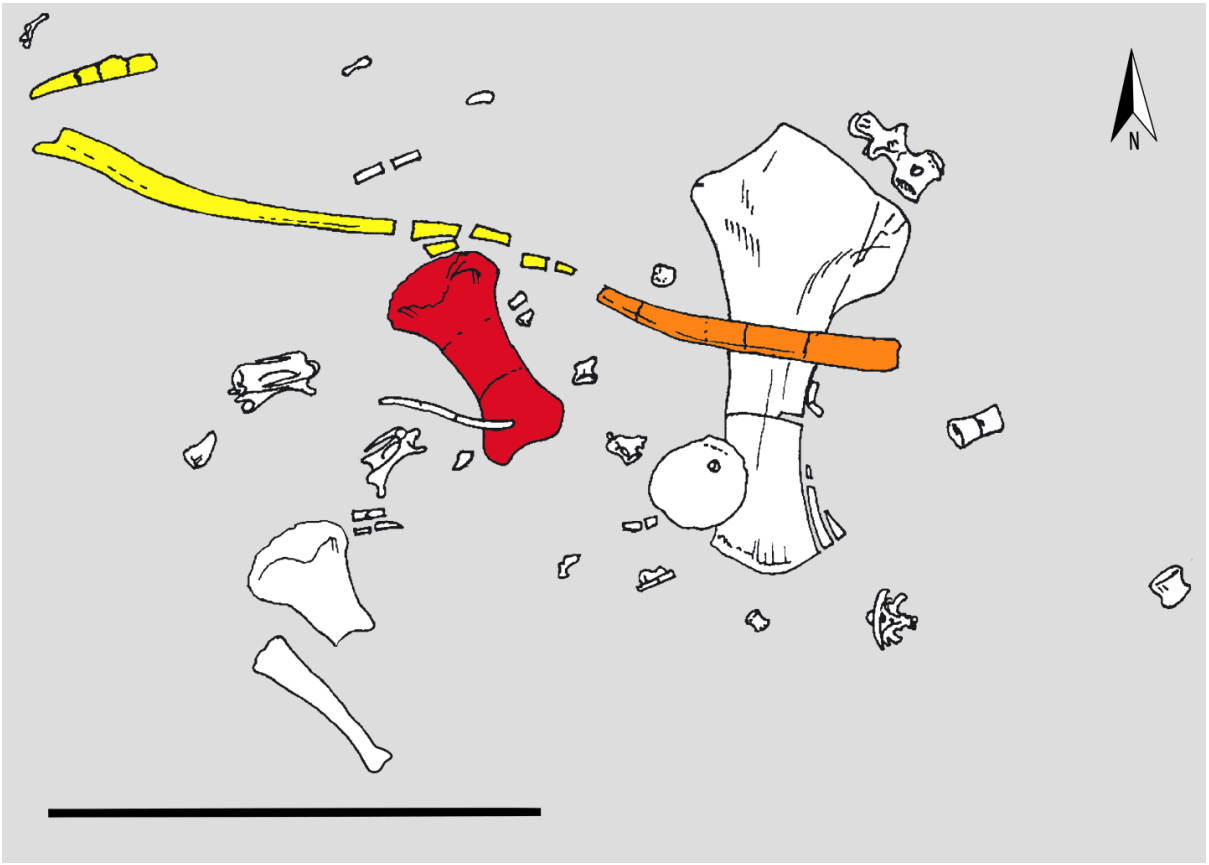

S.I. Fig. 4: Quarry map of *Suuwassea emilieae* (ANS 21122) found in Southern Carbon County (Montana, USA) in a layer most likely equivalent to the Brushy Basin Member of the Morrison Formation. Modified after Harris (2006). Note that additional elements possibly belonging to the same individual (including femur fragment) were found in 1 to 4m distance to the skeleton shown here. Dorsal ribs are marked in yellow. Sampled dorsal rib is marked in orange. Humerus used for size estimates is marked in red. Scale bar equals 1 m.

***Apatosaurus louisae* (SMA 0269)**

S.I. Fig. 5: Quarry map of *Apatosaurus louisae* (SMA 0269) nicknamed “Arapahoe”. The specimen was found at the Dana Quarry (Wyoming, USA) in the beds of the Upper Jurassic Morrison formation. Ribs are marked in yellow. Rib used for histological estimates of life history traits is marked in orange. Femur used for size estimate is marked in red. Scale bar equals 1 m.

***Brontosaurus parvus* (BYU 18531)**

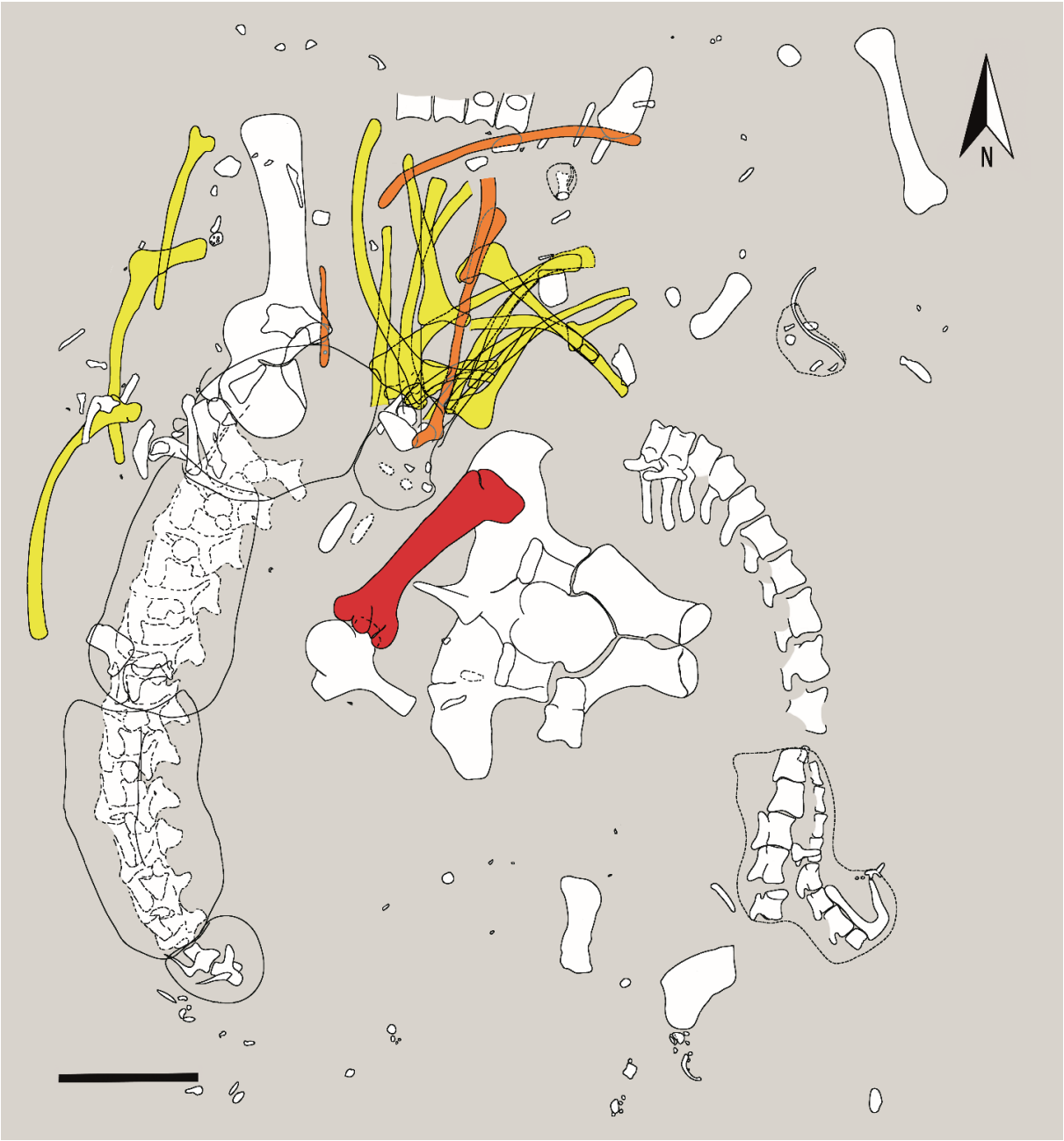

S.I. Fig. 6: Quarry map of *Brontosaurus parvus* (BYU 18531) found at the Mill Canyon (Utah, USA) in the Upper Jurassic Morrison Formation. Ribs are marked in yellow. Ribs used for histological estimates of life history traits are marked in orange. Femur used for size estimate is marked in red. Scale bar equals 1 m.

***Galeamopus pabsti* (SMA 0011)**

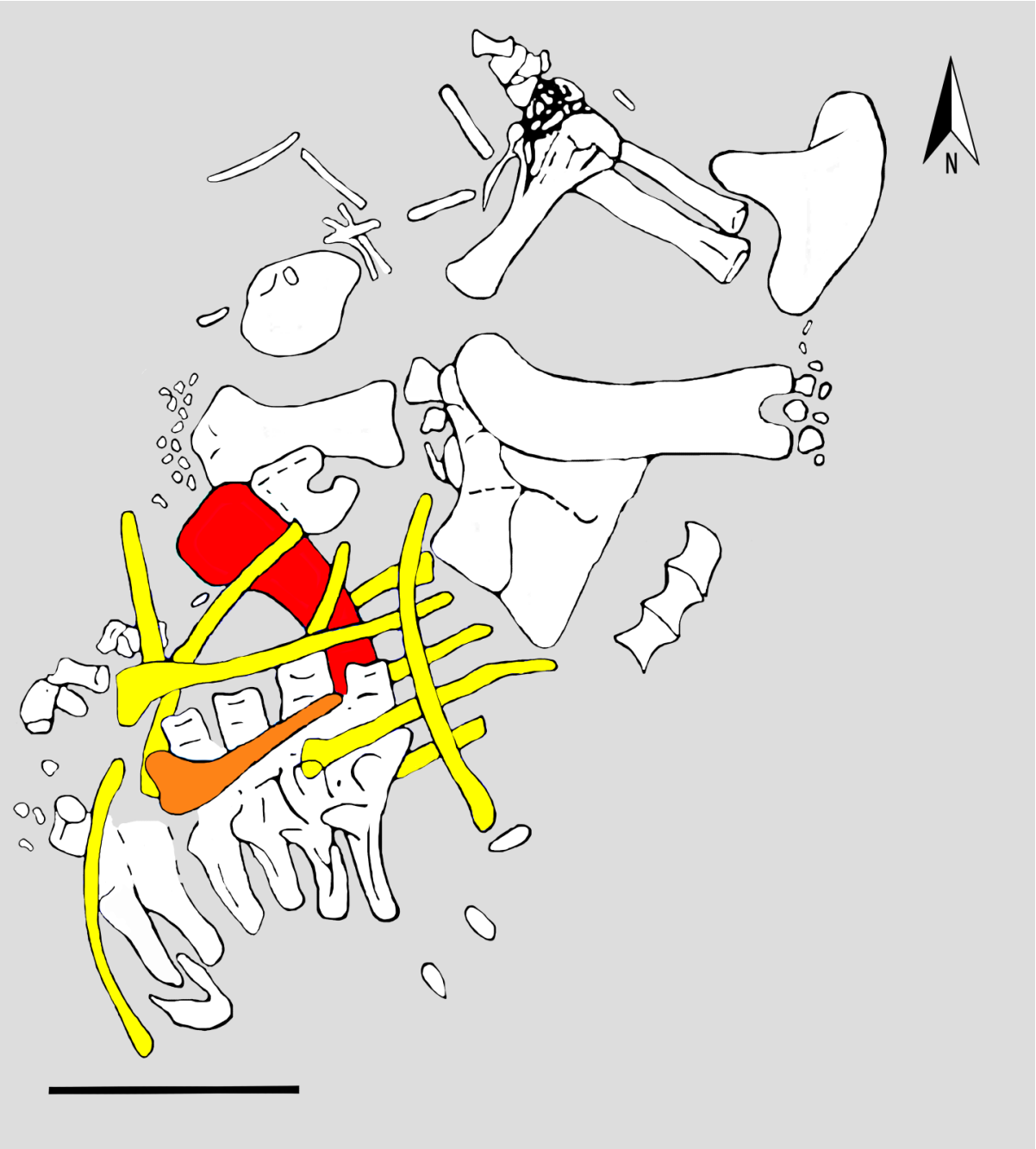

S.I. Fig. 7: Quarry map of the holotype *Galeamopus pabsti* (SMA 0011) found at the Howe Scott Quarry (Wyoming, USA) in the Upper Jurassic Morrison Formation. Note that the original quarry map consists of two separated partial skeletons that were thought to belong to the same specimen. Histological analysis of several dorsal ribs however, indicates that the two partial skeletons belong to two separate individuals. Thus, only one partial skeleton including a femur was used for this study and is pictured here. Ribs are marked in yellow. Rib sample used for life history estimates is marked in orange. Femur used for size estimation is marked in red. Scale bar equals 1 m.

***Diplodocus carnegii* (CM 84 and CM 94)**

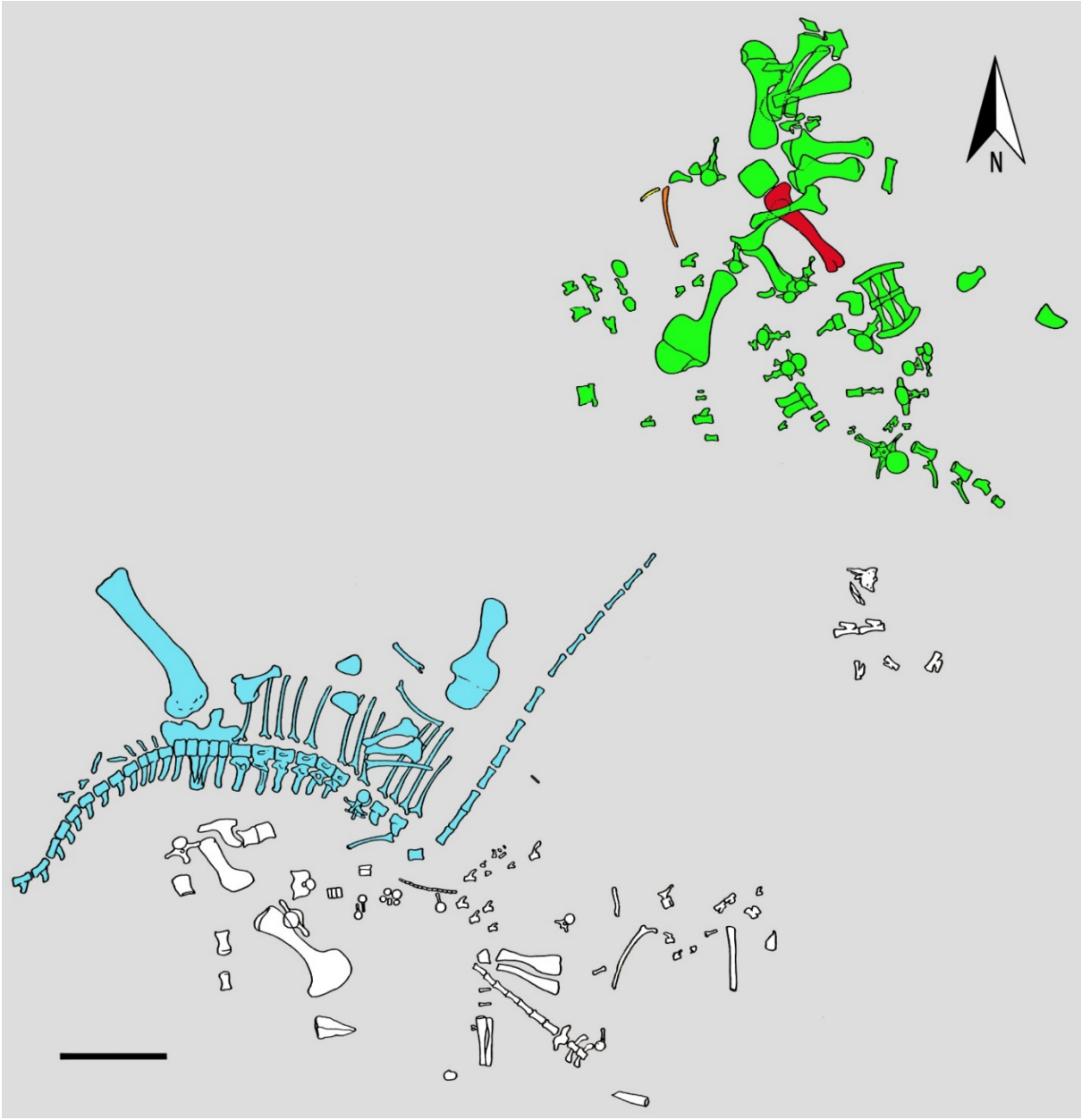

S.I. Fig. 8: Quarry map of the holotype and paratype of *Diplodocus carnegii* (CM 84 and CM 94) found at the Sheep Creek Quarry, Wyoming (Upper Jurassic Morrison Formation). Modified from Hatcher (1901). The Holotype (84) is marked in blue, the paratype (94) is marked in green. The sampled rib is marked in orange and the Femur used for size estimation in marked in red. White bones belong to other *Brontosaurus*, *Camarasaurus*, and *Stegosaurus* individuals found in the same quarry. Scale bar equals 1 m.

Diplodocinae indet. (SMA 0013)

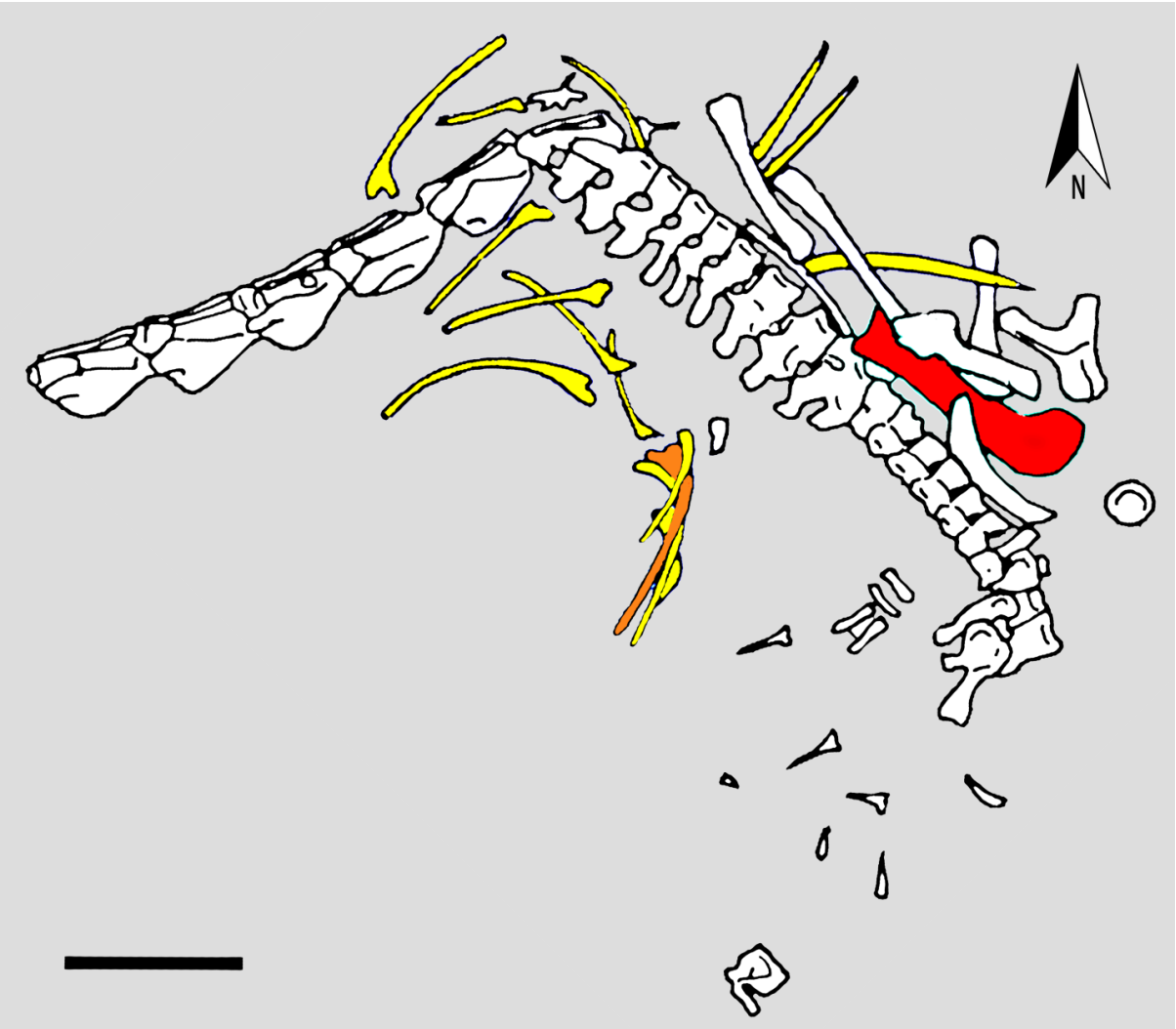

S.I. Fig. 9: Quarry map of Diplodocinae indet. (SMA 0013) nicknamed “Brösmeli” found at the Howe Stephens Quarry (Wyoming, USA) in beds of the Upper Jurassic Morrison Formation. Note that the original quarry map of this Diplodocine includes some more isolated vertebrates found in 2-5 m distance to the articulated skeleton pictured here. Ribs are marked in yellow. Rib used for histological estimates of life history traits is marked in orange. Femur used for size estimate is marked in red. Scale bar equals 1 m.

Diplodocidae indet. (SMA 0008)

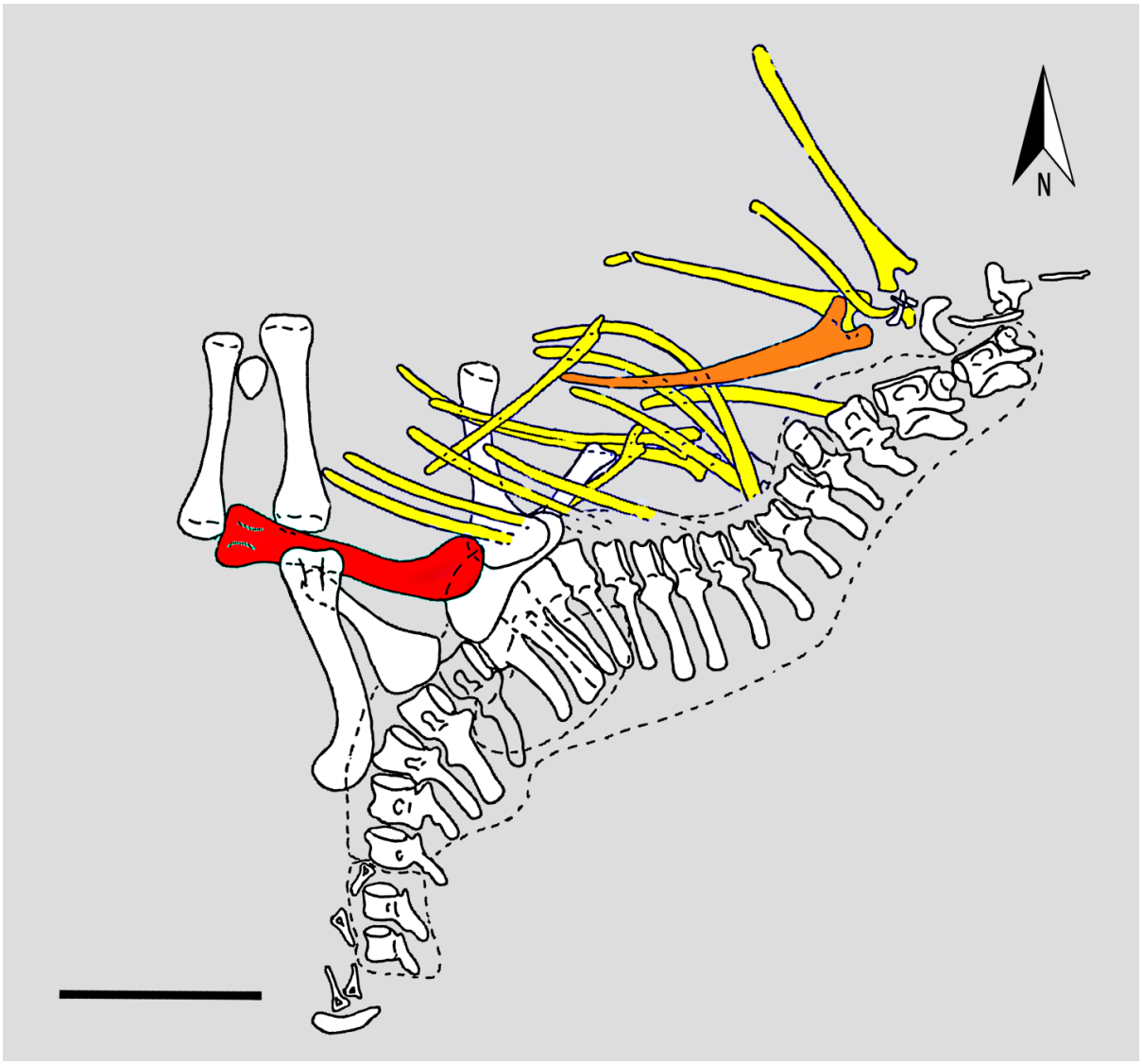

S.I. Fig. 10: Quarry map of Diplodocidae indet. (SMA 0008) nicknamed “Aurora” found in the Upper Jurassic Morrison Formation at Spring Hill Quarry (Wyoming, USA). Dorsal ribs are marked in yellow. Sampled dorsal rib is marked in orange. Femur used for size estimates is marked in red. Scale bar equals 1 m.

6.9.2. Dorsal rib growth records of sauropods

The following figures show the histology and individual growth records of all individuals sampled for this study that are not figured in the main manuscript. Note that some of the innermost growth marks are not visible as LAGs in microscopic view (photograph A) but only preserved as modulations or polish lines best visible in macroscopic view. These growth marks are figured in the drawings next to the photograph (drawing B). Drawings were produced by tracing the LAGs on high resolution sacnns of the thin sections or by using a camera lucida.

***Camarasaurus grandis* (YPM VP 001901)**

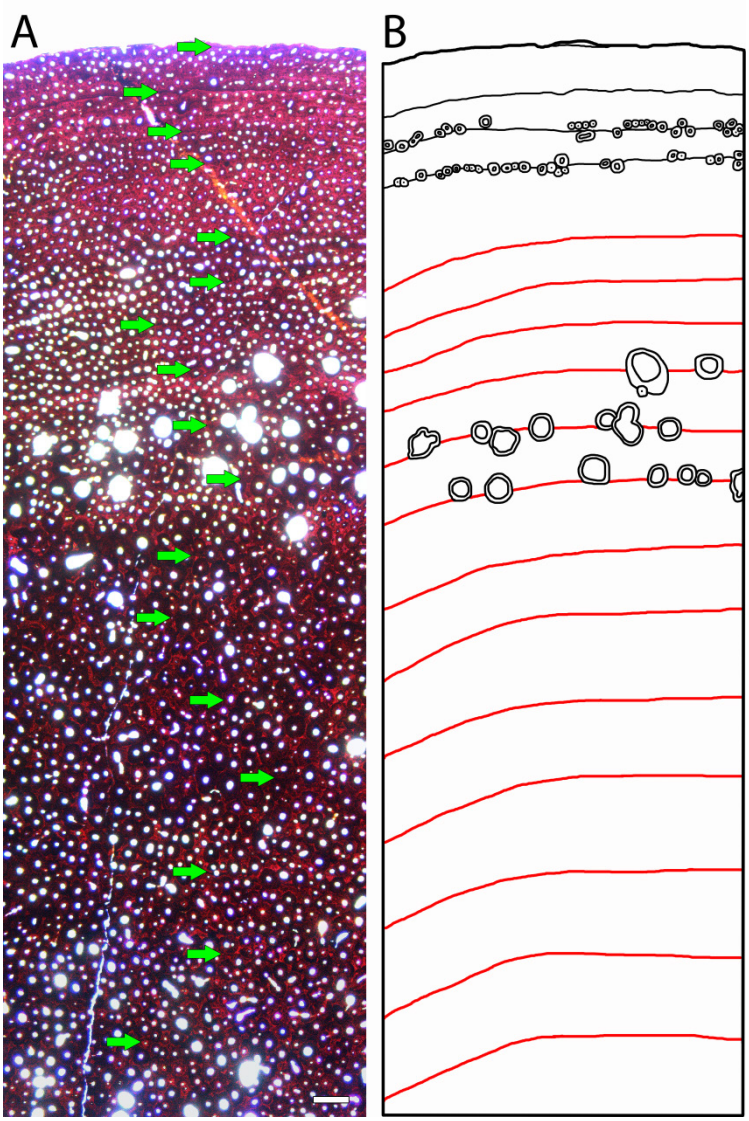

S.I. Fig. 11: Growth record preservation in the histological cross-section of the dorsal rib of *Camarasaurus grandis* (YPM VP 001901). **A**: Polarized light photograph. Green arrows indicate growth marks. Note that most of the growth marks are only preserved as polish lines not visible under the microscope. Scale bar equals 500 µm. **B**: Drawing of the visible growthmarks and the secondary osteons influencing the LAGs by destroying or tracing them marked in black. Polish lines are marked in red.

***Camarasaurus grandis* (YPM VP 001905)**

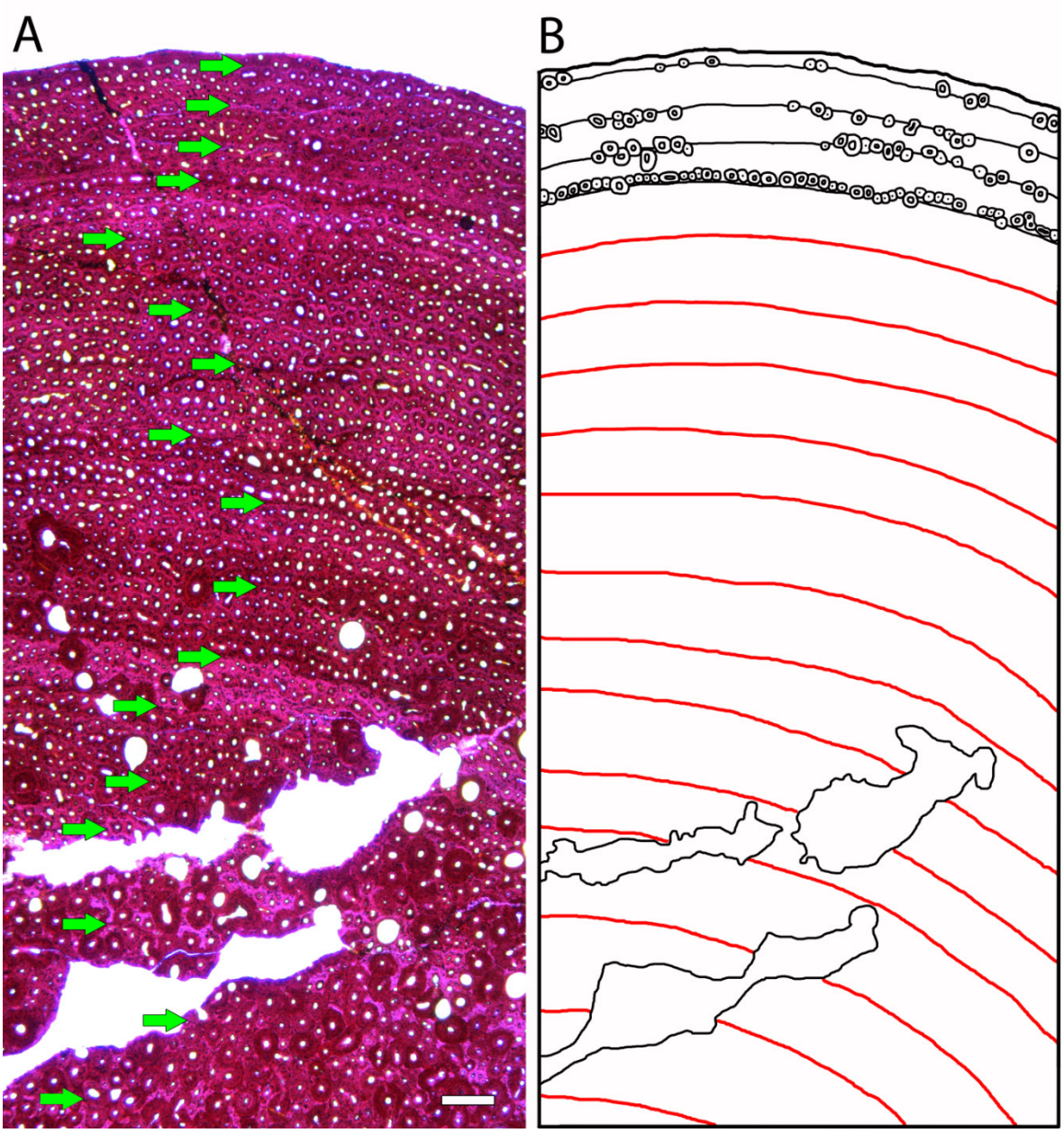

S.I. Fig. 12: Growth record preservation in the histological cross-section of the dorsal rib of *Camarasaurus grandis* (YPM VP 001905). Note that based on histology this rib sample most likely belongs to the same individual as sample (YPM VP 001901) figured before. **A**: Polarized light photograph. Green arrows indicate growth marks. Most of the growth marks are only preserved as modulations or polish lines not visible under the microscope. Scale bar equals 500 µm. **B**: Drawing of the visible growthmarks and the secondary osteons influencing the LAGs by destroying or tracing them marked in black. Polish lines not visible under the microscope are marked in red.

***Camarasaurus* sp. (SMA 274)**

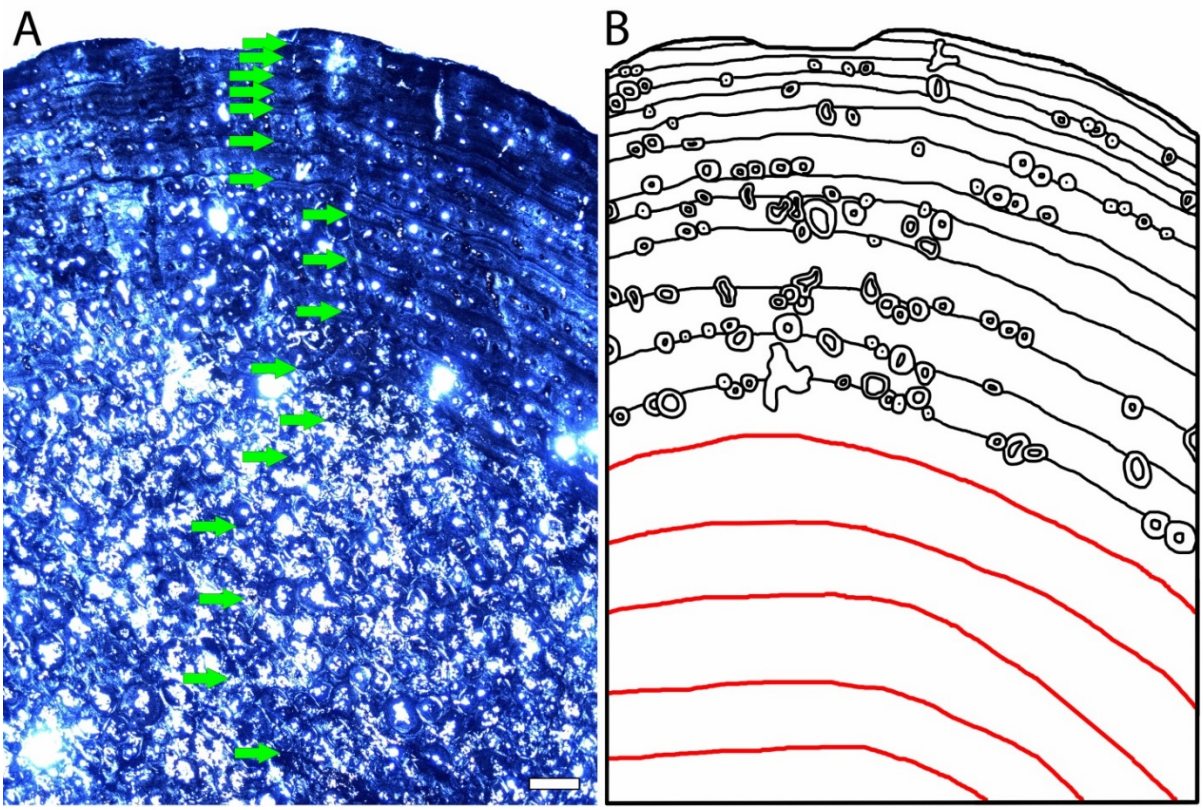

S.I. Fig. 13: Growth record preservation in the histological dorsal rib cross-section of *Camarasaurus* sp. (SMA 274). Note that the innermost cyhcles are not figured. **A**: Polarized light photograph. Green arrows indicate growth marks. Most of the growth marks are only preserved as modulations or polish lines not visible under the microscope. Scale bar equals 500 µm. **B**: Drawing of the visible growthmarks and the secondary osteons influencing the LAGs by destroying or tracing them are marked in black. Polish lines not visible under the microscope are marked in red.

***Camarasaurus* sp. (UW 46215)**

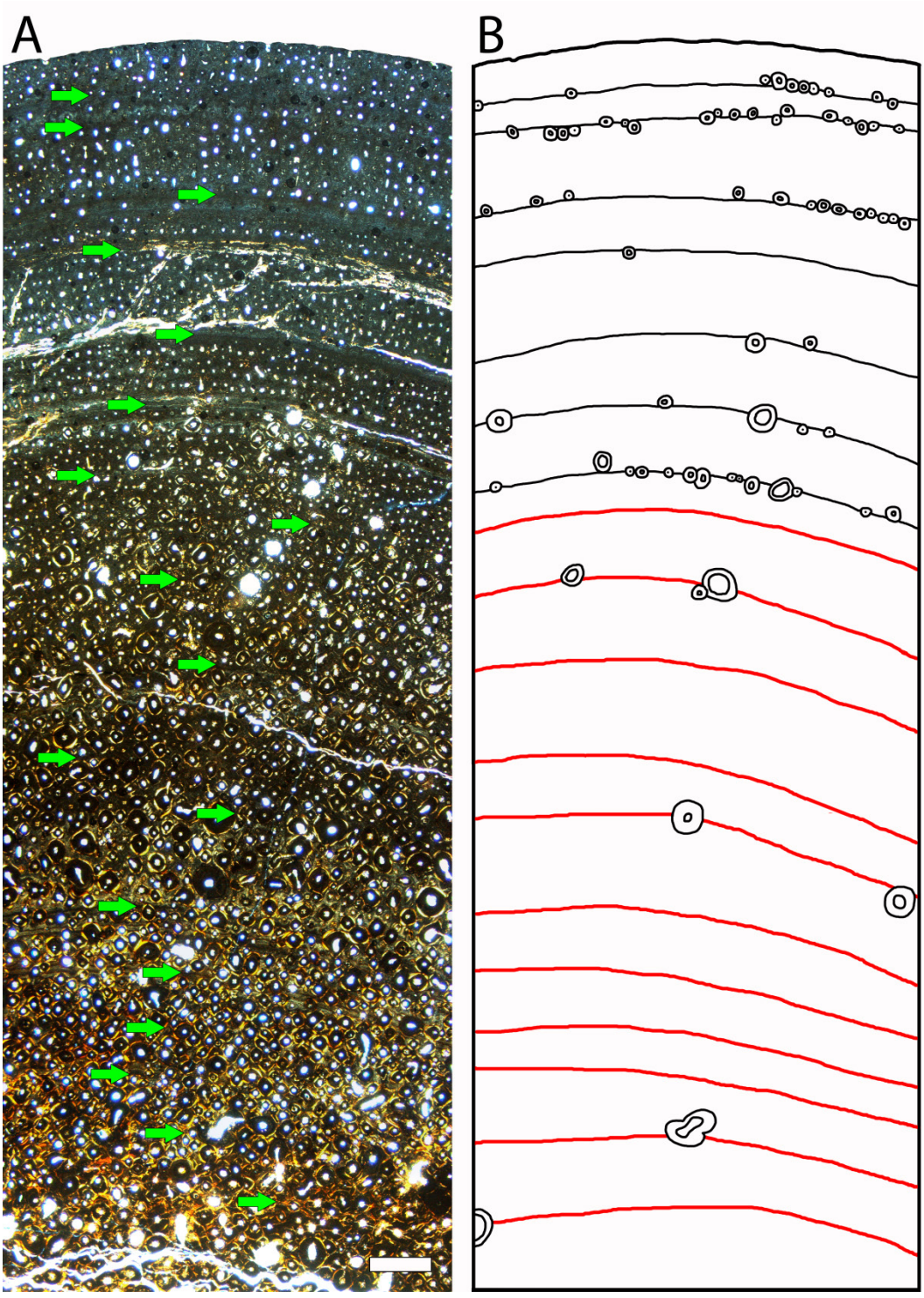

S.I. Fig. 14: Growth record preservation in the histological dorsal rib cross-section of *Camarasaurus* sp. (UW 46215). **A**: Polarized light photograph. Green arrows indicate growth marks. Note that most of the growth marks are only preserved as modulations or polish lines not visible under the microscope. Scale bar equals 500 µm. **B**: Drawing of the visible growthmarks and the secondary osteons influencing the LAGs by destroying or tracing them marked in black. Polish lines not visible under the microscope are marked in red.

***Camarasaurus* sp. (UW 46212)**

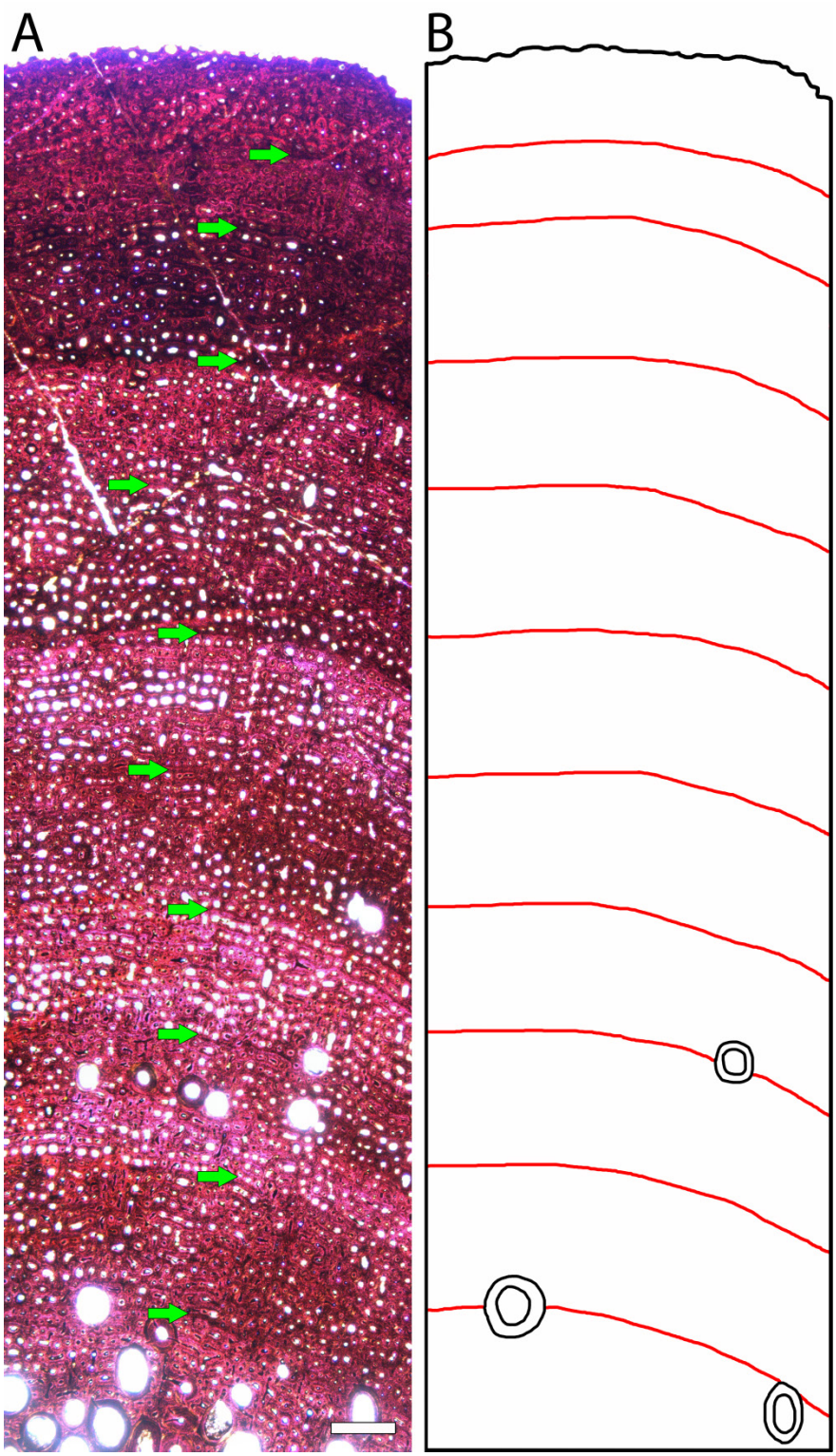

S.I. Fig. 15: Growth record preservation in the histological dorsal rib cross-section of *Camarasaurus* sp. (UW 46212). **A**: Polarized light photograph. Green arrows indicate growth marks. Note that all growth marks are preserved as modulations. Scale bar equals 500 µm. **B**: Drawing of the visible growthmarks (in red) and the secondary osteons influencing the growth marks by destroying them (in black).

***Camarasaurus* sp. (YPM VP 000619)**

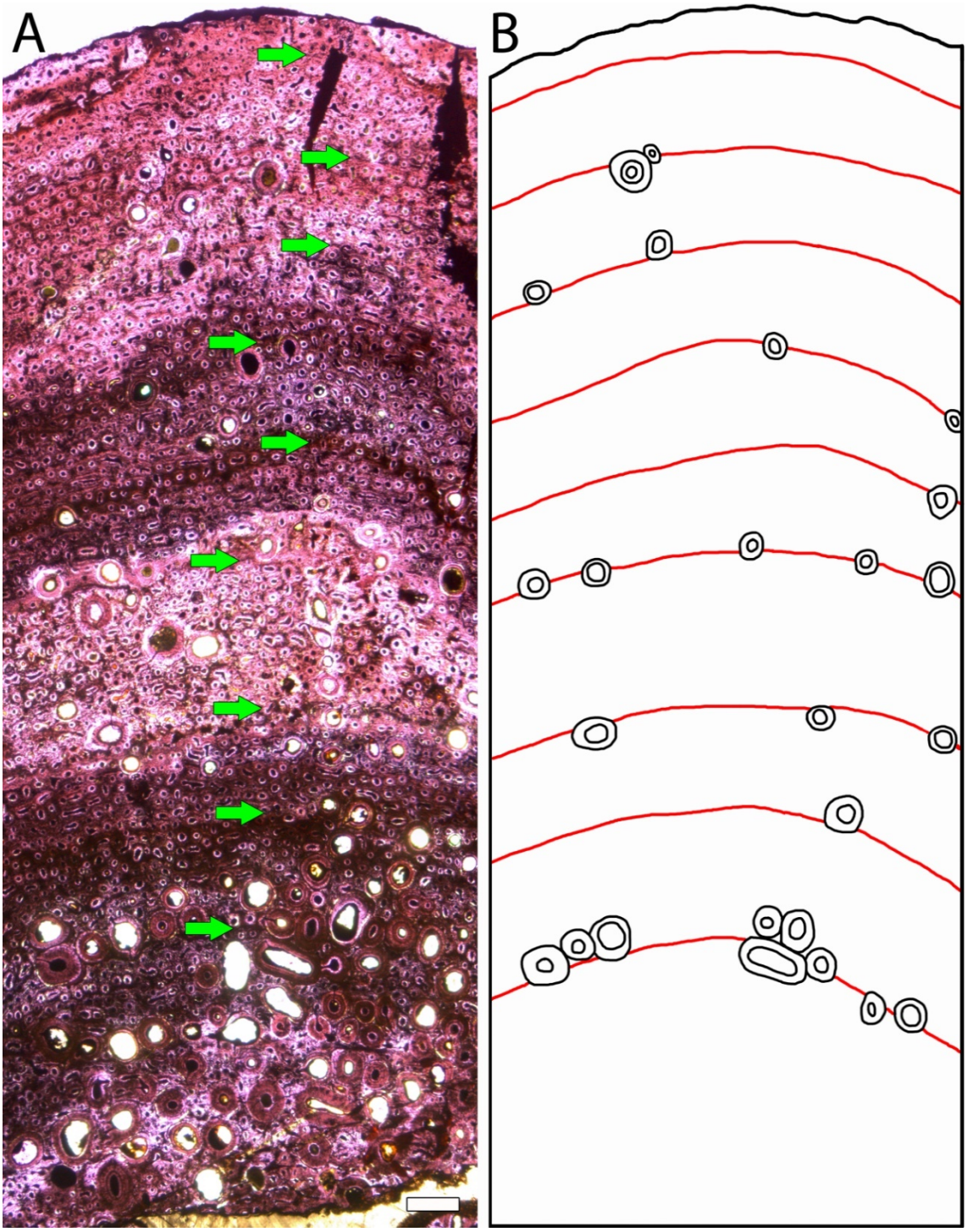

S.I. Fig. 16: Growth record preservation in the histological dorsal rib cross-section of *Camarasaurus* sp. (YPM VP 000619). **A**: Polarized light photograph. Green arrows indicate growth marks. Note that all growth marks are preserved as modulations. Scale bar equals 500 µm. **B**: Drawing of the visible growthmarks (in red) and the secondary osteons influencing the growth marks by destroying them (in black).

***Camarasaurus* sp. (UMNH 24802)**

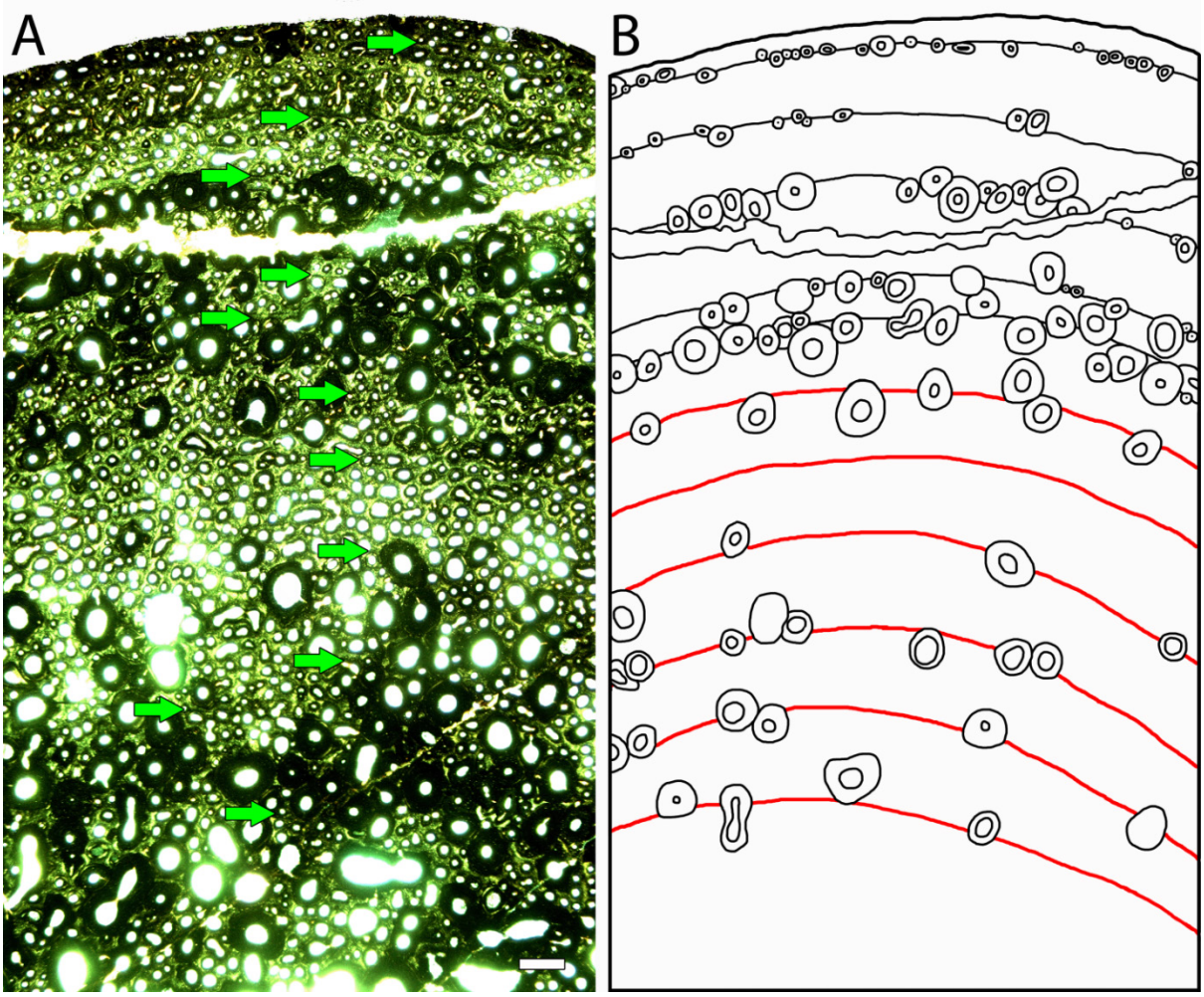

S.I. Fig. 17: Growth record preservation in the histological dorsal rib cross-section of *Camarasaurus* sp. (UMNH 24802). **A**: Polarized light photograph. Green arrows indicate growth marks. Note that most of the growth marks are only preserved as modulations or polish lines not visible under the microscope. Scale bar equals 500 µm. **B**: Drawing of the visible growthmarks and the secondary osteons influencing the LAGs by destroying or tracing them marked in black. Polish lines not visible under the microscope are marked in red.

***Camarasaurus* sp. (UMNH 5289)**

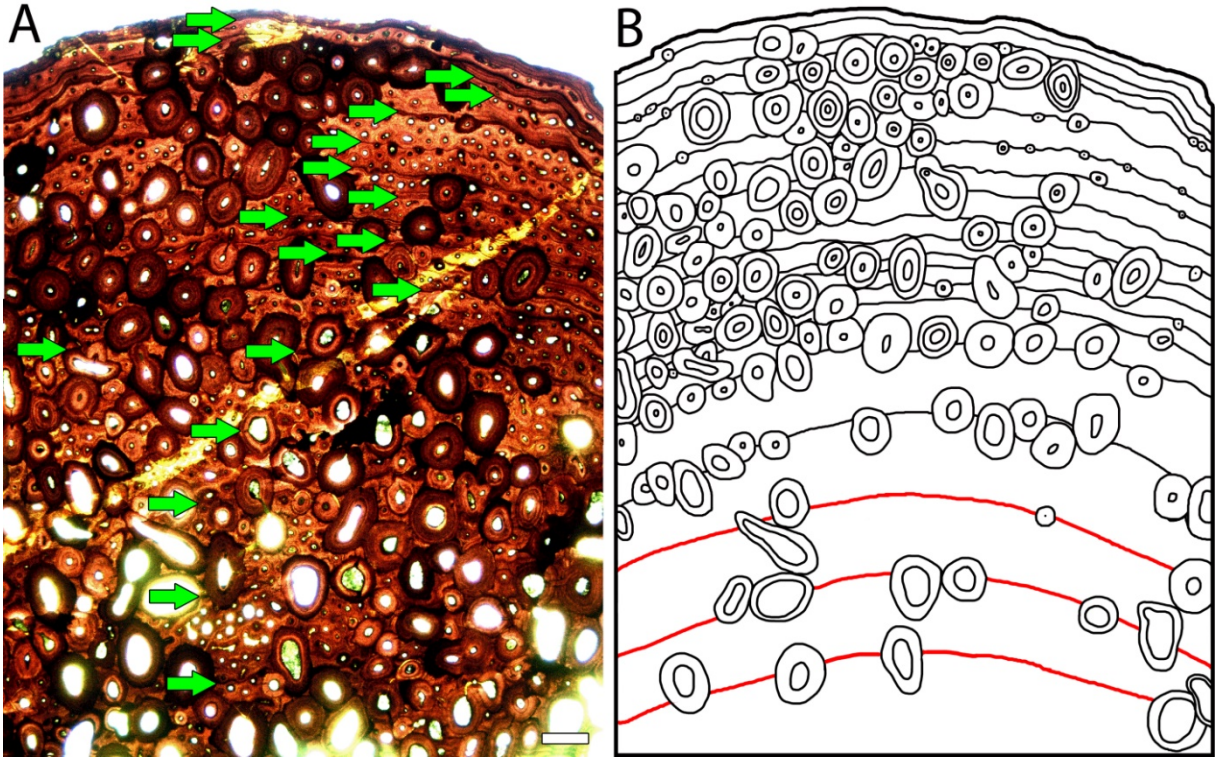

S.I. Fig. 18: Growth record preservation in the histological dorsal rib cross-section of *Camarasaurus* sp. (UMNH 5289). **A**: Normal light photograph. Green arrows indicate growth marks. Note that most of the growth marks are only preserved as modulations or polish lines not visible under the microscope. Scale bar equals 500 µm. **B**: Drawing of the visible growthmarks and the secondary osteons influencing the LAGs by destroying or tracing them marked in black. Polish lines not visible under the microscope are marked in red.

***Camarasaurus* sp. (UMNH 21608)**

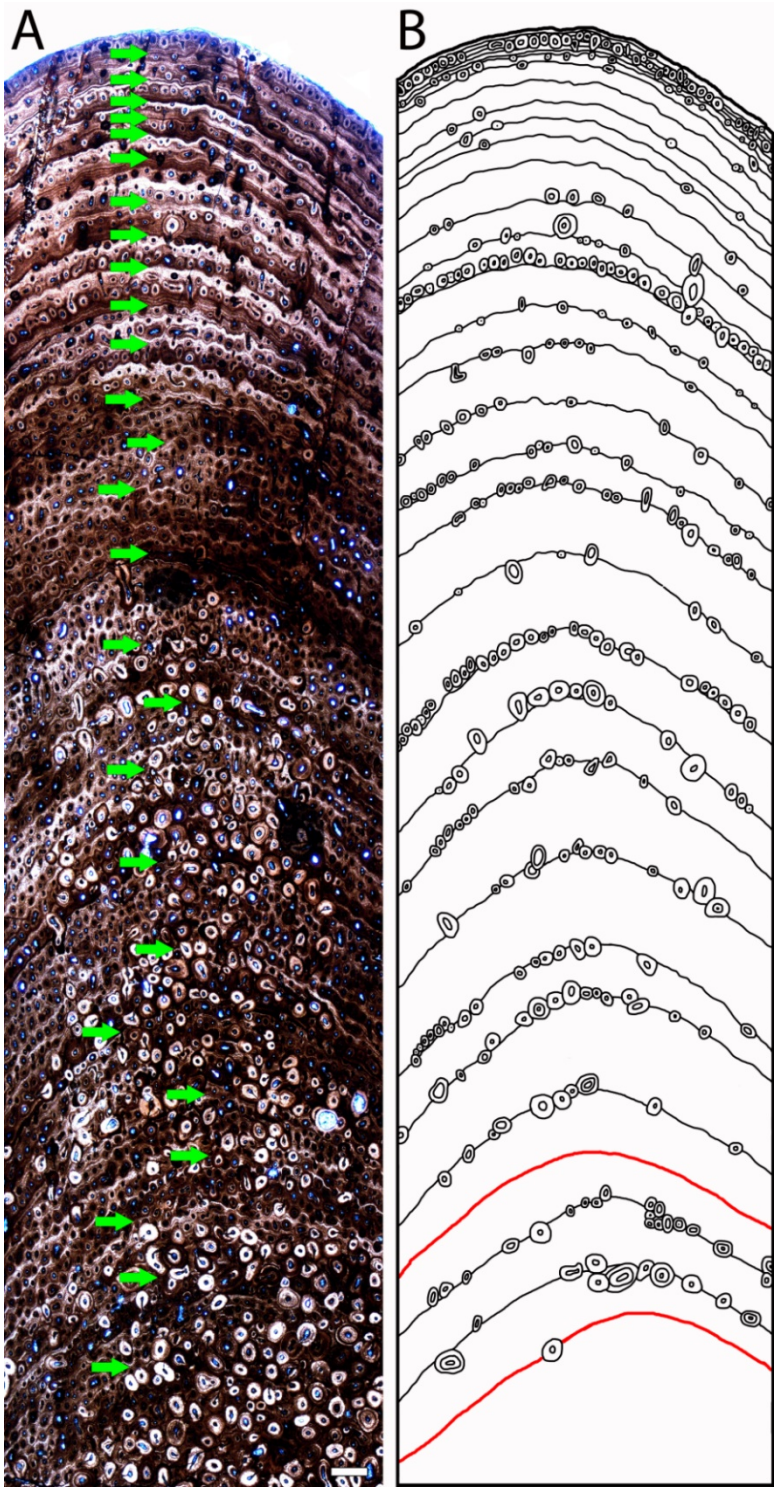

S.I. Fig. 19: Growth record preservation in the histological cross-section of the dorsal rib of *Camarasaurus* sp. (UMNH 24608). **A**: Normal light photograph. Green arrows indicate growth marks. Note that not all LAGs of the EFS are marked with arrows due to magnification of the figure. Scale bar equals 500 µm. **B**: Drawing of the visible growthmarks and the secondary osteons influencing the LAGs by destroying or tracing them. Modulations not developed as LAGs are marked in red.

***Camarasaurus* sp. (UMNH 24384)**

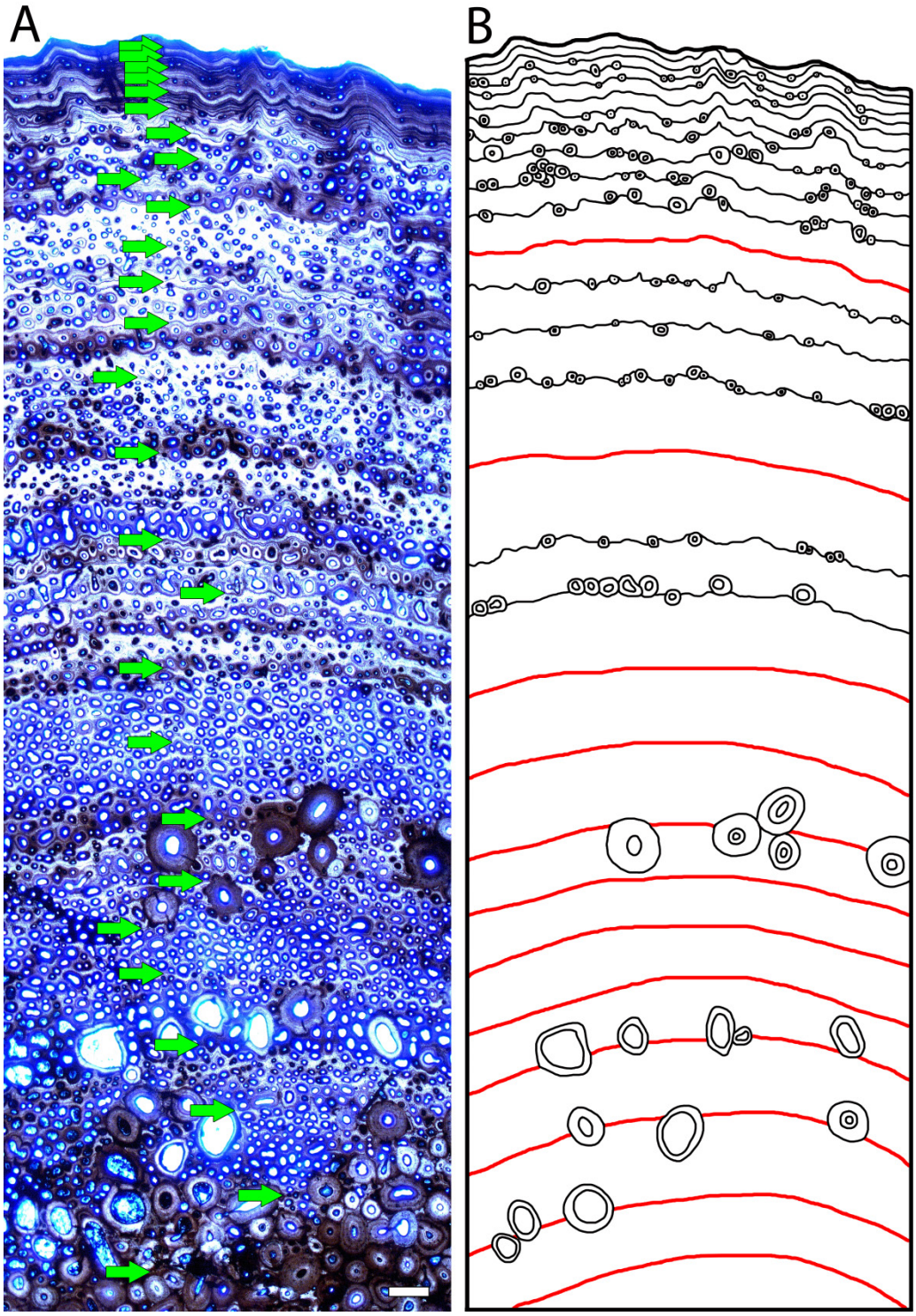

S.I. Fig. 20: Growth record preservation in the histological dorsal rib of cross-section of *Camarasaurus* sp. (UMNH 24384). Note that most of the visible growth marks are perseverd as multiple LAGs (up to five closely spaced LAGs completing one annual cycle) **A**: Polarized light photograph. Green arrows indicate growth marks some of which are only preserved as modulations or polish lines not visible in microscopic view. Scale bar equals 500 µm. **B**: Drawing of the visible growthmarks and the secondary osteons influencing the LAGs by destroying or tracing them. Modulations not developed as LAGs are marked in red.

***Camarasaurus* sp. (UMNH 20518)**

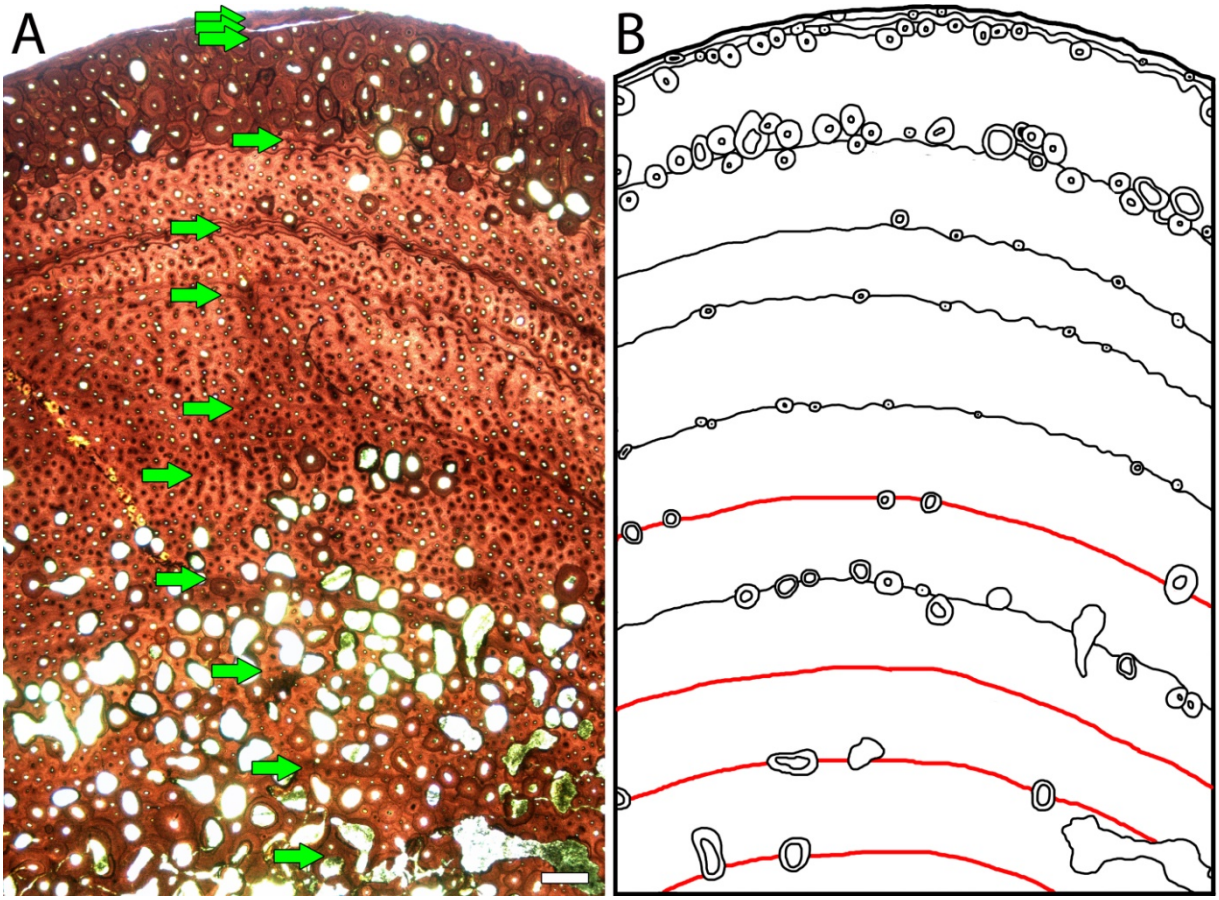

S.I. Fig. 21: Growth record preservation in the histological dorsal rib of cross-section of *Camarasaurus* sp. (UMNH 20518). Note that most of the LAGs of the EFS were destroyed due to remodeling at the posteromedial side pictured here. LAGs building the EFS are better visible in other parts of the thin section where they were counted. **A**: Normal light photograph. Green arrows indicate growth marks some of which are only preserved as modulations or polish lines not visible in microscopic view. Scale bar equals 500 µm. **B**: Drawing of the visible growth marks and the secondary osteons influencing the LAGs by destroying or tracing them. Some of the growth marks are perseverd as triple LAGs only one of which has been traced in the drawing. Modulations not developed as LAGs are marked in red.

***Camarasaurus* sp. (UMNH 24298)**

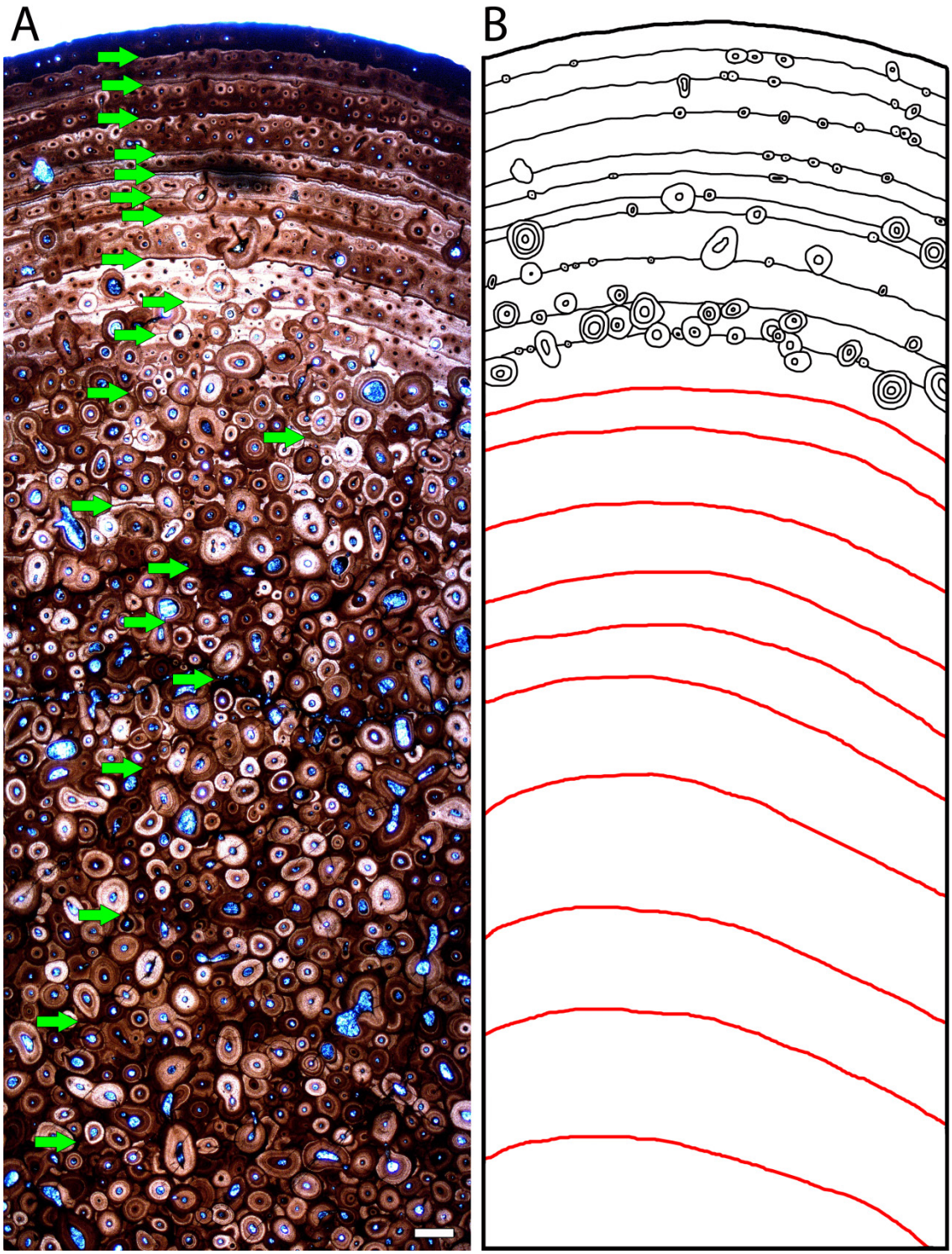

S.I. Fig. 22: Growth record preservation in the histological dorsal rib of cross-section of *Camarasaurus* sp. (UMNH 24298). Most of the innermost growth marks are only preserved as polish lines, tracing the original LAG poition in remodeled bone tissue (not visible in microscopic view). **A**: Normal light photograph. Green arrows indicate growth marks. Scale bar equals 500 µm. **B**: Drawing of the visible growthmarks and the secondary osteons influencing the LAGs by destroying or tracing them (marked in black). Polish lines are marked in red.

***Camarasaurus* sp. (UMNH 24803)**

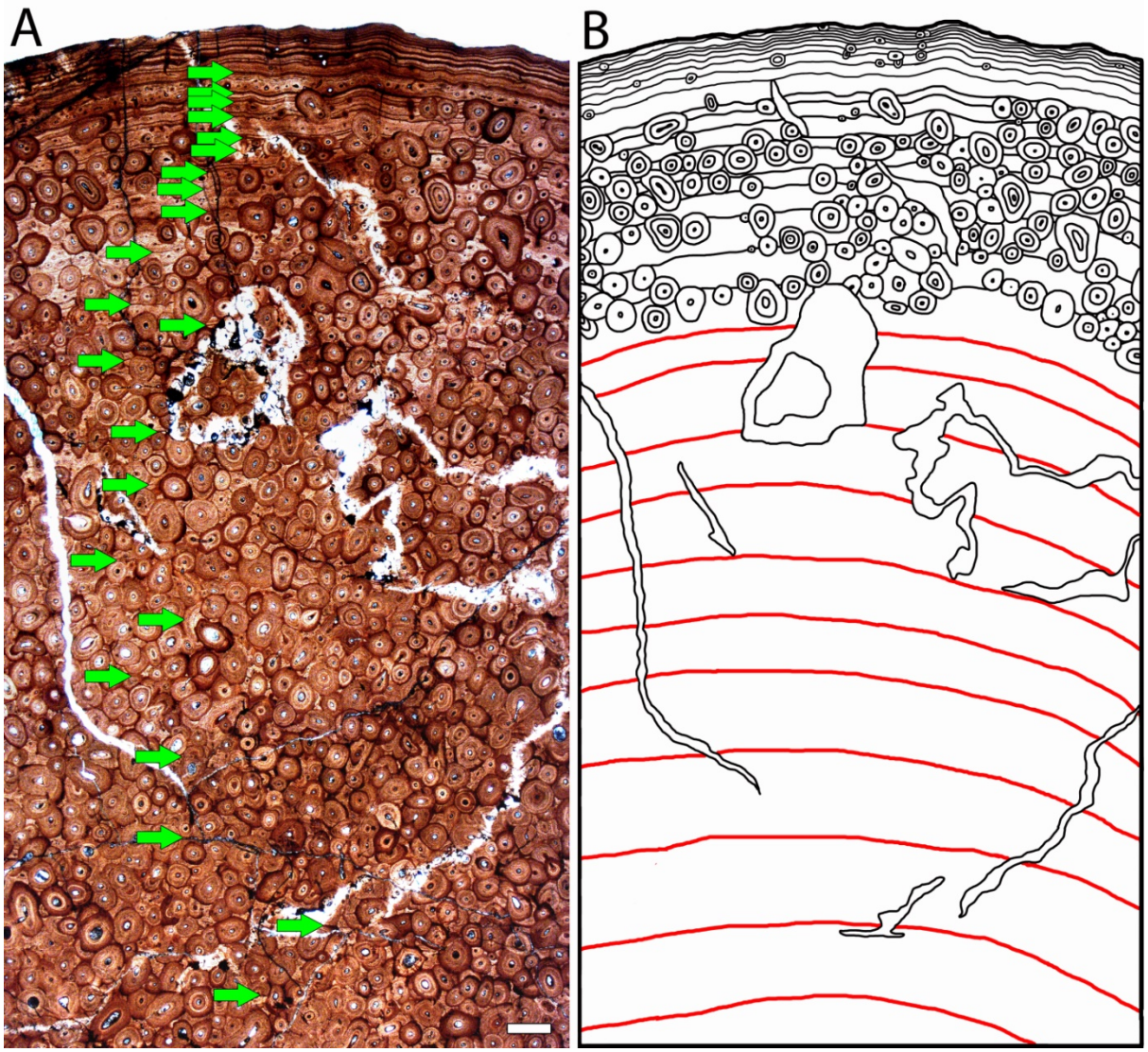

S.I. Fig. 23: Growth record preservation in the histological dorsal rib of cross-section of *Camarasaurus* sp. (UMNH 24803). Most of the innermost growth marks are only preserved as polish lines, tracing the original LAG poition in remodeled bone tissue (not visible in microscopic view). **A**: Normal light photograph. Green arrows indicate growth marks. Note that not all LAGs of the EFS are marked with arrows due to magnification reasons. Scale bar equals 500 µm. **B**: Drawing of the visible growthmarks and the secondary osteons influencing the LAGs by destroying or tracing them (marked in black). Polish lines are marked in red.

***Camarasaurus* sp. (UMNH 24805)**

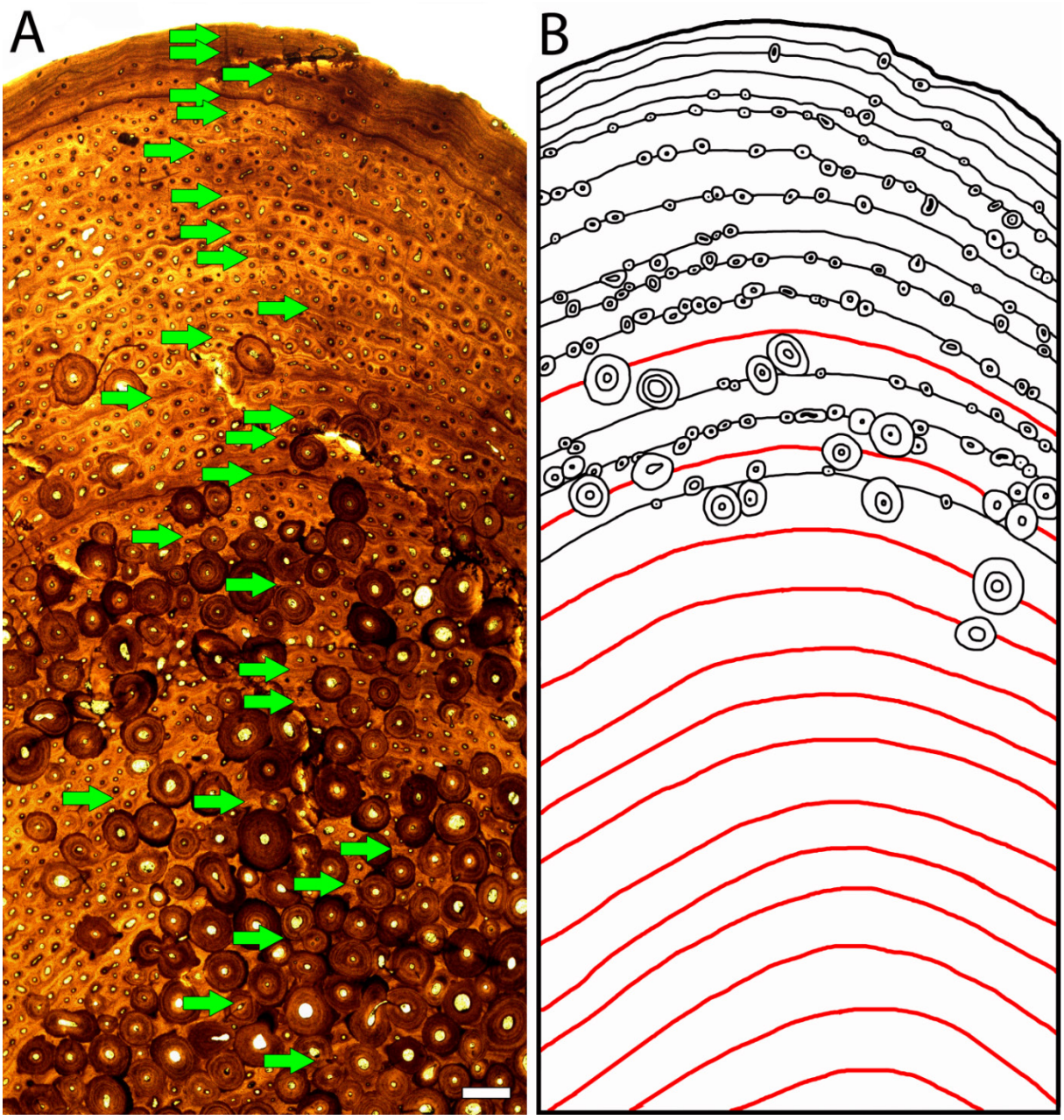

S.I. Fig. 24: Growth record preservation in the histological dorsal rib of cross-section of *Camarasaurus* sp. (UMNH 24805). Most of the innermost growth marks are only preserved as polish lines not visible in microscopic view. **A**: Normal light photograph. Green arrows indicate growth marks. Scale bar equals 500 µm. **B**: Drawing of the visible growthmarks and the secondary osteons influencing the LAGs by destroying or tracing them (marked in black). Polish lines are marked in red.

***Camarasaurus* sp. (UMNH 24806)**

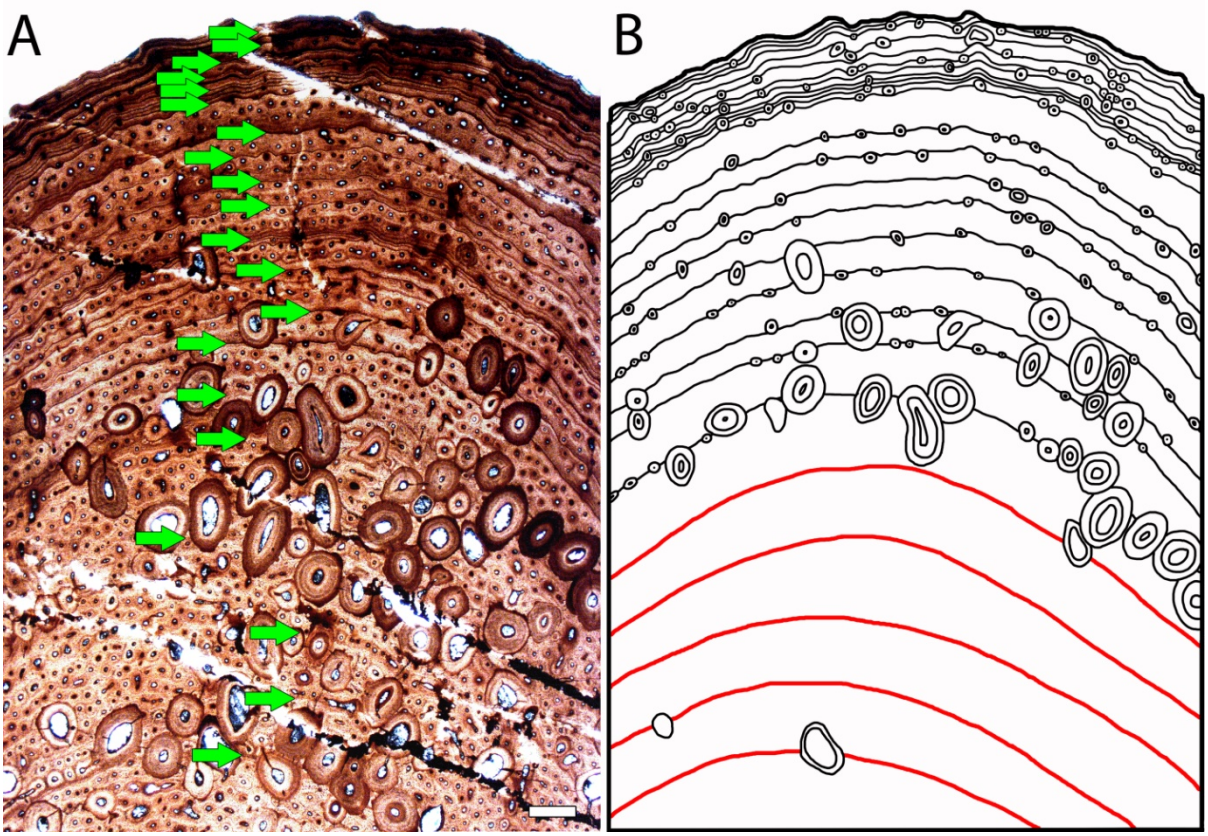

S.I. Fig. 25: Growth record preservation in the histological cross-section of the dorsal rib of *Camarasaurus* sp. (UMNH 24806). **A**: Normal light photograph. Green arrows indicate growth marks. Note that not all LAGs of the EFS are marked with arrows due to magnification of the figure. Scale bar equals 500 µm. **B**: Drawing of the visible growthmarks and the secondary osteons influencing the LAGs by destroying or tracing them. Modulations and polish lines not developed as LAGs are marked in red.

***Camarasaurus* sp. (UMNH 24807)**

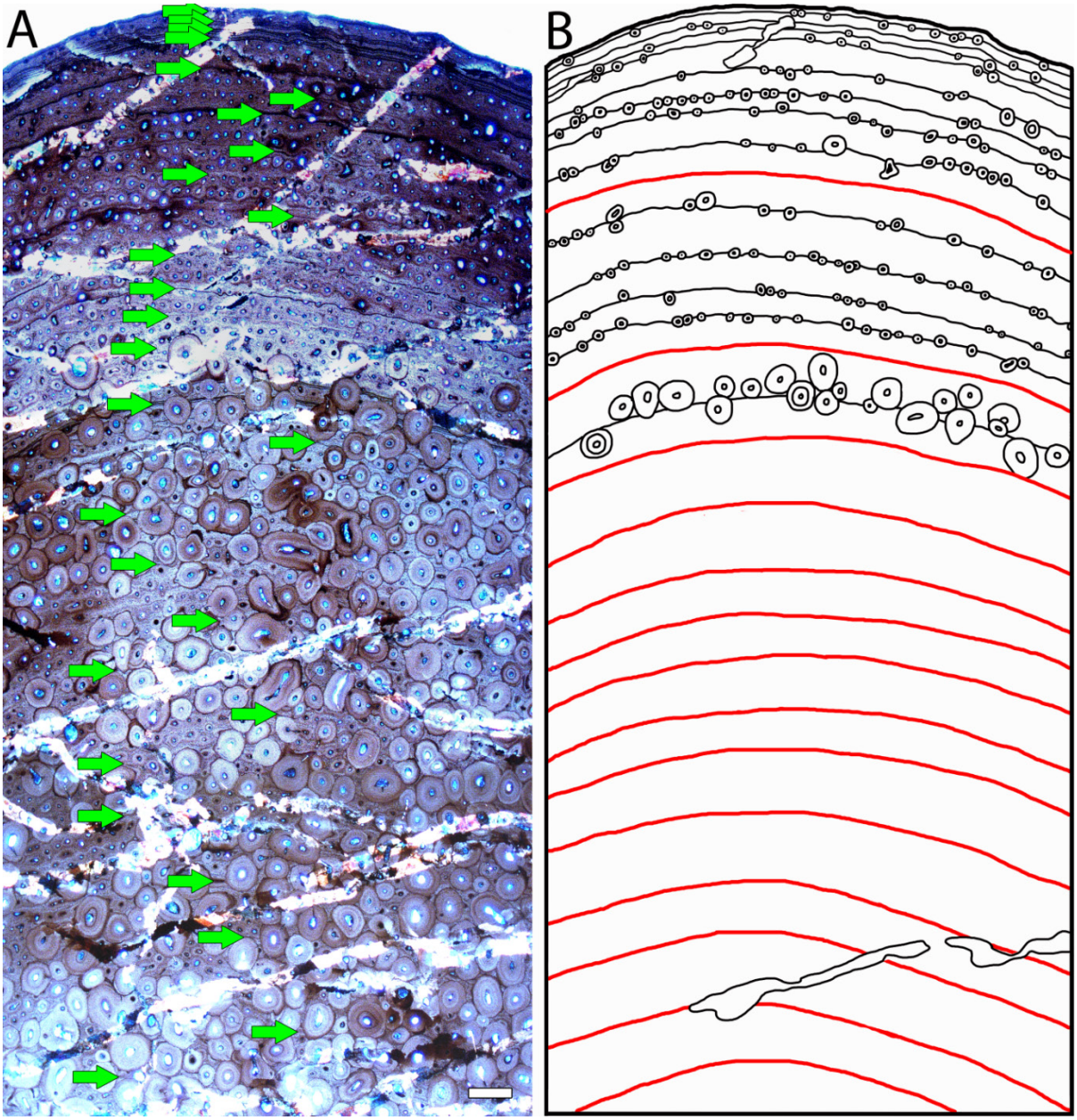

S.I. Fig. 26: Growth record preservation in the histological dorsal rib cross-section of *Camarasaurus* sp. (UMNH 24807). **A**: Polarized light photograph. Green arrows indicate growth marks. Note that most of the inner growth marks are only preserved as modulations or polish lines not visible under the microscope. Scale bar equals 500 µm. **B**: Drawing of the visible growth marks and the secondary osteons influencing the LAGs by destroying or tracing them marked in black. Polish lines not visible under the microscope are marked in red.

***Camarasaurus* sp. (UMNH 24808)**

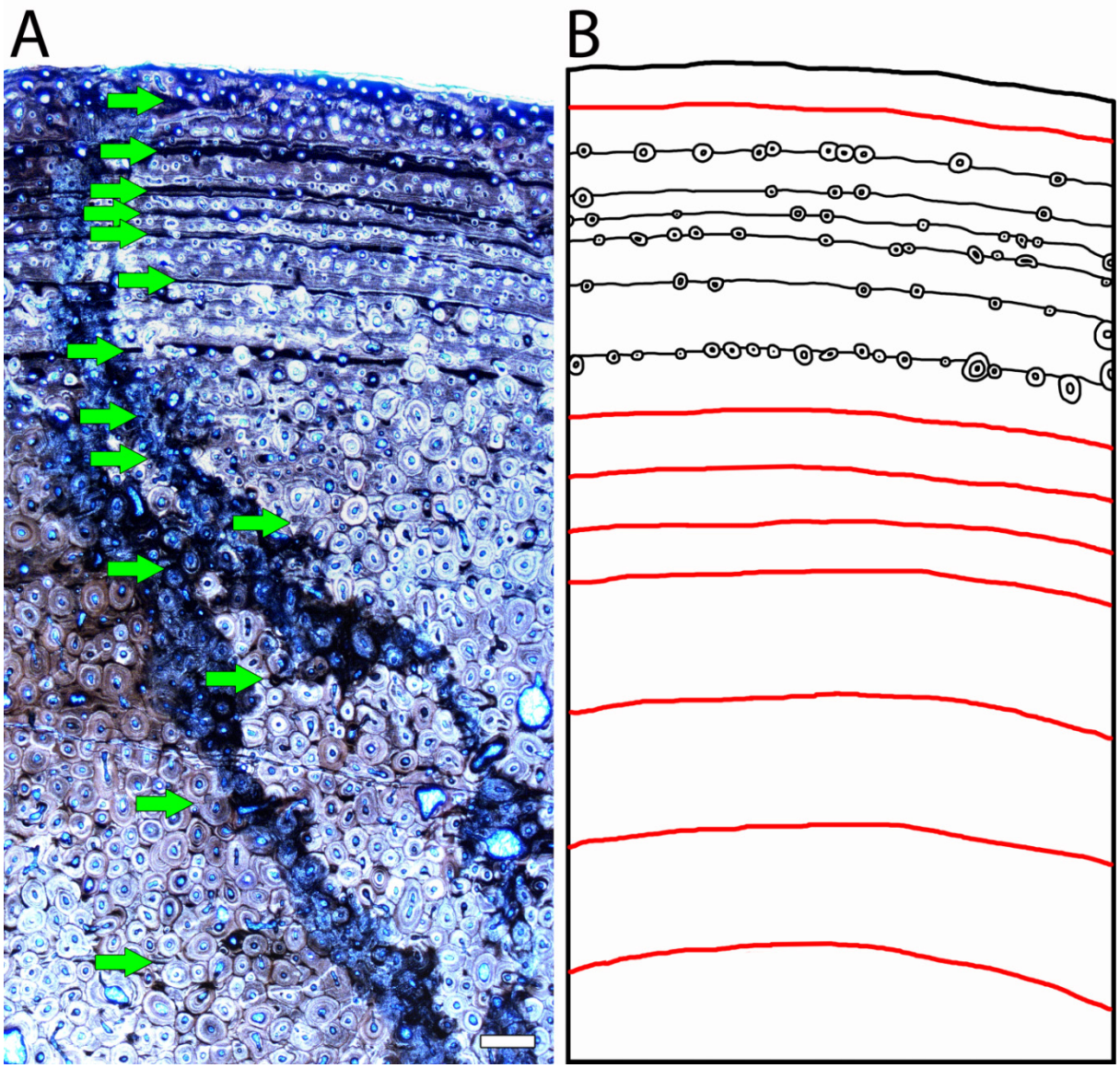

S.I. Fig. 27: Growth record preservation in the histological dorsal rib cross-section of *Camarasaurus* sp. (UMNH 24808). **A**: Polarized light photograph. Green arrows indicate growth marks. Note that most of the inner growth marks are only preserved as modulations or polish lines not visible under the microscope. Scale bar equals 500 µm. **B**: Drawing of the visible growth marks and the secondary osteons influencing the LAGs by destroying or tracing them marked in black. Polish lines not visible under the microscope are marked in red.

***Camarasaurus* sp. (YPM VP 060121)**

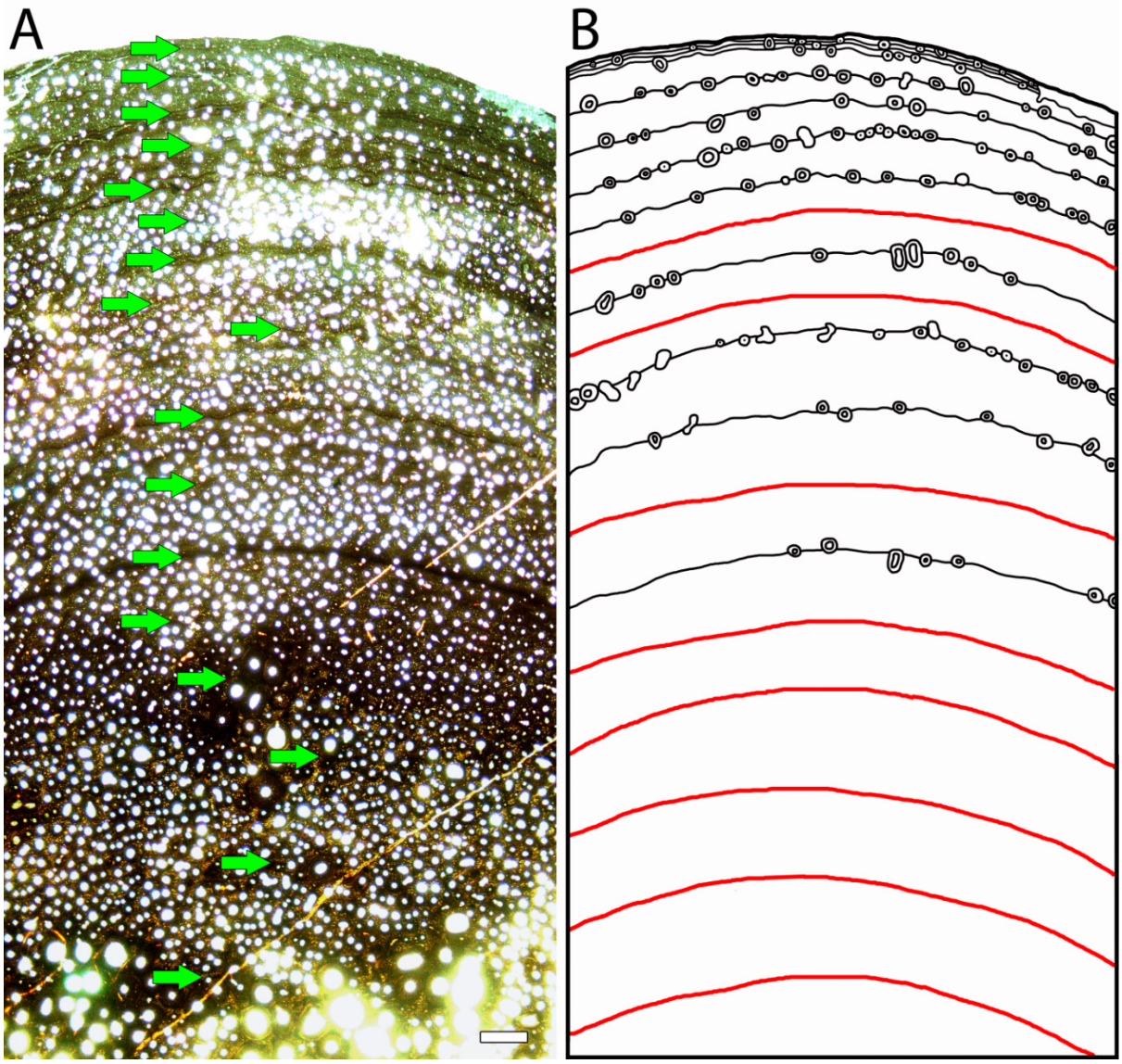

S.I. Fig. 28: Growth record preservation in the histological dorsal rib cross-section of *Camarasaurus* sp. (YPM VP 060121). **A**: Polarized light photograph. Green arrows indicate growth marks. Note that most of the inner growth marks are only preserved as modulations or polish lines not visible under the microscope. Scale bar equals 500 µm. **B**: Drawing of the visible growth marks and the secondary osteons influencing the LAGs by destroying or tracing them marked in black. Polish lines not visible under the microscope are marked in red.

***Brachiosaurus altithorax* (FMNH P25107)**

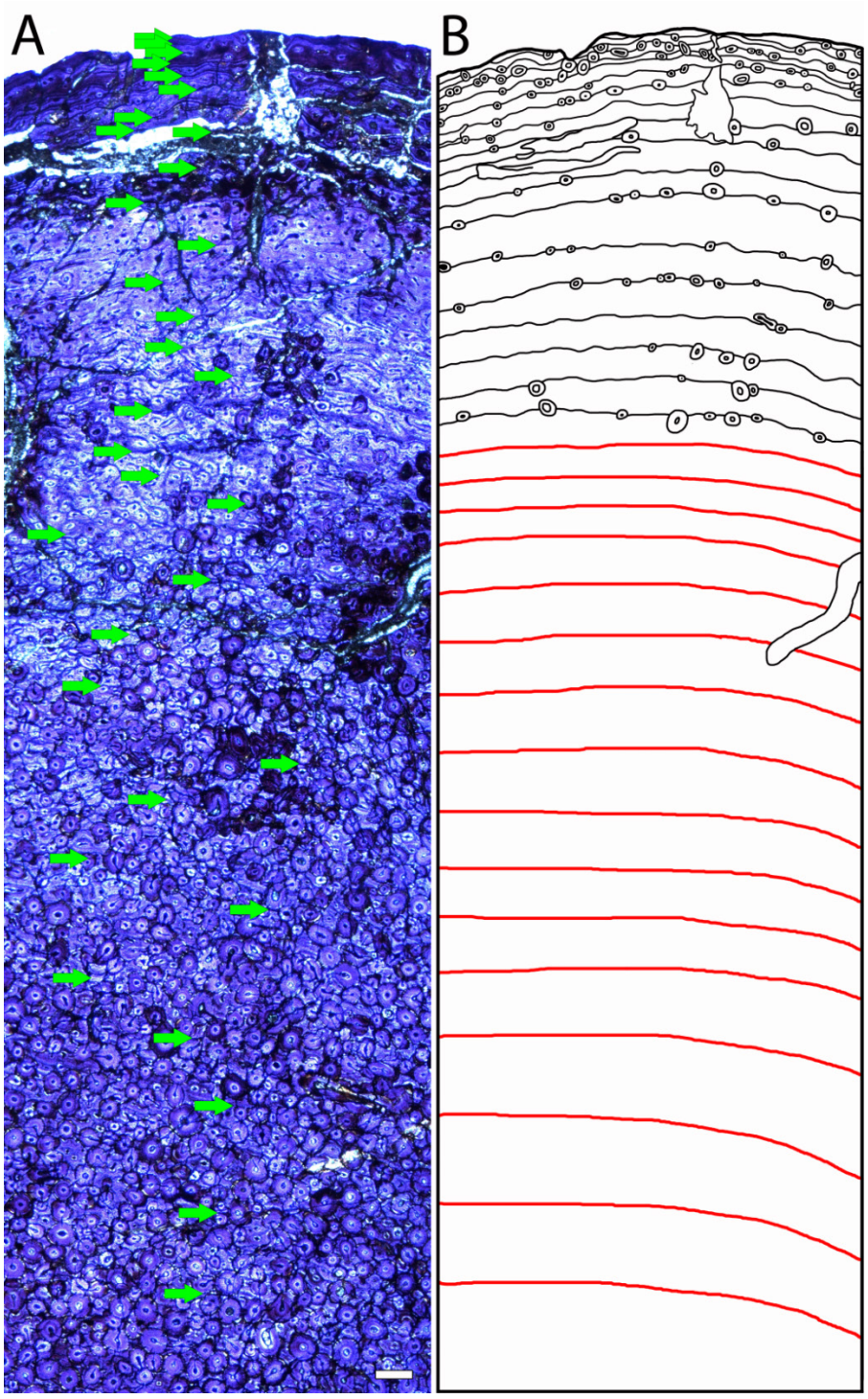

S.I. Fig. 29: Growth record preservation in the histological dorsal rib cross-section of *Brachiosaurus altithorax*. (FMNH P25107). **A**: Polarized light photograph. Green arrows indicate growth marks. Note that most of the inner growth marks are only preserved as modulations or polish lines not visible under the microscope. Scale bar equals 500 µm. **B**: Drawing of the visible growth marks and the secondary osteons influencing the LAGs by destroying or tracing them marked in black. Polish lines not visible under the microscope are marked in red.

***Brachiosaurus altithorax* (SMA 0009)**

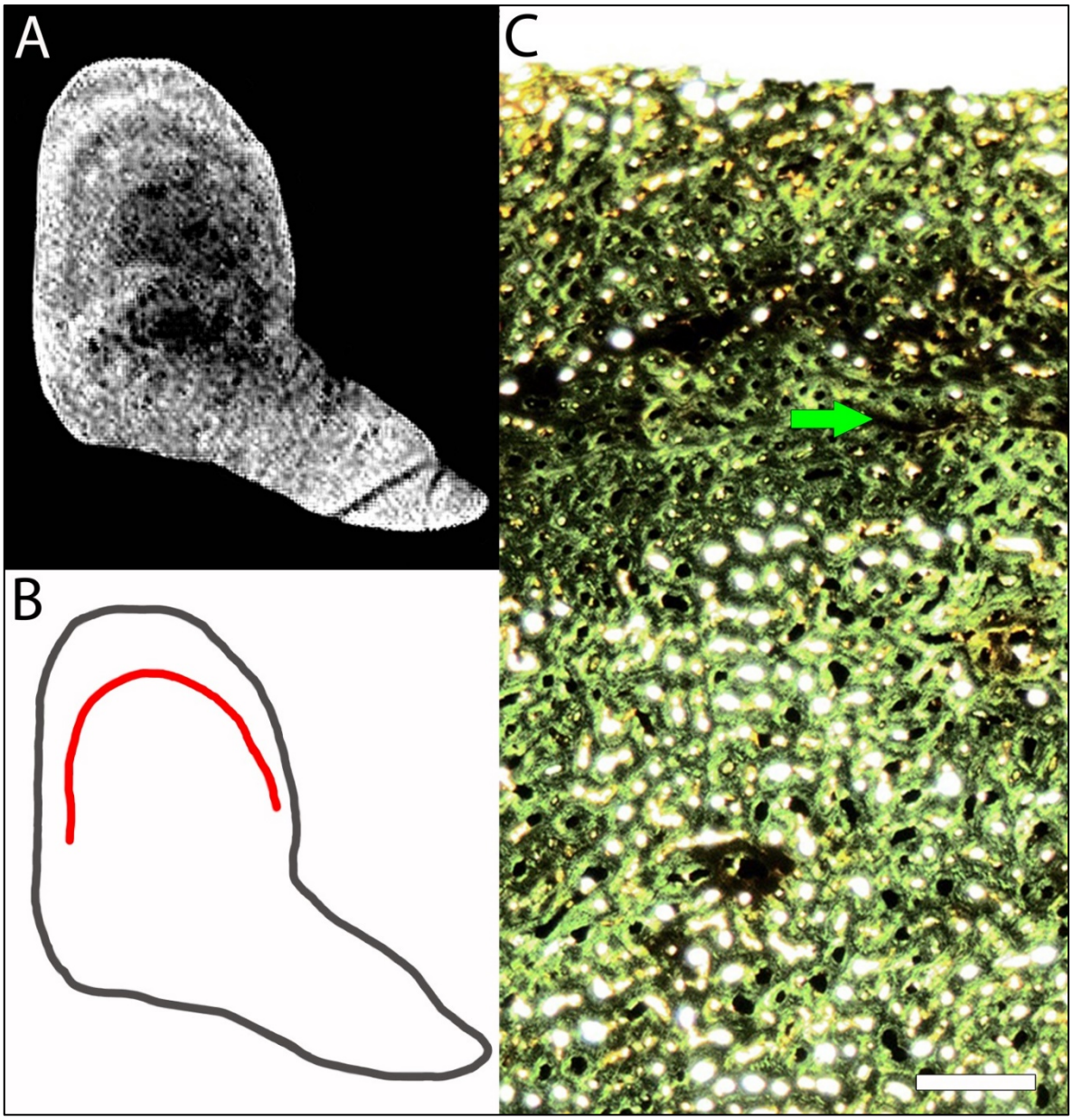

S.I. Fig. 30: Growth record preservation in the dorsal rib of *Brachiosaurus altithorax*. (SMA 0009). **A**: CT scan of the proximal rib shaft (cross-section similar in position to the histological sample). **B**: Drawing of the visible growth mark in the CT scan (marked in red). **C**: Polarized light photograph of a histological section. Green arrow indicates growth mark. Scale bar equals 500 µm. Note that CT scanning and histological sampling were performed on differing ribs belonging to the same individual. Due to the perfect completeness of the rib used for.scanning, a more incomplete fragment was used for destructive sampling.

***Brachiosaurus altithorax* (SMA 0314)**

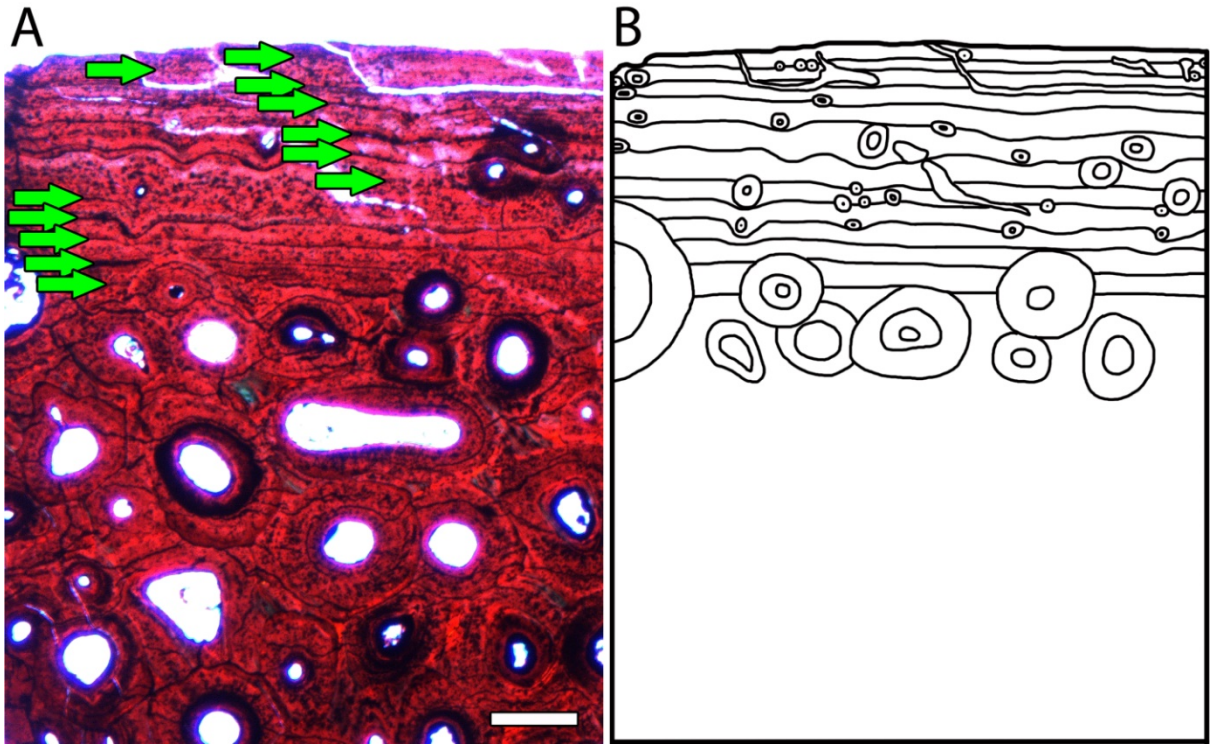

S.I. Fig. 31: External fundamental system (EFS) in the histological dorsal rib cross-section of *Brachiosaurus altithorax*. (SMA 0314). **A**: Polarized light photograph. Green arrows indicate growth marks. Scale bar equals 500 µm. **B**: Drawing of the visible growth marks of the EFS and the secondary osteons influencing the LAGs by destroying or tracing them.

Cf. *Giraffatitan* (J 12)

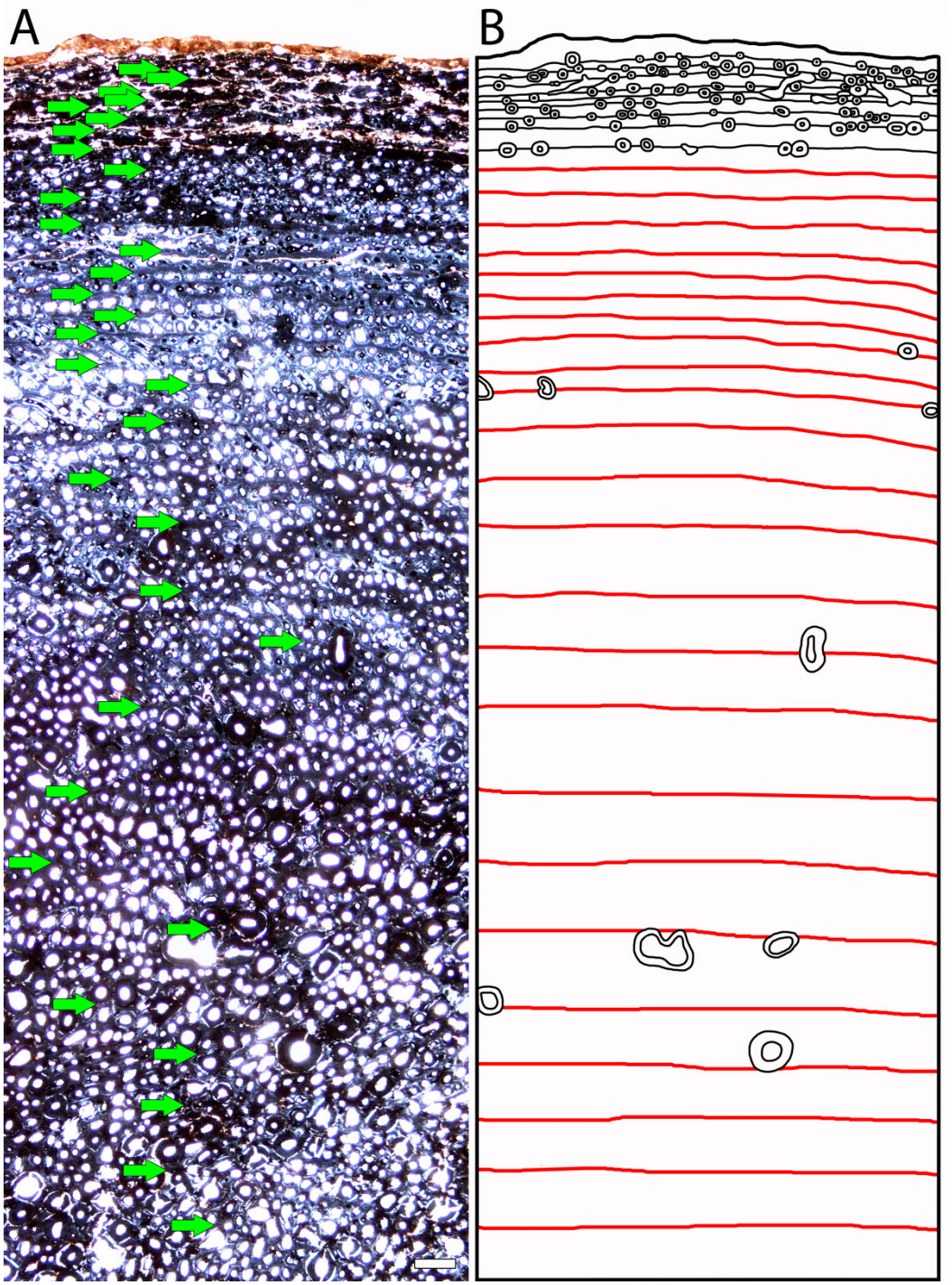

S.I. Fig. 32: Growth record preservation in the histological dorsal rib cross-section of Cf. *Giraffatitan*. (J 12). **A**: Polarized light photograph. Green arrows indicate growth marks. Note that most of the inner growth marks are only preserved as modulations or polish lines not visible under the microscope. Scale bar equals 500 µm. **B**: Drawing of the visible growth marks and the secondary osteons influencing the LAGs by destroying or tracing them marked in black. Polish lines and modulations are marked in red.

***Dicraeosaurus sattleri* (M 31)**

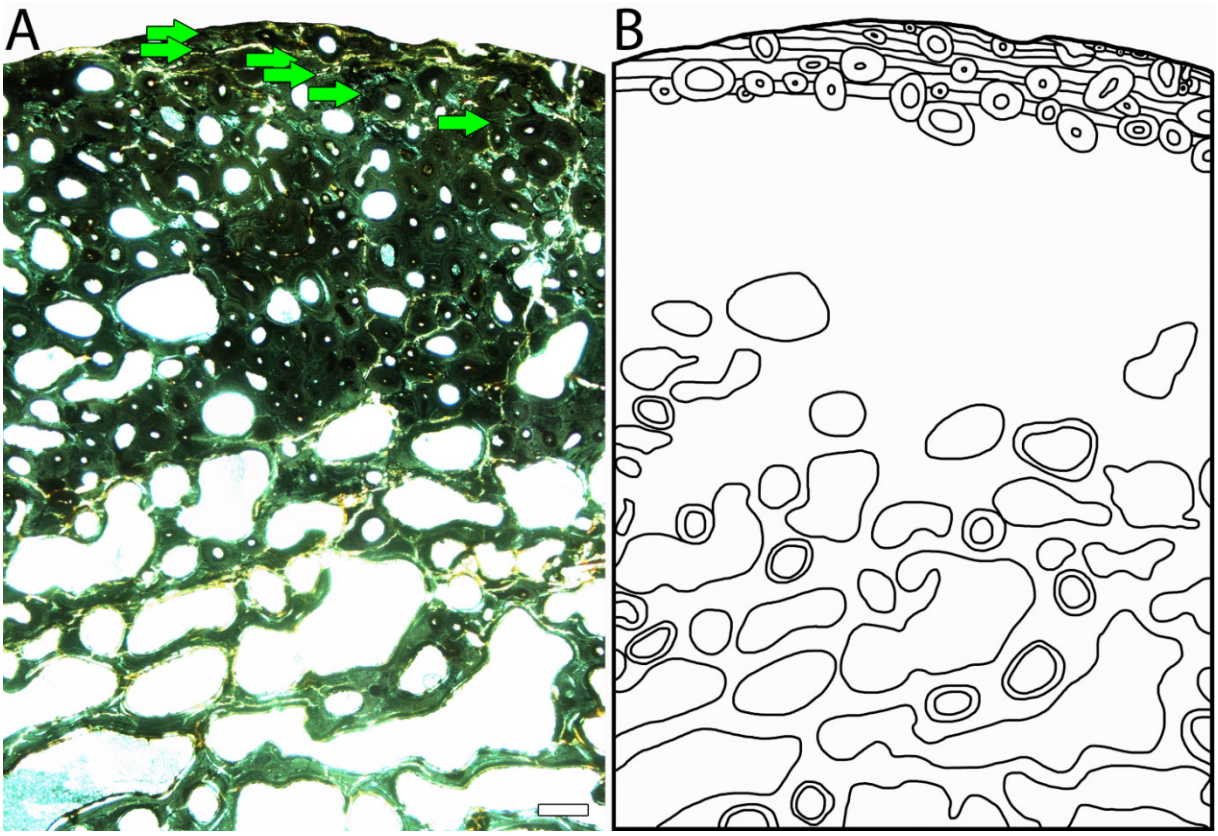

S.I. Fig. 33: External fundamental system (EFS) in the histological dorsal rib cross-section of *Dicraeosaurus sattleri*. (M31). **A**: Polarized light photograph. Green arrows indicate growth marks. Scale bar equals 500 µm. **B**: Drawing of the visible growth marks of the EFS and the secondary osteons influencing the LAGs by destroying or tracing them. Note the large cancellous bone area only occurring in *Dicraeosaurus* samples.

***Apatosaurus ajax* (YPM VP 001860)**

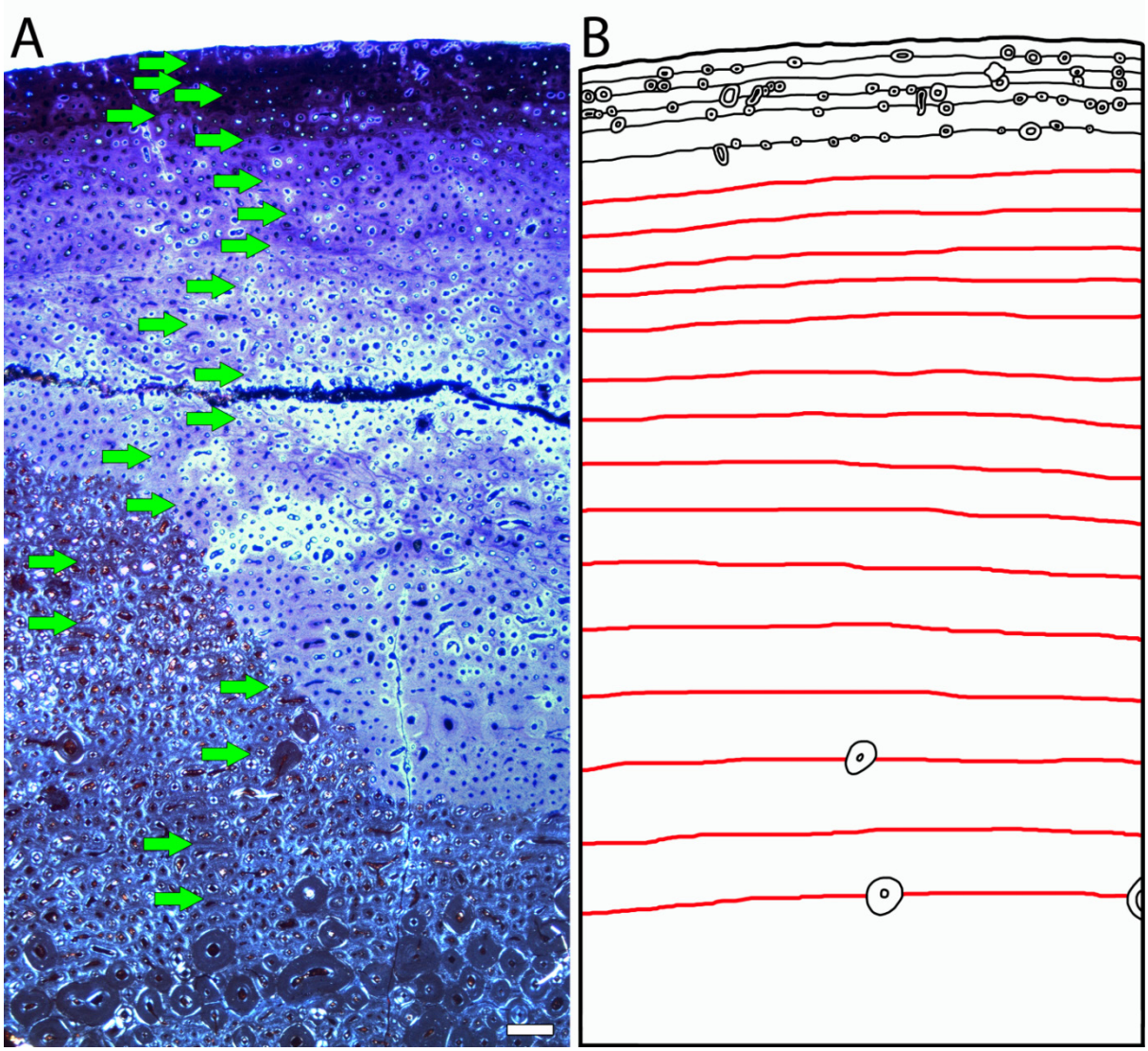

S.I. Fig. 34: Growth record preservation in the histological dorsal rib cross-section of *Apatosaurus ajax*. (YPM VP 001860). **A**: Polarized light photograph. Green arrows indicate growth marks. Note that most of the inner growth marks are only preserved as modulations or polish lines not visible under the microscope. Scale bar equals 500 µm. **B**: Drawing of the visible growth marks and the secondary osteons influencing the LAGs by destroying or tracing them marked in black. Polish lines and modulations are marked in red.

***Apatosaurus louisae* (SMA 0269)**

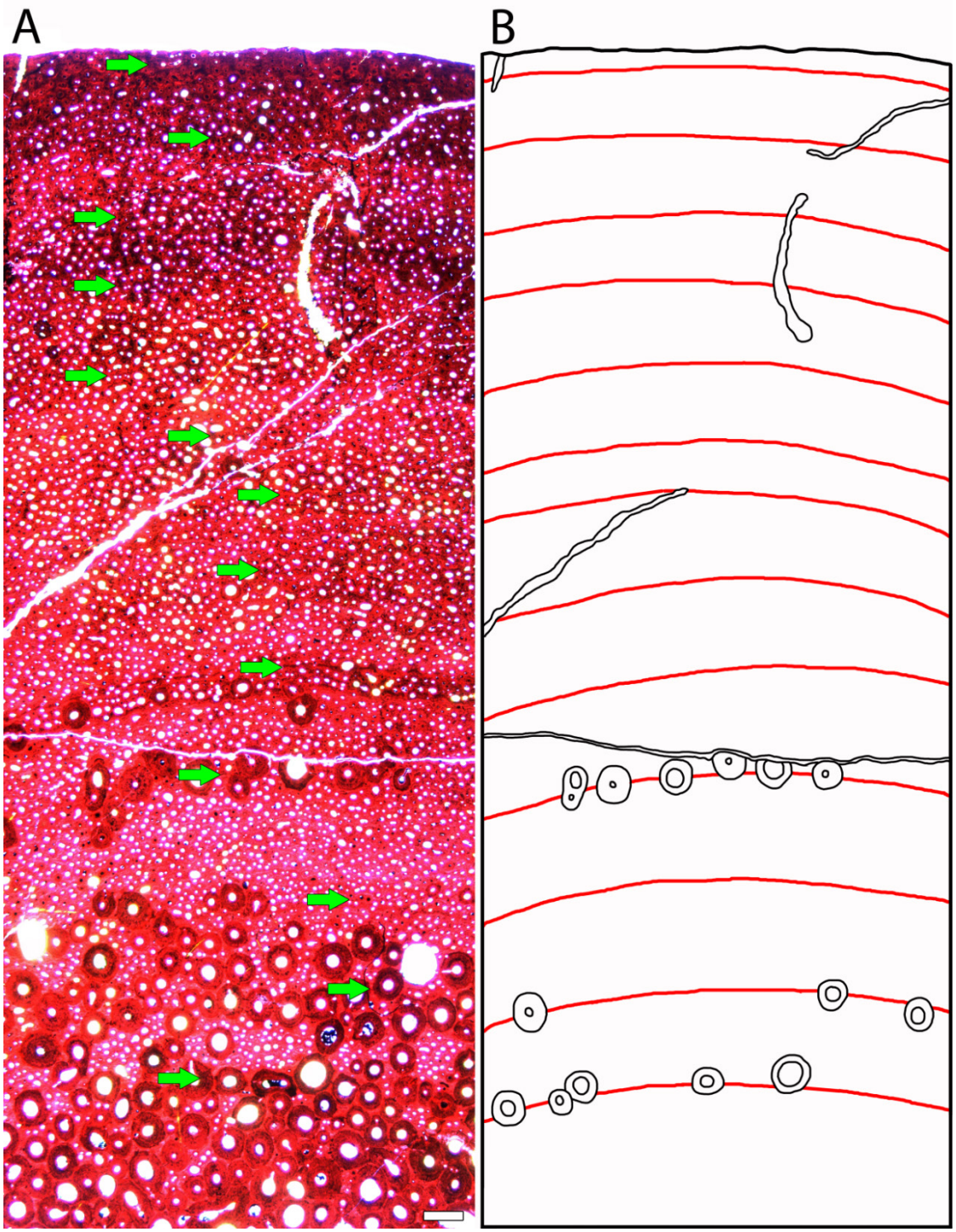

S.I. Fig. 35: Growth record preservation in the histological dorsal rib cross-section of *Apatosaurus louisae* (SMA 0269). **A**: Polarized light photograph. Green arrows indicate growth marks. Note that all growth marks are only preserved as modulations or polish lines not visible under the microscope. Scale bar equals 500 µm. **B**: Drawing of the visible growth marks (marked in red) and the secondary osteons influencing them by destroying or tracing the growth marks (marked in black).

***Apatosaurus* sp. (UW 46211)**

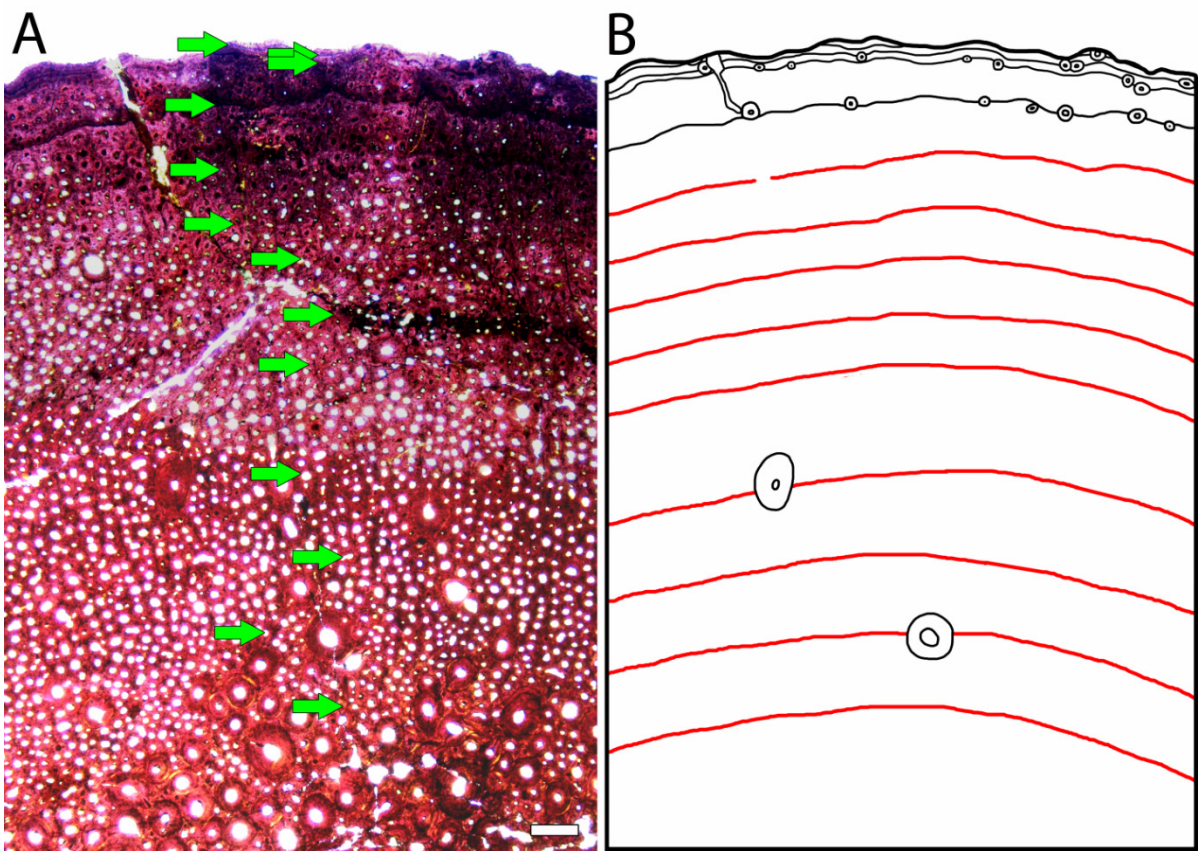

S.I. Fig. 36: Growth record preservation in the histological dorsal rib cross-section of *Apatosaurus* sp. (UW 46211). **A**: Polarized light photograph. Green arrows indicate growth marks. Note that most of the inner growth marks are only preserved as modulations or polish lines not visible under the microscope. Scale bar equals 500 µm. **B**: Drawing of the visible growth marks and the secondary osteons influencing the LAGs by destroying or tracing them marked in black. Polish lines and modulations are marked in red.

***Apatosaurus* sp. (MOR 957)**

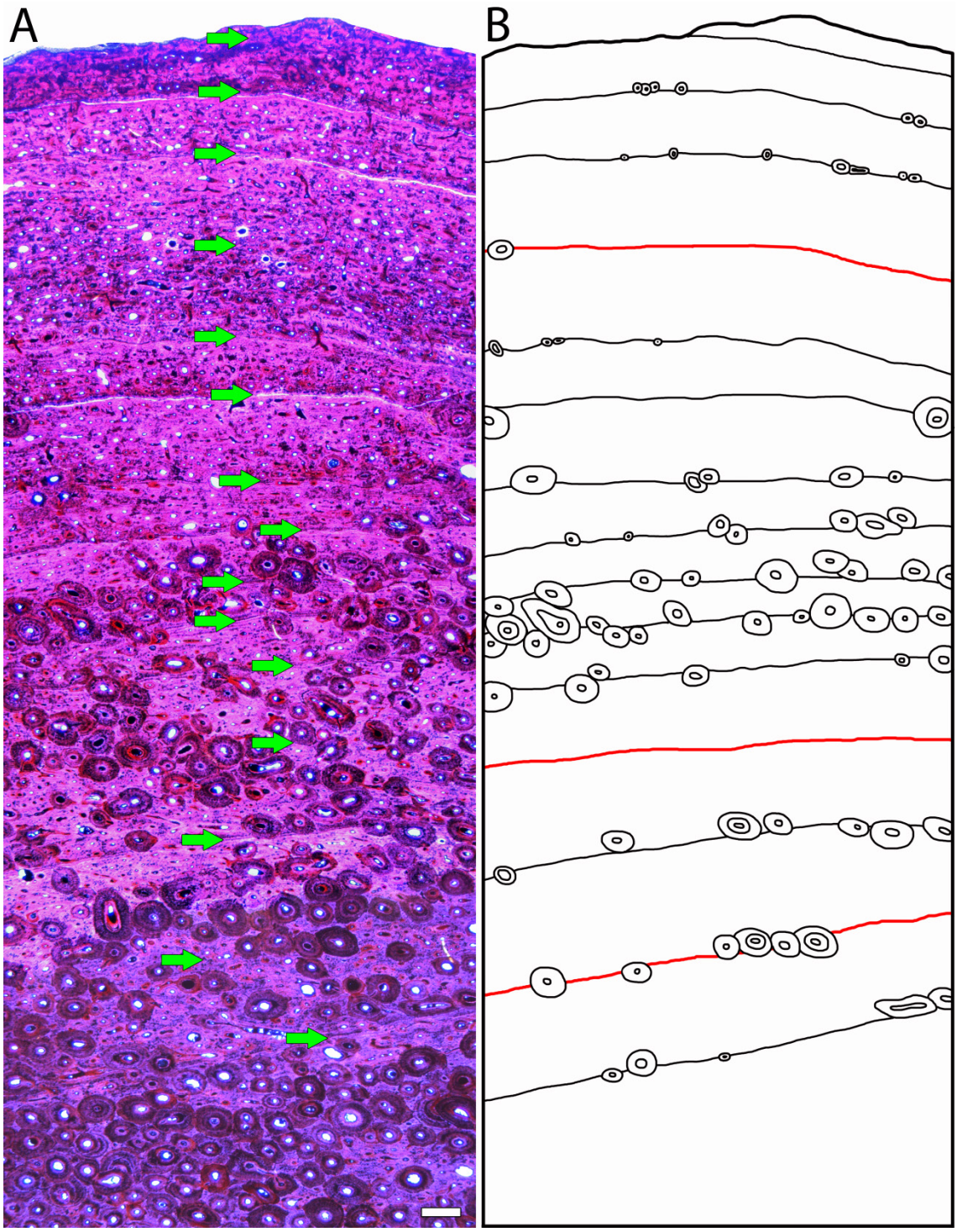

S.I. Fig. 37: Growth record preservation in the histological dorsal rib cross-section of *Apatosaurus* sp. (MOR 957). **A**: Polarized light photograph. Green arrows indicate growth marks. Note that some of the growth marks are only preserved as polish lines not visible under the microscope. Scale bar equals 500 µm. **B**: Drawing of the visible growth marks and the secondary osteons influencing the LAGs by destroying or tracing them marked in black. Polish lines are marked in red.

***Apatosaurus* sp. (YPM VP 004832)**

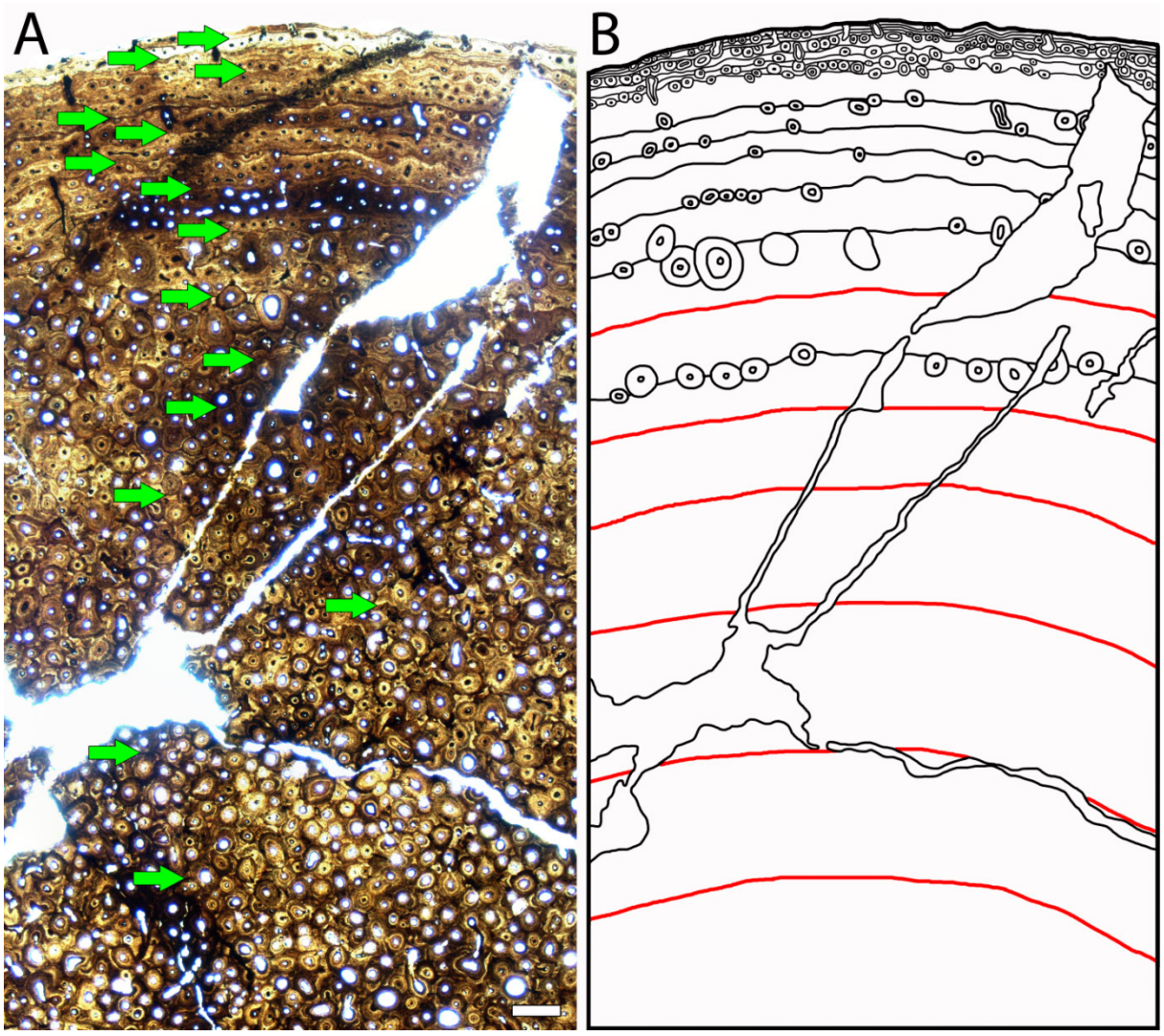

S.I. Fig. 38: Growth record preservation in the histological dorsal rib of cross-section of *Apatosaurus* sp. (YPM VP 004832). Most of the innermost growth marks are only preserved as polish lines, tracing the original LAG poition in remodeled bone tissue (not visible in microscopic view). **A**: Normal light photograph. Green arrows indicate growth marks. Note that not all LAGs of the EFS are marked with arrows due to magnification reasons. Scale bar equals 500 µm. **B**: Drawing of the visible growthmarks and the secondary osteons influencing the LAGs by destroying or tracing them (marked in black). Polish lines are marked in red.

***Brontosaurus excelsus* (YPM VP 001980)**

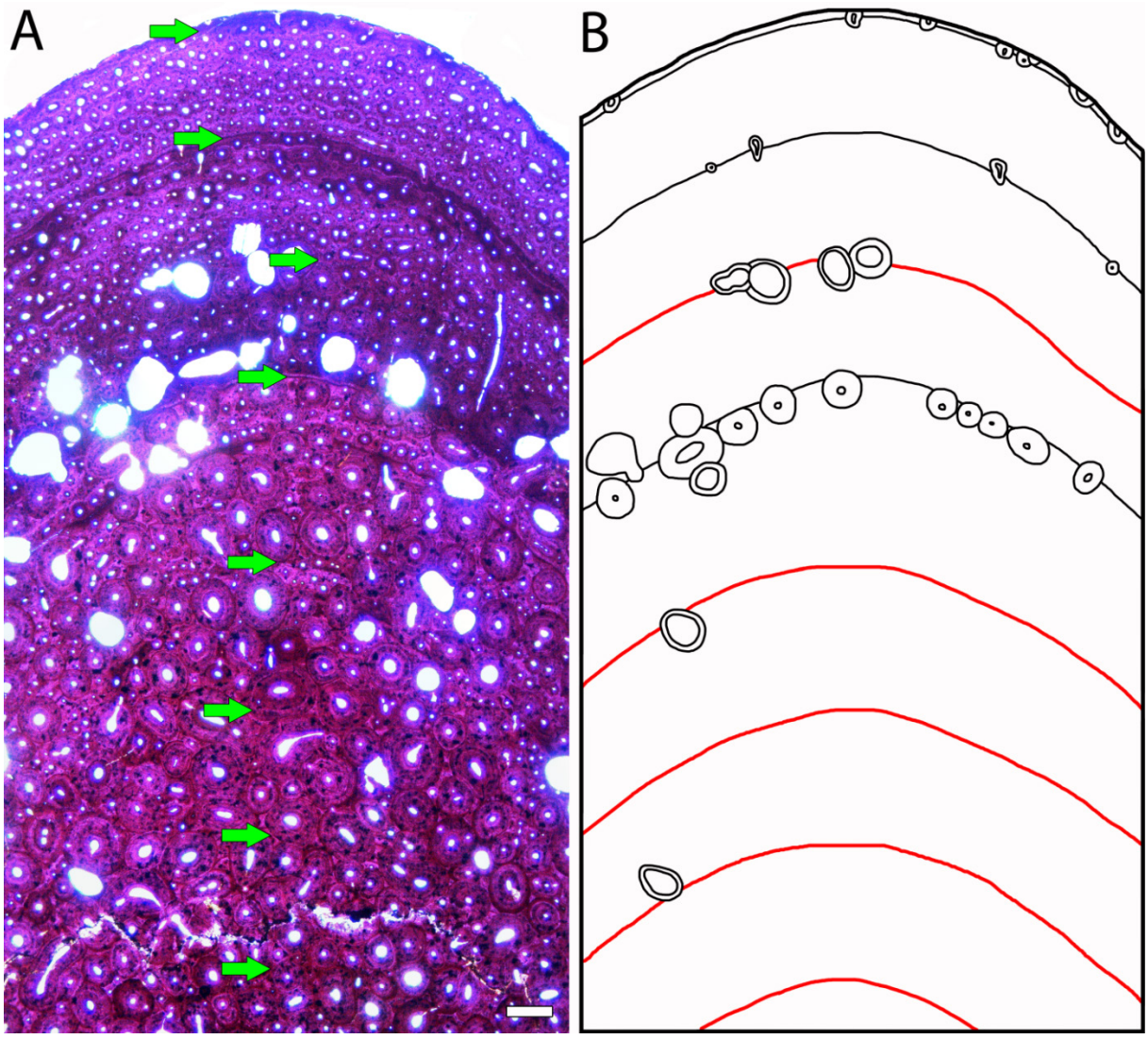

S.I. Fig. 39: Growth record preservation in the histological dorsal rib cross-section of *Brontosaurus excelsus* (YPM VP 001980). **A**: Polarized light photograph. Green arrows indicate growth marks. Note that some of the growth marks are only preserved as polish lines not visible under the microscope. Scale bar equals 500 µm. **B**: Drawing of the visible growth marks and the secondary osteons influencing the LAGs by destroying or tracing them marked in black. Polish lines are marked in red.

***Brontosaurus excelsus* (YPM VP 001981)**

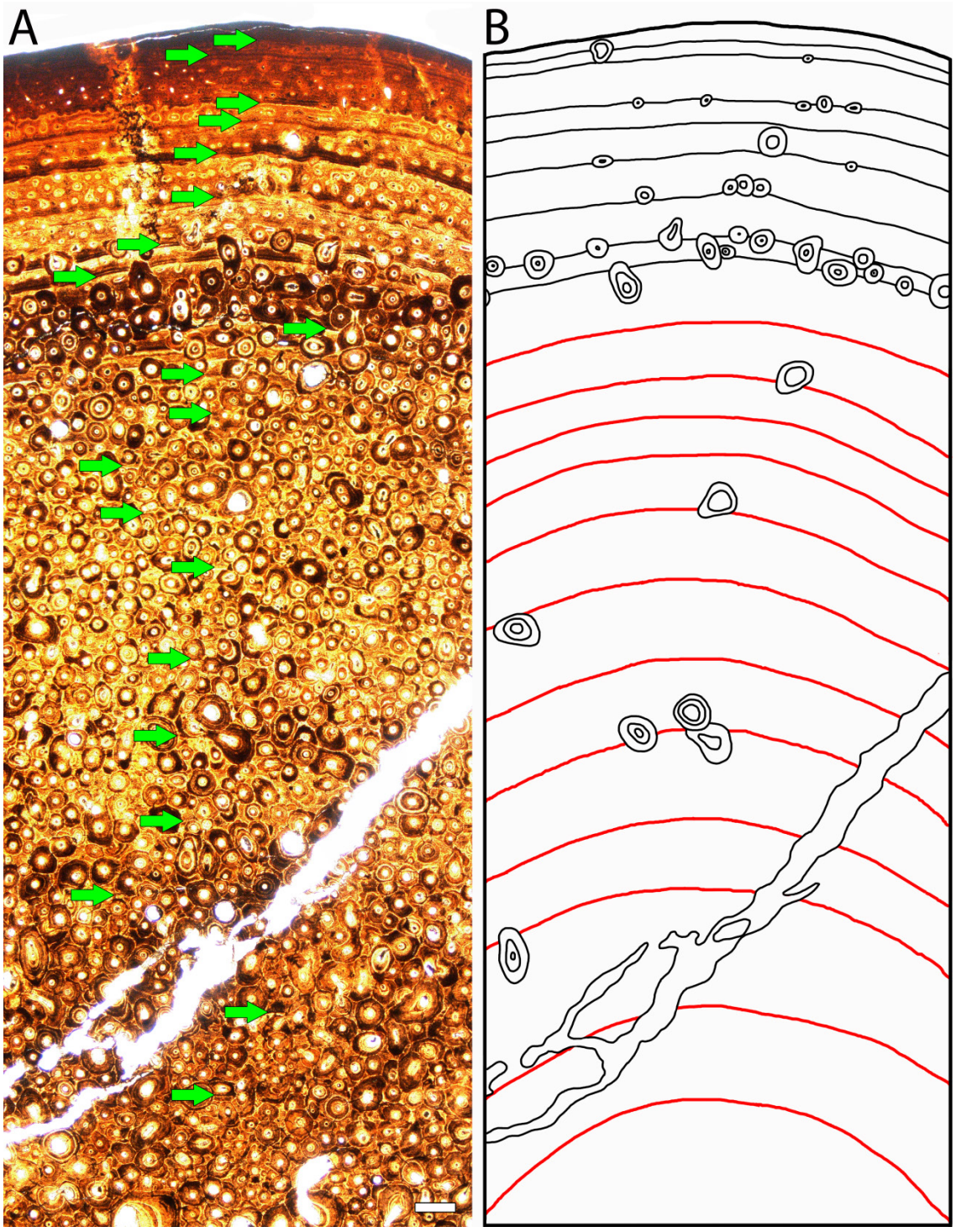

S.I. Fig. 40: Growth record preservation in the histological dorsal rib cross-section of *Brontosaurus excelsus* (YPM VP 001981). **A**: Normal light photograph. Green arrows indicate growth marks. Note that some of the growth marks are only preserved as polish lines not visible under the microscope. Scale bar equals 500 µm. **B**: Drawing of the visible growth marks and the secondary osteons influencing the LAGs by destroying or tracing them marked in black. Polish lines are marked in red.

Apatosaurinea indet. (BYU 18531)

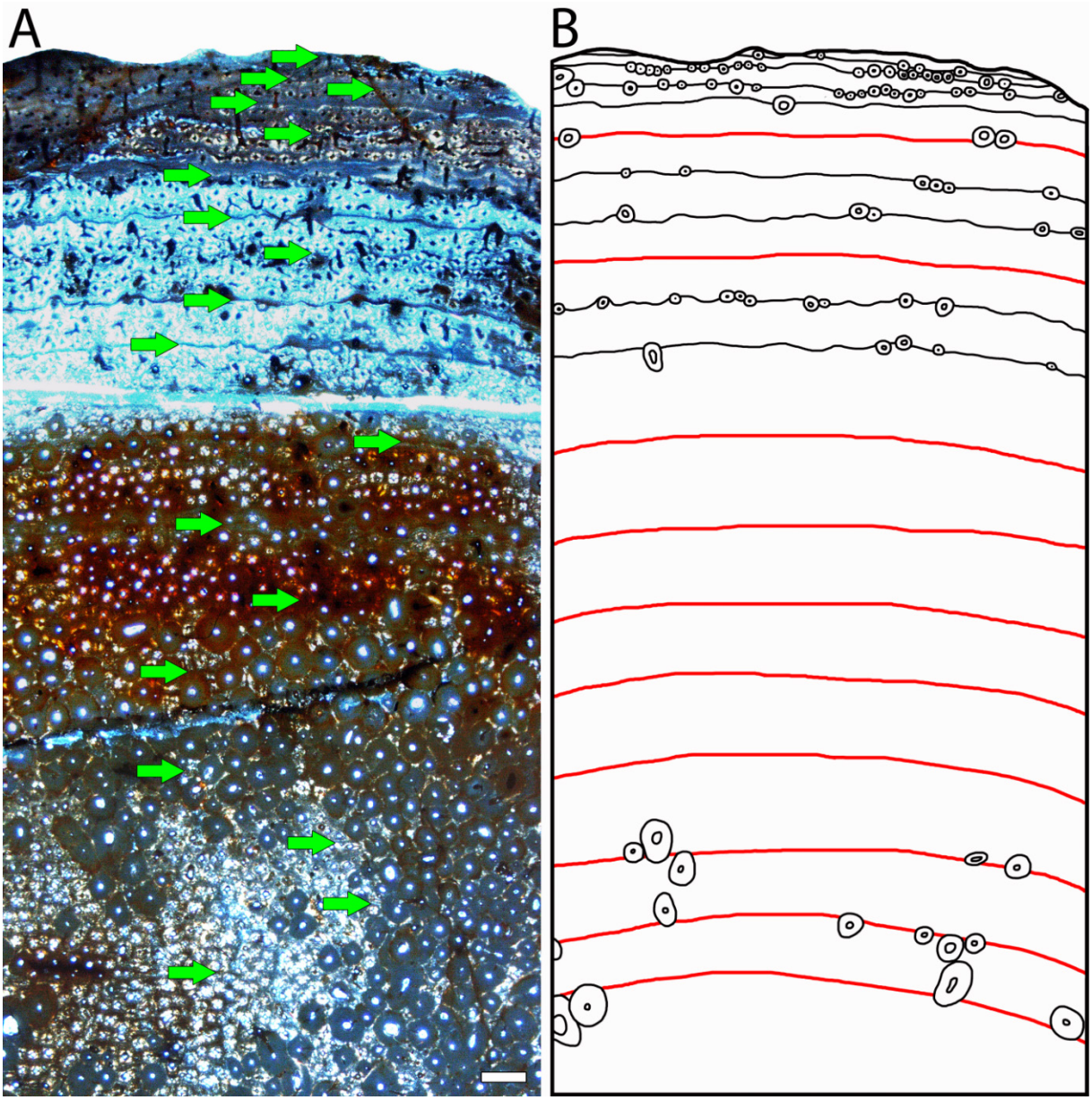

S.I. Fig. 41: Growth record preservation in the histological dorsal rib cross-section of Apatosaurinae indet. (BYU 18531). **A**: Polarized light photograph. Green arrows indicate growth marks. Note that the innermost growth marks are only preserved as modulations or polish lines not visible under the microscope. Scale bar equals 500 µm. **B**: Drawing of the visible growth marks and the secondary osteons influencing the LAGs by destroying or tracing them marked in black. Polish lines and modulations are marked in red.

***Galeamopus pabsti* (SMA 0011)**

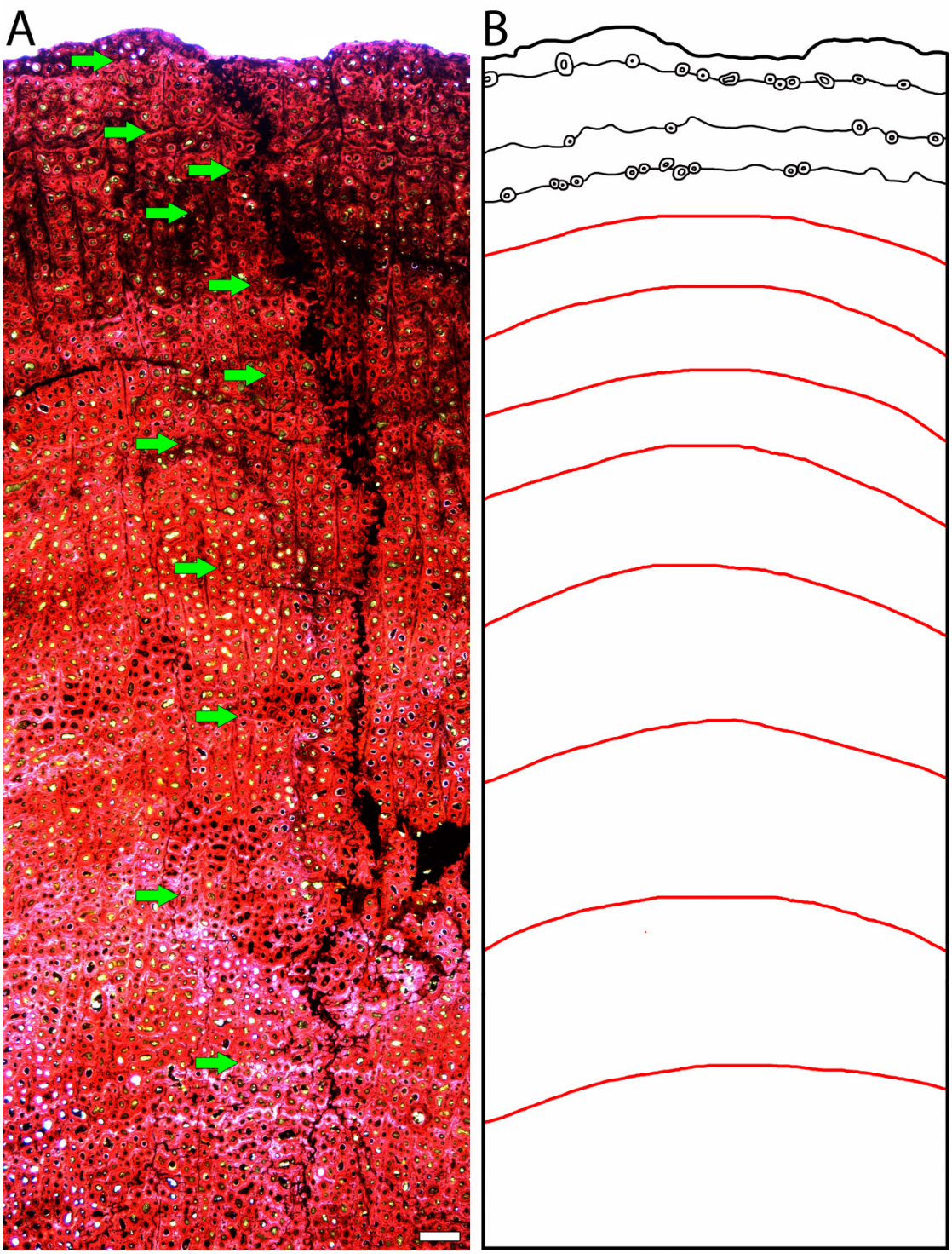

S.I. Fig. 42: Growth record preservation in the histological dorsal rib cross-section of *Galeamopus pabsti* (SMA 0011). **A**: Polarized light photograph. Green arrows indicate growth marks. Note that most growth marks are preserved as modulations or polish lines not visible under the microscope. Scale bar equals 500 µm. **B**: Drawing of the visible LAGs and the secondary osteons influencing them by destroying or tracing them (marked in black). Polish lines and modulations are marked in red.

***Diplodocus hallorum* (NMMNH P 3690)**

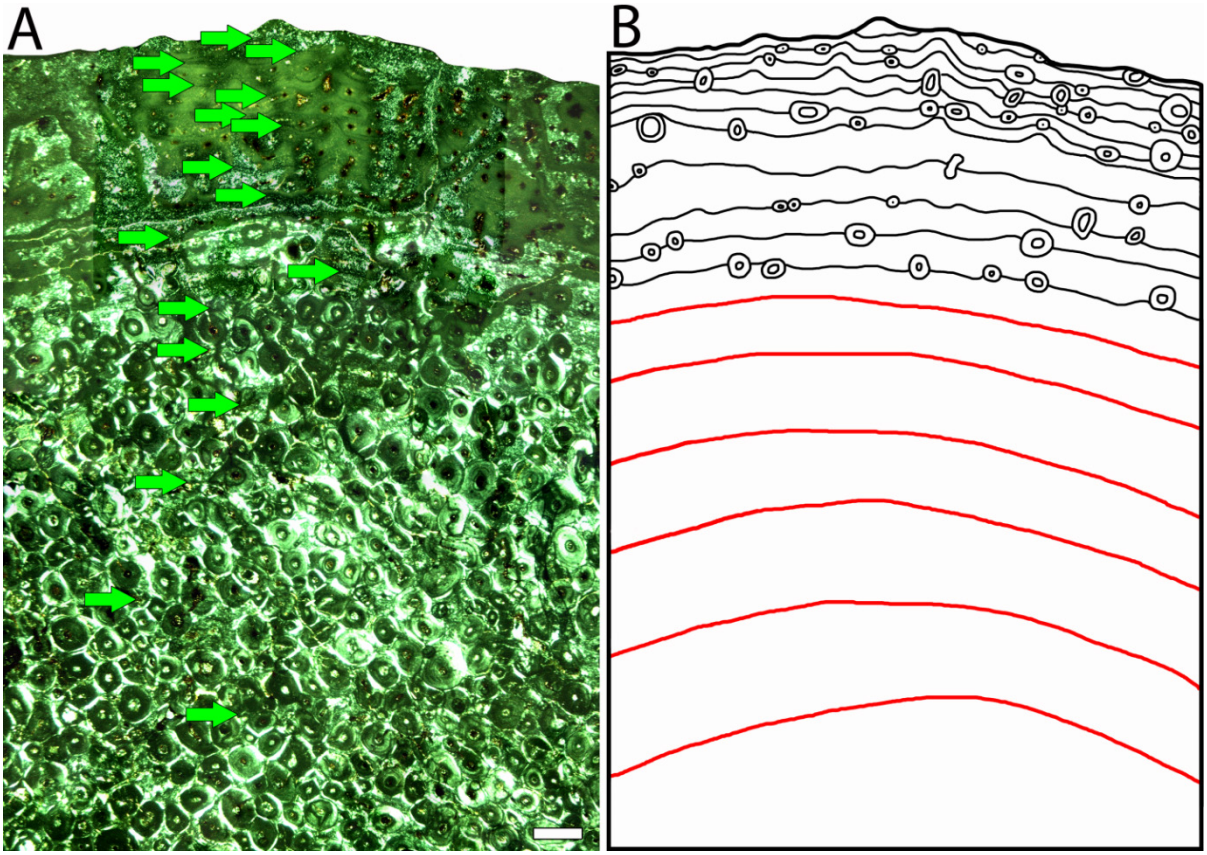

S.I. Fig. 43: Growth record preservation in the histological dorsal rib cross-section of *Diplodocus hallorum* (NMMNH P 3690). **A**: Polarized light photograph. Green arrows indicate growth marks. Note that the innermost growth marks are only preserved as modulations or polish lines not visible under the microscope. Scale bar equals 500 µm. **B**: Drawing of the visible growth marks and the secondary osteons influencing the LAGs by destroying or tracing them marked in black. Polish lines and modulations are marked in red.

***Diplodocus carnegii* (CM 94)**

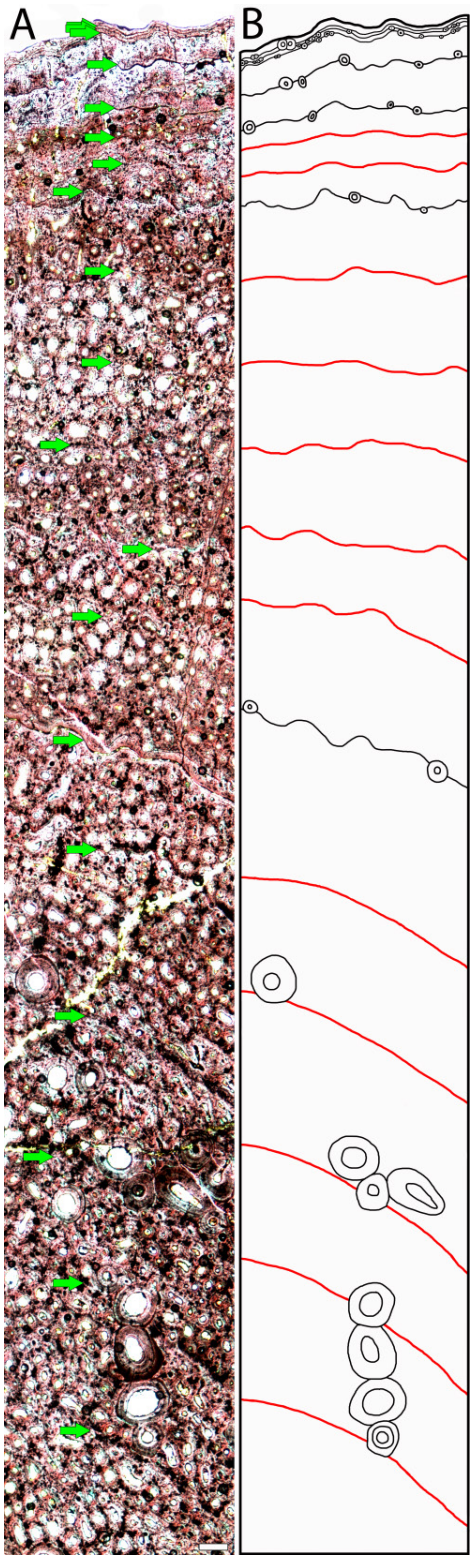

S.I. Fig. 44: Growth record preservation in the histological dorsal rib cross-section of *Diplodocus carnegii* (CM 94). **A**: Normal light photograph. Green arrows indicate growth marks. Note that the innermost growth marks are only preserved as modulations or polish lines not developed as LAGs and sparsely visible under the microscope. Scale bar equals 500 µm. **B**: Drawing of the visible growth marks and the secondary osteons influencing the LAGs by destroying or tracing them (marked in black). Polish lines and modulations (marked in red).

***Diplodocus* sp. MOR 592**

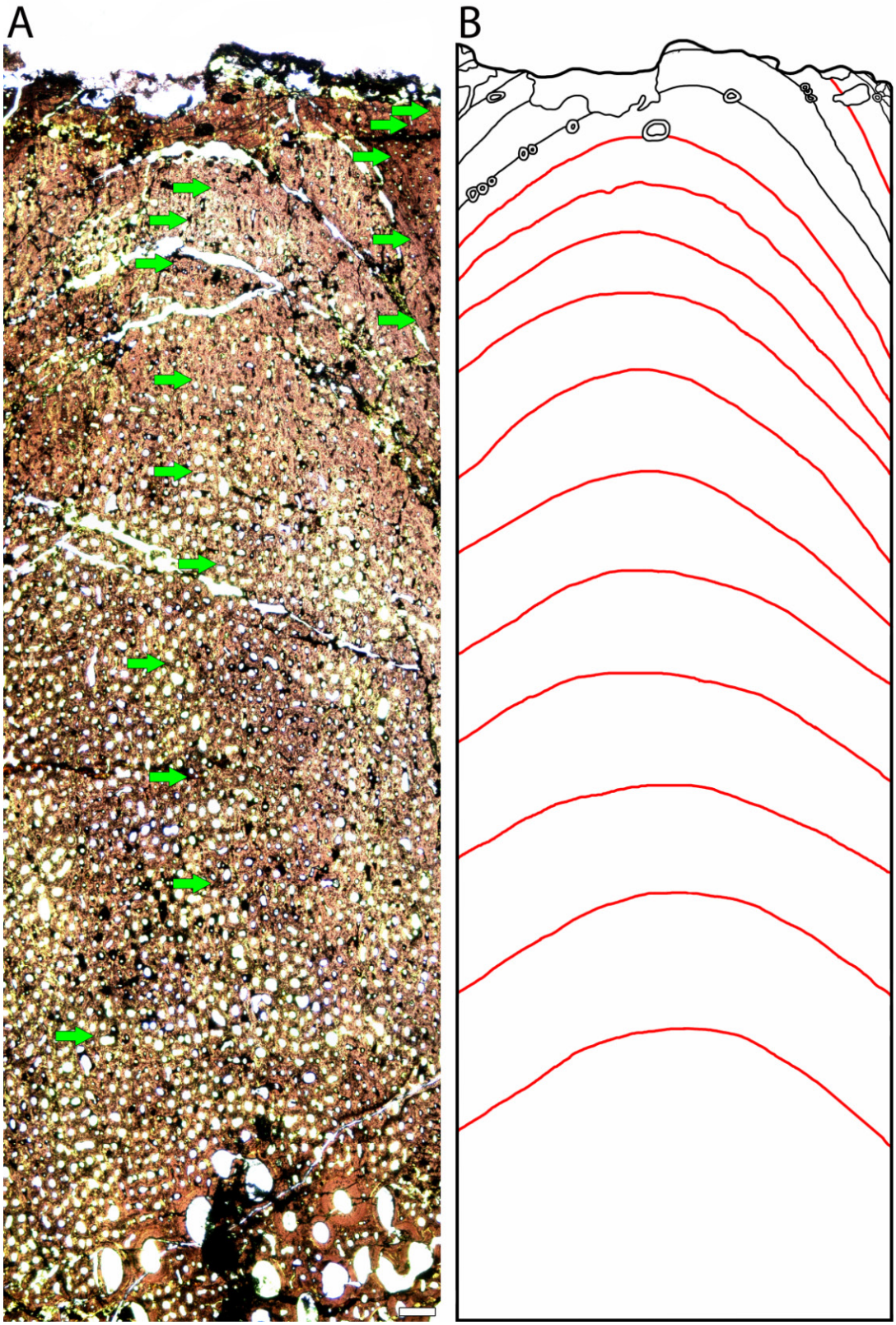

S.I. Fig. 45: Growth record preservation in the histological dorsal rib cross-section of *Diplodocus* sp. (MOR 592). **A**: Normal light photograph. Green arrows indicate growth marks. Note that most growth marks are only preserved as modulations or polish lines not visible under the microscope. Scale bar equals 500 µm. **B**: Drawing of the visible growth marks and the secondary osteons influencing the LAGs by destroying or tracing them (marked in black). Polish lines and modulations (marked in red).

***Barosaurus lentus* (YPM VP 000429)**

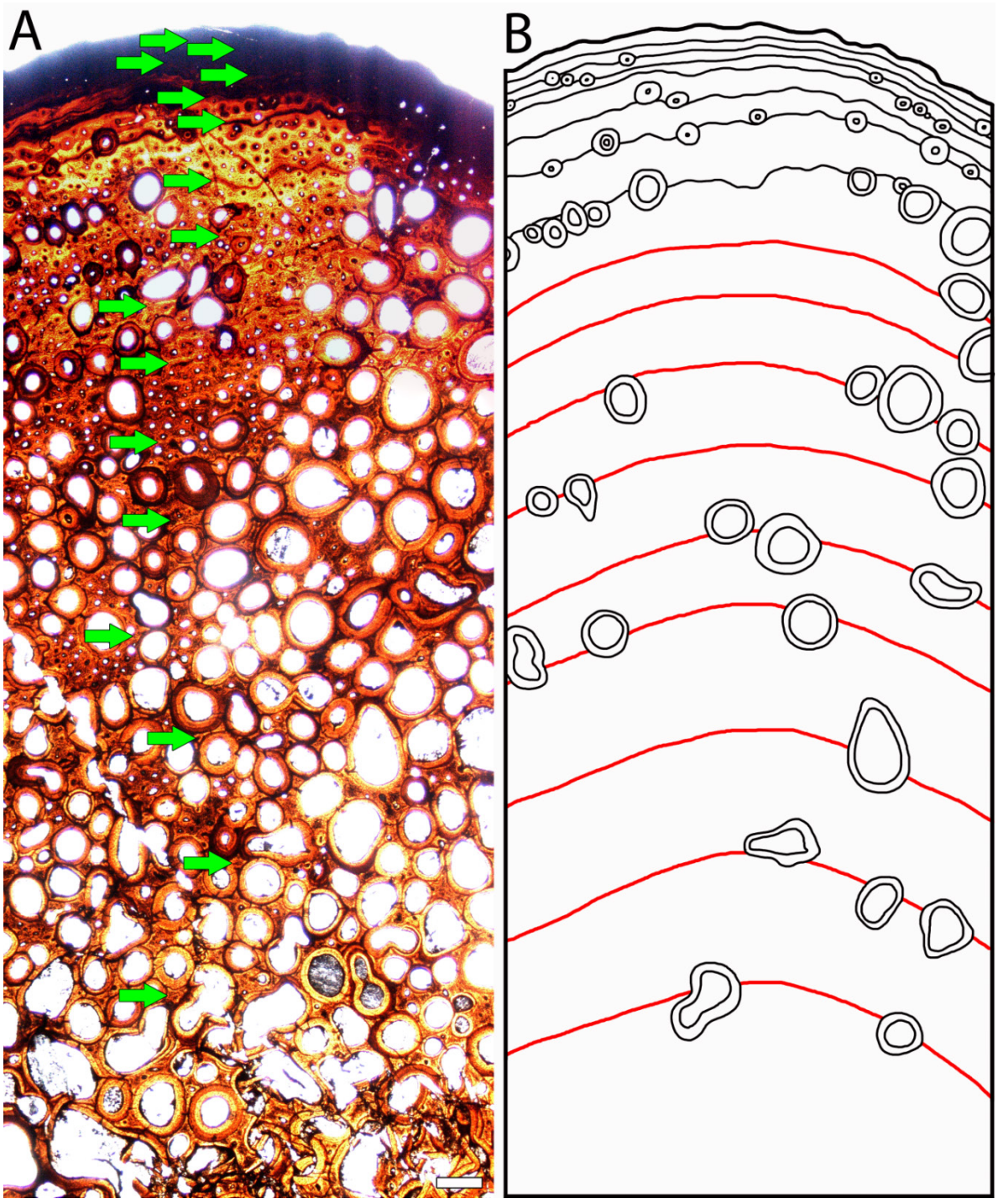

S.I. Fig. 46: Growth record preservation in the histological dorsal rib cross-section of *Barosaurus lentus* (YPM VP 000429). **A**: Normal light photograph. Green arrows indicate growth marks. Note that most growth marks are only preserved as modulations or polish lines not visible under the microscope. Scale bar equals 500 µm. **B**: Drawing of the visible growth marks and the secondary osteons influencing the LAGs by destroying or tracing them (marked in black). Polish lines and modulations (marked in red).

Diplodocine indet. (SMA 0013)

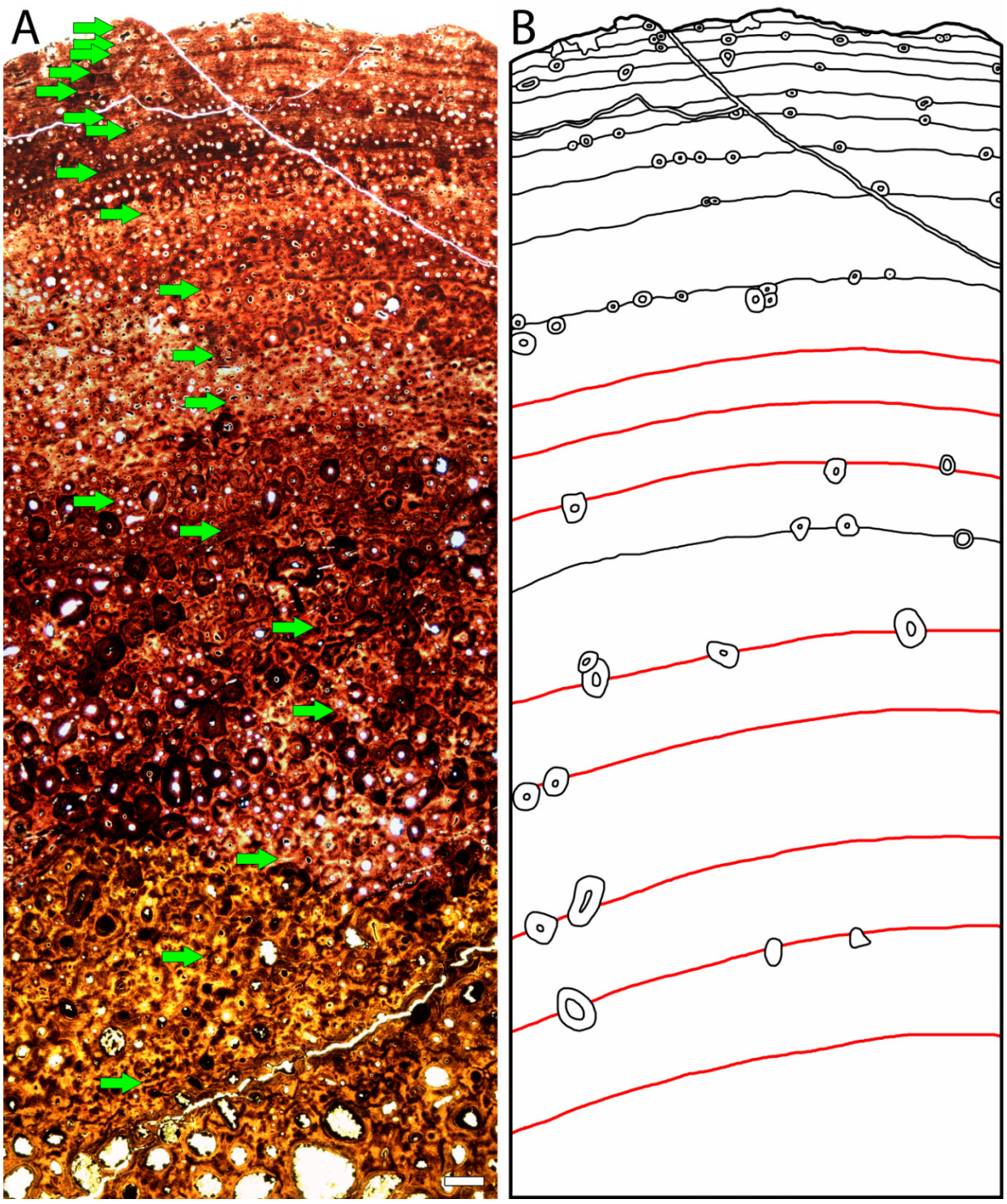

S.I. Fig. 47: Growth record preservation in the histological dorsal rib cross-section of Diplodocine indet. (SMA 0013). **A**: Normal light photograph. Green arrows indicate growth marks. Note that most of the inner growth marks are only preserved as modulations or polish lines not visible under the microscope. Scale bar equals 500 µm. **B**: Drawing of the visible growth marks and the secondary osteons influencing the LAGs by destroying or tracing them (marked in black). Polish lines and modulations (marked in red).

Diplodocine indet. (ML 418)

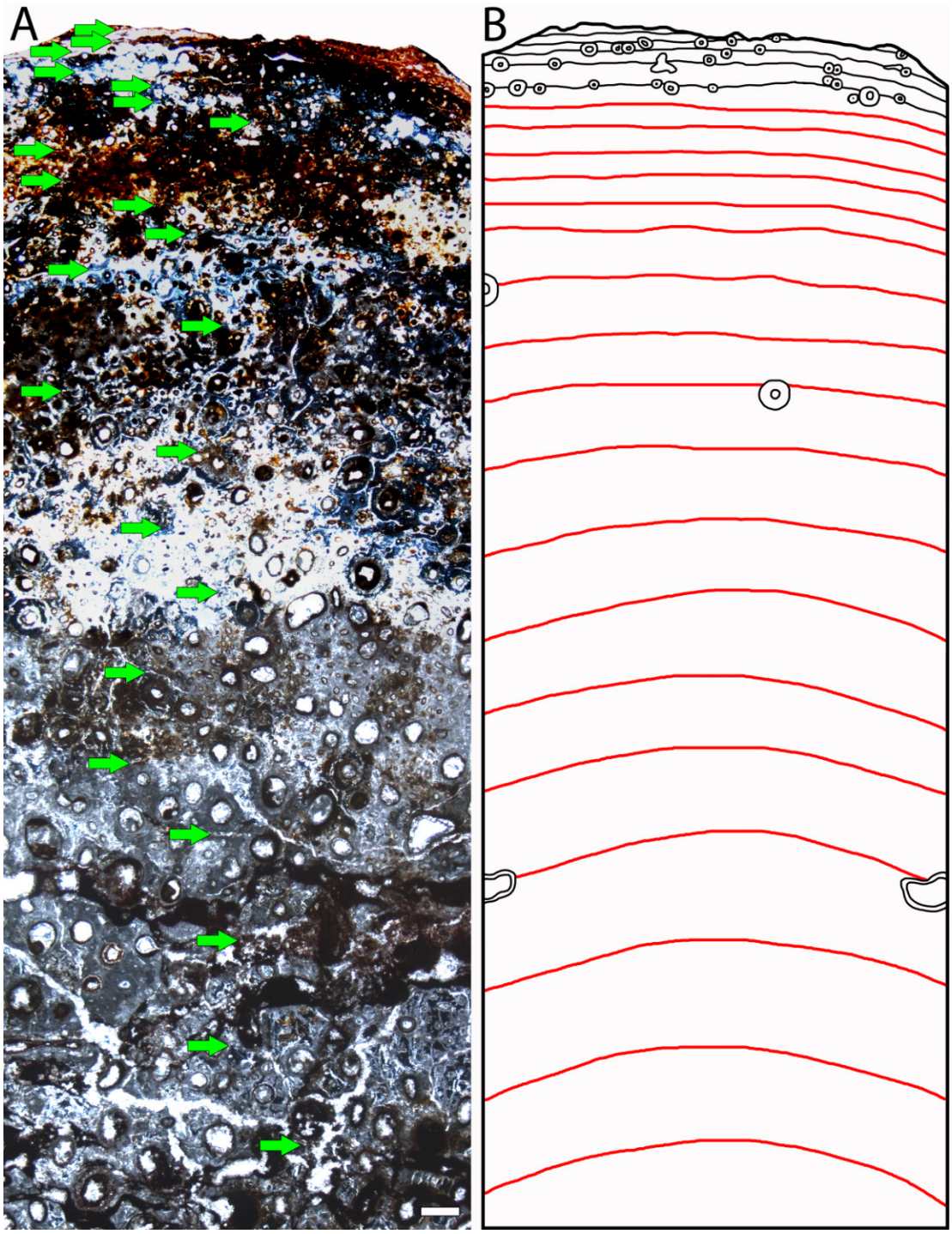

S.I. Fig. 48: Growth record preservation in the histological dorsal rib cross-section of Diplodocine indet. (ML 418). **A**: Polarized light photograph. Green arrows indicate growth marks. Note that most of the inner growth marks are only preserved as modulations or polish lines sparsely visible under the microscope. Scale bar equals 500 µm. **B**: Drawing of the visible growth marks and the secondary osteons influencing the LAGs by destroying or tracing them (marked in black). Polish lines and modulations (marked in red).

Diplodocinae indet. (MOR 790)

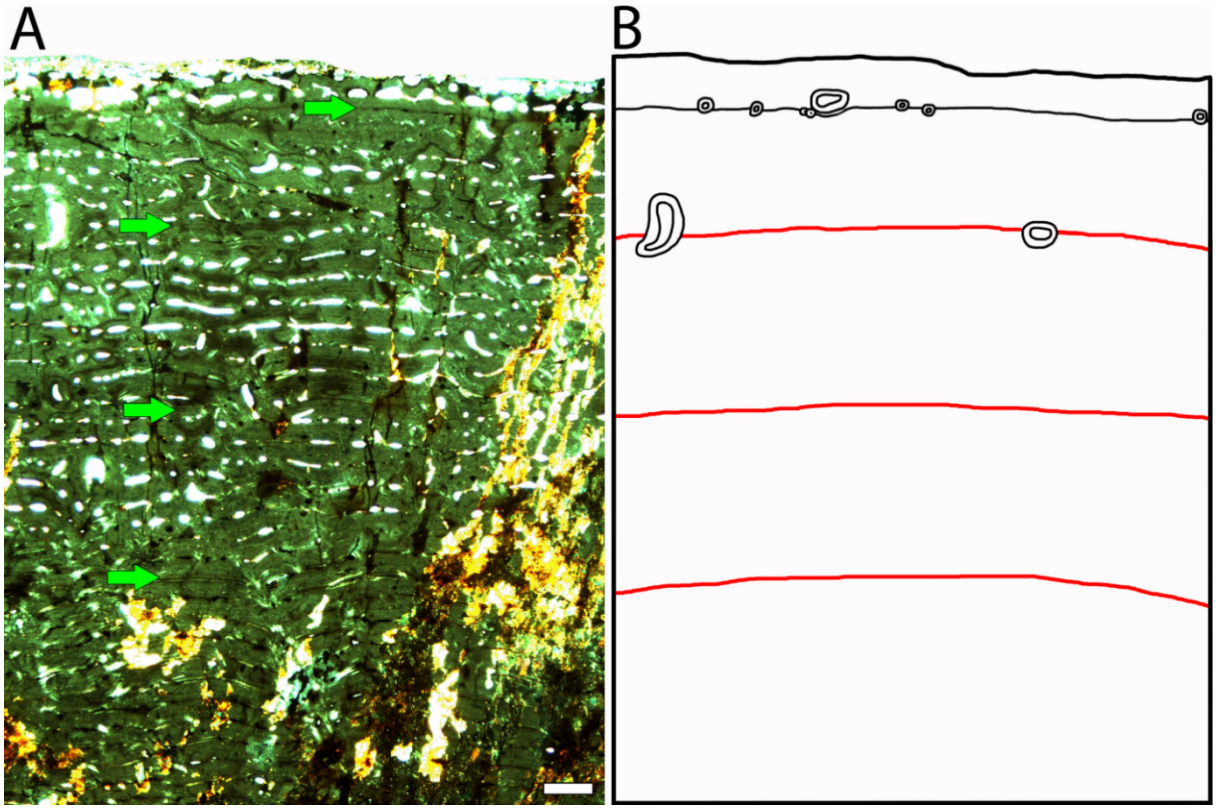

S.I. Fig. 49: Growth record preservation in the histological dorsal rib cross-section of Diplodocinae indet. (MOR 790). **A**: Polarized light photograph. Green arrows indicate growth marks. Note that the inner growth marks are only preserved as modulations or polish lines sparsely visible under the microscope. Scale bar equals 500 µm. **B**: Drawing of the visible growth marks and the secondary osteons influencing the LAGs by destroying or tracing them (marked in black). Polish lines and modulations (marked in red).

Diplodocidae indet. (SMA 0008)

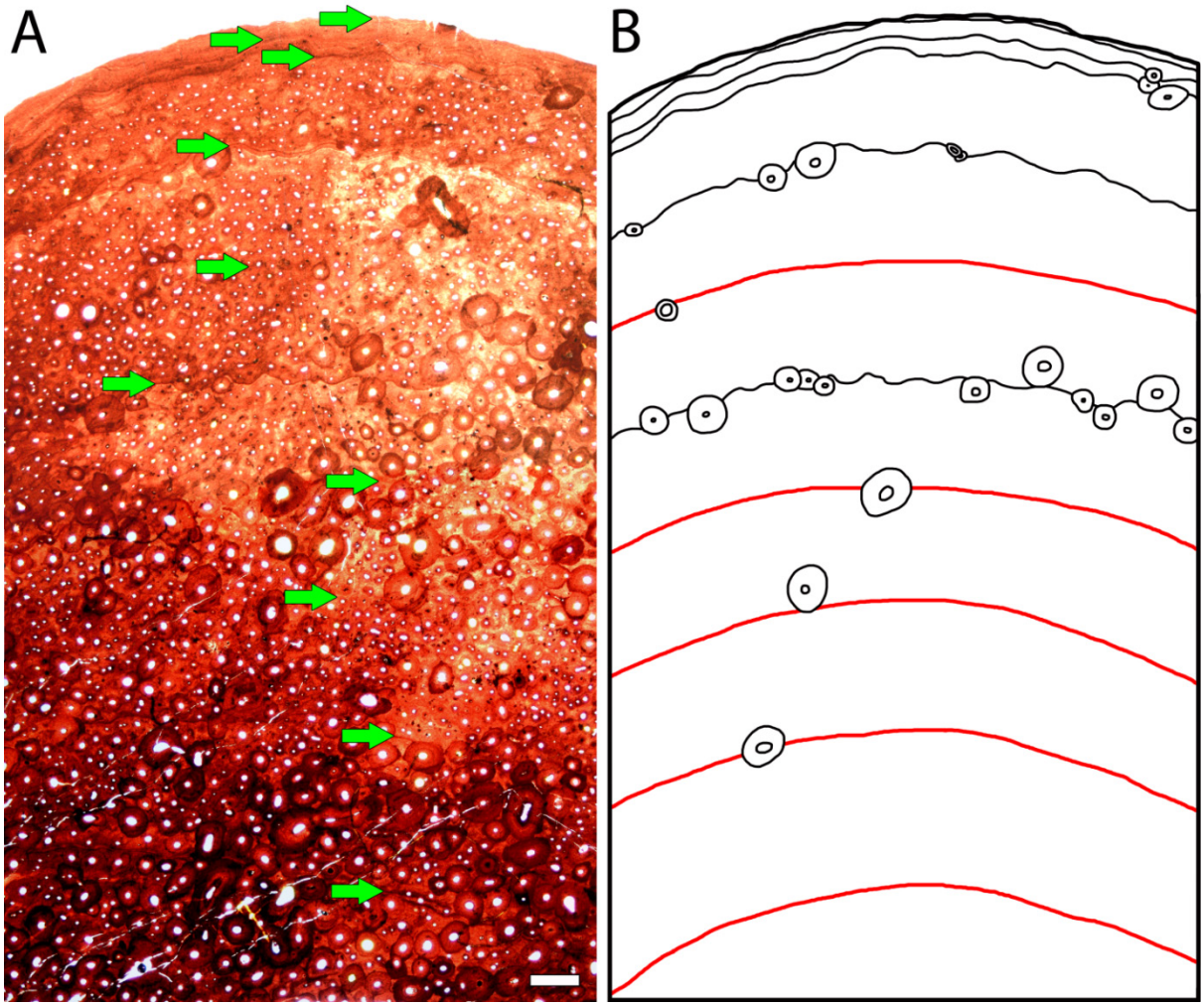

S.I. Fig. 50: Growth record preservation in the histological dorsal rib cross-section of Diplodocidae indet. (SMA 0008). **A**: Polarized light photograph. Green arrows indicate growth marks. Note that the inner growth marks are only preserved as modulations or polish lines sparsely visible under the microscope. Scale bar equals 500 µm. **B**: Drawing of the visible growth marks and the secondary osteons influencing the LAGs by destroying or tracing them (marked in black). Polish lines and modulations (marked in red).

Sauropoda indet. (YPM VP 007447)

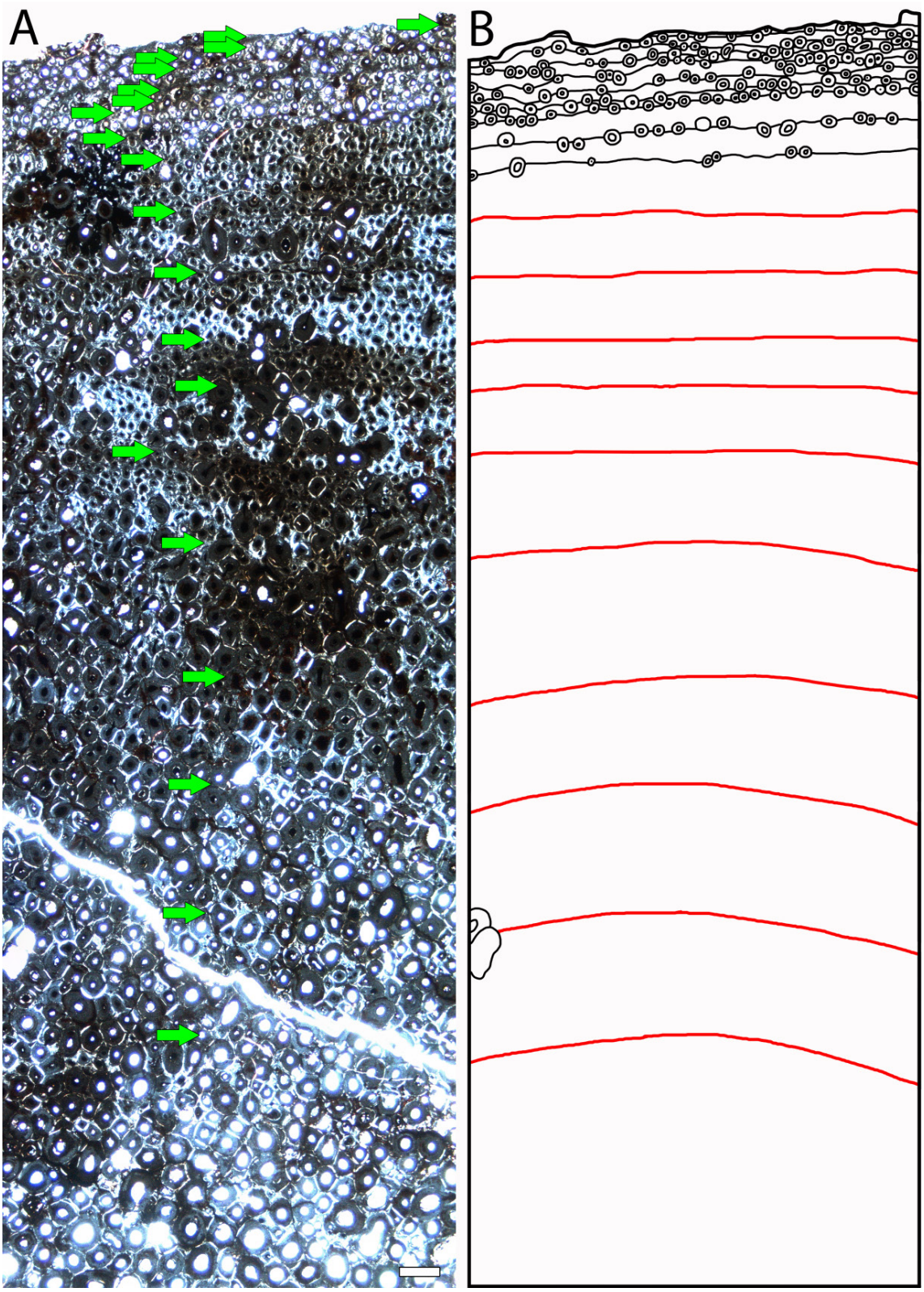

S.I. Fig. 51: Growth record preservation in the histological dorsal rib cross-section of Sauropoda indet. (YPM VP 007447). **A**: Polarized light photograph. Green arrows indicate growth marks. Note that most of the inner growth marks are only preserved as modulations or polish lines not visible under the microscope. Scale bar equals 500 µm. **B**: Drawing of the visible growth marks and the secondary osteons influencing the LAGs by destroying or tracing them (marked in black). Polish lines and modulations

Sauropoda indet. (YPM VP 060120)

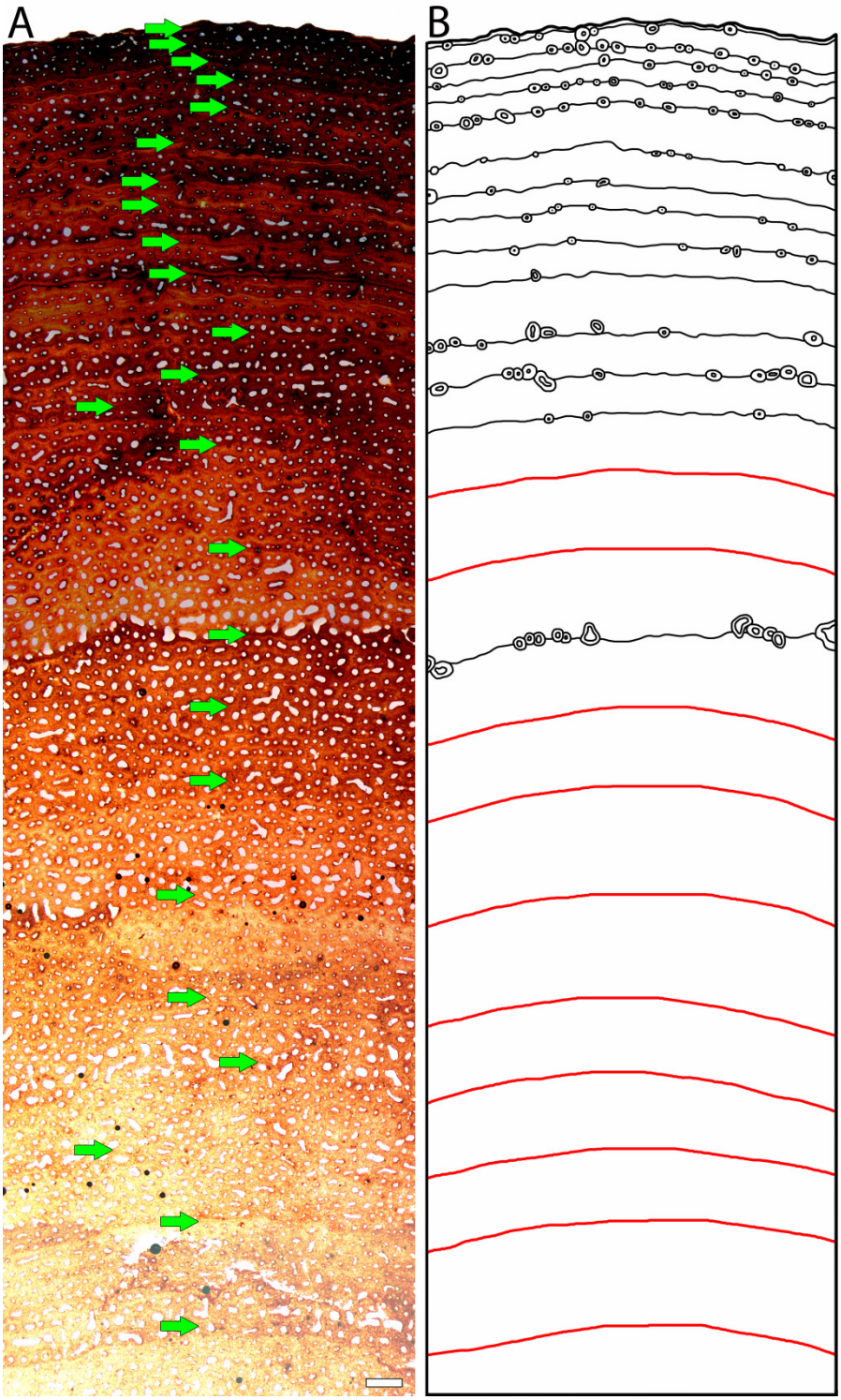

S.I. Fig. 52: Growth record preservation in the histological dorsal rib cross-section of Sauropoda indet. (YPM VP 060120). **A**: Normal light photograph. Green arrows indicate growth marks. Note that most of the inner growth marks are not developed as LAGs but preserved as modulations or polish lines best visible in macroscopic view. Scale bar equals 500 µm. **B**: Drawing of the visible growth marks and the secondary osteons influencing the LAGs by destroying or tracing them (marked in black). Polish lines and modulations

Sauropoda indet. (YPM VP 001911)

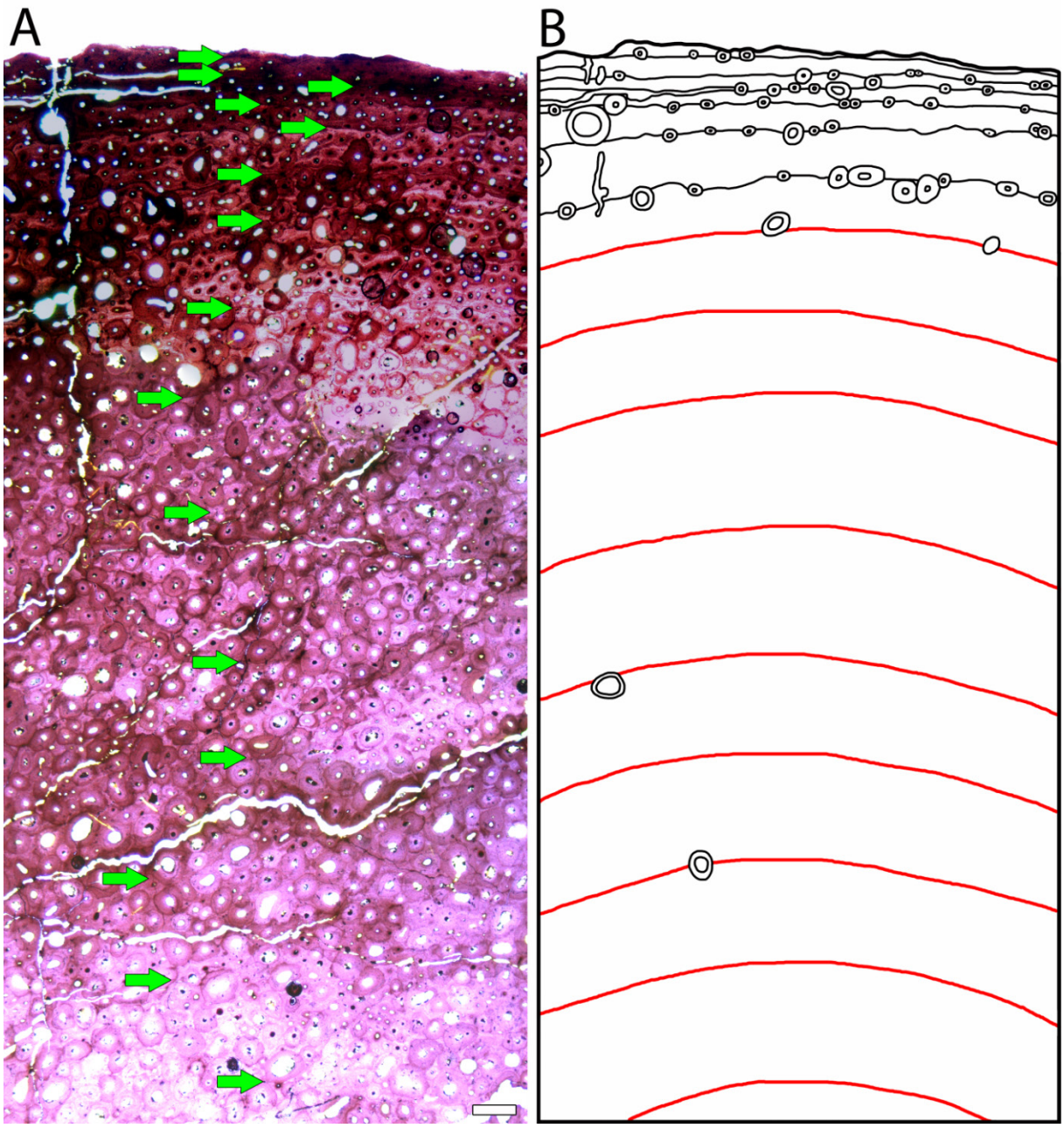

S.I. Fig. 53: Growth record preservation in the histological dorsal rib cross-section of Sauropoda indet. (YPM VP 001911). **A**: Polarized light photograph. Green arrows indicate growth marks. Note that most of the inner growth marks are only preserved as modulations or polish lines not visible under the microscope. Scale bar equals 500 µm. **B**: Drawing of the visible growth marks and the secondary osteons influencing the LAGs by destroying or tracing them (marked in black). Polish lines and modulations (marked in red).

Sauropoda indet. (Sa 22)

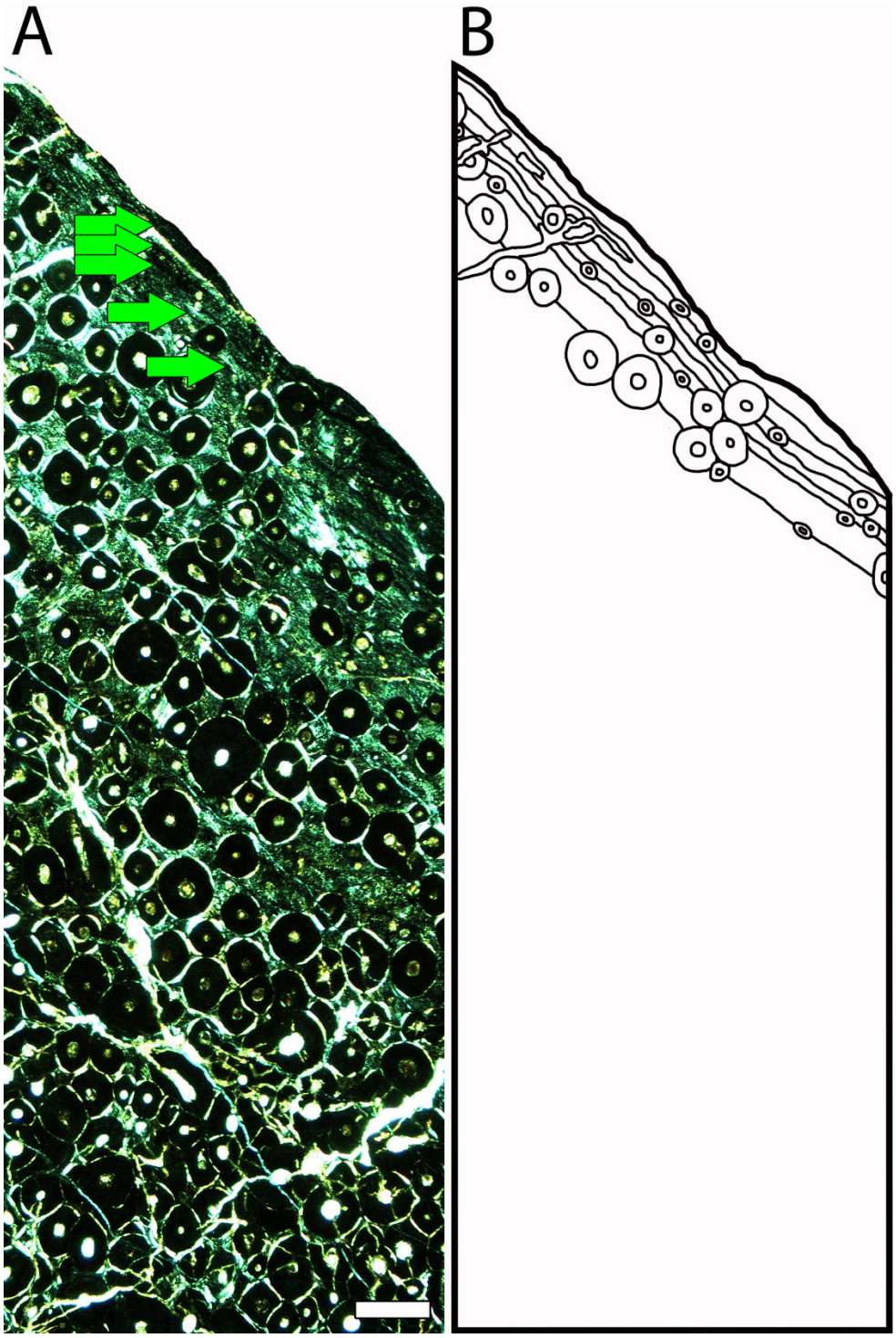

S.I. Fig. 54: Growth record preservation in the histological dorsal rib cross-section of Sauropoda indet. (Sa 22). **A**: Polarized light photograph. Green arrows indicate growth marks. Note that only the outermost cortex shows remains of the EFS and one additional cycle due to intense remodelling. Scale bar equals 500 µm. **B**: Drawing of the visible growth marks and the secondary osteons influencing the LAGs by destroying or tracing them (marked in black).

Sauropoda indet. (Sa 14)

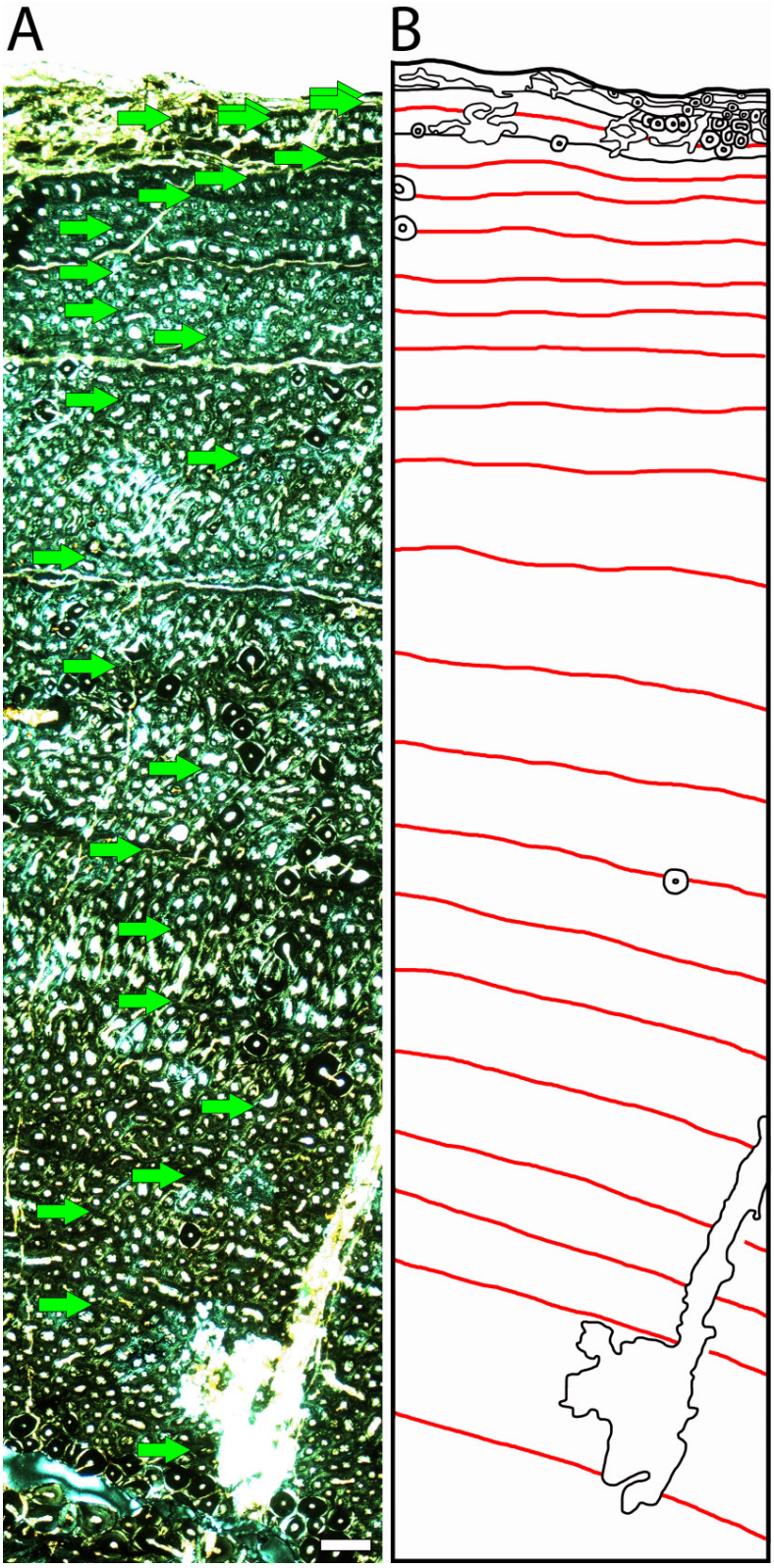

S.I. Fig. 55: Growth record preservation in the histological dorsal rib cross-section of Sauropoda indet. (Sa 14). **A**: Polarized light photograph. Green arrows indicate growth marks. Note that most of the inner growth marks are only preserved as modulations best visible in macroscopic view. Scale bar equals 500 µm. **B**: Drawing of the visible growth marks and the secondary osteons influencing the LAGs by destroying or tracing them (marked in black). Modulations are marked in red.

Sauropoda indet. (Sa 21)

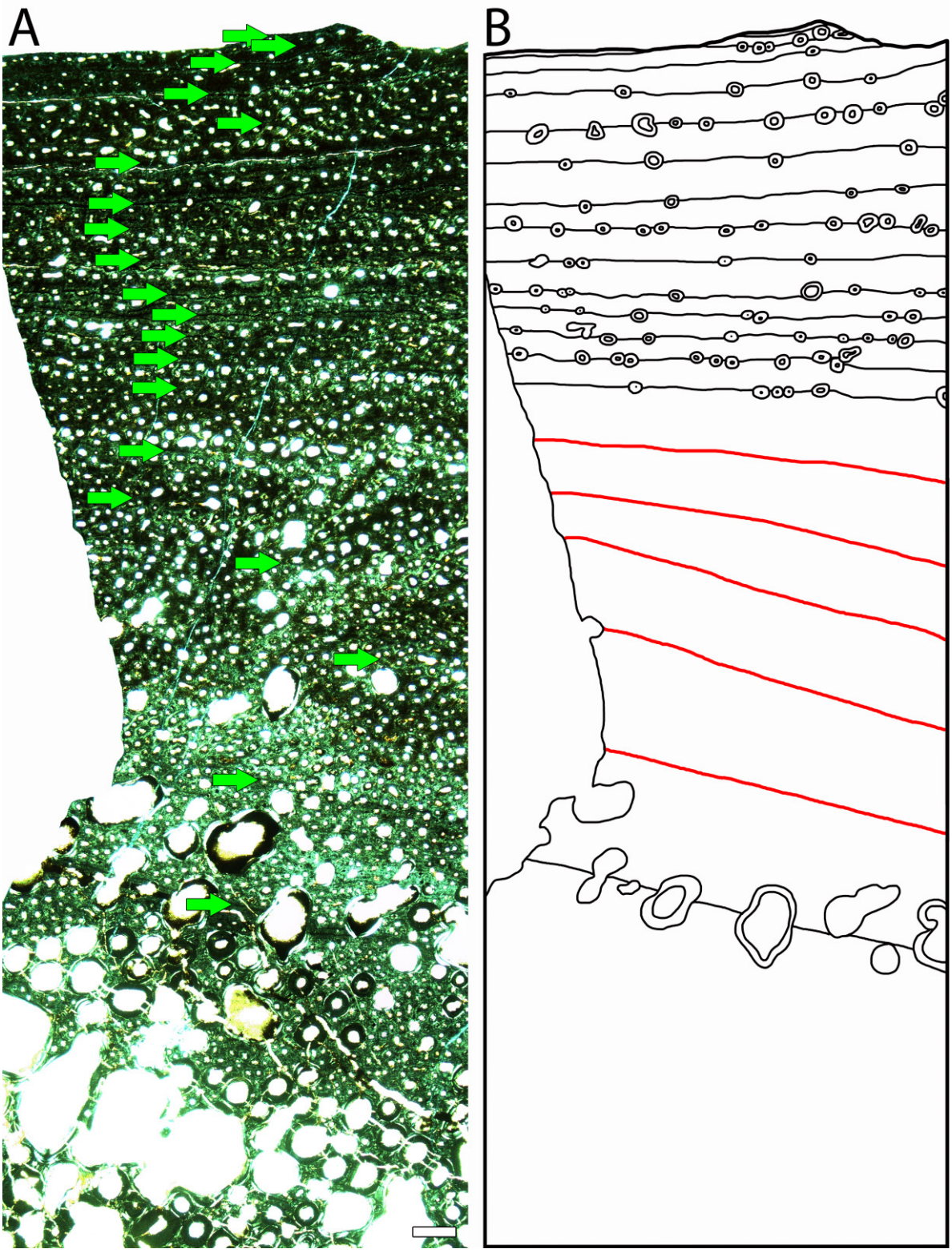

S.I. Fig. 56: Growth record preservation in the histological dorsal rib cross-section of Sauropoda indet. (Sa 21). **A**: Polarized light photograph. Green arrows indicate growth marks. Note that most of the inner growth marks are only preserved as modulations best visible in macroscopic view. Scale bar equals 500 µm. **B**: Drawing of the visible growth marks and the secondary osteons influencing the LAGs by destroying or tracing them (marked in black). Modulations are marked in red.

6.9.3. Dorsal rib growth curves of sauropods

The following figures show the dorsal rib growth curves of all individuals sampled for this study that are not figured in the main manuscript (excluding specimens showing less than ten cycles like, e.g., early stage juveniles or senescent individuals showing intense remodeling). In each graph measurements start with the first preserved cycle. Blanc spaces at the beginning of the curve indicate the number of missing innermost cycles estimated by retrocalculation. Purple arrows indicate the point of sexual maturity. Black arrows indicate point of skeletal maturity.

Note that the following two samples YPM VP 001901 and YPM VP 001905 most likely represent the same individual based on their remarkably similar growth records.

***Camarasaurus grandis* (YPM VP 001901)**

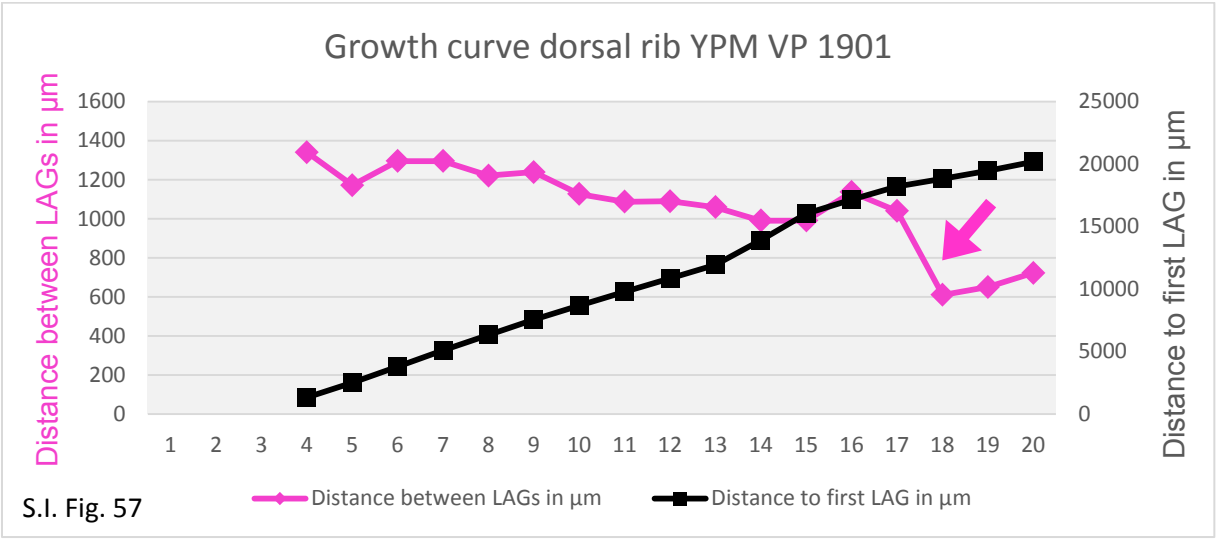

S.I. Fig. 57

***Camarasaurus grandis* (YPM VP 001905)**

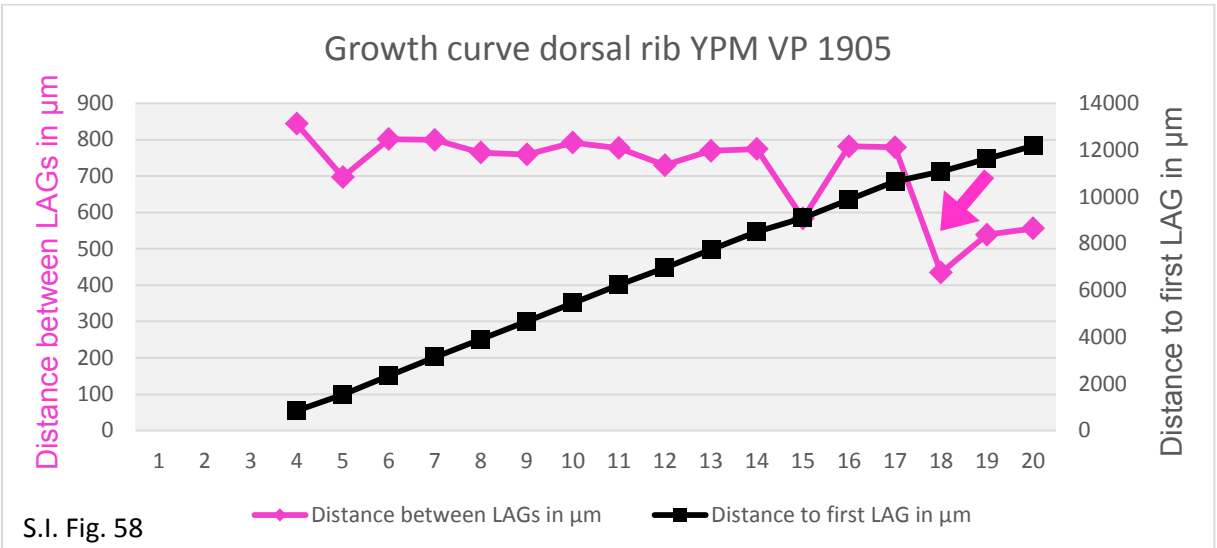

S.I. Fig. 58

***Camarasaurus* sp. (SMA 274)**

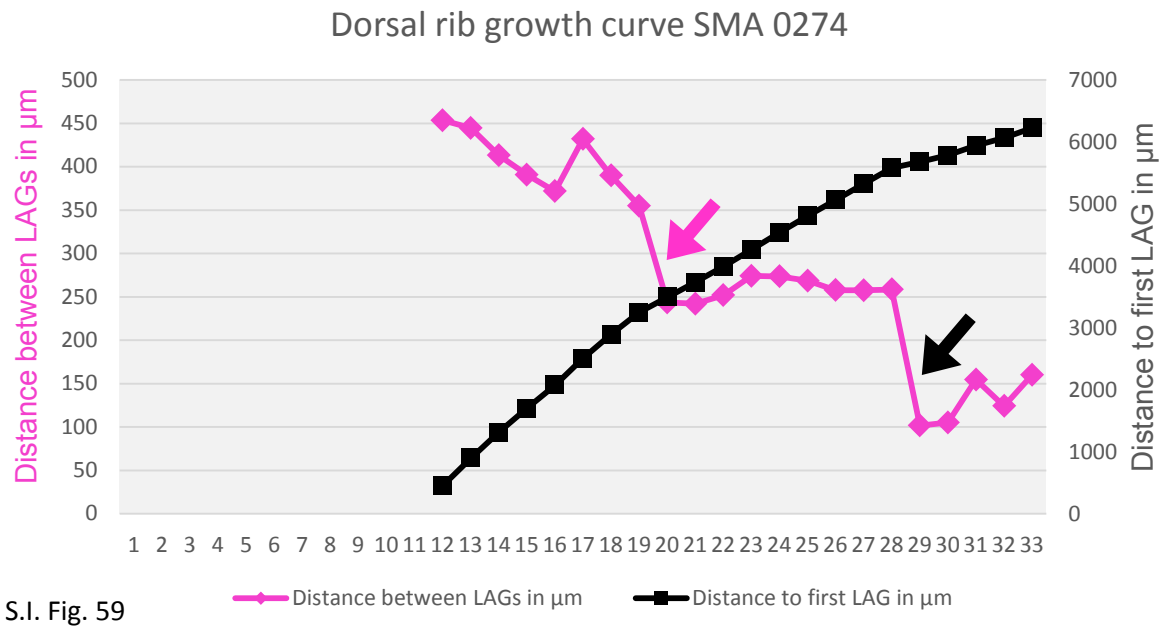

S.I. Fig. 59

***Camarasaurus* sp. (UW 46215)**

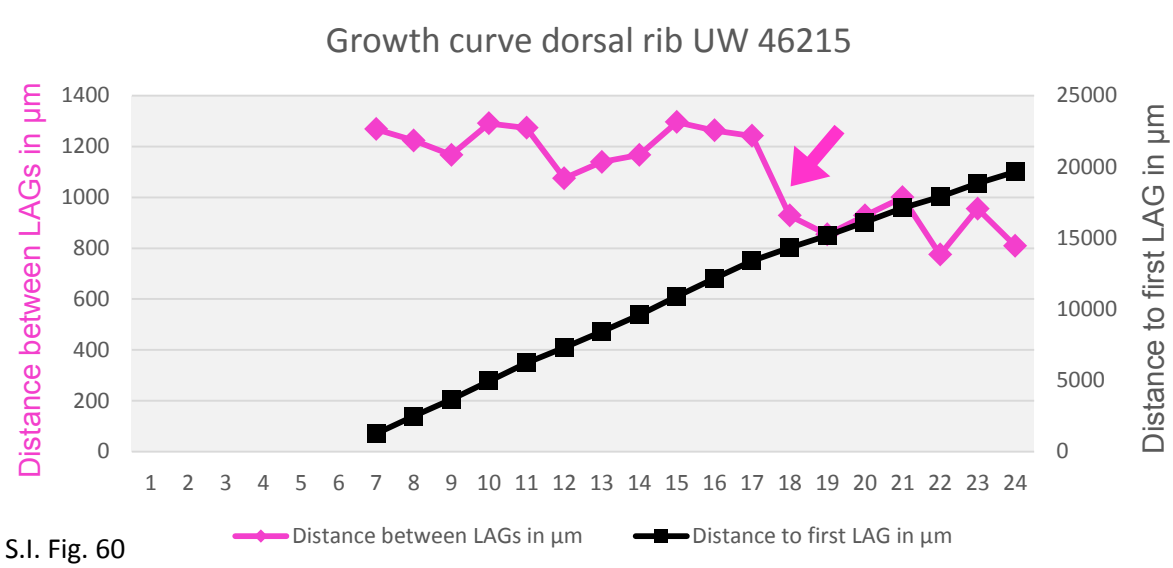

S.I. Fig. 60

***Camarasaurus* sp. (UW 46212)**

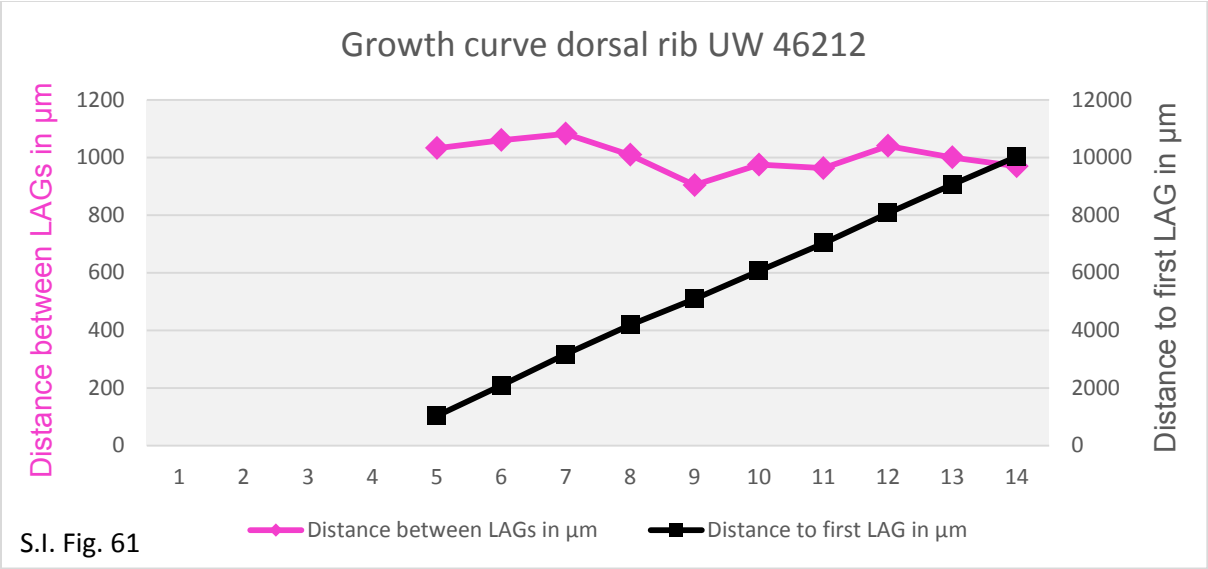

S.I. Fig. 61

***Camarasaurus* sp. (UMNH 24802)**

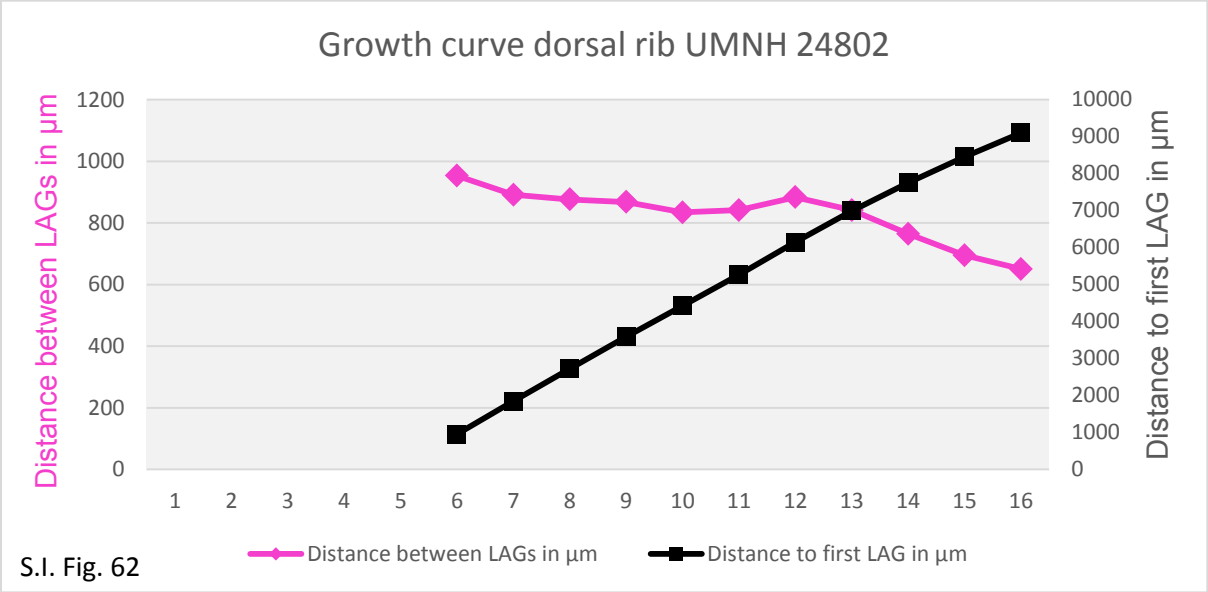

S.I. Fig. 62

Note that the following two samples UMNH 5289 and UMNH 5302 most likely represent the same individual based on their extremely similar growth records.

***Camarasaurus* sp. (UMNH 5289)**

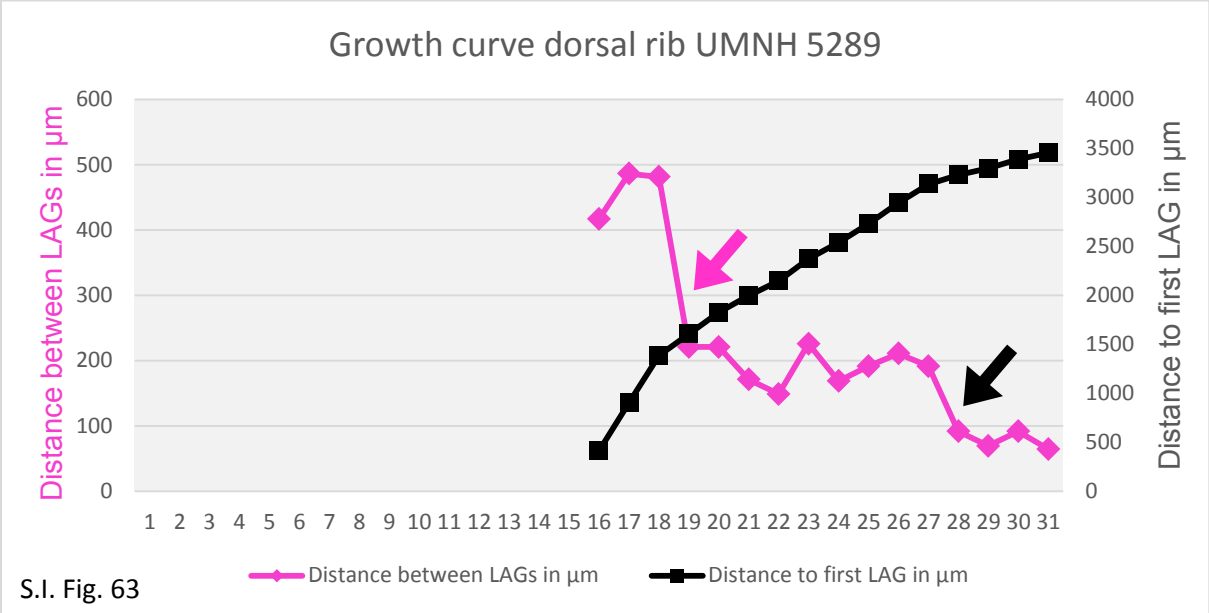

S.I. Fig. 63

***Camarasaurus* sp. (UMNH 5302)**

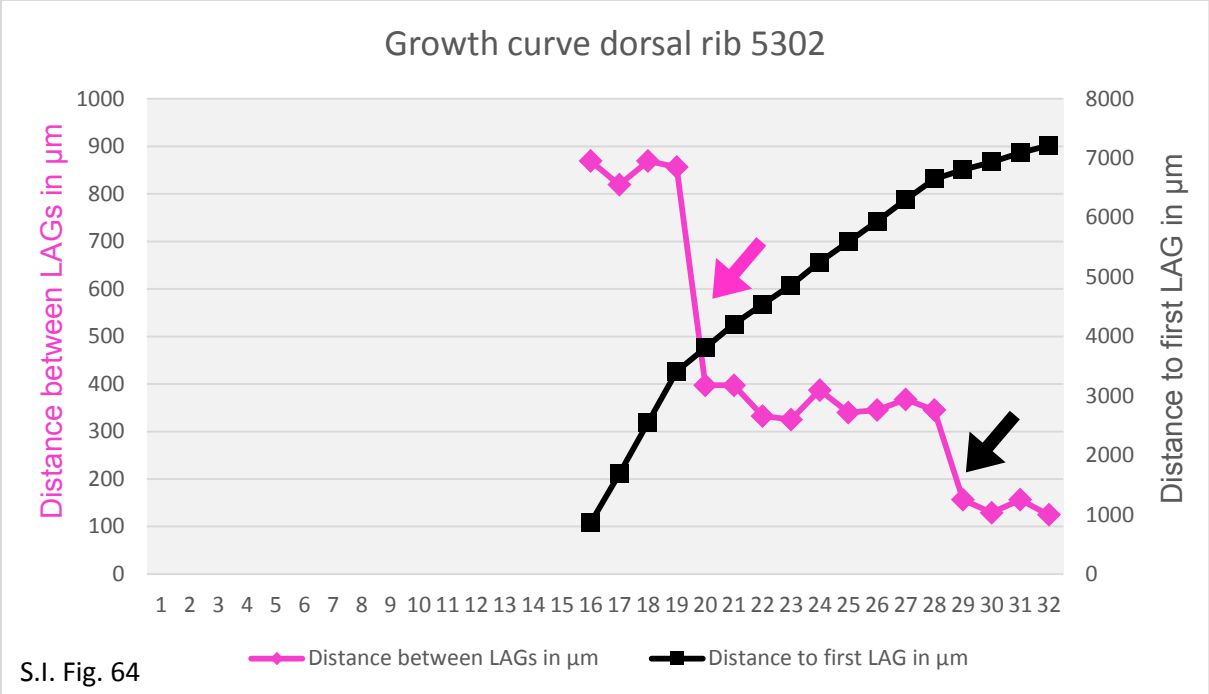

S.I. Fig. 64

Note that the following three samples UMNH 21608, 21606, and 24804 most likely belong to the same individual based on their very similar growth records.

***Camarasaurus* sp. (UMNH 21608)**

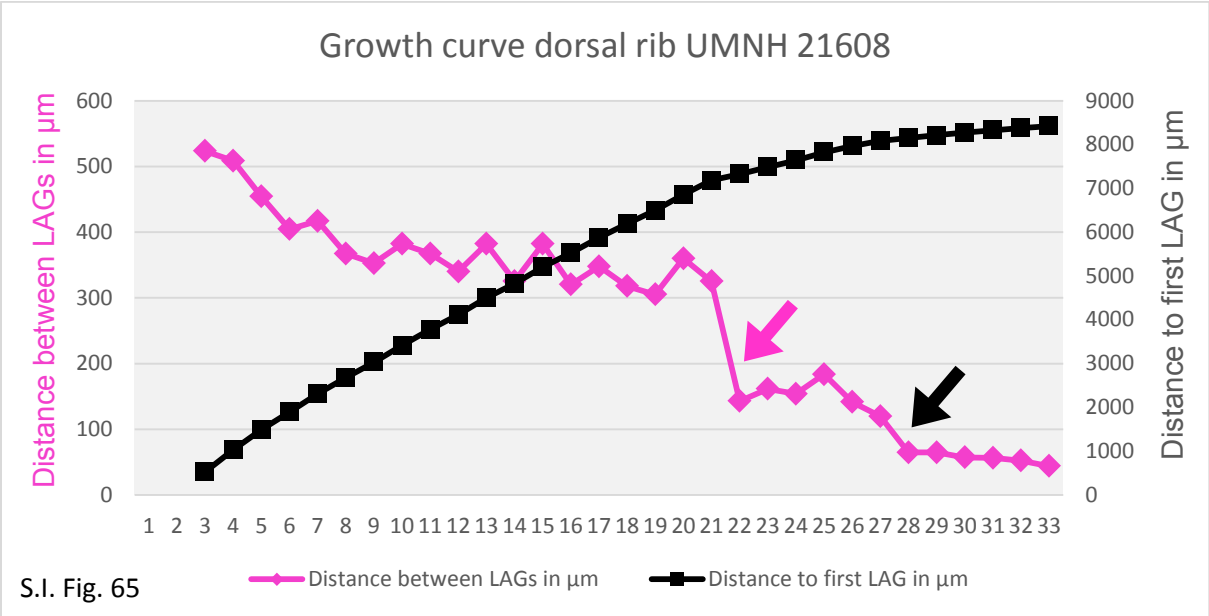

S.I. Fig. 65

***Camarasaurus* sp. (UMNH 21606)**

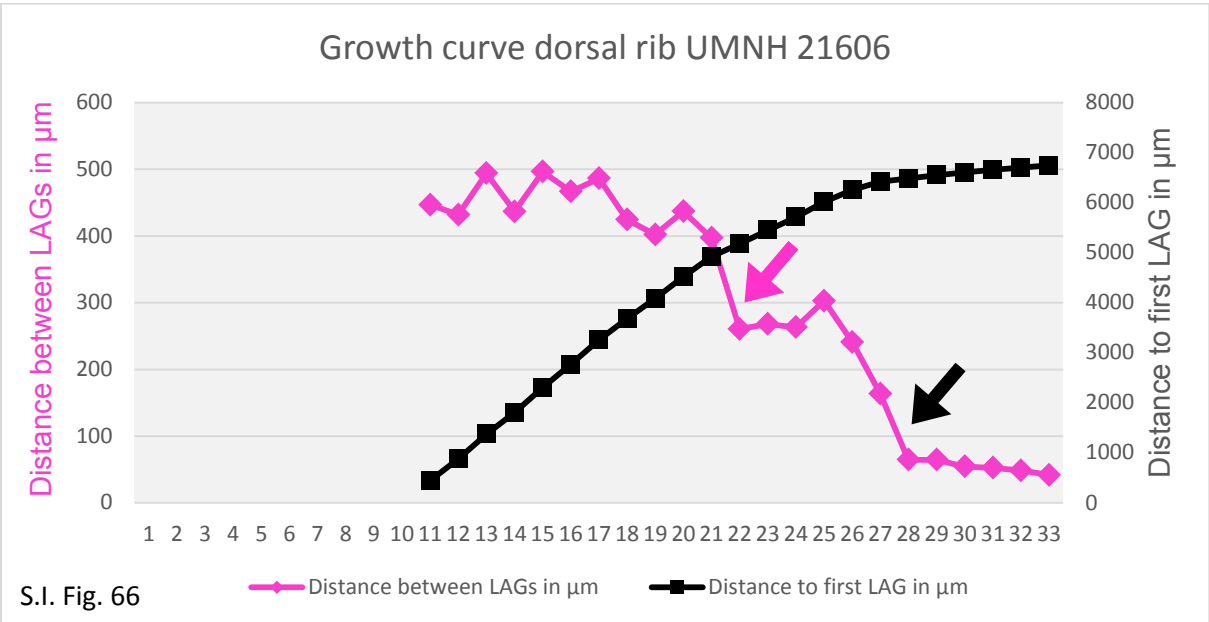

S.I. Fig. 66

***Camarasaurus* sp. (UMNH 24804)**

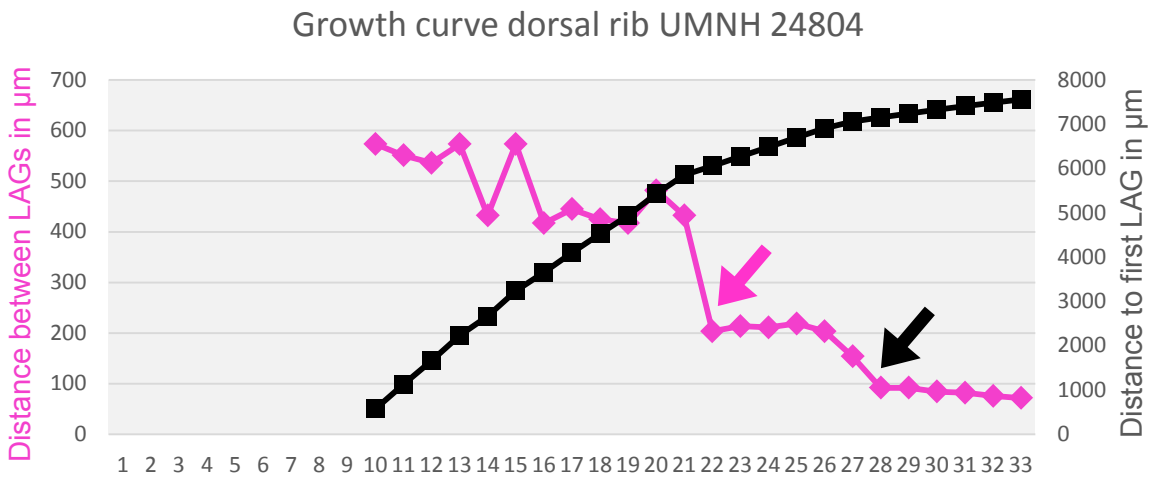

S.I. Fig. 67

Note that the following two samples UMNH 24384 and 24801 most likely belong to the same individual based on their very similar growth records.

***Camarasaurus* sp. (UMNH 24804)**

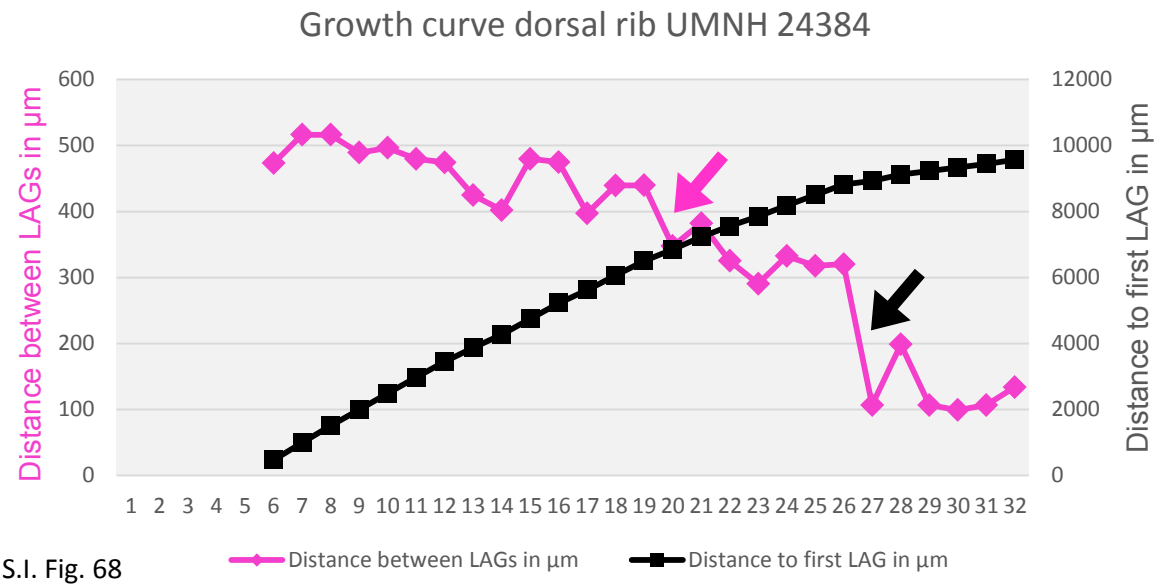

S.I. Fig. 68

***Camarasaurus* sp. (UMNH 24801)**

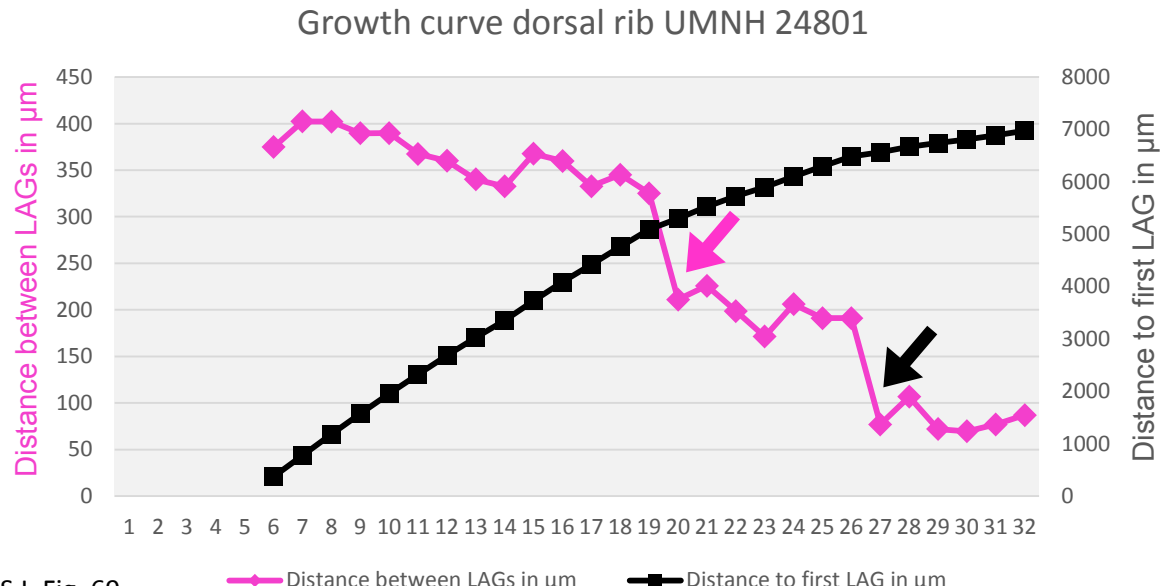

S.I. Fig. 69

***Camarasaurus* sp. (UMNH 20518)**

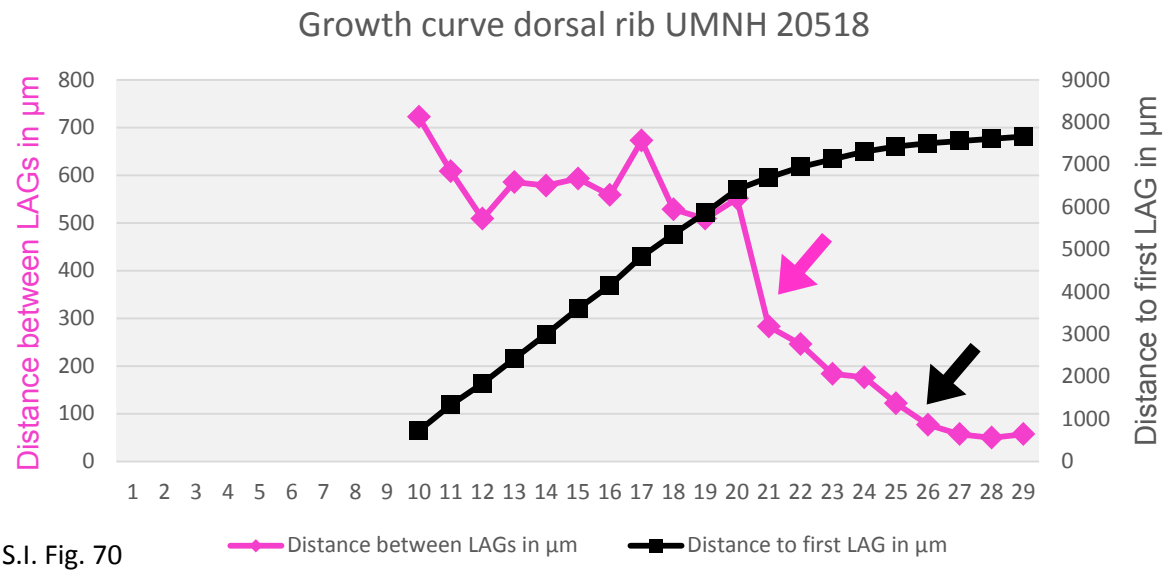

S.I. Fig. 70

***Camarasaurus* sp. (UMNH 24298)**

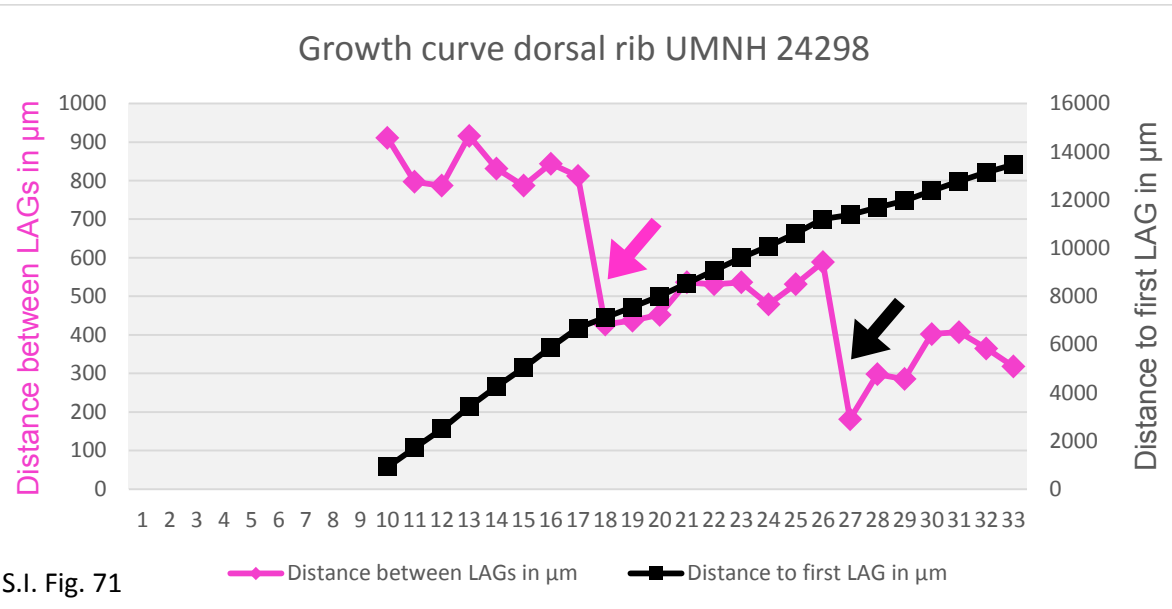

S.I. Fig. 71

***Camarasaurus* sp. (UMNH 24803)**

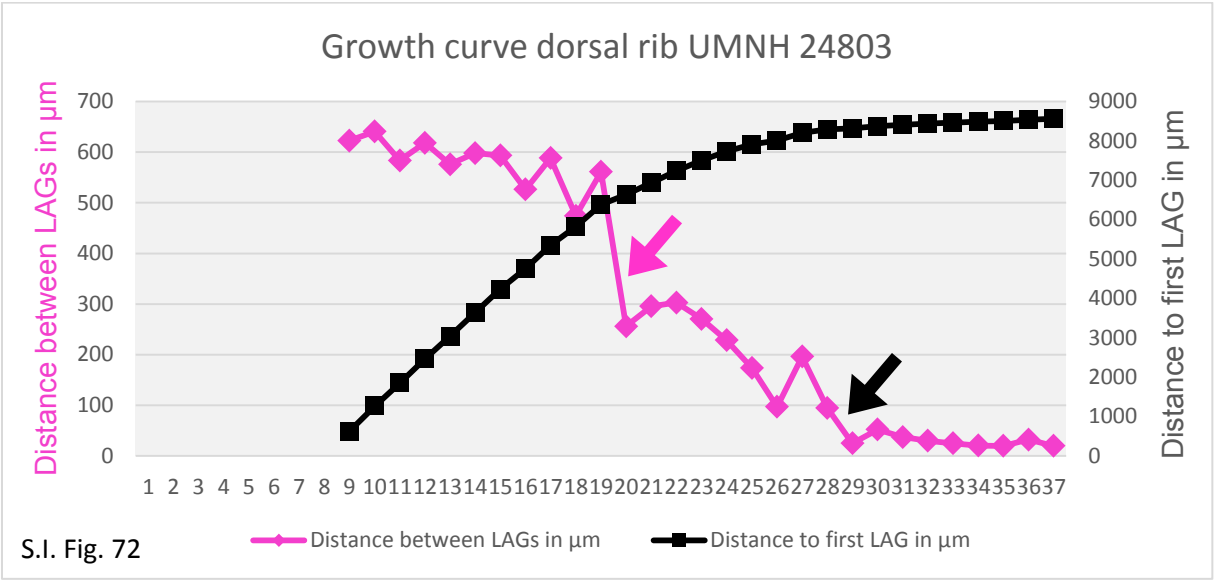

S.I. Fig. 72

***Camarasaurus* sp. (UMNH 24805)**

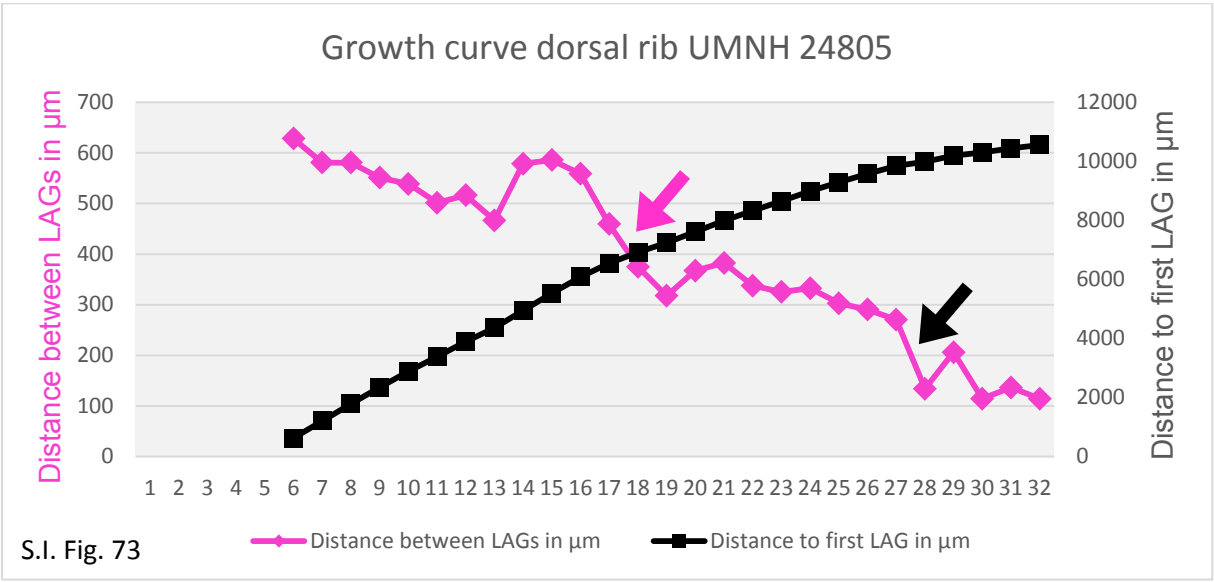

S.I. Fig. 73

***Camarasaurus* sp. (UMNH 24806)**

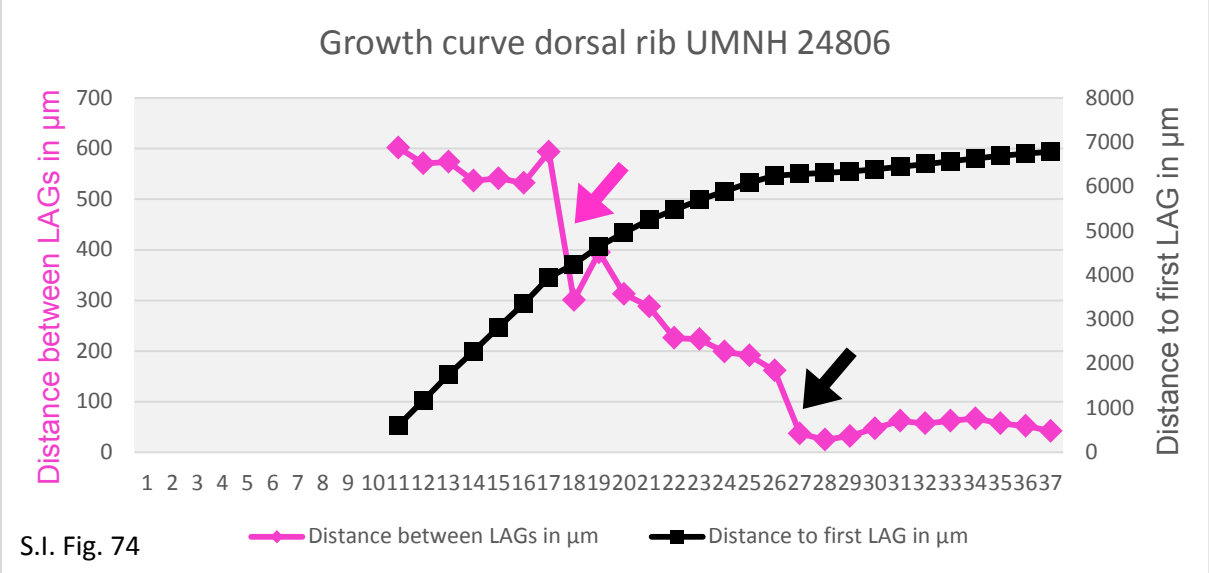

S.I. Fig. 74

***Camarasaurus* sp. (UMNH 24807)**

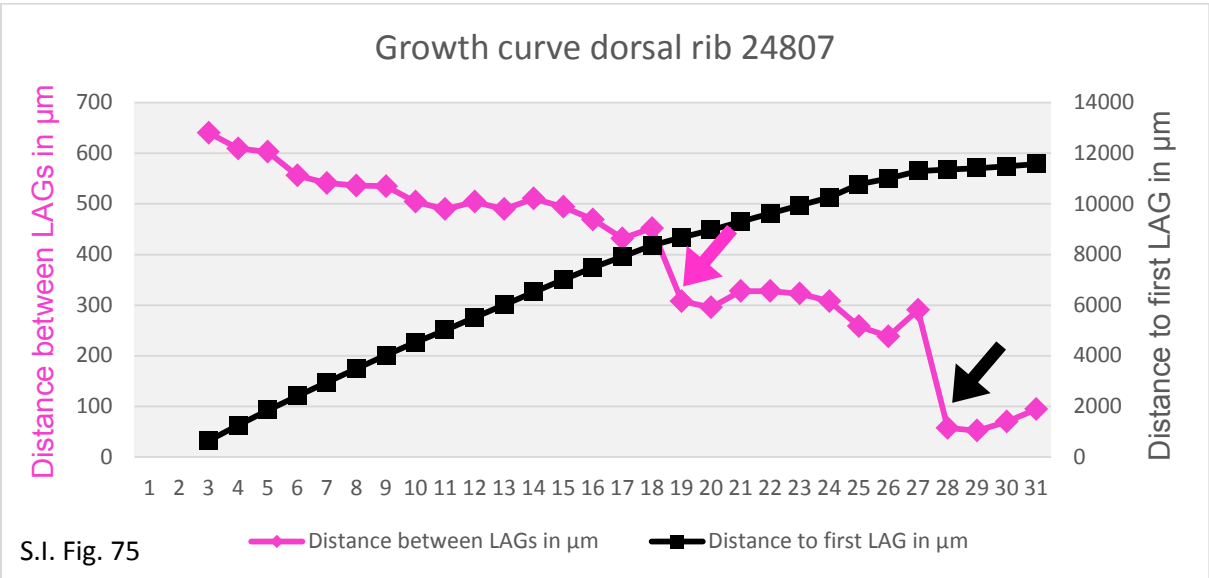

S.I. Fig. 75

***Camarasaurus* sp. (UMNH 24808)**

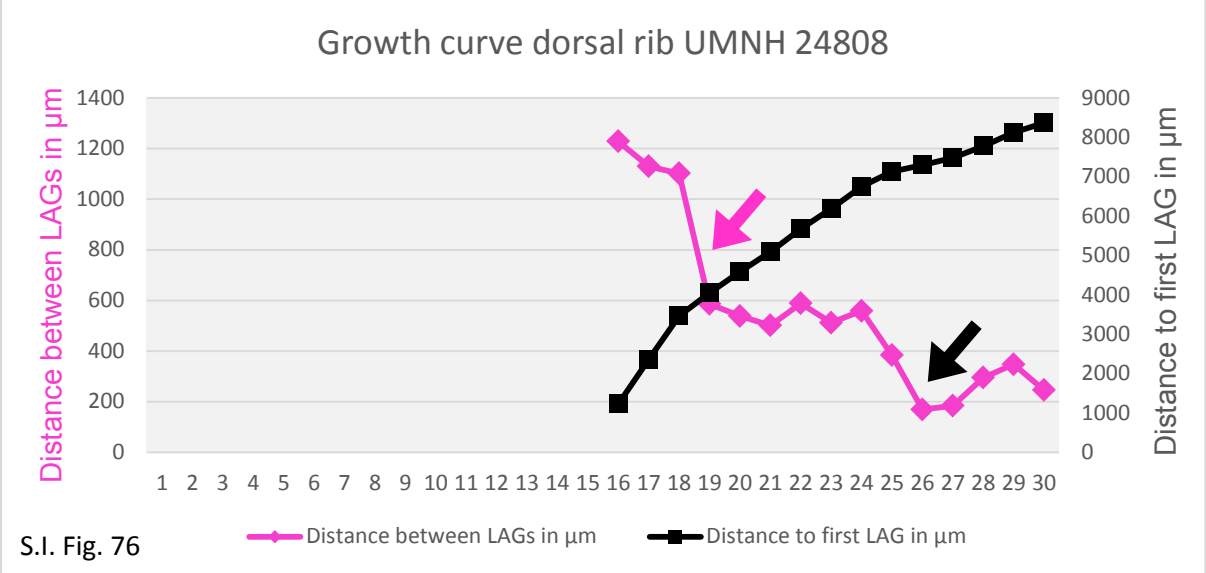

S.I. Fig. 76

***Camarasaurus* sp. (YPM VP 0060121)**

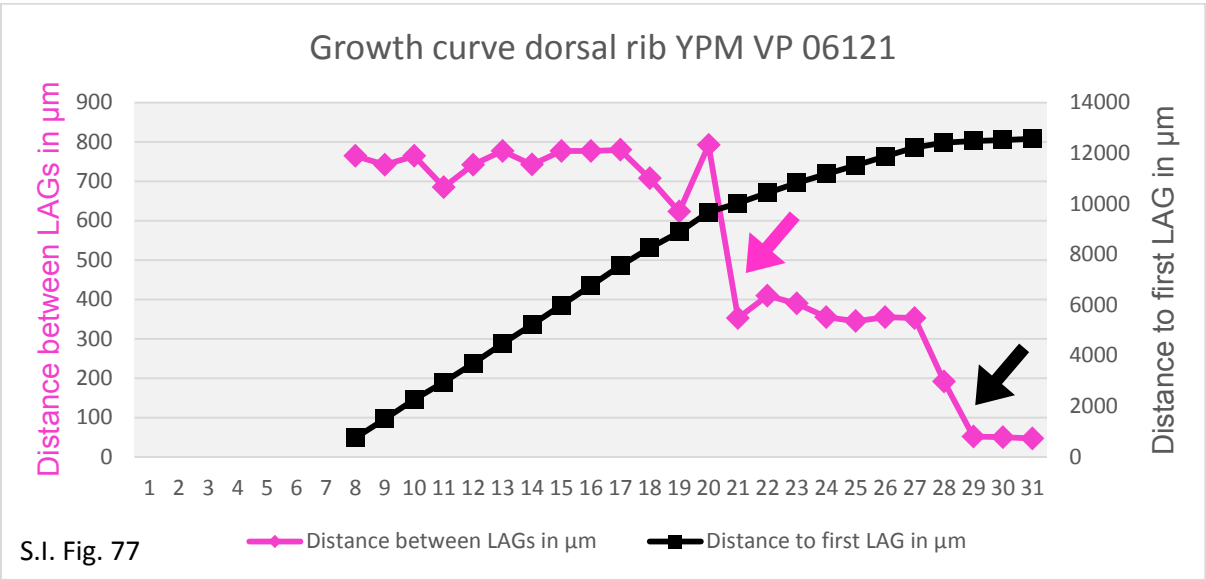

S.I. Fig. 77

***Brachiosaurus altithorax* (FMNH P25107)**

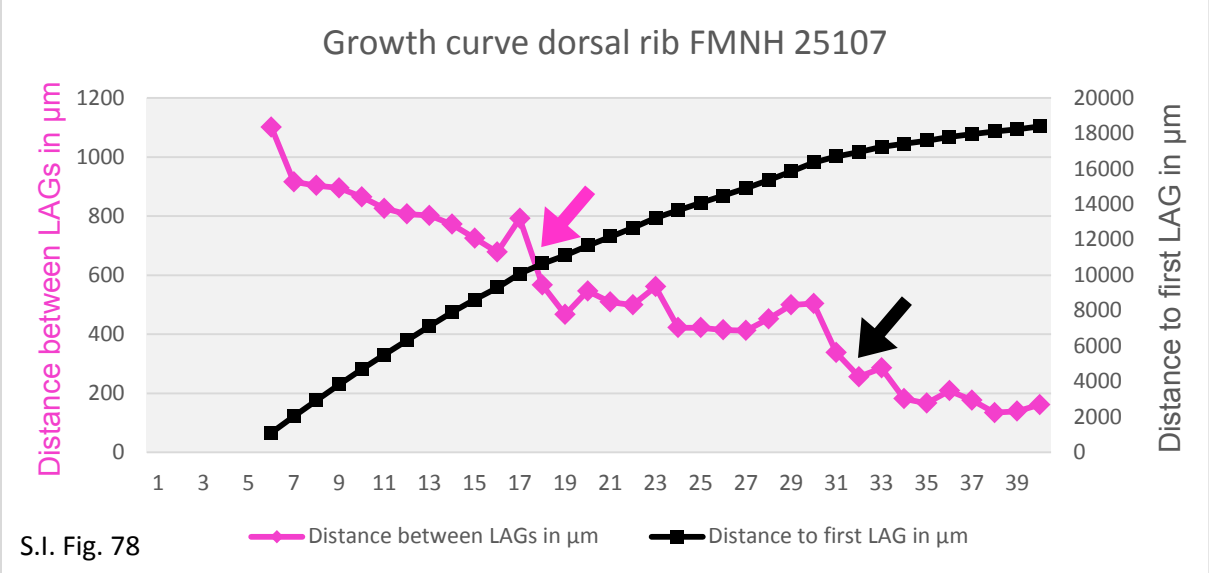

S.I. Fig. 78

Cf. *Giraffatitan* (J 12)

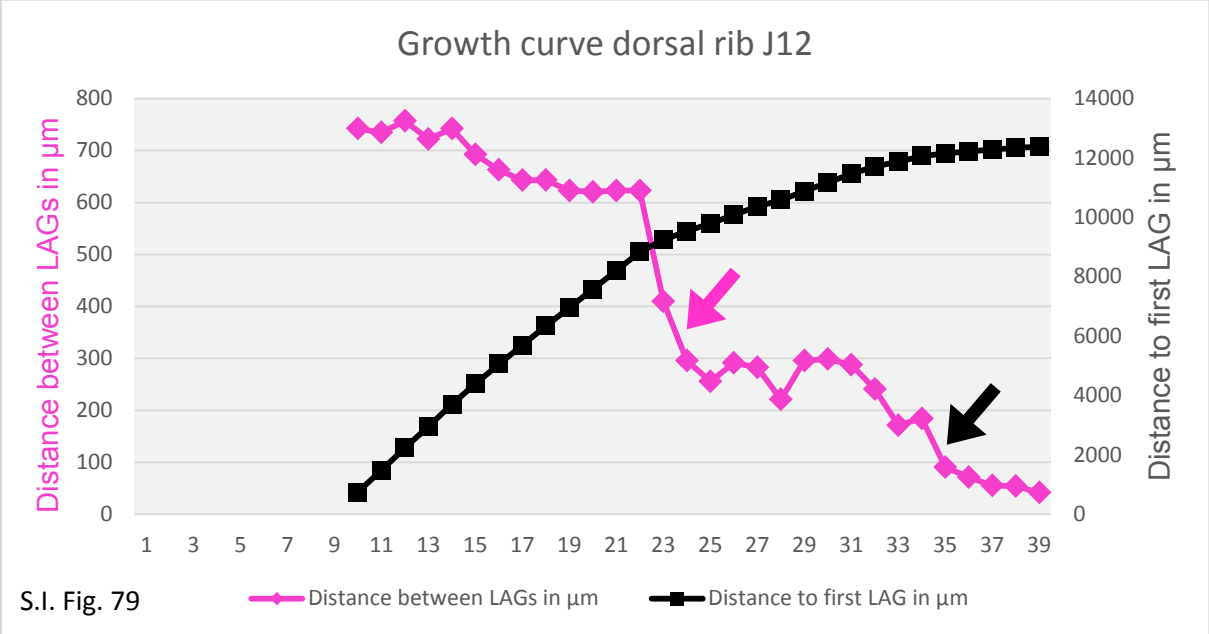

S.I. Fig. 79

***Apatosaurus ajax* (YPM VP 001860)**

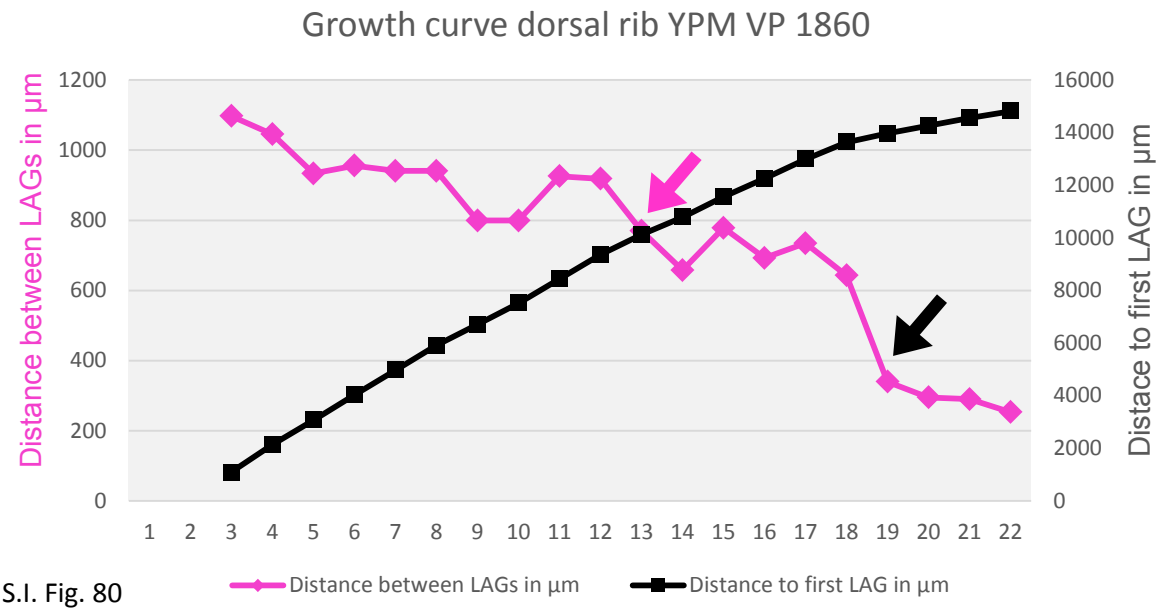

S.I. Fig. 80

***Apatosaurus louisae* (SMA 0269)**

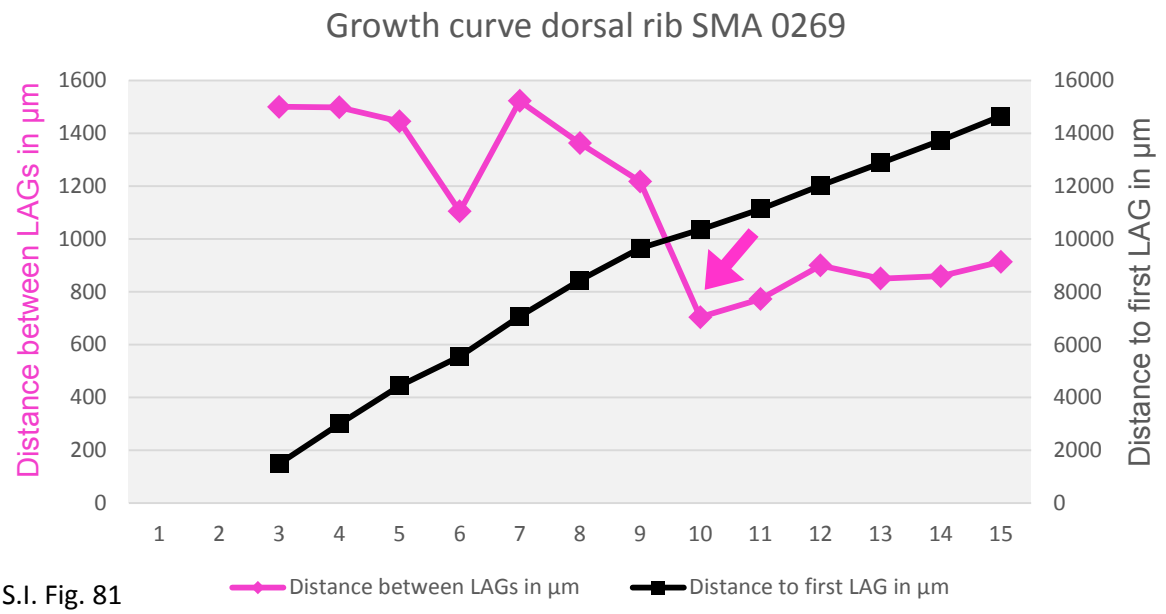

S.I. Fig. 81

***Apatosaurus* sp. (UW 46211)**

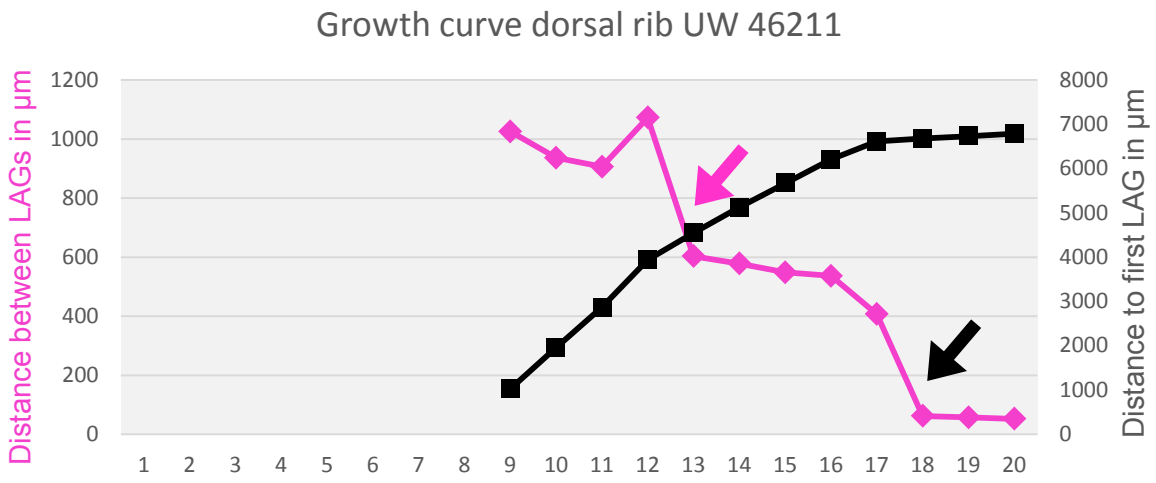

S.I. Fig. 82

***Apatosaurus* sp. (MOR 957)**

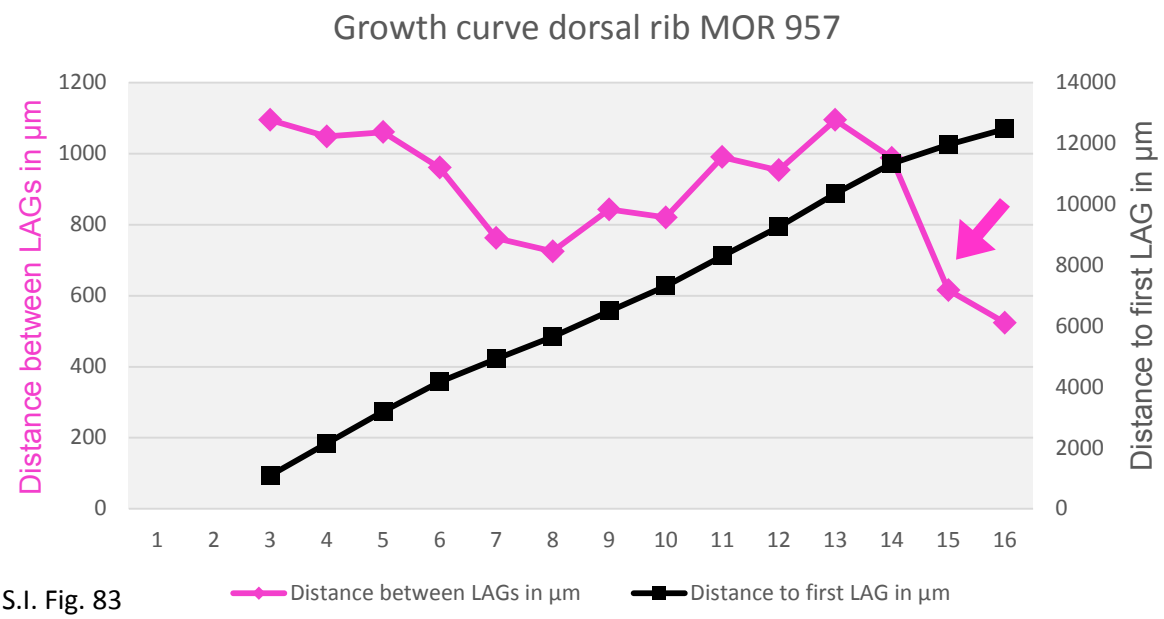

S.I. Fig. 83

***Apatosaurus* sp. (YPM VP 004832)**

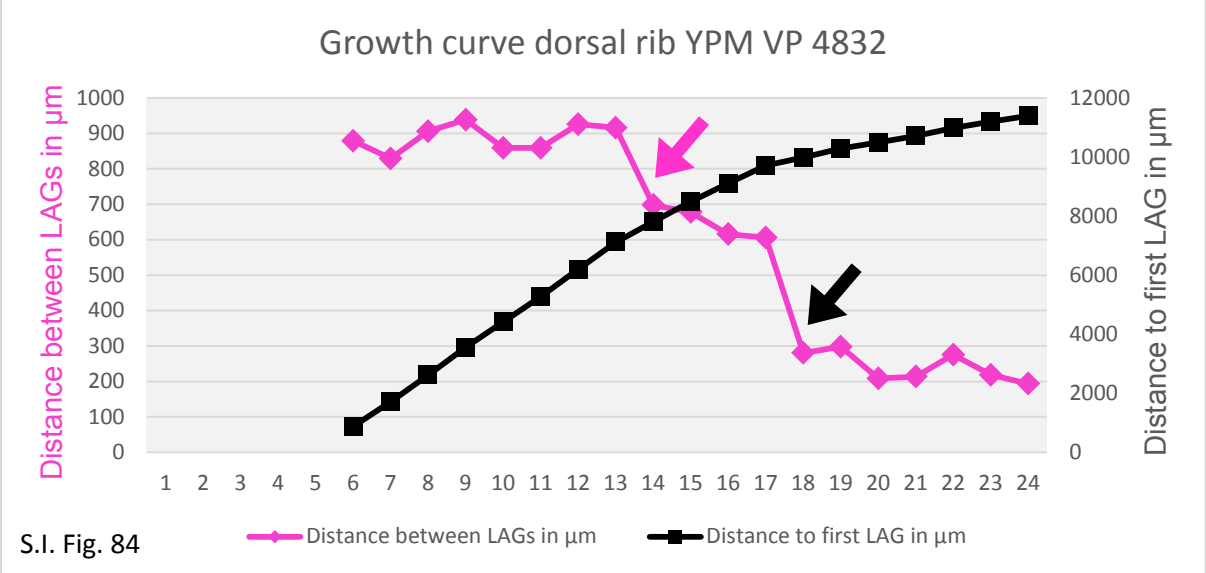

S.I. Fig. 84

***Brontosaurus excelsus* (YPM VP 001981)**

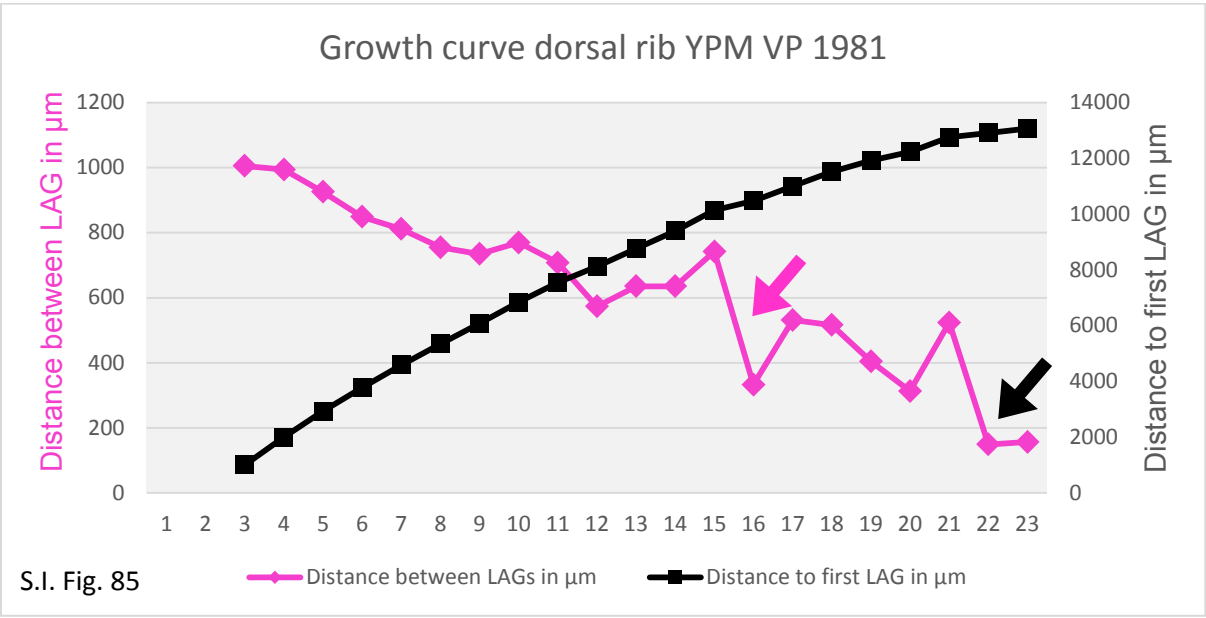

S.I. Fig. 85

Apatosaurinea indet. (BYU 18531)

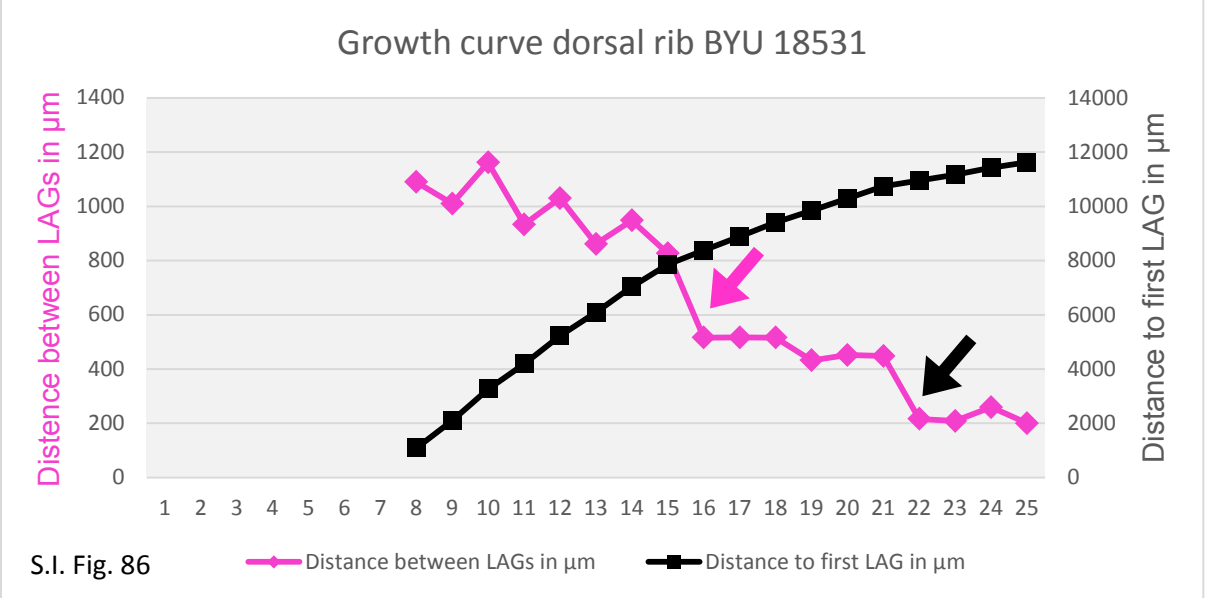

S.I. Fig. 86

***Galeamopus pabsti* (SMA 0011**

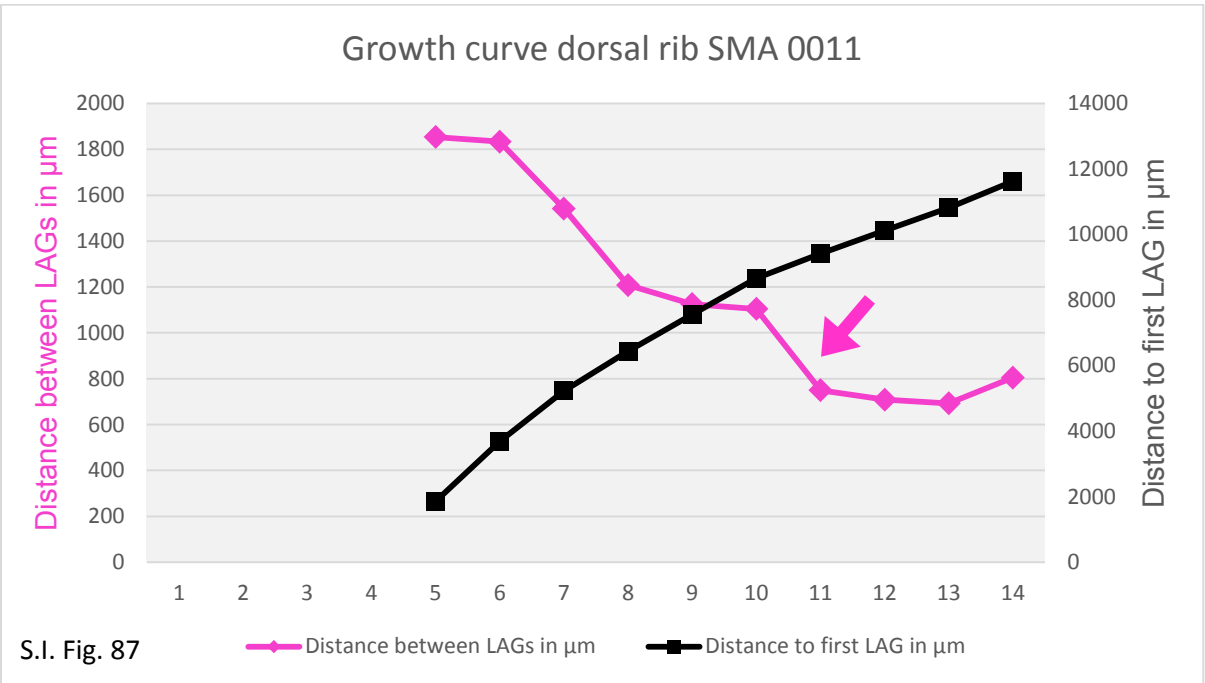

S.I. Fig. 87

***Diplodocus hallorum* (NMMNH P 3690)**

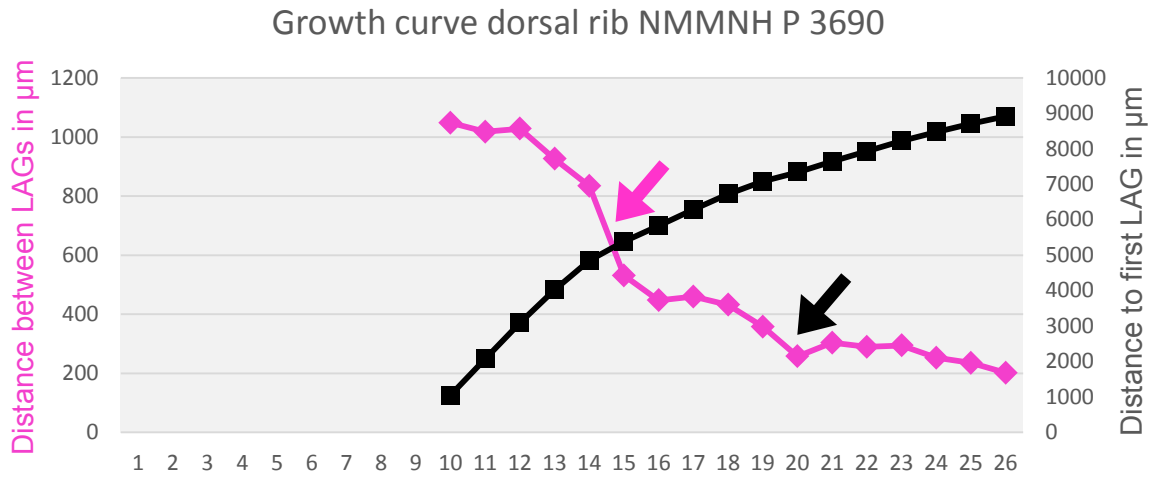

S.I. Fig. 88

***Diplodocus carnegii* (CM 94)**

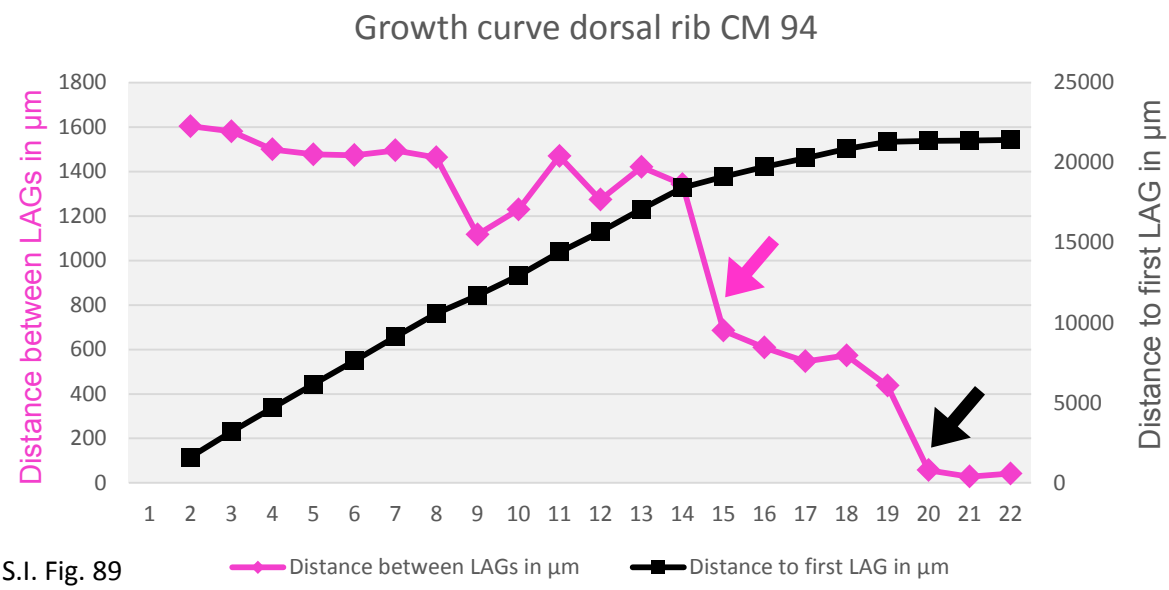

S.I. Fig. 89

***Diplodocus* sp. (MOR 592)**

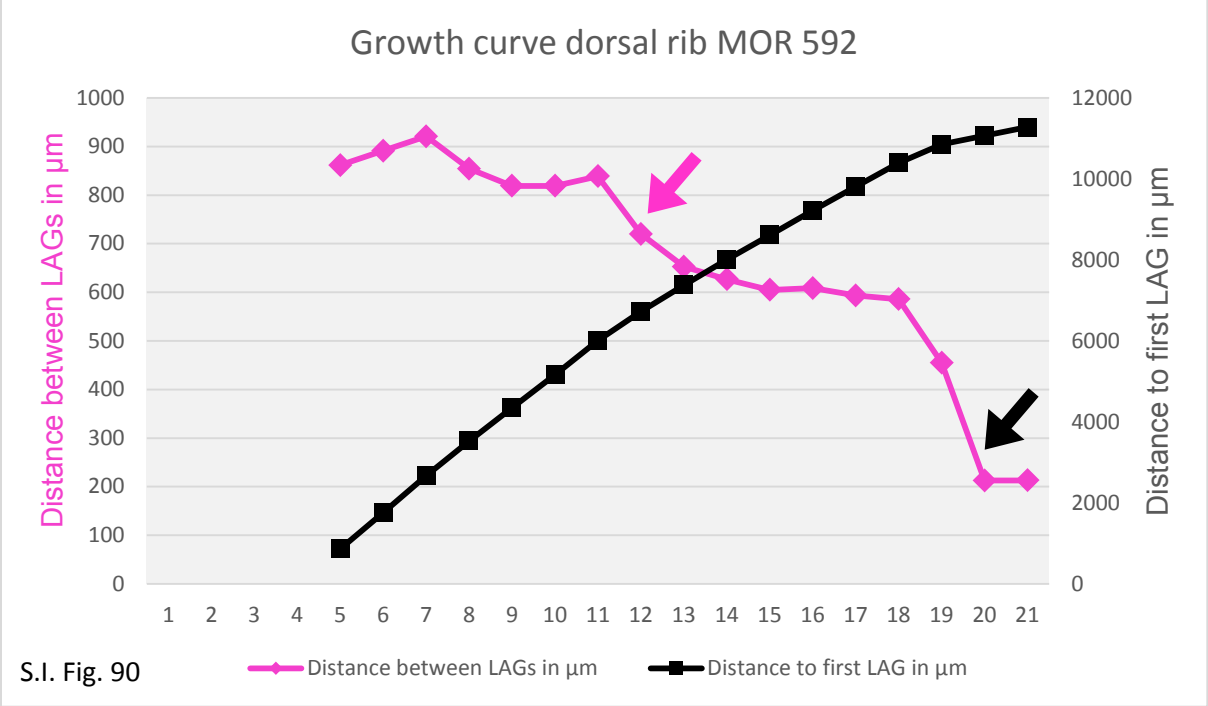

S.I. Fig. 90

***Barosaurus lentus* (YPM VP 000429)**

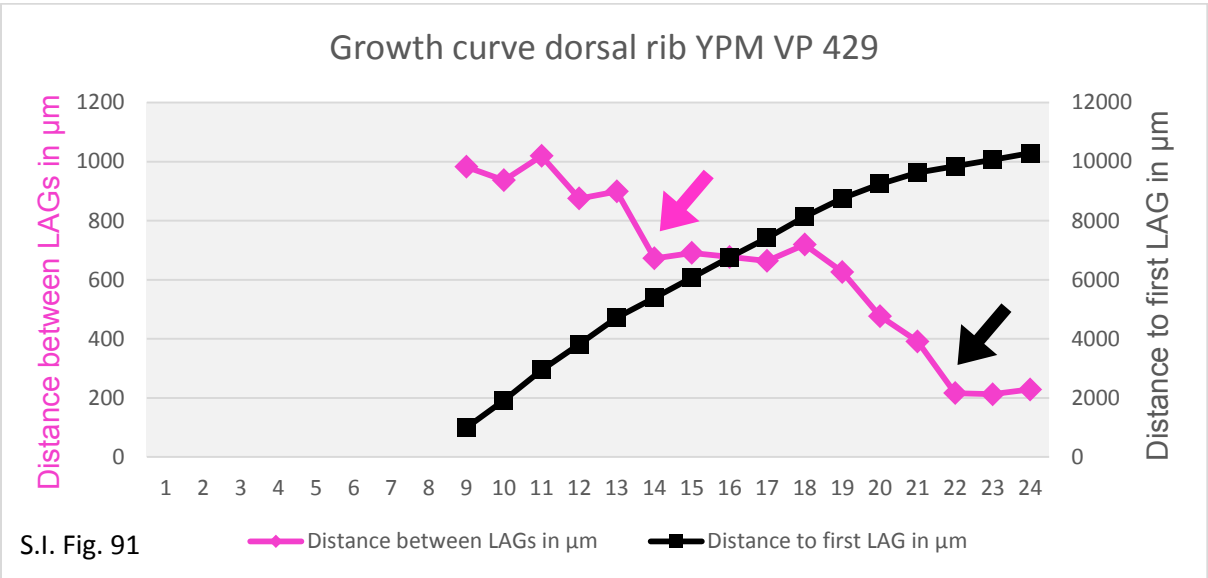

S.I. Fig. 91

Diplodocinae indet. (SMA 0013)

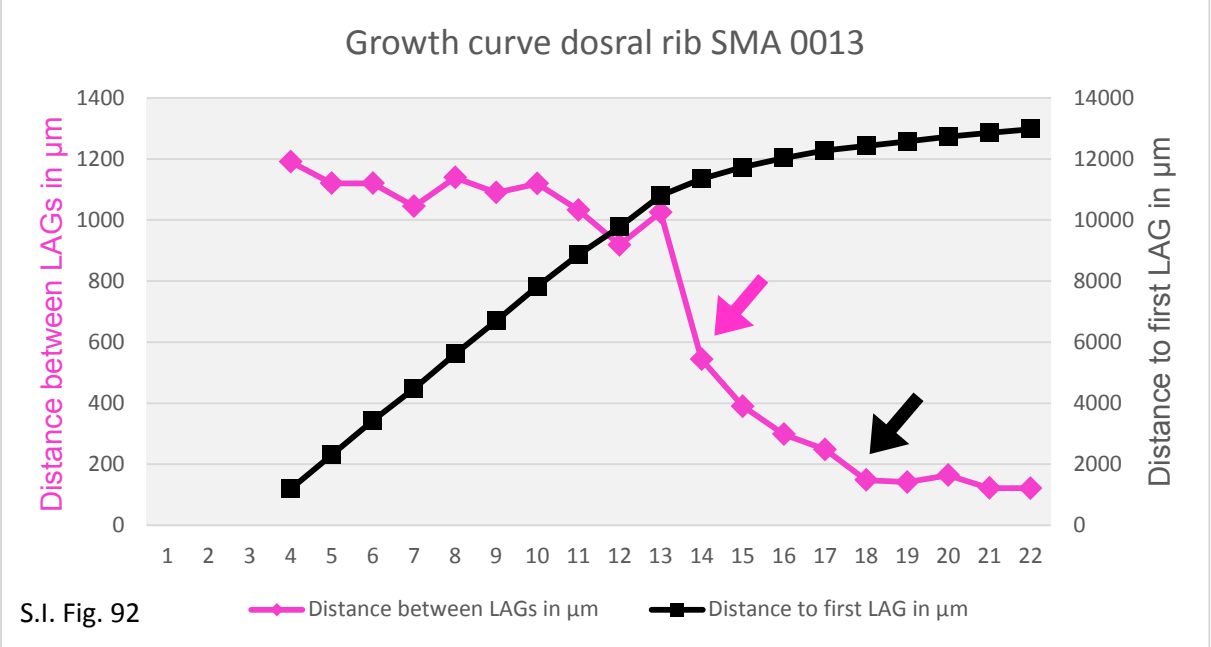

S.I. Fig. 92

Diplodocinae indet. (ML 418)

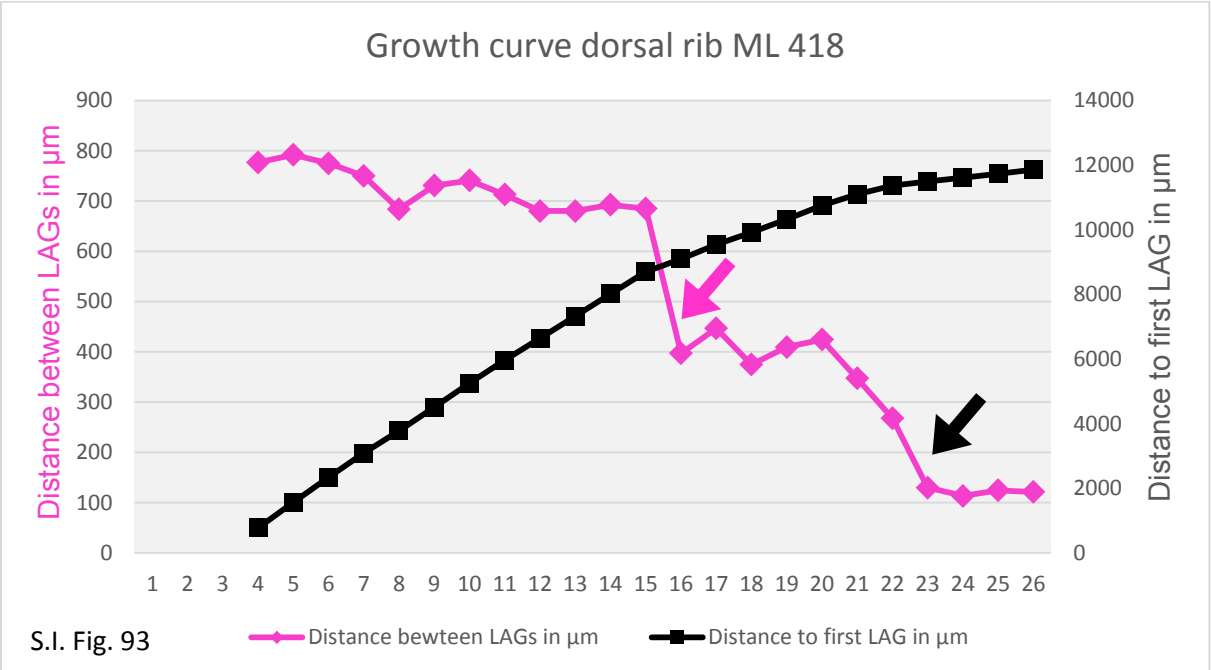

S.I. Fig. 93

Diplodocinae indet. (CMC VP 8020)

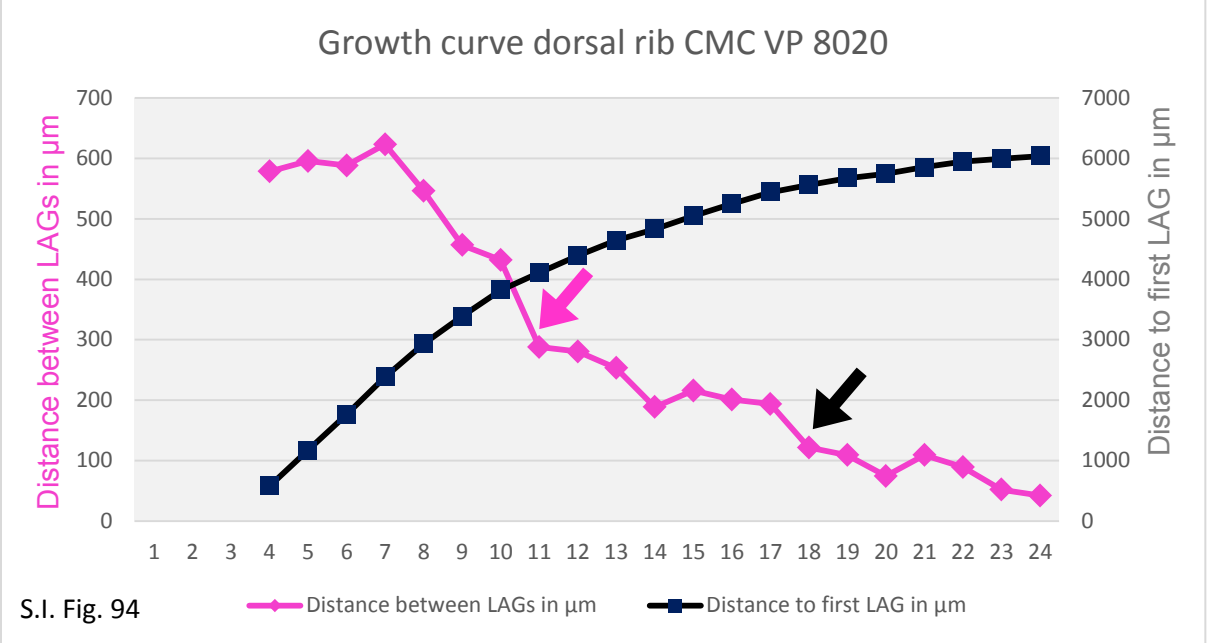

S.I. Fig. 94

Diplodocinae indet. (CMC VP 8038)

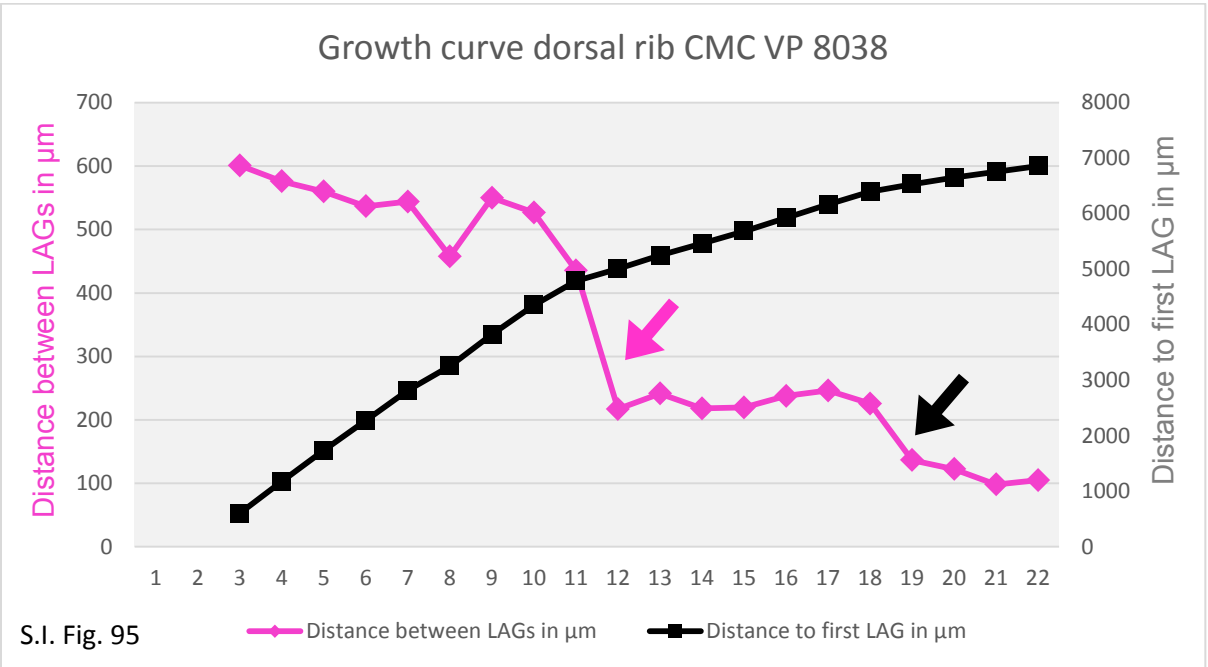

S.I. Fig. 95

Diplodocinae indet. (CMC VP 8991)

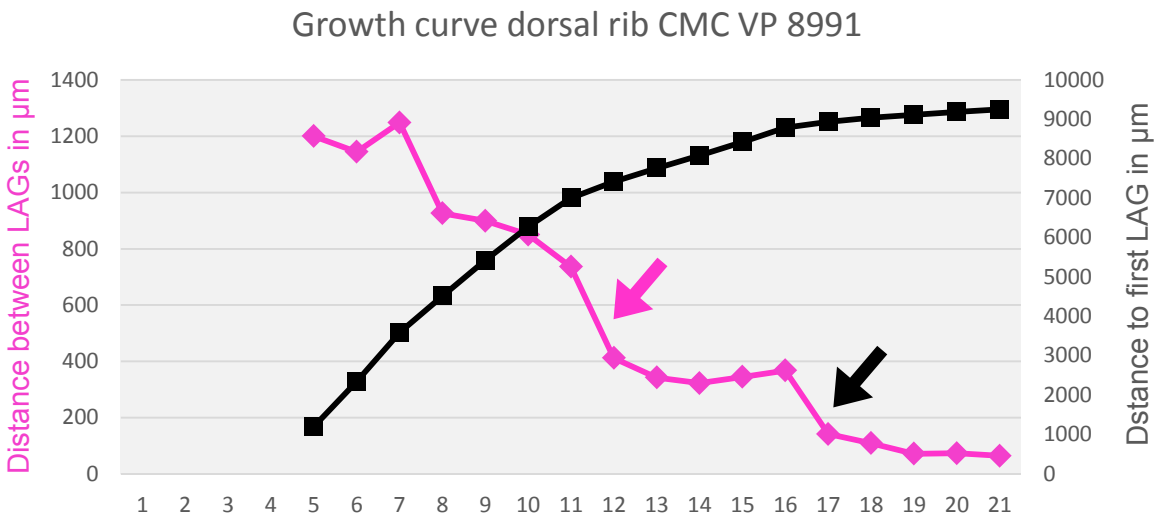

S.I. Fig. 96

Diplodocinae indet. (CMC VP 9930)

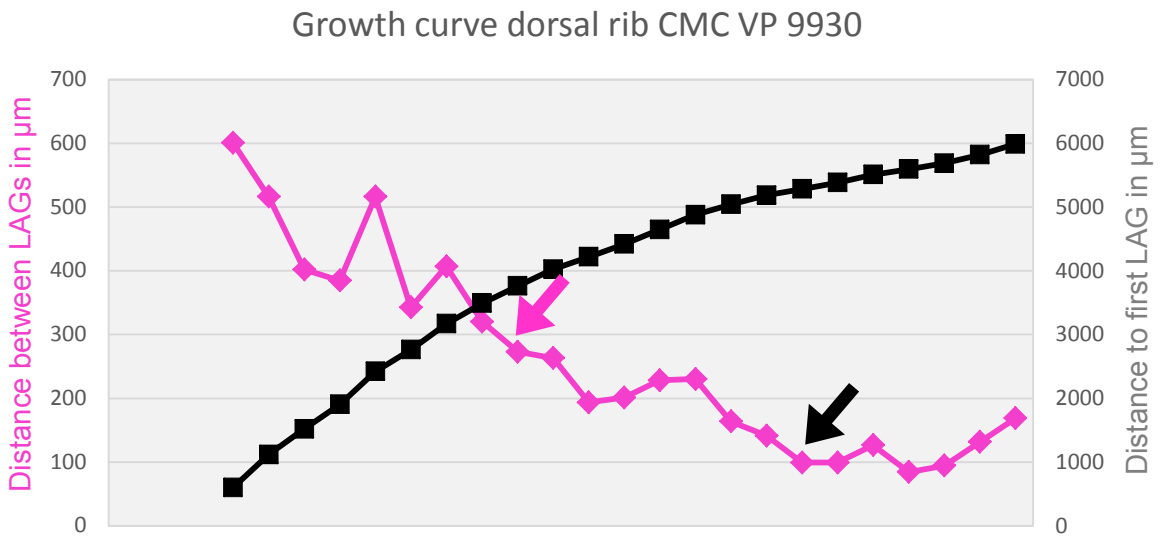

S.I. Fig. 97

Diplodocinae indet. (CMC VP 9932)

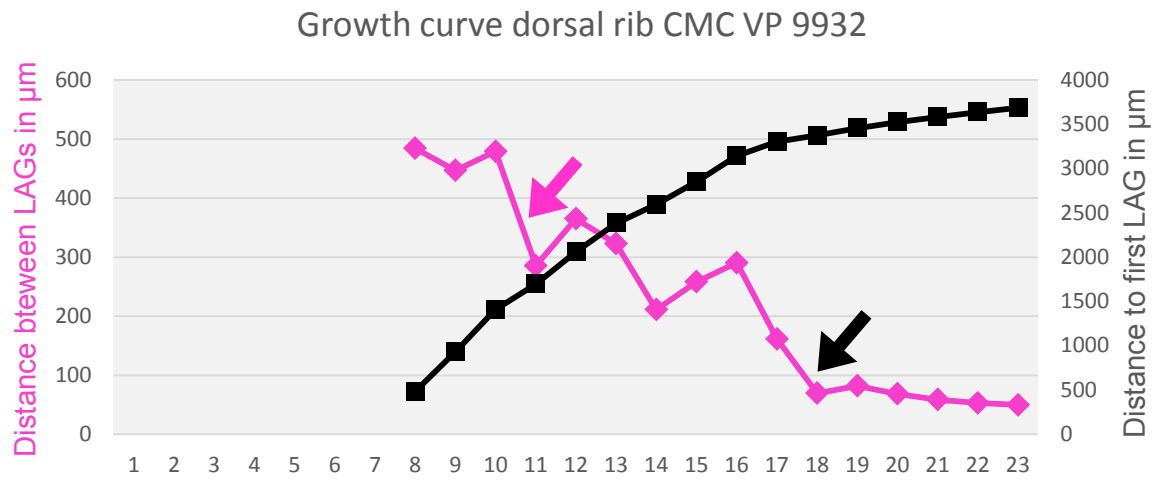

S.I. Fig. 98

Diplodocinae indet. (CMC VP 9948)

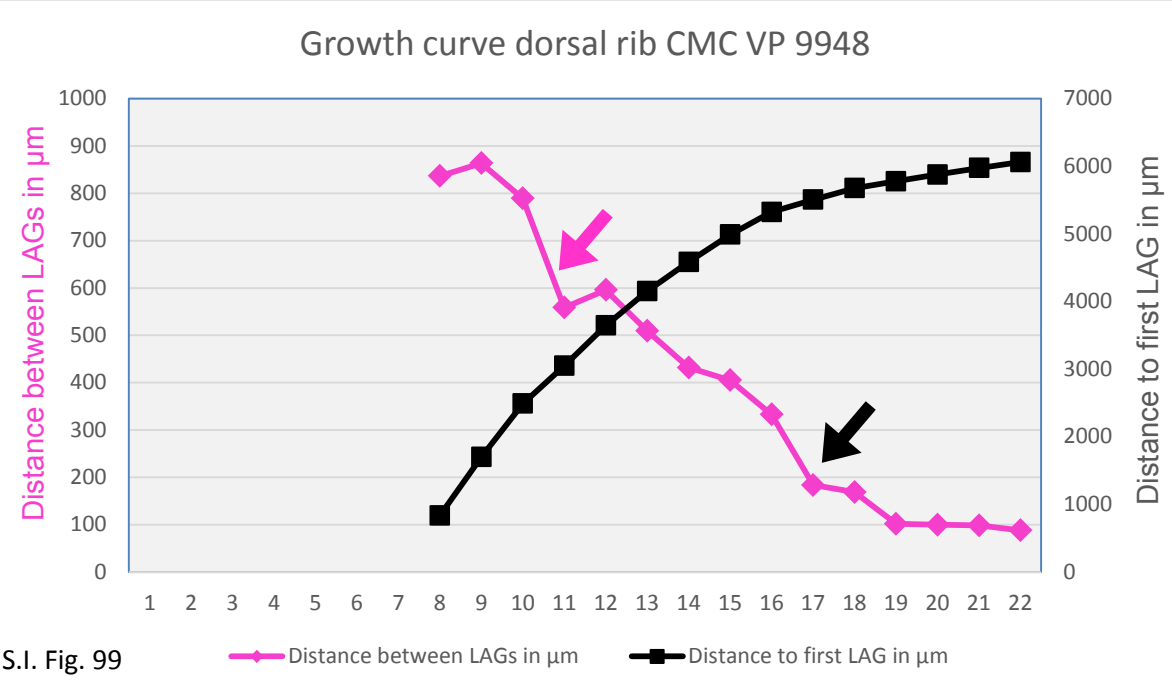

S.I. Fig. 99

Diplodocinae indet. (CMC VP 9956)

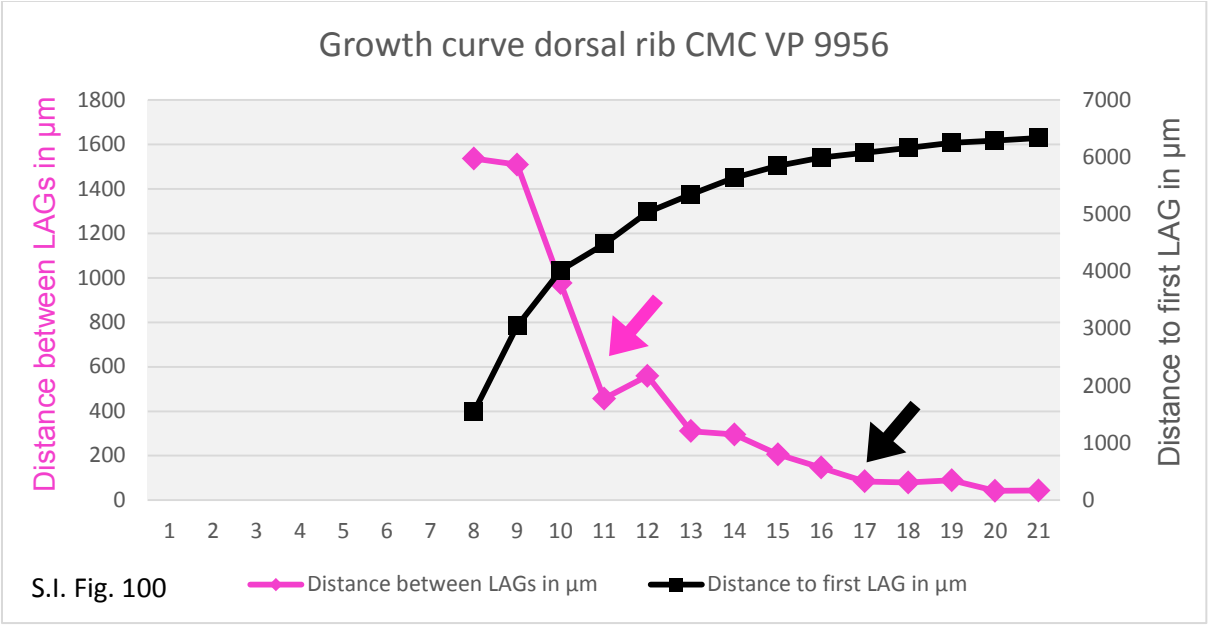

S.I. Fig. 100

Diplodocinae indet. (CMC VP 9977)

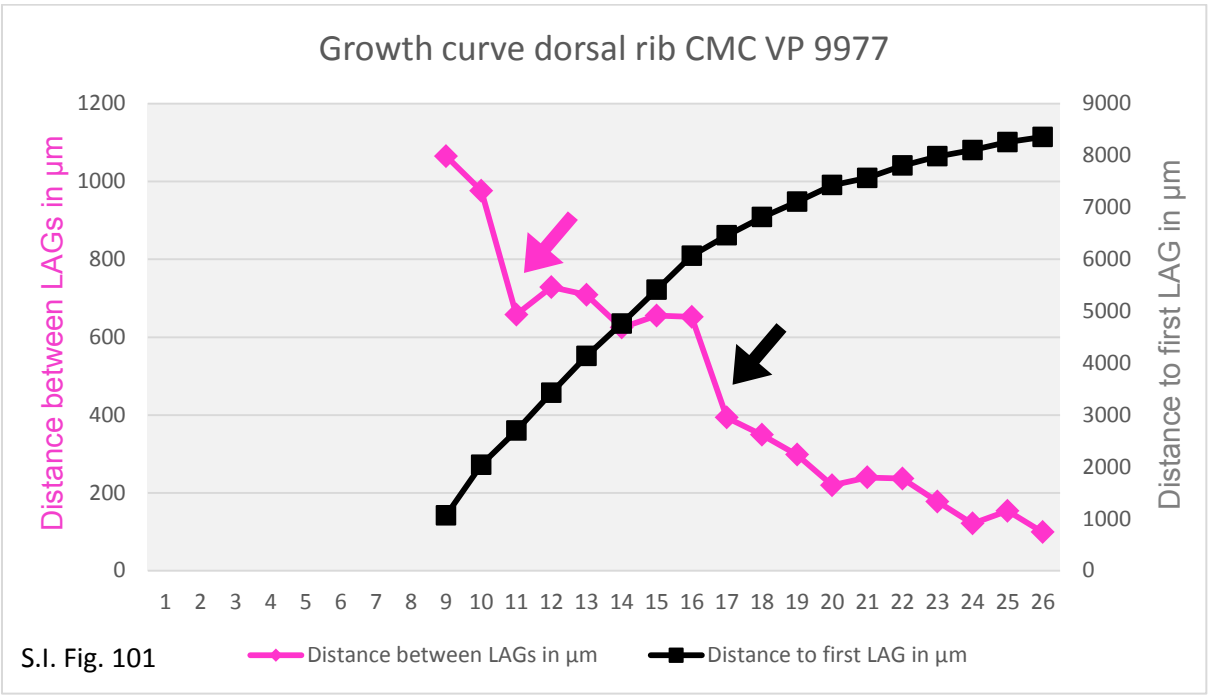

S.I. Fig. 101

Diplodocinae indet. (CMC VP 10666)

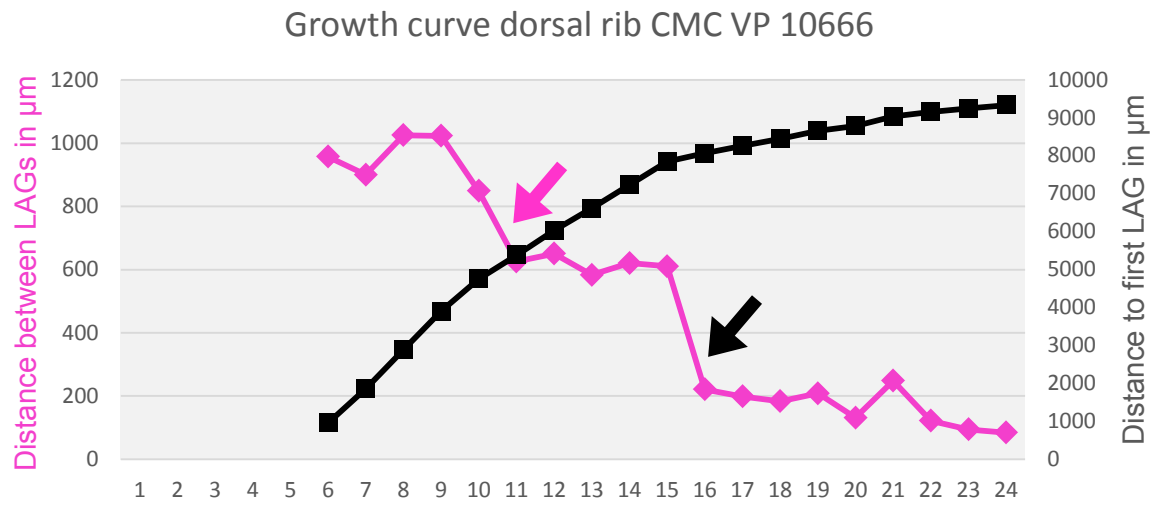

S.I. Fig. 102

Diplodocinae indet. (CMC VP 11339)

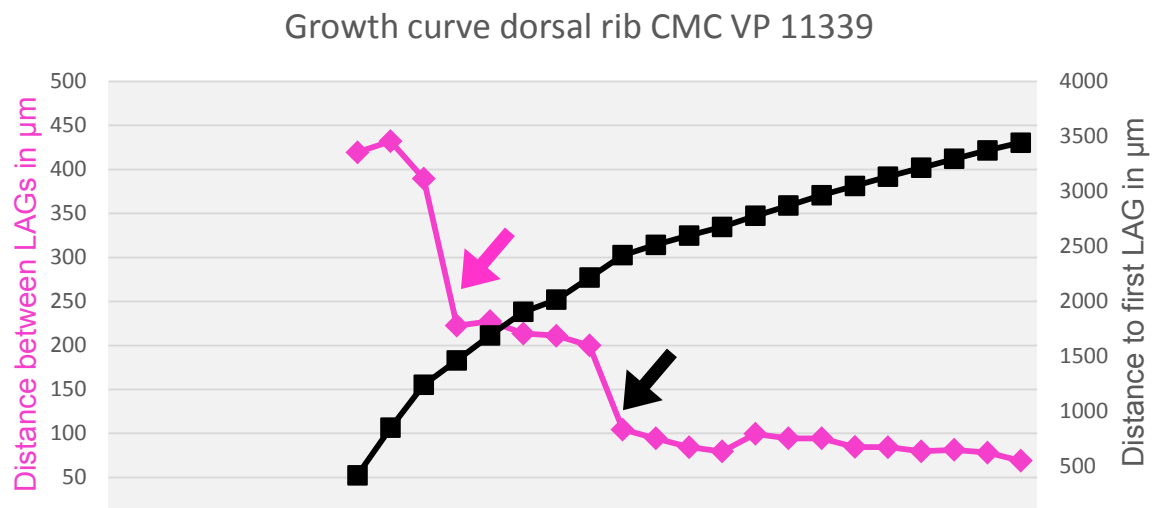

S.I. Fig. 103

Diplodocidae indet. (SMA 0008)

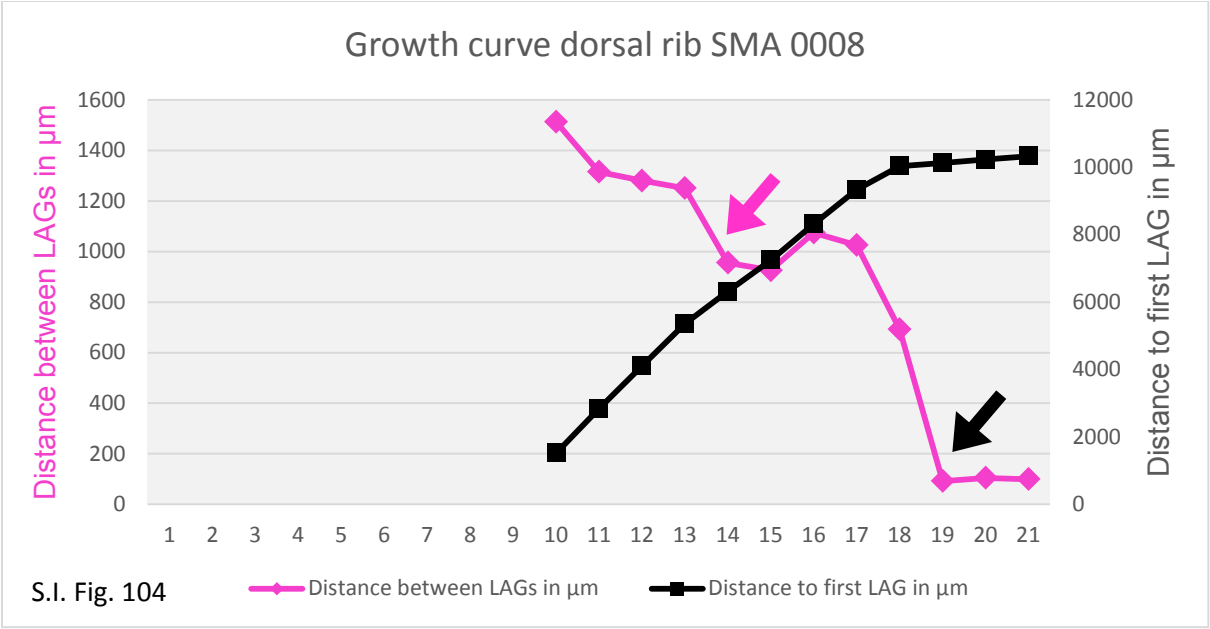

S.I. Fig. 104

Sauropoda indet. (YPM VP 007447)

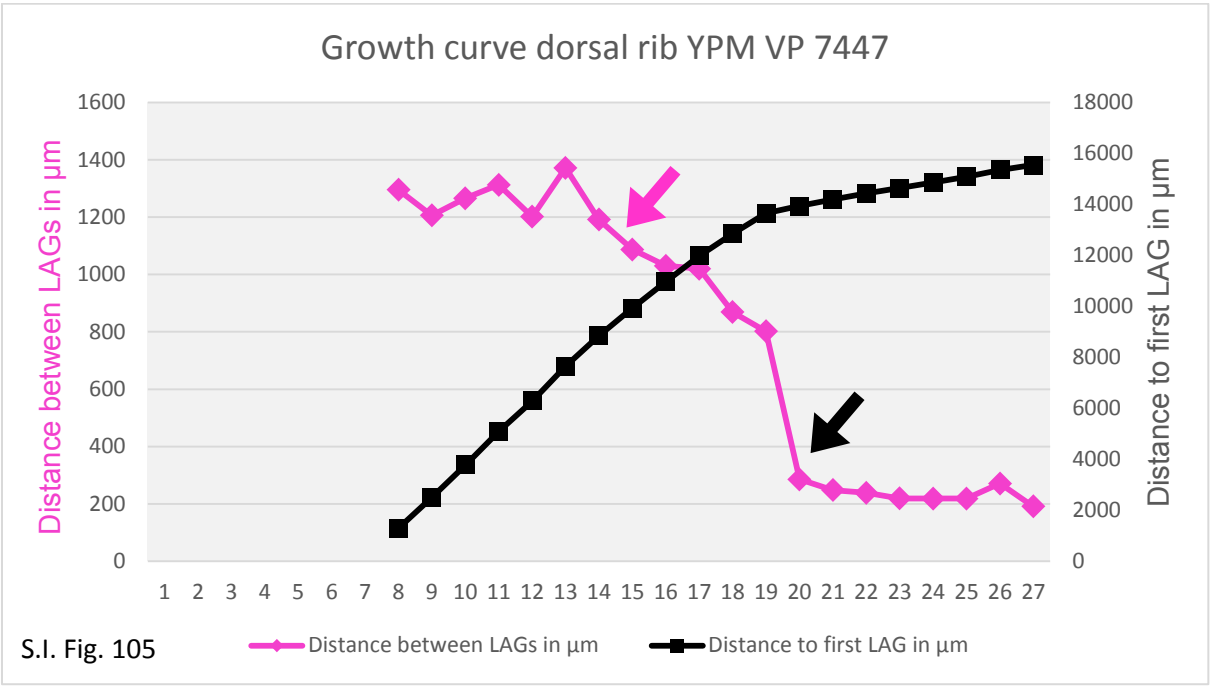

S.I. Fig. 105

Sauropoda indet. (YPM VP 060120)

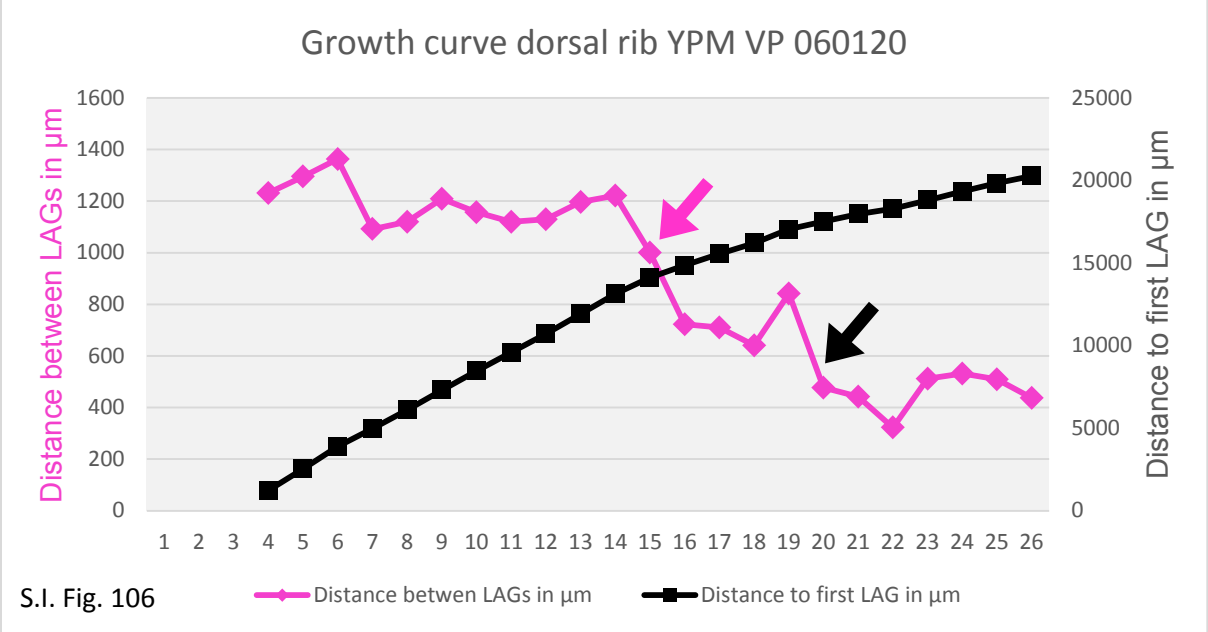

S.I. Fig. 106

Sauropoda indet. (YPM VP 001911)

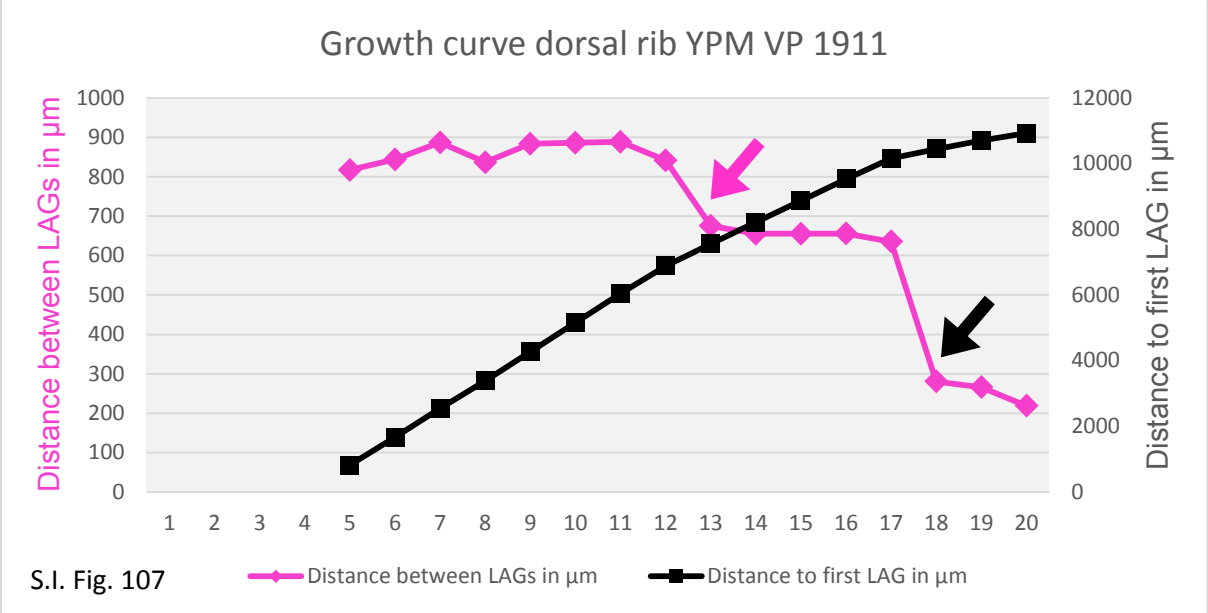

S.I. Fig. 107

“Da aber jede neue Entdeckung uns in eine neue Unwissenheit zurückwirft, und indem der eine Knoten sich löst, ein neuer sich schürzt, so ist begreiflich, dass die vollständige Entdeckung aller Zwischenglieder im Zusammenhang der Natur, dass also auch unsere Wissenschaft selbst eine unendliche Aufgabe ist.”

“Since every new discovery throws us back into a new ignorance, and as one knot loosens, another stretches, it is understandable that the complete discovery of all intermediates in the context of nature, that our science itself is an infinite task.”

Friedrich Wilhelm Joseph von Schelling

CHAPTER 7

Synthesis:
The advantages of dorsal rib histology – Reviewing the state of knowledge about life history traits, ecology, and evolution obtained by analyzing dorsal ribs of different vertebrate taxa

Katja Waskow

Abstract

Dorsal ribs of tetrapods for centuries have never been in focus of scientific interest in any of the main areas of research in biology or paleontology. However, new insights into rib inner structures reveal the importance of these underestimated skeletal elements that yield information about life history, ontogeny, ecology, and taxonomic assignment. Especially for extinct taxa this data stored in dorsal ribs often remains the only way to reconstruct the life history and mode of life of an animal. This study aims to review the state of knowledge ascertained by the analysis of dorsal ribs combining data collected from the literature with new methods preformed on ribs for this dissertation. Investigations on the microanatomy of ribs in differing taxa hint to ecological and evolutionary adaptations to a certain habitat or bauplan. The almost complete growth record preservation in dorsal ribs reveal important life history data on both, individual and taxonomic level including determination of age at sexual- and skeletal maturity, longevity and in some cases sex of the individual. In addition to that, dorsal rib skeletochronology can be used as a reliable tool for testing skeletal unity of bones found in disarticulation. Most of the studies stated herein are performed on dorsal ribs of sauropods because their long bone histology (in contrast to other taxa) lacks equivalent skeletochronological information. However, it is also shown that rib histology in general shows some advantages over the standard long bone sample including growth record completeness. Thus, this review should be considered as a starting point of data collection in dorsal ribs summing up results and methods that can be used as tool for investigations on life history in any kind of vertebrate in the future.

7.1. Introduction

7.1.1. History of research focusing on dorsal rib morphology

Beside the numerous descriptions of dorsal rib biomechanics in humans for medical purposes (e.g., Granik and Stein, 1973; Yoganandan and Pintar, 1998; Cormier et al., 2005; Kemper et al., 2007; Mohr et al., 2007, García- Martínez et al., 2016; Holcombe, 2016; Holcombe et al., 2017) scientific descriptions and drawings of dorsal rib in various vertebrate taxa most frequently occur in classical morphological descriptions of new taxa where they are described as part of the axial skeleton among all other skeletal elements (e.g., Osborn and Mook, 1921; Kammerer et al., 2008; Sallan, 2012). Only in some rare cases of anomalous dorsal rib or rib cage morphologies (like, e.g., the dorsal rib cage of turtles that fuses with the carapace and incorporates the shoulder blade) dorsal ribs are described in more detail (Cebra-Thomas et al., 2005; Lyson and Joyce, 2012; Hirasawa et al., 2015). Another area of research where ribs were considered for analysis more frequently is respiration. Because ribs are the most important bones serving in breathing, they were analyzed together with the intercostal musculature in several studies (Cowen, 1996; Schachner et al., 2009; Troyer and Boriek, 2011; Maina, 2017). The few studies focusing solely on rib morphology (e.g., Klein and Sichelschmidt, 2014) usually are motivated by the lack of more diagnostic skeletal elements.

7.1.2. Purpose of this paper

This paper aims to provide insights into the new perception of dorsal ribs as research objects. A variety of research areas may and will profit from more detailed analyses of dorsal rib microanatomy and histology the first case studies of which are summarized and presented herein. Even if some of the methods used for these analyses are already well established (Francillon-Vieillot et al., 1990; Chinsamy-Turan, 2005; Quémeneur et al., 2013), their application on dorsal ribs reveal information about environmental and ecological adaptations and almost complete growth records, which in turn provide several information about ontogeny and life history. This variety of information stored in dorsal rib bone tissue opens a new area of research that can be processed on ribs which are generally more abundant and easier to access compared to the usually sampled long bones.

In addition, new methods performed on ribs are presented. One method enables the testing of skeletal unity by correlating growth records of different dorsal ribs. Another one aims to reconstruct juvenile bone morphology based on Computed Tomography (CT) scans of an ontogenetically older individual. Even if performed on dorsal ribs, these methods might be used in the future to analyze other skeletal elements. The following chapter describes the advantages of dorsal ribs in differing fields of research in more detail combining literature knowledge and research performed in the different chapters of this dissertation.

7.2. Microanatomy of dorsal ribs

7.2.1. History of research on bone microanatomy

Bone microanatomy of extant and extinct vertebrates has become an important and frequently used tool to study their ecology, and phylogeny because it sheds light on biomechanical functions most of which are related to the mode of locomotion and habitat of the animal (Wall, 1983; Fish and Stein, 1991; Laurin et al., 2004; Germain and Laurin, 2005; Kriloff et al., 2008; Canoville and Laurin, 2009; 2010; Laurin et al., 2011; Quémeneur et. al, 2013; Nakajima et al., 2014; Houssaye et al., 2015; 2016, (chapter 3)). As usual, most of these microanatomical investigations have focused on the appendicular skeleton (particularly long bones). Even if some studies include axial skeletal elements (Hayashi et al., 2013; Amson et al., 2014; Houssaye et al., 2016, (chapter 3)) only a few focused solely on the microanatomy of vertebras (Dumont et al., 2013; Houssaye et al., 2014) or ribs (Buffrénil et al., 2010; Canoville et al., 2016). The quantitative analysis of Canoville et al. (2016) aimed to analyze the microanatomy of dorsal ribs in terms of habitat effects, body size and phylogeny on a broad taxonomic scale for the first time, while the study of Houssaye et al. (2016, (chapter 3)), broadened the scope of microanatomical investigations by comparing different skeletal elements including humeri, femora, and ribs in terms of habitational signals by analyzing the effect of graviportality and comparing it to the already well analyzed differences in bone microanatomy seen in terrestrial and aquatic taxa. The importance and implications of these analyses in terms of the ecological signal are further discussed herein.

7.2.2. Microanatomical implication for ecological habitat adaptation

The rib cage is a major part of the skeleton in nearly all amniote taxa. Thus, based on their great number, ribs contribute mainly to the body mass and density of an individual. This influence is comparable if not surpassing the influence the well-studied long bones have on skeletal mass (Canoville et al., 2016). Thus, decreases or increases of rib compactness most likely were caused by the same evolutionary habitat adaptations that have been observed in long limb bones (e.g., Germain and Laurin, 2005; Canoville and Laurin, 2010). A decrease in rib compactness and cortical thickness can be observed in flying or pelagic deep diving taxa, that try to reduce mass an increase maneuverability. Contrary an increase in mass and cortical thickness, that can be caused by, e.g., pachyostosis or osteosclerosis, occurs in taxa that live in coastal shallow water or swim close under the water surface (Houssaye et al, 2016, (chapter 3); Canoville et al., 2016). However, the observation of a thick compact cortex might also be misleading in terms on ecological habitat reconstruction as the analysis of Houssaye et al. (2016, (chapter 3)) shows. Graviportal animals like, e.g., sauropods, proboscideans, or rhinocerotids show similar mass increases in cortical thickness (in humeri, femora and dorsal ribs) than shallow water forms combined with narrow medullary cavities and large cancellous bone transition zones between cortex and medullary

region. This might be cause by bending, torsion and compression stresses that are stronger in large animals than in smaller taxa but needs further analysis to be completely understood. In general, the study of Houssaye et al. (2016, (chapter 3)) underlines that the microstructure of dorsal ribs and inferred habitat implications seems to be highly comparable to observations in long bones. Thus, dorsal rib should be considered for microanatomical investigations more frequently as also stated by Canoville et al. (2016).

7.3. Histology of dorsal ribs

7.3.1. History of research on dorsal rib histology

The presence of skeletochronological information preserved in dorsal ribs of differing archosaurs has already been reported in some scientific papers were ribs have been studied among other skeletal elements like, e.g., humeri and femora or even metatarsals or phalanges (Erickson, 2005; Erickson et al., 2007; Cerda and Chinsamy, 2012). Even if the examination of ribs in most cases were performed marginally or caused by the absence of the traditionally sampled long bones, dorsal rib histology of archosaurs in all cases shows excellent growth record preservation. In 2004, Erickson et al. started analyzing dorsal ribs by sampling the rib of a *Tyrannosaurus rex* (FMNH PR 2081). The rib showed clearly developed growth marks and an almost complete growth record preservation that enabled age estimation of the individual and lead Erickson to the erection of the first age-mass based growth curve for dinosaurs (Erickson et al., 2004). Even if reliability of such growth curves based on growth record preservation in dorsal ribs can be discussed controversially (see chapter limits and challenges of…), this was the first study that preformed age estimations based on nearly complete growth record preservation found in ribs. In 2007, Erickson and colleagues again performed further histological sampling on different dinosaur taxa on several skeletal elements including dorsal ribs, followed by another study by Cerda and Chinsamy (2012) who also included dorsal rib samples in their studies on several specimens of the ornithopod *Gasparinisaura cincosaltensis*.

The first study focusing primarily on dorsal rib histology instead of long bones was performed by Waskow and Sander (2014) who sampled the complete rib cage of an articulated *Camarasaurus* sp. (SMA 0002) to provide an overview about the histological variation in dorsal ribs from anterior to posterior and from proximal to distal. They detected the most complete growth record in ribs to be located at the proximal end of the rib shaft of the anterior dorsal ribs. Initially sauropod ribs were chosen for this study by the need to test growth record completeness in skeletal elements other than ribs because long bones of sauropods do not develop and preserve LAGs in their primary bone tissue caused by high rates of bone apposition and remodeling (Klein and Sander, 2008; Waskow and Sander, 2014; Mitchell and Sander, 2014). However, the excellent and nearly complete growth record preservation in *Camarasaurus* forced the authors to expand their database to other

archosaur- (Waskow and Mateus, 2017, (chapter 2)) and sauropod taxa (Waskow et al., submitted, (chapter 4); Waskow et. al., unpublished (chapter 6)). The histological analysis of dorsal ribs from different dinosaurs and a crocodylomorph taxa of Portugal (Waskow and Mateus, 2017, (chapter 2)) as well as revealed the usability of dorsal ribs for histological sampling in archosaurs by revealing almost complete growth records in all sampled taxa. The same is true for both studies of Waskow et al., (submitted, (chapter 4); unpublished, (chapter 6)) that analyzed dorsal rib skeletochronology in differing sauropod taxa. The estimations on life history data and their implications for ecology are described in the following chapters.

Contrary to this, mammals seem to have a generally increased remodeling rate (Enlow and Brown, 1958; Klevezahl, 2017) also observable in their dorsal rib bone tissue (de Buffrenil et al., 1990). This is not necessarily caused by differing basal metabolic rates (Padian and Horner, 2004; Sander and Andrássy, 2006) as has been argued by Chinsamy and Hillenius (2004) because mammals also do show growth marks in their bone tissue (Buffrénil, 1982; Chinsamy et al., 1998; Horner et al., 1999; Padian and Horner, 2004; Sander and Andrássy, 2006; Köhler and Moyà-Sola, 2009; Klevezahl, 2017) However, the generally higher remodeling rate results in the destruction of the primary growth records in most cases. Nevertheless, some recent studies on human ribs already considered their diagnostic potential for accurate ageing in forensic investigations, even if they do not focus on growth mark count but on differences seen in haversian bone tissue caused by ontogenetic ageing. (Bonicelli et al., 2017; Dellanoy et al., 2018).

7.3.2. Growth record preservation in dorsal ribs

In general, the growth record preservation in dorsal ribs is remarkably complete in all studied archosaur taxa (Erickson, 2004; Waskow and Sander, 2014; Waskow and Mateus, 2017, (chapter 2); Waskow et al., submitted, (chapter 4); Waskow et al., unpublished, (chapter 6)). Most of all sampled specimens show a growth record completeness of over 50% regardless of taxonomic assignment. Especially ontogenetically younger specimens that do not exceed young adult to skeletal mature age can easily reach growth record completenesses of over 80%. In early stage juveniles a complete growth record preservation can be assumed. Only some senescent individuals of very old ontogenetic age are limited in their growth record completeness caused by remodeling of the inner cortex. However, even those specimens still do show primary bone tissue preservation in their dorsal ribs, which seems to be contrary to long bones of the same individual that show higher remodeling rates. This difference in remodeling rate becomes most obvious in graviportal animals like, e.g., sauropods. The analysis of Waskow and Sander (2014) described a growth record completenesses of up to 87% for a senescent *Camarasaurus* individual the long bones of which are nearly completely remodeled. Possible explanations for such differences in remodeling are differences in bending, torsion and especially pressure loads between dorsal

ribs and weight bearing elements like long bones. The stresses in bone mentioned before are often discussed and proved to cause microcracks in the primary bone tissue that are then repaired by remodeling processes (Frost, 1960; Burr et al., 1985; Mori and Burr, 1993; Verborgt et al., 2000; Lee et al., 2002; Cardoso et al., 2009; Mitchell, 2017). Another explanation for remodeling, also known as Haversian bone formation is the mobilization of minerals stored in the bone (Parfitt, 2010). A verifiable influence of mineral mobilization in dorsal ribs bone tissue has been reported for female reindeer by Baski and Newbrey (1989). They found increased porosity of the bone tissue in July during antler growth than in samples taken in January. Implying mineral mobilization as main cause for remodeling in general, the differences in remodeling rate between different skeletal elements would imply a general genetical preference of mineral storage in long bones rather than in dorsal ribs.

Regardless of its causation, the lower remodeling rates observed in dorsal ribs result in more complete growth record preservation. Additionally, the special rib morphology and its ontogenetical development causes better growth record preservation compared to long bones even in unremodeled primary bone tissue. In long bones the formation of the medullary cavity that is described as the third front of bone development (resorption) by Mitchell and Sander (2014) causes the destruction of the innermost cortex and thus the juvenile growth record of the individual especially in ontogenetically more derived specimens. Dorsal ribs in contrast to that show a differing ontogenetic development. Caused by their growth direction from proximal to distal, the relative position of a certain point changes during ontogeny. What has been the distal end of a juvenile rib became incorporated into the proximal shaft later in ontogeny. These growth dynamics have been analyzed and described in more detail by Waskow and Sander (2014) in their analysis of a complete articulated rib cage of a *Camarasaurus* sp. individual. The shift in position allows the preservation of early stage juvenile primary bone in the inner cortex at the posteromedial side of the rib that would have been subject to resorption in a long bone of the same specimen.

7.3.3. Life history data collected from dorsal rib histology

The almost complete skeletochronology recorded in the proximal dorsal rib shaft of different vertebrate taxa yields several information about the life history of the sampled individual including ontogenetic age, sexual- and skeletal maturity and in some cases age at death. Two major decreases in growth have been observed in fully-grown individuals (Waskow and Sander, 2014; Waskow and Mateus, 2017, (chapter 2); Waskow et al., submitted, (chapter 4); Waskow et al., unpublished, (chapter 6)). The first one occurs approximately after 50% of the total growth time of the individual and has been interpreted as point of sexual maturity where the animal starts to use energy for reproduction that is then no longer available for growth (). The second one is the beginning of the external fundamental system (EFS) that consists of very closely spaced LAGs showing no significant

histological structures in between and is well established to represent skeletal maturity (Cormack, 1987; Sander, 2000; Starck and Chinsamy, 2002; Padian et al., 2004; Chinsamy-Turan, 2005; Erickson et al., 2004; Erickson, 2005; Turvey et al., 2005; Sander et al., 2011; Woodward et al., 2011; Andrade et al., 2015).

In taxa showing significant differences of ages at sexual maturity between males and females like, e.g., crocodiles thus sex can also be concluded by the examination of the growth record as it has been done by Waskow and Mateus (2017, (chapter 2)). Another important aspect of individual life history that can be ascertained by skeletochronology is age at death. By counting growth cycles and estimating the number of missing inner cycles in the cortex that have been lost due to remodeling, a reliable growth time can be estimated for the individual in question (Waskow and Sander, 2014; Waskow and Mateus, 2017, (chatper 2); Waskow et al., submitted, (chapter 4); Waskow et al., unpublished, (chapter 6)). In specimens that have not reached asymptotic growth and thus skeletal maturity before death this estimation represents the lifespan of the individual. For fully grown animals however, the estimated age solely represents individual growth time because it cannot be excluded that the animal in question lived on for several years after growth has stopped completely. The absence or presence of asymptotic lifetime growth versus growth completition in non-avian dinosaurs as well as in recent reptiles has been discussed controversially in the past (Richmond, 1965; Halliday and Verrell, 1988; Curry, 1999; Price et al., 2004; Congdon et al., 2013; Armstrong et al., 2018) and is still not completely understood.

7.4. Taxonomic assignment inferred from dorsal rib histology

Not only life history but also phylogeny influences growth patterns and tissue formation. Reversely, the examination of growth times, microanatomy and ontogeny obtained by sampling dorsal ribs can be used for taxonomic determination. As the analysis of Waskow et al. (chapter 4) shows, statistically significant taxonomical differences in ages at sexual- and skeletal maturity were found between the two major neosauropod clades Macronaria and Diplodocoidea. This allows taxonomic assignment of morphological undiagnostic rib material based on histology. Additionally, the study hints to further taxonomic differences on lower phylogenetical scale between, e.g., achievement of sexual- and skeletal maturity of the two macronarians *Camarasaurus* and *Brachiosaurus* or microanatomical differences between the two diplodocoidean taxa Dicraeosauridae and Diplodocidae both of which belong to the Fragellicaudata. These lower level taxonomical differences however are only based on a small sample size and thus need further sampling to verify statistical significance.

In the case of a special sampling locality, namely the Mother´s Day Quarry in Montana (USA), an Assemblage of former thought to be juvenile Diplodocids (Myers and Storrs, 2007; Storrs et al., 2012) were proofed to include many small, but skeletally mature

and thus adult individuals by growth record examination of dorsal ribs (Waskow et al., submitted, (chapter 4)). Hence, this examination of Waskow et al. revealed the presence of a dwarfed sauropod taxon within the Morrison Formation which is the first evidence for sauropod dwarfism in North America. The exact taxonomic affiliation of this dwarfed species is still to be analyzed as described in more detail in chapter 4. The histology of the dorsal rib samples of this site (Waskow et al., submitted, (chapter 4)) further revealed the presence of at least two different size-morphs within the Mother´s Day Quarry one of which is only represented by juveniles most likely belonging to an average sized sauropod. Further remains of this larger size morph including a relatively complete skull and a neck are morphologically and histologically (cervical rib samples) described by Woodruff et al. (2018, (chapter 5)). In conclusion the histological examination of the Mother´s Day Quarry material thus turns out to be the only way to recognize different morphotypes and with that the possible presence of different species within this morphologically very similar assemblage consisting almost exclusively of diplodocids. Other possible explanations like, e.g., sexual dimorphism and intraspecific variation are discussed by Waskow et al. (submitted, (chapter 4)) as well.

7.5. Ecological implications inferred from dorsal rib life history data

By collecting the life history data stored in dorsal ribs of many individuals found within a certain locality or environment age distribution in a death assemblage can be ascertained. This has been done by Waskow et al. (unpublished, (chapter 6)) who found that most fossil remains of their 66 histologically sampled sauropod specimens belong to adult or at least subadult individuals. This lack of juvenile sauropod remains has been reported in the literature before (Lehman and Coulson, 2002; Carballido et al., 2012). Most likely this age segregation in sauropods is caused by the large size ranges between hatchlings and adults that lead to occupation of different ecological niches at different ontogenetic ages and thus sizes (Myers and Fiorillo, 2009; Waskow et al., unpublished, (chapter 6)). The assumption of extreme size ranges between hatchlings and adults influencing ecological niche partitioning in different ontogenetic ages is underlined by the fact that no such an age segregation is found in dwarfed sauropod populations. Waskow et al. (unpublished, (chapter 6)) as well as Scheil (2018) found an age segregation including all ontogenetic stages from young juveniles to senescent adults in the island dwarf *Europasaurus* (Scheil, 2018) and the dwarfed sauropod population of the Mother´s Day Quarry (Waskow et al., submitted, (chapter 4); Waskow et al., unpublished, (chapter 6)).

Ontogenetic ecological nice partitioning in average sized sauropods is also supported by ontogenetical differences in tooth morphology that hint to ontogenetically differing food sources at it has been described by Woodruff et al. (2018, (chapter 5)). Even if the remains of the juvenile diplodocid skull that lead to this assumption was also found at the Mother´s Day Quarry, it most likely belongs to an average sized sauropod taxon occurring at the same site

that produced the dwarfed sauropod population. The study of Waskow et al. (submitted, (chapter 4)) reveals the presence of at least two size morphs at the site the largest of which is only represented by early stage juveniles which further underlines niche partitioning between juvenile and adults in average sized sauropods.

7.6. Implications of skeletochronological correlations in dorsal ribs

7.6.1. Testing skeletal unity using dorsal ribs

For centuries skeletal articulation of the individual in finding position was the only way to prove skeletal unity. Additional methods like, e.g., the count of single and paired skeletal elements that should or could be present in one individual have been used to evaluate the likelihood of the number of individuals present at a certain site. However, recently Wiersma et al., (in review) introduced histology as a proper tool for proving skeletal unity using the example of several sauropod skeletons found at the Howe Stephens Quarry (Morrison Formation, Wyoming, USA). Even if mainly focusing on long bones, the study shows, that comparison of histological features (including, e.g., histologic ontogenetic stage (HOS, described by Klein and Sander (2008)), vascularization, and remodeling) can be used to prove or disprove skeletal unity of bones. In their study Wiersma et al., only shortly commented on dorsal rib histology and referred to the work of Waskow and Sander (2014) who described similarities in skeletochronology in all ribs of the rib cage of an articulated *Camarasaurus* individual independent of the varying shape and microstructure from proximal to distal and anterior to posterior.

The skeletochronological information store in ribs (Waskow and Sander, 2014; Waskow and Mateus, 2017, (chapter 2)) is an even better tool to test skeletal unity based on the uniqueness of the individual growth record and histology comparable to a fingerprint. Even in if growth record completeness may vary between ribs or other skeletal elements, by correlating thinner and thicker LAGs a distinct sequence of relative distances of LAGs should be seen in one individual. This difference in cycle thickness is caused by annual variations in nutrition intake. The method has been used in Waskow et al. (submitted, (chapter 4); unpublished, (chapter 6)) to exclude multiple usage of one individual for, e.g., statistical analysis of age distribution. A more detailed analysis on testing skeletal unity using dorsal ribs of sauropods that includes more examples of individual conformity in skeletochronology is work currently in progress by Waskow and Sander.

7.6.2. Testing time periods of deposition

Another possible usage of dorsal rib histology might be the verification or disproval of death assemblages. By correlating the outermost growth records of different individuals that lived in the same environment and died in the same year, similar patterns of food supply recognizable as differing cycle thicknesses should be seen, even in taxonomically,

ontogenetically and histologically differing animals. These similarities may not be as significant as they are in samples of differing skeletal bones of one individual (as described above), but still should be recognizable. Conversely animals that do show extremely differing skeletochronological records in the outermost cortex must either have used differing food sources or died in differing years. This way the time frame of skeletal remain deposition in a certain locality can be tested. Animals that died together, e.g., in a catastrophic event or during the same drought season should show similar growth records in terms of cycle thickness at least in the outermost cortex. The method has some limitations because it is only applicable to individuals that did not reach skeletal maturity before death and thus stored environmental conditions until death and is still to be tested which is work currently in progress by Tschopp, Waskow and Moretti.

7.7. Advantages of studying dorsal ribs

7.7.1. Advantages regarding loan and sampling

Histological sampling and CT scanning of dorsal ribs has several advantages over the usual long limb bone sampling. Every vertebrate specimen has numerous dorsal ribs on each side of the body. Thus, the chances of fossil preservation are relatively high compared to other appendicular skeletal elements. Consequentially, dorsal ribs are one of the most abundant finds of postcranial elements found in the fossil record of vertebrates. Additionally, ribs show few morphological diagnostic characters. These two facts induce curators to allow destructive sampling methods more frequently because sampling of ribs is less invasive for the integrity of the specimen itself. Oftentimes not all dorsal ribs of certain taxa are mounted in an exhibit which allows easier access to samples. In contrast to long bones, ribs are no weight bearing elements. Therefore, even if mounted as part of an exhibit, they are more accessible based on their size and numbers. A single rib missing from an exbibit is likely to draw less to no attention at all from for, e.g., a visitor as compared to a missing humerus of femur.

7.7.2. Scientific advantages

Besides these numerous facts facilitating the sampling itself, the inner structures of dorsal ribs also do show some scientific advantages over long bone samples. The growth record of dorsal ribs in most cases is remarkably complete compared to long bones (Waskow and Sander, 2014; Waskow and Mateus, 2017, (chapter 2)). Most dorsal rib cross-sections show growth record preservations over 50% and easily reach growth record completeness of 80% to 100 % in juvenile to young adult individuals. This is not only true for sauropods, where histological dorsal rib sampling is literally the only way to obtain an almost complete skeletochronological record based on the high formation rates of primary and secondary bone tissue seen in the thick cortex of the long bones (for comparison: the most complete

growth record for a sauropod known so far has been reported by Wings et al., (2007) to be 60% for a *Mamenchisaurus* ulna.), it is also true for other vertebrate specimens that do show good growth record preservation in the primary bone tissue of, e.g., humerus or femur as it has been described in chapter 7.3.2. Thus, at least in terms of growth record completeness, dorsal ribs do have advantages over standardized long bone samples. In their microanatomical investigations on dorsal ribs Canoville et al. (2016) furthermore concluded that dorsal ribs might contain an even stronger ecological signal in terms of habitat use because ribs are no weight bearing elements and thus are free of biomechanical constrains. Additionally, dorsal rib sampling allows the ecological comparison of amniote taxa in a broader scope because limbless taxa like, e.g., snakes, anguids, and amphisbaenians or aquatic forms that lost their hindlimbs can also be included.

7.8. Limits and challenges of interpreting dorsal rib growth records

Even if the histological sampling of ribs has many advantages, there are still some challenges to face. While the growth record in most dorsal ribs is remarkably complete, the statistical analyses of the stored information still shows some difficulties. In contrast to, e.g., humeri or femora that have a nearly circumferential cross-section at the usually sampled mid shaft region, the shape of dorsal rib cross-sections are very variable caused by morphological changes during ontogeny and taphonomic deformation that has stronger influence on ribs than on long bones. Thus, the varying local bone apposition rates and deformation processes impede a direct correlation of mass and age based on the growth record of a single individual as it is usually applied in long bones (Anderson et al., 1985; Mazzetta et al., 2004; Campione and Evans, 2012; Campione et al., 2014). However, distinct changes in growth rates like, e.g., EFS-formation or accomplishment of sexual maturity are still visible and not obscured by ontogenetic morphological changes. The difficulties described above might be resolved in the future based on the results of Waskow et al. (2014). They detected LAGs that become visible in a CT scan of a dorsal rib. By following these LAGs that represent the former surface of the bone in an earlier ontogenetic stage of the individual, they were able to reconstruct the morphology of the juvenile rib and to print it out with a 3D printer. To date, this research has only been presented on the annual SVP conference. A more detailed description of the method and its advantages is still work in progress by Waskow and Sander. It the future however, this method might yield possibilities to create a correction formula that allow mass based dorsal rib growth curve interpretations by subtracting the mass of reconstructed juvenile ribs in several ontogenetic stages from the original dorsal rib sample and comparing it to the morphological changes and growth record seen in the histological sample.

7.9. Conclusion and future perspectives

Dorsal ribs of tetrapods are an important tool for interpreting the life history of extinct animals (Waskow and Mateus, 2017, (chapter 2)). Especially in sauropods that lack complete skeletochronological information in their long bones sampling of these underestimated skeletal elements is crucial to understand their life history. By analyzing the microanatomy (Houssaye et al., 2016, (chapter 3)), histology, and especially growth records important information regarding ontogenetic ages at death, sexual and skeletal maturity as well as taxonomic assignment (Waskow and Mateus, 2017, (chapter 2); Waskow et al., submitted, (chapter 4); Waskow et al., unpublished, (chapter 6)) can be determined. Ecological information including habitat and ecological niche preference can be ascertained by analyzing larger datasets (Houssaye et al., 2016, (chapter 3); Waskow et al., submitted, (chapter 4); Waskow et al., unpublished, (chapter 6)) that can complement other morphological and functional analyses aiming to interpret the ecology of extinct taxa (Woodruff et al., 2018, (chapter 5)). In addition to that correlation of growth records stored in dorsal ribs have the potential to verify skeletal unity (Waskow et al., submitted, (chapter 4); Waskow et al., unpublished, (chapter 6)) and might be used in the future for testing periods of bone deposition in different individuals and taxa that may hint to catastrophic events or long-term deposition of body fossils.

All these results presented in this dissertation show the diversity of information about extinct animals that can be detected by studying dorsal ribs, a skeletal element formerly thought to be relatively undiagnostic. Nevertheless, the analysis of dorsal rib material yields even more potential that is still to be discovered. This includes the 3D reconstruction of juvenile bone morphology out of an adult bone by following LAGs detected in the CT that represent the former bone surface which in turn might have the potential to create a correction formula for ontogenetic changes in bone apposition rate that would enable reliable mass- based growth curve compilation out of a single rib sample in the future. Phylogenetical and ecological adaptations that cause significant differences in dorsal rib primary bone tissue, growth record, and haversian bone might be used in the future for taxonomical assignment and environmental reconstructions on an even more detailed level then presented in this study. In conclusion, this thesis should be seen as a starting point of a more detailed analysis of dorsal rib histology, to answer old and new, upcoming questions and reveal the life history of extinct animals in even more detail in the future.

7.10. References

Amson, E., de Muizon, C., Laurin, M., Argot, C., and Buffrénil, V. de (2014). Gradual adaptation of bone structure to aquatic lifestyle in extinct sloths from Peru. Proceedings of the Royal Society of London B: Biological Sciences 281(1782), 20140192.

Anderson, J. F., Hall-Martin, A., and Russell, D. A. (1985). Long bone circumference and weight in mammals, birds, and dinosaurs. Journal of Zoology Series A 207, 53-61.

Andrade, R. C., Bantim, R. A. M., de Lima, F. J., dos Santos Campos, L., de Souza Eleutério, L. H., and Sayão, J. M. (2015). New data about the presence and absence of the external fundamental system in archosaurs. Cadernos de Cultura e Ciência 14(1), 200-211.

Armstrong, D. P., Keevil, M. G., Rollinson, N., and Brooks, R. J. (2018). Subtle individual variation in indeterminate growth leads to major variation in survival and lifetime reproductive output in a long-lived reptile. Functional Ecology 32(3), 752-761.

Baksi, S. N. and Newbrey, J. W. (1989). Bone metabolism during antler growth in female reindeer. Calcified Tissue International 45, 314–317.

Bonicelli, A., Xhemali, B., Kranioti, E. F., and Zioupos, P. (2017). Rib biomechanical properties exhibit diagnostic potential for accurate ageing in forensic investigations. PloS ONE 12(5), e0176785.

Buffrénil, V. de. (1982). Morphogenesis of bone ornamentation in extant and extinct crocodilians. Zoomorphology 99(2), 155-166.

Buffrénil, V. de, Ricqles, A. de, Ray, C. E., and Domning, D. P. (1990). Bone histology of the ribs of the archaeocetes (Mammalia: Cetacea). Journal of Vertebrate Paleontology 10(4), 455-466.

Buffrénil, V. de, Canoville, A., D'Anastasio, R., and Domning, D. P. (2010). Evolution of sirenian pachyosteosclerosis, a model-case for the study of bone structure in aquatic tetrapods. Journal of Mammalian Evolution 17(2), 101-120.

Burr, D. B., Martin, R. B., Schaffler, M. B., and Radin, E. L. (1985). Bone remodeling in response to in vivo fatigue microdamage. Journal of Biomechanics 18, 156–200.

Campione, N. E., and Evans, D. C. (2012). A universal scaling relationship between body mass and proximal limb bone dimensions in quadrupedal terrestrial tetrapods. BMC Biology 10(1), 60.

Campione, N. E., Evans, D. C., Brown, C. M., and Carrano, M. T. (2014). Body mass estimation in non-avian bipeds using a theoretical conversion to quadruped stylopodial proportions. Methods in Ecology and Evolution 5(9), 913-923.

Canoville, A., and Laurin, M. (2009). Microanatomical diversity of the humerus and lifestyle in lissamphibians. Acta Zoologica 90(2), 110-122.

Canoville, A., and Laurin, M. (2010). Evolution of humeral microanatomy and lifestyle in amniotes, and some comments on palaeobiological inferences. Biological Journal of the Linnean Society 100(2), 384-406.

Canoville, A., Buffrénil, V. de, and Laurin, M. (2016). Microanatomical diversity of amniote ribs: An exploratory quantitative study. Biological Journal of the Linnean Society 118(4), 706-733.

Canoville, A., Laurin, M., and Buffrénil, V. de (2017). Quantitative data on bone vascular supply in lissamphibians: Comparative and phylogenetic aspects. Zoological Journal of the Linnean Society 182(1), 107-128.

Carballido, J. L., Marpmann, J. S., Schwarz- Wings, D., and Pabst, B. (2012). New information on a juvenile sauropod specimen from the Morrison Formation and the reassessment of its systematic position. Palaeontology 55(3), 567-582.

Cardoso, L., Herman, B. C., Verborgt, O., Laudier, D., Majeska, R. J., and Schaffler, M. B. (2009). Osteocyte Apoptosis Controls Activation of Intracortical Resorption in Response to Bone Fatigue. Journal of Bone and Mineral Research 24, 597–605.

Cebra-Thomas, J., Tan, F., Sistla, S., Estes, E., Bender, G., Kim, C., Estes, E., Riccio, P., and Gilbert, S. F. (2005). How the turtle forms its shell: A paracrine hypothesis of carapace formation. Journal of Experimental Zoology Part B: Molecular and Developmental Evolution 304(6), 558-569.

Cerda, I. A., and Chinsamy, A. (2012). Biological implications of the bone microstructure of the Late Cretaceous ornithopod dinosaur Gasparinisaura cincosaltensis. Journal of Vertebrate Paleontology 32(2), 355-368.

Chinsamy-Turan, A. (2005). The microstructure of dinosaur bone: Deciphering biology with fine-scale techniques. Baltimore, Maryland, The Johns Hopkins University Press.

Chinsamy, A., and W. J. Hillenius. (2004). Physiology of non-avian dinosaurs. In: Weishampel, D.B., Dodson, P., and Osmólska, H., editors. The Dinosauria, second edition. Berkeley, California, University of California Press: 643-659.

Chinsamy, A., Rich, T., and Vickers-Rich, P. (1998). Polar dinosaur bone histology. Journal of Vertebrate Paleontology 18(2), 385-390.

Congdon, J. D., Gibbons, J. W., Brooks, R. J., Rollinson, N., and Tsaliagos, R. N. (2013). Indeterminate growth in long-lived freshwater turtles as a component of individual fitness. Evolutionary Ecology 27(2), 445-459.

Cormack, D.H. (1987). Ham's Histology. Philadelphia, JB Lippincott Company.

Cormier, J. M., Stitzel, J. D., Duma, S. M., and Matsuoka, F. (2005). Regional variation in the structural response and geometrical properties of human ribs. In: Annual Proceedings/Association for the Advancement of Automotive Medicine. Volume 49. Association for the Advancement of Automotive Medicine: 153.

Cowen, R. (1996). Locomotion and respiration in aquatic air-breathing vertebrates. Evolutionary Paleobiology, 337-354.

Curry, K. A. (1999). Ontogenetic histology of *Apatosaurus* (Dinosauria: Sauropoda): New insights on growth rates and longevity. Journal of Vertebrate Paleontology 19(4), 654-665.

Delannoy, Y., Colard, T., Cannet, C., Mesli, V., Hédouin, V., Penel, G., and Ludes, B. (2018). Characterization of bone diagenesis by histology in forensic contexts: A human taphonomic study. International Journal of Legal Medicine 132(1), 219-227.

Dumont, M., Laurin, M., Jacques, F., Pelle, E., Dabin, W., and Buffrénil, V. de (2013). Inner architecture of vertebral centra in terrestrial and aquatic mammals: A two-dimensional comparative study. Journal of Morphology 274(5), 570-584.

Enlow, D. H., and Brown, S. O. (1958). A comparative histological study of fossil and recent bone tissues. Part III. Texas Journal of Science 10, 187–230.

Erickson, G. M. (2005). Assessing dinosaur growth patterns: A microscopic revolution. Trends in Ecology and Evolution 20(12), 677-684.

Erickson, G. M., Curry Rogers, K., Varricchio, D. J., Norell, M. A., and Xu, X. (2007). Growth patterns in brooding dinosaurs reveals the timing of sexual maturity in non-avian dinosaurs and genesis of the avian condition. Biology Letters 3, 558-561.

Erickson, G. M., Makovicky, P. J., Currie, P. J., Norell, M. A., Yerby, S. A., and Brochu, C. A. (2004). Gigantism and comparative life-history parameters of tyrannosaurid dinosaurs. Nature 430(7001), 772-775.

Fish, F. E., and Stein, B. R. (1991). Functional correlates of differences in bone density among terrestrial and aquatic genera in the family Mustelidae (Mammalia). Zoomorphology 110(6), 339-345.

Francillon-Vieillot, H., Buffrénil, V. de, Castanet, J., Géraudie, J., Meunier, F. J., Sire, Y., Zylberberg, L., and Ricqlès, A. de (1990). Microstructure and mineralization of vertebrate skeletal tissues. In: Carter, J. G., editor. Skeletal biomineralization: patterns, processes and evolutionary trends 1. New York, Van Nostrand Reinhold: 471-530.

Frost, H. M. (1960). Presence of microscopic cracks in vivo in bone. Henry Ford Hospital Medical Bulletin 8(35), 158.

García-Martínez, D., Recheis, W., and Bastir, M. (2016). Ontogeny of 3D rib curvature and its importance for the understanding of human thorax development. American journal of physical anthropology 159(3), 423-431.

Germain, D., and Laurin, M. (2005). Microanatomy of the radius and lifestyle in amniotes (Vertebrata, Tetrapoda). Zoologica Scripta 34(4), 335-350.

Granik, G., and Stein, I. (1973). Human ribs: Static testing as a promising medical application. Journal of Biomechanics 6(3), 9-10.

Halliday, T. R., and Verrell, P. A. (1988). Body size and age in amphibians and reptiles. Journal of Herpetology, 253-265.

Hayashi, S., Houssaye, A., Nakajima, Y., Chiba, K., Ando, T., Sawamura, H., Inuzuka, N., Kaneko, N., and Osaki, T. (2013). Bone inner structure suggests increasing aquatic adaptations in Desmostylia (Mammalia, Afrotheria). PLoS ONE 8(4), e59146.

Hirasawa, T., Pascual-Anaya, J., Kamezaki, N., Taniguchi, M., Mine, K., and Kuratani, S. (2015). The evolutionary origin of the turtle shell and its dependence on the axial

arrest of the embryonic rib cage. Journal of Experimental Zoology Part B: Molecular and Developmental Evolution 324(3), 194-207.

Holcombe, S. (2016). The development of population-wide descriptions of human rib and rib cage geometry. Doctoral thesis, University of Michigan, Ann Arbor.

Holcombe, S. A., Wang, S. C., and Grotberg, J. B. (2017). The effect of age and demographics on rib shape. Journal of anatomy 231(2), 229-247.

Horner, J. R., Ricqlès, A. de, and Padian, K. (1999). Variation in dinosaur skeletochronology indicators: Implications for age assessment and physiology. Paleobiology 25(3), 295-304.

Houssaye, A., Tafforeau, P., and Herrel, A. (2014). Amniote vertebral microanatomy–what are the major trends? Biological Journal of the Linnean Society 112(4), 735-746.

Houssaye, A., Tafforeau, P., De Muizon, C., and Gingerich, P. D. (2015). Transition of Eocene whales from land to sea: Evidence from bone microstructure. PLoS ONE 10(2), e0118409.

Houssaye, A., Waskow, K., Hayashi, S., Cornette, R., Lee, A. H., Hutchinson, J. R. (2016). Biomechanical evolution of solid bones in large animals: A microanatomical investigation. Biological Journal of the Linnean Society 117, 350–371.

Kammerer, C. F., Flynn, J. J., Ranivoharimanana, L., and Wyss, A. R. (2008). New material of *Menadon besairiei* (Cynodontia: Traversodontidae) from the Triassic of Madagascar. Journal of Vertebrate Paleontology 28(2), 445-462.

Kemper, A. R., McNally, C., Pullins, C. A., Freeman, L. J., Duma, S. M., and Rouhana, S. W. (2007). The biomechanics of human ribs: Material and structural properties from dynamic tension and bending tests. Stapp Car Crash Journal 51, 235–273.

Kriloff, A., Germain, D., Canoville, A., Vincent, P., Sache, M., and Laurin, M. (2008). Evolution of bone microanatomy of the tetrapod tibia and its use in palaeobiological inference. Journal of Evolutionary Biology 21(3), 807-826.

Klein, N., and Sander, P. M. (2008). Ontogenetic stages in the long bone histology of sauropod dinosaurs. Paleobiology 34(2), 247-263.

Klein, N., and Sichelschmidt, O. J. (2014). Remarkable dorsal ribs with distinct uncinate processes from the early Anisian of the Germanic Basin (Winterswijk, the Netherlands). Neues Jahrbuch für Geologie und Paläontologie-Abhandlungen 271(3), 307-314.

Klevezal, G. A. (1996). Recording structures of mammals. Determination of age and reconstruction of life history. Rotterdam, A. A. Balkema.

Köhler, M., and Moyà-Sola, S. (2009). Physiological and life history strategies of a fossil large mammal in a resource-limited environment. Proceedings of the National Academy of Sciences of the United States of America 106, 20354–20358.

Laurin, M., Girondot, M., and Loth, M. M. (2004). The evolution of long bone microstructure and lifestyle in lissamphibians. Paleobiology 30(4), 589-613.

Laurin, M., Canoville, A., and Germain, D. (2011). Bone microanatomy and lifestyle: A descriptive approach. Comptes Rendus Palevol 10(5-6), 381-402.

Lee, T. C., Staines, A., and Taylor, D. (2002). Bone adaptation to load: Microdamage as a stimulus for bone remodelling. Journal of Anatomy 201, 437–446.

Lehman, T. M., and Coulson, A. B. (2002). A juvenile specimen of the sauropod dinosaur *Alamosaurus sanjuanensis* from the Upper Cretaceous of Big Bend National Park, Texas. Journal of Paleontology 76(1), 156-172.

Lyson, T. R., and Joyce, W. G. (2012). Evolution of the turtle bauplan: The topological relationship of the scapula relative to the ribcage. Biology letters 8(6), 1028-1031.

Maina, J. N. (2017). Biology of the Avian Respiratory System. Springer Verlag.

Mazzetta, G. V., Christiansen, P., and Farina, R. A. (2004). Giants and bizarres: Body size of some southern South American Cretaceous dinosaurs. Historical Biology 2004, 1-13.

Mitchell, J. (2017). Cortical Bone Remodeling in Amniota: A Functional, Evolutionary and Comparative Perspective of Secondary Osteons. Doctoral thesis, University of Bonn.

Mitchell, J., and Sander, P. M. (2014). The three-front model: A developmental explanation of long bone diaphyseal histology of Sauropoda. Biological Journal of the Linnean Society 112(4), 765-781.

Mohr, M., Abrams, E., Engel, C., Long, W. B., and Bottlang, M. (2007). Geometry of human ribs pertinent to orthopedic chest-wall reconstruction. Journal of Biomechanics 40(6), 1310-1317.

Mori, S., and Burr, D. (1993). Increased intracortical remodeling following fatigue damage. Bone 14, 103-158.

Myers, T. S., and Storrs, G. W. (2007). Taphonomy of the Mother's Day quarry, Upper Jurassic Morrison Formation, south-central Montana, USA. Palaios 22, 651-666.

Myers, T. S., and Fiorillo, A. R. (2009). Evidence for gregarious behavior and age segregation in sauropod dinosaurs. Palaeogeography, Palaeoclimatology, Palaeoecology 274(1), 96-104.

Nakajima, Y., Hirayama, R., and Endo, H. (2014). Turtle humeral microanatomy and its relationship to lifestyle. Biological Journal of the Linnean Society 112(4), 719-734.

Osborn, H. F., and Mook, C. C. (1921). *Camarasaurus*, *Amphicoelias*, and other sauropods of Cope. Bulletin of the Geological Society of America 30(1), 379-388.

Padian, K., and Horner, J. R. (2004). Dinosaur physiology. In: Weishampel, D. B., Dodson, P. and Osmólska, H., editors. The Dinosauria, second edition. Berkeley, California, University of California Press: 660-671.

Padian, K., Horner, J. R., and Ricqlès, A. de (2004). Growth in small dinosaurs and pterosaurs: The evolution of archosaurian growth strategies. Journal of Vertebrate Paleontology 24(3), 555-571.

Parfitt, A. (2010). Skeletal heterogeneity and the purposes of bone remodeling: Implications for the understanding of osteoporosis. In: Marcus, R. Feldman, D., Nelson, D., and

Rosen, C., editors. Fundamentals of osteoporosis. San Diego, California, Academic Press: 35–52.

Price, E. R., Wallace, B. P., Reina, R. D., Spotila, J. R., Paladino, F. V., Piedra, R., and Vélez, E. (2004). Size, growth, and reproductive output of adult female leatherback turtles *Dermochelys coriacea*. Endangered Species Research 1, 41-48.

Quémeneur, S., Buffrenil, V. de, and Laurin, M. (2013). Microanatomy of the amniote femur and inference of lifestyle in limbed vertebrates. Biological Journal of the Linnean Society 109(3), 644-655.

Richmond, N. D. (1965). Perhaps juvenile dinosaurs were always scarce. Journal of Paleontology, 503-505.

Sallan, L. C. (2012). Tetrapod-like axial regionalization in an early ray-finned fish. Proceedings of the Royal Society of London B: Biological Sciences 279(1741), 3264-3271.

Sander, P. M. (2000). Longbone histology of the Tendaguru sauropods: Implications for growth and biology. Paleobiology 26(3), 466-488.

Sander, P. M., and Andrássy, P. (2006). Lines of arrested growth and long bone histology in Pleistocene large mammals from Germany. Palaeontographica, Abt. A 277(1), 143-159.

Sander, P. M., Klein, N., Stein, K., and Wings, O. (2011). Sauropod bone histology and its implicatios for sauropod biology. In: Klein, N., Remes, K., Gee, C. T., and Sander, P. M., editors. Biology of the Sauropod Dinosaurs. Bloomington, Indiana, Indiana University Press: 276-302.

Schachner, E. R., Lyson, T. R., and Dodson, P. (2009). Evolution of the respiratory system in non-avian theropods: Evidence from rib and vertebral morphology. The Anatomical Record: Advances in Integrative Anatomy and Evolutionary Biology: Advances in Integrative Anatomy and Evolutionary Biology 292(9), 1501-1513.

Scheil, M., Wings, O., Knötschke, N. and Sander, P. M. (unpublished) The age structure of the *Europasaurus* assemblage from the Langenberg Quarry (Kimeridgian, Upper Jurassic, Lower Saxony, Germany). MSc thesis, University of Bonn.

Starck, J. M., and Chinsamy, A. (2002). Bone microstructure and developmental plasticity in birds and other dinosaurs. Journal of Morphology 254(3), 232-246.

Storrs, G. W., Oser, S. E., and Aull, M. (2012). Further analysis of a Late Jurassic dinosaur bone-bed from the Morrison Formation of Montana, USA, with a computed three-dimensional reconstruction. Earth and Environmental Science Transactions of the Royal Society of Edinburgh 103(3-4), 443-458.

Troyer, A. de, and Boriek, A. M. (2011). Mechanics of the respiratory muscles. Comprehensive Physiology 1(3), 1273-1300.

Turvey, S. P., Green, O. R., Holdaway, R. N. (2005). Cortical growth marks reveal extended juvenile development in New Zealand moa. Nature 435, 940–943.

Verborgt, O., Gibson, G. J., and Schaffler, M. B. (2000). Loss of osteocyte integrity in association with microdamage and bone remodeling after fatigue in vivo. Journal of Bone and Mineral Research 15, 60–67.

Wall W. P. (1983). The correlation between high limb-bone density and aquatic habits in recent mammals. Journal of Paleontology 57, 197–207.

Waskow, K. (2014). Reconstructing juvenile Morphology: A non-destructive method to detect histological structures in Computed Tomography (CT) and its potential for future research, using the example of sauropod ribs. 74st Annual Meeting of the Society of Vertebrate Paleontology 34:252.

Waskow, K., and Sander, P. M. (2014). Growth record and histological variation in the dorsal ribs of *Camarasaurus* sp. (Sauropoda). Journal of Vertebrate Paleontology 34(4), 852-869.

Waskow, K., and Mateus, O. (2017). Dorsal rib histology of dinosaurs and a crocodylomorph from western Portugal: Skeletochronological implications on age determination and life history traits. Comptes Rendus Palevol 16(4), 425-439.

Waskow, K., Griebeler, E. M, and Sander, P.M. (unpublished) Life history traits of different Jurassic sauropod taxa – Dorsal rib histology reveals differences in ages at sexual and skeletal maturity between macronarians and diplodocoids.

Waskow, K., Wiersma, K., Tschopp, E., Woodruff, D. C., Storrs, G., and Sander, P. M. (submitted). Histological evidence for dwarfism and different morphotypes of diplodocine sauropods within the Upper Jurassic Mother's Day Quarry (Morrison Formation, Montana, USA). Acta Palaeontologica Polonica.

Wiersma, K., Canoville, A., Siber, H.-J., and Sander, P. M. (in review). Testing hypothesis of skeletal unity using bone histology: The case of the sauropod remains from the Howe-Stephens and Howe Scott quarries (Morrison Formation, Wyoming). Palaeontologia Electronica.

Wings, O., Sander, P. M., Tütken, T., Fowler, D. W., and Sun, G. (2007). Growth and life history of Asia's largest dinosaur. Journal of Vertebrate Paleontology 27(3), 167A.

Woodruff, D. C., Carr, T. D., Storrs, G. W., Waskow, K., Scannella, J. B., Nordén, K. K., and Wilson, J. P. (2018). The smallest diplodocid skull reveals cranial ontogeny and growth-related dietary changes in the largest dinosaurs. Scientific Reports 8(1), 14341.

Woodward, H. N., Horner, J. R., Farlow, J. O. (2011). Osteohistological evidence for determinate growth in the American *Alligator*. Journal of Herpetology 45(3), 339-342.

Yoganandan, N., and Pintar, F. A. (1998). Biomechanics of human thoracic ribs. Journal of Biomechanical Engineering 120(1), 100-104.

Peer reviewed publications

Waskow, K., Wiersma, K., Tschopp, E., Woodruff, D. C., Storrs, G. W., and Sander, P. M. (submitted): Histological evidence for dwarfism and different morphotypes of diplodocine sauropods within the Upper Jurassic Mother's Day Quarry (Morrison Formation, Montana, USA). *Acta Palaeontologica Polonica.*

Waskow, K., Grzegorczyk D., and Sander, P. M. (2018): The first *Tyrannoneustes lythrodectikos* from the Callovian (Upper Mid-Jurassic) of Germany. *PalZ.*

Waskow, K. and Mateus, O. (2017): Rib histology and skeletochronology of Jurassic and Cretaceous dinosaurs and a crocodile from Western Portugal: implications on age determination and life history traits, *Comptes Rendus Palevol.*

Waskow, K and Sander, P. M. (2014): Growth record and histological variation in the dorsal ribs of Camarasaurus sp. (Sauropoda), Journal of Vertebrate Paleontology, 34:4, 852-869, DOI: 10.1080/02724634.2014.840645.

Houssaye, A., **Waskow**, K, Hayashi, S., Cornette, R., Lee, A. H., and Hutchinson, J. R. (2015): Biomechanical evolution of solid bones in large animals: a microanatomical investigation. *Biological Journal of the Linnean Society*.

Woodruff, D. C., Carr, T. D., Storrs, G. W., **Waskow**, K., Scannella, J. B., and Nordén, K. K. (2018): the smallest diplodocus skull: recapitulation of phylogeny and ontogenetic dietary changes in the largest dinosaurs. *Nature Communications.*